Seventh International Oil Sands Tailings Conference

Edmonton, Alberta, Canada: December 4-7, 2022
U of A Geotechnical Centre

IOSTC

SEVENTH INTERNATIONAL

OIL SANDS

TAILINGS CONFERENCE

Edmonton, Alberta
Canada

December 2022

Proceedings of the Seventh International Oil Sands Tailings Conference
4 - 7 December 2022, Edmonton, Alberta, Canada

Seventh International Oil Sands Tailings Conference

Edited by

Nicholas A. Beier, G. Ward Wilson & David C. Sego
University of Alberta Geotechnical Centre and
Oil Sands Tailings Research Facility

University of Alberta Geotechnical Centre Edmonton, Alberta, Canada

Published by: University of Alberta, Dept. of Civil & Environmental Engineering

ISBN 978-1-55195-489-9
Printed in Canada

FORWARD

It is with great pleasure that we present the **Seventh International Oil Sands Tailings Conference 2022 (IOSTC'22)**. In the tumultuous times during the unprecedented pandemic starting in early 2020, the oil sands industry needed to be flexible and adapt to changing workplace requirements on short notice. The oil sands industry demonstrated great resiliency in the face of the unknown and is well on its way to recovery. Our environmental obligations toward the treatment of legacy tailings remain, and the oil sands industry, in partnership with academia, consultancies and its regulator, continues to provide innovative technologies to tackle these challenges.

We are also aware of the growing interest of reclamation strategies and technologies from Indigenous communities and the public. Special to this year's conference, we are very pleased to include a panel session on "Indigenous perspectives on oil sand tailings management and reclamation" moderated by Jessica Vandenberghe, P.Eng., M.Sc., FEC, Assistant Dean, Engineering Community and Culture & Industrial Professor–Indigenous Engineering at the Faculty of Engineering, University of Alberta. Panelists include members of Athabasca Chipewyan First Nation and Mikisew Cree First Nation, as well as consultants who provide services to Indigenous communities situated in the oil sands region of Alberta.

Thank you to our Keynote Speakers, John Brogly, Paul Cavanagh and Heather Kaminsky, for sharing their experiences and expertise in managing different aspects of oil sands tailings, from water considerations and fluid fine tailings to designing deep cohesive tailings deposits. We are grateful for the strong support we received for **IOSTC'22** by the authors who have submitted their manuscripts, by the exhibitors who continue to support the conference and display their innovative technologies and most importantly by our sponsors who recognize the important contribution of this conference to meeting the challenges presented by oil sands tailings to the environment and the viability of this most important Alberta industry.

We want to personally thank members of the OSTRF and the University of Alberta Geotechnical Centre for their encouragement and support. The conference would not have been possible without the dedication of Vivian Giang, Jen Stogowski and especially Sally Petaske who provided so much assistance and leadership.

The technical challenges associated with fluid fine tailings (FFT), including legacy mature fine tailings (MFT), require novel and innovative approaches to ensure the sustainable development and environmental stewardship of Alberta's vast oil sands. It was with this in mind that the session themes and manuscripts were selected for presentation and inclusion in the proceedings. We want to thank our professional colleagues who willingly contributed their technical knowledge, experiences and especially their time to write the manuscripts that make the proceedings of this conference.

May you find further insights to enhance your understanding of the current state-of-practice in oil sands tailings management through **IOSTC'22**.

Nicholas A. Beier, G. Ward Wilson and David C. Sego
Co-Chairs, IOSTC 2022 Organizing Committee

IOSTC LAND ACKNOWLEDGEMENT

The oil sands mine sites and tailings structures we work with are situated on the traditional Indigenous territories in Treaty 8 and have an impact on Indigenous people, the land and communities. We would like to acknowledge that the University of Alberta and where we gather today in conference is located on Treaty 6 territory. We respect the histories, languages, and cultures of First Nations, Métis, Inuit, and all First Peoples of Canada, whose presence continues to enrich our vibrant community. We hope that we all can work towards reconciliation personally and in the professional realm through initiatives that increase equity, diversity and inclusion of Indigenous peoples.

The UofA Geotechnical Centre

OSTRF

Thank you to the following sponsors for their support in making the Seventh International Oil Sands Tailings Conference a huge success.

PLATINUM SPONSOR:

MIKISEW CONETEC

GOLD SPONSORS:

ALFA LAVAL

www.alfalaval.ca

cosia

ALFALUZ

HATCH

kemira

SNF

WIFI SPONSOR:

ALBERTA INNOVATES

LANYARD SPONSOR:

HATCH

TABLE OF CONTENTS

KEYNOTE ABSTRACTS:

MANAGING OIL SANDS MINE WATERS – A BALANCED PERSPECTIVE
J. Brogly *2*

THE STATE OF OIL SANDS FLUID FINE TAILINGS
H. Kaminsky *3*

DESIGNING DEEP COHESIVE OIL SANDS TAILINGS DEPOSITS
P. Cavanagh *4*

SESSION 1:

TAILINGS BEHAVIOUR TYPE TO PREDICT OIL SANDS TAILINGS CONSTITUENTS FROM THE GAMMA CONE PENETRATION TEST
I. Entezari, D. McGowan, J. Glavina and J. Sharp *6*

CHARACTERIZATION STUDY OF OIL SAND TAILINGS AT SUNCOR'S POND 5 TAILINGS STORAGE FACILITY
Y. Zhang, A.H. Abusaid, G.W. Pollock and D. Uffen *16*

ENHANCED IN-LINE FLOCCULATION OF FFT AND ITS CO-DEPOSITION WITH CST
R. Moussavi Nik and G. Sakuhuni *25*

SESSION 2:

CONE FORMATION DYNAMICS DURING DREDGING OF OIL SANDS TAILINGS PONDS – FIELD OBSERVATIONS AND COMPARISON WITH PREDICTION OF COMPUTATIONAL MODELS
T. Bugg, T. Bittner and B. Derakhshandeh *38*

INTEGRATED DAM BREACH AND GEOTECHNICAL MONITORING OF TAILINGS DAMS USING FIBER OPTICS SENSING TECHNOLOGY
Z. Anderson, S. Alkhaffaf and J. Furlong *48*

AUTOMATED SPECTROSCOPIC METHOD AND PLATFORM FOR ACTIVE CLAY AND WATER HARDNESS MEASUREMENT
R. Sun, D. Williams and L. McGilp *55*

CHARACTERIZATION OF NAPHTHENIC DILUENT IN OILSANDS TAILINGS STREAMS AND PONDS
C. Laborde-Boutet, W. Brown, E. Hollander and B. Derakhshandeh *64*

SESSION 3:

A PROTOCOL TO ASSESS AND SCREEN NEW FLOCCULANT FOR SUNCOR'S PASS PROGRAM PLANNING
Y. Li, H. Kaminsky, A. Revington and A. Sadighian *74*

NOVEL DEWATERING TECHNOLOGY TO TREAT FLUID FINE TAILINGS
W. Florman, C. Kujawa, G. Freeman, D. Sego, O. Ilkiw and E. Peluso *84*

SESSION 3 CONT'D:

APPLICATION OF NANOCELLULOSE FILAMENT (NFC) IN ENHANCING THE GEOTECHNICAL PROPERTIES OF OIL SANDS TAILINGS
Y. Zhang, N. Beier, K. Gourlay and G. Minhas *93*

HIGH-FINES SAND TAILINGS AS A NOVEL OIL SANDS TAILINGS TREATMENT TECHNOLOGY
S. Sun, E. Devereux, H. Kaminsky and M. Louis Catling *105*

SESSION 4:

GROWTH AND SURVIVAL OF NATIVE SPECIES IN SHALLOW CAPPED THICKENED TAILINGS: A MESO-SCALE GREENHOUSE STUDY
D. Degenhardt, A. Van Dongen, S.G. Schreiber and A. Bekele *118*

GROWTH AND SURVIVAL OF NATIVE WETLAND SPECIES IN SHALLOW CAPPED CENTRIFUGE TAILINGS AND CO-MIX TAILINGS: A MESO-SCALE GREENHOUSE STUDY
D. Degenhardt, A. Van Dongen, J. Hudson, N. Utting and S.G. Schreiber *131*

MONITORING NATIVE PLANT ESTABLISHMENT ON TREATED FLUID FINE TAILINGS USING WORLDVIEW 3 SATELLITE DATA
B. Rivard, A. Schoonmaker, J. Feng and M.Lipsett *147*

SESSION 5:

COMPLIANCE WITH TAILINGS MANAGEMENT FRAMEWORK OBJECTIVES – A 3RD PARTY PERSPECTIVE
J. Blum *159*

GOVERNMENT POLICY AND REGULATORY INFLUENCE ON OIL SANDS TAILINGS INNOVATION
J. Matthews *166*

WHAT DO WE MEAN BY "SAFE CLOSURE" FOR OIL SANDS TAILINGS FACILITIES?
G. McKenna *180*

SESSION 6:

ASSESSMENT TOOL FOR LANDFORMS CONTAINING POTENTIALLY FLOWABLE TAILINGS
G. Miller, B. Ramdharry, S. Martens, C. Isaka, A. James, A. Burnett, D. Bell, J. Law, J. Haverhals, N. Eenkooren, P.Cavanagh and W. Mimura *194*

COMPARING ADAPTIVE MANAGEMENT AND THE OBSERVATIONAL METHOD FOR MINE CLOSURE AND RECLAMATION
A. Paul, N. Beier and D. Barsi *208*

FLUID TAILINGS THERMAL DRYING: MORE PROMISING THAN YOU MIGHT THINK
J. Matthews *219*

SESSION 7:

INSIGHTS INTO DUTCH VACUUM CONSOLIDATION METHODS AND THEIR ABILITY TO IMPROVE STABILITY OF SOFT CLAY DEPOSITS FOR FILL PLACEMENT
J. Dijkstra and E. Meshkati *238*

CHEMICALLY-ENHANCED MODIFICATIONS TO IMPROVE DEWATERING PERFORMANCE FOR OIL SANDS TAILINGS
M. Pelaez, X.Yin and T. Fenderson *250*

PSEUDO TAILINGS AND FLOCCULATED FFT (FFFT) PIPELINE TRANSPORTATION PRESSURE LOSS METHOD
M. St-Cyr, A. Holik and M. Hujber *256*

SESSION 8:

ON THE MAGNITUDE AND RATE OF AGEING IN BOTH SOFT SOILS AND OIL SANDS TAILINGS
A. Patel and P. Simms *263*

A META-ANALYSIS OF POTENTIAL PRE-CONSOLIDATION BEHAVIOUR IN OIL SANDS TAILINGS
A. Abdulnabi, T. Moore, S. Proskin, N. Beier and D. Sego *273*

CONSOLIDATION-CREEP MODELING IN OIL SANDS TAILINGS DEPOSITS
N. Gheisari, P. Simms, S. Qi, F. Murphy, G. Gjerapic and D. Znidarcic *286*

MODELING OF TIME DEPENDENCY OF STRENGTH IN TAILINGS USING MATERIAL POINT MODELLING (MPM)- DELTAIC SAND CAPPING APPLICATION
M. Martinelli, E. Meshkati, D. Luger, A. Talmon, J.Greenwood and C. Tamagnini *298*

SESSION 9:

THE USE OF PRECIPITATED CALCIUM CARBONATE (PCC) IN FLUID FINE TAILINGS TREATMENT TO ENHANCE CIRCULAR ECONOMIES IN TAILINGS RECLAMATION
Y. Li, C. Romero, A. Sedgwick, R. Lacey, and B.M. Smith *310*

RESIDUAL BITUMEN RECOVERY FROM FLUID FINE TAILINGS AND ENHANCED DEWATERING PERFORMANCE WITH A NOVEL TECHNOLOGY – PURETAILS
M. Ghuzi, Y. Li, C. Romero, A. Sedgwick, G. Terry and N. Bosworth *316*

INFLUENCE OF CLAYS AND ORGANIC-RICH SOLIDS ON TAILING BEHAVIOUR
B. Patarachao, R. Way, A. Zborowski, J. Kung, M. Couillard, D. Tyo, Y. Li and H. Kaminsky *324*

International Oil Sands Tailings Conference

December 4 - 7, 2022
Edmonton, Alberta, Canada

Keynote Abstracts

OIL SANDS MINE WATER MANAGEMENT – A BALANCED PERSPECTIVE

John Brogly, Director, Water, COSIA

ABSTRACT

All oil sands commercial production facilities use water-based extraction. COSIA's water aspiration is to be world leaders in water management, producing Canadian energy with no adverse impact on water. For the oil sands mining sector, that means balancing multiple objectives through the use of the Integrated Water Management Framework: minimizing how much fresh water is used while minimizing other environmental effects of water management including increased salination of mine waters, increased green-house gas emissions, waste water disposal and delayed mine site reclamation. Topics covered include fresh water availability and use, trace elements in oil sands and their relative impact on the Athabasca River watershed, how the Integrated Water Management Framework has been used on oil sands mine sites, water treatment technology selection and deployment and finally, the importance of treated mine water release as a key element of responsible water management.

THE STATE OF OIL SANDS FLUID FINE TAILINGS

Heather Kaminsky, NSERC Industrial Research Chair, NAIT

ABSTRACT

The IOSTC conferences began in 2008 coincident with the release of Directive 074, targeted at addressing stakeholder concerns over the volume of fluid fine tailings. Since then, the conference has borne witness to results from hundreds of bench scale studies and dozens of pilot trials. This presentation reviews the current state of fluid fine tailings based on the publicly available regulatory reports including the current volume of fluid tailings, the technologies used to treat fluid tailings by the different operators, and the ready to reclaim criteria for each deposit.

DESIGNING DEEP COHESIVE OIL SAND TAILINGS DEPOSITS

Paul C. Cavanagh, Senior Principal, Global Dam Safety, Imperial

ABSTRACT

The Canadian Oil Sands Innovation Alliance (COSIA) created the Deep Deposit Working Group (DDWG) to identify and develop approaches and technologies for the design and implementation of deep cohesive tailings deposits and to explore different capping strategies for the reclamation of these deposits with a wetland or terrestrial landform.

The oil sands industry expects deep cohesive deposits to be included in operators' mine, tailings and closure plans, and supports their development when consistent with reclamation and land use objectives. Developing a deep deposit to support a closure landform at this scale is challenging, takes time, and is subject to changing expectations for performance and outcomes.

The Deep Deposit Design Guide (the Guide) was created to capture industry knowledge and experience, provide design and implementation guidance for deep deposit development, and outlines a design process based on an observational method so teams may prepare work scopes, assign responsibilities, and govern deposit development. The Guide advocates designing for most likely conditions and stewarding through execution using timely, pre-designed contingencies.

The Deep Deposit Design Guide:

- Is integral with and complimentary to existing corporate governance frameworks (e.g.; community relations);
- Summarizes deep deposit characteristics, knowledge, experience, available technologies and mitigations, and provides guidance for deep deposit development from concept to reclamation based on accepted engineering practice (e.g.; observational method);
- Provides practical comparative baselines for site-specific projects and applications; and
- Will be updated periodically as new information, knowledge and experience is acquired.

SESSION 1

TAILINGS BEHAVIOUR TYPE TO PREDICT OIL SANDS TAILINGS CONSTITUENTS FROM THE GAMMA CONE PENETRATION TEST

Iman Entezari, Dallas McGowan, Joseph Glavina, and James Sharp
ConeTec Investigations Ltd., Burnaby, BC, Canada

ABSTRACT

This paper presents an update on the development of an empirical relationship, called Tailings Behaviour Type (TBT), to estimate oil sands tailings constituents from in-situ gamma piezocone and piezoball penetration tests (GCPTu and GBCPTu). In this study, the 2020 development dataset was expanded to include not only more paired GCPTu and laboratory results but also to include paired GBCPTu and laboratory results. The TBT models were calibrated to work for both GCPTu and GBCPTu profiles. TBT models were developed to estimate % solids by mass, % 44 µm fines by mass, and methylene blue index (MBI). The TBT models are robust and capable of estimation of tailings properties from across the oil sands mining region. A Class A performance assessment showed TBT models can predict the contents of solids and total fines within 4.26 and 5.35 wt% error, respectively, assuming the laboratory data was perfectly accurate. MBI of oil sands tailings is predicted within 1.05 meq/100g error. TBT models enable mine operators to efficiently analyze the tailings constituents in-situ, saving time and expense.

INTRODUCTION

Background

In-situ testing, mainly gamma piezocone and piezoball penetration tests (GCPTu and GBCPTu), and laboratory analysis of ex-situ tailings samples are widely used to characterize oil sands tailings. Laboratory testing directly provides tailings constituents, while in-situ profiles directly and indirectly provide stratigraphy, strength, hydrogeological and engineering properties of the tailings.

Since 2012, TBT models have been increasingly utilized in the oil sands to estimate tailings properties from GCPTu data (Ansah-Sam et al. 2015, Styler et al. 2018 & Entezari et al. 2020). In TMW 2020, the preliminary results from whole-region TBT models to estimate tailings solids and fines content were presented (Entezari et al. 2020). Using a dataset of paired GCPTu and laboratory constituent data collected between 2011 and 2019, machine learning modelling was employed to calibrate models estimating tailings constituents from in-situ data. The performance assessment was performed on a test set selected randomly from the development dataset.

In this study, the development dataset was expanded to include additional paired GCPTu and laboratory results and to include paired GBCPTu and laboratory results. The TBT models were calibrated to work for both GCPTu and GBCPTu profiles. The TBT models were developed to estimate methylene blue index (MBI) of tailings in addition to total solids and fines contents. The aim of this publication is twofold: 1) to provide an update on the development and performance of the most recent regional TBT models and 2) to demonstrate how TBT models may be implemented and used in practice to provide rapid and continuous tailings properties and to identify potential laboratory issues.

GCPTu and GBCPTu

The piezocone penetrometer (CPTu) is a direct push probe routinely used for geotechnical site investigations worldwide. The CPTu measures tip resistance, sleeve friction, and pore pressure. The CPTu is advanced at a constant rate of 2 cm/s through the soil and all three measurements are made near continuously with depth. The piezoball penetrometer (BCPTu) is also used as a standard test for determining the undrained shear strength of soft tailings (DeJong et al. 2011). The test incorporates a standard cone penetrometer body and a large spherical tip that replaces the standard conical tip.

A variety of modules and sensors can be integrated with the penetrometer to provide additional in-situ data. The passive gamma module is a module useful for the characterization of oil sands tailings. This module responds to naturally occurring radioisotopes, namely radioisotopes of Potassium (^{40}K), Thorium (^{232}Th), and Uranium (^{238}U). The received gamma ray incidents are counted and reported as counts per second (cps). In tailings

where the fines include illite clay mineralogy, the gamma counts are proportional to the total fines content (Figure 1b). In addition, gamma is an efficient tool to delineate froth treatment tailings as these tailings are rich in Uranium and Thorium and so the measured gamma counts are substantially higher than other tailings materials (>> 60 cps).

DATASET DESCRIPTION

Samples and Lab Measurements

The samples used in this study were collected using fluid and sonic samplers (Ansah-Sam et al. 2015) from multiple tailings storage facilities (TSFs) operated by four oil sands mine operators anonymized as Mine Operators A, B, C, and D here. Tailings characteristics including the mass percent of solids and 44 µm fines, as well as the MBI were measured through laboratory programs. The laboratory measurements were from multiple commercial and owner-operated laboratories, using industry standard practices (e.g. Kaminsky 2014, Hiltz and McFarlane 2017). Methods such as oven-drying or Dean-Stark analysis are used to measure the solid content of tailings, while the fines content is normally measured through a sieve analysis or laser diffraction. It should be mentioned that not all the tailings constituents or index properties were analyzed for each sample.

In-situ Measurements

The in-situ variables used for modelling were the computed undrained shear strength, the linearity and slope of the dynamic pore water pressure, and the passive gamma rate. The undrained shear strength is used as an input parameter because it can be calculated by both GCPTu and GBCPTu measured penetration resistances, allowing both tests to work in the same prediction model.

During undrained penetration, the scaled net tip resistance is approximately equal to the undrained shear strength. It is recognized that only some of the results are truly undrained during penetration, but the calculated undrained shear strength from net tip resistance remains a useful intermediate parameter to equate CPTu and BCPTu results for this study regardless of the actual drainage conditions during penetration. To calculate the undrained shear strength, an estimate of total vertical stress is required which depends on the total unit weight of the tailings. The unit weight profile is typically calculated using the pore pressure dissipation (PPD) data (Styler 2018) or by using the laboratory results from adjacent samples. When such data was not available, in fluid tailings, the slope of the dynamic pore water pressure was used as the total unit weight. In non-fluid tailings, unit weights of 18.6 and 20.8 kN/m^3 were assumed for samples below and above the phreatic surface, respectively. In non-fluid tailings, slight variation in the unit weight assumption has a negligible impact on the undrained shear strength calculation because tip resistance is much larger than vertical stress in such tailings. It is also worth noting that the calculation of undrained shear strength from BCPTu is much less sensitive to estimated unit weight and total stress. Typically, any error in computed total stress will have one tenth the impact on BCPTu calculated shear strength compared to CPTu, due to full flow of tailings around the ball. Bearing factors for CPTu and BCPTu (N_{kt}, N_{ball}) of 15 and 11 respectively were used to scale the net tip resistance and calculate undrained shear strength for CPTu and BCPTu, respectively. The linearity and slope of the dynamic pore water pressure was calculated over a moving depth window of 1 m for both CPTu and BCPTu. Screening criteria was utilized to ensure that this slope (and hence fluid density) was not calculated for tailing exhibiting solid behaviour (Entezari et al. 2020).

Building Paired Dataset

To create the dataset of paired in-situ and laboratory results, ConeTec's geospatial database was queried to produce GCPTu, GBCPTu, and sample pairs collected from 2011 to 2021 in the oil sands region. The query was restricted such that only sample results falling within a 5-meter radius and 1-month time buffer from the in-situ sounding are paired with the in-situ measurements. This restriction criterion minimizes the potential temporal and spatial variability between the in-situ and laboratory results. For point fluid samples, the median GCPTu measurements over a 0.5 m depth window centered at the fluid sample elevation was paired with the laboratory results. For core samples (sonic), the window size was equal to the length of the sample core homogenized for the lab.
The result of the database query and pairing process led to a dataset of more than 30,000 data points.

Training and Test Sets

The dataset was split into training and test sets. The training set was used to calibrate the model whereas the test set was used to evaluate model

performance. For this study, the data collected from 2011 to 2019 was used as the training set (~85% of the development dataset) and the data collected in 2020 and 2021 as the test set (~15% of the development dataset). This allowed for performing a Class A evaluation of the model.

Dataset Exploration and Data Cleansing

The training and test sets were inspected to eliminate non-representative data. Examples of non-representative data are when samples and in-situ measurements are paired in non-homogenous layered deposits, native ground, or in froth treatment tailings. Froth treatment tailings contain heavy minerals, causing high gamma readings unrelated to clay content and fines. Subsequently, efforts were made to eliminate data points in recycle water, froth treatment tailings, natural ground, or near layer boundaries from both training and test sets. This was done by imposing screening criteria such as eliminating data pairs with gamma of less than 7 and greater than 60 cps to remove data pairs in recycle water and froth treatment tailings, respectively, and eliminating the data pairs in native ground using field descriptions. After initial screening, the relationship between laboratory and in-situ measurements were investigated to ensure data quality and representativeness (Figure 1).

Figure 1a shows the relationship between solids content and slope of pore water pressure in fluid tailings. Generally, there is a high correlation between solids content and slope of pore water pressure, which is representative of fluid tailings unit weight. The relationship between total 44µm fines content and gamma counts is shown in Figure 1b. Increasing total fines content corresponds to an increase in gamma counts. There are some data points with low total fines content and high gamma counts that are likely associated with mixtures of froth treatment tailings or lateral heterogeneity between in-situ test and sample hole locations that were not effectively screened out. The data points with high total fines content and low gamma counts are potentially due to lateral heterogeneity. The relationship between geotechnical fines content (mass of fines as a percentage of solids) and MBI is displayed in Figure 1c. As expected, MBI generally increases as geotechnical fines content increases. However, for a portion of test set, it is observed that the relationship does not follow the historic trend (from the training set) and shows lower MBI in high fines tailings (geotechnical fines between ~50-70 wt%). Further exploration also revealed that these samples show lower gamma counts compared to rest of the test set. These samples were found to be all from Mine Operator D collected in 2021. This atypical trend could be due to a potential lab issue or a new tailings treatment process resulting in capturing high contents of fine particles with low activity and thus low MBI. Ultimately, since such tailings from Mine Operator D were not represented in the training set, they were eliminated from the test set and the data collected in Fall of 2019 from Mine Operator D were removed from the trainings set and added to the test set instead.

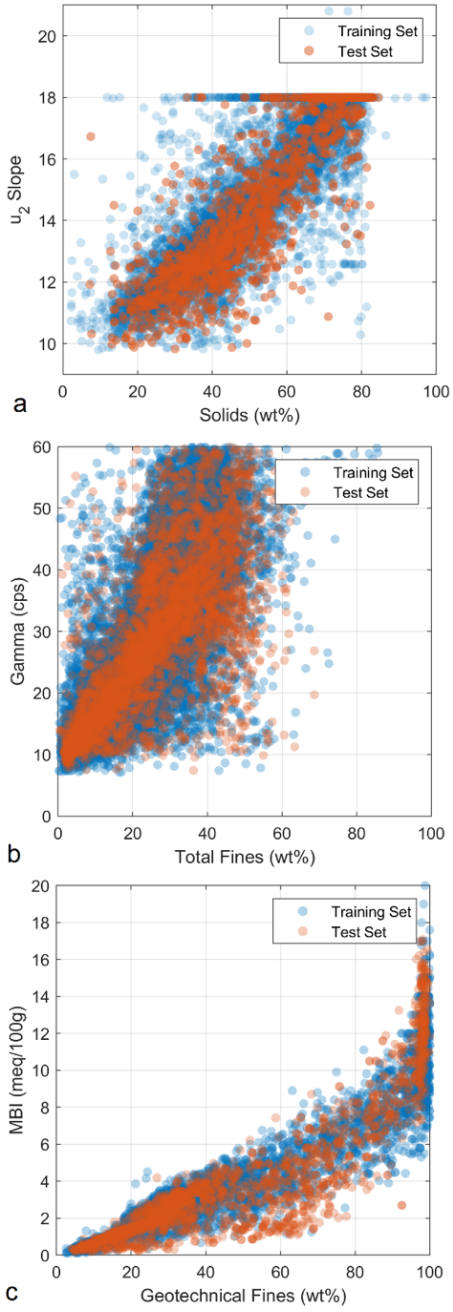

Figure 1. Relationships between some lab and in-situ measurements.

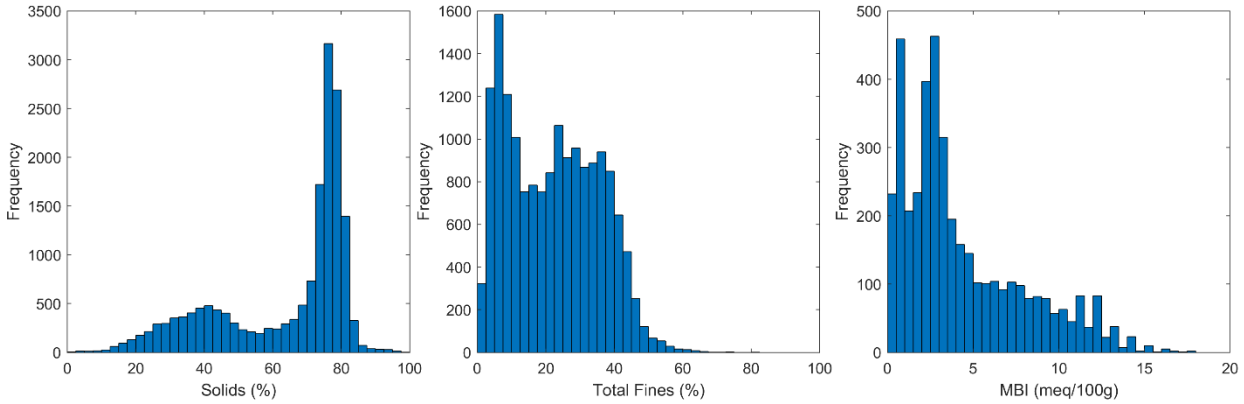

Figure 2. Histogram of tailings characteristics in the 2021 training set.

Table 1 compares the number of in-situ and laboratory data pairs (after the data screening process) in the training and test sets from each oil sands operator. The training and test sets include 16,993 and 3,281 data pairs, respectively. The histogram of solid and total fines contents and MBI for the training set is shown in Figure 2. A ternary diagram of the training set is shown in Figure 3. The ternary diagram shows that the tailings range from sandy soil-like tailings with high solids and low water content in the lower left corner to tailings with high fines, low sand, and high water content along the top-right edge. Overall, the training set contains a wide variety of materials paired with in-situ measurements collected from multiple TSFs operated by different mining companies and analyzed by multiple commercial laboratories over a ten-year period. Therefore, the models developed using this dataset are robust against equipment, sampling and laboratory procedures, regional geology, and temporal variations.

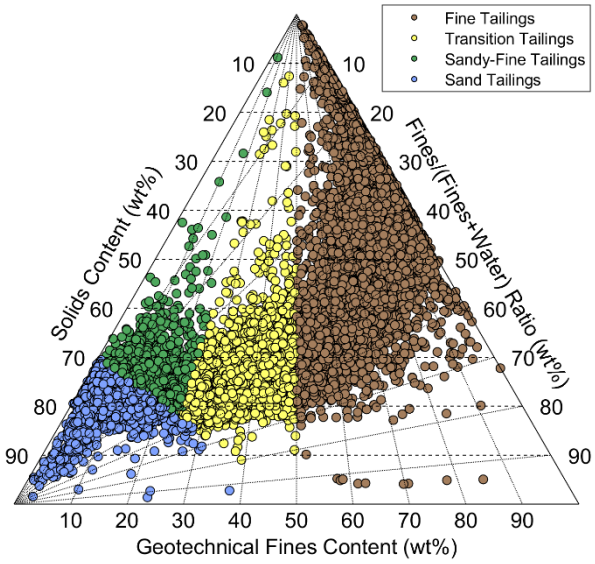

Figure 3. Ternary diagram of the training set.

Table 1. Number of paired in-situ and sample results in the training and test sets.

Mine Operator	Training Set		Test Set	
	GCPTu	GBCPTu	GCPTu	GBCPTu
A	9497	324	643	31
B	122	2327	26	616
C	3572	191	1467	288
D	719	241	59	151
Total	13910	3083	2195	1086

REGIONAL TBT MODELS

Machine Learning Modelling

The TBT models were trained using ensembles of neural networks, similar to our previous work (Entezari et al. 2020). The input in-situ features used for modelling included the undrained shear strength, the slope of the dynamic pore water pressure versus depth, the linearity of pore water pressure profile, the passive gamma rate as well as the mining property name where the data was collected. Because the dataset consisted of data from multiple sites, including the mine operator name as an input variable to the model added information about unquantified geological variances, as well as known variations in laboratory procedures (e.g. laser diffraction vs wet sieve).

The models were trained to predict the contents of solids and total fines, as well as MBI. The performance of the TBT models was evaluated by quantifying properties of the cumulative distribution function (CDF) of errors on the test set, while making the incorrect assumption that the laboratory data is perfect (Error = Lab -TBT).

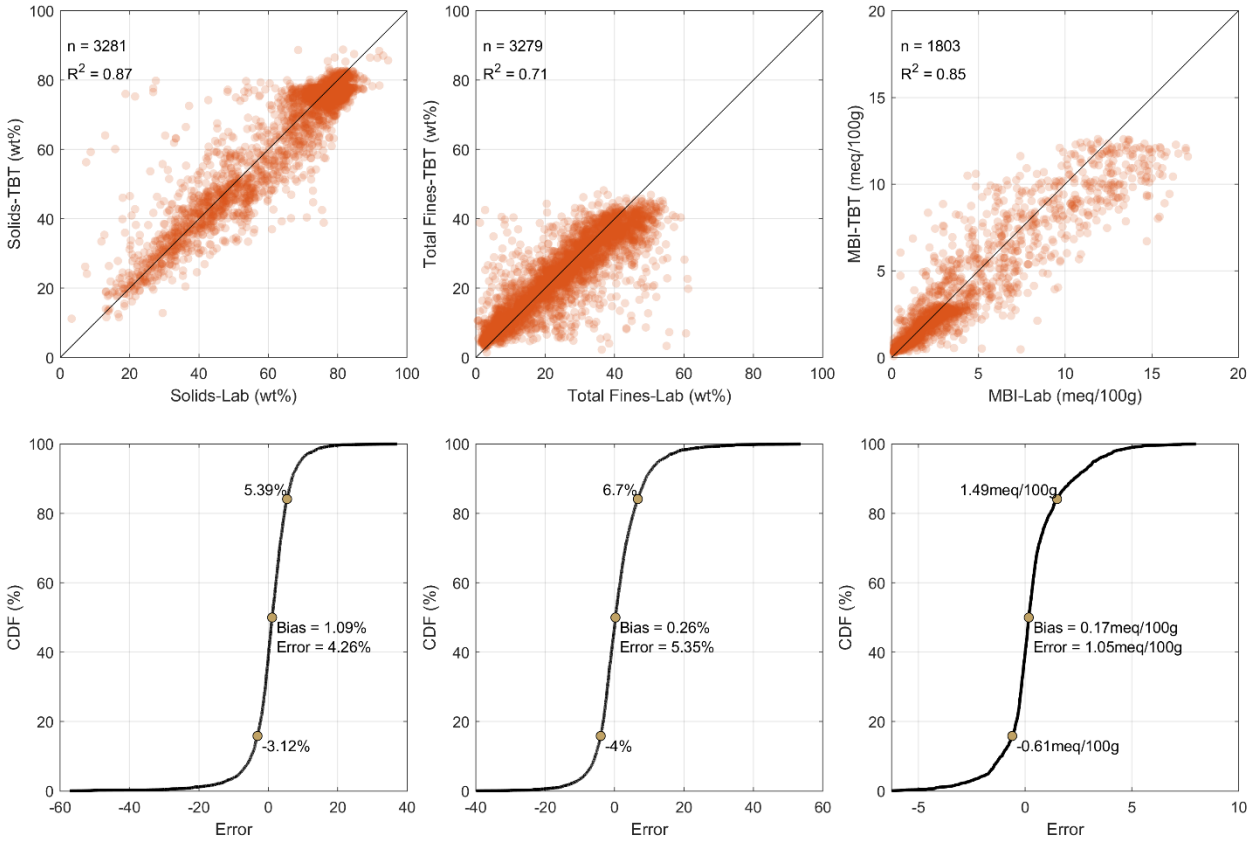

Figure 4. Relationship between TBT estimated vs laboratory measured tailings properties along with CDF of errors for the test set.

Performance Assessment

The relationships between the laboratory measured and TBT predicted tailings properties for the test set are shown in Figure 4. The CDF of errors on the test set is also shown for each model output. Table 2 summarizes the error values of the model outputs on the test set. There is a good correlation between the TBT predicted and laboratory results for all tailings characterizations. The bias of the estimated results is also very low and close to zero. For solids content estimation, the bias and error of the model was observed to be 1.09 and 4.26 wt%, respectively. This positive bias value means the model underestimates the laboratory solids content measurements by 1.09 wt%. The error of 4.26% means that one standard deviation (68.2% of the population) of the predicted solids content results fall within ±4.26 wt% of the laboratory measured solids content. For total fines content estimation, the bias and error were calculated to be 0.26 and 5.35 wt%, respectively. The model slightly underpredicts the total fines content by 0.26 wt%. For MBI, the bias and error were observed to be 0.17 and 1.05 meq/100g, respectively. The geotechnical fines can be estimated indirectly using the TBT estimated total fines and solids content. The bias and error for estimated geotechnical fines were calculated to be 0.02 and 8.8 wt%, respectively.

The performance of the models was also assessed for each individual mine operator. The error and bias of the models on tailings from each are listed in Table 2. It should be noted that Mine Operator A does not conduct MBI analysis in laboratory and Mine Operator B only performs MBI testing on a fraction of the samples in the laboratory. Therefore, although TBT could report MBI, it was not possible to compare TBT to laboratory results and perform an error analysis for MBI prediction for Mine Operator A.

A performance assessment was also performed on the test set based on the penetrometer type. The bias and error values for the predicted results were

separately calculated for GCPTu and GBCPTu test results using the data from all four mines (Table 2). Since the test set includes tailings samples from multiple TSFs operated by multiple oil sands operators, the developed TBT model is a regional model that can predict tailings properties from across the oil sands region. Therefore, the error assessment performed on the test set is considered the overall performance of the model, taking into account factors including but not limited to instrument repeatability, laboratory repeatability, laboratory variance, and field sub-sampling.

In general, the performance of the TBT model at each mine, and using each in-situ test, are comparable and similar while performing approximately the same as previously developed site-specific models.

Table 2. Bias and error values* of TBT model.

	Solids (wt%)	Total Fines (wt%)	MBI (meq/100g)
Overall	1.09±4.26	0.26±5.35	0.17±1.05
Mine A	1.1±4.12	0.43±6.38	NA
Mine B	-0.23±3.4	1.38±3.62	0.67±1.55
Mine C	2.06±4.24	-0.68±5.05	-0.1±0.71
Mine D	-0.59±5.05	3.7±6.44	0.72±1.01
GCPTu	1.5±4.16	-0.06±5.71	-0.04±0.64
GBCPTu	0.32±4.26	0.82±4.57	0.46±1.37

**The error values are absolute errors not relative.*

TBT IN PRACTICE

TBT in Fluid Fine Tailings (FFT)

Example TBT tailings characterization results estimated using a GCPTu sounding and the developed TBT model are presented in Figure 5. The GCPTu sounding was collected in 2020 and thus was part of the test set. The laboratory measured results are overplotted for visual comparison with TBT results. Evidently, the mudline is at 1.5 m based on the low cone tip resistance and rising gamma counts. The location includes FFT from 1.5 to 17 m with a gradual increase in solids content as depth increases. The TBT estimated constituents successfully follow the laboratory results over the entire tailings profile, while providing additional stratigraphic detail.

TBT in Soil-Like Tailings

Figure 6 shows an example profile of TBT results from a location tested with GCPTu where the samples were high solids tailings (solids content of ~75 wt%). The GCPTu sounding appears to be in high sand material with an average sand to fine ratio (SFR) of ~15. Overall, the TBT and laboratory results agree well for the entire profile.

TBT in Layered Deposits

One of the advantages of TBT model is that tailings properties can be estimated continuously with depth as opposed to sampling and laboratory analysis that average tailings properties over the length of sample core. This could be particularly important for layered deposits where sampling at certain depth intervals may not capture the variation present in the tailings. An example of TBT results from a test GCPTu collected with layered tailings deposits is shown in Figure 7. The TBT estimated and laboratory measured tailings properties are generally in good agreement, however there are narrow layers of high fines tailings that are not adequately characterized through sampling and laboratory testing.

TBT Using GBCPTu Data

The TBT model was developed to work with both GCPTu and GBCPTu data. Example TBT results estimated using a GBCPTu sounding is shown in Figure 8. The first 5.5 m has been drilled out through the coke material. Overall, a good agreement is observed between the laboratory results and the TBT estimated results using the GBCPTu data.

TBT and HSI

For locations with sampling, GCPTu or GBCPTu, and hyperspectral imaging (HSI) data (Entezari et al. 2021, 2022), multiple prediction methods can be utilized and compared to laboratory data. HSI and TBT prediction models have been developed independently using different technologies. Therefore, good agreement between the two is a good indicator of accurate tailings characterization, while poor agreement could indicate the need for laboratory analysis. HSI and TBT can also be employed to validate laboratory results and identify potential sampling, handling, or laboratory error including administrative error (mis-labelled samples).

Figure 9 illustrates an example profile showing TBT results from GCPTu along with HSI predictions of samples collected from a paired sonic sample hole. The laboratory results are overplotted to visually compare with the TBT and HSI results. The offset between the GCPTu sounding and the sample hole is 3 m. Importantly, the TBT results are predicted every 2.5 centimeters, whereas the samples and resulting lab and HSI measurements represent an average of the constituents over the cored interval of 1 meter. Also, there is tailings with gamma of greater than 60 cps from 5 to 7 m, which is indicative of froth treatment tailings, for which TBT cannot estimate tailings constituents. HSI models, on the other hand, have been trained to work for froth treatment tailings

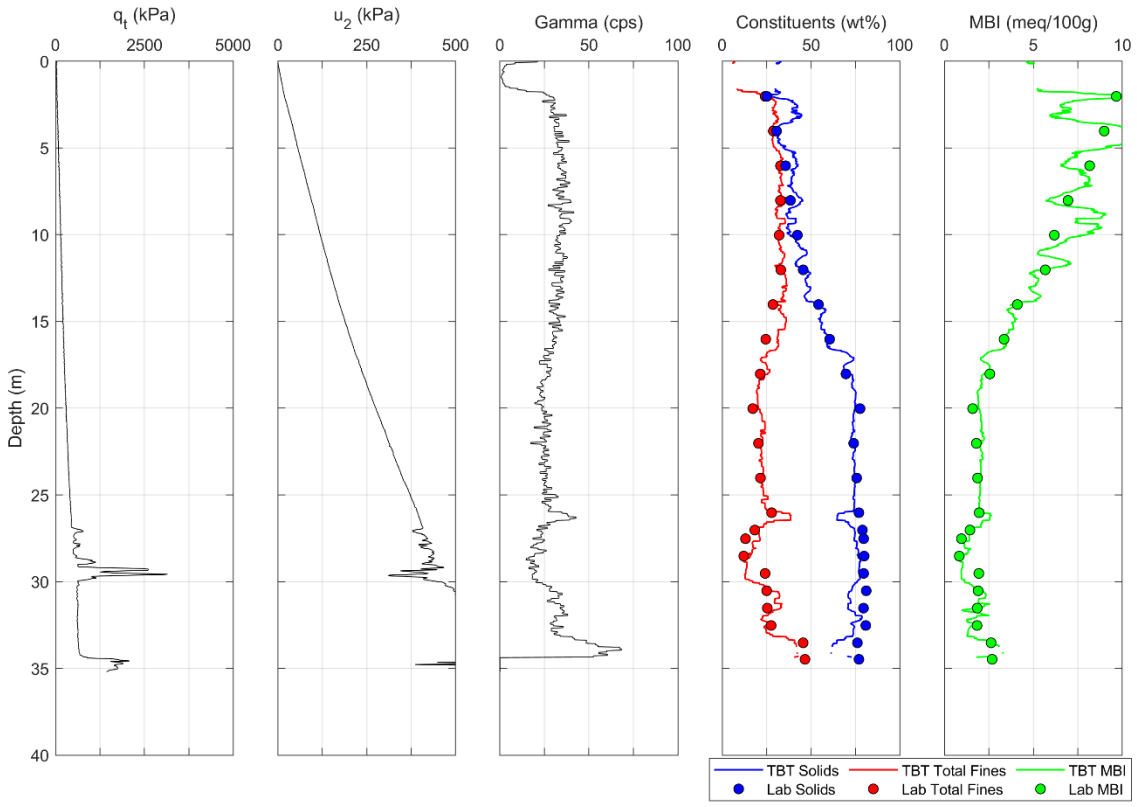

Figure 5. Example TBT profile in fluid and soil-like tailings.

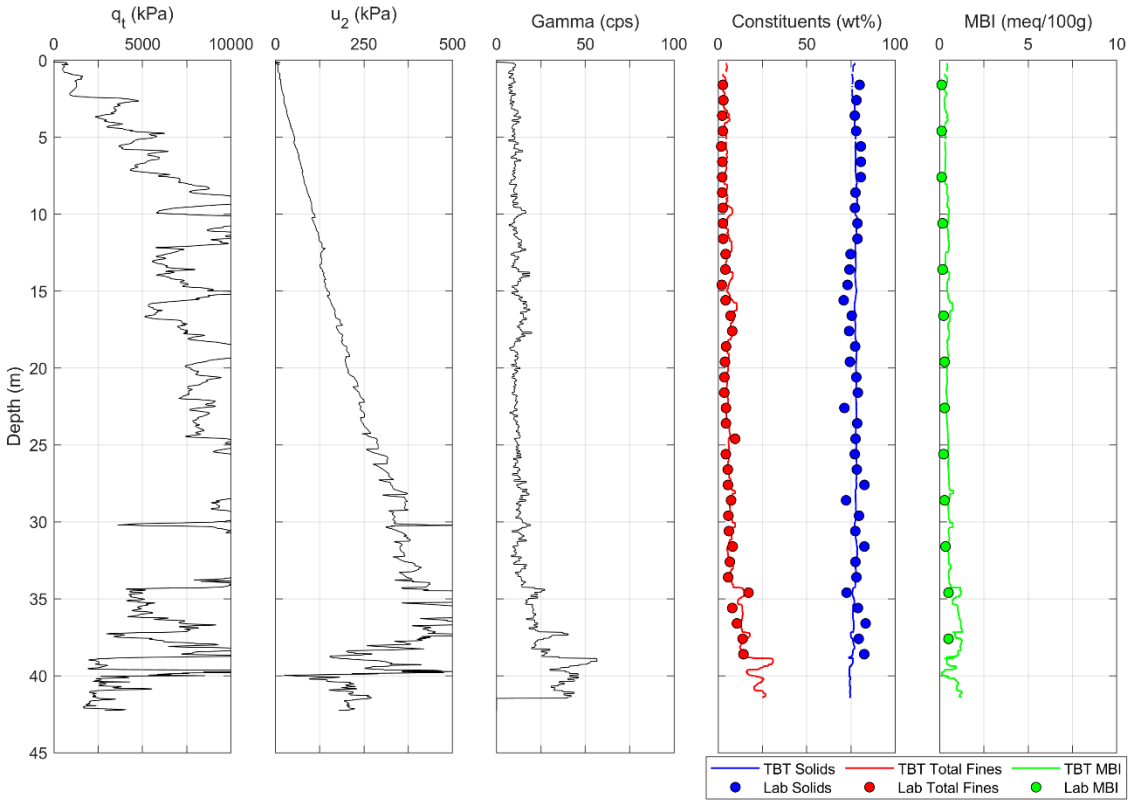

Figure 6. Example TBT profile in soil-like (beach) tailings.

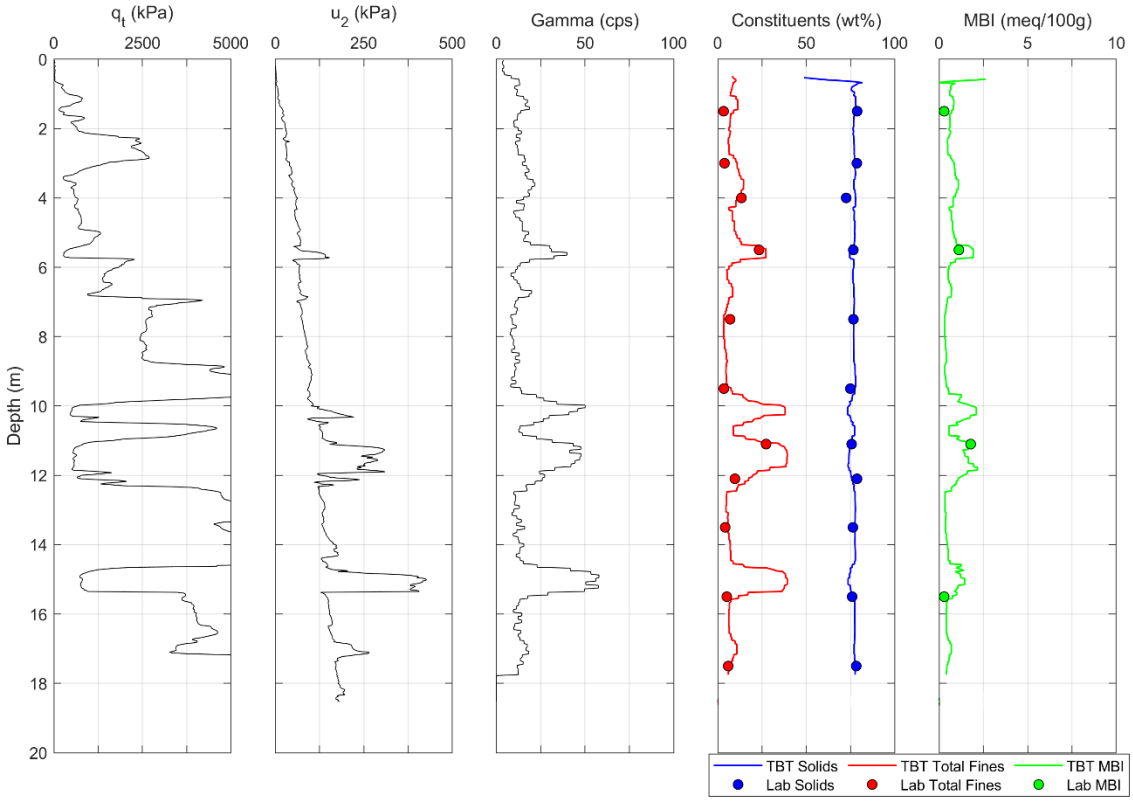

Figure 7. Example TBT profile in layered deposits.

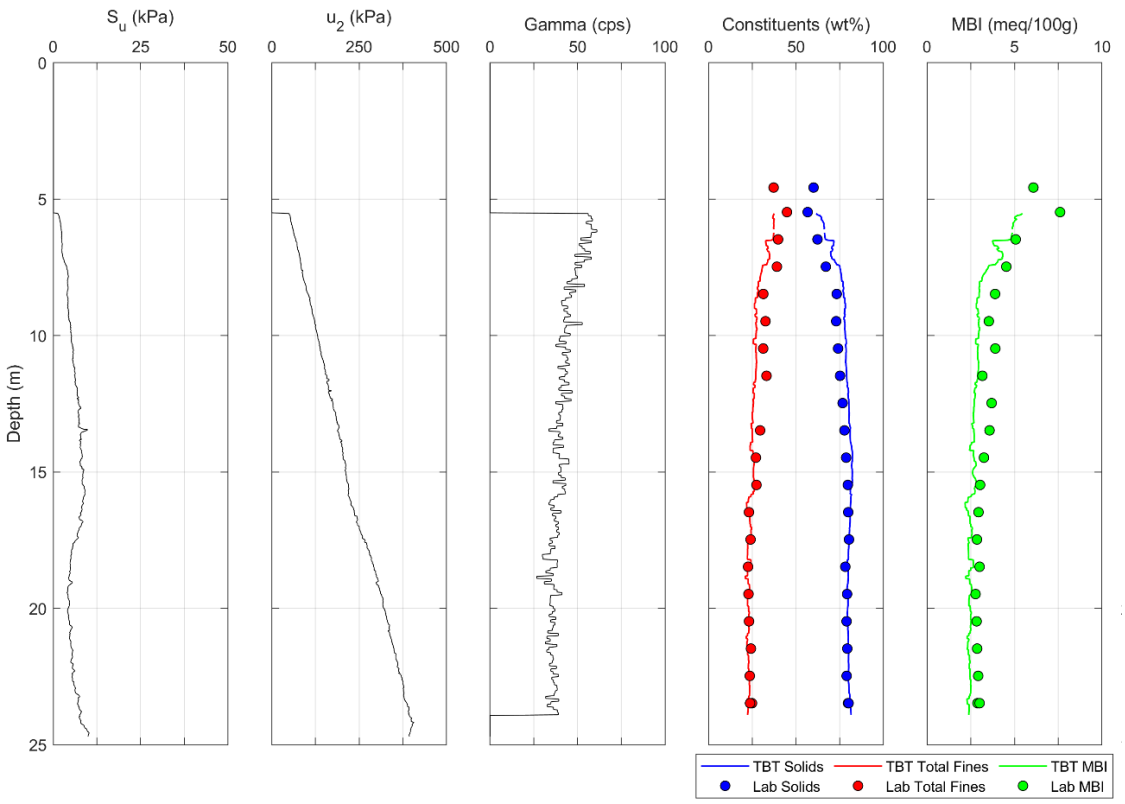

Figure 8. Example TBT profile using GBCPTu sounding.

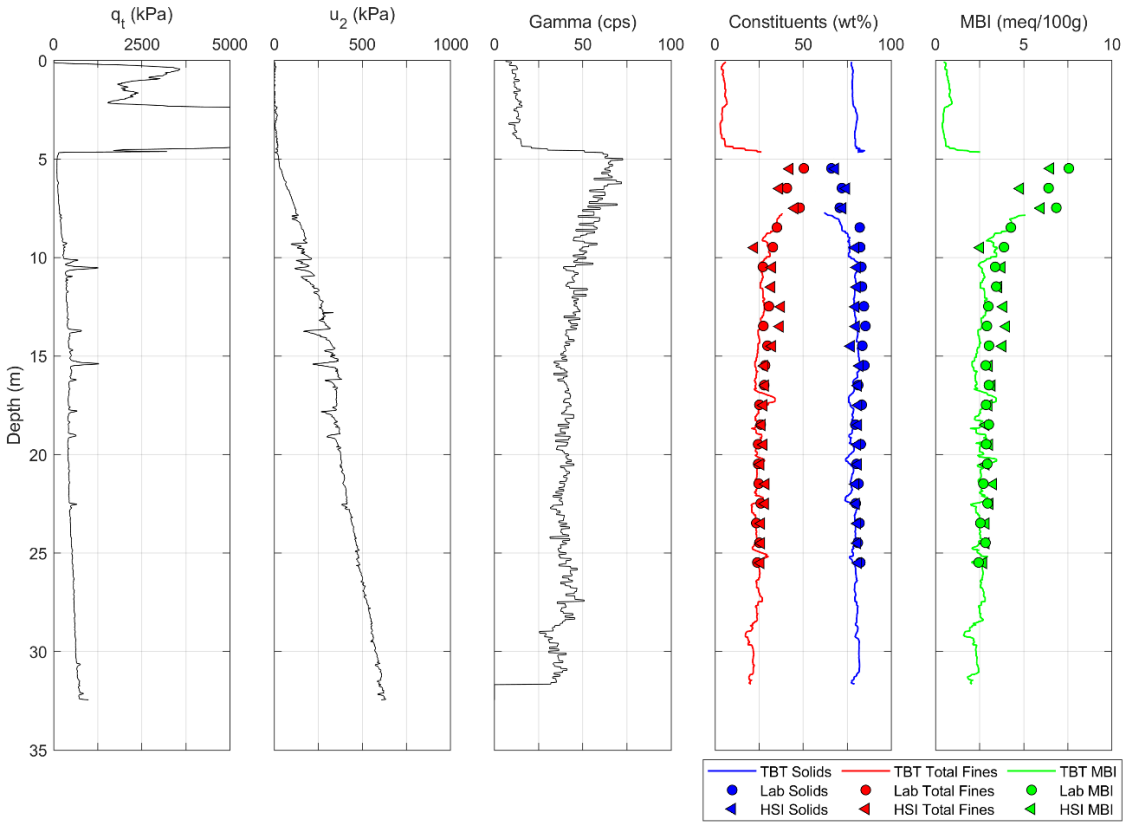

Figure 9. Example TBT profile along with HSI and laboratory test results.

CONCLUSIONS

The TBT model was calibrated using the training set consisting of ~17,000 paired in-situ and laboratory data from tailings samples collected across multiple TSFs at four oil sands mines. The model was trained to work with both GCPTu and GBCPTu soundings. The performance of the TBT model was evaluated using a Class A test set consisting of ~3,000 paired data points. This type of Class A error assessment properly evaluates the robustness of the predictions when applied on new data. Results showed TBT model can predict the solid and total fines contents with 4.26 and 5.35 wt% error, respectively, for the oil sands region. MBI is predicted with 1.05 meq/100g error. These errors incorrectly assume that all the laboratory data is perfect and repeatable.

TBT may be employed for rapid, repeatable, and objective tailings constituent, virtually eliminating the need for routine sampling and subsequent lab testing. TBT can also be used as a rapid and independent method to validate laboratory data, or to identify problematic data for re-analysis. Furthermore, TBT model may be employed to predict laboratory results using different laboratory techniques, or to objectively compare or translate data from one mine to another.

In the oil sands mining region, this new regional TBT negates the need for site-specific models, and enables operators to present their data in an objective and unified manner to practitioners and regulators.

REFERENCES

Ansah-Sam, M., Binczyk, T., Dobek, C., Geremew, A., Guo, C., Mimura, W., and Weerakone, S. 2015. Guidelines for tailings deposit sampling and measuring tools. Prepared by COSIA Geostatistical and Deposit Sampling Working Group.

DeJong, J.T., Yafrate, N.J., and DeGroot, D.J. 2011. Evaluation of undrained shear strength using full-flow penetrometers. Journals of Geotechnical and Geoenvironmental Engineering 137(1): 14-26.

Entezari, I., McGowan, D., and Sharp, J. 2020. Tailings characterization using cone penetration testing and machine learning. Proceedings of Tailings and Mine Waste 2020, Ft. Collins, Colorado: 695-704.

Entezari, I., McGowan, D., Glavina, J., and Parkinson, D. 2021. Hyperspectral imaging technology for oil sands tailings characterization: An update. Proceedings of Tailings and Mine Waste 2021, Banff, Alberta: 953-963.

Entezari, I., McGowan, D., and Glavina, J. 2022. Hyperspectral imaging (HSI) technology for oil sands tailings characterization: practical aspects. Proceedings of Tailings and Mine Waste 2022, Denver, Colorado, in press.

Hiltz, M. and McFarlane, R. 2017. Precision of particle size measurements for minus 44 micron solids from oil sands; an interlaboratory study. Prepared by InnoTech Alberta on behalf of COSIA.

Kaminsky, H. 2014. Demystifying the methylene blue index. Proceedings of 4th International Oil Sands Tailings Conference, Banff, Alberta: 221-229.

Styler, M.A., McGowan, D., & Sharp J. 2018. Characterizing soft oil sand tailings by gamma cone penetration testing. Proceedings of the 6th International Oil Sands Tailings Conference, Edmonton, Alberta: 112-120.

CHARACTERIZATION STUDY OF OIL SAND TAILINGS AT SUNCOR'S POND 5 TAILINGS STORAGE FACILITY

Ying Zhang[1], Ayman H. Abusaid[1], Gordon W. Pollock[1], and Derek Uffen[2]
[1]WSP E&I Canada Limited, Edmonton, Alberta, Canada, [2]Suncor Energy Inc., Calgary, Alberta, Canada

ABSTRACT

Suncor's Pond 5 tailings storage facility has been undergoing reclamation activities since 2009. A floating petroleum coke cover and vertical strip drains (VSDs) were installed as part of the reclamation of Pond 5. The area is now proposed to be used as a coke storage facility with additional coke being placed on top of the cover prior to final landscaping activities. Therefore, it was necessary to thoroughly characterize the tailings around the perimeter of the pond which would form the foundation of the storage facility slope. This paper presents the results of the extensive field and laboratory investigation conducted in 2020 to determine the tailings properties which could be used in future engineering analyses. The field program included Cone Penetration Tests (CPT), Ball Cone Penetration Tests (BCPT), electric Vane Shear Tests (eVST) and sampling. Correlations between the strength characterization methods were evaluated and are presented herein. Laboratory tests included index and density testing. The measured strength and density of the tailings were compared to those estimated using index properties and CPT data and compared to existing correlations available in the literature.

INTRODUCTION

Pond 5 is a tailings facility at Lease 86/17 of Suncor Energy Inc. (Suncor)'s Base Plant site and is approximately 35 kilometers (km) north of the city of Fort McMurray. The total area of the pond is approximately 500 hectares (ha) with approximately 200 ha of soft tailings, which consist of a layer of gypsum enriched Mature Fine Tailings (MFT) overlying Consolidated Tailings (CT). The CT process involves mixing tailings sand, MFT, and gypsum and it was used by Suncor in the 1990s. In support of Pond 5 reclamation, Suncor constructed an engineered floating coke cover (generally 2 meters (m) thick) over the soft tailings between 2009 and 2017. The coke cover has one layer of geogrid and one layer of geotextile between the MFT and coke. To facilitate the consolidation of the soft tailings, VSDs were installed in the soft tailings using the coke cover as a construction platform between 2011 and 2017. The extent of VSDs covered the footprint of the soft tailings except near the pond perimeter and along two main haul roads, as shown in Figure 1. The design of the coke cover was presented by Pollock et al (2010), and the construction methodology and activities were discussed by Abusaid et al (2011). To further enhance tailings consolidation and improve the stiffness of the engineered cover in support of closure activities, Suncor placed an additional 2 m of coke in 2019 and 2020 on the engineered cover to achieve a total coke thickness of 4 m. The construction work and the performance of the VSDs were published by Abusaid et al (2021).

Presently, the area is proposed to be used as a coke storage facility with additional coke being placed on top of the cover prior to landscaping activities. The soft tailings will form part of the foundation of the storage facility slope around the perimeter of the pond (where there are no VSDs), as shown in a typical profile along the pond perimeter in Figure 2. An extensive field and laboratory program was conducted in 2020 to delineate the soil stratigraphy and characterize the tailings around the perimeter of the pond. The locations of the CPT, BCPT, eVST, and sampling are shown in Figure 1. Laboratory testing was conducted on the samples to measure the tailings indices, including gradation, solids content, Atterberg limits, and bulk density.

This paper presents the characterization of the soft tailings and compares the measured values with those obtained using empirical correlations.

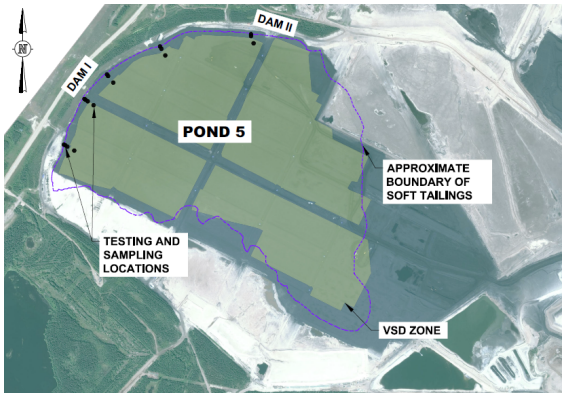

Figure 1. Site plan showing the testing and sampling locations

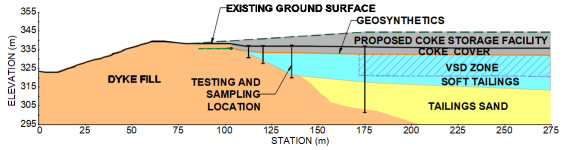

Figure 2. Typical profile of Dam I

OVERVIEW OF THE INVESTIGATION PROGRAM

The investigation program consisted of a field investigation and a laboratory testing program. The field investigation included fourteen sets of CPT, BCPT, and sonic sampling holes near Boundary Dyke (Dam I), and three sets near Exclusion Zone Dyke (Dam II), as shown in Figure 1.

CPTs were used to estimate the thickness of the coke, the undrained shear strength of the soft tailings, and the properties of the underlying tailings sand. The cone penetrometer had a base area of 15 square centimeters (cm^2), a net end area ratio of 0.8, and an apex angle of 60°. The penetrometer had a tip capacity of 150 megapascals (MPa), a sleeve capacity of 1.5 MPa, and a pore pressure capacity of 50 MPa.

BCPTs were conducted to estimate the undrained shear strength of the soft tailings at Pond 5. The ball plan area was 150 cm^2, the rod had a plan area of 15 cm^2, and the net end area ratio was 0.8. The ball penetrometer had a tip capacity of 37.5 MPa, a sleeve capacity of 1 MPa, and a capacity of 20 MPa for pore pressure transducer.

Seventeen eVSTs were performed at four test locations to estimate the undrained shear strength of the soft tailings at Pond 5. The capacity of the electric motor was 100 Newton-meter (N-m). The motor was situated in the extension rod right above the vane blade. Three different vane blade sizes (up to 150 millimeter (mm) in height) were used with a height to width ratio of two. The top and bottom taper angle of the vane blade was 45°.

Continuous sampling of the soft tailings was conducted using a drill rig with a sonic drill head and piston samplers (Aqualock AL50 system). Sampling started at the top of the soft tailings using samplers either one- or two-meters long. The samples were divided into approximately 0.5 m long sections and stored in sealed containers in the field before shipping to the laboratory.

Each sample was homogenized in the laboratory before testing. Dean Stark tests were performed on each sample to determine the mass of bitumen, minerals, and water. The minerals (soil particles) from Dean Stark tests were then washed on sieve # 325 (45 micrometers (μm)) to determine the fines content (< 45 μm). Atterberg limit tests were performed on the soft tailings samples and bitumen was removed prior to Atterberg limit tests.

RESULTS AND DISCUSSIONS

A ternary diagram, which is commonly used in classification of oil sands soft tailings and to indicate the required degree of dewatering to change the soft tailings to soil, was used to present the Pond 5 data. Figure 3 shows the Pond 5 soft tailings data on a ternary diagram by COSIA (2014). The definitions of the axes used in the figure are provided in the subsections below. As shown in Figure 3, the Pond 5 soft tailings are mainly in fluid state although part of the tailings is close to or has crossed the boundary from fluid tailings to soil.

Solids Content and Fines Content

Solids content is defined as:

$$SC = \frac{mass\ of\ bitumen, fines, and\ \ sand}{total\ mass\ of\ tailings}$$

where bitumen is considered as part of the solids.

Figure 4 shows the solids content profiles measured for the sampling locations at Pond 5. The solids

content was between 45% and 70% near the top of the soft tailings for Dam I and was close to 80% near the bottom of the soft tailings. The solids content was higher for Dam II, with 60% to 80% near the surface and slightly higher than 80% further down.

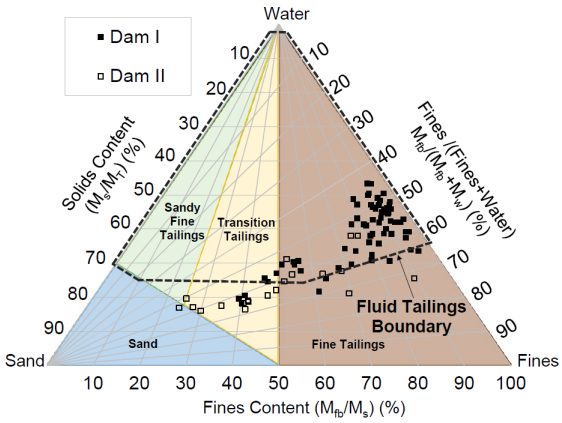

Figure 3. Pond 5 soft tailings on a ternary diagram (modified after COSIA, 2014)

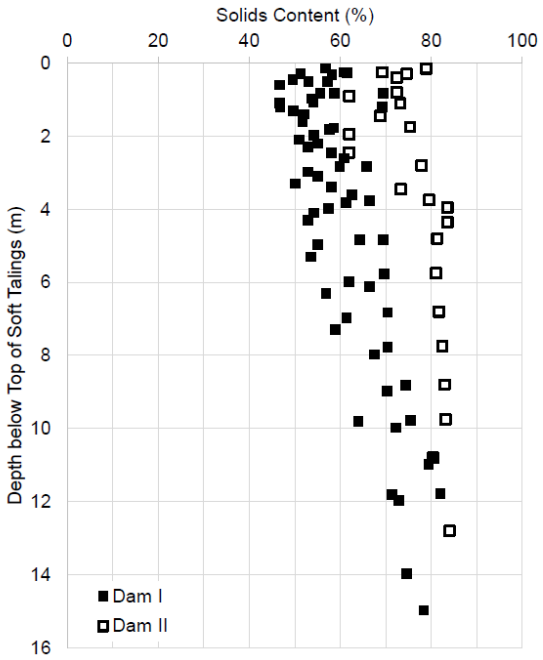

Figure 4. Solids content profiles

Fines content is defined as:

$$f = \frac{mass\ of\ fines\ and\ bitumen}{mass\ of\ fines, sand, and\ bitumen}$$

Where bitumen is considered as part of the fines. Other definitions of fines content are sometimes used in the oil sands industry, but are not presented herein.

Figure 5 shows the fines content profiles. The fines content of soft tailings was above 80% at the surface and was between 20% and 60% towards the bottom of the sampling locations of Dam I. The fines content was lower for Dam II, with 65% to 75% near the surface and between 20% and 30% near the bottom of the soft tailings. The trend of decreasing fines (or increasing sand content) with depth is typical of slurried deposits with a broad gradation and is indicative of sand settling through the matrix.

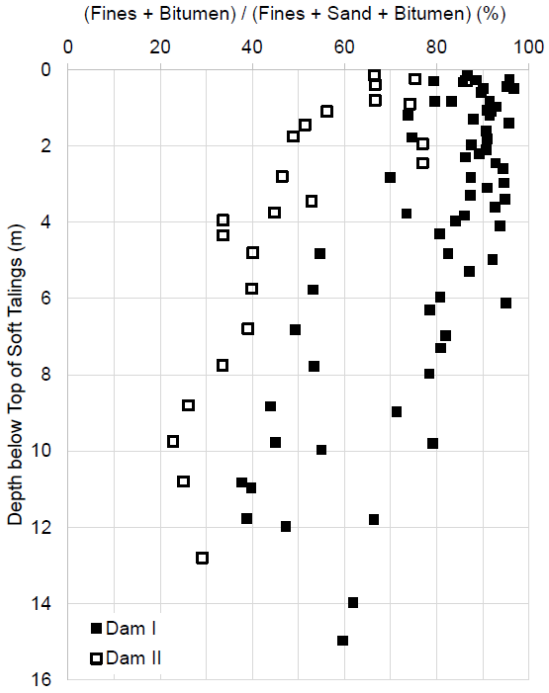

Figure 5. Fines content profiles

Fines-water ratio (FWR) is commonly used to classify the tailings and estimate the degree of dewatering. FWR is defined as:

$$fines\ water\ ratio = \frac{mass\ of\ fines, bitumen}{mass\ of\ fines, bitumen\ and\ water}$$

Where bitumen is considered as part of the fines.

Figure 6 presents the FWR profiles. The FWR was between 40% and 70% for the soft tailings at

Pond 5. The FWR ignores the sand in the matrix and therefore provides a better indication of whether consolidation or densification is occurring than solely considering solids content. For example, the data in Figure 4 shows an increase in solids content with depth. One may conclude that consolidation is occurring. However, Figure 5 shows the sand content increases with depth, likely due to segregation. The FWR profile in Figure 6 does not show as clear of a trend (i.e., no evident sign of consolidation) until down to a depth of 12 m at which point the FWR increases with depth.

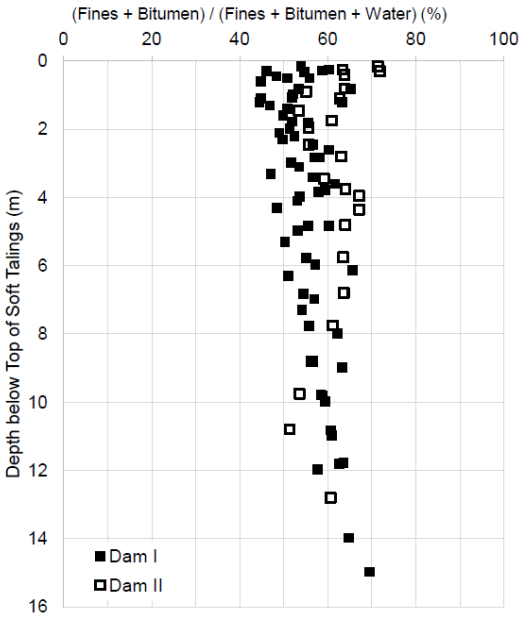

Figure 6. Fines-water ratio profiles

Unit Weight

Unit weight is required to determine the total stress accumulated with depth in soft tailings, which can then be used to estimate effective stress if pore pressure is known or to be used in other applications (e.g., CPT data interpretation).

Unit weight can be directly measured using undisturbed samples. It can also be estimated through various correlations with CPT data. Mayne et al. (2010) and Robertson and Cabal (2010) showed that some CPT correlations provide reliable estimation of unit weight for soils. Continuous unit weight profile can be obtained if CPT is carried out. However, it should be noted that unit weight of oil sands soft tailings is much lower than soils and the correlations for soils may not be applicable. There are other indirect estimation methods using electrical resistivity probes, gamma ray penetrometers, radioactive isotope modules, and dielectric measurements, however, they all have disadvantages, such as specialized device requirement, appreciable cost, or additional safety measures (Mayne et al, 2010).

For the current program, unit weight was estimated using laboratory testing on piston samples. The mass of minerals, bitumen, and water for each sample was determined using the Dean-Stark method. The unit weight of each sample was estimated using the following equations:

$$\gamma_b = \rho_b\, g$$

$$\rho_b = \frac{1}{\frac{SC}{\rho_w G_{mb}} + \frac{1-SC}{\rho_w}}$$

$$G_{mb} = \frac{1}{\left(\frac{mass\ of\ minerals}{(mass\ of\ bitumen\ and\ minerals)G_s} + \frac{mass\ of\ bitumen}{(mass\ of\ bitumen\ and\ minerals)G_b}\right)}$$

Where the specific gravity of the minerals (G_s) was assumed to be 2.65. The specific gravity of the bitumen (G_b) was assumed to be 1.01. The gravitational acceleration constant (g) is 9.81 m/s^2.

Unit weights determined through laboratory data are considered reliable however, such a method is not cost effective especially in applications where many tests are required. During the investigation program, unit weight was also estimated using the empirical CPT correlation proposed by Robertson and Cabal (2010).

$$\gamma/\gamma_w = \left[0.27[\log R_f] + 0.36\left[log\left(\frac{q_t}{p_a}\right)\right] + 1.236\right] G_s /2.65$$

Where q_t is the tip resistance. f_s is the sleeve friction, R_f is the friction ratio, $(f_s/q_t)100\%$. p_a is the atmospheric pressure in the same units as q_t. r_w is the unit weight of water.

Figure 7 shows the estimated unit weights versus the Sand to Fines Ratio (SFR). SFR is a commonly used tailings index to classify the oil sands soft tailings and is defined as:

$$SFR = \frac{mass\ of\ sand}{mass\ of\ fines}$$

Figure 7 indicates that the Robertson and Cabal (2010) method obtained lower unit weight compared with lab determined values, and the underestimate could be larger than 5 kN/m^3 for the soft tailings at Pond 5.

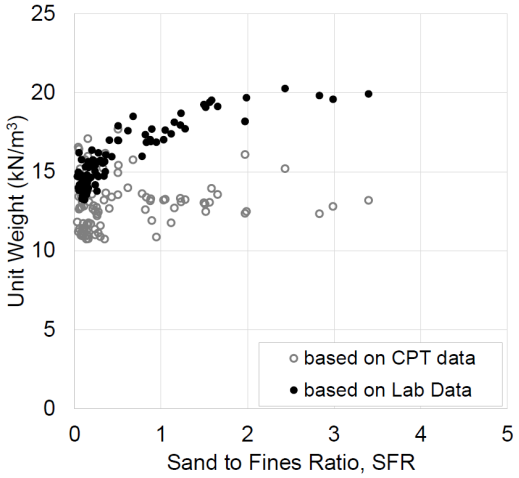

Figure 7. Unit weights based on lab data and CPT data

An exercise was carried out to calibrate the CPT based unit weight using the lab determined unit weight. The coefficients in the Robertson and Cabal (2010) correlation were replaced with A, B, and C, as shown below.

$$\gamma/\gamma_w = \left[A\left[\log R_f\right] + B\left[log\left(\frac{q_t}{p_a}\right)\right] + C\right] G_s/2.65$$

Where G_s considered the presence of bitumen.

The lab determined unit weights were divided into three groups based on SFR. Figure 8 shows that the unit weight estimated from CPT data using adjusted coefficients matched well with that from lab data. Table 1 summarizes the calibrated coefficients for each SFR group. In the absence of lab data, the modified Robertson and Cabal (2010) method can be used to estimate the unit weight of Pond 5 soft tailings.

Table 1. Calibrated coefficients for the Robertson and Cabal (2010) method

Coefficient	SFR < 0.3	0.3≤SFR<1	1≤SFR<4
A	0.05	0.05	0.05
B	0.22	0.15	0
C	1.65	1.8	2.02

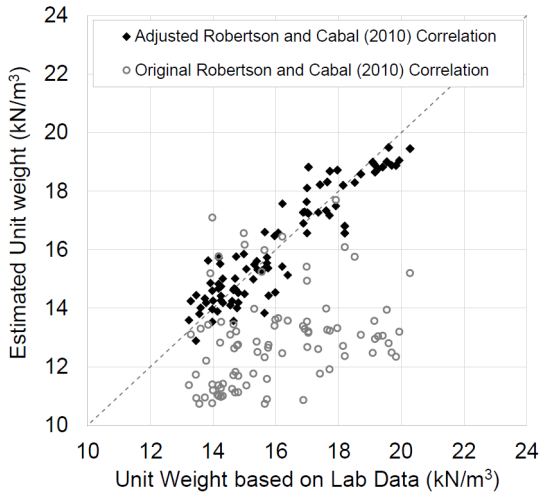

Figure 8. Calibrated unit weights based on lab data

Atterberg Limits

Figure 9 shows the Atterberg limits data for the soft tailings at Pond 5. The soft tailings with higher fines contents (e.g., SFR < 1) were medium plastic to high plastic. The soft tailings with lower fines contents (e.g., 1≤SFR<3) were mainly in the low plastic range. Figure 10 shows the correlation between liquid limit and SFR. Liquid limit is higher for lower SFR, but does not show any evident increase when SFR is lower than 0.1.

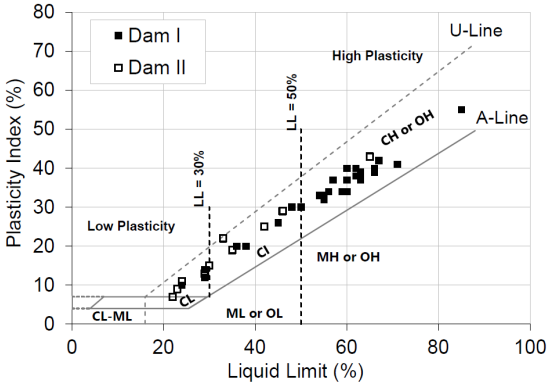

Figure 9. Atterberg limits of the soft tailings at Pond 5

Undrained Shear Strength

During the investigation program, the undrained shear strengths of soft tailings at Pond 5 were measured in the field using eVST, BCPT, and CPT. Shear strength was also estimated using empirical

correlations between undrained shear strength and liquidity index.

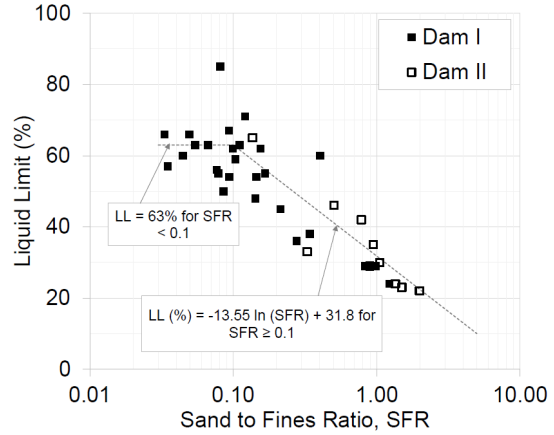

Figure 10. Liquid limit versus SFR

eVST provides accurate undrained shear strength measurements since it uses a load cell with digital data collection system and the load cell is situated above the vane blade. Figure 11 presents the measured peak and residual shear strengths of the soft tailings at Pond 5. The measured peak undrained shear strengths of the soft tailings ranged from 0.5 kilopascals (kPa) to 45 kPa. The measured residual shear strengths of the soft tailings were between 0.1 kPa and 7 kPa. The measured shear strength is recommended to be corrected for shear rate and plasticity index prior to its use in applications such as slope stability analyses (ASTM, 2002).

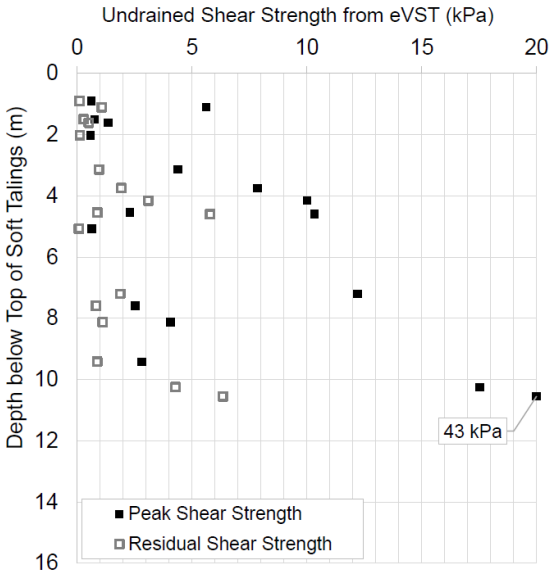

Figure 11. Undrained shear strength of soft tailings measured by eVST

BCPT was also used in measuring the undrained shear strength of the soft tailings at Pond 5. The ball shaped penetrometer has a much larger equivalent plan area than that of CPT (e.g., 10 times the area for cone penetrometer and extension rod). Therefore, BCPT is much more sensitive to changes in density and strength. A continuous peak undrained shear strength profile was obtained using BCPT test. Remolded (cyclic) tests were carried out at specific depths over a range of 0.5 m. The peak and remolded undrained shear strength of BCPT can be estimated below:

$$S_u = \frac{q_{bnet}}{N_{ball}}$$

Where q_{bnet} is the net ball tip resistance, N_{ball} is a conversion coefficient, which is typically calibrated using VST, DMT, laboratory testing, or other tests. N_{ball} values between 5 and 15 were reported by Schaeffers and Weemees (2012), Colreavy et. al. (2010), Boylan et. al. (2007), and DeJong et. al. (2011). For the soft tailings at Pond 5, an upper bound of typical N_{ball} values of 15 was found applicable for both peak and residual undrained shear strengths, as shown in Figure 12. Figure 12 only shows the data with q_{bnet} below 200 kPa. The data for q_{bnet} above 200 kPa indicated a similar N_{ball} but is not presented.

The accuracy of CPT in measuring the undrained shear strength of soft tailings is questionable due to the lack of sensitivity of the apparatus in very soft soils or slurries (i.e., relatively large capacity of the load cells and relatively small end area of the penetrometer comparing to BCPT). Nevertheless, in this program, the CPT data was used to estimate the undrained shear strength of Pond 5 soft tailings using the equation below as continuous CPT data profiles were available.

$$S_u = \frac{q_{tnet}}{N_{kt}}$$

Where q_{tnet} is the net cone tip resistance, N_{kt} is a conversion coefficient, typically in the range of 10 to 20. N_{kt} tends to increase with increasing plasticity and decrease with increasing soil sensitivity (Robertson and Cabal, 2015). Wroth (1984) recommended CPT data should be calibrated with other testing (e.g., VST) for undrained shear strength estimation. The remolded undrained shear strength can be assumed to be equal to the sleeve friction (f_s), which is the average shear resistance around the sleeve of the penetrometer (Robertson and Cabal, 2015). Figure 13 indicates an upper

bound of the typical N_{kt} values of 20 is applicable to the Pond 5 soft tailings for peak undrained shear strength estimation. The data for q_{net} above 200 kPa indicated a similar N_{kt} but is not shown herein. As expected, the correlation between CPT data and eVST data are not as good as that for BCPT data for the Pond 5 soft tailings with very low undrained shear strength. CPT measurement is expected to be more reliable when the soft tailings consolidate and become more soil-like.

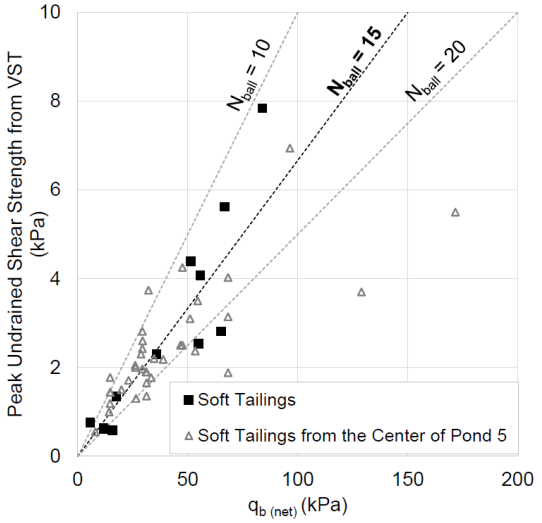

a) Peak undrained shear strength

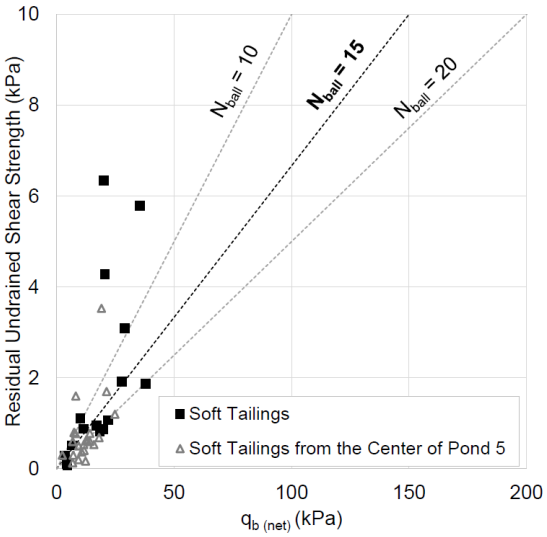

b) Residual undrained shear strength

Figure 12. N_{ball} calibration using eVST

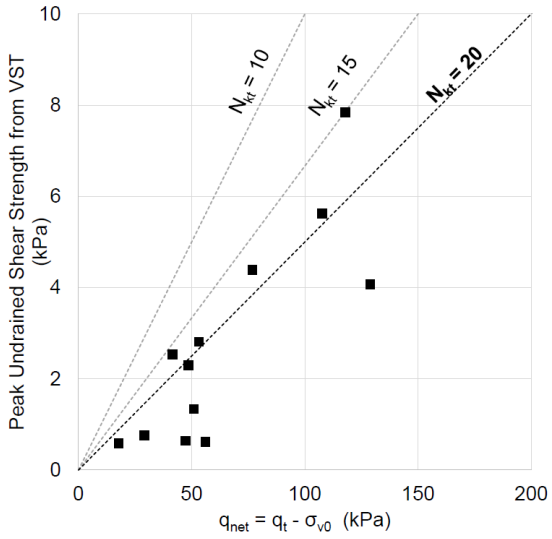

a) Peak undrained shear strength

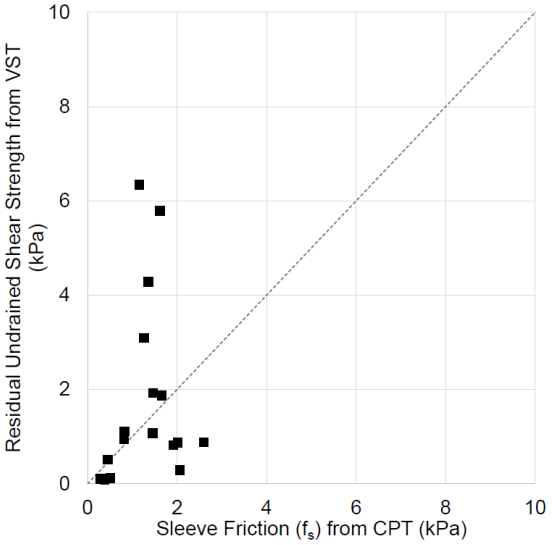

b) Residual undrained shear strength

Figure 13. N_{kt} calibration using eVST

The correlation between the residual undrained shear strength from eVST and the liquidity index of the soft tailings was examined against the data compiled by Beier et al (2013), as shown in Figure 14. In general, the Pond 5 data matched well with the data in Beier et al. (2013) and the correlation proposed by Locat and Demers (1988), while it is recognized that the variation in undrained shear strength can be over one order of magnitude for the same liquidity index. A similar match was observed for the residual undrained shear strength estimated using BCPT and CPT data. Therefore, in the absence of data, the Locat and Demers (1988) relationship can be used, however, it should be

recognized that the strength data can vary over an order of magnitude, particularly at low liquidity index values.

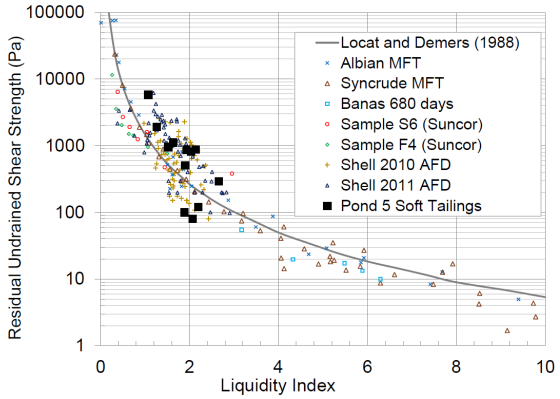

Figure 14. Residual undrained shear strength versus liquidity index

SUMMARY

An extensive field and laboratory investigation program was conducted to characterize the oil sands tailings along the perimeter of Suncor's Pond 5 and to evaluate correlations between different testing methods that could be used for future characterization of Pond 5 soft tailings and possibly soft tailings at other mine sites.

This paper presents the characterization data, including solids content, fines content, FWR, Atterberg limits, unit weight, and undrained shear strength.

The lab determined unit weight was compared to that estimated using CPT based correlation established for soils by Robertson and Cabal (2010). The empirical correlation by Robertson and Cabal (2010) was calibrated using the soft tailings data at Pond 5.

The undrained shear strengths of the soft tailings at Pond 5 were measured using eVST, BCPT, and CPT. The strength measured by eVST was considered to be representative of the field strength. The BCPT and CPT data was calibrated against the eVST data, where a N_{ball} of 15 was applicable for BCPT and N_{kt} of 20 was suitable for CPT. Also, the empirical correlation between residual undrained shear strength and liquidity index proposed by Locat and Demers (1988) was found valid for the Pond 5 soft tailings, although the data is scattered to some extent.

ACKNOWLEDGEMENT

The authors would like to recognize Yvonne (Yirao) Qiu of WSP E&I Canada Limited for her assistance in processing the data and preparing the figures of this paper.

REFERENCES

American Society of Testing and Materials (ASTM). 2002. ASTM D2573-01, Standard test method for field vane shear test in cohesive soil, ASTM International, West Conshohocken, PA

Abusaid, A., Pollock, G., Fear, C., McRoberts, E., & Wells, S. 2011. An Update to the Construction of the Suncor Oil Sands Tailings Pond 5 Cover, Proceedings from Tailings & Mine Waste' 11. Vancouver, BC

Abusaid, A., Zhang, Y., Pollock, G., & Uffen, D., 2021. An Update on the Construction and Performance of the Suncor Tailings Pond 5 Coke Cover, Proceedings from Tailings & Mine Waste'21. Banff, AB

Beier, N., Wilson, W., Dunmola, A., & Sego, D. 2013. Impact of flocculation-based dewatering on the shear strength of oilsands fine tailings. Canadian Geotechnical Journal, 50: 1001-1007

Boylan, N., & Long, M. 2007. Characterization of peat using full flow penetrometers. Soft Soil Engineering: Proceedings of the Fourth International Conference on Soft Soil Engineering, 403-414.

Colreavy, C., O'Loughlin, C.D., Long, M., Boylan, N., & Ward, D. 2010. Field experience of the piezoball in soft clay. 2nd International Symposium on Cone Penetration Testing, CPT' 10, Huntington Beach, CA, USA.

COSIA, 2014. Guidelines for Performance Management of Oil Sands Fluid Fine Tailings Deposits to Meet Closure Commitments.

DeJong, J.T., Yafrate, N.J, & DeGroot, D.J. 2011. Evaluation of undrained shear strength using full-flow penetrometers. Journal of Geotechnical and Geoenvironmental Engineering, ASCE, 137(1): 14-26.

Locat, J., & Demers, D. 1988. Viscosity, yield stress, remolded strength, and liquidity index relationships for sensitive clays. Canadian Geotechnical Journal, 25: 799-806.

Mayne, P.W., Peuchen, J., & Bouwmeester, D. 2010. Soil unit weight estimation from CPTs. 2nd International Symposium on Cone Penetration Testing, CPT' 10, Huntington Beach, CA, USA.

Pollock, G., Liu, X., McRoberts, E., Williams, K., Wells, S., & Fournier, J. 2010. Suncor Oil Sands Pond Capping Project, Proceedings from Tailings & Mine Waste' 10. Vail, Colorado.

Robertson, P.K., & Cabal, K.L. 2010. Estimating soil unit weight from CPT. 2nd International Symposium on Cone Penetration Testing, CPT' 10, Huntington Beach, CA, USA.

Robertson, P.K. & Cabal, K. L. 2015. Guide to cone penetration testing for geotechnical engineering, 6th edition.

Schaeffers, J., & Weemees, I. 2012. Comparison of in-situ shear strength measurement techniques of soft clays.

Wroth, C.P. 1984. The interpretation of in situ soil tests. Géotechnique, 34(4), 449-489.

ENHANCED IN-LINE FLOCCULATION OF FFT AND ITS CO-DEPOSITION WITH CST

Reza Moussavi Nik, and Givemore Sakuhuni
Imperial Oil – Calgary, Alberta, Canada

ABSTRACT

Imperial piloted an advanced fluid tailings treatment technology using an enhanced chemistry regime in two phases. Phase 1, conducted in 2019, compared the performance of "Enhanced In-Line Flocculation" (eILF) treatment of FFT (consisting of flocculant, colloidal silica, and coagulant) with a single flocculant treatment. Two test cells, each covering an area of about 80m by 15m and a depth of about 2.5 m were built and instrumented, and the FFT amended by each treatment method was poured into them. The resultant deposits were monitored for one year. Comparison of the data obtained from site investigation and instrumentation indicated superior performance of the eILF treatment.

Phase 2 of the pilot, conducted in 2020, focused on co-deposition of eILF treated FFT with coarse sand tailings (CST) using two different discharge methods (spigots and single pipe). The main objectives of Phase 2 pilot were to evaluate the fines capture and distribution achieved by each discharge method, and to understand the operational requirements associated with each scenario. The present paper provides a summary of the learnings from each pilot.

INTRODUCTION

Background

At Kearl, Imperial's oil sands mining operation, thickeners are utilized to reduce FFT accumulation by combining FFT and Flotation tailings into settling vessels where a polymer (i.e. flocculant) is added. The thickened underflow is treated once more with a flocculant before deposition into the thickened tailings (TT) panels, a dedicated terrestrial area for TT storage. Left as is, most of the TT material should achieve the reclamation criteria set out by Imperial's Directive 085 Tailings Management Plan, which was submitted to the Alberta Energy Regulator (AER) in 2016.
Additional fines treatment technologies are required in order to keep Kearl's FFT profile flat. One of these technologies, developed internally at Imperial, is eILF (enhanced In-Line Flocculation). In 2010, Imperial began developing the eILF technology using Chemically Induced Micro-Agglomeration (CIMA) chemistry as an alternative to thickening (Lin et al., 2013). The CIMA recipe chemically agglomerates the clay particles via aluminosilicate bonds, creating a material with higher solids content and enhanced dewatering compared to single-polymer treatment. The silicate also acts as a binder that provides deposit strength after initial dewatering. Another major advantage of CIMA is that it allows a much wider operating window for feed, meaning it can handle process fluctuations much better than traditional in-line flocculation technologies. CIMA was scaled up successfully in 2013 at the Saskatchewan Research Council (SRC) where its deposition behavior was investigated in 10 m^3 flumes. An improved performance (versus single-polymer treatment) was observed for solids content, strength gain, and enhanced ability to condition the incoming feed. As such, it was concluded that the next phase of eILF development would require a field pilot.

In 2018 a modification on the CIMA technology (Enhanced inline flocculation [eILF]) involving changing the order of chemical additives was implemented to enable piloting the technology at Kearl (Sakuhuni et al., 2021). The main difference between CIMA and EILF is that whilst CIMA requires long conditioning time of the chemicals, eILF requires short conditioning time which enables use of shorter pipe lengths between chemical additions. Figure 1 shows the difference between the CIMA and eILF chemicals treatment technologies.

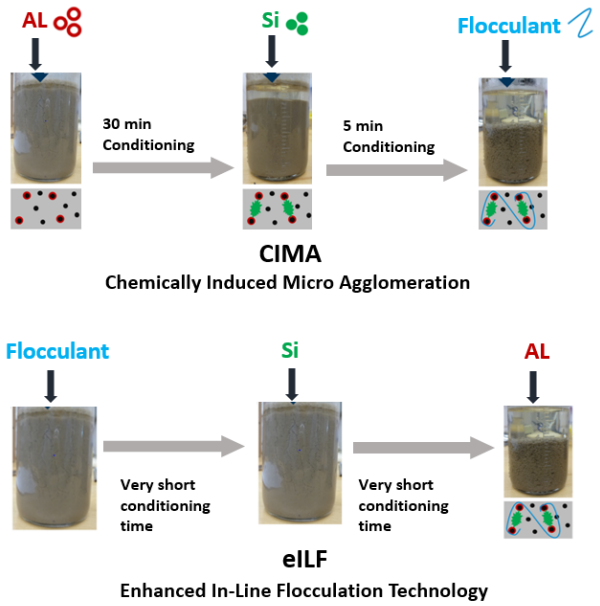

Figure 1. Distinguishing eILF from CIMA chemical treatment process

The Enhanced In-line Flocculation (eILF) trial was conducted in 2019 treating FFT from the TT panels (SFR 0.3) and it demonstrated successful deposit performance (improved deposit strength and release water clarity) for treating FFT using the three chemical treatment (polymer, colloidal silica [CSi] and Aluminum Sulfate [ALS]) in comparison to the single flocculant treatment. Phase 2 eILF pilot was conducted in 2020 treating WETA FFT (SFR 0.01) and co-depositing the treated eILF tailings with CST. Two discharge methods (Single pipe and spigots) were evaluated. The results demonstrated feasibility of co-depositing treated eILF FFT with CST. The following sections provide further details on each field trial.

2019 eILF PILOT

Objectives

The 2019 pilot was focused on comparing two different tailings treatment as shown in Figure 2:

- A base case of using a single flocculant to treat FFT (typical of in-line flocculation [ILF]); and,
- An enhanced ILF (EILF) treatment which utilizes a three chemical combination (flocculant, colloidal silica and coagulant) to treat FFT.

The flocculant used was a PAM polymer, which was very similar to the PAM that was approved for secondary chemical treatment of TT. The coagulant was aluminum sulfate and the colloidal silica functioned as a binder in this chemical treatment system.

The objectives of the pilot were as follows:

1. Monitor the deposit performance and evaluate the robustness of both treatments to fluctuations in the feed;
2. Validation of enhanced chemistry for FFT treatment in a thin lift deposition; and,
3. Comparing the deposit performance (net water release, strength, fines capture and segregation) of the single flocculant to the three chemical treatment.

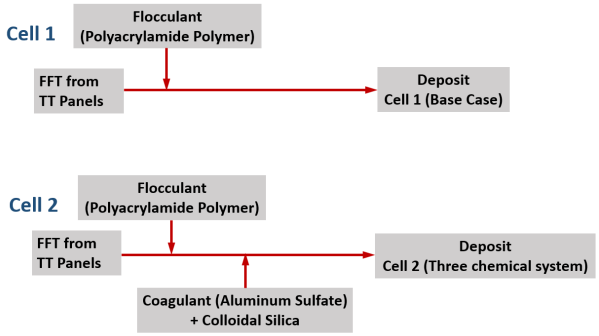

Figure 2. High level flow chart of the 2019 pilot

Deposition

The single flocculant (ILF) and three-chemical (eILF) treated FFT streams were deposited into two purpose-built cells located outside of the TT panels within the ETA footprint. Figure 3 shows aerial photos of the two cells, about six days after completion of the pour.

Both cells were approximately 120 to 140 m long by 33 m wide at the surface and varied in depth from 2.5 to 5.5 m. The base of the cells were approximately 80 m long by 15 m wide and sloped at 2% along the length. The soil material at the base was sand and clays. A volume of about 1000 m^3 of treated FFT was poured into each receptive cell within one day.

Figure 3 - Aerial Photo of the two test cells (six days after completion of the pour). The arrows show the position of discharge outlet at each cell.

Monitoring Plan – 2019 Pilot

A surveillance plan was developed to monitor the key performance indicators of the process and deposit during the pilot. The plan leveraged readily available instrumentation (inline for the process, and clusters of instruments installed on two posts in each cell for monitoring the deposit). In addition, field sampling combined with laboratory testing of the samples, and visual, videographic and photographic monitoring was also carried out during deposition.

The key process indicators monitored during the pilot included:

- FFT characterization (solids content, MBI, clay content, bitumen content, particle size distribution);
- Dilution water characterization;
- Treated FFT solids rate, flowrate and density;
- Treated FFT Sand to Fine Ratio (SFR);
- Chemical dosage;
- Capillary suction time; and
- Net water release.

The key deposit indicators monitored during the pilot were solids content, SFR, shear strength, pore water pressure dissipation, settlement, and release water characterization.

Below is the summary of operating conditions for each cell:

Cell 1 (ILF) - Single flocculant

- The feed solids content range was between 25-30 wt.% and dilution of the feed to 16-25 wt.% was not feasible due to pump limitations.
- Average feed MBI was 7.3 meq/100 g of solids; bitumen content was 1%wt, and SFR was 0.3.
- The feed flow rate was in the range of 200-220 m^3/hr.
- In order to monitor performance, KPIs were measured including Capillary Suction Time for both solids and release water, net water release (NWR) and yield stress. The strategy was to maintain polymer dosage throughout the deposition process in order to evaluate the robustness of the treatment to fluctuations in feed properties. Therefore, polymer dosage was maintained constant despite achieving KPI targets. The targeted KPIs were met initially but as the deposition continued, Capillary Suction Time measurement indicated polymer overdose. As the KPIs continued to fail during the deposition, the flocculant dosage had to be adjusted to match required dosage.

Cell 2 (eILF) – Three chemical treatment

- The injection rate for all the chemicals remained constant throughout the process.
- The feed solids content range was between 30-35 wt.%, and dilution of the feed to 16-25 wt.% was not feasible.
- Feed flow rate was 200-220 m^3/hr for the first one hour of the pilot and dropped to 180 m^3/hr to simulate the feed fluctuation without adjusting the dosages.
- All the KPIs (Capillary Suction Time, strength, NWR) met the target ranges throughout the deposition process without any adjustment to the chemicals dosages.

Release Water Analysis – 2019 Trial

Release water samples were taken from both cells during deposition and submitted to a local laboratory for water chemistry testing. The release water (Figure 4) from eILF treatment was observed to have significantly higher clarity but had higher dissolved metals.

Figure 4. Release water samples collected form the ILF and eILF cells during deposition.

Whilst the results showed differences in water chemistry between the two treatments, the actual impact on pond water chemistry is dependent on dilution, clay cationic exchange reactions and thermodynamics equilibrium, which were evaluated using OLI water modeling software. Figure 5 shows results for OLI modeling results for divalent cations.

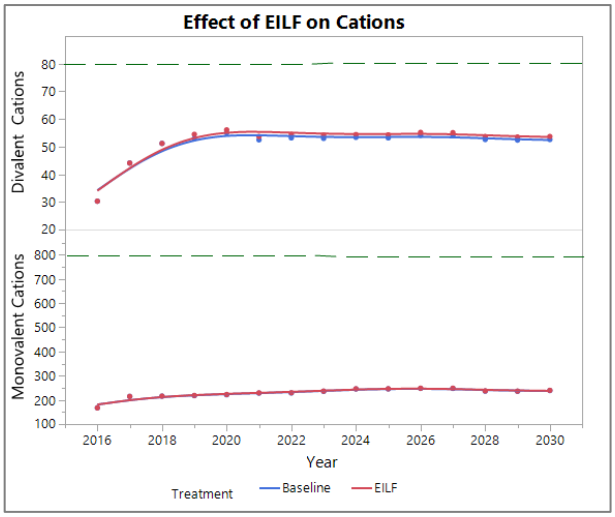

Figure 5. OLI modeling results comparing pond water chemistry with and without eILF release water inflow to the pond.

Deposit Performance – 2019 Trial

The tailings deposits in the two cells were monitored during the pour and for one year after the pour.

A scaffolding and platform system with sampling ports/openings were assembled in both cells to allow safe access to the deposits during the site investigations (visible in Figure 3). An initial site investigation program was conducted about ten days after the pour. This included in-situ tests of ball cone penetration (BCPT) and vane shear tests (VST) at three locations along each deposit, also core sampling from five to six locations along the cell. A second site investigation was conducted about one year after the pour, to evaluate the effect of freeze-thaw and evaporation on variations of solids/water content and strength of the deposits.

Two instrumentation posts/clusters were installed within each cell prior to the tailings pour to enable continuous monitoring of the water content, temperature and pore-water pressure of the tailings deposits during pour and afterwards.

2019 Pilot Results and Observations

Cell 1 (Single flocculant treatment):

Figure 6 shows an image of Cell 1 (ILF) during the pour of tailings treated with a single flocculant. The tailings deposit was observed to form a gentle slope of about 2% and to spread relatively evenly along the cell length and across the width. Multiple small

channels and few erosion gullies were observed, directing the release water towards the edges and downstream of the cell. A large pond (covering over 1/3 of the cell area) was formed at the downstream. Figure 7 shows the appearance of deposit in Cell 1 less than 24 hours after the pour. A thin layer water still appeared on surface of the deposit and traces of bitumen delineated the erosion gullies/channels.

Cell 2 – eILF (Three chemical treatment):

Figure 8 shows an image of Cell 2 (eILF) during the pour of tailings treated with three chemicals. Formation of a series of narrow/shallow channels was observed on the deposit surface, originating around the discharge area and evenly distributing across the width. These channels conveyed the release water towards the edges and front of the deposit. The surface of the deposit looked more 'solid' compared to Cell 1. As depicted in Figure 9, less than 24 hours after the pour, dry looking zones and crack formation could be observed on the surface of the deposit. The ponded water at the downstream of the cell was observed to recede a few hours after the pour, indicating potential infiltration into the cell base due to higher permeability of the tailings material. As shown in Figure 10, this hypothesis was confirmed at the lab by conducting funnel tests on treated FFT: eILF treated FFT showed better water drainage confirming a more porous structure. (The raw FFT used in this lab test was from the same source as field trials).

Figure 6. View of the tailings pour in Cell 1. Dominant channeling can be observed on the South side of the cell.

Figure 7. View of Cell 1 approximately 15 hours after ceasing pour operations. Surface of the deposit looks wet and stains of bitumen delineate the erosion gulley.

Figure 8. View of the tailings pour in Cell 2. Evenly distributed channeling can be observed.

Figure 9. View of the East Cell approximately 15 hrs after cease of pour operations.

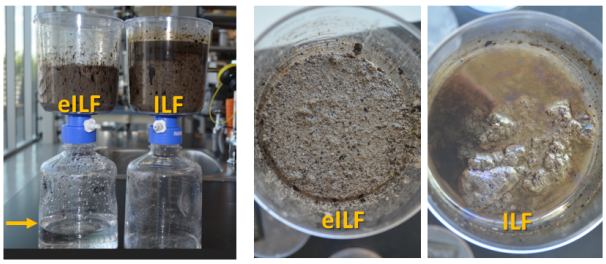

Figure 10. Funnel tests on ILF and eILF treated FFT, indicating higher permeability as a result of eILF treatment

Deposit Characterization – 2019 Pilot

Three days after the pour, the release water was pumped off from the two test cells. The objective was to evaluate the volume of release water from each cells and to collect additional water samples for turbidity measurements and chemical analysis. Figure 3 shows an aerial view of the two test cells after pumping off the majority of release water.

Surface of the tailings deposits was surveyed about six days after completion of the pour. The objective was to evaluate the thickness and volume of the deposits in the two test cells.

Eight days after completion of the pour, a site investigation program was started at the two test cells. A third party vendor supported the investigations by conducting core sampling and in-situ shear strength testing (BCPT and VST). The samples from the field investigation were tested at a third party vendor laboratory for index testing (including particle size distribution (PSD), Dean-Stark analysis, MBI, specific gravity and solids content).

Deposit Profile and Solids Content – 2019 Pilot

Cross-sections of the tailings deposits in the two test cells were prepared using the survey data. It was observed that the deposit at Cell 1 (ILF) formed a gentle slope of about 2% and a relatively uniform thickness along the cell, while the deposit in Cell 2 (eILF) formed a steeper slope of ~ 5.4% at the discharge location (i.e. thicker deposit at upstream), converting to a gentler slope of ~2% (resulting in a thinner layer downstream).
The solids content profiles at different sampling locations for each cell were also prepared. The solids content values for the upstream of Cell 1 (ILF) were varying from 51% to 59% from top to bottom of the deposit 8 days after the pour, while the upstream of Cell 2 (eILF) deposit showed a solids content variation of 61 to 67% from top to bottom 11 days after the pour. Considering the slightly higher thickness of deposit at the upstream of Cell 2, this difference in solids content indicates higher permeability and better dewatering of tailings in Cell 2 as a result of the three chemical treatment. The average solids content of the Cell 1 and Cell 2 samples were 56.1% and 59.4%, respectively.

Variations of strength – 2019 Pilot

Peak Shear Stress values from the Vane tests were significantly higher in the eILF Cell (~ 6kPa) compared to the ILF Cell (1.5 to 2 kPa). Pore Pressure dissipation tests indicated a more porous deposit in eILF Cell (i.e. higher permeability resulting in higher dewatering rate).

Another site investigation was conducted about one year after the pour to evaluate the consolidation and strength gain after one freeze-thaw and evaporation cycle. Table 1 shows the variations of average solids content in each cell after one year. The shear strength of both deposits had also improved after one year, due to combined effect of consolidation, freeze-thaw and evaporation.

Table 1 – Variations of average solids content in Cells 1 and 2

Test Cell	Average Solids Content (%)	
	~10 days after pour	One-year after pour
Cell 1 (ILF)	56	69
Cell 2 (eILF)	60	78

2020 Pilot – Co-Deposition of eILF treated FFT and CST

Following successful completion of the 2019 pilot and the improved performance observed for the eILF treated FFT, a follow up pilot (Phase 2) was conducted in 2020. Phase 2 pilot focused on learning about co-depositing eILF treated FFT with coarse sand tailings (CST) to generate a deposit with a sand-to-fines ratio (SFR) of 3 to 5. The target average SFR can be chosen a lower value in commercial operations, depending on the final depth and expected consolidation time and desired fines storage efficiency of the tailings deposit. It is anticipated that co-deposition of eILF treated FFT with another sandier tailings stream (e.g. CST, TT) will generate a deposit with higher SFR that will consolidate at a shorter time frame, and as a result,

will accelerate closure and reclamation, and will reduce the need for fresh water import.

The flocculant (PAM polymer) used during the 2020 co-deposition was similar to the PAM polymer utilized for the secondary injection system in the thickening process, and the coagulant and binder were similar to the 2019 pilot (i.e. aluminum sulfate and Colloidal Silica).

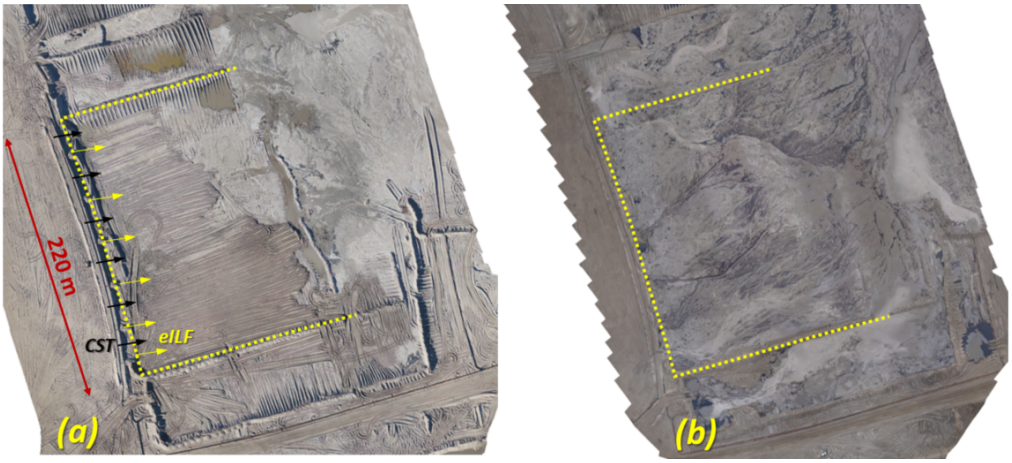

Figure 11. Aerial view of Cell 1 (co-deposition by spigots): (a) Prior to tailings pour; (b) Three days after completion of tailings pour

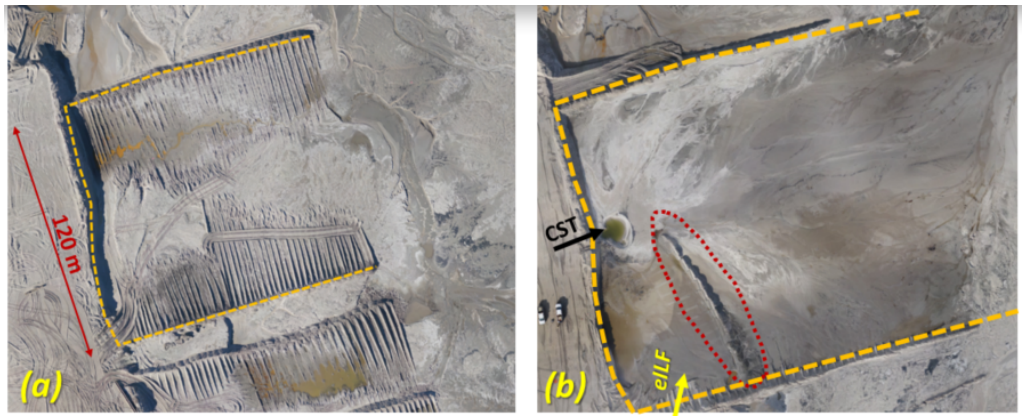

Figure 12. Aerial view of Cell 2 (co-deposition by single pipes): (a) Prior to tailings pour; (b) Two days after completion of tailings pour

Based on the 2019 trial experience, the enhanced chemistry treatment resulted in robust agglomerates of fine particle that maintain their integrity during pipeline transport and at discharge. Co-deposition of treated FFT with sand is expected to capture more fines, either in the void space of the sand matrix, or as individual layers, and result in a deposit with better dewatering and strength characteristics compared to a fines dominated deposit.

The objectives of the Phase 2 pilot were as follows:

- Compare two different discharge methods (spigots versus single pipe) for co-deposition of treated FFT and CST

- Identify the operational challenges associated with co-deposition of the two streams at field scale

Feed Characteristics – 2020 Pilot

The feed FFT for the 2020 trial was from West External Tailings Area (WETA) with the following average characteristics:

- MBI = 10.4 meq/100 g of solids
- Bitumen content = 0.6%wt
- Clay content was about 75%.

Deposition

The CST and treated FT streams were co-deposited into two open-ended cells located in the non-structural zone of the beach within East ETA. Approximate dimensions of the two test cells, along with position of the CST and eILF discharge lines are shown on aerial photos of the cells in Figures 11(a) and 12(a). The design specifications of the cells were as follows:

Cell 1 (Discharge by spigots):

- Base width: 220m
- Average slope of the cell base: 2%
- Spacing between treated FFT spigots: 32 to 36m
- Spacing between CST spigots: 32 to 36m
- Spacing between each CST spigot and its adjacent treated FFT spigot: 16m to 18m

Cell 2 (Discharge by two single pipes):

- Base width:120m
- Average slope of the cell base: 1.5%
- Distance between the single treated FT pipe and single CST pipe: ~60m

Treated FFT was poured continuously during the deposition period into each Cell, and CST was poured intermittently (based on a designed pour schedule) to ensure achieving an overall SFR of 3 to 5 for the feed to the cells.

Monitoring – 2020 Pilot

A field investigation was completed about 14 days after completion of the pour to run in-situ tests (CPT and VST) and to collect representative samples from the deposits). No in-situ instrumentation was installed in the cells for long term monitoring of the deposit, because the test area could not to be maintained beyond three months after the tailings deposition due to the need for CST pour in the area during dyke construction activities.

The CST and FFT flow rates were recorded using in-line flow meters and the density was measured using an in-line density meter. To optimize the process parameters for dosage and mixing requirements, during the commissioning FFT samples were collected from the pipeline and analyzed at the Kearl lab. The main KPIs measured for chemical optimization was the structure of the flocs by visual observation and the capillary suction time.

Based on the measured KPIs, the dosages were adjusted to obtain the required performance. This exercise was critical to optimize the process parameters to achieve an on-spec deposit.

The deposit build-up was monitored by visual observation, time-lapse photography and videography. Also, a handheld LiDAR scanner was utilized to determine the deposit thickness during the pour. This information was used to adjust the pour duration and to ensure a thick enough beach for site investigation was formed.

A tailings pour schedule, identifying the required durations of treated FFT and CST pour to obtain an average SFR of 3 to 5, was designed for each cell. Tailings operations followed the designed schedule and recorded the durations (i.e. start and end times) of the pour into the cells. This information was used to calculate the total mass of fine and sand fractions poured into each cell. Tables 2 and 3 provide total volume of tailings and mass of sand and fines poured into Cells 1 and 2. As indicated in the tables, the average SFR of the feed (FFT+CST) into Cells 1 and 2 is equal to 3.96 and 4.26 accordingly.

Table 2- Volume and mass of sand and fine tailings poured into Cell 1

Parameter	Treated FT	CST
Total Volume (m^3)	29,384	46,891
Average Solids Content (%wt.)	14.51	58.89
Mass of solids poured (tonne)	5,676	43,598
Average Fines Content (>44m)	96%	12%
Fines mass (tonne)	4,504	5,232
Sand mass (tonne)	181	38,367
Average SFR of the feed to Cell 1	**3.96**	

Table 3 - Volume and mass of sand and fine tailings poured into Cell 2

Parameter	Treated FT	CST
Total Volume (m^3)	38,993	80,021
Average Solids Content (%wt.)	15.8	59.6
Mass of solids poured (tonne)	6,832	75,772
Average Fines Content (>44m)	96.7%	12%
Fines mass (tonne)	6,606	9,093
Sand mass (tonne)	225	66,679
Average SFR of the feed to Cell 2	**4.26**	

Figure 11 (b) shows an aerial views of Cell 1 about three days after completion of treated FFT and CST co-deposition. An aerial survey was conducted before and after the pour, and the thickness of co-deposited beach was determined to be between 0.4 m to 1.25 m.

Figure 12 (b) shows aerial view of Cell 2 about two days after completion of treated FFT and CST co-deposition. The thickness of co-deposited beach in Cell 2 was determined to be between 0.5 m to 1.75 m. In this figure, the dotted redline marks a dry dyke in Cell 2 that was constructed by field operations during the first hour of the tailings pour. The intent was to direct the treated FFT towards the CST outlet, to ensure interaction of the two streams.

Pilot Results – 2020 Trial

A geotechnical site investigation program was conducted at Cells 1 and 2 about two weeks after the completion of the pour and was concluded in about 11 days. The objectives were to:

- Collect representative samples across the tailings deposits to characterize the solids and fines content.
- Run in-situ tests (Cone Penetration and Vane Shear) to assess the variations of strength across the deposits.

A parky piston sampler was used to collect relatively undisturbed samples. The sample cores collected at each location were sub-divided into ~30cm segments and each were tested to determine the solids content and fines content/SFR. The test results were then used to calculate the weighted average solids content and SFR at each sampling location.

SFR and Beach Fines Capture in Cell 1 (Discharge by Spigots)

Figure 13 illustrates the variations of weighted average solids content in Cell 1. In-situ peak and remolded shear strength values at select locations of the deposit are shown in Figure 14 (peak values shown in blue and remolded values in red), overlaid on the SFR distribution map. The average SFR for the whole deposit in Cell 1 is equal to 4.95.

The following observations can be made from Figures 13 and 14:

In Figure 13, except for a small zone in the north eastern part of the deposit (~15m diameter, shown in violet), the rest of the deposit had a solids content higher than 65% at the time of investigation. The average SFR in the identified small zone is less than 1 (see Figure 14) and the peak and remolded shear strength values measured by vane are the lowest across the cell (1.87 kPa and 1.54 kPa respectively), indicating generation of a small softer zone. In operational scale, generation of such zones can be reduced by annual monitoring of the deposit and alternating the CST pour and discharge locations.

The central zones with lower SFR of 1.3 to 2 have a solids content higher than 75%. Considering that the site investigation was conducted about two weeks after completion of the pour, this means that this zone has enough time to consolidate and gain enough strength to allow reclamation in a reasonable time frame.

This co-deposition method has resulted in a deposit with an average fines content of ~20%, which is significantly higher than the fines content of regular CST beaches.

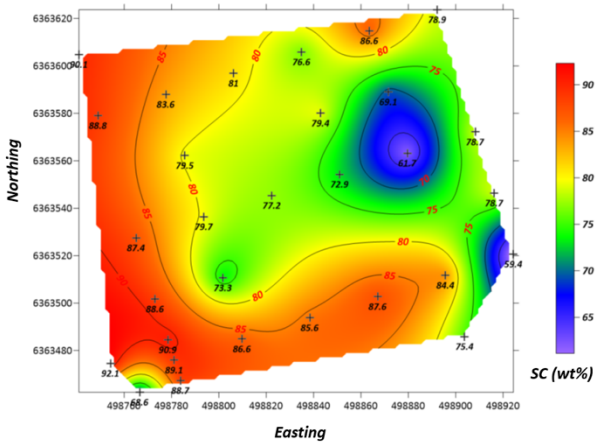

Figure 13. Variations of weighted average solids content in Cell 1

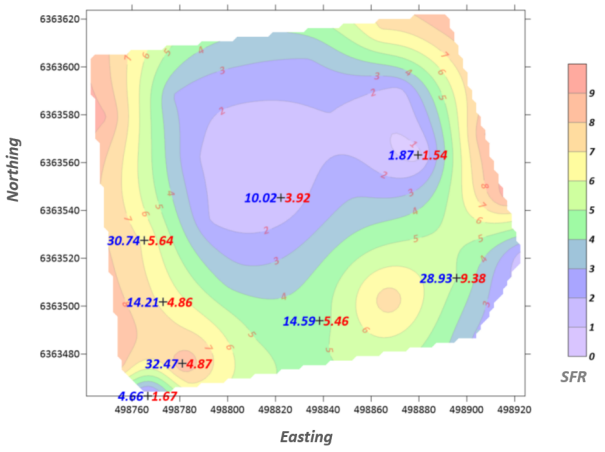

Figure 14. In-situ measurements of peak and remolded shear strength (kPa) in Cell 1, on the SFR distribution map

Calculated Fines Capture in Cell 1:

Fines capture was calculated by using the simplified method suggested in the COSIA Beach Fines Capture Study (AMEC, 2013):

$$Fines\ capture = \frac{SFR_S}{SFR_D} \times 100\% \qquad \text{(Equation 1)}$$

Where SFR_D is the sand to fine ratio of the beach; and SFR_S is the sand to fine ratio of the tailings stream. The SFR calculation is based on the percent finer than 44 microns. The fines capture parameter assumes all the sand in the tailings stream is retained within the beach deposit and only the fines and water flow away into the pond.

As indicated in Table 2, the average SFR of the feed into Cell 1 is equal to 3.96. Therefore:

Fines Capture in Cell 1 = 3.96/4.95 = 80%

This is higher than the fines capture in beaches of commercial scale ETFs and the commercial scale co-disposal case listed in the COSIA Beach Fines Capture Study (AMEC, 2013). Considering the limited duration of the pour in this trial and the additional operational controls, this value shows a potential upper limit of fines capture for co-deposition with spigots and the actual fines capture rates in full scale operations could be lower due to variations of the feed and upset conditions.

SFR and Beach Fines Capture in Cell 2 (Discharge by Single Pipes)

Figure 15 illustrates the variations of weighted average solids content in Cell 2. In-situ peak and remolded shear strength values at select locations of the deposit are shown in Figure 16, overlaid on the SFR distribution map (peak values shown in blue and remolded values in red). The average SFR for the whole deposit in Cell 2 is equal to 5.05.

The following observations can be made from figures:

In Figure 15, the solids content of the deposit at the south part of Cell 2 (close to the treated FFT discharge point) is varying from about 44% to 55%. The SFR values for this zone, shown in Figure 14, change from 0.04 to <1, indicating generation of a soft fines dominated zone.

In Figure 15, the solids content of the north western part of the deposit (close to the CST discharge point) is higher than 85%. The SFR values for this zone, shown in Figure 16, change from 7 to about 13, indicating generation of a low fines content CST beach. Intermixing of the two streams at the central parts of the cell has generated a deposit with an average SFR between 2 to 5 and weighted average solids content of about 70% to 80%.

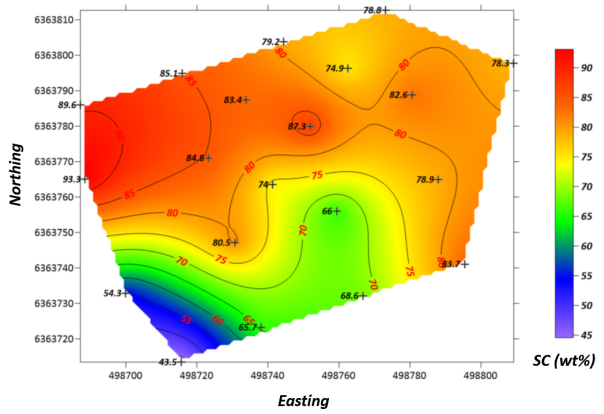

Figure 15. Variations of weighted average solids content in Cell 2

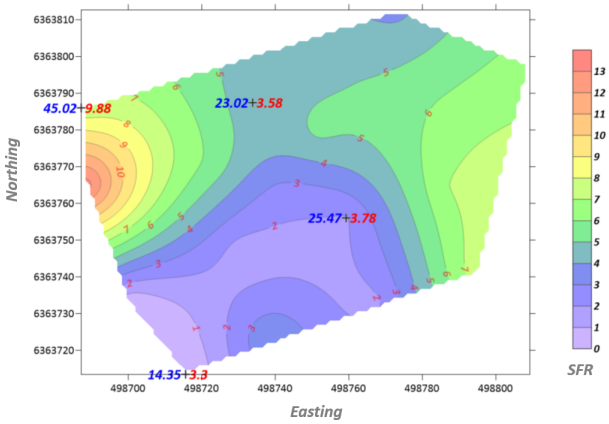

Figure 16. In-situ measurements of peak and remolded shear strength (kPa) in Cell 1, on the SFR distribution map

Similar to Cell 1, this co-deposition method has resulted in a deposit with an average fines content of ~20%, which is significantly higher than the fines content of regular CST beaches and allows taking advantage of the void space between sand particles for storage of fines. However, use of two single pipes rather than spigots has generated a fines dominated zone close to the treated FT discharge area, and in general a lower SFR material in the southern part of the cell and a higher SFR material in the northern part. This suggests that on an operational scale, interchanging CST and treated FFT pour locations might provide better co-deposition.

Also as shown in Figure 12 (b), operations had to build a dry dyke to direct the treated FT stream towards CST and ensure mixing of the two streams. Construction of such a dyke could be challenging on a soft deposit in commercial application. Alternative methods to encourage mixing of the two streams should be explored.

Calculated Fines Capture in Cell 2:

As indicated in Table 3, the average SFR of the feed into Cell 2 is equal to 4.26. Using Equation 1:

Fines Capture in Cell 2 = 4.26/5.05 = 84%

It should be noted that entrance of the tailings from Cell 1 into the eastern part of Cell 2 changed the topography of the cell base and altered its open ended design. This back-end effect has increased the fines capture beyond the values that would be expected in field scale operations.

CONCLUSIONS

The enhanced in-line flocculation (eILF) shows superior performance compared to single polymer treatment of FFT and is more robust to fluctuations of feed characteristics.

The co-deposition of eILF treated FFT and CST using the spigot and single pipe discharge methods showed promising results with respect to fines content and fines capture in the resultant beaches. Entrapment of fines (either as fine layers within coarser tailings layers, or as fine particles/agglomerates within the void space of coarse tailings) reduces the volume of fines dominated zones, and accelerates closure. The spigot discharge system generated relatively a more uniform deposit. The single pipe discharge method generates a soft fines dominated zone close to the FFT discharge point, which can be managed by alternating the CST and FFT discharge points in operational scale.

Imperial will consider the findings of these trials for increasing the fines capture efficiency and enhancing the reclamation timeline in tailings deposits.

ACKNOWLEDGMENT

The valuable support of our colleagues at Kearl Technical and Research teams, in particular, Atoosa Zahabi, Anu Saini, Thuan Ngo and Amjad Ali during these field trials is highly appreciated.

REFERENCES

Lin, C., Speirs, B.C, Sarkar, A., Zhu, R. and Lunn, S.R.D. (2013). Method of using a silicate-containing stream from a hydrocarbon operation or from a geothermal source to treat fluid tailings by chemically-induced micro-agglomeration. Canadian Patent 2823459.

Sakuhuni, G., Lin, C., Ngo, T.T., Forgeron, G.S., Cebula, S., Zahabi, A. (2021) Oilsand tailings treatment using flocculation and treatment with coagulant and silicate. Canadian Patent reference for eILF Patent 3048297

AMEC, Beach Fines Capture Study, submitted to COSIA. June, 2013. Link on web: https://cosia.ca/uploads/documents/id8/Fines%20Capture%20Report_Jun2013.pdf

ABBREVIATIONS

AER: Alberta Energy Regulator
CIMA: Chemically Induced Micro-Agglomeration
CST: Coarse Sand Tailings
eILF: enhanced In-Line Flocculation
ETA: External Tailings Area
ETF: External Tailings Facility
FFT: Fluid Fine Tailings
ILF: In-Line Flocculation
TT: Thickened Tailings
WETA: West External Tailings Area

SESSION 2

CONE FORMATION DYNAMICS DURING DREDGING OF OIL SANDS TAILINGS PONDS – FIELD OBSERVATIONS AND COMPARISON WITH PREDICTION OF COMPUTATIONAL MODELS

Trevor Bugg, Taryn Bittner, and Babak Derakhshandeh
Suncor Energy Inc., Calgary, Alberta, Canada

ABSTRACT

In this paper we provide a comprehensive overview of cone formation dynamics during dredging of fines dominated oil sands tailings ponds. Prediction of computational fluid dynamics models (CFD) will be compared with field scale data collected from dredging of several different ponds at Suncor's Baseplant operations. Impacts of pond rheology, depth, density and dredge operating variables on the extent and the rate of density reduction in outflow from the commercial assets will be reviewed. We will show that shallow ponds and/or those with a high rheology inventory exhibit a rapid cone formation requiring frequent asset relocation every 2 weeks to 2 months depending on the available dredging depth. Deeper ponds with a low rheology inventory exhibit slow dynamics with cone formation rates of approximately 5 to 15 times slower than other ponds. Comparison between commercial scale data and those predicted by the CFD models indicate that computational models consistently over-predict the size of cones formed and, hence, underpredict the rate of cone formation, potentially due to numerical limitations and complexities involved in incorporation of density and rheological models capable of representing the non-homogenous ponds. Furthermore, real world variables such as the pond geometry, nearby dykes, multiple dredge operations, and tailings inflow cannot be captured reliably in CFD leading to mismatch between the model predictions and cone formation dynamics at commercial scale. Based on the work performed by Suncor, it is concluded that CFD models can only provide directional information for planning purposes and should not be used to accurately predict cone formation at commercial scale.

ACRONYMS AND DEFINITIONS

CFD – computational fluid dynamics
CWR – mass of clay to mass of water ratio
Mudline – the sharp interface boundary between the fluid tailings deposit and the watercap in a tailings pond

BACKGROUND

Dredging is typically undertaken in oil sands tailings to manage fluid containment in a pond by transferring tailings from one pond to another, or to provide volume to support tailings treatment operations. The industry has historically experienced challenges sustaining predictable and long-term dredging operations in oil sands fluid tailings. Frequently, a rapid decrease in dredged fluid tailings density occurs, requiring unplanned and frequent on-pond dredge asset relocations to achieve desired fluid tailings quality and dredging objectives.

Fines dominated oil sands tailings are viscoplastic suspensions possessing a yield stress and a time-dependent flow behavior referred to as the thixotropy. Tailings exhibit slow dynamics, ageing and shear banding like those observed in colloidal suspensions (Derakhshandeh 2016) (Adeyinka 2009). The unique rheology of tailings combined with the non-homogeneity of their properties in the pond contribute to the experienced challenges in oil sands dredging operations. Tailings withdrawal at a consistent density or solids content is often not possible for long periods of time due to formation of a "cone" resulted by the breakthrough of the surface water to the pump's inlet at depth in the tailings deposit. Once a cone is formed, the effective density of the harvested material will be lower due to dilution with surface water.

Coning is not specific to the oil sands operations. Cone formation in a two-layer fluid system is a classical fluid mechanics problem that has been the subject of various academic studies in the past. Cone formation in oil reservoirs has attracted the most attention in the field, where oil extraction imparts an upward driving force on the underneath water layer creating an upward cone towards the ground surface. Experimental methods and semi-empirical approaches have been used to specify

the production rates that define the onset of coning for specific geometries (Wojtanowicz 2019). Such studies cannot be applied to the tailings/water systems given differences in the physics, the rheological behaviors of the fluids (Newtonian vs non-Newtonian) and the boundaries defining the system (closed in the case of a reservoir vs free surface in the case of tailings ponds).

The only approximate theoretical analysis of coning in tailings has been provided by Rayland and Shook (Shook 1996). Semi-empirical relationships were developed to predict the onset of cone formation as a function of tailings properties and the depths of the fluid layers. The relationships developed by Rayland and Shook provide the steady-state solution of the problem and ignore the time-dependent rheological behavior of tailings as well as the combined impacts of shear-thinning and yield stress on coning behavior.

Application of CFD modelling to oil sands tailings coning has been found to provide only “directional” information incapable of accurately predicting the field-scale behavior, likely due to the way the models are developed or the method by which rheological variation in the pond is incorporated into the computational models.

CFD has been employed by Suncor to predict dynamics of cone formation in 4 tailings ponds with different configurations and fluid tailings properties at Suncor’s Baseplant facility. Field-scale experimental data has also been collected during operations to evaluate the capability of the CFD models in predicting large scale coning behavior. This paper provides a summary of the main conclusions from these studies. A comparison between experimental data and CFD models will be provided and important variables in control of large-scale cone formation dynamics will be presented.

DEVELOPMENT OF CFD INPUTS

Pond Assessments & Properties

Tailings pond volumes and properties are assessed annually, which includes analysis and modelling of field data. Samples from the pond are collected for compositional analysis, as well as several downhole tools are used to obtain material properties. Statistical and geospatial analysis is conducted on the field data to develop a block model representation of the pond and fluid tailings properties. The mudline of the oil sands tailings deposit is measured using a sonar survey where there is a watercap or by an aerial survey such as LiDAR, air photo, or satellite image interpretation where there is no water cap. Data from these pond assessment models were used both as inputs, pre-dredging, to the CFD coning simulations, and, post-dredging, as comparison of field observations to CFD predictions.

The 4 different tailings ponds evaluated in this study are: Pond A – a shallow pond with lower rheology tailings; Pond B – a deep pond with deep dredging of lower rheology tailings; Pond C – a deep pond with relatively shallow dredging of high rheology tailings; and Pond D – a deep pond with planned deep dredging of high rheology fluid tailings. It should be noted that dredging in Pond D has not yet occurred and CFD predictions only are available for comparison to the other three ponds. See Table 1 for a comparison of pond properties.

Table 1. Comparison of Pond Properties

	Pond Depth	Dredging Depth	% solids	CWR	Fluid Rheology
Pond A	Shallow	6m	High	Medium	Low
Pond B	Deep	21m	High	Medium	Low
Pond C	Deep	13m	High	High	High
Pond D	Deep	N/A	High	High	High

Cross sections from the pond block model are used to compare pond properties with depth along a vertical plane in one direction across the pond. The cross-section comparisons for Clay to Water Ratio (CWR) are shown in Figure 1 and for solids content by weight percent in Figure 2 for each of the 4 ponds assessed in this study. The depth scale (y-axis) in Figures 1 & 2 are consistent between the 4 ponds to illustrate the relative differences in pond depth. The color heatmap for CWR and solids content shown in Figures 1 and 2 are also consistent between the 4 ponds for comparison. The properties range for the heat map are provided in Figures 3 and 4.

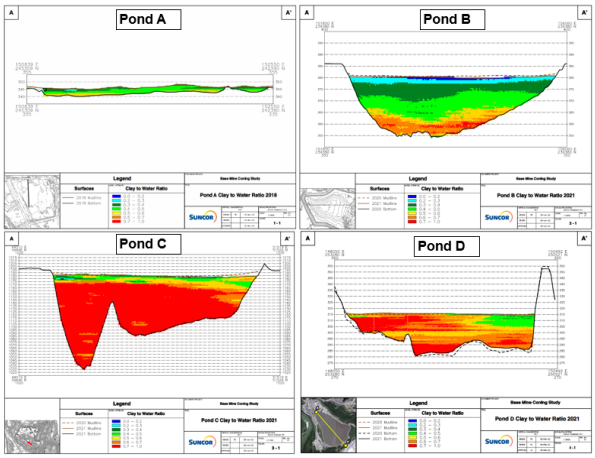

Figure 1. Comparison of pond depth and CWR

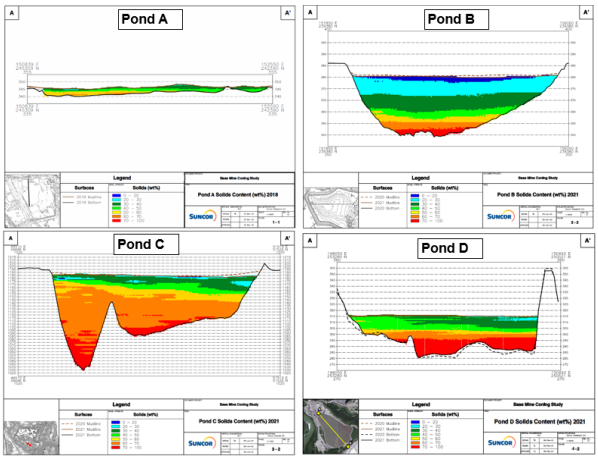

Figure 2. Comparison of pond depth and solids content by weight percent

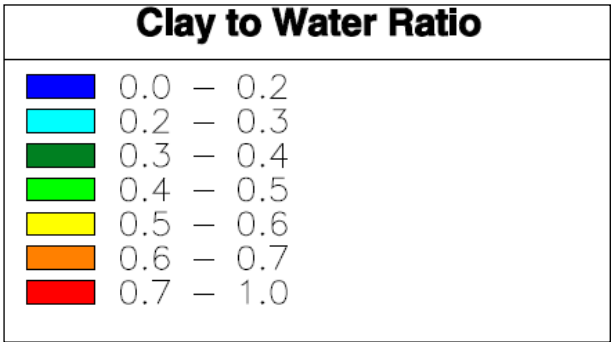

Figure 3. Color ranges for cross sections of Clay to Water Ratio

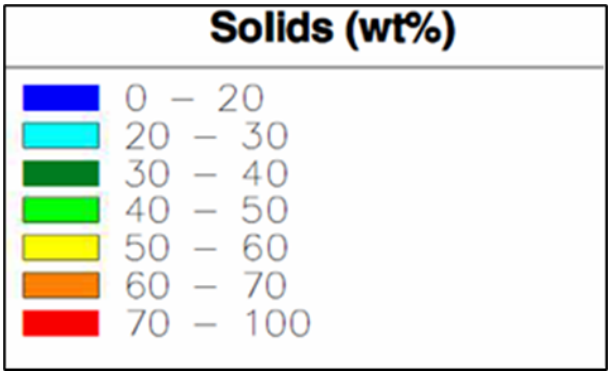

Figure 4. Color ranges for cross sections of Solids content

Composition Correlations

ANSYS Fluent, 2016 CFD software was used for CFD modelling. The ponds were modelled in two dimensions of radius from dredge location and depth in the pond with an assumption that the pond is axi-symmetric. A modelling domain of 1500m radius was used. Modelled pond depth, dredging depth, and dredging flowrate were set to expected field operating conditions specific to each pond. Pond and dredge depth are provided in Table 1, with the notable exception that, for Pond C, a dredging depth of 13m was realized in operations versus CFD modelling basis of 6m depth. Modelled flowrate was varied between 2200m3/hr and 5000m3/hr reflective of the size of the dredging asset planned to be used in operations in each specific pond. From the pond assessment data, for each of the 4 ponds, an average compositional profile versus depth was developed for clay mineral, non-clay mineral, and water content. Rheology correlations for static yield stress, and viscosity were also produced from lab measurement of samples from each of the ponds. These correlations were used as initial starting conditions (pre-dredging) for the CFD simulations.

As shown in Figure 2, there is uniformity or only small, gradual change in solids content versus depth across the multiple sample locations and cross section within each pond. This provides confidence in the representativeness of correlations used for CFD modelling for water and total mineral content. However, as illustrated in Figure 1, CWR versus depth within individual ponds is non-homogenous and varies quite significantly between sample points, driven by variability in clay content in the pond. This

variability in clay is created by the depositional history including type and locations of different tailings inflows, along with any previous dredging history in the pond.

Rheology Correlations

Fluid tailings samples from the pond assessment program from Ponds A, B, and C were measured in the lab for yield stress and plastic viscosity to develop rheology models for input to the CFD software. Samples were allowed to sit, undisturbed, for greater than 2 months prior to rheology measurements to allow for stabilization of rheology after disturbance from sample collection and shipping operations. Specifically for Pond C, periodic rheology measurements over time were taken on a subset of samples to verify rheology conditions had reached steady state and no further meaningful time-dependent strength gain was occurring, prior to analyzing the samples.

Pond A and B, being lower density, actively consolidating tailings ponds, with similar source tailings material, were found to have low rheology that correlated most closely to CWR results of the samples. Combined with the CWR compositional profiles, rheology data was translated into rheology versus depth correlations for each pond. Figure 5 shows the static yield stress and Figure 6 the viscosity versus depth correlations for Ponds A, B, and C. The marker on each trendline denotes target dredging depth for CFD simulations. In Pond C, CFD simulated dredging depth was selected as 6m below mudline. Realized dredging depth in Operations was deeper at 13m as provided in Table 1.

Pond C and D are higher density consolidated deposits with a different depositional history from Ponds A & B. Pond C rheology was found to be significantly higher than Ponds A and B, as shown in Figures 5 and 6. Pond C rheology was also found to be highly variable and did not correlate well with depth or compositional properties as shown in Figure 7. This may be due to potential non-representativeness of lab samples to in-situ field conditions for rheology; challenges in measuring fluid rheology given the high rheology of the samples; or other chemical or unknown factors affecting demonstrated rheology in the samples. Given the high variability, for CFD modelling purposes, only the data from sample locations nearest the dredge were used, which generally had measured yield stresses of 170 Pa or less. Data from the sample locations with measured yield stress above 170Pa were excluded as not representative of the planned dredging footprint in Pond C.

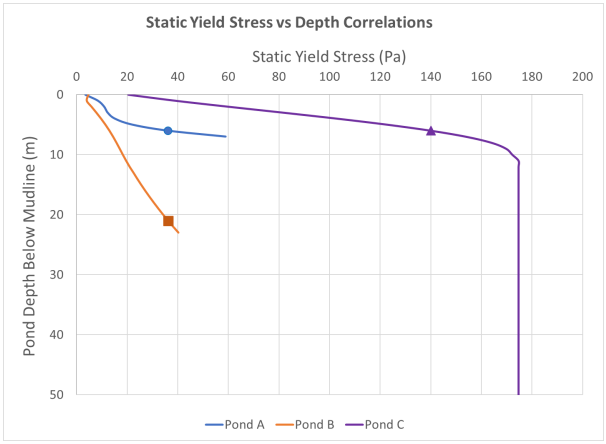

Figure 5. Static yield stress to depth correlations for Ponds A, B, and C.

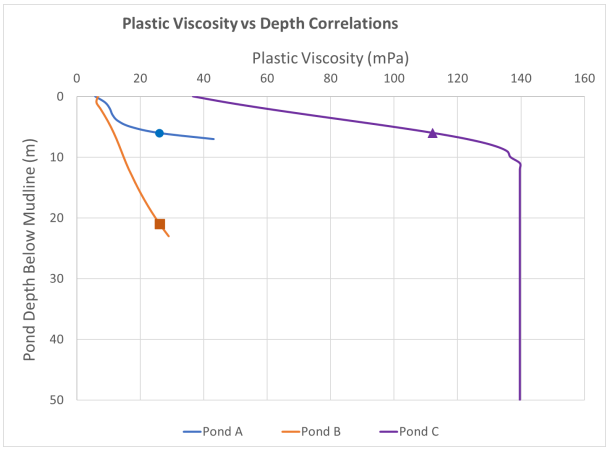

Figure 6. Plastic viscosity to depth correlations for Ponds A, B, and C.

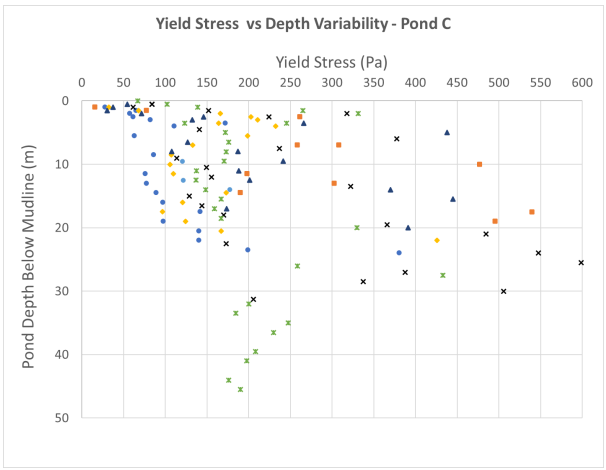

Figure 7. Variability in static yield stress versus depth in Pond C

Samples from Pond D were not measured for rheology. Pond D, at planned dredging depth, has similar source tailings material as Pond C. At the time of CFD modelling for Pond D, field data for coning performance in Pond C was available. An adjustment factor of double the initial assumed Pond C rheology models for yield stress and viscosity was required to make Pond C CFD and field coning results match. As Pond D and C have similar source tailings, Pond D rheology correlations for CFD models was assumed to be double that used in Pond C CFD simulations.

The high lateral variability in clay content and rheology versus depth within each pond had potential to impact the accuracy of the CFD model inputs and hence the CFD predictions. Inherently any given dredging location within the pond will have higher or lower compositional properties and rheology than the assumed average correlations for CFD modelling. Consequently, the CFD predictions should be treated as an average expected outcome and may or may not match conditions for dredging at any given specific location in the pond.

CONING RESULTS AND DISCUSSION

CFD Modelling Results

CFD modelling sensitivity analysis was conducted for Pond A on the impact of dredged flowrate to coning performance and is shown in Figure 8. The simulations predicted that tailings fluid removal rate had negligible impact to shape and volume of produced cones. The inference is that coning is driven only by pond characteristics; both depth and width of the pond itself, and the composition and rheological properties of the tailings deposit. Given a fixed cone shape outcome, higher dredging flowrates only serves to proportionally accelerate the timeline and rate of coning; increasing the rate of density decrease and frequency of required dredge relocations. This finding is not surprising if we consider that both the CFD predicted, and field observed dimensions for cones formed in oil sands tailings deposits are greater than 400m radius compared to typical dredge intake piping diameters of less than 1m or less than 0.2% of the cone size. In short, the size of cones formed in oil sands tailings ponds dwarf and render inconsequential the size and flowrate of the dredging asset itself.

If we assume these simulation results, showing negligible impact of flowrate on cone size, can be reliably translated to field operations, it eliminates dredge size and flowrate as a variable and enables direct comparison of field coning observations between the different dredging operations in each pond.

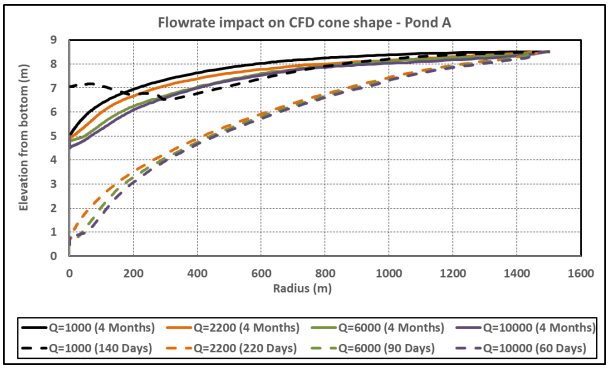

Figure 8. CFD simulations of effect of tailings removal rate on cone shape.

CFD simulations were also developed for cone recovery potential for Pond A, wherein, upon complete coning and water breakthrough at the suction intake pipe, fluid removal was stopped in the simulation and the CFD software predicted, over time, the degree to which fluid tailings continued to flow into the coned area. In these simulations, there was no active tailings deposition to the pond. Any fluid tailings migration into the coned area was solely due to non-steady state conditions with over-steepened cone slopes driving ongoing fluid mobility in the pond until reaching an equilibrium slope defined by the yield stress characteristics of the specific tailings material. The purpose of this simulation was to gain insight into the extent to which coned areas regenerated fluid tailings volume and expected timeline before the same area could be dredged again. Pond A cone recovery simulations are shown in Figure 9. After 2 months simulated time there was negligible cone recovery observed in the CFD predictions and the simulation was stopped. Implications of these results are that, in the absence of new tailings inflow to the pond, there is effectively no cone recovery, and no area of the pond can be dredged twice.

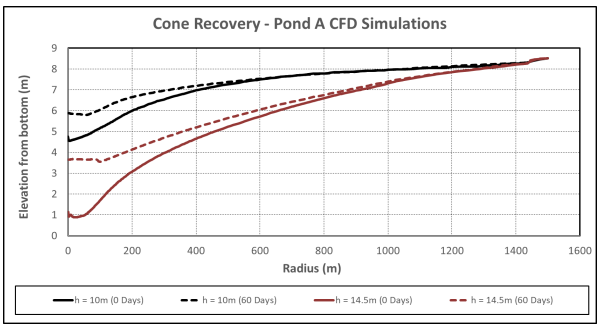

Figure 9: Pond A CFD cone recovery simulations

Cone Dimensions - Field Observations:

Observed coning, in the field, during dredging operations was highly variable depending on the pond. In general, field observed cone shapes had significantly steeper slopes and a smaller radius than CFD predictions. In Pond A, the tailings cones that formed during dredging operations were determined from mudline sonar scans as pond assessment sample spacing did not have high enough resolution to show coning at depth within the tailings deposit. Coning seen at the mudline was small and restricted, with only a maximum radius of 425m compared to CFD predictions of 1500m. See Figure 10 for a plan map of annual changes in mudline, showing coning at the mudline around the multiple dredging locations.

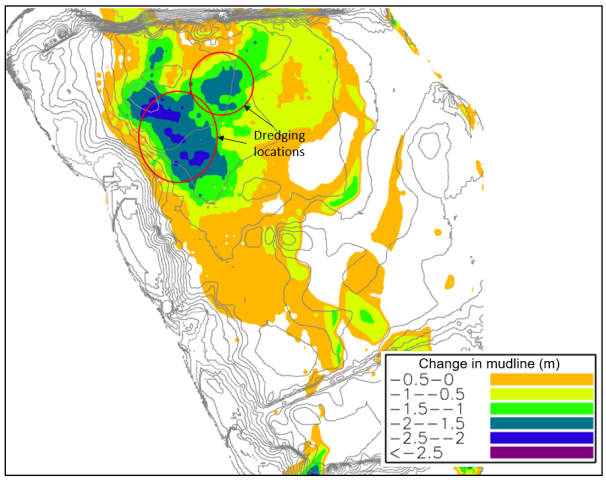

Figure 10. Annual changes in mudline in Pond A

Field data showed no mudline coning in Pond B, which aligned with CFD predictions, as the top layers of the pond have very low rheology. Field data does appear to show coning at depth, with a maximum cone radius of 650m measured in the higher CWR and higher rheology layers of the pond. This is in directional agreement with CFD models in Pond B. However, again, the CFD models predicted a much larger cone radius of up to 1500m expected at depth in the pond. See Figure 11 for a cross section showing field coning of CWR compared to CFD cone predictions in Pond B.

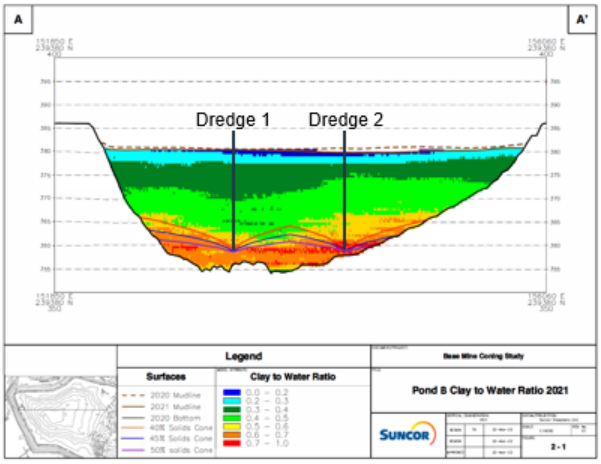

Figure 11. Comparison of field measured coning to CFD in Pond B

Field coning in Pond C had high variability from one dredging location to the next due to localized variability in oil sands tailings rheology. Similar to Pond A, sample spacing from the pond assessment program was not of high enough resolution to detect coning at depth within the tailings deposit. Mudline scans on Pond C detected dredged cone radius of, on average, 500m compared to CFD predictions of up to 1500m. See Figure 12 for a cross section comparison of field cones to CFD predicted coning in Pond C. See Figure 13 for a plan map of annual changes in mudline, which shows coning at the mudline around the dredging location.

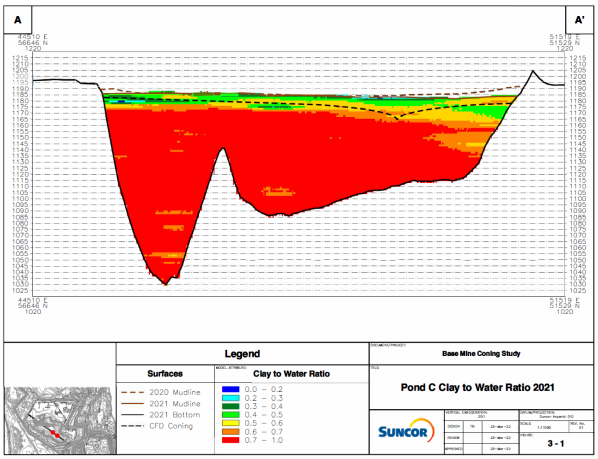

Figure 12. Comparison of field measured coning to CFD in Pond C

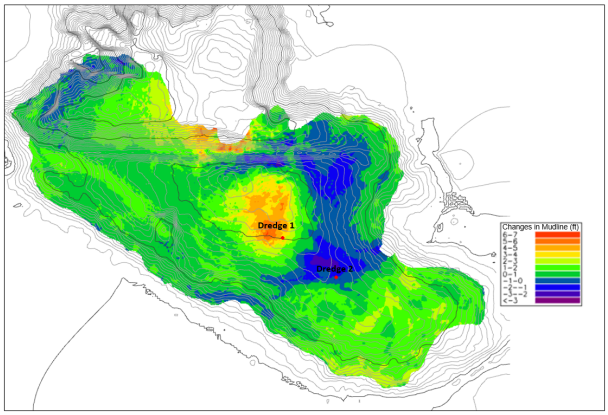

Figure 13. Annual changes in mudline in Pond C

Across all 3 ponds with dredging operations at Suncor's Baseplant facility, CFD modelling consistently and significantly overpredicted the size and shape of the cone compared to that measured in the field dredging operations. This indicates the apparent in-pond tailings rheology is higher and fluid mobility lower than predicted by CFD. The cause for overprediction in CFD was not able to be determined in this study. Potential contributing causes include non-representative rheology measurements associated with differences between lab samples and in-situ behavior, non-homogenous pond properties for both composition and rheology, variable pond geometry, and inability to account for dykes and multiple dredge operation in CFD, or other unknown factors. See Figure 14 for a comparison between the depth and radius of realized field dredging cones in operations and the CFD predictions.

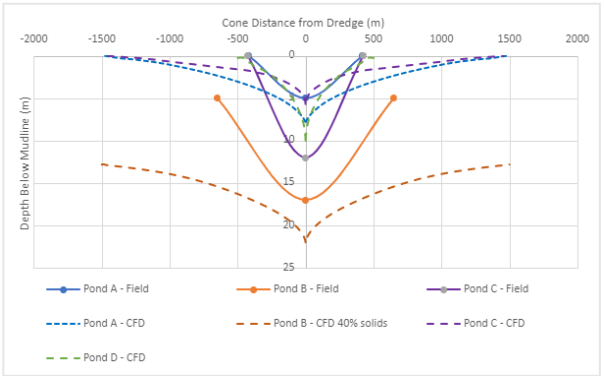

Figure 14. Comparison of CFD predicted and field measured cone dimensions

Dredged Density Change - Field Observations

Field results for realized dredged density in each pond were also below and decreased more rapidly than predicted by CFD. Representative dredged density data at three different locations in Pond A for the first year of dredging operations, compared against CFD model predictions, are presented in Figure 15. Density data are presented as achieved density from start of dredging (day zero) in a new on-pond location, to ending density at the same location, immediately prior to dredge relocation.

As shown in Figure 15, realized initial dredged density in Pond A was always lower than, and rate of density decrease significantly faster than, predictions by CFD. For the first year of dredging in Pond A, given the rapid rate of density decrease observed, dredges were required to be relocated every 2 to 4 weeks to sustain fluid tailings pumping rates. This was much quicker than expected and operationally planned for based on the CFD predictions. Based on CFD simulations showing lack of cone recovery (Figure 9), dredge relocations in Pond A, as well as in the other ponds, was always to new, not previously dredged, locations.

Pond A did not receive new tailings inflow during the 3 years of dredging. Consequently, the depth of the tailings deposit progressively reduced with dredging over time. Figure 16 shows significant deviation in field results to CFD models for achieved density in years 2 and 3 of dredging in Pond A. Dredging operations experienced progressively lower realized density and more frequent relocation requirements as the deposit depth and time to coning decreased.

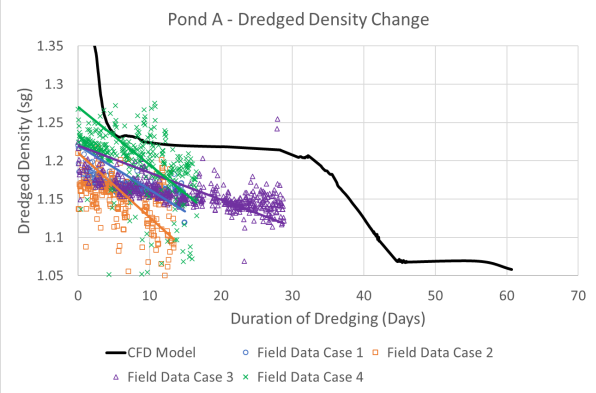

Figure 15. Comparison Dredged Density to CFD predictions for Pond A

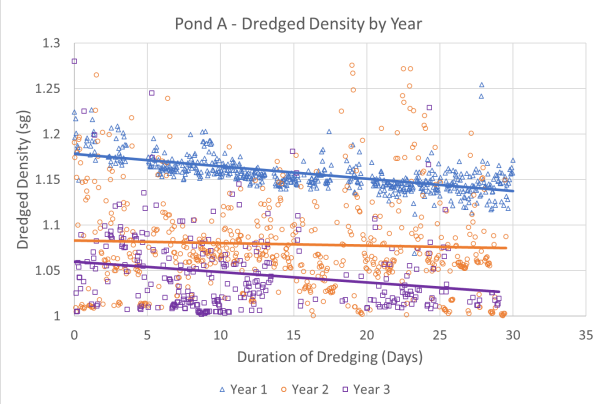

Figure 16. Comparison 3 years of Pond A dredged density results

Three years of seasonal (spring to fall) dredging field density data for Pond B, compared against CFD predictions, are presented in Figure 17. Pond B, due to the low rheology tailings and high pond depth, experienced a significantly slower rate of density decrease compared to Ponds A and C. As a result, the dredge did not require relocation and tailings removal occurred in approximately the same location for each of the 3 years of operating data shown.

Consistent with observations for Ponds A, initial dredged density in Pond B was much less than, and rate of density decrease much quicker than, CFD predictions. Notably, given the large depth and low rheology of Pond B, CFD models predicted higher density tailings would continue to flow towards the dredge suction sustaining effectively a constant dredged high density over time. This was not observed in field operations with initial higher densities of 1.35sg observed in year 1 of dredging, dropping to below 1.20sg after 6 months of operation. Initial dredged tailings density in Pond B for year 2 and 3 was much lower than year 1.

As dredging only occurred for 6 months of the year in Pond B, it gave a 6-month "winter" window between dredging seasons for potential cone recovery to occur, wherein fluid tailing could migrate and potentially replenish volume of higher density tailings within the dredged and coned footprint of the pond. However, despite year-round new tailings inflow into Pond B, low dredged density results in year 2 and 3 suggest no cone recovery occurred within the 6-month "winter" window of no dredging operations. This is consistent with the CFD cone recovery simulations discussed above (Figure 9).

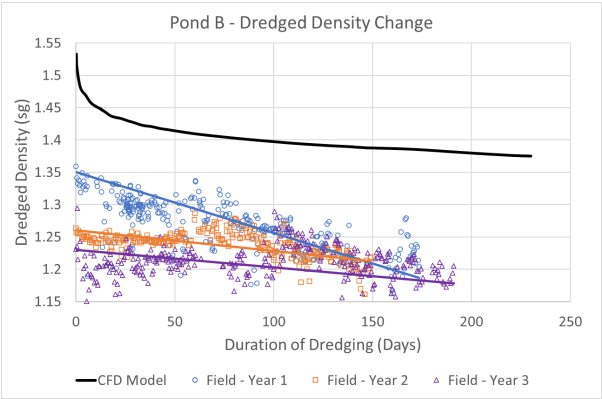

Figure 17. Comparison Dredged Density to CFD predictions for Pond B

Figure 18 compares dredged density in Pond C to CFD models for dredging in multiple on-pond locations within the same year. Consistent with the high variability in composition and rheology in Pond C (Figures 1 and 7 above), achieved density and rate of density decrease at each of the different on-pond dredging locations was highly variable. Given the low achieved initial dredged density and rapid rate of density decrease, the dredge was required to be relocated every 3 to 4 weeks in Pond C to sustain tailings removal operations.

Two CFD models were developed for Pond C. In model #1, a dredging depth of 9m (6m below mudline) with pond depth limited to 15m was used. In model #2, dredging depth was kept at 9m with the actual pond depth of 30m used. The results between the models are very different with model #1 showing a very rapid drop in dredged density and model #2 showing no expected drop in density. The interpretation of the CFD models is

that model #2 predicted an upwelling of high-density tailings from depth towards the dredge intake, sustaining high density of the pumped and removed tailings fluid. In contrast, by placing a depth cutoff at 15m, model #1 effectively rendered a majority of the fluid tailings volume at depth below the dredge suction intake inaccessible and immobile leading to rapid coning given the high rheology of the tailings.

Realized initial dredged density in operations was lower than both models predicted despite operational dredging depth in Pond C of 13m being much deeper than the 6m depth simulated in CFD. Field dredging results in Pond C more closely aligned to model #1 suggesting that, despite a total pond depth of 30m, versus dredging depth of 13m, the tailings fluid at and below dredging depth had higher demonstrated in-situ rheology and lower mobility towards the dredge suction than predicted by the CFD.

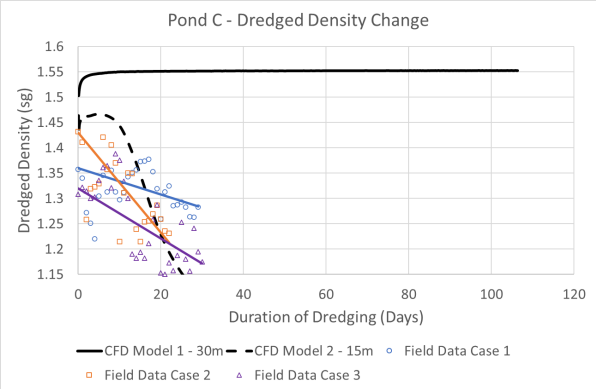

Figure 18. Comparison Dredged Density to CFD predictions for Pond C

The Pond C CFD models were subsequently revisited to make CFD predictions match observed field performance, to achieve complete coning within 4 weeks, consistent with average field observations. It was found that an adjustment factor of 1.5 to 2 times the previously assumed yield stress and viscosity correlations for Pond C CFD modelling was required to make the CFD predictions and field density data align. Wherein rheology increases very quickly with depth in the tailings deposit, this accomplished a similar effect as model #1 in Figure 18 to progressively restrict with depth, the mobility of fluid tailings towards the dredge intake. This does not necessarily affirm rheology measurement accuracy as the causal factor for discrepancy between CFD and field observations. Any of the previously mentioned factors could also individually or cumulatively contribute to the tendency for CFD under-prediction of timelines for coning.

As discussed above in Figure 8, if we presume dredging flowrate has negligible impact to cone size, direct comparison of field coning results between the different ponds is possible and is provided in Table 2. Given different dredging rates in each pond, “coning rate” was normalized by dividing the rate of density change (Δsg units / time) by the specific pond dredging rate (m^3/hr) to create an equivalent rate of density change per unit volume pumped (Δsg / million m^3 pumped) metric. Despite Pond A (shallow depth and low rheology) and Pond C (shallow dredging and high rheology) having very different tailings deposit properties, the data in Table 2 indicate they demonstrate very similar rapid coning behavior with small coning radius of approximately 425m, frequent dredge relocation requirements of every 2-4 weeks, and similar rate of density change of 0.04 to 0.17 sg units per million m^3 pumped. Both ponds are effectively restricted driving rapid and small cone size formation. Pond A is dimensionally restricted for size by shallow pond depth and Pond C is restricted by high rheology limiting tailing fluid mobility to the dredge. In contrast Pond B is not restricted, having both high dredging depth and low rheology which greatly increases the size and volume of cone formed. As a result, rate of density decrease in pond B was 5 to 15 times slower than in Pond A and C at approximately 0.01 sg units decrease per million m^3 pumped.

Dredging in pond D has not yet occurred. CFD predictions, which were based on doubling the rheology used in Pond C, gave an expected cone radius of approximately 500m and an expected rate of density change of approximately 0.1sg units per million m^3 pumped. These results are similar to both Ponds A and C and 10 times faster than Pond B, suggesting Pond D is expected to produce similar restricted cone sizes due to the high rheology of the tailings. As dredging in Pond D is expected to be deeper than Ponds A and C, dredge asset relocation frequency is predicted to be less frequent at approximately every 2 months compared to 2-4 weeks in Ponds A and C.

Table 2. Comparison field coning performance between ponds

	Dredge move frequency	Field Cone Radius (m)	Coning Rate (∆sg units/1,000,000 m3 pumped)
Pond A	13 – 29 days	420	-0.06 to -0.14 sg/ 1Mm3
Pond B	Not required	650	-0.01 sg / 1Mm3
Pond C	22 – 30 days	425	-0.04 – 0.17 sg/ 1Mm3
Pond D	~ 60 days		-0.1 sg / 1MM3 *(CFD basis)*

CONCLUSION

Cone formation during dredging of oil sands tailings ponds is primarily affected by dredging depth and fluid rheology. Ponds with a shallow depth and/or high rheology have a restricted cone volume and therefore have rapid rates of coning. Frequent dredge relocation in these ponds is required, from 2 weeks to 2 months depending on available dredging depth. Ponds with high dredging depth and low rheology tailings have very slow coning rates, at 5 to 15 times slower than other ponds. Coning still occurs in these deeper, low rheology ponds, as high-density tailings, at depth in the deposit, is depleted over time in the region of dredging activities. Sustained dredging in one location results in progressive deterioration of dredged tailings density and quality achieved.

CFD modelling may be used directionally for predictions of coning; however, there are limitations to prediction capabilities. In all cases, CFD overpredicted cone size and underpredicted the rate of coning, with higher starting densities and a slower rate of density decrease than observed in dredging operations. Potential contributing causes include non-representative rheology measurement associated with differences between lab samples and in-situ behavior, non-homogenous pond properties for both composition and rheology, variable pond geometry, including depth and width, and inability to account for dykes, tailings inflow, and multiple dredge operation in CFD models.

This study also demonstrated that dredging and cone performance differs between individual ponds and is driven exclusively by pond geometry and tailings deposit properties specific to each pond. This means that operational experience for coning in one pond cannot be used as a reliable prediction of expectations for dredging in a new and different pond. The study also indicates that dredge asset design and selection factors such as flowrate and suction intake dimensions appear to have negligible influence on coning outcomes with increased dredge pumping rates only serving to accelerate the rate of density decrease and dredge relocation frequency; but ultimately not affecting the overall cone shape and volume created.

REFERENCES

Adeyinka, S. S. Z. X. J. M. OB. 2009. Effect of particle size on the rheology of Athabasca clay Suspensions. Canadian Journal of Chemical Eng 422-434.

Derakhshandeh, B. 2016. Kaolinite suspension as a model fluid for fluid dynamics studies of fluid fine tailings. Rheologica Acta 749-758.

Shook, D. K. R. a. C. A. 1996. Coning of a slurry during withdrawal of a settled layer from a tailings pond. Hydrotransport 13 335-345.

Wojtanowicz, S. Prasun and A. K. 2019. Semi-analytical prediction of critical oil rate in naturally fractured reservoirs with water coning. Journal of Petroleum Science and Engineering 779-792.

INTEGRATED DAM BREACH AND GEOTECHNICAL MONITORING OF TAILINGS DAMS USING FIBER OPTICS SENSING TECHNOLOGY

Zara Anderson, Saman Alkhaffaf, Jon Furlong
Silixa Canada, Silixa UK

ABSTRACT

Distributed Fiber Optics Sensing (DFOS) technology provides a high spatial and temporal resolution monitoring platform for tailing storage facilities. Using a single cable, extended for tens of kilometers, the platform monitors ***seepage*** via DTS, ***deformation*** via DSS and ***seismic*** via DAS.

In its basic set up, the monitoring platform detects dam failure (localized or broad) and issues alerts within seconds to initiate evacuation protocols.

A temperature-based seepage monitoring can be added to the monitoring platform through DTS technology. Real-time seepage detection and flow is identified through variations in the diurnal and seasonal temperature profiles for the region. The calculated annual mean seepage flow is typically in the order of a few centiliters per second per meter. Ideally, the fiber cable is installed during the construction of the dam to ensure a comprehensive monitoring platform with high spatial accuracy for seepage detection and quantification.

Deformation surveys is another layer of monitoring that can be integrated into the platform. The same fibre cable can be used for monitoring gradual or sudden movements or subsidence in and around the monitoring volume with micro-strain resolution using DSS interrogator.

In its most advanced set up, the DFOS platform can also be used to acquire passive and active seismic data and provide sub-surface imaging via DAS. Using the same fiber cable, DAS records seismic signals detecting changes in material, seepage and/or internal erosion within the dam walls.

Since Fiber Optics cable is buried within the dam structure it requires little maintenance and can operate for many years including post-closure of tailings facilities.

This paper discusses the capabilities and limitations of fibre optics sensing as an integrated temperature, strain, and seismic platform for monitoring the structural integrity of TSF.

DFOS: *distributed fibre optic sensing*
DTS: *distributed temperature sensing*
DBV: *dam breach verification module*
DAS: *distributed acoustic sensing*
DSS: *distributed strain sensing*
ANI: *ambient noise interferometry*
MASW: *multichannel analysis of surface waves*
TSF: *tailing storage facility*

INTRODUCTION

Tailings storage facilities are some of the largest manmade structures and prone to failure. Failure of TSF can have a devastating impact on human life, infrastructure, and environment, especially if TSF is storing toxic material. The most recent failure occurred at Jagersfontein diamond mine tailings facility in South Africa in September 2022 as we are writing this paper.

The causes of dam failures can range from overtopping, seepage, foundation and/or design issues, seismic events among others. Figure 1 (iCOLD 2001, Chambers 2017) lists causes of TSF failures. Increased rate of mining extraction (excess capacity of tailings) as well as climate change can further contribute to increased risk of TSF failure as the stability conditions exceed the design criteria.

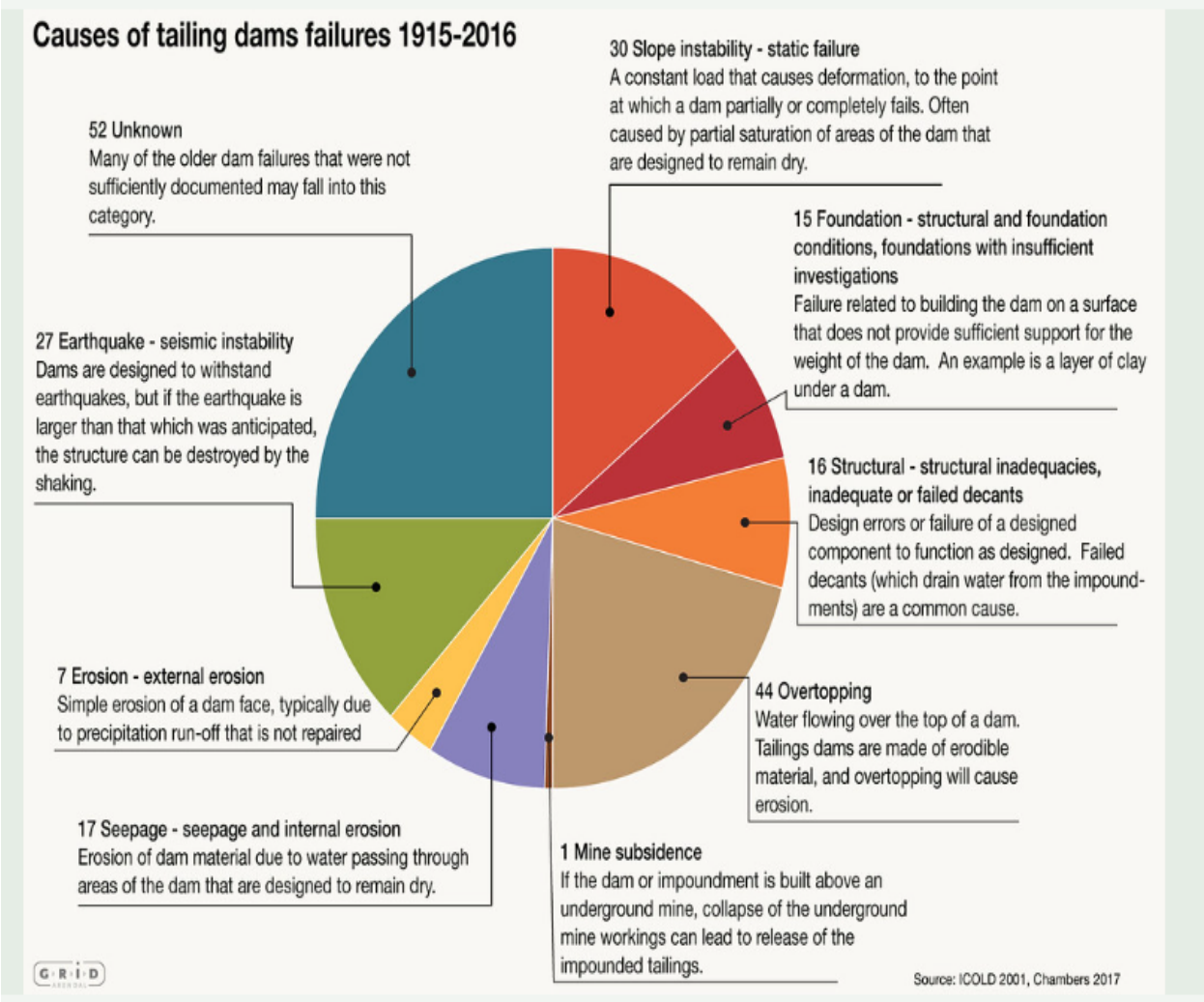

Figure 1 Causes of Tailings Dam Failure *(*iCOLD 2001, Chambers 2017*).*

Distributed Fibre Optics Sensing Technology (DFOS)

DFOS enables continuous and real-time measurements along the full length of an optical fibre for tens of kms. DFOS is suitable for 3-D for tens of kms. DFOS is suitable for 3-D monitoring of large structures with high spatial resolution.

DFOS has been used extensively in alternative energy (Binder G, 2021), environmental and earth sciences (Becker, 2019), infrastructure (Akira Fujimoto, 2021), carbon capture and utilisation (Hopkins M, 2018), oil and gas (Garth Naldrett, 2019), and mining (Riedel M, 2018);(Gilles Bellefleur, 2019). In DFOS, the optical fibre is the sensing element without any additional sensors in the optical path. The interrogator transmits a sequence of light pulses into the optical fibre connection and records the return of the naturally occurring scattered signal against time. At the end of the fibre, not all of the light emitted by the interrogator is received. During transmission, some light is attenuated as a result of dispersion and absorption (Figure 2). The different light scattering processes, measured in distributed sensing are Rayleigh, Brillouin, and Raman. Elastic scattering of light (Rayleigh) maintains wavelength while inelastic scattering of light (Raman and Brillouin) change wavelength based on the amount of energy absorbed or released (i.e., Stoke shift).

The backscattered light has the same frequency as the input light in Rayleigh scattering. As the fibre deforms, the glass functions as a weak mirror that is magnified, resulting in a stronger backscatter reaction. The interaction of the laser pulse and the

intrinsic vibrations of the glass results in much decreased Brillouin and Raman scattering interactions. Figure 2 depicts several backscattering phenomena measured by optical interrogators. Interrogators measure ambient characteristics such as acoustics, temperature, and strain by capturing a specific scattering interaction. Fibre interrogators are designed to analyse backscattered light caused by various scattering events. Brillouin and Raman backscattering can be used to measure strain and temperature with resolutions of 1 microstrain and 0.01°C, respectively. Rayleigh backscattering can be used to accurately assess both acoustics and dynamic strain (Parker TR, 1997); (Jousset, 2018).The result of using backscattered light as signal has the effect of turning many kilometres of fibre into a dense array of sensors, with a channel output density as high as every 0.10 m. For reference, a 10 km long fibre optical cable interrogated via an DAS system writing data every meter is analogous to having 10,000 one-component geophones lain end-to-end. Acoustic amplitude, phase, and frequency are all captured making DAS a full solution for seismic applications.

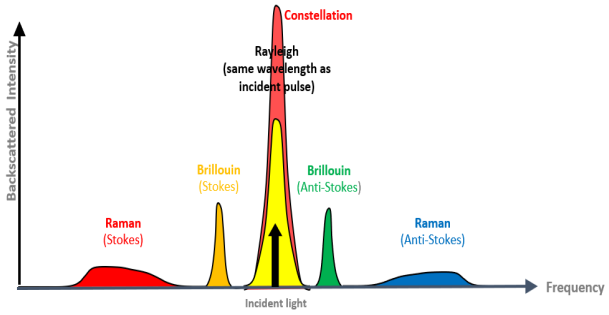

Figure 2. Wavelength/frequency of light scattering phenomenon recorded by interrogators.

TSF monitoring using DFOS

Fiber Optics sensing technology has been used for monitoring of infrastructure, including hydro dams and tailings dam for over a decade. The advances in technology now allows for an integrated dam breach and structural integrity monitoring in semi-real time.

The fibre optics cable, designed specifically for tailings dams to withstand erosion and load build up, is installed during the construction of tailings and/or the raise of the dam wall. The cable is typically installed in 20-50 cm deep narrow trenches (Figure 3). The cable often has multiple fibers inside to allow for monitoring of temperature (DTS), strain (DSS) and acoustic (DAS) simultaneously or periodically as needed (Figure 4).

Figure 3. Installation of fibre optic cable at a TSF site

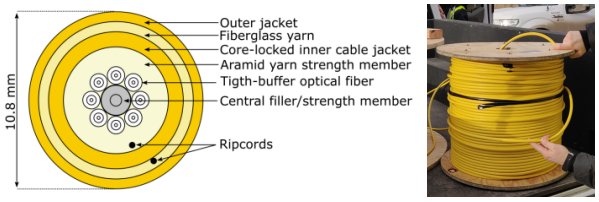

Figure 4. Cross section and a reel of fibre optic cable typically used for embankment dams.

Most operators evaluate their tailings facilities and assign a failure risk. The risk assessment enables operators to put in place the necessary monitoring processes and instrumentation. Based on site conditions, a variety of monitoring tools such as point measurement systems (i.e., piezometers, inclinometers), surface measurement systems (such as satellite imagery and Radar), and more recently fibre optics systems can be implemented to provide proactive monitoring of the TSF and alarming tools in the event of a failure. In the following sections different components of a fibre-based monitoring platform for TSF monitoring are discussed (Figure 5).

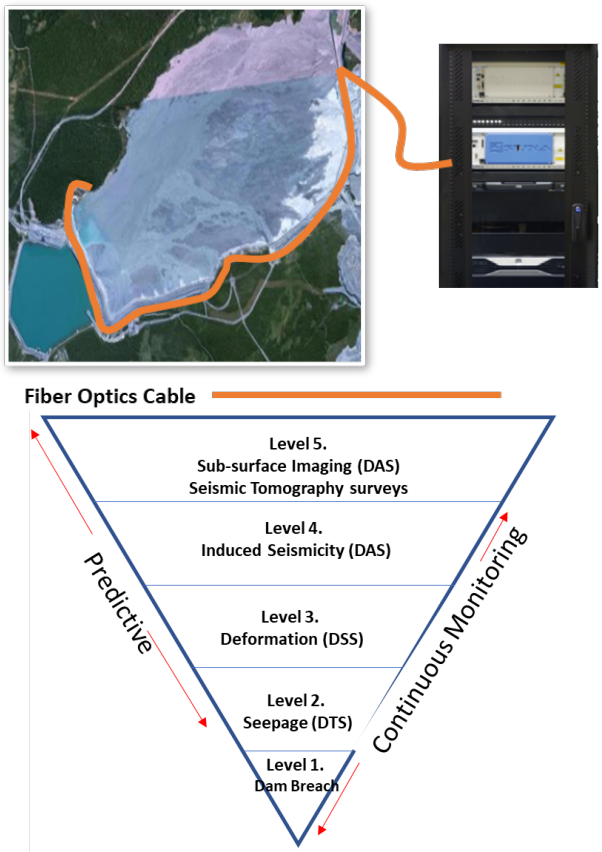

Figure 5. Schematic of fibre optics cable in a TSF to monitor dam breach and geotechnical monitoring using DAS, DTS, DSS.

Dam breach alerting based on DFOS

A fibre optics-based breach detection system detects signal attenuation or loss in the fibre as a result of cable loading or dam failure. Depending on the site conditions and infrastructure available, the system can be configured using DTS and DBV or a DSS unit. The DTS/DBV system is suitable for remote dam sites where solar/wind energy can power the system on site. The system monitors for fibre breaks or damage and the DTS unit is used to locate the location of the potential damage or failure (Figure 7).

A cloud server or a remote desktop server can be used for distant data processing. The alarms in the relevant software can be adjusted to send emails when specific abnormal situations or breaches occur. A variety of communication protocols can be used for data export (i.e., Modbus over Wireless AND Modbus TCP). It is possible to support temperature, attenuation, and alerts for several zones.

Figure 6 depicts a DTS/DBV system schematic.

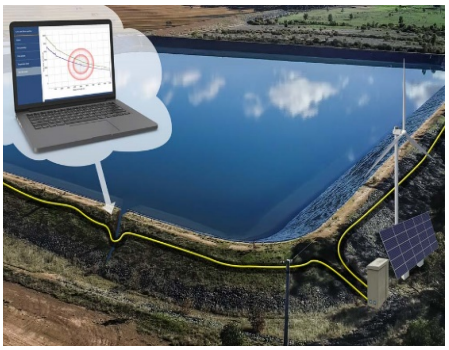

Figure 6. DTS/DBV stand-alone system for dam failure detection. Fibre optic cable is trenched in critical areas within the dam.

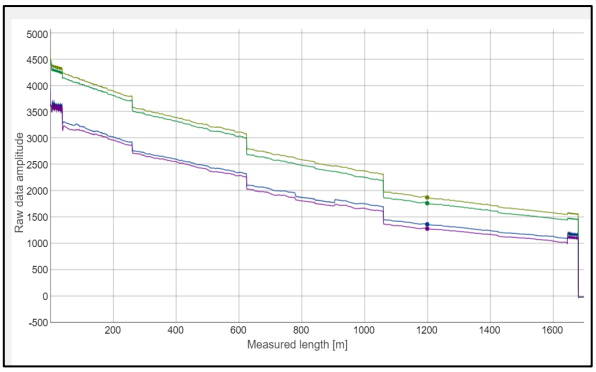

Figure 7. Raw fiber data showing amplitude over length of fiber (XSeepT software courtesy of HydroResearch).

A DSS based system can also be deployed for dam failure detection. It can be a more reliable system that indicates detail fiber data and signal attenuation data. More importantly the system can detect a strain build-up before a failure. A DSS unit can also provide location as well as real time and comprehensive signal analysis.

A DSS based system, however, requires power on site. Another option is to extend the fiber cable from the tailings site to a server room a few kilometers away if terrain conditions allow.

A DSS based system can also be used on a period basis to perform strain monitoring surveys along the Fiber optics in the dam structure and to track small scale movement over time. Figure 8 shows absolute strain survey conducted across 500-meter section

of a tailing dam with strain resolutions of two meter and five meters respectively.

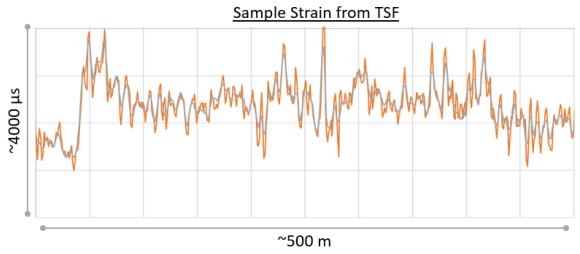

Figure 8. TSF Strain survey across 500 m length of fibre cable with 2 m strain resolution (orange) and 5 m strain resolution (grey).

Using Brillouin scattering, we can determine the absolute strain experienced by the entire cable. By coupling the fibre to the object, the strain experienced by an object of interest, such as a wall, the earth, or a borehole, can also be measured. Because strain is also affected by temperature, accurate strain calculations in a dynamic environment require temperature affects to be removed. This requires an independent temperature measurement from a DTS. When temperature modification is required, the DTS quality used can reveal the genuine strain resolution limit. In a temperature controlled, or temperature corrected environment, this maximum resolution is 1-2 micro-strains.

The benefit of DSS is that it is possible to measure absolute strain over long periods of time at a spatial resolution as high as 25 cm. The DSS surveys reported here provide a valuable baseline and repeat time-lapse surveys will be possible for the infrastructure that will be exposed to variable conditions over many months and years.

Temperature based seepage monitoring

Temperature-based seepage monitoring using DTS has been deployed in over 100 embankment dams since early 2000 (Johansson, 1997);(Sjödahl, 2017); (Johansson S. S., 2021); (Boleve A., 2012). Seepage flow and rate is detected in real time based on seasonal temperature variations representative of the annual mean seepage flow, typically in the order of a few centi-litres per second per meter. Sudden seepage flow rate changes caused by internal erosion is also detected and located. The system issues custom set alarms on abnormal seepage conditions. Ideally the fiber cable should be installed during the construction of the dam to allow for high resolution seepage detection, although the application could be retrofitted for some dams or during construction at the toe/drainage of the dam. Figure 9 shows temperature variation and seepage rate over months of monitoring at a dam site (HydroResearch).

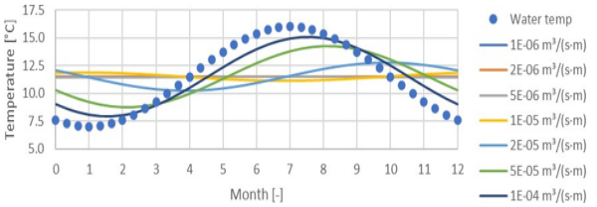

Figure 9 Seasonal temperature and flow rates over a 12-month period.

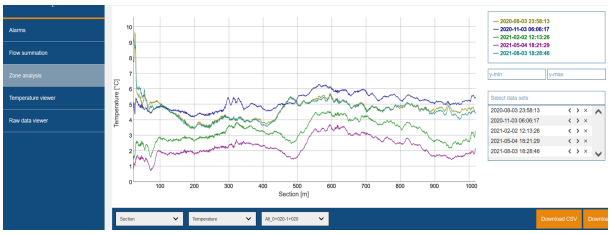

Figure 10 Temperature variations over 1000 m of fiber installed at a dam showing temperature variations along the cable in different seasons.

A DTS-based seepage monitoring system requires an initial calibration using high accuracy temperature sensors in addition to annual calibration analysis based on seasonal temperature variations to establish data trends and enhance reporting and alarming capability.

Volumetric seismic imaging of dam interior using DAS

Geophysics-based technologies and analytical methods have advanced significantly over the past decade. For seismic geophysical surveys, historically geophones and accelerometers have been the common instrument. However, with advances in technology, it is feasible to perform most seismic application using DAS and Fiber Optics.

The result of using backscattered light as signal has the effect of turning many kilometres of fibre into a dense array of sensors, with a channel output density as high as every 0.10 m. For reference, a 10 km long fibre optical cable interrogated via an DAS system writing data every meter is analogous to having 10,000 one-component geophones lain

end-to-end. Acoustic amplitude, phase, and frequency are all captured making DAS a full solution for seismic applications (Anderson & Furlong, 2022)

With modern enhanced DAS interrogators and engineered fiber, signal to noise ratios can be improved by 20db (100x) over standard fibres. With these improvements to the noise floor, DAS can provide equal or better detection than geophones in many circumstances.

The differences between the various optical fibres used for acoustic sensing are outlined in Figure 11.

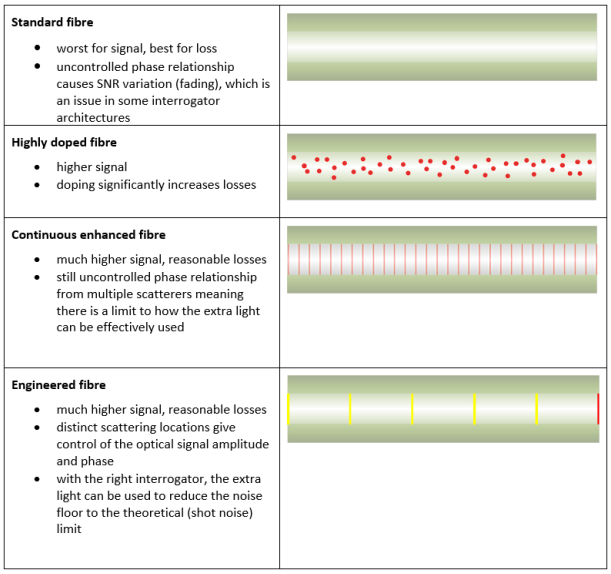

Figure 11 Types of Fiber Optics for seismic applications.

DAS seismic surveys are suitable for high resolution subsurface imaging of large volumes at depth. Both active and passive seismic surveys can be conducted using optical fiber. One of the more recent applications in monitoring the structural integrity of tailings dams is the Ambient Noise Interferometry (ANI) using DAS. ANI uses background noise recordings and processing to create a subsurface image that characterises seismic velocity changes over time and space. Seepage, material movement within the dam, piping, can all impact the seismic velocity within the dam that can be captured using ANI. (Olivier, 2019) At a test site in Sweden, ANI analysis was carried out using DAS (Johansson & Hellström, 2021) The test site was designed with premeditated defects unknown to the researchers to validate the DAS based ANI imaging technique. The results presented in Figure 12 outline seismic velocity profile in the dam.

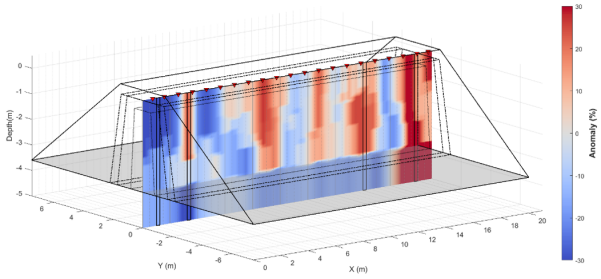

Figure 12 Imaging dam sub-surface using ANI (Johansson et al., 2021, Energiforsrk report).

Depending on the location of the Fiber optics cable, the DAS system can also be used for induced microseismic monitoring and seismic hazard. Since DAS has a broadband frequency and flat response to DC, it can detect a range of seismic event magnitudes.

CONCLUSIONS

Depending on the monitoring objectives, miners may benefit from a continuous or periodic measurement method. Because of the benefits of DFOS, future mines might be safer, have lower carbon footprints, and collect data more effectively. Optical fibre online monitoring is standard practise in all new tailings' dams in Sweden. Distributed Fibre Optic Sensing (DFOS) devices are used to detect local safety warnings and signal losses caused by large movements. These installations, which first appeared in tailings dams in 2008, are in accordance with the most recent Global Industry Standard on Tailings Management developed by ICMM, UNEP, and PRI (Aug 2020).

The entire structure can be used as a distributed array for temperature, strain, and acoustic sensors by putting fibre into active and passive TSF assets. Typically, a suitable cable must be located and custom-made for each TSF. Cables will be put all over the TSF. The data analysis and presentation software will be set up as a cloud-based system. All data will be displayed using real-time web-based software, and a subset of it will be available to the client's monitoring system.

Increasing prices and increased energy consumption, accompanied by minimal hardware, are some of the primary management and control objectives of mining operators. Most TSF

monitoring methods have caused a considerable change toward two or more of these criteria, and potentially others, which have had a significant impact on efficiency, production, and ESG measures. The tailing dam integrity solution is expanding, and the platform's partnership is bringing interesting innovations to the system, such as accelerated data processing, increased measurement derivatives, and Artificial Intelligence and Predictive analytics. These are components of a larger tailing dam integrity monitoring solution that will be researched and developed further in the coming years to align with industry standards and mining operators' long-term goals.

REFERENCES

Akira Fujimoto, T. L. (2021). https://silixa.com/resources/technical-papers/. Retrieved from www.silixa.com: https://library.seg.org/doi/abs/10.1190/segj2021-006.1

Anderson, Z., & Furlong, J. (2022). Distributed acoustic sensing/distributed strain sensing technology and its applications for block caving progress monitoring, rock mass preconditioning and imaging.

Becker, M. W. (2019). Distributed Acoustic Sensing of Strain at Earth Tide Frequencies. Sensors.

Binder G, A. Z. (2021). Joint microseismic event location with surface geophones and downhole DAS at the FORGE geothermal site. In First International Meeting for Applied Geoscience & Energy (pp. 2001-2005), Society of Exploration Geophysicists.

Boleve A., V. J. (2012). Dyke leakage localization and hydraulic permeability estimation through self-potential and hydro-acoustic measurements: Self-potential ‘abacus’ diagram for hydraulic permeability estimation and uncertai.

Garth Naldrett, A. V. (2019, September). Cluster Flow Identification During Multi-Rate Testing Using a Wireline Tractor Conveyed Distributed Fiber Optic Sensing System With Engineered Fiber on a HPHT Horizontal Unconventional Gas Producer in the Liard Basin. Retrieved from www.silixa.com: https://onepetro.org/SPEATCE/proceedings-abstract/19ATCE/1-19ATCE/D011S016R004/217734

Gilles Bellefleur, E. S. (2019). Vertical seismic profiling using distributed acoustic sensing with. British Columbia, Canada.

Hopkins M, R. R. (2018). Leinster cave seismic risk management: a block cave solution. In Caving 2018: Proceedings of the Fourth International Symposium on Blockand Sublevel Caving (pp. 591-606)’. Australian Centre for Geomechanics.

Johansson, S. (1997). Seepage Monitoring In Embankment Dams. Stockholm: Royal Institute Of Technology.

Johansson, S. S. (2021). Distributed Acoustic Sensing for detection of seepage and internal erosion in the Test Dam at Älvkarleby.

Johansson, S., & Hellström, G. (2021). DamTemp Manual - Ver. 1.0, HydroResearch and NeoEnergy, 25p. (2007). Experiences from Distributed Strain Measurements in Five Embankment.

Jousset, P. R. (2018). Dynamic strain determination using fibre-optic cables allows imaging of seismological and structural features. Nature Communications.

Olivier, G. F. (2019). Monitoring the stability of tailing dam walls with ambient seismic noise. The Leading Edge.

Parker TR, F. M. (1997). A fully distributed simultaneous strain and temperature sensor using spontaneous Brillouin backscatter. IEEE Photonics Technology Letters.

Riedel M, C. C. (2018). Underground vertical seismic profiling with conventional and fibre-optic systems for exploration in the Kylylahti Polymetallic Mine, Eastern Finland', Minerals, 8(11),

Sjödahl, S. J. (2017). Fibre-optic temperature monitoring for seepage detection in embankment and tailings dams. Prague: ICOLD 85th Annual Meeting.

AUTOMATED SPECTROSCOPIC METHOD AND PLATFORM FOR ACTIVE CLAY AND WATER HARDNESS MEASUREMENT

Ruijun Sun, David Williams and Lesley McGilp
Saskatchewan Research Council, Saskatoon, Saskatchewan, Canada

ABSTRACT

The mining industry requires automated instrumentation to improve process efficiency, reduce costs and to achieve cleaner and greener operation. The Saskatchewan Research Council has developed an automated spectroscopic method which correlates spectra absorbance of filtrates to the titrant volume for process parameter measurement. An automated and online platform is developed based on the automated spectroscopic method. Slurry or process water samples can be automatically withdrawn from a live process and transferred into a mixing chamber where the sample can be conditioned and treated by reagents. After the titrant solution is added to the sample in increments, a series of filtrates can be automatically extracted from the sample mixture and measured by a spectrophotometer. The spectra absorbance of the filtrates can be correlated to determine active clay content in minerals or water hardness in process water.

The platform is designed to measure challenging samples, such as samples with elevated levels of active clays or oily specimens from processes with hot temperature and high pressure. This paper will present field validation results for the active clay analysis on oil sands tailings, along with active clay results from model clay mixtures and samples from potash and kimberlite industries. Preliminary water hardness results for liquid samples taken from oil sands SAGD process will also be presented.

INTRODUCTION

There are increasing demands from the mining industry for automated measurement of key process parameters so the operators can have more control of the process and rapid reaction to the change of conditions such as feed properties. Active clays are swelling clays that do not agglomerate, settle, or consolidate easily when mixed with water, they can cause significant challenges for mining operators by tying up large volumes of water and requires extra resources for treatment. Their presence complicates rheological, pipe flow and solids settling behaviors, causing difficulties in many mineral processes, such as extraction, flotation, flocculation, thickening, hydro transportation, and consolidation.

In 2019, Canadian oil sands industry produced 1.6 million barrels of bitumen every day. It was estimated that for every barrel (~205 L) of produced bitumen, there is about 3.3 m^3 of tailings to be discharged into the tailings pond (Masliyah et al. 2011), which is on top of 1.2 billion m^3 legacy fluid fine tailings (FFT) already stored in various tailings ponds in Canada's northern Alberta region (Government of Canada 2019). Active clays in oil sands tailings hinder the quick solids settling and consolidation and complicate the effective solid-water separation and process water recovery. Oil sands is not the only mining industry challenged by active clays from ore to tailings, as the kimberlite industry has the similar challenges (Strydom 2015).

Active clays need to be monitored closely to achieve economic and environment objectives. For example, if active clays can be detected and quantified during mine planning, ore deposits with high active clay content can be managed through proper ore sorting and/or ore blending, avoid carrying clay lumps to down-stream process and affect ore processibility; tailings with high active clay can be re-routed to designated storage area so to avoid cross-contamination in the main tailings pond; dosages of process aids such as coagulant and flocculant can also be optimized and controlled to improve efficiency and reduce cost.

One effective tool to detect and quantify active clays is the Methylene Blue Index (MBI) test. Methylene Blue (MB) is a cationic dye which has strong affinity to clay particles and can replace cations on clay external surfaces, edges, and interlayers. The consumption of MB at given concentration can be correlated to clay activity and clay quantity in the sample (Hang 1970).

Visible spectroscopy had been utilized to determine cation exchange capacities and surface areas of clay minerals treated by MB (Cenens et al. 1988, Currie et al. 2014). However, it remained as a lab procedure because either high speed centrifuges

were required to separate the supernatant before spectroscopic analysis, or diluted sample were measured directly without separating the solids, affecting accuracy of the results. Therefore, the manual spectroscopic method has not been developed nor widely adopted as an alternative to the visual and halo MBI method in the mining industry.

Online water hardness measurement is required for heating equipment such as boilers and heat exchangers to improve efficiency, reduce cost and Green House Gas (GHG) emission. Due to challenges from live processes with high pressure, elevated temperature and sometimes samples containing solids and dissolved hydrocarbons, such as those from Steam Assisted Gravity Drainage (SAGD) operation in Canada's oil sands industry, no satisfactory instrument is available to provide the online and automated water hardness measurement.

This paper presents an automated and online spectroscopic method and measurement platform as an active clay analyzer capable of detecting and quantifying active clays in mineral samples. The system can also be utilized for automated and online complexometric titration such as water hardness measurement. The paper will share some validation results from the automated active clay analyzer, as well as some preliminary results for automated water hardness measurement.

AUTOMATED SPECTROSCOPIC METHOD AND MEASUREMENT PLATFORM

Automated Spectroscopic Method for Active Clay Detection and Quantification

We started the development of automated spectroscopic method with active clay detection and quantification. Currently commercial labs measure active clays by the MBI test which is performed based on ASTM C837-09 (ASTM International 2014). Details of the MBI procedure are described elsewhere (Omotoso & Morin 2004, Kaminsky 2014). The CANMET method is a modified version of ASTM C837-09 for oil sands samples (Kaminsky 2014).

The MBI value can be calculated using Equation 1:

$$MBI = \frac{V_{endpoint} N_{MB}}{m_{solids}} \times 100 \quad (1)$$

Where $V_{endpoint}$ is MB solution in mL, m_{solids} is the dry mineral sample in g (or equals the solids fraction multiplied by the slurry mass), and N_{MB} is the normality of the MB solution in meq/mL. The MBI is typically expressed as milliequivalent per 100 grams (meq/100g).

The $V_{endpoint}$ is the MB volume required to complete the cation exchange process, which can be determined through titration on conditioned samples by identifying a permanent blue color halo around a droplet on a filter paper as shown in Figure 1. Both ASTM C837-09 and the modified ASTM method are time consuming as it requires minimum 6 hours including manual sample preparation, conditioning, and titration; it is subjective as different operators can have different interpretations of the halo endpoint.

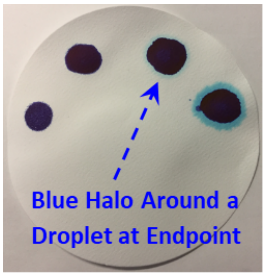

Figure 1. A Blue Halo Around a Droplet on Filter Paper Indicating the Endpoint of MB Titration

The blue halo on the filter paper represents excess MB in aqueous phase after MB molecules adsorbed onto the clay edges, interlayers, external and internal surfaces, which appears even before reaching the titration endpoint. The amount of residual MB molecules in aqueous phase progressively increases as the MB molecules approach full coverage on the clay surfaces.

Figure 2 shows that filtrates were extracted during the MBI titration with fifteen increment MB additions, each filtrate was scanned by a spectrophotometer from 500 to 750 nm. The Spectra Absorbance (ABS) at 664 nm of each filtrate is the highest and most sensitive peak on the MB spectrum (Figure 2a). The ABS value at 664 nm was then plotted against the cumulative MB volume (Figure 2b). There is a transition between two distinctive curves representing the spectroscopic titration endpoint (red circle). The V_{MB} derived from the spectroscopic

endpoint is slightly less than the V_{MB} interpreted from the visual halo endpoint (solid red dot) measured from the identical sample. This is because spectrophotometer is more sensitive than human eyes, it is consistent and less subjective.

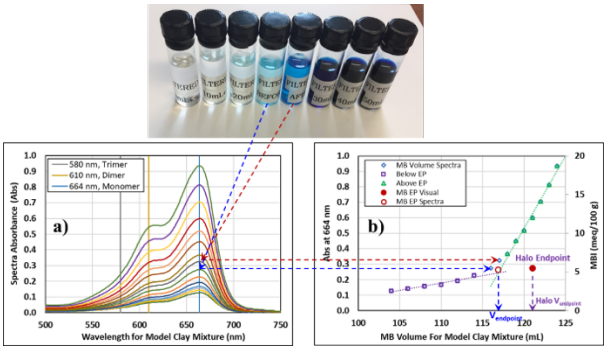

Figure 2. ABS of Filtrate Containing Residual MB Molecules During MB Titration

Concept of Automated Spectroscopic Method

A novel approach has been developed to automate the spectroscopic method for online active clay analysis using MB as the indicator. As illustrated by Figure 3, an auto sampler A can be installed on a process (e.g., slurry pipeline, mixing tank etc.). A controlled volume of slurry sample can be withdrawn from the process and carried by a controlled volume of dilution water injected into the sampler A. The diluted mixture is transferred into a mixing chamber where the sample mixture is conditioned by sonication, dispersion, and pH adjustment etc.

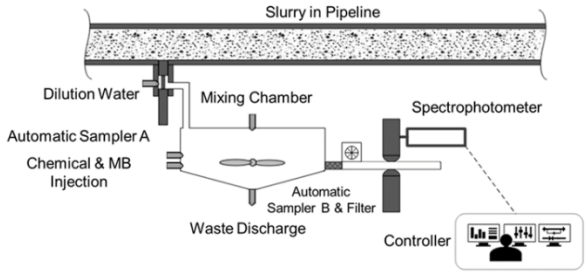

Figure 3. Concept of Automated and Online Spectroscopic Method and Measurement Platform

A controlled volume of MB solution is then injected into the sample mixture in increments. After each MB injection and mixing, an aliquot of the sample mixture is extracted and filtered by an auto sampler B equipped with an auto filter changer. The filtrate is then transferred through an optical flow cell where it is measured by a spectrophotometer. The ABS value (e.g., at 664 nm) of the filtrates are plotted against the cumulative MB volume, and the spectroscopic endpoint can be determined from the correlation. Since the slurry sample volume and MB solution normality are known, solids content in the slurry can be determined from slurry concentration provided by other devices (e.g., inline nuclear densitometer) installed on the process near the active clay analyzer, the MBI value can be determined automatically.

After the MBI value is determined, the spent sample mixture is flushed via an auto drain valve at the bottom of the mixing chamber. The analyzer system is auto cleaned by injecting wash water or solution via auto sampler A through the mixing chamber and the auto drain valve. It takes approximately 1 hour to measure one slurry sample with fifteen data points for the correlation. The measurement time can be reduced if less than 15 data points are required for process control purpose, e.g., comparing the filtrate ABS data to a pre-set target value.

The main advantage of this concept is that it is online as it can connect to live process and, all procedures are performed automatically. Other advantages include tolerance for trace amounts of residual bitumen in the sample, larger sample sizes (>7 mL) from the process for improved sample representation, and the capability to measure samples with remarkably high MBI values (exceeding 40 meq/100 g) such as kimberlite. It can also be used as an at-line active clay analyzer where dry solids or slurry sample is manually loaded into the mixing chamber and analyzed.

Development of the Automated Measurement Platform

System Control and Automation

The automated measurement platform was first developed as an automated and online active clay analyzer. To automate the entire procedures from sampling, sample preparation/titration, filtrate extraction/scanning, spent mixture flushing, to data correlation/reporting, several control elements were necessary. The primary control elements and sensors are illustrated in Figure 4.

Actuation of automatic samplers and filter changer is provided by compressed air and controlled by a

manifold of valves. The same compressed air is also used to control the drain valve. The chemical solution pumps are peristaltic pumps and stepper motor drives are used to allow fine control of the chemical dosing. Process sensors include pH and temperature measurement of the sample in the mixing chamber, as well as a pressure sensor at the outlet of the automatic sampler B.

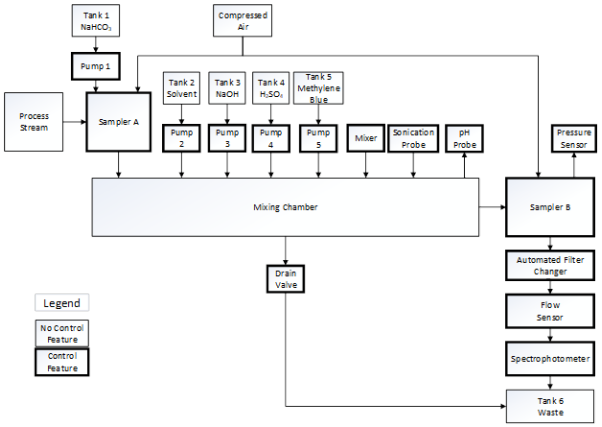

Figure 4. Control Block Diagram for the Automated and Online Active Clay Analyzer

The filter changer is a custom design which engages a filter in line with the automated sampler B and allows a filter to be changed with no operator intervention. A magazine allows storage of five filters or more. Filter change could be initiated manually by user or automatically by the sampling software. This can be done by decoupling the existing filter from the automated sampler B, and a new filter is dropped from the magazine. An actuator pushes the new filter under the sampler B ejecting the existing filter in the process, and then the new filter is mated to the sampler B and is ready to be used.

Four linear actuators control the motion of the filter through the process, and sensors provide feedback on the presence of a filter and position of the actuators.

Automation Control Flow

The automated analysis process begins when the operator clicks on the start button. The basic flow diagram is shown below in Figure 5 and consists of three primary stages.

The first stage is sampling and sample preparation, where sample is loaded into the mixing chamber, the chemical solutions are added to the sample in the mixing chamber, and the sample is mixed and sonicated. The second stage is titrating the sample, where the predetermined number of sub-samples are extracted, filtered, and measured by the spectrophotometer. The final stage is using the completed measurement data to calculate the MB $V_{endpoint}$ at titration endpoint and the MBI value.

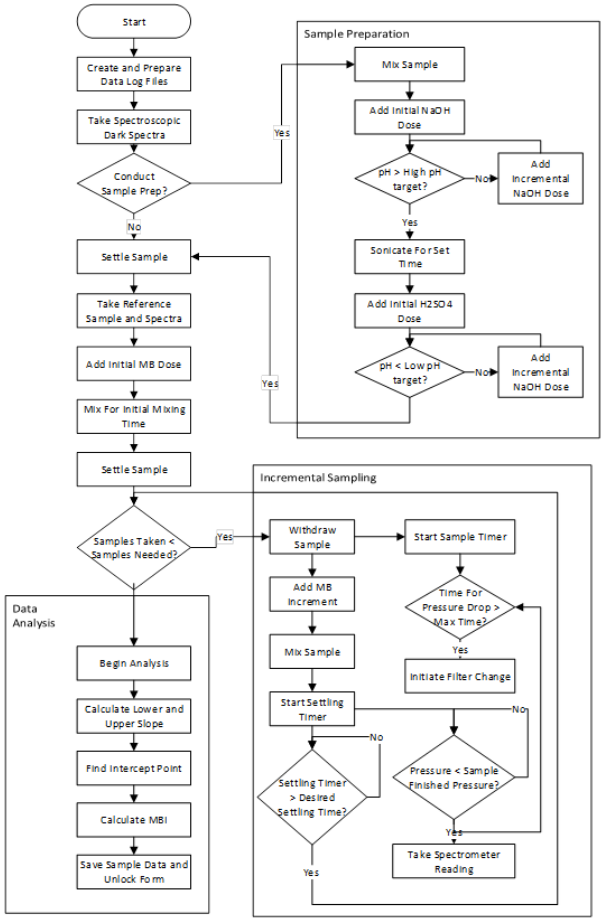

Figure 5. Automated Analysis Process Flow

During sample preparation, a combination of fixed values and feedback loops are used to control the addition of chemical solutions to the sample. For pH adjustment at both the basic and acidic steps, an initial dose is added to sample, and then smaller doses are added while the pH is monitored to reach the desired pH target for that step.

In the primary titrating phase, several timers and flags are run concurrently with dependencies between them. The sampler B begins by withdrawing an aliquot of sample from the mixing

chamber and begins pushing it through the filter and the filtrate into the optical flow cell of the spectrophotometer.

As soon as the aliquot is withdrawn, it is isolated from the mixing chamber and so the next increment MB volume is added, and the mixing process resumes. When the mixing time ends, the settling time for the next aliquot begins. Two concurrent flags are set here that must be cleared before the next aliquot can be taken. First, the settling time must be reached. Second, the system needs to have determined that the entire aliquot has passed through the filter and a spectrophotometer scan can begin. Once these two conditions are met, the filtrate is scanned by spectrophotometer, and the next aliquot is taken if needed.

Should the system determine that the filter performance has degraded enough that it slows filtering, a new filter will be inserted prior to the next aliquot. When a set number of aliquots has been taken, the system can flush the remaining sample mixture through the drain valve to the waste tank followed by auto cleaning, and the new cycle of sample analysis begins.

The system stores the full ABS data from 500 to 750 nm (or any wavelength range user defined) for every filtrate scanned at each increment volume of MB solution. These point pairs (ABS vs. MB volume in Figure 2a and 2b) are graphed, and a simple linear regression is performed. The spectroscopic endpoint is determined from the intersection of the two lines, and the volume of MB ($V_{endpoint}$) at the spectroscopic endpoint is used to calculate the final MBI value.

The primary analysis only uses the ABS at 664 nm (MB monomer) for this application, but it can analyze ABS at any other wavelength or multiple wavelengths e.g., 610 nm for MB dimer and 580 nm for MB trimer (Figure 2a) as the data is already collected from the scan.

RESULTS AND DISCUSSION

Validation for the Concept of Automated Active Clay Analyzer

Numerous MBI tests have been performed during the development of the automated spectroscopic method and active clay analyzer. Results obtained by the automated spectroscopic method and modified ASTM method are presented for direct comparison. Figures 6 and 7 show the MBI values of pure kaolinite and pure bentonite respectively from the two MBI methods.

Results from the modified ASTM method were scattered due to manual operation and visual halo endpoint interpretation, which are known shortcomings of the modified ASTM method. As these results are generated by three operators from the same lab, the data is expected to be more scattered if more operators and/or labs are involved.

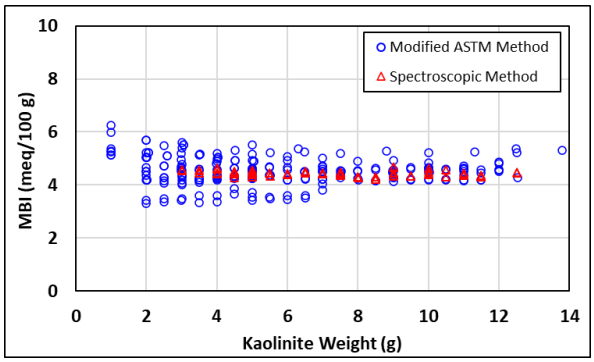

Figure 6. MBI Results of Pure Kaolinite by Modified ASTM and Spectroscopic Method

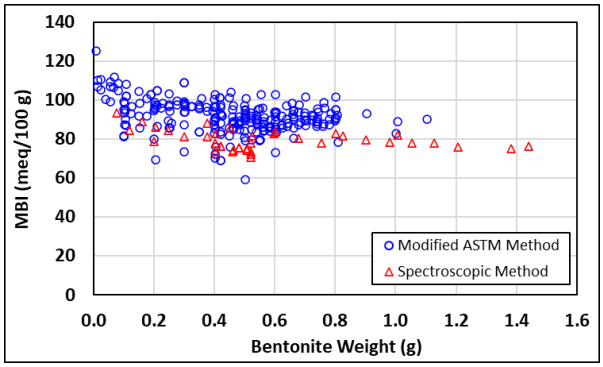

Figure 7. MBI Results of Pure Bentonite by Modified ASTM and Spectroscopic Method

The MBI results generated by the spectroscopic method are more consistent with narrower scattering. It is more objective than the visual halo endpoint determination in which different operators may interpret the endpoint differently. The data continued to be consistent as high slurry sample weights were measured, which is an advantage of the automated active clay analyzer system design. Larger samples can be withdrawn by industrial size

auto sampler from a live process, expanding the capability and feasibility of this system.

Figure 8 shows the MBI value as a function of active clay (i.e., bentonite) fraction in the model clay mixture composed of kaolinite, bentonite, and silica flour. For method development purposes, the active clay ratio covered wide range of MBI values commonly seen in samples from oil sands, potash, and kimberlite industries.

The modified ASTM method again generated scattered data, with more scattering at the high active clay fractions. On the other hand, the data by the automated spectroscopic method was more consistent and more objective as it eliminated the common issues associated with manual operation and visual halo interpretation.

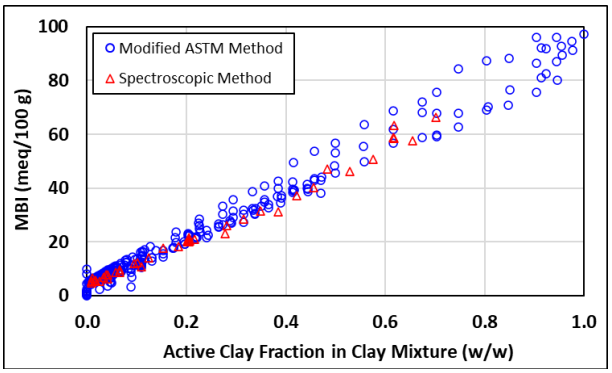

Figure 8. MBI Results of Model Clay Mixture by Modified ASTM and Spectroscopic Method

Table 1. MBI Results of Industrial Samples by Modified ASTM and Spectroscopic Method

Sample ID	MBI by Modified ASTM Method (meq/100g)	MBI by Spectroscopic Method (meq/100g)
FFT-A	4.5	4.7
FFT-B	4.6	5.2
FFT-C	6.5	7.5
FFT-D	8.6	9.9
FFT-E	11.3	10.9
Kimberlite A	44.0	43.2
Kimberlite B	23.2	23.8
Kimberlite C	25.0	24.0
Kimberlite D	23.4	23.9
Kimberlite E	37.2	36.5
Kimberlite F	33.6	33.7
Potash Slimes	6.8	7.4
Potash Tailings	5.7	8.5

The MBI results of industrial samples generated by the two methods are presented in Table 1. Each set of data was determined based on an average of 2-8 repeats.

For oil sands samples, the MBI difference between the two methods was larger for samples FFT-C and FFT-D, due to higher bitumen contents in each sample (up to 3 wt.%). The active clay analyzer was able to handle kimberlite samples with MBI values 5 to 10 times higher than those of oil sands FFT and the results from the modified ASTM and spectroscopic methods were very close.

The spectroscopic method for potash samples is under development, as the difference between the two methods is relatively large. This is partly due to high dissolved salt content in potash samples which interferes with the spectra absorbance. Extra sample conditioning is being investigated to counter the impact of dissolved salt in potash.

Field Validation for the Active Clay Analyzer

A field validation trial was conducted at Suncor Energy's plant site in Fort McMurray, Canada during the summer of 2021. A prototype of the active clay analyzer (Figure 9) was evaluated, along with the at-line active clay analyzer developed by the Northern Alberta Institute of Technology (NAIT). NAIT's at-line active clay analyzer and the data were discussed elsewhere (Jason Ng, et al., 2021).

Figure 9. Prototype of Automated Active Clay Analyzer Used in Suncor Field Validation Trial

Total of 22 FFT samples were taken from a live oil sands tailings pipeline and tested on site. Identical samples were sent to AGAT lab in Edmonton Canada and measured by the modified ASTM method. MBI values from both methods are presented in Table 2 for comparison. About ten MBI results generated by the active clay analyzer are over ± 1 MBI unit than those from the AGAT lab analysis. However, six out of ten of these discrepancies were generated during the week of July 22-29 when the operator started independently operating the analyzer after only ½ day training, indicating a learning curve is required for operating the active clay analyzer. The discrepancy quickly reduced during the following week of operation.

Table 2. MBI Results Obtained During Suncor Field Validation Trial

FFT Sample Test Date	FFT Sample #	MBI By AGAT Lab (meq/100g)	MBI by SRC Clay Analyzer (meq/100g)
21-Jul	1	8.87	Commission
21-Jul	2	7.57	Commission
22-Jul	3	8.54	9.10
22-Jul	4	9.29	9.91
22-Jul	5	9.48	9.32
22-Jul	6	8.77	10.35
23-Jul	7	9.13	9.77
23-Jul	8	7.95	5.11
26-Jul	9	8.89	9.34
27-Jul	10	9.29	11.40
27-Jul	11	8.60	5.97
28-Jul	12	7.39	4.13
28-Jul	13	8.52	7.97
28-Jul	14	8.08	9.60
29-Jul	15	8.43	17.32
29-Jul	16	8.25	8.07
30-Jul	17	8.69	8.01
30-Jul	18	8.51	5.93
09-Aug	19	9.61	14.31
09-Aug	20	9.57	8.79
10-Aug	21	10.24	11.74
11-Aug	22	11.04	11.38
11-Aug	23	9.82	10.10
12-Aug	24	10.06	10.55
12-Aug	25	10.32	No sample

Automated Platform for Water Hardness Measurement

The automated spectroscopic method and the measurement platform can also be applied to online complexometric titration. One example is online measurement of water hardness under challenging situations such as high pressure, hot temperature, and oily samples.

The measurement platform automated the ASTM D1126-17 method (ASTM International 2017). A chemical indicator such as blue color Eriochrome Black T (EBT) is added into the process water sample automatically withdrawn from the process and it complexes with calcium (Ca) and magnesium (Mg) ions which are major water hardness ions in the sample. The liquid color becomes wine pink as shown in Figure 10.

A known concentration titrant such as Ethylene Diamine Tetra Acetate (EDTA) dihydrate or similar format is added in increments into the liquid sample. Since EDTA has stronger complexing power to Ca and Mg ions than EBT, EDTA complexes with Ca and Mg and releases EBT so the liquid color returns to blue. The concentration of EDTA and its cumulative volume at the titration endpoint can be used to determine the Ca and Mg ion concentration hence the water hardness based on Equation 2.

$$Water\ Hardness\ (epm) = \frac{V_{EDTA}}{S_{sample}} \times 20 \qquad (2)$$

Where V_{EDTA} is the standard EDTA solution volume injected when reach the endpoint in mL, S_{sample} is the liquid sample volume in mL. The water hardness is calculated as equivalent parts per million.

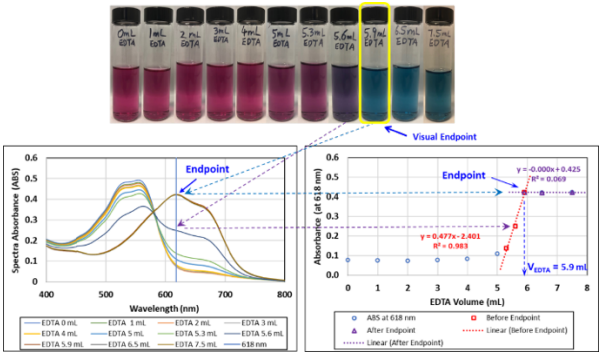

Figure 10. Water Hardness Determined by Automated Spectroscopic Method

Figure 10 shows liquid samples obtained from Canadian oil sands SAGD process, which were analyzed by the automated measurement platform for water hardness. A manual titration following the ASTM D 1126-17 for the identical samples resulted the EDTA visual endpoint at 5.9 mL. After correlating the filtrate ABS at 618 nm against the cumulative EDTA volume, the analyzer using the

automated spectroscopic method generated the spectroscopic endpoint at 5.9 mL (Figure 10) which matches the visual EDTA endpoint volume determined from lab titration. The difference is that the automated platform can be connected to a live process with high pressure and elevated temperature, and the operation is automated and continuous, where the data can be available in 15 minutes or less.

CONCLUSIONS

An automated spectroscopic method and an automated and online measurement platform have been developed which correlates spectra absorbance of a filtrate to the titrant volume for process parameter measurement. The filtrate is automatically extracted from a slurry or process water sample which is automatically withdrawn from a live process and conditioned in a mixing chamber. It can be utilized to determine active clay content in mineral samples or water hardness in process water.

The automated measurement platform as an active clay analyzer has been validated using a wide range of model clay mixtures and industrial samples from oil sands, potash and kimberlite industrials; it also completed a field validation trial at Suncor Energy's plant in the summer of 2021. The analyzer generated MBI results matched values from identical samples measured by the modified ASTM method in a commercial lab.

The automated spectroscopic method and measurement platform can also be utilized to measure water hardness for oily samples taken from the oil sands SAGD process. The spectroscopic water hardness results match to the manual lab results based on ASTM D1126-17.

Optimization of the automated measurement platform is ongoing, including full automation and online capabilities.

ACKNOWLEDGEMENTS

The authors would like to acknowledge and appreciate Natural Resource Canada (NRCan) for the financial support to this research work through the Clean Growth Program (CGP) funding. The authors would acknowledge and thank the collaborations from Northern Alberta Institute of Technology (NAIT) and Suncor Energy (Suncor) during the development, and assistance from SRC team in conducting the experiments.

The authors would also acknowledge the mineral samples provided by oil sands, potash and kimberlite industrials from Alberta, Saskatchewan, Canadian and International mining companies.

REFERENCES

ASTM *C837-09 (2014):* "Standard Test Method for Methylene Blue Index of Clay". ASTM International 2014.

ASTM *D1126-17 (2017):* "Standard Test Method for Hardness in Water". ASTM International 2017.

Cenens, J. & Schoonheydt, R.A. 1988. "Visible Spectroscopy of Methylene Blue on Hectorite, Laponite, B, and Barasym in Aqueous Suspension". *Clays and Clay Minerals* 36(3): 214-224.

Currie, R., Bansal, S. & Mian, H. 2014. "An Investigation of the Methylene Blue Titration Method for Clay Activity of Oil Sands Samples". Edmonton: Oil Sands Research and Information Network.

Government of Canada, www.nrcan.gc.ca/science-data/data-analysis/energy-data-analysis/energy-facts/crude-oil-facts

Hang, P.T., & Brindley, G.W. 1970. "Methylene Blue Absorption by Clay Minerals. Determination of Surface Areas and Cation Exchange Capacities". (Clay-Organic Studies XVIII). *Clays and Clay Minerals* 18: 203-212.

Kaminsky, H. 2014. "Demystifying the Methylene Blue Index". *Proceedings of the 4th International Oil Sands Tailings Conference*. Banff: University of Alberta Geotechnical Centre.

Masliyah, J., Czarnecki J. & Xu, Z. 2011. "Handbook on Theory and Practice of Bitumen Recovery from Athabasca Oil Sands Volume 1: Theoretical Basis". Edmonton: Kingsley Knowledge Publishing.

Ng., J, Sun, R., Rizvi, S., et. al., 2021. "Automated Clay Analyzers to Rapidly Measure Methylene Blue Index of Oil Sands and Mining Slurries". Tailings and Mine Waste 21'.

Omotoso, O. & Morin, M. 2004. “Standard Operating Procedure 0043-SOP – Methylene Blue Titration: Sludges, Slurries and Dean-Stark Solids”. Devon: Natural Resources Canada.

Strydom, J., 2015. “The Effect of Kimberlite Weathering on the Behavior of Waste Material at Cullinan Diamond Mine, South Africa”. Master Thesis, North-West University.

CHARACTERIZATION OF NAPHTHENIC DILUENT IN OILSANDS TAILINGS STREAMS AND PONDS

Cedric Laborde-Boutet[1], Wayne Brown[1], Elco Hollander[2], Babak Derakhshandeh[2]
[1] Coanda R&D, Edmonton, Alberta, Canada
[2] Suncor Energy Inc., Calgary, Alberta, Canada

ABSTRACT

The presence of residual diluent and associated biodegradation in Froth Treatment Tailings (FTT) has been identified as a potential issue in aquatic reclamation structures of oilsands operations. Due to the complexity of the sample matrix, and the ill-defined chemical nature of naphtha, producing a reliable measurement technique is difficult.

The quantification of naphtha in a typical FTT-affected tailings sample by flashing the sample successively under controlled conditions showed significant discrepancies with the results given by 'standard' analyses, which were based on solvent-extraction followed by Gas Chromatography. Inefficiencies in the solvent-extraction step were identified as the root cause for the underestimation of the naphtha content in the samples. A novel method for quantifying naphtha in naphthenic FTT relying on the use of an amphiphilic solvent with high solubility for hydrocarbons was developed to address this issue. The results obtained by this new protocol matched the naphtha quantification given by the successive vapour-slurry flashes.

INTRODUCTION

Background

In oilsands operations, the bitumen froth from primary extraction is subjected to the froth treatment process to yield a clean bituminous product and reject water and solids. The naphthenic froth treatment process consists in adding naphtha as a processing agent to facilitate the segregation of the hydrophobic from the hydrophilic components of the bitumen froth in gravity separators. While most of the naphtha is recovered from the hydrocarbon product after separation, a very small quantity is discharged with the tailings into storage ponds. Quantifying the amount of naphtha exiting with the tailings stream or residing within the ponds is important for both economic and environmental reasons, namely since the presence of naphtha can hinder the reclamation of aquatic structures (Foght et al., 2017).

Suncor has historically relied on several analytical laboratories for naphtha analysis of its tailings samples and noted large discrepancies between the results produced by the various labs. To investigate the issue, Suncor leveraged the experimental capabilities at Coanda where an apparatus designed for the Vapour-Liquid partitioning of tailings samples had been commissioned. By performing successive Vapour-Liquid flashes on a standard tailings sample and characterizing the naphtha content in the vapour of each flash, an estimate of the naphtha content in the tailings sample could be obtained. While this 'Vapour Flash method' could yield naphtha estimates with relative certainty, it is too onerous to be implemented as a routine test method. Thus, since no analytical laboratory could produce results comparable to the 'Vapour Flash method', a new analytical method for the quantification of naphtha in tailings was required.

The Analytical Task

To identify potential causes in analytical discrepancies and attempt to resolve them, it is important to review the four main steps of the analytical process, which are:

1. Subsampling
2. Test sample preparation
3. Quantitative analysis
4. Data processing and result output

Subsampling consists in the collection of a small portion of the original material for analytical testing purposes. If the test portion of the material is not representative of the original material, the analytical result will not be relevant. Subsampling oilsands tailings stream or pond material presents challenges given the heterogeneity of the material, which exhibits dispersed solids and hydrocarbon domains. Additional precautions should also be taken with respect to the volatile nature of the analyte of interest (naphtha).

Test sample preparation describes the set of laboratory steps to transform the subsample into a matrix that can be quantitatively analyzed. Naphtha analysis conducted in commercial laboratories mostly rely on liquid extraction to transfer the analyte of interest into a phase where it can be quantified. In the 'Vapour Flash method', the sample preparation steps consist in subjecting the sample to Vapour-Liquid flashes, followed by gas-liquid absorption of the vapours into a solvent where the analyte is recovered.

Quantitative analysis is the measurement process itself. Gas Chromatography using a Flame Ionization Detector (GC-FID) is commonly used for the quantification of hydrocarbons as it is a reliable, precise and accurate technique. The components of the prepared test sample are separated based on their affinity with the GC column stationary phase and their boiling points, whereas the FID produces an integrated response proportional to the mass of each component.

Following GC analysis, data processing consists in the integration of the chromatograms, blank chromatogram subtraction, comparison of the processed chromatogram to calibration data to infer the concentration of the analyte in the prepared test sample. Finally, the concentration of the analyte in the material can be calculated following the test sample preparation steps.

MATERIALS

Composition

The reference material used in this study was a FTT-affected Mature Fine Tailings (MFT) provided by Suncor. Dean-Stark analyses of duplicate samples gave estimates of 69.7 wt.% solids, 4.5 wt.% bitumen and 25.8 wt.% water in this FTT-affected MFT sample.

3rd party analyses of the naphtha content in the reference FTT-affected MFT following Protocol A and Protocol B, which differed by the preparation of the test sample (i.e. Step 2 of the Analytical Task) prior to GC analysis. Protocol A consisted in the extraction of the tailings material with Tetrahydronaphthalene followed by GC of the extract, whereas Protocol B consisted in the extraction of the tailings material with Methanol, also followed by GC of the extract. Naphtha analysis by Protocol A and B gave estimates of 450 and 1847 ppmw, respectively.

Subsampling

Subsampling of the FTT-affected MFT was carried out while homogenizing the material inside a 20 L pail fitted with four 1"-wide baffles using a Pitch-Blade Turbine impeller at 400 rpm. To minimize naphtha devolatilization while subsampling, the procedure was conducted under refrigerated conditions (i.e. ~4 °C), with a cover placed onto the pail. Subsamples of FTT-affected MFT were withdrawn using large syringes fitted with a 3/8" OD drawing tube, to avoid material segregation during collection.

VAPOUR FLASH METHOD

Theoretical basis

The evaluation of the quantity of naphtha in a tailings samples can be can be derived from mole balances, given that the Vapour-Liquid equilibria of hydrocarbons from naphthenic froth treatment tailings samples is known to follow Raoult's law (Brown et al., 2018), i.e. naphtha and bitumen form an ideal liquid solution dispersed in the tailings samples (1):

$$\boldsymbol{x_n\, P_n^{SAT} = y_n\, P} \qquad (1)$$

Where P_n^{SAT} is the saturation pressure of naphtha, P is the total pressure, while x_n and y_n are the mole fractions of naphtha in the liquid hydrocarbon phase and in the gas phase, respectively.
Hence, during the i[th] vapour-liquid flash:

$$\frac{\boldsymbol{n_{n,L,i}}}{\boldsymbol{n_{n,L,i}+n_B}}\boldsymbol{P_n^{SAT}} = \frac{\boldsymbol{n_{n,V,i}RT}}{\boldsymbol{V}} \qquad (2)$$

And:

$$\boldsymbol{n_{n,L,i-1} = n_{n,L,i} + n_{n,V,i}} \qquad (3)$$

Where $n_{n,L,i}$ and $n_{n,V,i}$ are the number of moles of naphtha in the slurry and vapour phases during the i[th] flash, whereas n_B is the number of moles of bitumen in the slurry, which was assumed to be constant throughout the vapour-liquid flashes (i.e., bitumen is considered as purely non-volatile). Introducing the naphtha molar recovery χ_i on the i[th] vapour-liquid flash as the ratio $n_{n,V,i}/n_{n,L,i-1}$, equations (2) and (3) can be rewritten as:

$$\frac{(1-\chi_i)n_{n,L,i}}{(1-\chi_i)n_{n,L,i}+n_B} P_n^{SAT} = \chi_i \frac{n_{n,L,i}RT}{V} \quad (4)$$

$$\frac{n_{n,V,i}}{\chi_i} = \frac{n_{n,V,i+1}}{\chi_{i+1}} + n_{n,V,i} \quad (5)$$

Experimentally, both vapour-liquid flashes were conducted under the same temperature T and volume V. If the vapour pressure of naphtha is considered to be constant during both flashes (approximating naphtha to a single pseudo-component), it follows from equation (4) that the recovery χ is constant throughout the vapour-liquid flashes regardless of the flash number i. This simplifies equation (5), which can be re-arranged as:

$$1 - \chi = \frac{n_{n,V,i+1}}{n_{n,V,i}} \quad (6)$$

With $n_{n,V,1}$ and $n_{n,V,2}$ being measured, the naphtha molar recovery χ can be estimated by (6). The number of moles of naphtha initially present in the slurry $n_{n,L,0}$ can then be determined by the ratio $n_{n,V,1}/\chi$. The value obtained for $n_{n,L,0}$ is then multiplied by an estimate of the naphtha molecular weight to give a mass of naphtha in the sample, $m_{n,L,0}$. Dividing the mass of naphtha present in the sample by the initial mass of FTT-affected MFT yields the weight fraction of naphtha in the tailings material.

Overview of Vapour-Liquid Flash Experiments

Vapour-Liquid flash experiments were conducted using the 'VLE' (Vapour-Liquid Equilibration) apparatus, whose design was inspired from the unit built by Dr. Peng from the University of Saskatchewan for the VLE characterization of oilsands tailings (Brown et al., 2018, Peng et al., 2016). The primary function of the VLE apparatus is to produce liquid and vapour phases that are in thermodynamic equilibrium. The unit was designed specifically to process complex mixtures of oilsands FTT, consisting of water, solids, bitumen, and light hydrocarbons. There are three primary steps to the process.

1. Sample Preparation, to collect the sample in a specifically designed cell and remove air from the sample cell headspace.
2. Equilibration, to allow the liquid and vapour to reach equilibrium at the desired temperature and total volume.
3. Analysis, in which the composition of the vapour and liquid phases are determined.

Each of these steps are described in detail in the following sections.

Sample preparation for Vapour-Liquid Flash

A selected sample of fluid tailings was homogenized and withdrawn with a syringe connected to a dip tube to fill specifically designed Liquid Sample Cells ('LSC'). Two LSCs were filled with approximately 50 mL of fluid tailings, with samples 'VLE01' and 'VLE02' being 68.716 g and 63.742 g, respectively. Since the objective of the experiments was to flash hydrocarbon vapours from the slurry, and that water does not impact the VLE of hydrocarbons from tailings, samples were mixed with approximately 50 mL of deionized water (exact mass recorded) to facilitate sample mixing and vapour-liquid contacting. The air headspace present in the Liquid Sample Cell was then removed through a 'Degassing' procedure.

In the Degassing procedure, the air was removed from the LSC through the application of vacuum in a stage-wise fashion, using the apparatus shown in Figure 1. The LSC to be degassed was separated from the vacuum pump by an empty sample cell (the 'Vacuum Cell'). The LSC was immersed in an ice bath to decrease the vapour pressure exerted by the slurry and minimize sample loss.

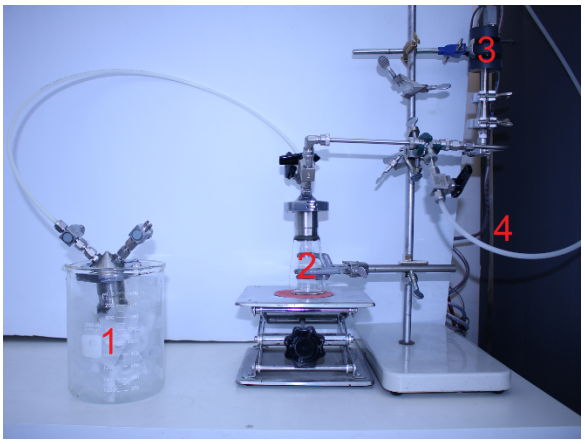

Figure 1. Degassing unit. 1) Liquid Sample Cell. 2) Vacuum sample cell. 3) Pressure sensor. 4) Line to vacuum pump.

Each stage of the Degassing procedure involves: 1) physically isolating the Vacuum Cell from the LSC, 2) Fully evacuating the Vacuum Cell, 3) Isolating the vacuum pump from the fully evacuated Vacuum Cell, and 4) enabling communication between the Vacuum Cell and the LSC, allowing the pressures

to equilibrate. During the initial stages, the equilibrated pressure decreases geometrically. As the air was removed, the vapour pressure approaches the equilibrium pressure of the liquid sample at 0 °C. For naphthenic froth treatment tailings samples, this equilibrium pressure was slightly above the vapour pressure of water at 0 °C (i.e. 0.089 psia), given that hydrocarbons also exert their partial pressure. A typical evolution of the pressure of the Liquid Sample Cell with the number of Degassing stages is presented in Figure 2.

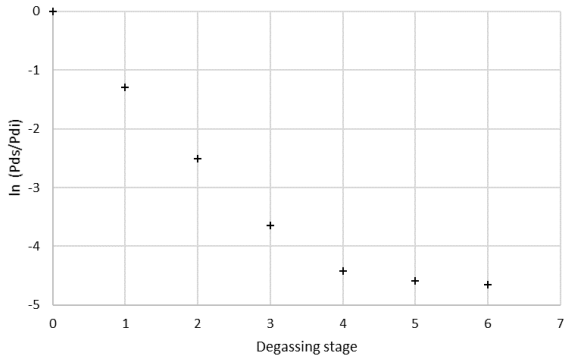

Figure 2. Sample pressure profile in a Liquid Sample Cell associated with the degassing process (sample: process water).

In the case described in Figure 2, this stage-wise removal of air induces a geometric decrease in pressure inside the cell till the 4th Degassing stage. A significant decrease in slope steepness occurs beyond that point, which was indicative of the predominant removal of the vapours which are produced by the sample itself. Therefore, it was important to track where the system pressure started to deviate from a geometric reduction with each stage and stop the Degassing procedure before compromising sample integrity.

Once the air in the headspace was removed from the Liquid Sample Cell, the LSC was weighed before installation in the VLE Apparatus.

Vapour-Liquid Flash Equilibration

A schematic diagram of the VLE Apparatus is presented on Figure 3. The whole assembly is contained in a temperature-controlled enclosure, as shown in Figure 4.

Initially, the valves to the degassed Liquid Sample Cell are closed. The setup was then tested for leaks. This was accomplished by a 'pressure decay' method. A vacuum was applied to the system, and then the system was isolated. The internal pressure was then monitored for indication of leaks. When the setup was deemed leak-free, it was then evacuated and heated to the desired setpoint temperature.

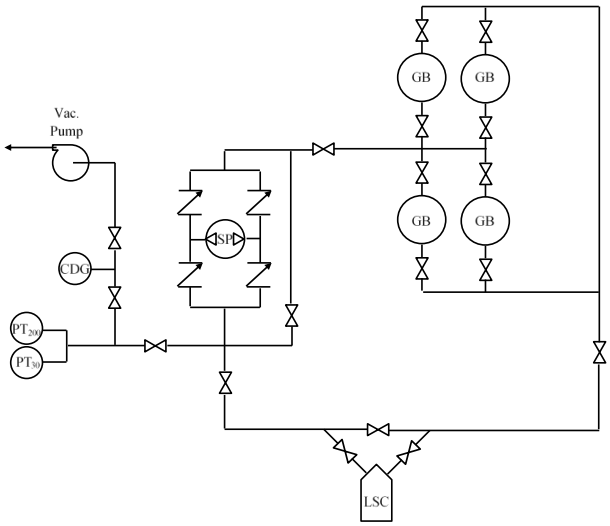

Figure 3. Plumbing associated with the VLE Apparatus. LSC: Liquid Sample Cell; GB: Glass Bulb; SP: Solenoid Pump; CDG, PT_{30} and PT_{200} are pressure sensors. Air circulation and heater not shown.

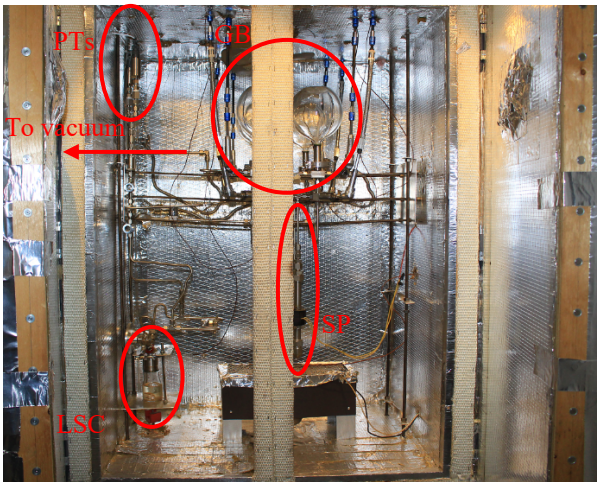

Figure 4. VLE Apparatus used to generate results at Coanda. LSC: Liquid Sample Cel ; GB: Glass Bulb; SP: Solenoid Pump; PTs are pressure sensors.

The pressure was monitored by two transmitters, PT_{30} and PT_{200}, rated to 30 and 200psi, respectively. The PT_{30} transmitter provided improved sensitivity. The split range was required to accommodate the

higher pressures associated with elevated operating temperatures. The temperature of the air inside the enclosure was monitored by a high-accuracy platinum Resistance Temperature Detector (RTD) and was controlled by an on/off programmable Proportional-Integral-Derivative (PID) temperature controller. In this PID control loop, the RTD temperature was used as the input and a 150 W electrical resistance strip heater was used to supply heat.

During the Equilibration process, the sample was exposed to a constant temperature and fixed system volume. The volume selected implicitly dictated the final equilibrium pressure. In all the vapour-liquid flashes executed in this project, the flash temperature setpoint was 120 °C, whereas the vapour volume was set to 3634 mL. The four glass bulbs had a total volume of 3419 mL whereas the tubings of the unit had an internal volume of 215 mL. These conditions were the maximum temperature and volume conditions the unit was designed for, and were chosen to maximize the amount of naphtha that would flash to the vapour phase.

Once the temperature was stable at the setpoint, and the pressure was stable at approximately 0 psi, the valve to the vacuum pump was closed. The outlet valve of the liquid sample cell was slowly opened, allowing the vapor pressure to build up in the setup. A custom solenoid pump was activated to circulate the vapor through the glass bulbs and back into the liquid sample cell, thereby increasing mass transfer and enabling phase equilibration. The equilibration process typically lasted 12 to 16 hours and was monitored by following the evolution of pressure. Once the pressure remained stable within approximately ± 0.001 psi for 1 hour, the system was assumed to reach equilibrium. Following equilibration, the glass bulbs and LSC were isolated, before the setup was cooled down.

After each vapour-liquid flash, the glass bulbs were removed from the setup in order to analyze the vapours as described in the following section. At the end of the first vapour-liquid flash, the LSC remained connected to the setup. Before the second vapour-liquid flash, the lines and the glass bulbs were purged and evacuated. After the second vapour-liquid flash, the LSC was also disconnected from the setup to complete the liquid compositional analyses.

Analysis of Flash Vapours

The Analysis of post-flash vapours were done using a combination of gravimetrics, gas chromatography, and Karl Fisher titration. They were achieved by extracting the glass bulb contents with ~25 mL of a solution of ethanol spiked with n-hexadecane internal standard at ~1000 ppmw. Extractions were conducted by submerging the glass bulb in an ice bath to facilitate gas-liquid absorption. Ethanol extracts were then analyzed by Karl-Fisher and gas chromatography to determine the weight of water and hydrocarbons, respectively.

A Mettler Toledo C20S Coulometric KF titrator was used for estimating the water content in ethanol extracts. The titration relied on the stoichiometric reaction of the water present in the sample with iodine, which was electrochemically generated in situ. Knowing the water content in the extract, the mass of ethanol injected, and the amount of trace water present in the ethanol solution prior to extraction, the amount of water inside the glass bulb at the end of a Vapour-Liquid flash was calculated.

The hydrocarbons in the post-flash vapours were analyzed by GC of the ethanol extracts. The GC hardware consisted of an Agilent 6890N unit, equipped with a 30 m Restek RTX-1 fused silica column with 0.53 mm ID. The stationary phase was a cross-bonded, 100% dimethyl-polysiloxane, of 1.5 µm thickness. The method used for the analysis was as follows: 40 °C initial temperature, followed by a 15°C/min temperature ramp until reaching 240°C, with a final hold time of 5 min at 240 °C. Sample injection was performed by an autosampler, with an injection volume of 1 µL and a split ratio of 20:1, with a GC inlet temperature of 200°C. A constant flow of helium (9.5 mL/min at 40°C) was used as carrier gas. The quantity of analytes at the end of the column was determined by a FID, maintained at 275°C. The GC calibration was carried out with a set of 5 calibrants made with process naphtha diluted in ethanol (spiked with n-hexadecane internal standard at ~1000 ppmw) with a concentration ranging from 0.01 wt.% to 1 wt.%.

The mean molecular weight of naphtha in the vapour extracts was estimated from a correlation with boiling point (7), after having mapped the boiling points of hydrocarbons to their retention times in the GC analyses (Table 1).

Table 1. GC retention times and boiling points of linear alkanes.

n-alkane	Boiling Point (°C)	GC retention time (min)
n-C_6	68.0	2.08
n-C_7	98.4	3.04
n-C_8	125.0	4.38
n-C_9	151.0	5.92
n-C_{10}	174.1	7.51
n-C_{11}	196.0	9.05
n-C_{12}	216.3	10.52
n-C_{16}	286.9	15.61

$$\boldsymbol{BP = 49.5\ CF^{0.2791}\ M^{0.5039}} \quad (7)$$

Note that CF in equation (7) is the atomic fraction of carbon in the hydrocarbon, which was assumed to be ≈ 0.33 for naphtha hydrocarbons (equivalent to an average chemical formula of C_nH_{2n}).

The hydrocarbon and water content in the vapours estimated by KF and GC, respectively, were systematically cross-checked with two other experimental data:

- Glass bulbs weights were measured before and after the Vapour-Liquid flashes. The addition of the mass of water measured by KF with the mass of hydrocarbons measured by GC was compared to the total weight of vapours collected.

- Combining the mass of the hydrocarbons measured by GC with the estimation of the mean naphtha molecular weight using equation (7) and Table 1 gave an estimate of the number of moles of naphtha in the vapour phase. The number of moles of water in the vapour phase was estimated from the KF results, using the molecular weight of water. The total number of moles in the vapour phase was cross-checked against the measured pressure, temperature, and volume of the vapours, based on ideal gas law.

RESULTS

The pressure, volume, and temperature of the first and second vapour-liquid flashes on samples VLE01 and VLE02 are reported in Table 2 and Table 3, respectively. Based on ideal gas law, the VLE01 sample generated 0.225 and 0.217 moles of vapour in its first and second flash, respectively. The VLE02 sample generated 0.218 and 0.215 moles of vapour on its first and second flash, respectively.

Table 2. V,T conditions in the first vapour-liquid flash of each sample and resulting vapour pressures.

	VLE01 – Flash 1	VLE01 – Flash 2
V (mL)	3643.3	3643.3
T (°C)	120.01	120.03
P (psi)	29.291	28.215

Table 3. V,T conditions in the first vapour-liquid flash of each sample and resulting vapour pressures.

	VLE02 – Flash 1	VLE02 – Flash 2
V (mL)	3643.3	3643.3
T (°C)	120.03	120.02
P (psi)	28.215	28.010

The total mass of vapours determined by gravimetry, as well as the mass of water determined by KF analyses, and the mass and moles of hydrocarbons determined by GC analyses are reported in during the first and second flash are reported in Table 4 and Table 5 for samples VLE01 and VLE02, respectively.

Table 4. Vapour mass and compositions resulting from the first and second vapour-liquid flashes of sample VLE01.

Vapour quantity	VLE01 Flash 1	VLE01 Flash 2
Vapour mass (g)	4.263	3.966
Water mass (g)	4.118	3.939
Naphtha mass (g)	0.145	0.027
Naphtha molecular weight (g/mol)	109.4	124.7
Naphtha millimoles	1.327	0.217

Table 5. Vapour mass and compositions resulting from the first and second vapour-liquid flashes of sample VLE02.

Vapour quantity	VLE02 Flash 1	VLE02 Flash 2
Vapour mass (g)	4.082	3.959
Water mass (g)	3.928	3.929
Naphtha mass (g)	0.154	0.030
Naphtha molecular weight (g/mol)	115.0	128.3
Naphtha millimoles	1.343	0.231

The consistency of the molar quantities of vapour generated during each flash can be cross-checked between the P, V, T data and the analytical results provided by KF and GC analysis (using 18.015 g/mol as the molecular weight of water), as reported in Table 6.

Table 6. Molar quantities generated during each flash, estimated from P, V, T data and estimated from KF and GC results.

Flash	Vapour moles (P, V, T estimate)	Vapour moles (KF, GC estimate)
VLE01, Flash 1	0.225	0.230
VLE01, Flash 2	0.217	0.219
VLE02, Flash 1	0.218	0.219
VLE02, Flash 2	0.215	0.218

Estimates of molar quantities in the vapours of each flash are very consistent. However, the quantities of vapour produced are largely dominated by water, which is more abundant than hydrocarbons in the vapour phase by 3 orders of magnitude, on a molar basis.

Using the molar quantities of naphtha recovered from each flash (Table 4 and Table 5) into equation (6), the naphtha vapour phase recovery was estimated at 83.6% and 82.8% for samples VLE01 and VLE02, respectively. Using these recovery values, the molar quantities of naphtha initially present in the samples, given by $n_{n,V,1}/\chi$, are 1.586 and 1.622 mmol for samples VLE01 and VLE02, respectively. GC analysis of a neat sample of process naphtha supplied by Suncor provided an estimate of the mean naphtha molecular weight of 113.6 g/mol. Using this estimate of the molecular weight of naphtha, the mass of naphtha initially present in the samples can be evaluated at 0.180 g and 0.184 g for samples VLE01 and VLE02. These naphtha contents are close to the mass of naphtha collected in the vapours during both flashes for each sample (0.172 g and 0.184 g for samples VLE01 and VLE02, respectively). Since samples VLE01 and VLE02 had an initial mass of 68.716 g and 63.742 g, respectively, their naphtha concentrations amount to 2623 ppmw and 2891 ppmw. These quantities, averaging at 2757 ppmw, are substantially higher than the analytical results provided by Protocols A and B, which were 450 and 1847 ppmw, respectively.

DEVELOPMENT OF A NEW METHOD FOR NAPHTHA ANALYSIS IN TAILINGS

Diagnostic

Estimates of the naphtha content given by the Vapour Flash method were significantly higher than those given by Protocol A and Protocol B. An investigation on the details of Protocols A and B was conducted to determine the possible causes for the discrepancy in the naphtha estimates. Considering the different steps in the execution of the Analytical Task, the major difference between Protocols A, Protocol B and the Vapour Flash method lied in the "Test sample preparation step".

Rapid bench-top tests were conducted to understand the challenges in the solvent extraction of oilsands tailings samples. Contacting tailings material with a non-polar hydrocarbon solvent, such as Tetrahydronaphthalene, resulted in the formation of an emulsion, which is unsuitable for GC analysis. These emulsions were most likely stabilized by the bi-wettable clays and the asphaltenic hydrocarbons from the sample. Hydrocarbon extraction with toluene or carbon disulfide led to similar observations. Further consultations with the analytical laboratory executing Protocol A pointed out that avoiding emulsion formation when contacting the tailings with THN required "gentle" contacting with minimal mixing energy. However, the minimization of the mixing action during the extraction process is very likely to cause incomplete mass transfer of the hydrocarbons from the tailings into the extraction solvent, resulting in the underestimation of the naphtha content in the tailings sample that was observed.

The formation of an emulsion during the extraction process can be eliminated by using an amphiphilic solvent where both the water and the hydrocarbon phase of the tailings can be dissolved. This was partially accomplished by using Methanol in Protocol B. While water is completely soluble in Methanol, this solvent remains poor for solubilizing bituminous hydrocarbons. It is likely that the underestimation of the naphtha content in the tailings samples by Protocol B came from the poor solubility of the tailings hydrocarbon phase in the extraction solvent of choice.

Modification of the test sample preparation step

While the Vapour Flash method offered many datapoints to cross-check the quality of the measurements, it is a very onerous method which is

not suited for routine analysis. In contrast, Protocols A and B provided an adequate framework for routine analysis, however it was diagnosed that the solvents used in these protocols were ill-suited for this purpose. For the extraction of naphtha hydrocarbons from oilsands tailings, a suitable solvent should offer complete solubility for both water and bituminous hydrocarbons, while exhibiting minimal interference in the following chromatographic process. To estimate the ability for a solvent to dissolve bituminous hydrocarbons, a comparison can be made on the basis of Hildebrand solubility parameters: the closer the Hildebrand solubility parameter between bitumen and a solvent, the better the solubility. The Hildebrand solubility parameter of Athabasca bitumen was estimated between 18.25 and 20.2 $MPa^{½}$ (Gray, 2015). Since Methyl-Ethyl-Ketone (i.e. 2-Butanone, or 'MEK') has a solubility parameter of 19.3 $MPa^{½}$ and has good water solubility, it was screened as an ideal solvent candidate for the extraction method of interest.

Using MEK as an extraction solvent for oilsands tailings sample, the sample:solvent extraction ratio was set as the compromise that could maximize the analytical response of the hydrocarbons while achieving complete water solubility. The optimum extraction ratio was 1:7 sample:solvent on a mass basis, which is applicable to tailings samples with a solids fraction above 20 wt.%. More solvent might be required to achieve complete water solubility at lower solids fractions in the tailings materials. Complete hydrocarbon extraction was achieved after homogenizing the sample with the solvent for 10 minutes on a wrist-shaker and letting the extract rest for 24 hours. Afterwards, extracts were processed through 0.44 µm syringe filters to supply the aliquots required for GC analyses.

Gas Chromatography of MEK extracts

The GC analyses of the MEK extracts were carried out using a Gas Chromatograph equipped with a non-polar fused silica column (Restek RTX-1, crossbond dimethyl-polysiloxane stationary phase) with the following specifications: 0.53 mm ID, 1.5 µm stationary phase thickness, 30 m long. The method used for the analysis was as follows: 40 °C initial temperature, followed by a 10 °C/min temperature ramp until reaching 240°C, followed by a second temperature ramp of 25 °C/min until reaching 300 °C with a final hold time of 22 min at 300 °C. Sample injection was performed by an autosampler, with a volume of 1 µL injected in splitless mode to maximize the analyte response. The GC inlet temperature was set to 275°C. A constant flow of helium (9.5 mL/min at 40°C) was used as carrier gas. The quantity of analytes at the end of the column was determined by a FID maintained at 330 °C with H2 flow at 40 mL/min, air flow at 400 mL/min and He makeup flow at 20 mL/min.

The GC calibration was carried out with a set of 5 calibrants made with process naphtha diluted in MEK (spiked with n-hexadecane internal standard at ~1000 ppmw) with a concentration ranging from 0.01 wt.% to 1 wt.%. The calibration curve was obtained by normalizing the sum of the peak areas from naphtha hydrocarbons to that of the n-hexadecane internal standard, and reporting it against the calibrant concentration. It should be noted that at low concentration, some of the minor naphtha chromatogram peaks are susceptible to fall below detection threshold. As a result, the calibration curve exhibits non-linearity in the low concentration range.

Several considerations should be accounted for while processing the chromatograms of MEK extracts of tailings samples. MEK is not commonly available at purities greater than 99.5 wt.%, and solvent impurities have a high likelihood of interfering with the chromatographic response of the analytes of interest (i.e. naphtha hydrocarbons). Common impurities include but are not limited to: acetone, propanol, butanol, ethyl-acetate, tetrahydrofuran, pentanone, t-butyl acetate and n-propyl acetate. While the shorter oxygenates from this list generally elute at smaller retention times than the analytes of interest, the larger oxygenates may coelute with naphtha hydrocarbons. Hence, solvent blank subtraction is required when processing extract chromatograms. The solvent blank subtraction process presents some challenges because the water contained in the sample extracts can cause some changes in the retention times and the shape of the peaks associated with MEK impurities, as well as baseline drift.

RESULTS

Naphtha analyses were conducted in triplicates on the reference FTT-affected MFT material supplied by Suncor, using the new protocol relying on MEK extraction followed by GC as previously described. The naphtha content in the material was estimated at 2912 ± 341 ppmw. These results offer a very good match to the data obtained by the Vapour Flash method. The data confirmed that the Test

sample preparation step was the main aspect of the analytical procedure that needed to be revised to close the gaps between the various analytical results. It can be noted that the analyses, whether from the Vapour Flash method or the MEK extraction method, exhibit a significant variability (~10% relative standard deviation). Subsequent GC re-analyses of extracts have shown that the variability associated with the chromatographic process and the related data processing was within 2% relative standard deviation. These results suggest that most of the analytical variability is attributable to tailings subsampling.

CONCLUSIONS

Estimations of the naphtha content in tailings samples using the Vapour Flash method have revealed very large gaps between the true naphtha content in tailings materials and standard protocols that were used by analytical laboratories. On a reference FTT-affected tailings sample, an average naphtha content of 2757 ppmw was determined by the Vapour Flash method, whereas Protocols A and B only found 450 and 1847 ppmw, respectively. The gaps in the analytical results were attributed to an incomplete extraction of hydrocarbons through standard protocols.

Therefore, a new analytical procedure was developed with MEK as an extraction solvent with the aim of fully solubilizing bituminous hydrocarbons and water. This approach produced naphtha estimates of 2912 ppmw, which closely aligns with the data obtained by the Vapour Flash method. This analytical method can be used as a basis for a new standard.

As presented, the analytical method would benefit from several improvements. First, improvements on material subsampling would address the main source of variability in analytical results. Secondly, more robust calibration and integration techniques, especially to refine accuracy and precision at concentrations below 100 ppmw on an extract basis.

REFERENCES

Foght, J.M., Gieg, L.M, Sidique, T. 2017. The microbiology of oil sands tailings: past, present, future. FEMS Microbiology Ecology, **93**: 1-22.

Brown, W., Laborde-Boutet, C., McCaffrey, W.C., Gaskin, L., Naikyar, E., Peng, D.Y., Hollander, E. (2018). Thermodynamic limit for the recovery of naphtha from oilsands tailings, 2018 COSIA Innovation Summit, Calgary, Alberta, June 7-8, 2018.

Peng, D.Y., Moran, K. (2016). Vapour-liquid equilibria and solvent recovery from oil sands froth treatment tailings streams, 66th Canadian Chemical Engineering Conference, Quebec City, Quebec, October 16-19, 2016.

SESSION 3

A PROTOCOL TO ASSESS AND SCREEN NEW FLOCCULANT FOR SUNCOR'S PASS PROGRAM PLANNING

Yunhui Li[1], Heather Kaminsky[1], Adrian Revington[2], and Ardalan Sadighian[2]
[1] Northern Alberta Institute of Technology, Edmonton, Canada
[2] Suncor Energy Ltd., Calgary, Alberta, Canada

ABSTRACT

Oil sands fluid fine tailings (FFT) are a byproduct of oil sands mining and are considered a major liability in oil sands mining due to environmental and financial challenges. In 2018, Suncor Energy Inc. (Suncor) commercialized a novel and proprietary tailings treatment approach named Permanent Aquatic Storage Structure (PASS). The PASS program combines the use of an inorganic coagulant and a polymer flocculant applied during the tailings transport process. To support this program, NAIT Centre for Oil Sands Sustainability (COSS) and Suncor have worked together and developed a benchtop-scale methodology to evaluate and screen new polymeric tailings treatment technologies for PASS program.

The developed protocol is designed for polymers that will replace the current polyacrylamide (PAM) in the combination of alum and PAM. This protocol involves four stages: coagulation and flocculation to treat fluid fine tailings (FFT) and shearing the treated FFT using a custom-built shearing device to simulate the conveyance process; settling on conveyed treated FFT to produce release water and observe the short-term consolidation; modified filter press test to indicate the long-term consolidation performance and produce enough release water for water analysis; water chemistry analysis including total suspended solids (TSS), routine water chemistry (pH, alkalinity, electrical conductivity, major cations and anions, etc.) and dissolved organic carbon (DOC). The protocol is defined in stages with key Pass/Fail criteria at each stage.

This protocol is a necessary step to reducing the cost to technology providers and Suncor by the bench-scale testing as the first step of polymer screening. It ensures polymers to be tested in the pilot/field have a good chance of success and provides information on expected dosage and performance behavior to evaluate the business case of new polymers.

INTRODUCTION

Background

Since 1967, surface mining of the oil sands deposits in Northern Alberta has been a significant contributor to Canada's economy. Oil sands mining, however, has created by-products and environmental challenges in the form of tailings ponds and fugitive emissions. Bitumen extraction of oil sands leaves behind a waste product composed of a combination of sand, silt, clay, and water. Sand fractions are recovered for other uses relatively easily, leaving behind a slurry of water, residual solids, and bitumen known as FFT. By 2020, the FFT inventory in Alberta had grown to 1,360 Mm^3 (AER, 2021). FFT is stored in large ponds until final treatment and placement. These ponds represent a major concern as they require perpetual construction, maintenance, and observation, increasing long-term liabilities for the industry (Gulley and MacKinnon, 1993).

The oil sands tailings ponds represent a large and growing liability for the province of Alberta and its citizens (EDC and NRDC, 2017). In response to growing tailings stockpiles and environmental concerns, the Alberta Energy Regulator (AER) released Directive 085, which requires oil sands mine operators to ensure that all fluid tailings are returned to a reclamation-ready state 10 years after the end of mine life (AER, 2016). Suncor is a major oil sands operator and reported 292 Mm^3 of total fluid tailings inventory as of 2020 (AER, 2021). Suncor is striving to reduce liabilities from tailings waste by speeding up the path to reclamation through a new tailings treatment technology in its commercial-scale implementation of the PASS project (Omotoso et al, Patent CA 2921835). PASS creates a substrate that can be reclaimed into a

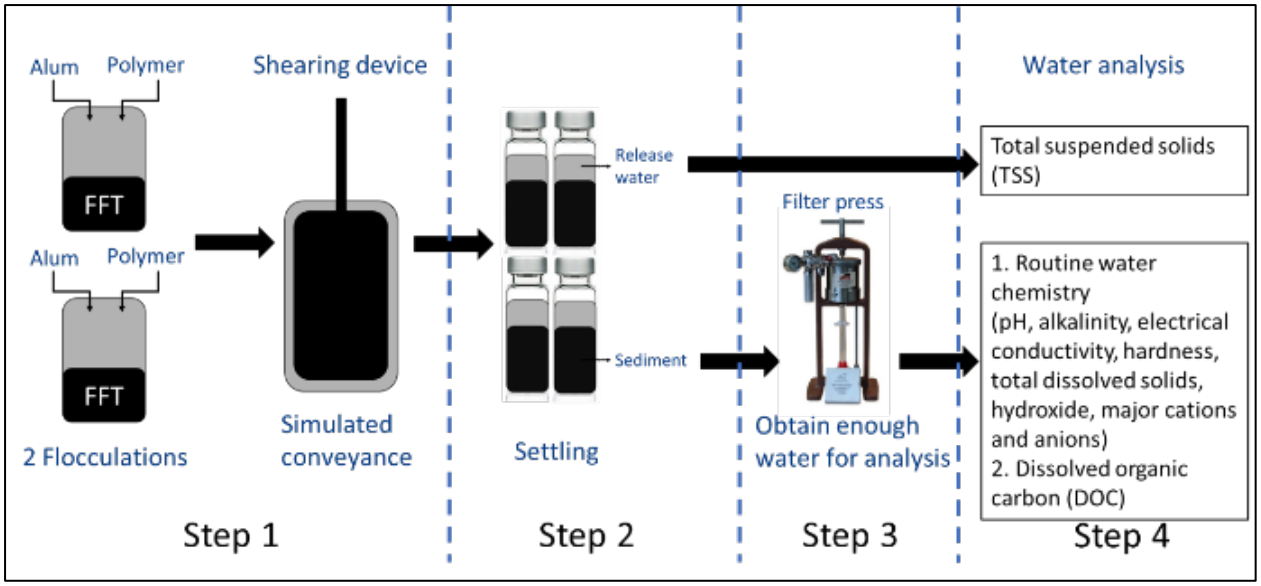

Figure 1. Experimental process of PASS screening protocol at lab scale.

Table 1. PASS Screening Process for Qualifying Alternative Technology

Stage	Description	Criteria	# of Tests	Man days	Timeline
Materials	• 1 benchmark polymer • 1 new polymer • Coagulant alum • 3 FFT samples				
0	Characterization of FFT samples	• Composition by Dean & Stark (D&S) • Particle size distribution (PSD) • Methylene blue index (MBI) • Water chemistry		• Done in advance as we received FFT	
1	Determination of the concentration of the new polymer			3 days	3 days
1	• Dosage map using the capillary suction time (CST) • 5 dosages to cover 2 under dosage, optimal dosage, and 2 overdosages	• CST is within 20% of the benchmark or lower • The optimal dosage window is within 20% of the benchmark or wider	• 138 flocculations • 54 conveyance tests • 252 CST tests	20 days	30 days
2	• Settling for 1 month	• The release water is clear and colorless at optimal dosage	• 216 settling tests	5 days	30 days
3	• Modified filter press test	• The time to achieve 0.65 CWR of filtered cake is within 20% of the benchmark or shorter	• 216 filter press tests	20 days	30 days
4	• Water analysis	• Water chemistry is within 10% tolerance of benchmark or better	• 16 TSS tests • 54 routine water analysis • 54 DOC	10 days	14 days
5	• Report			10 days	14 days
			Total	**68 days**	**4.5 months**

man-made freshwater lake shortly after the end of deposition in a mined-out pit.

PASS treatment is a two-step process (Figure 1). Step 1 starts with a coagulant treatment to immobilize, through precipitation and chemisorption, the contaminants of potential concerns in a freshwater lake such as some metals, organic acids, hydrocarbons, and ultrafines (COSIA, 2019). This is followed by the addition of a flocculant that aids the rapid release of water from the treated FFT. The treated FFT is subsequently conditioned and conveyed through a pipeline to a deposition area that acts as a settling basin. In Step 2, the treated FFT is analogous to lake sediment settling over long periods after the end of the deposition. As settlement of the treated FFT occurs, pore water (water surrounding the individual solid particles of the treated FFT) is continuously expressed or released from the treated FFT to an overlying water cap, which is connected to the surrounding watershed. The immobilization process ensures geotechnical stability of the lake landform such that seepage through the pit walls or expressed water to the lake meets federal and provincial guidelines for the protection of aquatic life.

PASS SCREENING PROTOCOL

To support Suncor for regulator asks – Directive 085 requires proof of performance before changing to new polymers, NAIT COSS and Suncor developed a lab-scale screening method for Suncor's PASS application (Figure 1). This protocol is designed for polymers that will replace the current HPAM in the Alum + PAM PASS program. Through this lab-scale protocol as the first step of polymer screening before the pilot or field testing, both technology providers and Suncor can reduce costs greatly. The results from this protocol will provide information on expected polymer dosages and performance behavior to evaluate the business case of new polymers, and ensure polymers tested in pilot or field have a good chance of success.

Overall Evaluation Program

The chemical evaluation program was run through a stage evaluation process with key Pass/Fail criteria at each stage. In order for a chemical to reach the stage of full field trials, it has to pass through each of the stages outline in Table 1. The time frame for a successful chemical to make it through all four steps in this protocol is 4.5 months. The protocol identified the chemical that has been used in the Suncor's PASS program as the incumbent superior polymer.

Stage 0 – Materials and Characterization

Three types of FFT were used in this study and characterized on Dean & Stark (D&S) for the composition (Dean and Stark, 1920), Methylene blue index (MBI) for the surface clay activity (Kaminsky, 2014), particle size distribution (PSD) for the fines content (COSIA, 2015), and water chemistry (Table 2 and Table 3). Process effluent water (PEW) was also characterized and used to prepare diluted FFT (D4400) and polymer solutions. Alum was used as the coagulant at a fixed dosage of 950 ppm (Equation 1). Three polymers were used in the protocol study: incumbent as the benchmark, polymer-A, and polymer-N.

Equation 1.

$$V\ (ml) = \frac{D}{10^6} \times \frac{1/C}{G} \times m_{water}$$

Where V is the volume of alum (ml), D is the dosage of alum in ppm, C is the concentration of alum (48.76%), G is the specific gravity of alum (1.33 g/ml), and m is the mass of water in sample (g).

Table 2. Characterization of FFT Samples.

FFT	Minerals wt%	Bitumen wt%	Water wt%	MBI (meq/100 g)	Fines wt%	SFR	Density (kg/m^3)
ES4400	32.45	2.15	65.40	10.6	90.60	0.104	1213
ES3152	30.98	2.87	66.15	8.1	89.30	0.120	1215
D4400	25.78	1.60	72.62	10.3	90.50	0.105	1161

Table 3. Concentrations of major cations and anions of FFT samples and PEW. Unit is ppm.

Sample	Cl^-	NO_2^-	Br^-	NO_3^-	SO_4^{2-}	Li^+	Na^+	NH_4^+	K^+	Mg^{2+}	Ca^{2+}
ES4400	785	1.3	3.6	8.9	209	0.1	942	9.2	13.4	8.9	13.0
ES3152	684	1.4	3.6	8.6	160	0.1	858	9.7	12.5	7.1	11.7
D4400	859	13.9	9.3	4.9	351	0.4	1150	0.0	20.1	9.5	12.7
PEW	583	0.0	3.8	5.2	258	0.1	754	0.0	11.8	6.4	7.3

Table 4. Water Chemistry of FFT Samples and PEW.

Sample	EC (µS/cm)	pH	Total alkalinity as $CaCO_3$ (ppm)	NAFC (ppm)	DOC (mg/L)
ES4400	4267	8.7	561	72.5	70.6
ES3152	3920	8.7	565	57.8	79.8
D4400	4190	9.1	836	62.7	66.4
PEW	3370	9.2	632	20.4	38.1

Stage 1 – Dosage Map

This stage was to screen a new polymer based on the dosage curves against the benchmark polymer. Two main treatments were in this stage: coagulation and flocculation, and over-shearing to simulate conveyance. The pass criteria of this stage were as follows.

- Clay to water ratio (CWR) of conveyed flocs at optimal dosage was within 20% of benchmark or higher.
- Capillary suction time (CST) at optimal dosage was within 20% of benchmark or lower.
- The optimal dosage window was within 20% of the benchmark or wider (robustness)

Determination of the polymer solution concentration. The concentrations of the tested polymers were determined by the viscosity properties of the polymer solutions. Each polymer was prepared to the concentrations from 0.1 wt% to 1.0 wt% and tested to determine the consistency index (CI) using a rheometer and Power Law Model. Based on the experience provided by Suncor, a CI of 1000 – 1500 cp range was a good match for mixing the polymer into the FFT (Sadighian, et al. 2018). One concentration of each polymer in this range of CI was chosen for further assessment. In this example, 0.45 wt% of all three polymers were used for the protocol study.

Coagulation and flocculation. The 6” cup technique (Figure 2) was used to coagulate and flocculate FFT; it used a torque monitoring overhead (Heidolph Hei-Torque 100 Precision Base) with a paddle mixer and a baffled beaker. This technique named the “torque-oriented mixing technique” was a semi-automatic method and easy to operate providing repeatable and reproducible flocculation results (Li, et al. 2011; Li, et al. 2022). Each test was conducted using a 1 L FFT sample. Mix the FFT sample for 1 min at 300 rpm to pre-shear the slurry. Inject the desired volume of alum (Equation 1) using a 1 ml syringe within 1 second while mixing at 300 rpm. Mix for 10 seconds, and then decrease the mixing speed to 80 rpm and continue to mix for 13 minutes. The 13 minutes of mixing was to simulate the transportation of the alum-treated FFT in the field. Increase speed to 300 rpm and inject the desired volume of polymer solution using a peristaltic pump (ColeParmer Drive/DISP MFLX BENCH 115/230) at a fixed flow rate of 1200 ml/min. The filler nozzle with 1/4" ID for polymer injection was inserted into the FFT slurry at a depth of 5 mm. Continue mixing at 300 rpm while monitoring torque response on the overhead mixer screen. When torque reached a peak value and began to decrease, immediately decrease mixing speed to 50 rpm. Condition the flocs by mixing at 50 rpm for 15 seconds.

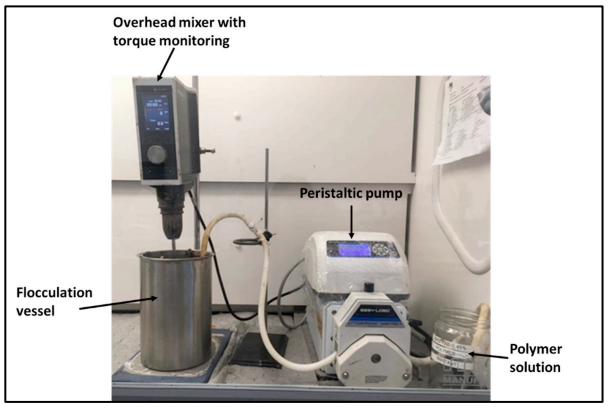

Figure 2. Coagulation and flocculation setup.

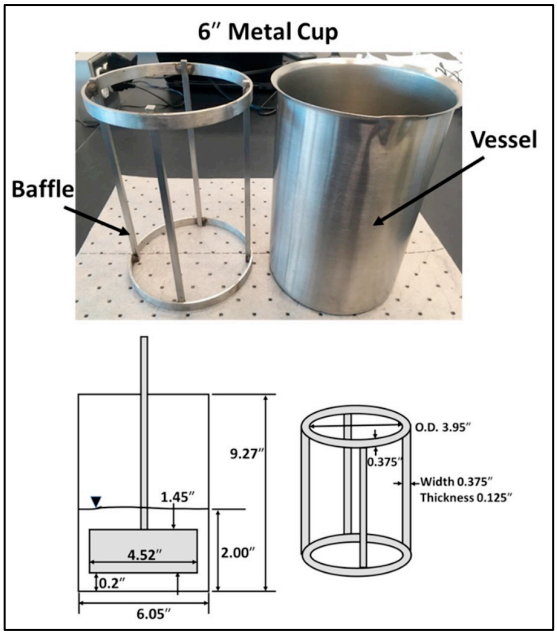

Figure 3. Schematic dimensions of coagulation and flocculation vessel, baffles, and impeller.

Conveyance Treatment (Li, et al. 2022). A custom-built small-scale shearing device (conveyance tester), which was designed with a rotating inner cylindrical bob inside a stationary outer cup, was used to simulate the energy input onto treated tailings delivered by shear during pipeline transport to the tailings pond (Figure 4). The size of the bob assembly was 23.2 cm in diameter and 54.7 cm in height. The cup assembly was 24.4 cm in diameter

and 55.3 cm in height. The gap between cup and bob was 5 mm. Eight evenly spaced baffles on the bob and cup surfaces minimized sample wall slip. To prevent the build-up of bitumen on the testing surfaces, the conveyance tester was thoroughly cleaned between each run. Testing setpoints for the rotational speed of the bob and duration of shearing were calculated to represent field pipeline size and tailings transportation flow rate.

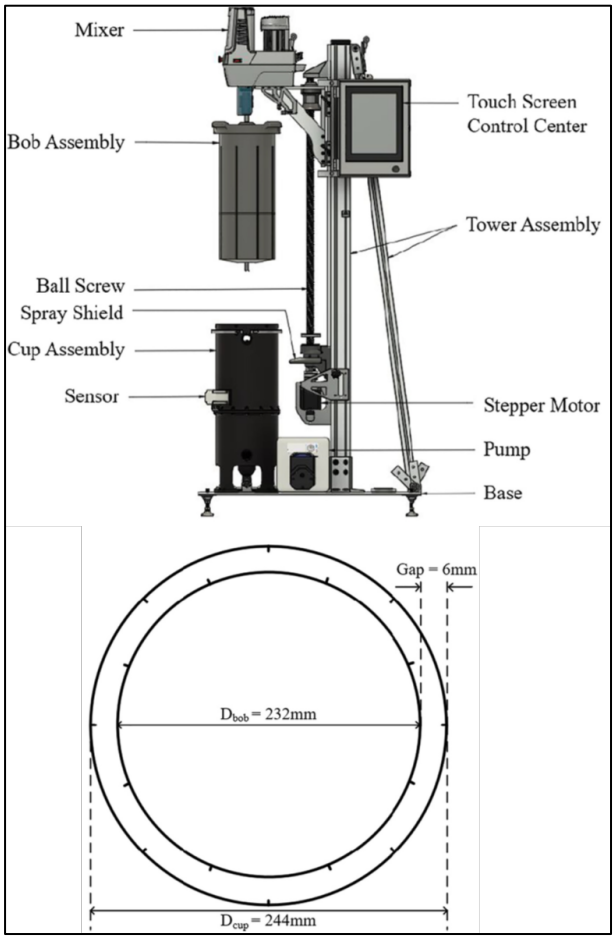

Figure 4. Schematic of the shearing device (top) and overhead view of cup/bob (right) with key measurement (bottom).

In this protocol, the conveyance condition was designed based on the field pipeline (22" in diameter and 1000 m in length) and treated tailings flow rate (1950 m^3/h) to simulate the shear energy input (~1500 kJ/m^3) into the treated tailings by transportation in the pipeline to the tailings deposit. Two batches of coagulated and flocculated FFT were treated for one batch of conveyance testing.

Dosage map. In general, the flocculation performance of the polymer increases with the dosage up to a certain optimum point and then decreases with further addition of the polymer due to the repulsion between the polymer-covered particles (Vedoy, et al. 2015). Full dosage response curves including under dosages, optimal dosages, and overdosages were performed for all three polymers on all three FFT samples (Figure 5 for both solids-based dosages and clay-based dosages). CST tests on the conveyed flocs were used to obtain the dosage curves. CST is designed to test homogenous and well-mixed slurry samples which can be applied to the conveyed flocs. According to the results in Figure 5, the optimal dosage window range of polymer-A was smaller and out of 20% of the benchmark for the FFT ES4400 and ES3152. This indicated that polymer-A was less robust than the benchmark to treat different types of FFT. The robustness of polymer dosage is critical to mitigating the variance of FFT compositions at the field. As a result, polymer-A failed on FFT ES4400 and ES3152 for the optimal dosage window at this stage. Polymer-N was a better candidate than the benchmark because the optimal dosage window shifted to a lower dosage range.

Stage 2 – Settling Test

This step was to screen a new polymer based on the release water quality (color and clarity) against the benchmark polymer after 1-month of settling. The pass criteria included that

- The release water was clear and colorless at the optimal dosage
- Total suspended solids (TSS) in the release water were within 20% of the benchmark or lower.

Figure 6 shows that the FFT without treatment or treated with a very low polymer dosage did not settle in 1 month. The polymer added in the range of optimal-500 ppm and optimal+500 ppm had a significant effect on the short-term water release. The release water at under dosages, optimal dosage, and optimal+250 ppm were clear and colorless.

Figure 7 shows that both polymer-A and polymer-N produced clear and colorless water at under dosages and optimal dosages. But overdosing leads to poor water quality. The TSS results (Figure 8) combined with Figure 7 results indicate that both polymer-A and polymer-N passed this stage.

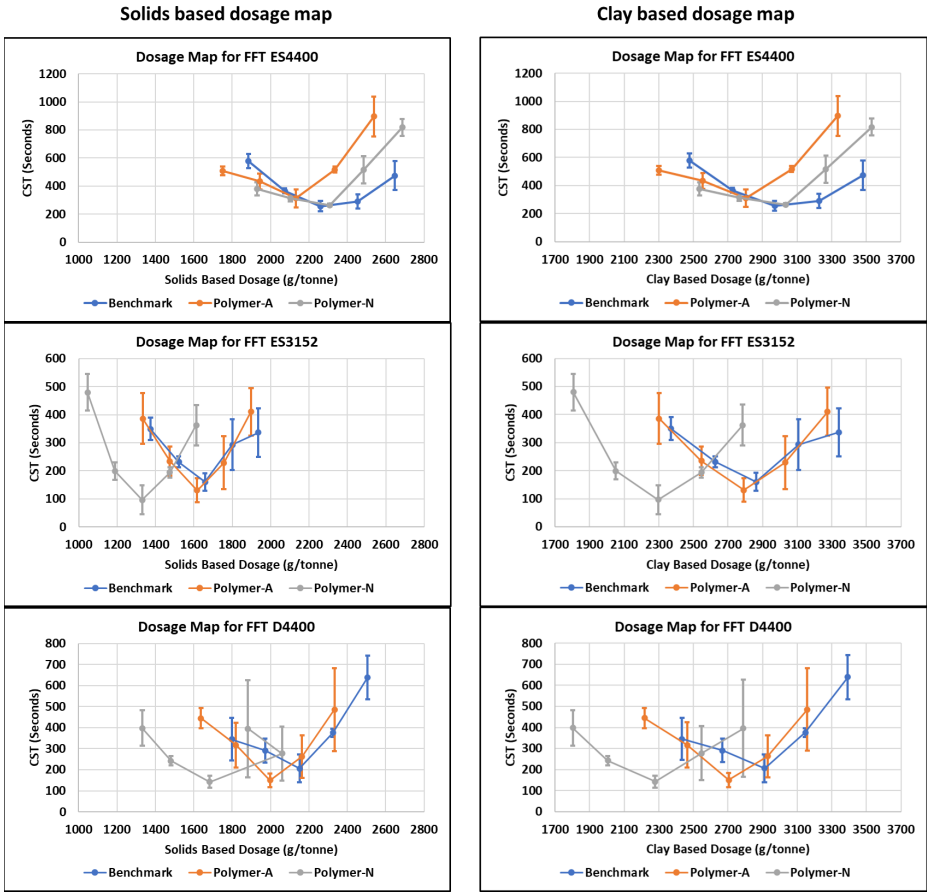

Figure 5. Dosage curves of three polymers (benchmark, polymer-A, and polymer-N) treatments on three FFT samples.

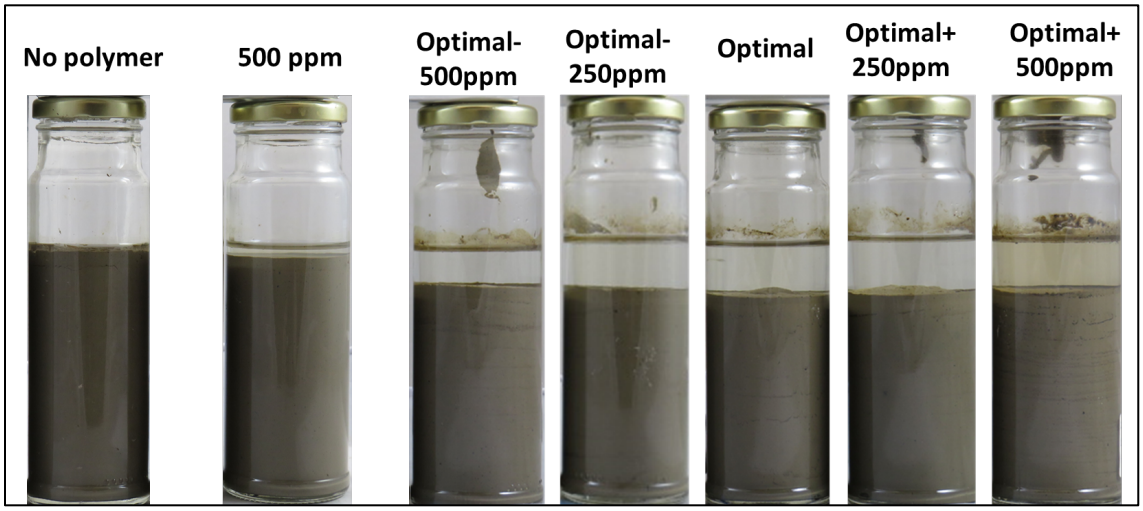

Figure 6. Photos of FFT ES4400 treated with alum and bench polymer after 1-month of settling.

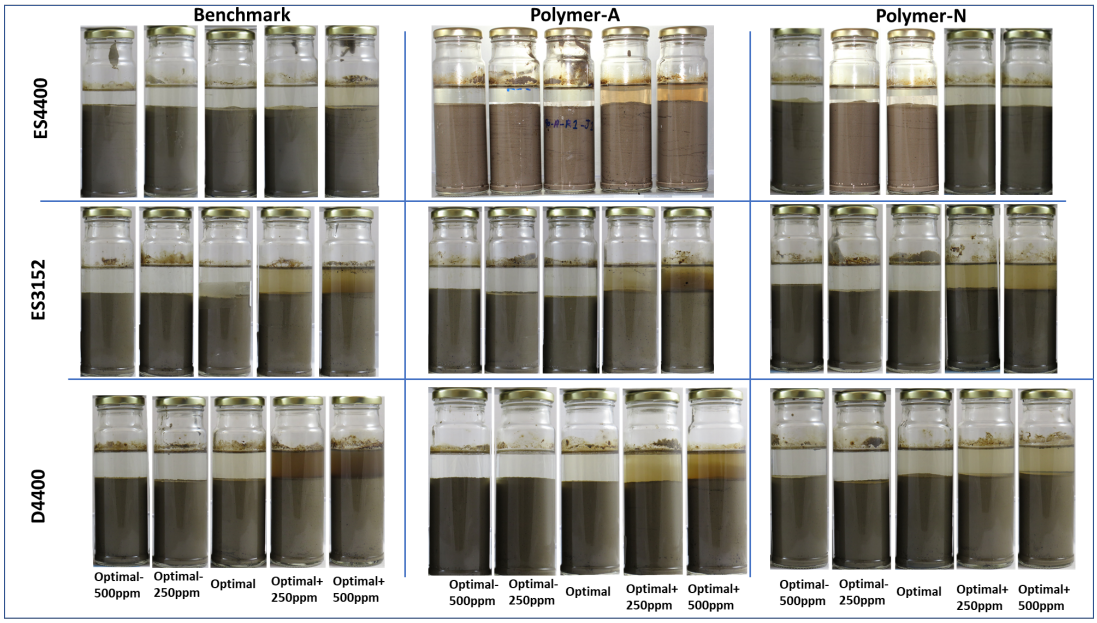

Figure 7. Photos of three types of FFT treated with alum and three tested polymers after 1-month of settling.

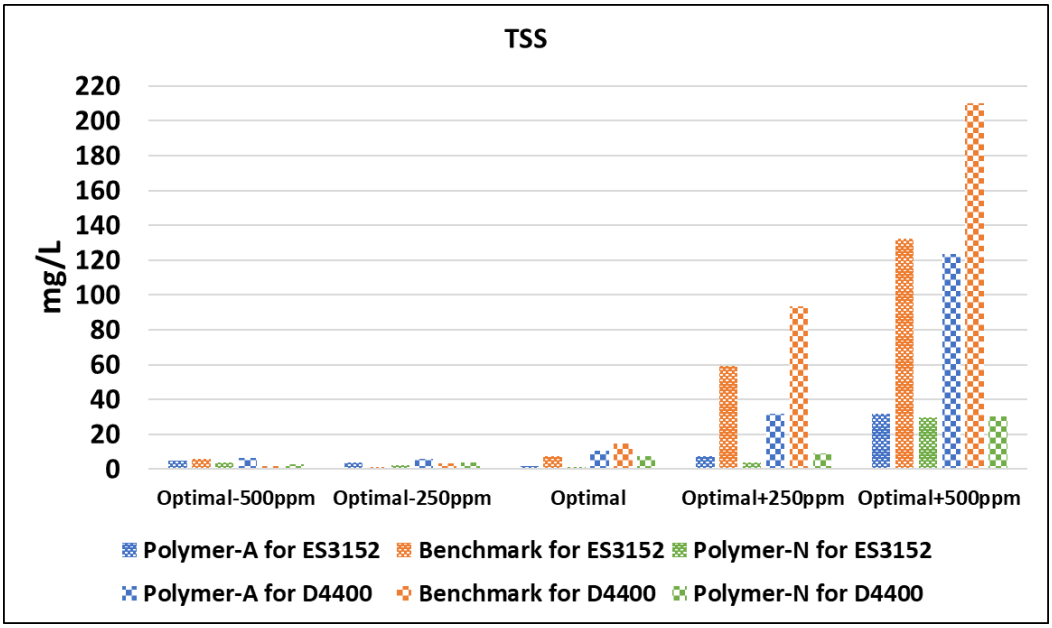

Figure 8. The total suspended solids (TSS) contents of the release water after 1-month settling.

Stage 3 – Modified Filter Press Test

This step was to obtain enough water for water analysis and to indicate the long-term consolidation performance of the FFT treated with different polymers using a modified filter press. The filter press modified by NAIT COSS applied gas pressure to the sample but removed the limitation on dewatering time due to cracking (Li, et al. 2021). This permitted an assessment of dewatering performance of different tailings treatments at much higher solids contents. It was believed that pressure filtration could be an indicator of long-term consolidation trends. The criteria of Stage 3 was that the filtration time to achieve 0.65 CWR of filtered cake is within 20% of the benchmark or shorter.

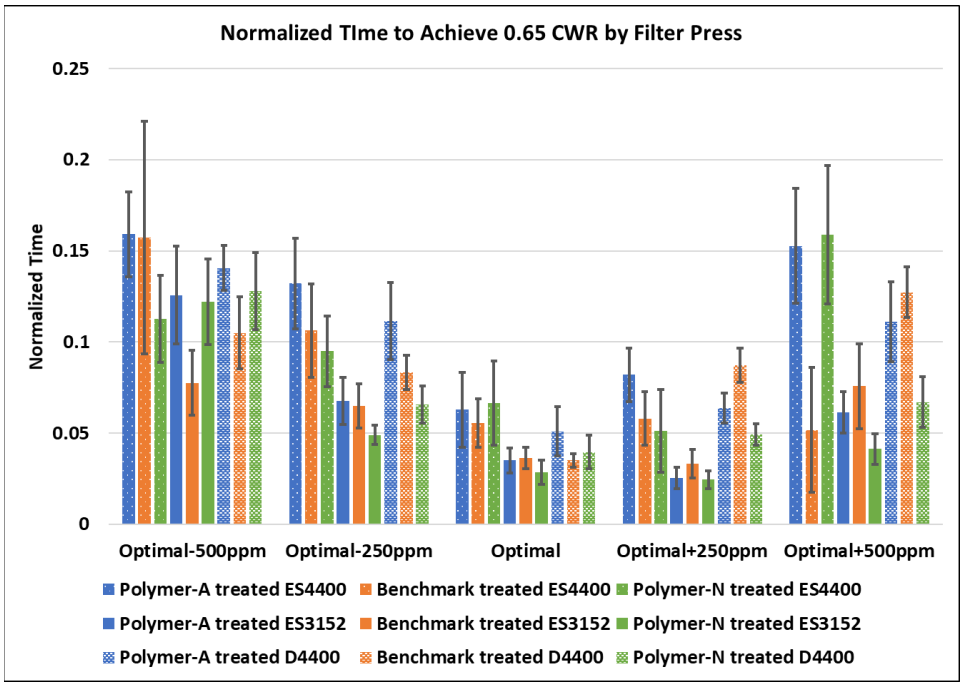

Figure 9. Normalized time to achieve 0.65 CWR of filtered cakes for three types of FFT treated with alum and three tested polymers.

Figure 9 shows the normalized time (Equation 2) to achieve the targeted 0.65 CWR increased substantially at under dosages or overdosages (optimal+500 ppm) compared with optimal dosages Compared with the benchmark polymer, polymer-A failed on the FFT D4400 and polymer-N passed this stage.

Equation 2.

$$Normalized\ time = \frac{t_{0.65}}{T_{0.65}}$$

Where $t_{0.65}$ is the time to achieve 0.65 CWR of the treated FFT; $T_{0.65}$ is the time to achieve 0.65 CWR of the untreated FFT.

Stage 4 – Water Analysis

The purpose of this stage was to use regular and low-cost water analysis to screen the polymeric flocculant. The filtrates from Stage 3 produced by different treatments on 3 FFT samples were tested on routine water chemistry (pH, alkalinity, electrical conductivity (EC), hardness, total dissolved solids (TDS), hydroxide, major cations, and major anions) and dissolved organic carbons (DOC). The criterion of stage 4 was that the release water chemistry was within 10% tolerance of benchmark or better. Representative water chemistry results of DOC, dissolved Calcium, and EC are shown in Figures 10-12. Polymer-A failed at the DOC testing on the FFT D4400 and polymer-N passed this stage.

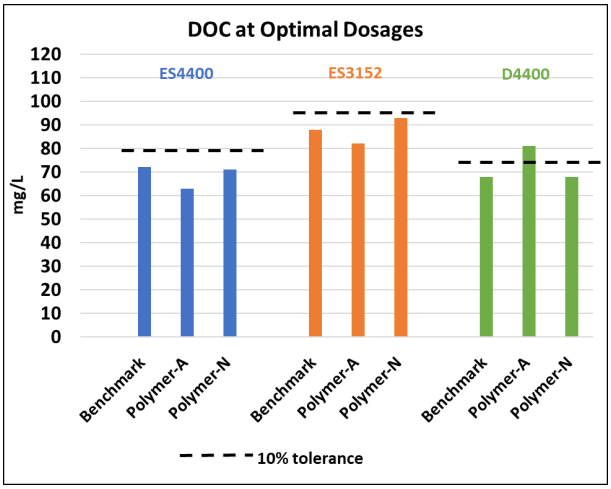

Figure 10. DOC results of water produced by three types of FFT treated with alum and three tested polymers at the optimal dosages.

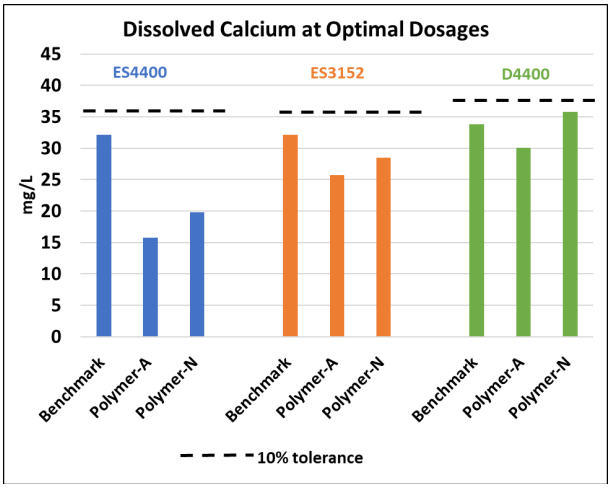

Figure 11. Dissolved calcium concentrations of water produced by three types of FFT treated with alum and three tested polymers at the optimal dosages.

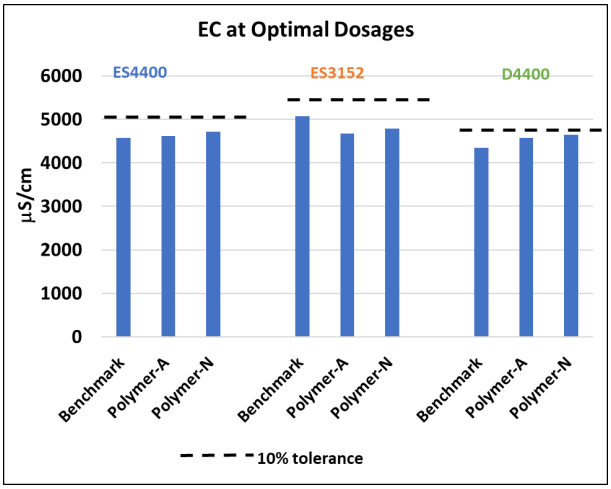

Figure 12. EC results of water produced by three types of FFT treated with alum and three tested polymers at the optimal dosages.

Timeline of the Screening Protocol

The Screening protocol has two phases and takes 4.5 months to screen one new polymer alongside the benchmark polymer on three types of FFT (Table 5). If the new polymer fails in Phase 1, Phase 2 will not proceed. In this case, the client will only be charged for Phase 1 scope.

Table 5. Timeline of the PASS screening protocol.

Phase	Stage	Timeline
1	0-2 and report	80 days
2	3-4 and report	60 days
Total		4.5 months

IMPORTANCE OF DOSAGE MAP

One of the key findings from this research is the importance of testing polymers on multiple FFT and in evaluating the performance over a range of dosages. For example, while the benchmark polymer has an optimal point just shy of 3000 g/t for all three FFTs with a CST of ~200 s the optimal point for Polymer N varies greatly – from ~3000 g/t for ES4400 to ~2250 g/t for the other two FFTs. This variation may point to the issue of achieving stable performance in the field with Polymer N. Understanding the potential range of performance can allow for better predictions of overall deposit performance knowing that there is a range of dosages that will be applied to a range of FFT in the field.

CONCLUSION AND FUTURE WORK

The present work uses three polymeric flocculants combined with the incumbent PASS coagulant alum as examples to present the bench scale screening protocol for Suncor's PASS program. There are a large number of chemicals proposed by various vendors for tailings treatment. Chemical screening is cumbersome, expensive, and long in duration from laboratory screening to field test – the shortest development timeframe is 12 months. This protocol should allow polymers passing this 4.5-month bench scale process to skip the expensive pilot loop process and go directly to a field scale trial while providing a larger degree of certainty to the regulator about the expected performance of the polymers.

REFERENCES

Alberta Energy Regulator (AER) (2016). Fluid Tailings Management for Oil Sands Mining Projects.

Alberta Energy Regulator (AER) (2021). State of Fluid Tailings Management for Mineable Oil sands, 2020.

Alexander, M. (1999). Biodegradation and Bioremediation. 2nd ed. Academic Press, San Diego, California, 409-433.

COSIA Fines Measurement Working Group. (2015). Unified Fines Method for Minus 44 Micron Material and for Particle Size Distribution.

COSIA Tailings EPA. (2019). Permanent Aquatic Storage Structure for Fluid Fine Tailings. 2018 Tailings Research Report, 57-59.
Environmental Defence Council (EDC) and Natural Resources Defense Council (NRDC) (2017). One Trillion Liters of Toxic Waste and Growing: Alberta's Tailings Ponds.

Gosselin, P., Hrudey, S.E., Naeth, M.A., Plourde, A., Therrien, R., Van Der Kraak, G., and Xu, Z. (2010). Environmental and Health Impacts of Canada's Oil Sands Industry. The Royal Society of Canada Expert Panel Report.

Gulley, J.R. and MacKinnon, M. (1993). Fine Tailings Reclamation Utilization Using a Wet Landscape Approach. AB Chamber Resource, AOSTRA, Energy, Mines & Resources Canada, Oil Sands: Our Petroleum Future Conference, Edmonton, Alberta, April, 23.

Holowenko, F.M., MacKinnon, M.D., and Fedorak, P.M. (2000). Methanogens and Sulfate-Reducing Bacteria in Oil Sands Fine Tailings Waste. Canadian Journal of Microbiology, 46, 927-937.

Kaminsky, H. (2014). Demystifying The Methylene Blue Index. Proceedings of Fourth International Oil Sands Tailings Conference, Banff, Canada.

Li, Y., Kaminsky, H., Gong, X.Y., Sun, Y.S., Ghuzi, M., and Sadighian, A. (2021). What Affects Dewatering Performance of High Density Slurry? Materials, 11: 761-777.

Li, Y. Kaminsky, H., Romero, C., Gong, X.Y., Ghuzi, M., and Tacas, J. (2021). Assessing Dewatering Performance of Treated Fluid Fine Tailings With A Modified Bench-Scale Filter Press. Proceedings of Tailings and Mine Waste 2021 Conference, Banff, Canada, November 7-10, 2021.

Li, Y., Kaminsky, H., Sadighian, A., Sun, Y.S., Murphy, F., Gong, X.Y., Ghuzi, M., and Rima, U. (2022). Impact of Chemical and Physical Treatments on Freeze-Thaw Dewatering of Fluid Fine Tailings. Cold Regions Science and Technology 193, 103385.

Omotoso, O., Revington, A., Melanson, A., Kone, M., Guest, R., and Wells, S. (2017). Treatment of Thick Fine Tailings Including Chemical Immobilization, Polymer Flocculation and Dewatering. Canadian Patent 2921835.

Roche, C., Thygesen, K., and Baker, E. (2017). Mine Tailings Storage: Safety Is No Accident. A UNEP Rapid Response Assessment. United Nations Environment Programme and GRID-Arendal, Nairobi and Arendal.

Sadighian, A., Revington, A., Kaminsky, H., Moyls, B., Li, Y., and Omotoso, O. (2008). A New Protocol to Assess the Quality of Tailings Flocculation/Coagulation: A Collaboration to Improve Tailings Treatment at Suncor Energy. Proceedings of Sixth International Oil Sands Tailings, Edmonton, Alberta, December 9-12, 2008. 81 pp.

Vedoy, D.R.L., Soares, J.B.P. (2015). Water-Soluble Polymers for Oil Sands Tailings Treatment: A Review. Can. J. Chem. Eng. 93: 889-904.

Disclaimer

NOVEL DEWATERING TECHNOLOGY TO TREAT FLUID FINE TAILINGS

William Florman[1], Christian Kujawa[1], Gavin Freeman[1], David Sego[2], Orest Ilkiw[3] and Enzo Peluso[3]
[1]Extrakt Process Solutions LLC, Kentucky, USA
[2]University of Alberta, Edmonton, Alberta, Canada
[3] Bantrel, Calgary, Alberta, Canada

ABSTRACT

The Canadian oil sands operators have implemented various tailings technologies over the past 25 years with mixed success. Challenges with high capital and operating costs as well as less-than-optimal results in progressing the ultimate reclamation of the mine site have been seen.

The dewatering of fluid fine tailings (FFT) from the Canadian oil sands operations is a critical issue. The objective of enabling low risk sustainable mine closures has driven evaluation of technologies ranging from atmospheric drying to managing a fluid slurry. Process options such as thickening, centrifugation and filtration have also been pursued. Depending upon the tailings structure the ability to drain the fluid tailings and thereby reduce the potential tailings liquefaction is an important consideration.

Extrakt Process Solutions has developed a novel and effective high-rate dewatering technology, named TNS™; which is able to treat high clay content streams (<20-micron clays and slimes).

This novel dewatering technology quickly and efficiently dewaters tailings to produce a potentially stackable material while producing a clear supernatant water stream. The test program carried out using a laboratory centrifuge confirmed these benefits. These results show well-defined dewatering patterns when using TNS™ technology, including a very fast rate of initial water release, in which most of the water is released shortly after treatment. As a result, an additional 18% volume of FFT can be accumulated in the deposit in this first year of operation. Furthermore, the robustness of this technology was demonstrated by the low impact of mixing shear and precise chemical dosing on its performance.

As a result of the efficient tailings dewatering, TNS™ technology offers flexibility for placement strategy and final configuration of the tailing's storage facilities. Data using other feedstocks suggest that improvements in solid-liquid separation efficiency make it possible to achieve stackable geo-stable filtered tailings.

INTRODUCTION

Background

Extracting bitumen from surface-mined oil sands produces a fluid tailings stream that is composed of sand, fines (silts and clays), water and lesser amounts of unrecovered bitumen. Due to the poor engineering properties of these fluid tailings, its storage and disposal is a challenge for industry.

Oil sands tailings management is a major challenge for the Alberta oil sands industry, both operationally and in meeting the environmental protection requirements and government regulations (Znidarcic and Miller 2011).

Much of the FFT is stored in tailings ponds, where consolidation of the fine solids progresses at a very slow rate. Experimental data collected by multiple Alberta oil sands operators shows that solid particles in a tailings pond settle out of the water at different rates that are related to particle size and density, sand particles settle quickly while smaller particles (44μm or less) tend to remain suspended for decades (AER 2021).

Oil sand operators have been seeking innovative ways to manage fluid fine tailings; most of the Alberta oil sands companies have been considering multiple options. The existing tailings dewatering technologies involve making use of natural dewatering processes (e.g., self-weight consolidation, atmospheric drying, freeze/thawing) and physical/mechanical processes (e.g., filtration, centrifugation,) or mixing tailings with varied materials and wastes to improve the dewatering (BGC, 2010). Some of these technologies have proven difficult and costly to implement commercially while others have limited applicability. The trend in the mining companies beyond the oil sands industry is often towards higher performing

thickeners and filters to produce geo-stable tailings. Often the best available practice is to dewater the tailings via filtration to reduce the potential for liquefaction, which can lead to dam failures and potentially devastating consequences.

The objective of government regulations in this area is to establish directives to manage and decrease liability and environmental risk associated with the accumulation of fluid on the landscape. In 2015, the "*Lower Athabasca Region: Tailings Management Framework for Mineable Oil Sands (TMF)"* was released to increase the rate of reclamation and enhance the reduction of tailings ponds, while Directive 085 (2016 and updated in 2017) under the *Oil Sands Conservation Act* enables implementation of TMF and aligns with the *Lower Athabasca Regional Plan* (AER 2021).

TNS™ Technology

Extract Process Solution has developed a tailings solution which is applicable for the oil sand tailings. The TNS™ technology is novel, economic and sustainable solution for the treatment of fluid fine tailings. This technology excels where other processes often fail in its ability to process and dewater high clay content streams (<20µm clays and slimes).

TNS™ technology is an innovative approach to solids/liquids separation that overcome one of the fundamental technical issues with clay slurries from oil sands tailings (low permeability and high compressibility). TNS™ differs from conventional technologies by disrupting the surface charge of the particles, by altering and/or destabilizing the surface electrical charge of the particles, allowing the particles to coagulate, flocculate and consolidate.

The innovative chemical formulation of the TNS™ solution allows a faster and more efficient phase separation (solid/liquid) than other formulations on the market.

The sedimentation test results of Mature Fluid Tailings (MFT) show that the TNS™ treated sample mixtures settle very rapidly compared to the untreated MFT that takes years to settle.

Figure 1 shows that the untreated and TNS™ treated Albian MFT undergo similar compression when subjected load (effective stress). This shows that these materials release water in a similar manner when deposited and placed under self-weight or additional load.

However, Figure 2 shows that they dewater to achieve this final volume quite differently. This is important since the time to release water and thus increase the solids content governs the storage volume required and the strength that develops within the deposit. Figure 2 shows that the TNS™ treated MFT maintains a hydraulic conductivity about 10 time greater than the untreated Albian MFT for all void ratios. Comparison of the TNS™ treated MFT with the conventional polymer treated MFT shows that while the conventional polymer treated MFT may have greater hydraulic conductivity for void ratios higher than between 2.5, the TNS™ treated MFT shows significantly higher hydraulic conductivity at lower void ratios. The important observation from this test data is that while the conventional polymer-only treatment dewaters well to ~54% solids content, but above 54% solids content, the TNS™ treatment will dewater the sample much faster. It should be noted that at a void ratio of 1.5 (solids content 64%) the TNS™ treated MFT sample dewaters approximately 10 times faster than the conventional polymer-only treated MFT sample.

Figure 3 shows the variation of shear strength with decreasing void ratio for the TNS™ treated samples. At a void ratio of 1.5 (64 % solids content) the material has strengths of between 4 and 7 kPa. This strength increases to between 20 and 40 kPa as the void ratio decreases to 1.0 (73 % solid content) for the samples tested. This strength data indicates that at solid contents greater than 70% the strength is sufficient to cap a deposit and the begin reclamation using lightweight earth moving equipment

Florman et al (2021), uses the TNS™ technology to treat a different variety of tailings (phosphate slimes tailings and porphyry copper tailings) using different operational parameters for the solids-liquid separation. Also, a high-level economic analysis demonstrates the efficacy of TNS™ technology as a sustainable solution to solids-liquid separation applications to achieve stackable filtered tailings

Extract Process Solution (2017) carried out a MFT treatment pilot plant study in Canada. In these test runs two tanks, one containing MFT and the second containing the TNS, were connected to a positive displacement pump. The slurry was then pumped through a length of pipe. The length of pipe could be varied to change mixing time. The slurry then emptied onto a simple wooden flume to allow gravity drainage, as shown in Figure 4. As the TNS/MFT slurry emerged from the mixing pipe onto the flume

the solids had already partially separated from liquids. The latter appeared to be a mostly clear stream with minimal suspended particles. The slurry quickly drained to give a material that could be pressed by hand to give a cohesive solid ball, again with a solids content of 75%, as shown in Figure 5.

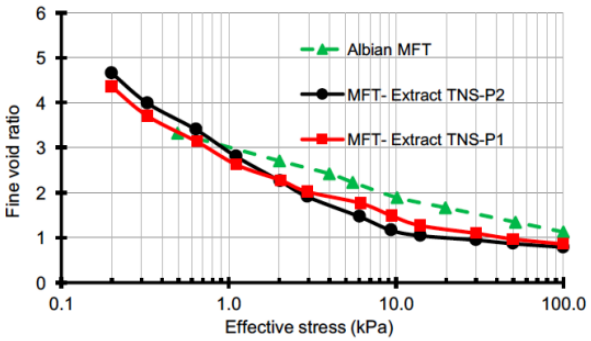

Figure 1. Compressibility Curves for TNS™-MFT-Polymer Samples and Untreated Albian MFT

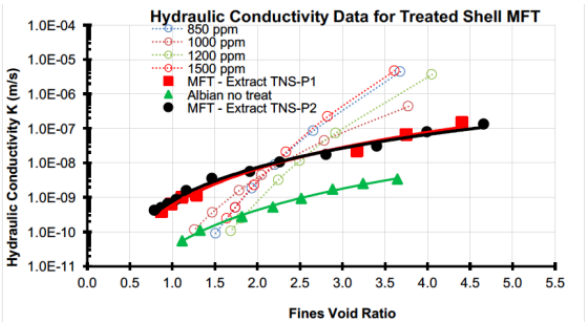

Figure 2. Hydraulic Conductivity Curves for TNS™-MFT_Polymer Samples, Untreated MFT and Polymer Treated MFT Albain Samples (Bereket et al 2017)

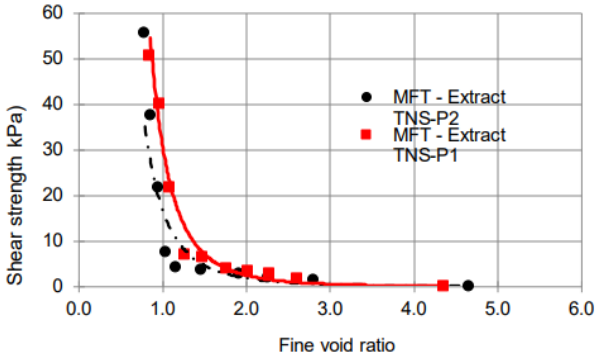

Figure 3. Shear Strength vs Fine Void Ratio Curves for Extrakt TNS™-P1 and Extrakt TNS™-P2 Samples.

Figure 4. Slurry emerging from the pipes on a flume to give simple gravity dewatering

Figure 5. Slurry squeeze by hand to give a consolidate material with a solids content of about 75 wt.%

These results suggest that this novel dewatering technology (TNS™) potentially can produce a stackable stable tailing with enhanced water recovery. TNS™ technology allows for flexibility in placement strategy and final configuration of the tailing's storage facilities.

As is well known, each oil sand operator has a different configuration and logistics regarding the tailing ponds; the interconnection between each pond is different. Therefore, the best process configuration of the TNS™ technology for each case will depend on the characteristics of the material to be processed and the final purpose for the water recovered using this technology. As part of this paper a generic TNS™ process configuration, will be discussed.

SETTLEMENT AND CONSOLIDATION TESTING

A test program was conducted using a bench-top centrifuge developed by Suncor and COANDA. These centrifuges are used for modelling self-weight consolidation and for deriving consolidation parameters of soft soils. Experimental data obtained using this equipment has confirmed the prior results from conventional large strain consolidation tests.

The flocculants/polymer type has a major influence on the settling/consolidation behavior of the tailings; the main objective of this study is to compare these performances of a commercial flocculant used in the oil sand operation against the TNS™ technology.

MATERIALS and METHODS

Materials Characterization

The basis properties of fine fluid tailing (FFT) material and the oil sands process water (OSPW) used for this investigation are reported in Tables 1 and 2.

Apparatus

The bench-top centrifuge allows four samples to be evaluated simultaneously using the same FFT while the laser displacement sensor follows the consolidation process as a function of time. The machine is coupled with centrifuge modelling techniques software that can predict the consolidation process in an accelerated manner. One hour of centrifugation time is equivalent to approximately one year of self-weight consolidation in the field. Details about centrifugation of oil sands tailings is available in several references (Sorta et al 2012), (Sorta et al 2013), (Sorta et al 2015), (Sorta, 2015).

Table 1. FFT Basic Properties

Properties	FFT
Density, g/ml	1.217
Bitumen Content, wt%	1.7
Solid Content, wt%	28.6
MBI, meg/100ml	11.1
Clay Content, wt% (< 2 μm)	80
Fines Content, wt% (< 44 μm)	96.9
Sand to Fines Ratio	0.03

Table 2. Oil Sands Process Water (OSPW) - Basic Properties

Properties	OSPW
pH	7.9
Conductivity, μS/cm	1580
Hardness ($CaCO_3$), mg/L	245
Alkalinity (Total as $CaCO_3$), mg/L	405
Total Dissolved Solids (TDS), mg/L	1120
Naphthenic Acids, mg/L	22

Test Methodology

Both reagents (commercial polymer and TNS™ solution) were prepared using OSPW and following the typical standard procedure provided by the polymers' manufacturer. The polymer solution dosage was prepared in the typical range used in the day-to-day operation of the Canadian oil sands industry (1000 to 1400 g/tonne of tailings solids). While for the TNS™ solution, different dosages were explored.

The preparation of the samples to be evaluated in the centrifuge were prepared following the same procedure for both reagents. The FFT material and the reagents are properly mixed and then transfer to the centrifuge container as shown in Figure 6. The sample volume for all centrifugation experiments was the same.

Different centrifugation times were explored to simulate different field consolation times, all data as a function of time for the separation process were recorded numerically and via video (Figure 7).

After centrifugation, the liquid and solids are separated, the supernatant liquid is collected and weighed, while the solid is transferred to a previously weighed container and then dried in a conventional oven at 105 ºC for 24 hours (Figure 8). The weight of the container, the weight of the material transferred to the container as well as the weight of the container with the dried solid are recorded to determine the final of solids content at different centrifugation times.

The polymer dosage in the TNS™ solution is between 13 to 50 wt.% lower than the typical industrial dosage, depending on the process configuration and characteristics of the material to be processed.

Figure 6. FFT treated with TNS™ solution before centrifugation

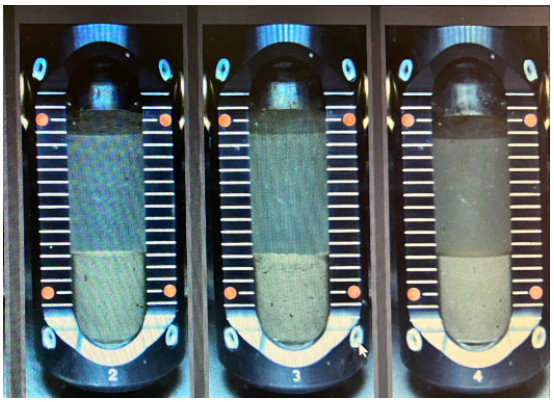

Figure 7. Treated FFT samples during centrifugation / consolidation process

Figure 8. Centrifuge Cake sample for FFT samples treated with TNS™ Technology

RESULTS AND DISCUSSION

Effect of TNS™ Solution Dosage

The first set of centrifuge experiments evaluated the effect of TNS™ concentration on the final solid concentration in the cake. Three TNS™ dosage were tested, one the normal TNS™ dosage while the other two has a TNS™ concentration ± 8% with respect at the normal TNS™ dosage.

The results of the impact of TNS™ dosage on the solid concentration for the 1 year of consolidation (1 hour of centrifuge) are plotted in Figure 9. The overall performance of the TNS™ technology is slightly affected by TNS™ dosage, however in the early stages on the consolidation process (before 60 days) the higher TNS™ dosage show a higher dewatering rate than the other two dosages.

Other criteria used to select the proper TNS™ dosage was the clarity of the supernatant water obtained after the centrifugation process, for the three dosages used, no significant differences were observed.

Figure 9 illustrates one of the potential benefits of the TNS™ technology, which is to provide some flexibility on the day-to-day operation in terms of adjusting chemical dosage without large performance impacts. This ability to treat FFT with a range of dosages will be beneficial in dealing with of the expected variability of the FFT composition.

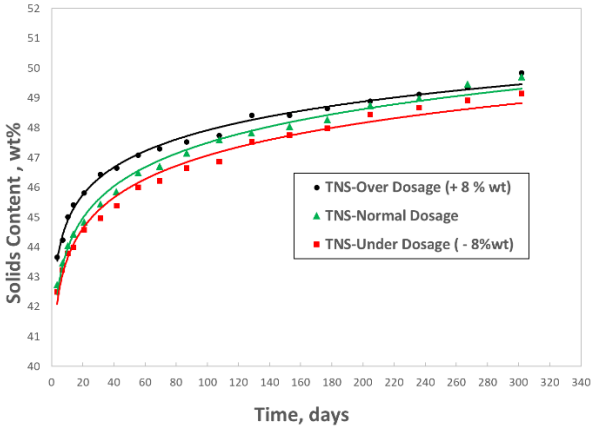

Figure 9. Effect of TNS™ solution dosage on final slurry solids content.

Effect of Mixing Shear on TNS™ Performance

One of the operator's challenges during the flocculation of a FFT stream is to prevent the flocs from breaking from applied shear during the mixing of the chemical and the FFT; this can be a critical issue depending on the FFT-chemistry interaction, and in certain cases leads to an irreversible loss of flocculation and dewatering performance.

Using the normal dose of TNS™, another series of experiments was carried out in which the impact of mixing shear on the final solids content of the cake was investigated. In the first FFT sample, the TNS™ solution was added and mixed until the first flocs appeared. While in the second sample (at the same dose of TNS™) the mixing time was much longer and more intense."

Figure 10 shows that the TNS™ technology shows a similar dewatering rate for both cases with normal flocs obtained under the most typical mixing conditions currently used in the industry, while “small flocs” are obtained under longer time at higher mixing shear.
This result show that the difference in mixing shear has a minimal impact on TNS™ treated FFT performance (final solid content in the cake) which is also indicative of the robustness of this technology.

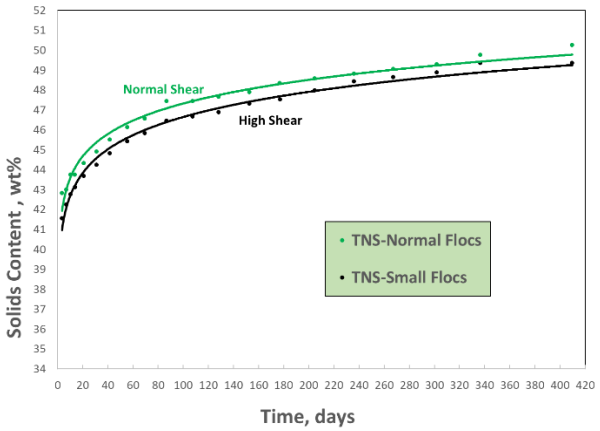

Figure 10. Effect of Mixing Shear on TNS™ Performance

Effect of TNS™ on the Tailings Dewatering Process

The impact of TNS™ technology on the dewatering process of an FFT material was investigated and compared with the results obtained for an FFT treated with a commercial polymer. Figure 11 summarizes the results for both reagents for a centrifugation time equivalent over 14 years of consolidation time. For reference, centrifugation data for untreated FFT is also presented. The same FFT is used in all cases.

Figure 11 shows an initial rapid dewatering process for the TNS™ technology compared to the conventional polymer, as expected, the performance of both reagents exceeds the performance of the untreated FFT. Figure 11 also shows that after extended periods of time (over 14 years) all treatments reach similar solids contents.
From Figure 11, the dewatering process with the TNS™ technology can be described in 3 regions:

1. A very rapid rate of dewatering shortly after treatment. This is one of the main advantages of this technology.

2. The observed efficient water release for the next ~two years resulting in the rapid plateauing of slurry solids contents.

3. The ultimate final solids content is attained after only 3 years, with only minor change thereafter.

Another qualitative observation from these experiments is the consistency of the solid cake after the centrifugation process (Figure 8). The solid cake obtained for the TNS™ technology has more structural integrity and is easier to transfer from the centrifugate container to the aluminum pad than the cake from conventional polymer; finally, as expected an unstable solid cake was obtained from centrifuged untreated FFT.

Certainly, further characterization is required to quantify this experimental observation about the characteristics of the solids obtained from the TNS™ technology, but this initial observation may be related to the ability to support sustained drainage from a deposit, also suggesting that TNS™ treatment of high-clay material may allow FFT to be processed efficiently in a thickener or pressure filter.

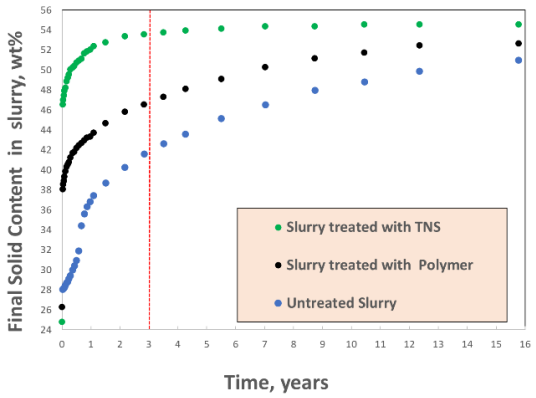

Figure 11. Effect of Reagents on FFT Consolidation Process as Function of Time (prolonged period of time).

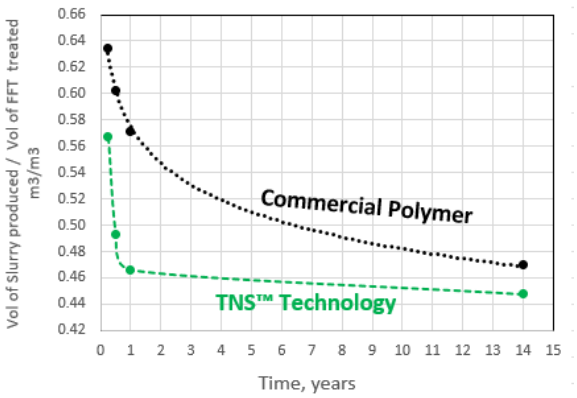

Figure 12. Impact of TNS™ Technology on the Management of Tailings Ponds Capacity.

Impact of TNS™ Technology of the Oil Sands Tailings Ponds Facilities

It is reasonable to expect that rapid dewatering process will have an impact on the management of the storage capacity with time.

To estimate this potential impact a very simple mathematical model has been developed using the experimental data obtained from the centrifugation experiments. The ratio between the volume of slurry produced after centrifugation (SV2) and the volume of slurry treated (SV1) is estimated.

A lower ratio between slurry volume produced (after centrifugation) and the volume of FFT treated implies a lower amount of material to be deposited in the deep deposit. In other words, TNS™ technology enables better management of the tailings deposit capacity as a function of time as shown in Figure 12.

For 1 year period

- The TNS™ technology will produce 0.47m^3 of slurry per m^3 of FFT treated while the conventional polymer will produce 0.57m^3 of slurry per m^3 of FFT treated
- As result an additional 18% volume of FFT can be accumulated over this frame time (1 year) for the same deep deposit capacity when using TNS™ technology.

For the whole 14-year period

- TNS™ technology will allow an additional 38% volume of FFT over this frame time (14 years) for the same deposit capacity.

Process Configuration for the TNS™ Technology

TNS™ technology can be adapted to different process configurations that are defined based on client requirement and needs.

Figure 13 shows a generic process configuration for the TNS™ technology based on the results obtained in this work.

- The tailing pond material (FFT) is mixed with the TNS™ solution, different mixing choices can be explored (pipeline turbulence, online mixer, etc.).
- In the context of this work, a centrifugal device was used as a solids-liquid separation device; however, other solids-liquid separation equipment and a combination of them (thickener, vacuum filter, filter press, or pressure filter) have been used on a small scale with similar feedstock in the facilities of Extrakt in the USA. Selection of solids/liquid separation devices depends on the client's need and the final disposal of the solid (for instance deep deposit).
- The Water Treatment System (WTS) has the main objective of delivering a water to specification for future intended purpose. One of the advantages of the TNS™ technology is the clarity of the supernatant stream obtained after solid-liquid separation step, which will have a positive impact on the design of the WTS.
- Another important consideration in the design of the WTS is the expectations and needs of the

client regarding the management and use of the water recovered through the treatment process. This can range from being used for utility services (steam production), use in the bitumen extraction process or to be discharged back to environment.

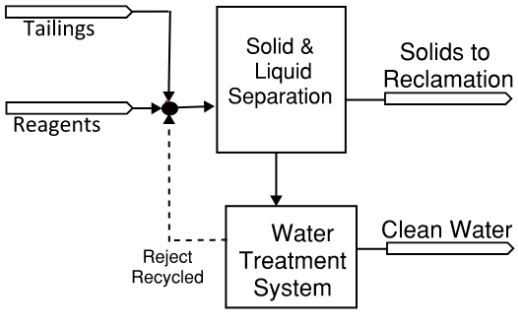

Figure 13. Generic Process Configuration for the TNS™ Technology

SUMMARY

- Accelerated Dewatering 18% additional water release achieved in first year compared to commercial polymer technology. TNS™ technology offers a high rate of initial dewatering.
- TNS™ technology allows better management of deposit capacity by producing a lower settled slurry volume per volume of FFT treated.
- This enhances Deep Deposit performance reducing volume contained and significantly increasing volume of expressed water for recycle or treatment.
- TNS™ treatment produces a clear supernatant water stream indicating high fines capture.
- TNS™ technology reduces the time required to complete solids settlement and consolidation in the ponds.
- TNS™ technology offers flexibility in dosage and shear used during the mixing with the FFT stream providing a large, robust operating window.
- Plug and Play TNS™ technology can be implemented using a similar process as currently being used for FFT treatment and can use a single injection point for reagent addition.
- High reproducibility for the TNS™ technology ensures a reliable day-to day operation with a robust and flexible process.
- High water release provides the operator with ability to reduce long term lability associated with slower consolidation rates.

FUTURE WORK

The TNS™ technology is ready to be implemented in the Alberta oil sands industry.

From previous results and those reported in this work, it can be concluded that the TNS™ technology has a significant impact on changing the behavior of FFT solids and opens the possibility of improving the operation of centrifuges, thickeners, and pressure filters, as well as for deep cohesive deposits for the Alberta oil sands industry.

Extrakt has the technological and infrastructure capacity to perform test work relevant to the unique situation of each oil sands operator.

ACKNOWLEDEMENTS

The authors acknowledge the technical support and assistance of Ian Mountain, we greatly appreciate his help in facilitating the lab scale centrifuge tests.

REFERENCES

Alberta Energy Regulator (2021), State of Fluid Tailings Management for Mineable Oil Sands, 2020, September 2021

BGC Engineering Inc, (2010). Oil Sands Tailings Technology Review. OSRIN, University of Alberta, School of Energy and the Environment, Edmonton, Alberta. OSRIN Report No. TR-1. 136 pp

Bereket, T.F, Wilson, G.W., and Simms, P.H. 2018. Assessment of self-weight consolidation of flocculated fluid fine tailings under various environmental Condition. 21st International Seminar on Paste and Thickened Tailings, Perth, Australia., DOI:10.36487/ACG_rep/1805_23_Fisseha

Florman, W., Kujawa, C., Sego, D., (2021) Novel Dewatering Technology by Extrakt Process Solutions, Tailings Mine Waste Conference, Banff 07-10 Nov 2021

Sorta, A. R., Sego C. D., and Wilson W. (2012), Effect of thixotropy and segregation on centrifuge modelling. International Journal of Physical Modelling in Geotechnics, V4, Issue 4, 143-161.

Sorta, A. R. (2015) Centrifugal Modelling of Oil Sands tailings Consolidation, PhD Dissertation Thesis in Geotechnical Engineering Department of Civil and Environmental Engineering, University of Alberta.

Znidarcic, D., and Miller, R. (2011), Consolidation testing of Oil Sand Fine Tailings, Proceedings Tailings and Mine Waste 2011, Vancouver, BC, November 6 to 9, 2011.

Sorta, A. R., Sego C. D., and Wilson W (2013)., Behaviour of oil sands fines-sand mixture tailings. Surface Mining Vol 4 No4, , V4, 265-280.

Sorta, A. R., Sego C. D., and Wilson W., (2015) Physical modelling of oil sands tailings consolidation. International Journal of Physical Modelling in Geotechnics.

APPLICATION OF NANOCELLULOSE FILAMENT (NFC) IN ENHANCING THE GEOTECHNICAL PROPERTIES OF OIL SANDS TAILINGS

Yunhai Zhang[1], Nicholas Beier[1], Keith Gourlay[2] and Gurminder Minhas[2]
[1]University of Alberta, Edmonton, Alberta, Canada
[2]Performance BioFilaments Inc, Canada

ABSTRACT

Nanofibrillated Cellulose (NFC), a novel renewable material derived from wood fibers, has unique mechanical, rheological, and physical properties. Its high performance has been proven in various applications when used as reinforcement agents or rheology modifiers. This study evaluated the performance of NFC to enhance the strength and density of the oil sands tailings, in support of reclamation and closure of the tailings deposits. The dose based on dry solid mass in fluid fine tailings (FFT) samples, mixing speed, and mixing time were evaluated to understand the impact of NFC combining different sample preparation processes on the behavior of FFT related to reclamation. The short-term settling characteristics and the long-term geotechnical behavior of different tailings mixtures including NFC amended FFT, NFC amended centrifuged FFT, and FFT treated by NFC combined with polymer were evaluated. The laboratory results indicated that by adding NFC, the yield stress, and the long-term shear strength gain under atmospheric drying of FFT samples were enhanced. A target NFC: FFT dose of 0.2 wt.% was determined as a promising long-term shear strength gain was observed under atmospheric drying. However, the settling behavior and the freeze-thaw were not effectively enhanced by adding NFC.

INTRODUCTION

The oil sands industry has produced a significant volume of tailings for over half a century. In northern Alberta, the footprint of tailings storage facilities is over 220 km^2. These fine-grained slurry wastes, known as fluid fine tailings (FFT), have now surpassed 1 billion cubic meters and continuously growing each year (AER report 2019). With a solid content of about 35 wt.% (by mass) and containing mainly silts and dispersed clays, FFT presents a poor consolidation property and low strength. Various coagulants and flocculants have been evaluated as dewatering aids to reduce the overall volume and increase the strength of tailings for effective reclamation (Matthews et al. 2002, Jeeravipoolvarn 2009, Beier et al. 2013, Beveridge et al. 2015, Mizani et al. 2017, Afacan et al. 2019). Due to the bridging effect of the amendments, tailings particles bond together, forming a non-segregating deposit, which enhances the water release, consolidation rate, and strength gain of tailings (Vajihinejad et al. 2018). Similar to the coagulants and flocculants, nanocellulose can also function as a cross-linking agent attributed to the bridging effect in some scenarios (Martin et al. 2017). Considering the bridging effect and the eco-friendly nature of nanocellulose, it may be regarded as a potential reinforcing agent to improve the dewatering rate and the subsequent strength of oil sand tailings.

Nanocellulose can be obtained from the most abundant renewable and biodegradable material on earth - plants - such as cotton, wheat, banana, bamboo, any softwood or hardwood, etc (Besbes et al. 2011, Khalil et al. 2016, Mousa et al. 2016, Martin 2017). As described in the review articles, nanocellulose can typically be grouped into three categories according to the material sources and manufacturing processes, namely cellulose nanocrystals (CNC), Bacterial nanocellulose (BNC), and fibrillated nanocellulose (NFC) (Klemm et al. 2011, Moon et al. 2011, Osong et al. 2015, Moon et al. 2016, Martin 2017). In this study, the material employed to treat FFT is limited to NFC, which is disintegrated from wood fibers into 10-100 nm in width and up to several micrometers in length using mechanical shearing with some pretreatment strategies (Zimmermann et al. 2010, Oson et al. 2015). For example, Besbes et al. (2011) isolated nanofibrillated cellulose with a diameter ranging from 5 to 20 nm from alfa, eucalyptus, and pine fibers using the homogenization process and peroxidization of the source fibers.

With a larger aspect ratio and the ability to form a highly porous mesh, NFC shows high water-trapping properties, low gas permeability, high elastic modulus, and high tensile strength. The application of NFC has extended to various areas, including transparent films (Bhatnagar and Sain 2005, Fernandes et al. 2010), packaging materials (Khali et al. 2016, Ferrer et al. 2017), and the papermaking industry (Brodin et al. 2014, Osong et al. 2015, Bouf et al. 2016), etc. Bhatnagar and Sain (2005) tested the stiffness and mechanical strength of NFC reinforced polyvinyl alcohol (PVA), and the results showed a remarkable reinforcing potential of the nanofibers. In the geotechnical field, nanofibrillated cellulose has been increasingly recognized as a potential reinforcement agent. Correia et al (2018) studied the capability of NFC in particle packing and decreasing the growth rate of microcracks in cement-based material, the high specific surface area of NFC improves the adhesion between the cement particles. Hunek et al (2019) discovered that it directly influences the resistance to freeze-thaw of concretes by adding NFC. Stanislas et al (2022) demonstrated that adding NFC in earth-based composites satisfactorily increases the density and flexural strength and decreases the apparent void volume of the composite.

In addition to the lower cost, higher strength, better thermal properties, and biodegradability, another feature of NFC is to form an aqueous gel, which indicates NFC could be used as a potential rheological modifier or rheology-control agent in many areas (Zimmermann et al. 2004). Studies of the advances in NFC derived from different sources for water treatment have been highlighted (Shak et al, 2018, Salam et al, 2021). Salama et al (2021) investigated the adsorption properties of NFC in water wastewater treatment, this nanoflocculant induces the bridging of the suspended particles in contaminated wastewater by neutralizing the surface charge of the particles, which exhibits a similar bridging effect of polymer used in tailings dewatering. However, there is no case being reported using NFC or nanocellulose in tailings management. Given the extraordinary properties of NFC regarding strength and unique aspect ratio, the objective of the research is to explore the use of NFC as a potential strategy for the reclamation of tailings storage facilities.

MATERIAL AND METHODS

Characterization of Oil Sands Tailings

The oil sand fine tailings samples used in the study were characterized to determine the physical, chemical, and mineralogy properties. The FFT sample had a liquid limit of 52%, and contained 3.9% hydrocarbons, while the centrifuged FFT (cFFT) was characterized to have a liquid limit of 57%, and hydrocarbon content of 5.7 %. From the grain size distribution analysis, FFT had a sand-to-fines ratio (SFR) of 0.06 with a fine content (≤ 0.044 mm) of 94%, as centrifuged tailings had an SFR of 0.15 with a fine content of 87%. According to Methylene Blue Index (MBI) analysis and the X-ray diffraction (XRD) analysis, FFT samples used in this study had a clay content of 54 % which mainly consisted of 87 % kaolinite and 13% illite, and centrifuged tailings had a clay content of 35% which mainly consisted of 68% kaolinite and 32% illite. The clay content was determined based on the Methylene Blue Index (MBI) (Kaminsky, 2014). The typical characteristics of FFT and cFFT are listed in Table 1.

Table 1. Summary of characterization properties of tailings

Characteristic	FFT	cFFT
Initial solids content (%)	53	53
Hydrocarbons content (%)	3.9	5.7
Specific gravity	2.20	2.24
Liquid limit (%)	52	57
Plastic limit (%)	32	26
Plasticity index (%)	20	32
Fine content (<0.044 mm) (%)	94	87
Clay content from MBI (%)	54	35

Sample preparation

In this study, the NFC samples were provided by Performance BioFilaments Inc. (PBI). Figure 1 illustrates the process of manufacturing NFC products from forests. The tested oil sands tailings samples were amended with different NFC doses under various mixing conditions to evaluate the NFC treatment process in both short-term and long-term performance including water release and strength gain behavior. The variables investigated including the mass fraction of NFC dilution, NFC: FFT dose, and mixing speed and duration. The received NFC products with an

original mass fraction of 8% were first dispersed to 1 wt.% and 4 wt.% in beakers. The dilutions were stirred for one hour at 200 rpm with a 4-blade impeller and then were sealed for 24 hours to reach an equilibrium status before adding to homogenized tailings. The NFC: FFT doses of 0.2, 0.5, 1.0, 2.0, 5.0, 7.0, and 10.0 wt.% based on the dry mass of the solid were first selected for evaluating the impact on yield stress. The NFC-FFT mixtures were stirred at different mixing speeds of 250, 600, and 900 rpm for 60, 90, and 180s, respectively. In this stage, all the tests were carried out with 33 wt.% solid FFT. Mixed samples were separated and sealed in identical test jars (250 mL). Yield tests using a rheometer (Brookfield DV3T rheometer) were carried out followingly to evaluate the short-term strength of the samples. Subsequently, the dose of 0.25 wt.% was used for evaluating the impact of the mixing time and mixing speed using FFT samples with 33 wt.% and 53 wt.% solid. Settling tests of samples with the NFC: FFT dose of 1.0, 2.5 and 5.0 wt.% prepared using 1 wt.% NFC dilution was also conducted to study the impact of NFC on the settling behavior of FFT.

Long-term Geotechnical Test

The treatment combinations resulted in favorable short-term strength gain and water release were further tested subsequently to determine the long-term geotechnical behavior of NFC amended FFT (NFC-FFT) samples. Atmospheric drying tests and near-surface shear strength tests of these samples were conducted at room temperature (≈ 21 ℃). The daily mass changes were determined to analyze the evaporation behavior of these samples. Meanwhile, a container filled with water of the same volume was placed next to the samples, which served as a control to measure the potential evaporation (PE) and then compared it with the actual evaporation (AE) of the NFC amended tailings specimen. Either a rheometer or a laboratory vane-shear apparatus was employed to determine the shear strength of the samples on different days. The shear strength was measured at a depth of approximately 3 cm in the samples. The rheometer was more accurate to determine the shear strength below 8 kPa, while the vane-shear apparatus was used to determine the shear strength over 8 kPa. Furthermore, to evaluate the

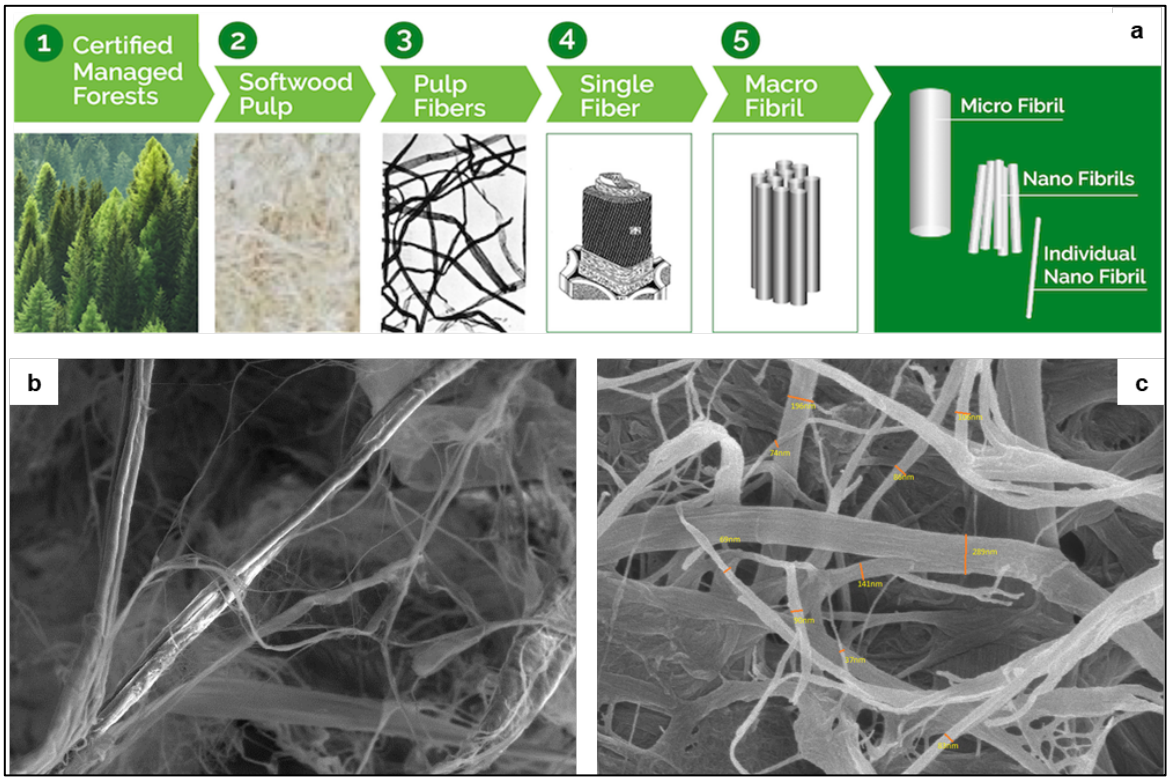

Figure 1. **Schematic description of the manufacturing and structure of NFC** (provided by BioFilaments Inc.) **b** and **c** are the scanning electron microscope (SEM) images reveal the network of micro-fibrils and nano-fibrils

potential performance of NFC in combination with other tailings treatment technologies, the NFC dilutions were added to cFFT samples and polymer-treated FFT (fFFT) samples prepared using the same FFT samples. Freeze-thaw tests were also conducted on these samples with the subsequent shear strength measurements in addition to the tests demonstrated above. The temperature range of freeze-thaw was from -15 ℃ to room temperature.

RESULTS AND DISCUSSION

NFC dilution, dose, and mixing parameter

To investigate the impact of the mass fraction of NFC dilution, the energy required (quantified as mixing speed and mixing time) for dispersing the NFC dilutions and the yield stress of the NFC-FFT samples were evaluated. The 8 wt.% NFC product was diluted with deionized water. A mixing speed of 250 rpm was first selected to prepare NFC-FFT mixtures based on the advice from PBI to minimize the damage to the NFC fibers due to shearing. Figure 2 concludes the measured yield stress of the samples prepared at the NFC: FFT dose of 0.5 wt.%, 1 wt.%, and 5 wt.% using 1 wt.%, 4 wt.%, and 8 wt.% NFC dilutions over 20 days. The samples were sealed in identical 300 mL containers to prevent drying in the atmosphere. The yield stress of the samples prepared using 4 wt.% NFC dilution was 7 Pa, 11.6 Pa, and 46.3 Pa at each dose, respectively. The yield stress of samples mixed with 1 wt.% NFC dilution was 9.2 Pa, 8.6 Pa, and 15.7 Pa at each dose. Meanwhile, the yield stress of the samples prepared using the original NFC product with a mass fraction of 8% reached the yield stress of 5 Pa, 41.2 Pa, and 99.2 at each NFC: FFT dose. The yield stress of the samples with lower FNC: FFT doses of 0.5 wt.% and 1 wt.% are similarly lower despite the mass fraction of the NFC dilutions used. A higher yield stress gain was observed in samples mixed with 8 wt.% NFC dilution. However, homogeneously dispersing the 8 wt.% NFC dilution in FFT was more challenging compared to NFC dilution with a lower mass fraction. Meanwhile, a considerable amount of water was added to the samples when the 1 wt.% NFC dilution was used, which is adverse for sample dewatering. Therefore, 4 wt.% NFC dilution was determined as a target dilution as it required less effort to prepare and mix with FFT compared to 8 wt.% NFC dilution. In addition, it also introduced relatively less water compared to 1 wt.% NFC dilution.

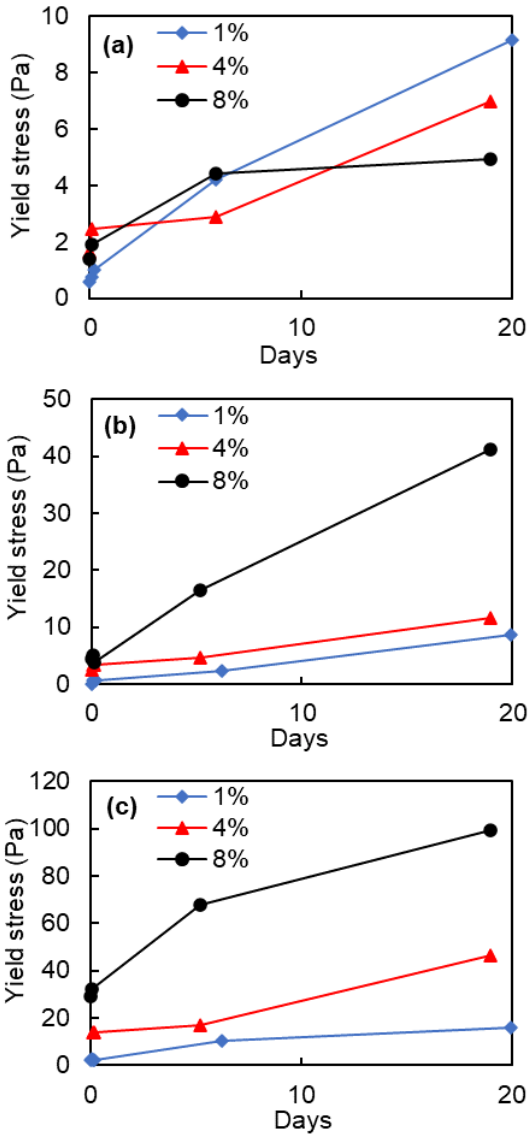

Figure 2. Yield stress of NFC-FFT samples with 33 wt.% solid at different doses: (a) 0.5 wt.%, (b) 1 wt.%, (c) 5 wt.%

Based on the dry mass of the FFT samples, 7 NFC- FFT samples with doses varying from 0.2 wt.% to 10 wt.% were prepared using the same method mentioned above for evaluating the yield stress gain. Figure 3 shows the results of the yield stress of the 7 samples prepared using 4 wt.%

NFC dilution over 20 days. The yield stress increases as the dose increases. Less variation in yield stress was observed at lower doses (below 5 wt.%), however, at higher doses (over 5 wt.%), the yield stress started decreasing after the peak values were reached. Considering the economic purpose of the field application, the NFC: FFT dose of 2.5 wt.% was chosen as the target dose for the next tests.

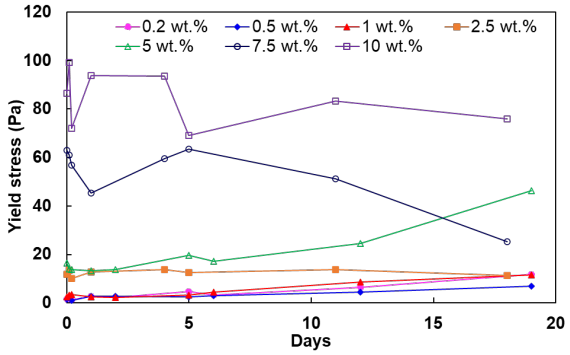

Figure 3. Yield stress of NFC-FFT samples with 33 wt.% solid at different dose

Dispersion of the NFC within an amended NFC-FFT mixture is critical to maximizing the treatment potential. Based on the study (Reis et al. 2016, Mizani et al. 2013) on the impact of mixing speed and mixing duration on polymer-treated oil sands tailings, mixing speeds of 600 rpm and 900 rpm were investigated subsequently in this study. Results of the samples with 33 wt.% solid at the NFC: FFT dose of 2.5 wt.% trails mixed for less than 90s and 180 s are shown in Figure 4. (Note: after the screening tests, the mixing speed of 250 rpm was excluded due to the lowest stress gain of the samples at 11-days.) Similarly, tests were conducted on samples with 53 wt.% solid at the NFC: FFT dose of 2.5 wt.% mixed for 180 s and 360 s. The results are illustrated in Figure 5.

From Figure 4 and Figure 5, it can be seen NFC-FFT samples mixed at a mixing speed of 600 rpm show a higher stress gain compared to samples prepared at 900 rpm. In addition, for samples mixed at 600 rpm, as the mixing time increases, the initial yield stress is increased. However, the final stress gain at 11-days of samples with a solid content of 33 wt.% are roughly the same as the mixing time increases from 90 s to 180 s. In Figure 5, as the samples with 53 wt.% solid mixed at 600 rpm for 360 s, the initial yield stress increases from 254 Pa to 334 Pa, while the stress gain at 11-days increases from 463 Pa to 602 Pa compared to samples mixed for 180 s. Besides, it is worth noting that for samples mixed at 900 rpm, the yield stress is only boosted for the sample with 33 wt.% solid when the mixing time increases.

It can be concluded that the initial yield stress of NFC-FFT samples is increased by 30% to 50 % with an increased mixing time when mixed at 600 s. However, for samples of 33 wt.% solid, it seems that 90 s is sufficient for sample preparation as the stress gain at 11-days are approximately the same with the sample mixed for 180 s. For samples with higher solid content of 52 wt.%, it is obvious that a longer mixing duration is required to homogenize the NFC in FFT. A peak yield stress of 600 Pa was observed when the sample was mixed at 600 rpm for 360 seconds. In summary, 600 rpm was targeted for further tests as it resulted in a higher initial yield stress. As for mixing time, 180 s was selected for samples of 33 wt.% solid, and 360 s is selected for samples of 53 wt.%.

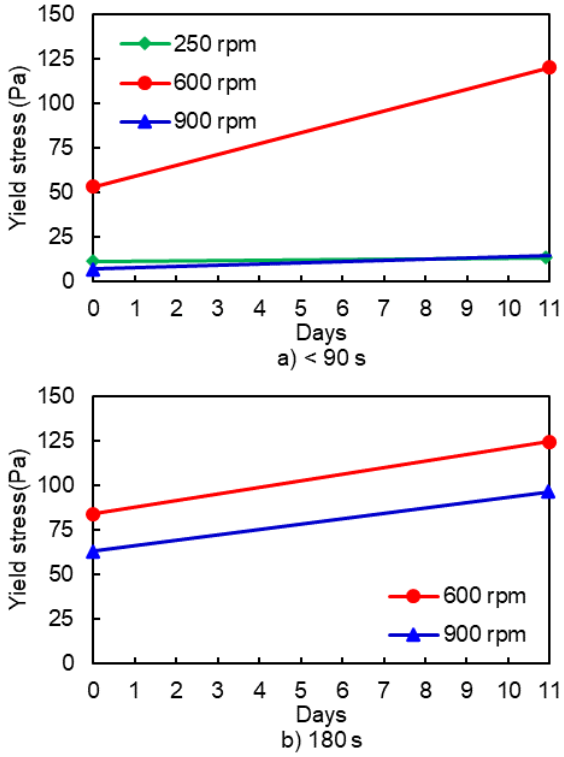

Figure 4. Stress gain of NFC-FFT with 33 wt.% solid mixed at 250, 600 and 900 rpm

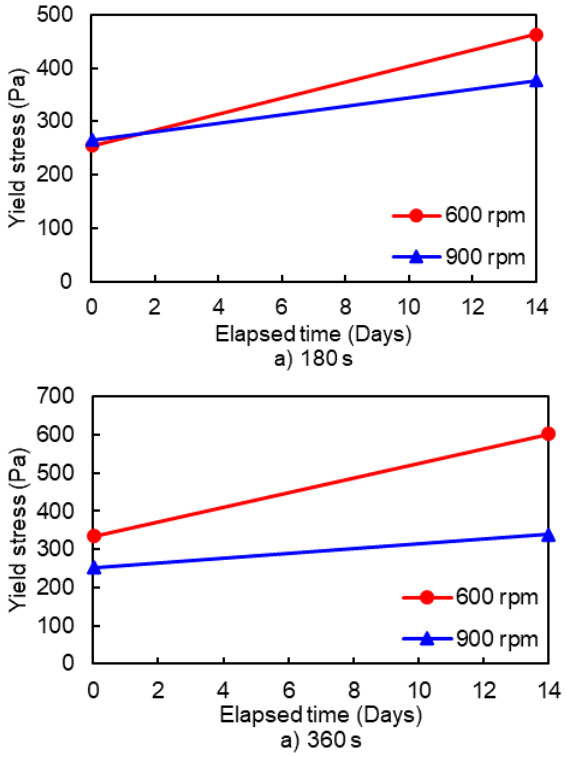

Figure 5. Stress gain of NFC-FFT with 53 wt.% solid mixed at 600 rpm and 900 rpm

Settling Test

In the earlier stage of screening the NFC dilution, samples prepared using 1 wt.% NFC dilution exhibited an improved performance in the settling behavior. Figure 6 demonstrates the settling tests with around 1 L~ 1.2 L NFC-FFT samples dosed at 1, 2.5, and 5 wt.% using 1 wt.% NFC dilution. Figure 7 shows the results of the solid content and net water release (NWR) of the samples over a time of period of 8 days. The samples at a higher dose of 5 wt.% yield a higher degree of settlement of approximately 50% initial height of the column. A significant increase of 71.3 % in the solid content of 5 wt.% dose sample is observed, while the change of the solid content is only 5.3 % and 17 % respectively of samples dosed at 1 wt.% and 2.5 wt.%. A similar trend of the NWR is observed that the highest NWR is 82 % sample dosed at 5 wt.%, while it remains negative for the samples with lower doses. In addition, it was noted that the turbidity of the release water over the sample at the dose of 5.0 wt.% is much higher than that of the other two samples. The higher dose seems not sufficient in capturing the fine particles in the mixture. The higher turbidity release water would not fulfill the requirement of water recycling.

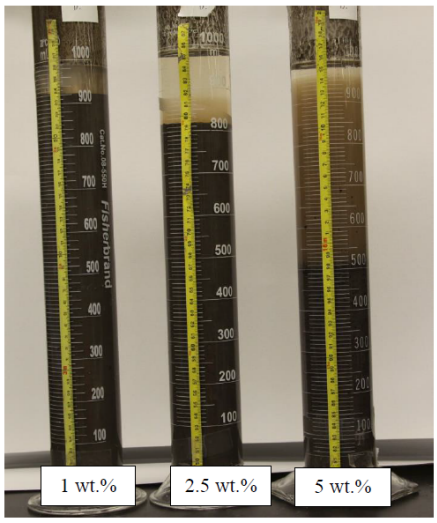

Figure 6. Settling test of NFC-FFT samples at doses of 1, 2.5 and 5 wt.%

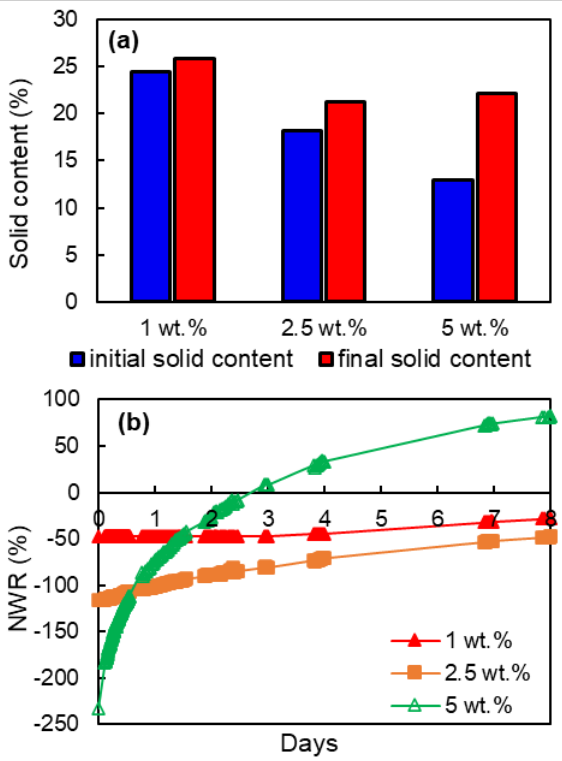

Figure 7. Settlement (a) and NWR (b) of NFC-FFT samples at doses of 1, 2.5 and 5 wt.%

Atmospheric Drying Test

Atmospheric drying tests were conducted to study the drying behavior of NFC-FFT, NFC-cFFT, and NFC-fFFT samples. The solid content of all the samples in this stage of the test was 54 wt.%. The polymer dose used in this study was 850 g/t, which was selected based on the results of previous research (Mizani, 2016). The near-surface shear strength was measured to characterize the long-term shear strength gain of NFC amended tailings during natural drying in the laboratory. The AE/PE over time was calculated and plotted in Figures 8 and 9.

In the early drying stage, the evaporation rate was mainly controlled by the climate condition. Due to the saturation at the surface of the samples, the surface moisture is initially allowed to evaporate at the rate of free water drying, the AE/PE approximately equals 1 (Kabwe et al. 2022). Figure 8 shows, the stable stage of AE/PE of the NFC-FFT samples dosed above 0.2 wt.% are before Day 21, while the stable stage for samples with a lower dose of 0.05 wt.% and 0.1 wt.% are before Day 10. The value of AE/PE of all the samples ranged between 1.0 and 1.6. This deviation can be attributed to variations in the aerodynamic resistance in the air spaces above the water and soil evaporation containers (Wilson et al. 1997). The evaporation rate starts declining at the moment of sample desaturating, where the drying behavior is controlled by the properties of the samples such as hydraulic conductivity. After the declining stage, the samples dry at a relatively lower evaporation rate subsequently when the water availability in the samples remains low, then the drying is controlled by both the climate and the sample's properties. Considering the dewatering rate, the samples prepared at a lower dose between 0.1 wt.% and 1 wt.% yield a relatively higher evaporation rate.

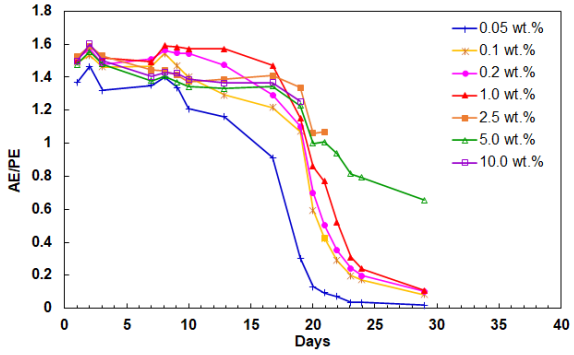

Figure 8. Drying curve of NFC-FFT samples over time

Figure 9 shows the AE/PE versus time for NFC-FFT samples, NFC-cFFT samples, NFC-fFFT samples and FFT samples. In the early drying stage, the AE/PE of the NFC-FFT samples at the dose of 0.2 wt.% and 2.5 wt.% are both around 1.5, which are higher compared to the other samples at the same dose correspondingly. The AE/PE of the NFC-cFFT samples and the NFC-fFFT samples in the early stage are similar, while it starts around 1 and subsequently increases to 1.3 before dropping of the FFT control sample. The temporary increase of AE indicates the formation of cracks at the surface of the FFT sample. NFC-cFFT sample dosed at 0.2 wt.% entered the first transition zone earlier than the other samples even with a lower evaporation rate, which could be attributed to the higher solid content or the lower water availability of the sample. As the dose increased from 0.2 wt.% to 2.5 wt.%, the transition zone or the desaturating point of the NFC-FFT and NFC-cFFT samples were pushed back from day 10 to day 19. However, the desaturating point of NFC-fFFT samples occurred at the same time period on day 19 with an increase in the NFC dose.

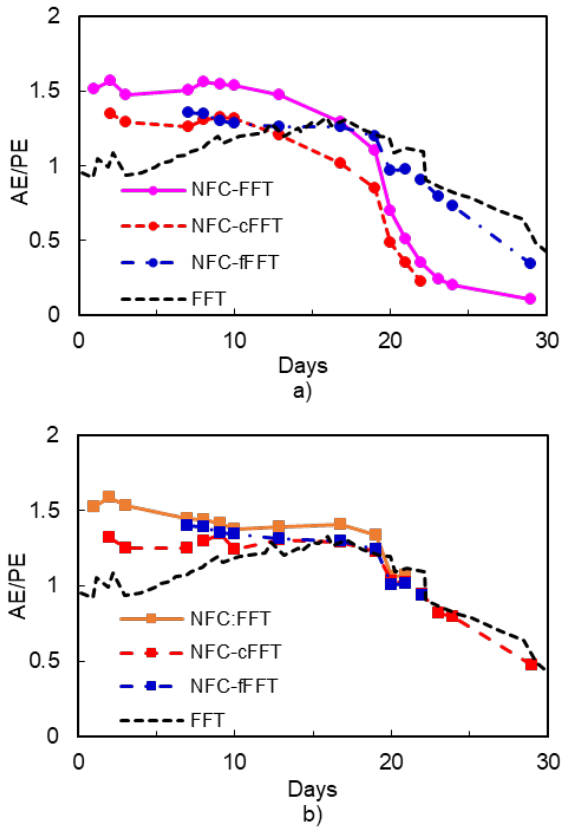

Figure 9. Drying curve of NFC amended FFT, centrifuged FFT and polymer treated FFT with a dose of (a) 0.2 wt.%, (b) 2.5 wt.%

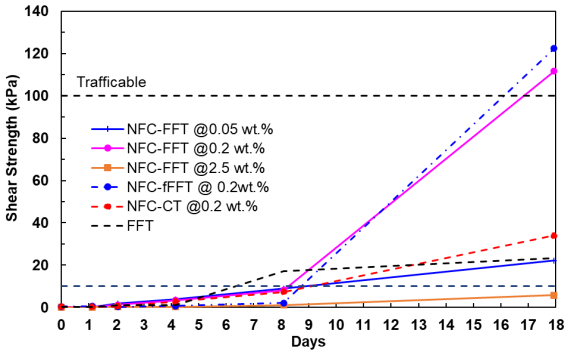

Figure 10. Near-surface shear strength of atmospheric drying samples

Figure 10 shows the shear strength gain of the samples in the atmospheric drying test, the NFC-FFT and the NFC-fFFT samples with the dose of 0.2 wt.% show significant strength gains over 18 days of drying. Both samples reached and exceeded the targeted 100 kPa trafficable shear strength. Meanwhile, the other samples reached the shear strengths between 6 kPa and 34 kPa on day 18. For NFC-FFT samples, the relationship between the NFC dose and the shear strength gain was not strictly positively correlated, which exhibits some similarity to the polymer-treated FFT with a ranged dose. As the NFC: FFT dose increases from 0.05 wt.% to 2.5 wt.%, the shear strength first increases and declines after a peak value of 112 kPa is reached at the dose of 0.2 wt.%. It is assumed that the NFC: FFT dose of 2.5 wt.% probably resulted in the overdosing of the sample. However, the mechanism behind this is unknown. The shear strength of the NFC-cFFT sample is only around 34 kPa, which is unexpectedly lower than that of the NFC-FFT and the NFC-fFFT samples. A potential cause of the lower shear strength gain of the NFC-cFFT samples could possibly be the inconsistent homogenizing of the NFC fibers in the cFFT samples.

Freeze-Thaw Test

Previous research has shown that freeze-thaw process would cause significant dewatering of oil sands tailings (Dawson and Sego, 1993; Johnson et al., 1993, Proskin, 1998). In this study, a radial freeze-thaw set-up was employed to conduct the freeze-thaw tests on 6 samples over - 15 ℃ to 21 ℃. Table 2 shows the sample matrix used in this part of the test. The samples were first frozen at - 15 ℃, once the samples were thawed at room temperature, the released water was removed from the samples, and the yield stress was measured using the rheometer.

Table 2. Freeze-thaw samples matrix

Sample	Sample details
a	NFC-FFT at 2.5 wt.% (FFT began at 53 wt.% solids)
b	NFC-fFFT at 2.5 wt.%, (flocculated FFT prepared using 54 wt.% solids FFT with polymer at 0.04 wt.%)
c	NFC-CT at 2.5 wt.%, (CT began at 48 wt.% solids)
d	FFT, (30 wt.% solids)
e	FFT, (42 wt.% solids)
f	FFT, (53 wt.% solids)

Figure 11 shows that as the increase of the solid content of the FFT samples, a non-linear increase in yield stress can be observed while the thaw strain decreases. The yield stress of the FFT samples increases from 18 Pa at 30 wt.% solid to 314 Pa at 53 wt.% solid with a decline of the thaw strain. This is expected as the increased solid content of material results in lower water contents, thus allowing for higher strengths to be attained. The freeze-thaw strain is 3% of the NFC-FFT sample (a) with 53 wt.% solid, which is slightly lower when compared to 8% of the FFT sample with the same solid content (f). With the comparable solid contents (53 wt.%, 54 wt.%, and 48 wt.%) as well as equivalent freeze-thaw strains (3%, 5%, and 6%), the yield stress of the NFC-FFT sample (a) is 607 Pa followed by 485 Pa and 398 Pa of the NFC-fFFT sample (b) and the NFC-cFFT (c) respectively. However, it should be noted that in Figure 5 the NFC-FFT samples with 53 wt.% solid dosed at 2.5 wt.% reached approximate yield stress of 602 Pa without undergoing the freeze-thaw process. It demonstrates that the impacts of the freeze-thaw process on the NFC-FFT samples regarding yield stress and thaw strain are not appreciable. The yield stress gain of the NFC-FFT samples is mainly due to the addition of NFC rather than a combination with freeze-thaw.

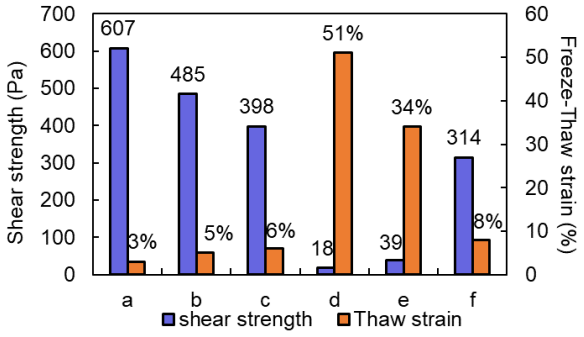

Figure 11. Freeze-Thaw results of samples

CONCLUSION

The amendment of FFT with NFC was investigated to determine the impact on the dewatering behavior and geotechnical properties of oil sands tailings deposits. The findings from this study are summarized below:

1. For samples prepared using 33 wt.% solid FFT, as the dose increased from 0.2 wt.% to 10 wt.%, the initial yield stress of NFC-FFT samples increased. Especially for samples with doses higher than 5 wt.%, however, the yield stress of the NFC-FFT samples decreased over time.

2. Adding NFC is not effective in enhancing the settlement of FFT samples, adding NFC dilution at a higher dose of 5 wt.% could potentially lead to high turbidity of the supernatant.

3. The results of the atmospheric dry tests emphasize that NFC fiber influences the drying rate of the FFT, cFFT, and polymer-treated FFT samples. Dose below 0.2 wt.% would be more effective in accelerating the desaturation of the samples.

4. The NFC-FFT and NFC-fFFT samples dosed at 0.2 wt.% NFC experienced the greatest near-surface shear strength gain. The shear strength of the samples reached and exceeded the 100 kPa trafficable target on day 18.

5. The influence of the freeze-thaw process on the stress gain of FFT samples is inappreciable when combined with adding NFC. Also, the small differences in thaw-strain between NFC amended samples indicate that the freeze-thaw of the NFC-FFT samples was not enhanced by NFC.

ACKNOWLEDGEMENTS

The authors would like to express their gratitude to NSERC and MITACS for their financial support, and to Performance BioFilaments Inc (PBI) for the technical support and the nanocellulose product provided for this project. Meanwhile, great thanks to Kelsey Stienwand and Hilary Smith for their great contribution to the laboratory work and reporting.

REFERENCES

AER report (2019). State of Fluid Tailings Management for Mineable Oil Sands, 2018.

Abdul Khalil, H. P. S., Y. Davoudpour, C. K. Saurabh, M. S. Hossain, A. S. Adnan, R. Dungani, M. T. Paridah, M. Z. Islam Sarker, M. R. N. Fazita, M. I. Syakir and M. K. M. Haafiz (2016). "A review on nanocellulosic fibres as new material for sustainable packaging: Process and applications." Renewable and Sustainable Energy Reviews 64: 823-836.

Afacan, C., R. Narain and J. B. P. Soares (2019). "Water soluble polymeric nanofibres for rapid flocculation and enhanced dewatering of mature fine tailings." The Canadian Journal of Chemical Engineering 98(1): 96-103.

Vajihinejad, V., S. P. Gumfekar, B. Bazoubandi, Z. Rostami Najafabadi and J. B. P. Soares (2018). "Water Soluble Polymer Flocculants: Synthesis, Characterization, and Performance Assessment." Macromolecular Materials and Engineering 304(2).

Beier, N., W. Wilson, A. Dunmola and D. Sego (2013). "Impact of flocculation-based dewatering on the shear strength of oil sands fine tailings." Canadian Geotechnical Journal 50(9): 1001-1007.

Besbes, I., M. R. Vilar and S. Boufi (2011). "Nanofibrillated cellulose from Alfa, Eucalyptus and Pine fibres: Preparation, characteristics and reinforcing potential." Carbohydrate Polymers 86(3): 1198-1206.

Beveridge, A., P. Mutz and D. Reid (2015). Tailings co-disposal case study – art or science? Proceedings of the 18th International Seminar on Paste and Thickened Tailings: 505-520.

Bhatnagar, A. and M. Sain 2005. "Processing of Cellulose Nanofiber-reinforced Composites." Journal of Reinforced Plastics and Composites 24(12): 1259-1268.

Boufi, S., I. Gonzalez, M. Delgado-Aguilar, Q. Tarres, M. A. Pelach and P. Mutje (2016). "Nanofibrillated cellulose as an additive in papermaking process: A review." Carbohydr Polym 154: 151-166.

Brodin, F. W., Ø. W. Gregersen and K. Syverud (2014). "Cellulose nanofibrils: Challenges and possibilities as a paper additive or coating material–A review." Nordic Pulp & Paper Research Journal 29(1): 156-166.

Da Costa Correia, V., S. F. Santos, R. Soares Teixeira and H. Savastano Junior (2018). "Nanofibrillated cellulose and cellulosic pulp for reinforcement of the extruded cement based materials." Construction and Building Materials 160: 376-384.

Danuta Barnat-Hunek, M. S.-C., Monika Jarosz-Hadam, Grzegorz Łagód (2019). “Effect of cellulose nanofibrils and nanocrystals on physical properties of concrete.” Construction and Building Materials 223: 1-11.

Fernandes, S. C. M., C. S. R. Freire, A. J. D. Silvestre, C. Pascoal Neto, A. Gandini, L. A. Berglund and L. Salmén (2010). "Transparent chitosan films reinforced with a high content of nanofibrillated cellulose." Carbohydrate Polymers 81(2): 394-401.

Ferrer, A., L. Pal and M. Hubbe (2017). "Nanocellulose in packaging: Advances in barrier layer technologies." Industrial Crops and Products 95: 574-582

Jeeravipoolvarn, S., Scott, J.D., and Chalaturnyk, R.J. (2009). "Geotechnical characteristics of laboratory in-line thickened oil sands tailings." Proceedings of Tailings and Mine Waste 2009, Banff, Alta., 1–4 November 2009. Information Technology, Creative Media: Vancouver, B.C: pp. 813–828

Klemm, D., F. Kramer, S. Moritz, T. Lindstrom, M. Ankerfors, D. Gray and A. Dorris (2011). "Nanocelluloses: a new family of nature-based materials." Angew Chem Int Ed Engl 50(24): 5438-5466.

'Lokendra Pal a (2017). "Rheology of Nanocellulose-rich Aqueous Suspensions: A Review."

Matthews, J. G., W. H. Shaw, M. D. MacKinnon and R. G. Cuddy (2002). "Development of Composite Tailings Technology at Syncrude." International Journal of Surface Mining, Reclamation and Environment 16(1): 24-39.

Martin A. Hubbe, a. P. T., a Michael Joyce,a Preeti Tyagi,a Margaret Kehoe,a,b Katarina Dimic-Misic,c and Lokendra Pala 2017. "Rheology of Nanocellulose-rich Aqueous Suspensions: A Review."

Matthews, J. G., et al. 2002. "Development of Composite Tailings Technology at Syncrude." International Journal of Surface Mining, Reclamation and Environment 16(1): 24-39.

Mizani, S. (2016). Experimental Study and Surface Deposition Modelling of Amended Oil Sands Tailings Products. PhD, Carleton University.

Mizani, S., et al. 2017. "Rheology for deposition control of polymer-amended oil sands tailings." Rheologica Acta 56(7-8): 623-634.

Moon, R. J., A. Martini, J. Nairn, J. Simonsenf and J. Youngblood (2011). "Cellulose nanomaterials review: structure, properties and nanocomposites." Chem. Soc. Rev 40: 3941-3994.

Moon, R. J., G. T. Schueneman and J. Simonsen (2016). "Overview of Cellulose Nanomaterials, Their Capabilities and Applications." Jom 68(9): 2383-2394.

Mousa, M. H., Y. Dong and I. J. Davies (2016). "Recent advances in bionanocomposites: Preparation, properties, and applications." International Journal of Polymeric Materials and Polymeric Biomaterials 65(5): 225-254.

Osong, S. H., S. Norgren and P. Engstrand (2015). "Processing of wood-based microfibrillated cellulose and nanofibrillated cellulose, and applications relating to papermaking: a review." Cellulose 23(1): 93-123.

Salama, A., R. Abouzeid, W. S. Leong, J. Jeevanandam, P. Samyn, A. Dufresne, M. Bechelany and A. Barhoum (2021). "Nanocellulose-Based Materials for Water Treatment: Adsorption, Photocatalytic Degradation, Disinfection, Antifouling, and Nanofiltration." Nanomaterials (Basel) 11(11).

SavastanoJuniorf, T. T. C. K. R. N. A. M. W. H. M. F. T. A. O. (2022). "Potential of raffia nanofibrillated cellulose as a reinforcement in extruded earth-based materials." Case Studies in Construction Materials Volume 16.

Shak, K. P. Y., Y. L. Pang and S. K. Mah (2018). "Nanocellulose: Recent advances and its prospects in environmental remediation." Beilstein Journal of Nanotechnology 9: 2479-2498.

Zimmermann, T., E. Pöhler and T. Geiger (2004). "Cellulose Fibrils for Polymer Reinforcement." Advanced Engineering Materials 6(9): 754-761.

Dawson, R.F. and Sego, D.C. 1993. Design concepts for thin layered freeze-thaw dewatering systems. In Proceedings of the 46th Canadian Geotechnical Conference, Saskatoon, SK, September 27-29, 1993. Canadian Geotechnical Society, Saskatoon, SK, pp. 283-288.

Johnson, R.L., Pork, P., Allen E.A.D., J., and Koverny, L. 1993. Oil sands sludge dewatering by freezethaw and evaporation. RRTAC 93-8, Alberta Environmental Centre, Edmonton, AB.

Mizani, S., Soleimani, S., and Simms, P. 2013. Effects of polymer dosage on dewaterability, rheology, and spreadability of polymer-amended mature fine tailings. In Proceedings of the 16th International Seminar on Paste and Thickened Tailings, Belo Horizonte, Brazil, June 17-20, 2013. Australian Centre for Geomechanics, Perth, Australia, pp. 117-131.

Proskin, S., Sego, D., and Alostaz, M. 2012. Oil sands MFT properties and freeze-thaw effects. Journal of Cold Regions Engineering, 26(2): 29-54.

Reis, L.G., Oliveira, R.S., Palhares, T.N., Spinelli, L.S., Lucas, E.F., Vedoy, D.R.L., Asare, E., and Soares, J.B.P. 2016. Using acrylamide/propylene oxide copolymers to dewater and densify mature fine tailings. Mineral Engineering, 95: 29-39.

Kabwe, L.K., Wilson, G.W., Beier, N.A., and Barsi, D. 2022. Effects of sand and flyash on unsaturated soil properties and drying rate of oil sands tailings. In Proceedings of the Twenty-Fifth International Conference on Tailings and Mine Waste, Banff, Alberta, Canada, November 7-10, 2021. University of Alberta Geotechnical Centre & SOTRF, pp. 892-903.

Wilson, G.W., Fredlund, D.G., and Barbour, S.L. 1997. The effect of soil suction on evaporative fluxes from soil surfaces. Canadian Geotechnical Journal, 34(1): 145-155.

Wilson, G.W., Fredlund, D.G., and Barbour, S.L. 1994. Coupled soil-atmosphere modelling for soil evaporation. Canadian Geotechnical Journal, 31(2): 151-161.

HIGH-FINES SAND TAILINGS AS A NOVEL OIL SANDS TAILINGS TREATMENT PROCESS

Y. Simon Sun[1], Emily Devereux[1], Heather Kaminsky[1], Mitchell Catling[2]
[1]Northern Alberta Institute of Technology, Edmonton, Alberta, Canada
[2]BASF Corporation, Tucson, Arizona, United States of America

ABSTRACT

Extracting bitumen from Canada's oil sands generates large volumes of fluid fine tailings (FFT), a waste material that presents significant environmental and economic challenges to consolidation and remediation. Chemical company BASF developed a novel technology known as High-Fines Sand Tailings (HFST), which combines FFT with coarse sand and two reagents to create a substrate composed of fine particles filling the interstitial voids between successively larger particles. Given the highly variable nature of FFT, operability testing was conducted to understand the impact of sand and FFT characteristics, reagent dosages, shearing time, and sand-to-fines ratio (SFR) on the performance of the technology.

Pressure filtration results indicated that at optimal dosage, HFST-treated FFT had the potential to release water up to 50 times faster than untreated FFT. Underdosed samples released water twice as quickly as untreated materials. Unlike incumbent polymer technologies, HFST was insensitive to overdosing. Performance of the HFST technology was not significantly impacted by clay content, but type of sand used as well as the water chemistry of the FFT and process effluent water (PEW) affected the required reagent dosages. Both sand types used had good performance at SFR 2, with the acid generating sand being optimal at SFR 2 and the non-acid generating sand performing even better at SFR 3. The treated substrate showed increased signs of fines segregation when exposed to 300s of shearing versus 30s. A conservative estimate showed that with sufficiently dosed reagent, the clay capture for all HFST-treated materials was over 96%.

INTRODUCTION

Mining and processing minerals generate a waste stream commonly known as tailings. In Alberta's oil sands sector, fluid fine tailings (FFT) are a complex, problematic material consisting primarily of water and fine clay particles (Dhadli et al., 2012) that require extensive and expensive dewatering treatments to target reclamation objectives and process water recycling. Due to environmental, economic, and social pressures, oil sand producers in Alberta are motivated to reduce FFT inventories and reclaim land currently occupied by fluid tailings. However, the reclamation of oil sands tailings is accompanied by significant challenges. Current industry practices of building tailings containment facilities carry extreme risk as a single dam failure would be catastrophic. Alternatives in the form of end-pit lakes introduce other complexities, such as the need to maintain a freshwater cap, and the risk of methane production. As many oil sands mines are quickly approaching end-of-life, the requirement for tailings to reach a "ready-to-reclaim" status as outlined by the Alberta Energy Regulator's Directive 85 (Alberta Energy Regulator, 2016) has become a priority.

Few of the oil sands industries' implemented tailings treatment technologies have achieved reclamation goals thus far. Chemical company BASF has developed a novel physio-chemical tailings treatment technology called "High Fines Sand Tailings" (HFST) that combines FFT, coarse sand particles, and two reagents to form a highly water-permeable matrix that also traps fines. Laboratory tests conducted by BASF from September 2017 to February 2020 indicate clear potential towards creating upland landforms in compliance with the ready-to-reclaim criteria outlined by the Alberta Energy Regulator (AER). The technology bears some resemblance to composite tailings (CT) or non-segregating tailings (NST), but it operates at a lower sand content than typical CT or NST. The intent of BASF's technology is to create stable aggregates of sand and flocculated clays, transforming large fluid tailings ponds into dry landforms that can be reclaimed using conventional land reclamation techniques. The direct treatment of recombined oil sands waste achieved by HFST has potential to significantly reduce greenhouse gas (GHG) emissions associated with material rehandling and need for water covers associated with current oil sands

tailings treatments. Furthermore, the process creates an opportunity for optimizing tailings storage areas thereby limiting land disturbance while reducing existing and future liabilities associated with fluid fine tailings on oil sands surface mines.

The NAIT Technology Access Centre for Oil Sands Sustainability has been evaluating the efficacy of the HFST technology, providing a critical assessment of the technology's promises and shortcomings though an operability study. To be considered successful, the HFST process would need to demonstrate resilience by achieving acceptable performance indicators under a wide range of process conditions, as lack of process robustness and control have been identified as critical weaknesses in other sand-based tailings treatment technologies. The key performance indicators evaluated over this study were the solids content achievable in the filter cake following pressure filtration, the clay capture within the treated substrate, and the mitigation of segregation. The objective of the evaluation at bench scale was to assess the ability of the HFST process to accommodate changes in reagent dosage, mixing intensity, and FFT feed characteristics.

EXPERIMENTAL METHOD

Materials

Three types of FFT were chosen for this study to represent a range of clay content based on Methylene Blue Index (MBI), an estimate of clay% derived empirically from x-ray diffraction and particle size distribution (Equation 1) (Sethi, 1995)

$$\%clay = \frac{MBI+0.04}{0.14} \quad [1]$$

The FFTs were combined with one of two process effluent waters (PEWs) based on shared process source. FFT-1, with a mid-range MBI of 6.2, was paired with PEW-1. FFT-3 was sourced from the same operation, and was also combined with PEW-3, and had a high MBI value of 12.8. FFT-2 had the lowest MBI of the FFTs in this study at 5.6 and was paired with PEW-2. Initially, the study evaluated just one type of sand. However, it was discovered during early tests that the sand produced acid when exposed to process water (acid generating sand, AGS), and significantly influenced flocculation performance and required dosages. A second sand was subsequently sourced and verified to be a non-acid generating sand (NAGS). The majority of the operability investigation was conducted using NAGS. The novel HFST process relied on two reagents – DP-OMC-1509 (henceforth known as "polymer") and DP-OMC-1510 (henceforth known as "Nexus reagent"). Reagent storage and preparation protocols followed instructions provided by BASF.

Characterization

All FFTs, PEWs, and sands were characterized using pH, electrical conductivity (EC), and leachate assessed for major cations and anions using ion chromatography (IC). In addition, FFT and sand were further characterized using the Dean and Stark analysis (Dean & Stark, 1920), MBI (Currie et al., 2014; Kaminsky, 2014), and particle size distribution (PSD) (Currie et al., 2015). Sand-to-fines ratio (SFR) is defined by Equation 2, where fines are defined as particles passing through a 44µm sieve.

$$SFR = \frac{1-fines\ wt\%}{fines\ wt\%} \quad [2]$$

Key characterization details are shown in Tables 1-3.

Table 1. Key characterization items for FFT.

Item	FFT-1	FFT-2	FFT-3
MBI	6.2±0.16	5.6±0.16	12.8±0.69
Solid%	24.0±0.28	44.88±0.24	18.92±0.004
Water%	73.15±0.49	54.74±0.35	80.52±0.05
Bit.%	1.71±0.57	0.94±0	0.86±0.003
SFR	0.29	0.99	0.07
pH	7.81±0.49	7.62±0.056	7.55±0.02
EC[µS/cm]	1201±47	1390±5.2	1496.6±20.9
SAR	15.9	5.8	9.4
CST	719.32±27.24	1249.93±22.3	397.87±32.19

Table 2. Key characterization items for sand.

Item	AGS	NAGS
pH	2.2	6.7
EC [µS/cm]	331	1945
Solid%	97.4	96.4
Water%	3.1	3.1
Bitumen%	0.2	0.2

Table 3: Particle size distribution details for FFT and sand.

Item	D_{10}[µm]	D_{50}[µm]	D_{60}[µm]	D_{90}[µm]
FFT-1	4.77	12.71	17.80	74.42
FFT-2	6.00	20.45	75.13	192.16
FFT-3	4.21	10.52	12.40	27.70
AGS	109.90	252.93	258.85	392.61
NAGS	75.51	127.91	129.69	191.30

Equipment

A Heidolph Hei-Torque 100 Precision Base overhead mixer with a flat blade impeller was used to mix the substrate at a controlled speed during the flocculation process. Specific details for mixing vessel dimensions and reagent injection methods and locations are withheld to preserve confidentiality. Specific resistance to filtration (SRF) testing (Li, Kaminsky, Romero, et al., 2021) was performed using a modified OFITE Low Pressure Filter Press assembly using carbon dioxide bulbs. The pressure filter cup consisted of a stainless-steel test cell with a 250µm screen. No filter paper was used as part of the setup to provide a more challenging test when evaluating for fines capture. A photo of the SRF assembly is shown in Figure 1.

Figure 1. SRF assembly with scale.

Samples were dried for solids content determination using an oven set to 105°C. The SRF cakes were weighed on a laboratory top-loading scale with an accuracy of 0.01g. The settling column sediment and supernatant water, as well as the SRF release water, were weighed on an analytical balance with an accuracy of 0.001g.
The Triton Type 319 multi-purpose capillary suction time (CST) device, with Triton default CST paper and 18 mm diameter funnels, were used for the CST tests on the settling column sediments. To determine the turbidity level of the supernatant column water, a clarity wedge with readings up to 46 was used. Supernatant column water colour was determined using an in-house water colour reference scale, shown in Figure 2.

Procedures

Flocculation procedures, including reagent preparation and details related to injection location and mixing, have been withheld to preserve confidentiality. Following flocculation, 300g of HFST-treated material was transferred into the test cell using a small sieve. WinWedge software was used to record the weight of released water each minute as the sample was filtered for at least 10 minutes under an applied pressure of 30psi. Following pressure filtration, the SRF filter cake was transferred to an aluminum pan for determination of solids content by oven drying. For samples pressed for longer than 10 minutes, the solid content at the 10-minute mark was back calculated. The released filtrate water was also subsampled for solids content measurement, done by drying the samples overnight in an oven set to 105°C.

The flocculated substrate left over after SRF subsampling was transferred into a transparent 1L settling column. As the time required to load the SRF was variable, the settling column was capped and inverted once to simulate initial deposition. The total sample level in the column was marked and the mudline tracked at 1 minute, 10 minutes, 30 minutes, 24 hours, and 1 week. Photos of the settling columns were taken after 24 hours and 1 week of settling, at which the columns were dismantled. During dismantling, the supernatant water was decanted from the settling column, subsampled for solid content determination, and its turbidity was assessed using a clarity wedge. Supernatant colour was assessed using an internal standard colour scale reference (Figure 2).

While high/dark coloured water is not necessarily a concern for process recycle, it can be an indicator that the water is problematic for environmental release. However, the testing required for evaluation of eco-toxicological properties falls beyond the scope of the present study.

Upon column dismantling, sediment was removed from the column and the top and bottom 4cm of treated materials were sampled into separate containers. Homogenized subsamples were taken for CST testing and to determine their solid content by drying the sample overnight in an oven set to 105°C.

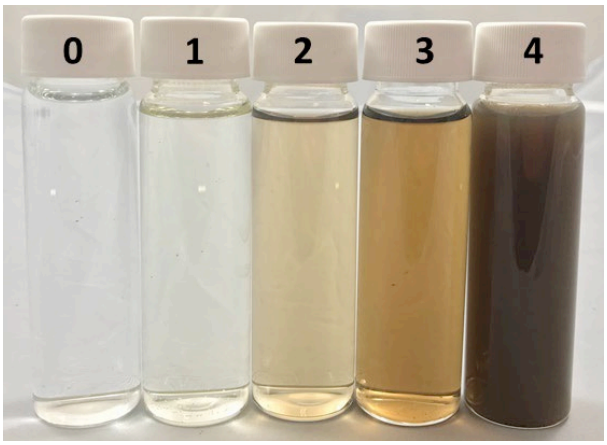

Figure 2. Supernatant colour scale reference.

Test conditions

A partial factorial study was designed to assess the impact of FFT clay content, sand type, sand-to-fines ratio (SFR), dosage of each of the two chemical reagents, and shearing time on HFST performance. SFRs of 1, 2, and 3 were initially evaluated, with a target optimal at SFR 2. SFR 1.5 was later added as a partial factorial level to assess performance at slightly below-spec SFR. A 5-point polymer dose sweep was used to assess flocculant requirements for optimal performance, but it was quickly determined that flocculant dosage depended heavily on the type of sand used. For NAGS, polymer doses were 150ppm; 300ppm; 450ppm; 600ppm; 750ppm. For the relatively few experiment runs using AGS, a significantly higher polymer dose sweep was used (900ppm; 1050ppm; 1200ppm; 1500ppm; 1800ppm). To evaluate the effect of the Nexus reagent, Nexus dose was varied between 50ppm and 150ppm. For both polymer and Nexus, dosages are based on the total solids within the given substrate. To assess the ability of HFST-treated materials to withstand increased shearing, mixing times of 30s vs 300s were compared.

Prior to flocculation each substrate was prepared to be 35wt% solids, while obeying the target SFR.

Key performance indicators

In this study, the SRF pressure filter was used to provide an index to assess short- and long-term dewatering. Running the test for 10 minutes at 30psi allowed for rapid screening of how easily water was released from treated substrates. Based on criteria initially outlined by BASF, HFST-treated material is considered optimal if the SRF cake exceeds 65wt% solids following a 10-minute press at 30psi. Solids in the release water should not exceed 0.5wt%. Treatment results were considered marginally acceptable if the SRF cake solids surpassed 50wt% after a 10-minute press at 30psi with solid content in the release water under 1.0wt%. To assess for fines segregation, no filter paper was added in the SRF device. Instead, only the 250µm mesh providing bottom containment of the sample tested in the SRF was used.

Following one week of settling, columns containing HFST-treated material were dismantled. Solid content and capillary suction time (CST) of the top 4cm and bottom 4cm of the settled bed of treated materials was compared. Low solid content at the sediment top and high solid content at the sediment bottom indicated poor fines capture, subsequent segregation, and increased concentration of sand at the bottom of the column. The ratio of the solids content between column bottom and top was considered optimal if it fell below 1.1, and marginally acceptable if it fell below 1.3. A ratio of solids content between column bottom and top more than 1.3 was an indicator of significant segregation of clay from sand and therefore unacceptable performance.

Although not the primary focus of this study, release water colour was also assessed at the time of column dismantling. Based on the scale provided in Figure 2, colour between 0 and 2 were optimal, 3 was acceptable, and 4 was unacceptable.

RESULTS AND DISCUSSION

Impact of polymer dose

To be a robust process, HFST must not be significantly negatively impacted by polymer overdose. A range of five polymer dosages was defined to be centered around the expected optimal dose, and increased or decreased by 150ppm per step increment. Unlike many other tailings flocculation applications, reagent dosing for HFST is based on total solids, instead of clay-based dosing, allowing for more straightforward dose calculation.

Figure 3 shows the SRF cake solids and solids content of release water solid content as a function of polymer dose. The shaded green and yellow areas on the graph denote the areas of optimal (green) and marginally acceptable (yellow) performance, respectively. Reagent dosages are

based on total solids in substrate. As most of the testing was done using NAGS, only the dose range relevant to NAGS is displayed. SRF performance results indicate that 150ppm of polymer is underdosed, and insufficient to achieve target performance by either SRF cake or release water KPIs.

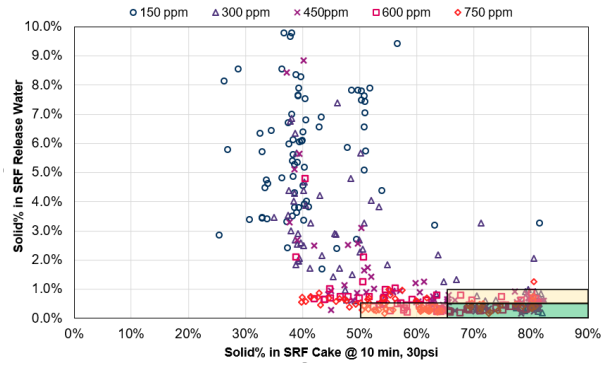

Figure 3. Key performance indicators derived from SRF, based on polymer dose.

As polymer dose increased, solid content in SRF release water decreased indicating more effective fines capture. Polymer doses of 450ppm, 600ppm and 750ppm performed best overall, with over 70% of the tested conditions achieving acceptable criteria. Figure 4 shows a comparison of sediment solid content based on sampling location for the five polymer doses tested with NAGS. A higher solid content at the sediment bottom indicates segregation, where coarse sand and fine clays have separated in the column.

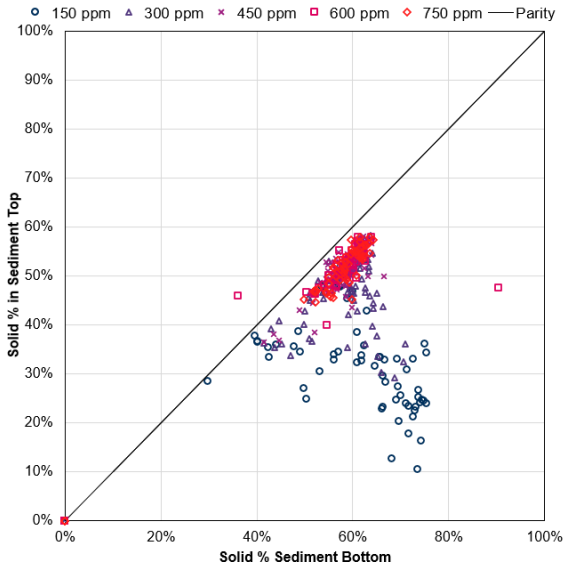

Figure 4. Key performance indicators derived from settling column, based on polymer dose.

Fines segregation is most consistently apparent for 150ppm and 300ppm polymer dosages. This observation is consistent with the previously discussed SRF KPIs, confirming that 150ppm of polymer is an insufficient dose to achieve proper flocculation. At 450ppm, 600ppm, and 750ppm polymer dosages, the solids content at the sediment top and bottom tended to be more comparable. However, they are not expected to be identical as the sediment at the bottom of each column is further compressed by the 7-10cm of solids that rest on top of the materials at the bottom of the column.

Coloured release water was consistently observed in HFST testing with the NAGS, with supernatant colour becoming apparent at optimal dose and growing darker as polymer dose increased. The effect was seen in all three FFTs, though it was most apparent for FFT-3. Figure 5 compares a 5-dose polymer sweep in ascending dosage for each of the three FFTs.

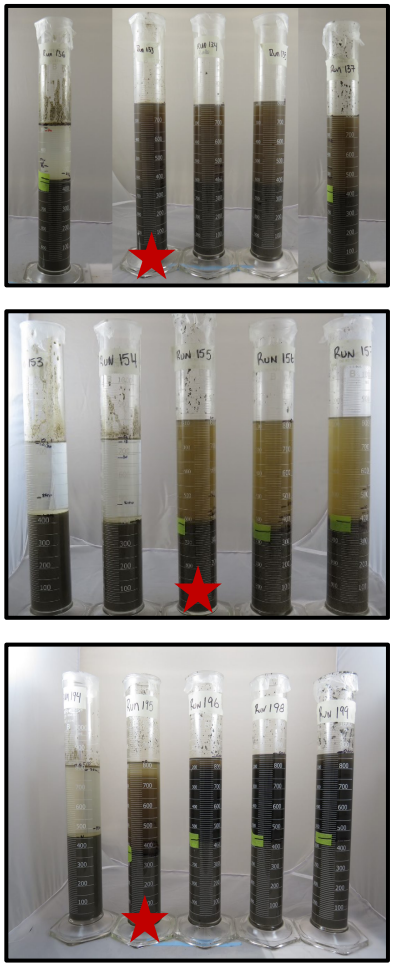

Figure 5. Dark release water at optimal and overdose for FFT-1 (top), FFT-2 (middle), and FFT-3 (bottom). Star symbol indicates optimal dose.

It should be noted that following a very limited preliminary investigation, the darker supernatant colour is not due to suspended particles, since in most cases, the solid content in the supernatant remained below 0.5wt%. Testing of the dark release water using a coagulant that targets organic material indicates the colour may be due to the presence of some organic substance, though investigations are still ongoing.

When combining results from SRF and settling column, a polymer dosage of 150ppm was generally insufficient to achieve adequate flocculation and often resulted in failure. As polymer dose increased, performance increased. When paired with the NAGS, 450ppm was observed to be the optimal polymer dose. As polymer became overdosed, it should be emphasized that SRF and settling column solid content and segregation performance remained strong, with supernatant colour as the detriment. Increasing polymer dose from the typical optimum of 450ppm to 750ppm did not have a detrimental effect on filter cake and sediment performance, despite this representing a 67% overdose. This observation suggests the HFST process exhibits a broad acceptable dose window and is resilient to overdosing. In this way, HFST contrasts with typical FFT flocculation, as increasing polymer dose by 50% over optimal historically results in poor performance (Li, Kaminsky, Gong, et al., 2021).

Impact of FFT type

Three FFTs were tested in this study spanning three levels of MBI and sources from two different oil sands operators. FFT-1 and FFT-3 were obtained from the first source, with MBI of 7.6 and 13, respectively. FFT-2 originated from a different site, with a relatively low MBI value of 5.6. Figure 6 describes the performance of the three tailings samples based on solid content of the SRF cake after 10 minutes of pressing, and solid content in the release water. As previously discussed, experiment runs where polymer was insufficiently dosed performed poorly for all FFTs tested and are excluded from the analysis.

Although all three FFT types display the potential to give optimal results, FFT-1 performance was most likely to fall outside the range of acceptability. Only 66% of conditions tested with FFT-1 meet passing criteria based on SRF results even after the polymer underdosed runs were removed from consideration. Conversely, the low-MBI FFT-2 provided acceptable results in 93% of the optimal- and overdosed-polymer conditions.

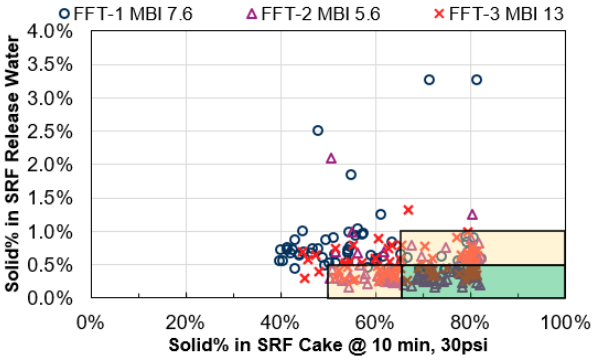

Figure 6. Key performance indicators derived from SRF, based on FFT type. Samples with underdosed polymer excluded.

When comparing the three FFTs tested, clay content is unlikely to fully explain the differences in performance, as the worst performing FFT-1 exhibited a mid-range MBI. FFT-1 had the highest sodium absorption ratio (SAR) of the 3 FFTs tested. FFT-1 and 3 have a SAR above 9 which is a known threshold for coagulating vs dispersing behavior. This difference in water chemistry may have led to a more dispersive environment and hampered fines capture. FFT-2 performed the best when comparing the overall KPIs.

Impact of shear

To understand the ability for HFST-treated tailings to withstand shear, two mixing times were defined following the addition of Nexus reagent and polymer. Table 4 shows the percentage of test conditions which belong to each settling column sediment category, where R represents the ratio between solid% of the bottom portion of sediment vs solid% of the top portion. When R falls between 0.9 and 1.1, minimal segregation is observed and performance is optimal. R values between 1.1 and 1.3 were considered to be marginally acceptable, but R exceeding 1.3 indicates significantly more solids at the bottom of the column, and segregation has occurred. For consistency, only substrates with SFR 2 were included in this analysis.

For each of the three FFTs, the percentage of settling columns achieving optimal segregation performance decreased significantly when shearing time increased from 30s to 300s. FFT-1 and -3 saw a proportional increase in the percentage of tests where segregation exceeded acceptable levels. However, when FFT-2 was subjected to increased shearing, the percentage of marginally acceptable results increased without much change in the number of unacceptable results. This indicated that FFT-2 was less susceptible to segregation as shear increased. This could again be due to the more dispersive water chemistry of FFT-1, FFT-3, and their corresponding PEW relative to FFT-2. Overall, HFST-treated FFT is better suited to withstand increased shear conditions than other flocculated FFT materials, which break down quickly when oversheared (Li, Kaminsky, Gong, et al., 2021). Therefore, HFST-treated FFT is expected to better withstand shear forces associated with pipeline transport over long distances relative to rival flocculation techniques.

Table 4. Effect of shearing time on settling column sediment ratio at SFR 2.

FFT	Shear time	0.9<R<1.1	1.1<R<1.3	1.3<R
FFT-1	30s	10%	70%	20%
	300s	0%	70%	30%
FFT-2	30s	39%	43%	18%
	300s	8%	73%	19%
FFT-3	30s	33%	52%	14%
	300s	0%	55%	45%

Impact of HFST treatment on FFT dewatering

The rate at which solid content increased in the SRF cake was calculated based on the original mass of HFST-treated materials placed into the SRF container, and the rate at which water was released during pressing at 30psi. To ensure all testing was completed in a timely manner, most SRF tests were stopped after 10 minutes of pressing. However, select runs were run for an extended period to the point at which solids content in the SRF reached a plateau, to further probe the dewatering effect of HFST-treatment.

Figure 7 shows the SRF solid content increase over time of HFST-treated substrate containing FFT-3 at SFR 2 with NAGS, 50ppm of Nexus reagent, and five increasing doses of polymer. The baseline substrate behaviour (FFT-3, sand, and PEW combined to form a 35wt% substrate, but with no HFST treatment) is also shown for comparison.

While the baseline substrate requires over 500 minutes (over 8 hours) to reach completion, even underdosed HFST-treated materials may reduce the time to completion by 50%. When optimally dosed, HFST-treated substrate containing FFT-3 was able to achieve a final solid content of 80% as quickly as 10 minutes, an improvement of over 50x faster than the substrate without HFST treatment. Under overdosed conditions (750 ppm polymer), 40 minutes was required for data to plateau. This is longer than optimal conditions, but still a vast improvement over the untreated and underdosed materials. In an independent study, HFST also significantly outperformed a rival flocculation technique on FFT with a combination of polyacrylamide flocculant and alum-based coagulant, which required nearly 25x longer to fully dewater at the same pressure, and achieved a lower solid content at plateau relative to HFST (Li, Kaminsky, Romero, et al., 2021). Given that dewatering time scales with deposit depth these differences in dewatering rates could conceptually translate to differences of centuries at field scale. Better numerical model predictions require the use of longer and more complex consolidation testing some of which could be validated by creating a meso-scale field deposit and adequate depth and planar dimensions. Furthermore, HFST treatment also improves fines capture and suppresses fugitive solids in the release water (Figure 8).

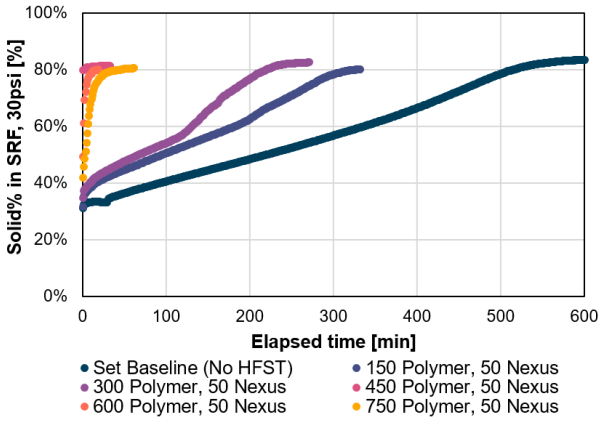

Figure 7. Solid content increase in SRF with HFST treatment. Reagent dosage shown in ppm, based on total solids.

For the untreated baseline substrate, the release water contained nearly 5wt% solids. For this FFT, sand, and Nexus reagent combination, underdosed polymer was able to reduce released solids to 2-3wt%. When polymer was optimally dosed, solids in the release water was further reduced to just over 0.5wt%.

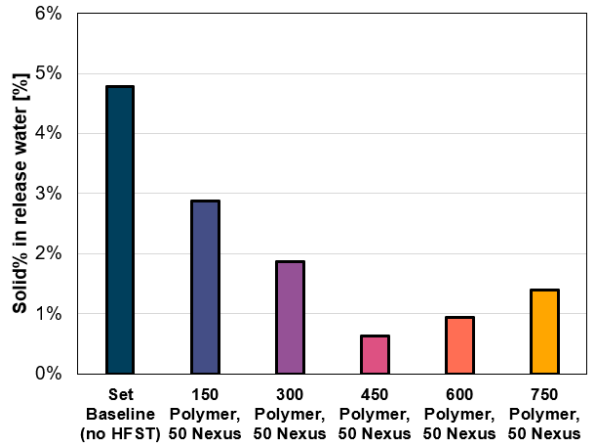

Figure 8. Solid content in release water with HFST treatment. Reagent dosage shown in ppm, based on total solids.

Impact of Nexus reagent on HFST performance

Two dosages of BASF's novel Nexus reagent, 50ppm and 150ppm, were chosen to investigate if an overdose of Nexus reagent could be detrimental to HFST performance. Since minimal differences were observed between 50ppm and 150ppm, further investigations were made in the impact of excluding the Nexus reagent altogether. Figure 9 shows the SRF solid content increase over time of HFST-treated substrate containing FFT-3 at SFR 2 with NAGS, and five increasing doses polymer, but in the absence of any Nexus reagent.

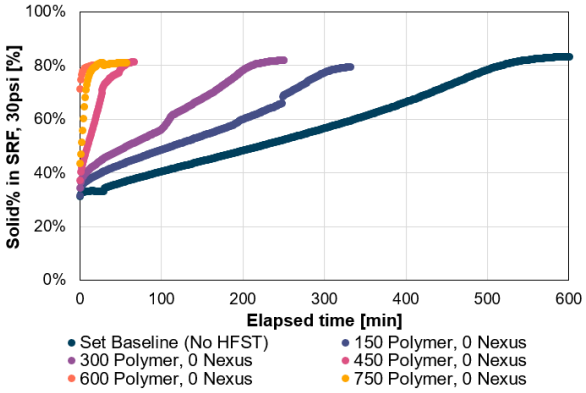

Figure 9. Solid content increase in SRF with HFST treatment with no Nexus reagent. Reagent dosage shown in ppm, based on total solids.

Compared to Figure 7, SRF performance at all polymer doses except 450ppm are similar. The 450ppm polymer dose condition releases water more slowly in the absence of Nexus reagent, indicating that Nexus serves as a process aid and boosts dewatering performance when polymer dose is on the cusp of sufficiency. When polymer is overdosed, adding Nexus reagent does not further increase dewatering rate.

Impact of sand on polymer dose requirements

Overall, the biggest impact on polymer dose requirement was the type of sand used. Originally, only one type of sand was included as part of the overall test plan. However, when it was discovered that the original sand was generating significant amounts of acid, a second sand type was added to the test plan to compare differences. The acid generating sand required a significantly higher polymer dosage relative to NAGS to achieve optimal flocculation results. This finding is consistent with the known reduction in polymer efficiency in acidic environments if the polymer's anionic content isn't adjusted to perform in this lower pH environment (Brien et al., 1977). If the acid-generating sand is present at an application site, the anionic content could be optimized to improve dose efficiency. Figure 10 shows the relationship between sand type, HFST performance, and polymer dose at the target SFR of 2. While the AGS required more polymer to achieve optimal flocculation at the same SFR relative to NAGS, better quality flocculation was also acheivable, indicated by higher solid% in the SRF at optimal dose, and less of a performance drop when dose

exceeded optimal. Dosage differences to achieve optimal flocculation based on sand type, while significant, are not expected to present a problem for field application. This is because the acid-generating characteristics of sand are expected to be measurable at any site and constant over the time of HFST tailings treatment operation.

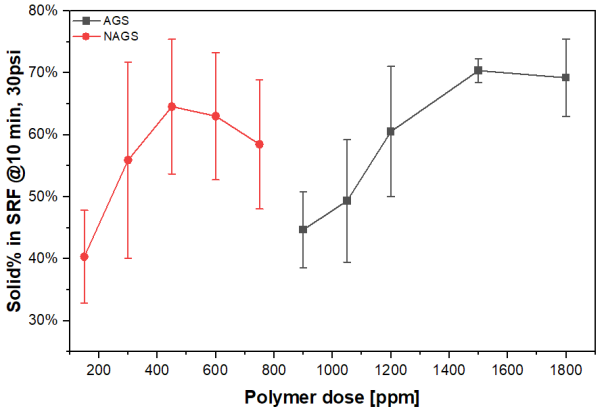

Figure 10. SRF solid% performance.

SFR also impacted HFST performance. HFST was originally designed to give optimal performance at an SFR of 2, significantly less than competing technologies like CT and NST, which require SFRs starting at 4. Lower sand requirement in composite substrates is desirable because it reduces the overall volume of treated tailings, and because sand is also required for road and berm construction.

Figure 11 shows the pressure filter performance of HFST-treatment of the two sand types tested at each SFR investigated in this study.

For AGS, optimal performance was consistently reached at SFR 2. As AGS content increased, the additional acid was likely responsible for causing decreased performance. In contrast, performance for NAGS was best at an SFR of 3, with nearly all tested conditions meeting minimum satisfactory SRF performance criteria (Above 65wt% solids in SRF cake, and below 1 wt% solids in release water). At SFR 2, 67% of the NAGS conditions were acceptable. Below SFR 2, sand content was not sufficient to produce acceptable results for either sand type. SFR 1.5 was not tested for the AGS.

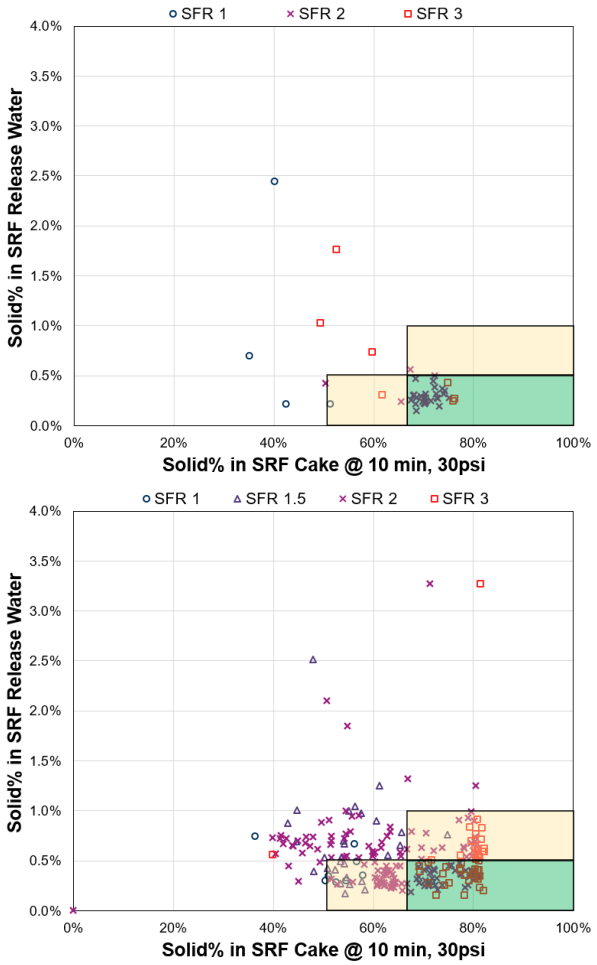

Figure 11. Pressure filter performance of HFST at various SFR, for AGS (top) and NAGS (bottom).

Performance of HFST treatment was compared the Co-efficient of Uniformity (C_u) for each substrate, defined as the particle size D_{60}/D_{10}. The C_u is a measure of the variability of the particle sizes in a sampled material with higher values indicating better ability for smaller particles to fit within the interstitial spaces between successively larger particles and form a material fabric which may be described as a "well-graded material" in geotechnical terminology. Figure 12 indicates that HFST treatment is most effective when substrate C_u exceeds 20 for the substrates tested.

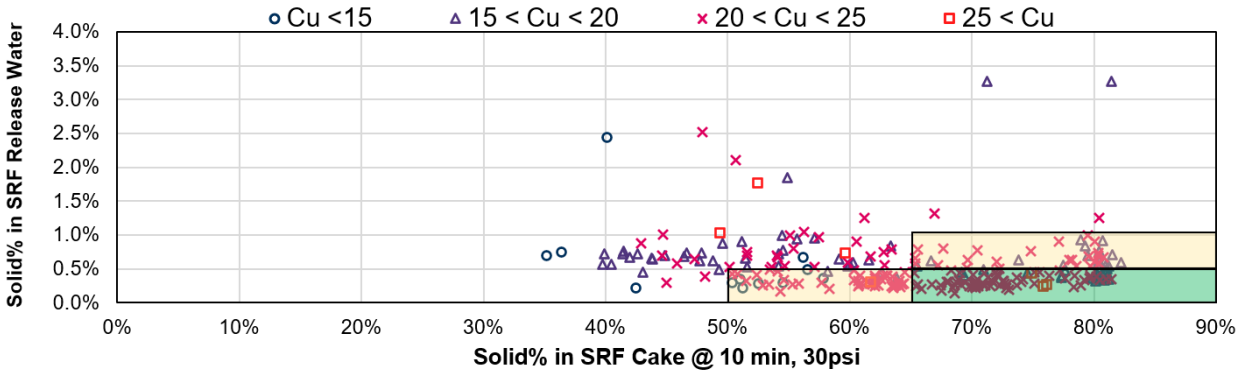

Figure 12. HFST performance by Co-efficient of Uniformity of substrate.

Clay capture

Figure 13 shows the solid content in the water released through the 250µm SRF bottom screen during pressure filtration as a function of polymer dose and FFT type. For all three FFTs so long as polymer was not underdosed, low solids (<1wt%) were present in the release water, indicating excellent capture of fine particles.

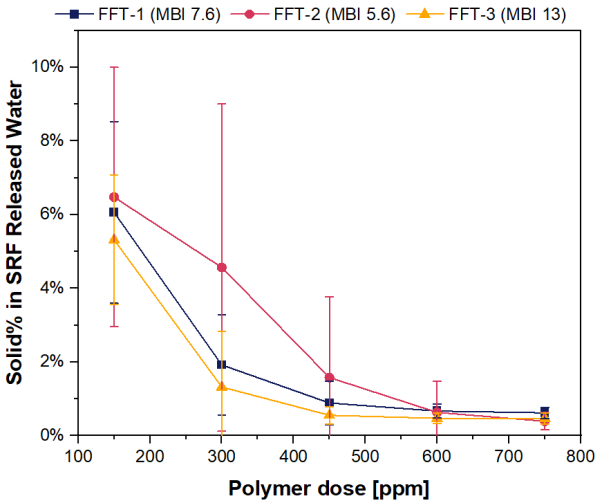

Figure 13. Impact of polymer dose on solid content of SRF release water.

Aside from solids released during SRF testing, MBI was used to assess the fraction of clays able to escape into the supernatant water in the settling column. It was assumed that the most significant source of clays in the substrates was the FFT itself, and that sand and PEW introduced negligible clay content. Clay capture was calculated by comparing the milli-equivalents (meq) of methylene blue into the system versus the meq of methylene blue leaving through the released water. Equations 3 and 4 describe the calculations used to assess clay capture.

$$meq_{in} = MBI_{FFT} \times M_{FFT} \times Solid\%_{FFT} \quad [3]$$

$$meq_{out} = MBI_{Water} \times M_{Water} \times Solid\%_{Water} \quad [4]$$

The mass of the supernatant was also estimated based on the settling column mudline after 1 week of settling. Clay capture is then calculated by Equation 5. Figure 14 demonstrates over 96% clay capture in settling column sediment for all three FFTs even when polymer was underdosed.

$$Clay\ capture = 1 - \frac{meq_{out}}{meq_{in}} \quad [5]$$

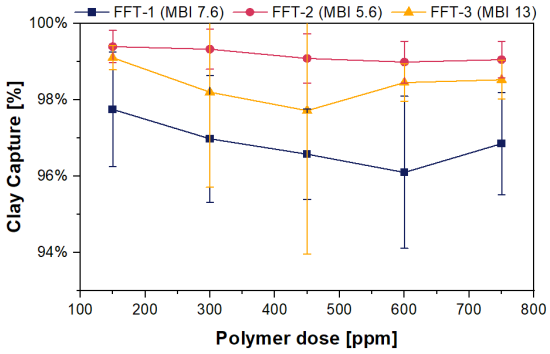

Figure 14. Impact of polymer dose on clay capture.

CONCLUSIONS

Through independent verification of BASF's HFST process, the following conclusions are made:

At a targeted SFR of 2, pressure filter dewatering tests demonstrated that the time to achieve 80wt% solids under 30psi applied pressure was approximately 15 minutes for HFST-treated materials, while untreated material required over 500 minutes to reach the same solids content. Optimal polymer treatments produced rapid dewatering for all substrates tested, relative to untreated FFT and blends of untreated FFT with sand. Overall, overdosing polymer is better than underdosing, which is encouraging given the tendency for tailings treatment operations to err on the side of overdosing chemical reagents. When polymer was underdosed, HFST performed poorly overall, with significant solids released into pressure filter filtrate and settling column supernatant, indicating fines segregation.

Insignificant differences in performance were noted between a Nexus reagent dosage of 50ppm and 150ppm, though in some cases where the polymer dose was marginally adequate / nearing underdose, the presence of the Nexus reagent helped achieve performance targets. For most of the tested cases, adding Nexus reagent also helped decrease the solids in the SRF release water, so long as polymer was not underdosed. In summary, some Nexus reagent is better than no Nexus reagent, but more Nexus reagent is not necessarily better than using the recommended amount of Nexus reagent, especially when combined with an optimal dosing of the polymer used in the HFST treatment process.

When mixing time was increased from 30 seconds to 300 seconds following reagent dosing, the optimal polymer dose did not change overall. However, evidence of segregation became more apparent for two of the FFTs (FFT-1 and FFT-3) tested. FFT-2 was relatively resilient to increased shearing, which may be attributed to lower clay content, but potentially also due to the relatively coagulating water chemistry of FFT-2's process source.

Recommendations

Sand source was found to have a significant impact on the results, where the acid content of one of the sand types significantly increased the polymer dose required to achieve optimal flocculation. Testing other sand sources, in parallel with larger scale testing is recommended to assess how widespread acidic sands are, and to further probe impacts caused by sand pH and particle size distribution.

Dark coloured release water was observed for optimal and overdosed HFST-treated samples, especially for FFT-3. Further investigation is required to determine its cause and nature, and to identify if mitigation is required should the water be required to be returned for use in extraction or as part of the water treatment that will be needed prior to eventual discharge to the environment.

REFERENCES

Alberta Energy Regulator. (2016). *Directive 85*. https://static.aer.ca/prd/documents/directives/Directive085.pdf

Brien, J. H. O., Novak, J. T., Brien, J. H. O., & Novak, J. T. (1977). *Effects of pH and Mixing on Polymer Conditioning of Chemical Sludge*. *69*(11), 600–605.

Currie, R., Bansal, S., Khan, I., & Mian, H. (2014). *An Investigation of the Methylene Blue Titration Method for Clay Activity of Oil Sands Samples*.

Currie, R., Zhao, B., & Khan, I. (2015). *Design of Experiment Study in Support of Development of a Standard for Fines Measurement in Oil Sands*.

Dean, E. W., & Stark, D. D. (1920). A convenient method for the determination of water in petroleum and other organic emulsions. *Industrial and Engineering Chemistry*, *12*(5), 486–490. https://doi.org/10.1021/ie50125a025

Dhadli, N., Fair, A., Hyndman, A., Langer, A., McEachern, P., Nadeau, S., Nickerson, A., Payne, F., Penner, B., Shaw, B., & Sission, R. (2012). *Technical Guide for Fluid Fine Tailings Management*.

Kaminsky, H. (2014). Demystifying the methylene blue index. *4th International Oil Sands Tailings Conference*, *October*.

Li, Y., Kaminsky, H., Gong, X. Y., Sun, Y. S., Ghuzi, M., & Sadighian, A. (2021). What affects dewatering performance of high density slurry? *Minerals*, *11*(7). https://doi.org/10.3390/min11070761

Li, Y., Kaminsky, H., Romero, C., Gong, X. Y., Ghuzi, M., & Tacas, J. (2021). Assessing dewatering performance of treated fluid fine tailings with a modified bench-scale filter press. In N. Beier, W. Wilson, & D. C. Sego (Eds.), *Tailings and Mine Waste 2021* (pp. 862–872). University of Alberta Geotechnical Center.

Sethi, A. (1995). Methylene blue test for clay activity determination in fine tailings. *MRRT Procedures*.

SESSION 4

GROWTH AND SURVIVAL OF NATIVE SPECIES IN SHALLOW CAPPED THICKENED TAILINGS: A MESO-SCALE GREENHOUSE STUDY

Dani Degenhardt[1], Angeline Van Dongen[1], Stefan G. Schreiber[2], and Asfaw Bekele[3]
[1]Natural Resources Canada, Canadian Forest Service, Northern Forestry Center, Edmonton, AB
[2]EnviroStats Solutions Inc., Edmonton, AB
[3]Imperial Oil Resources Limited., Calgary, AB

ABSTRACT

This three-year meso-scale greenhouse study used 55-gallon columns to evaluate the survival and growth of boreal upland and wetland communities on thickened tailings (TT) with 0, 10, and 30 cm peat-mineral mix (PMM) reclamation cap. While survival was high in all treatments, the PMM cap treatments showed significant improvement in overall plant growth, cover, and above-ground biomass compared to the uncapped treatment, with the 30 cm PMM cap outperforming the 10 cm PMM. The plant growth response was similar between the two communities and the top performing species, in terms of survival and growth, were *Cornus sericea, Populus tremuloides*, *Salix bebbiana,* and *Scirpus microcarpus*.

INTRODUCTION

In the Athabasca oil sands region (AOSR) of Alberta, approximately 4,800 km^2 of oil reserves are recoverable by surface-mining (Ma et al., 2021). A warm-water bitumen extraction process is used to recover bitumen from the oil sands deposits; this process also generates large volumes of tailings, a fluid waste stream containing sand, silt, clay, water, residual bitumen, salt, and trace metals which are stored temporarily in containment ponds (Alberta Energy Regulator, 2022). There are currently over 1.25 billion m^3 of tailings in large containment ponds across the AOSR that must eventually be reclaimed into landforms prior to mine closure (Alberta Energy Regulator, 2020; Cossey et al., 2021).

Tailings thickening techniques are being used by mine operators around the world to enhance dewatering and consolidation of fluid tailings, a practise which has recently been adopted in the AOSR with the goal of reducing the water content and increasing deposit density and strength required for restoring tailings ponds to dry landscapes (Boswell et al., 2015; Demoz, 2022). At Imperial's Kearl Operation, tailings are managed by thickening the middlings (specific gravity of 1.05-1.2) with secondary in-line chemical treatment of thickener underflow prior to deposition. This process creates a thickened tailing (TT) with a sand to fine ratio (SFR) of 0.5–2 and a solids content >65%. In general, TT can achieve geotechnical stability to start reclamation activities (Imperial Oil Resources Limited, 2020).

Once TT deposits are placed in their final landscape position and meet specified performance criteria, they can be reclaimed into terrestrial landscapes with wetlands to facilitate the return of equivalent land capability to the pre-disturbance landscape (Alberta Energy Regulator, 2020, 2022). TT are suitable for capping with solid materials, such as coarse sand tailings, to create a trafficable surface for reclamation (COSIA, 2012). Adequate capping material, known as a substrate cap, is required to increase the strength and stability of the landform while hydraulically isolating the tailings from the surface and vegetation rooting zone (Alberta Energy Regulator, 2018; Sutton & Price, 2020). A reclamation cap, or cover soil, is placed above the substrate cap to support vegetation establishment and development of a productive ecosystem through nutrient cycling and water retention (Stack et al., 2021; Zhuang et al., 2008). Peat material, salvaged from bogs and fens, is commonly used as a cover soil in oil sands reclamation due to the abundance of peatlands within the local mining footprint (Rowland et al., 2009; Stack et al., 2021). Finally, the reclaimed landscape is revegetated with a native plant community through a variety of processes including germination from propagules (seeds or vegetative fragments) in cover soils, immigration from natural processes, and active planting of seedlings (Farnden, 2021).

While reclamation of overburden dumps and sand-dominated tailings deposits has been implemented at Syncrude's Sandhill Fen, South Bison Hill, and Gateway Hill (Grant et al., 2013; Syncrude Canada Ltd., 2013; Wytrykush et al., 2012), reclamation of treated fine tailings deposits is still in its infancy. A

few greenhouse capping studies have been conducted using centrifuge tailings (Lalonde et al., 2020; Omari et al., 2020); however, this type of treated fine tailings have different chemical and physical properties from TT (Cossey et al., 2021). Most research involving TT (or consolidated tailings) has focused on the phytotoxicity of its release water (Armstrong et al., 2010; Cutter, 2013; Renault et al., 1998, 2003) or its physical properties and consolidation behaviour (Demoz, 2022; McKenna et al., 2016; Wilson et al., 2018). There is a need to better understand how TT affects native plant establishment and how reclamation cover soil caps might mitigate these limitations to inform reclamation capping designs.

Greenhouse studies provide an opportunity to assess plant performance in tailings with different soil caps in a controlled environment with reduced complexity relative to field studies. In this study, we omitted the recommended substrate cap between the tailings and soil reclamation cap to represent a scenario where tailings are not isolated from the rooting zone. The objective of this three-year, meso-scale greenhouse study was to understand the effect of TT on the survival and growth of native upland and wetland species and the potential improvement in plant response with the addition of a relatively thin (10 cm and 30 cm) soil reclamation cap of peat mineral mix (PMM).

MATERIALS AND METHODS

Experimental design

Columns were assembled in 55 gallon (208 L) plastic cylindrical barrels (54 cm in diameter and 90 cm in height) using TT and PMM freshly salvaged by Imperial Oil Resources, Canada. Three different capping treatments were tested: 0, 10, and 30 cm PMM (Figure 1).

Each column was planted with one of two plant communities: wetland or upland; comprised of common species found in the boreal forest. The upland community included *Populus tremuloides* Michx. (aspen), *Pinus banksiana* Lamb, (jack pine), *Cornus sericea* L. also referred to as *Cornus stolonifera* Michx. (red-osier dogwood), and *Elymus trachycaulus* ssp. *trachycaulus* (Link) Malte (slender wheat grass). The wetland community included *Salix bebbiana* Sarg. (Bebb's willow), *Scirpus microcarpus* J. Presl and C. Presl (Small-fruited bulrush), *Triglochin maritima* L. (sea-side arrow grass), *Rumex salicifolius* Weinm. (willow dock), and *Carex aquatilis* Wahlenb (water sedge). Each of the three capping depth treatments with each of the two plant communities were replicated in four columns for a total of 24 columns.

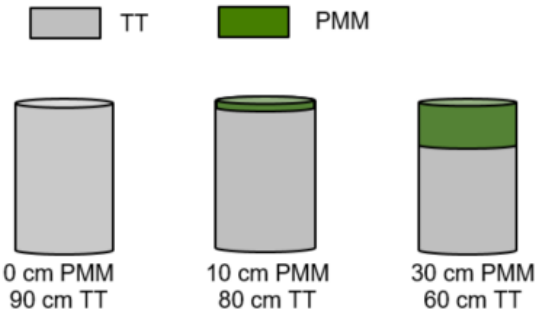

Figure 1. Tailings capping treatments with varying depths of peat mineral mix (PMM) on top of thickened tailings (TT) in columns.

One-year old seedlings were planted into the columns in May 2019. In the upland community, three individual plants per species were planted for a total of 12 plants per column. In the wetland community, three plants per species were planted, with the exception of *S. bebbiana* where only two plants were planted, for a total of 14 plants per column. No fertilizer was applied post-planting. Over-head irrigation was applied consistently to all treatments to mimic precipitation. Column temperature and moisture were monitored and greenhouse conditions were altered to mimic seasonal temperatures (summer temperatures: 18 – 22◦C day, 10 - 12◦C night; winter temperature: 2 - 4◦C day / night).

Initial material characterization

Composite samples of the TT and PMM were collected prior to column assembly for characterization (Table 1). The TT used in this study were a coarse tailings with a sands to fines ratio (SFR) of 2.8 (Table 1). TT has a low cation exchange capacity (CEC) and available water holding capacity (AWHC) due to the sandy loam texture. Petroleum hydrocarbon concentrations exceeded the Alberta Tier 1 guideline levels for coarse textured soil (Alberta Environment and Parks, 2019). The TT were also relatively low in nutrients and high in sodium and sulfur compared to the PMM (Table 1).

The PMM's values were within the general range of PMM coversoil used for reclamation in this region

(MacKenzie & Quideau, 2012; Schott et al., 2016; Stack et al., 2020, 2021).

Table 1. Thickened tailings (TT) and peat mineral mix (PMM) properties expressed as mean ± standard deviation.

Properties	*Parameter*	*PMM (n=3)*	*TT (n=12)*
Physio-chemical	pH	6.9±0.2	8.7±0.1
	Electrical Conductivity (dS/m)	0.5±0.1	1.0±0.1
	Sodium Adsorption Ratio	0.2±0.02	1.9±0.1
	Cation Exchange Capacity (cmol/kg)	43.8±10.2	3.0±1.1
	Solids (%)		79.3±1.0
	Sand to Fines Ratio		2.8±0.5
	% sand (2 mm – 50 µm)		70±7
	% silt (2 – 50 µm)		17±3
	% clay (< 2 µm)		14±5
	% moisture at field capacity (1 bar)		9±1.6
	% moisture at wilting point (15 bar)		3.9±0.9
	% Available water holding capacity		5.1±0.7
	Total Carbon (mg/kg)	8.6±1.4	0.9±0.3
	Total Organic Matter (mg/kg)	16.6±2.8	1.4±0.3
Inorganics	Exchangeable Ca^{2+} (mg/kg)	8820±1148	332.8±52.2
	Exchangeable Na^{+} (mg/kg)	87.9±10.2	156.8±17.1
	Exchangeable K^{+} (mg/kg)	67.0±13.8	47.5±6.2
	Exchangeable Mg^{2+} (mg/kg)	1261±23	106.2±17.4
	Extractable P (mg/kg)	2.1±0.3	2.3±0.2
	Extractable S (mg/kg)	43.7±10.7	71.8±7.4
	NO_3-N (mg/kg)	22.1±9.1	3.0±1.0
	NH_4-N (mg/kg)		10±1
	Total Nitrogen (mg/kg)	0.3±0.04	0.005±0.005
Trace metals	Boron (mg/kg)		1.0±0.2
	Barium (mg/kg)		0.1±0.01
	Copper (mg/kg)		0.02±0.003
	Iron (mg/kg)		0.02±0.009
	Manganese (mg/kg)		1.2±0.7
	Strontium (mg/kg)		1.1±0.2
	Zinc (mg/kg)		<DL
Organics	PHC F1 C6-C10 (mg/kg)		<DL
	PHC F2 C10-C16 (mg/kg)		521±197
	PHC F3 C16-C34 (mg/kg)		3689±1316
	PHC F4 C34-C50+ (mg/kg)		1862±673
	PHC F5 (mg/kg)		1816±670
	Naphthenic Acids* (mg/kg)		227±85
	Bitumen (%)		0.61±0.2

***** Napthenic acids analysed using Headley et al.'s method (Headley et al., 2002, 2011)

Assessment and monitoring

Vegetation assessments were conducted at the time of planting and at the peak (August) of each growing season and included evaluations of plant survival and vegetative cover for plants of all species, as well as stem diameter, height, and growth increment (leader growth) for the woody species (*P. tremuloides, P. banksiana, C. sericea,* and *S. bebbiana*). Vegetative cover was assessed as the percent of the total circular area of the column covered by each individual plant.

At the end of Year 3, composite samples of the TT and PMM were collected throughout the depth of the material, combining all replicates for each treatment, and analyzed. In addition, the living aboveground biomass was collected for each

species from each column. The total aboveground biomass per species was determined after drying for three days at 40 °C.

Data analysis

Data analysis and visualizations were carried out using the R language and environment for statistical computing (R Core Team, 2021), the *glmmTMB* package (Brooks et al., 2017) as well as the *tidyverse* packages (Wickham et al., 2019). Linear and generalized linear mixed-effects models (Bolker et al., 2009; Gelman & Hill, 2006; Zuur et al., 2013) were used to model the effect of capping treatment and community type on survival, above-ground biomass, plant cover, and woody species growth (stem diameter, height, height increment) in Year 3. The random effect that was used for all models was "column" to account for non-independent measurements within each column. Furthermore, whenever possible, species nested in the community were used as an additional random term. Wald chi-square tests were conducted to test the fixed effects for their significance via the *Anova()* function of the *car* package (Fox & Weisberg, 2019). Estimated marginal means were calculated using the *emmeans* package (Lenth, 2020) based on the fitted models. P-values for multiple mean comparisons were adjusted using the Tukey method.

RESULTS

Changes in substrate properties

There were some notable changes in the physical and chemical properties of the TT after three growing seasons. In particular, the vane shear strength increased in all treatments while pH of the TT decreased, likely as a result of plant respiration (Table 2). The EC increased across all three treatments, while the SAR remained relatively constant. Exchangeable cation concentrations were all higher in the upland columns compared to the wetland columns. The other discernible change observed was the PHC concentration, which saw a decline in all three treatments across all PHC fraction groups measured (Table 2).

After three growing seasons, a notable increase was observed in EC and SAR in the PMM, while a decrease was observed in exchangeable Ca^{2+} (Table 3).

Table 2. Chemical properties of thickened tailings (TT) composite samples expressed as mean ± standard deviation at the beginning of the experiment (Initial) and at the end of Year 3 (Final) for each treatment: 0 cm PMM, 10 cm PMM, and 30 cm PMM

Parameters	***TT Initial*** *(n=12)*		***TT Final***		
			0 cm PMM (*n*=1)	10 cm PMM (*n*=1)	30 cm PMM (*n*=1)
Vane shear strength (kPa)	7±7	Upland	33 ± 7 *	50 ± 17*	20 ± 3*
		Wetland	40 ± 20*	36 ± 3*	33 ± 7*
pH	8.7±0.1	Upland	7.3	7.1	6.9
		Wetland	7.4	7.4	6.9
Electrical conductivity (dS/m)	1.0±0.1	Upland	3.33	2.07	2.15
		Wetland	0.95	0.96	1.79
Sodium adsorption ratio	1.9±0.1	Upland	3.33	1.97	1.99
		Wetland	1.12	1.26	1.66
Exchangeable Ca^{2+} (mg/kg)	332.8±52.2	Upland	227	190	207
		Wetland	74	72	153
Exchangeable Na^{+} (mg/kg)	156.8±17.1	Upland	339	149	156
		Wetland	51	60	110
Exchangeable K^{+} (mg/kg)	47.5±6.2	Upland	69	40	48
		Wetland	45	36	34
Exchangeable Mg^{2+} (mg/kg)	106.2±17.4	Upland	100	73	80
		Wetland	30	30	64
Extractable S (mg/kg)	2.3±0.2	Upland	227	117	172
		Wetland	53	54	118
NO_3-N (mg/kg)	71.8±7.4	Upland	<DL	2.35	2.22

		Wetland	2.01	0.78	2.26
PHC F1 C6-C10 (mg/kg)	<DL	Upland	<DL	<DL	<DL
		Wetland	<DL	<DL	<DL
PHC F2 C10-C16 (mg/kg)	521±197	Upland	210	229 ± 74#	221 ± 48#
		Wetland	235 ± 22#	279 ± 95#	206 ± 96#
PHC F3 C16-C34 (mg/kg)	3689±1316	Upland	1670	1890 ± 537#	1840 ± 368#
		Wetland	1895 ± 163#	2320 ± 297#	1615 ± 700#
PHC F4 C34-C50+ (mg/kg)	1862±673	Upland	850	946 ± 232#	964 ± 193#
		Wetland	961 ± 84#	1245 ± 120#	814 ± 348#
PHC F5 (mg/kg)	1816±670	Upland	870	974 ± 221#	1102 ± 54#
		Wetland	910 ± 13#	1335 ± 106#	674 ± 518#

* *n*=4, #n=2

Table 3. Chemical properties of peat mineral mix (PMM) composite samples expressed as mean ± standard deviation at the beginning of the experiment (Initial) and at the end of Year 3 (Final) for the 10 cm PMM and 30 cm PMM treatments. DL = Detection Level

Properties	***PMM Initial*** *(n=3)*	***PMM Final***		
			10 cm PMM (*n*=1)	30 cm PMM (*n*=1)
pH	6.9±0.2	Upland	7.4	7.4
		Wetland	7.3	7.4
Electrical conductivity (dS/m)	0.5±0.1	Upland	2.6	1.8
		Wetland	1.5	0.7
Sodium adsorption ratio	0.2±0.02	Upland	2.2	1.5
		Wetland	1.3	0.8
Exchangeable Ca^{2+} (mg/kg)	8820±1148	Upland	269	186
		Wetland	156	71
Exchangeable Na^{+} (mg/kg)	87.9±10.2	Upland	199	100
		Wetland	77	34
Exchangeable K^{+} (mg/kg)	67.0±13.8	Upland	48	62
		Wetland	104	39
Extractable S (mg/kg)	43.7±10.7	Upland	344	239
		Wetland	194	94
NO_3-N	22.1±9.1	Upland	3.4	2.3
		Wetland	1.5	3.2
Total P (mg/kg)	2.1±0.3	Upland	0.6	1.1
		Wetland	1.0	0.7
PHC F1 C6-C10 (mg/kg)	-	Upland	<DL	<DL
		Wetland	<DL	<DL
PHC F2 C10-C16 (mg/kg)	-	Upland	<DL	<DL
		Wetland	<DL	<DL
PHC F3 C16-C34 (mg/kg)	-	Upland	152 ± 39#	74 ± 4#
		Wetland	111 ± 19#	108 ± 4#
PHC F4 C34-C50+ (mg/kg)	-	Upland	120 ± 14#	<DL
		Wetland	124 ± 25#	52 ± 73#
PHC F5 (mg/kg)	-	Upland	108 ± 44#	172 ± 55#
		Wetland	39 ±13#	98 ± 61#

#n=2

Plant growth response

The probability of plant survival after three growing seasons was high (> 75%) across all capping treatments and both communities; however, there was a significantly higher (P = 0.005) probability of plant survival in the 30 cm PMM capped tailings compared to the uncapped tailings for both upland and wetland communities (Figure 2A). Above-

ground biomass and vegetation cover at the end of the third growing season increased significantly ($P < 0.001$) with increasing PMM depth within both the upland and wetland plant communities (Figure 2B, C).

For the woody species, mean stem diameter and mean height both increased significantly with increasing PMM depth ($P < 0.001$) in both the upland and wetland communities after three growing seasons (Figure 3A,B). Incremental height growth in Year 3 was significantly higher ($P < 0.001$) in the 10 and 30 cm PMM treatments compared to the uncapped tailings in both communities; however, there was a significant difference in growth increment between the communities ($P < 0.001$), with the wetland community achieving higher incremental growth than the upland community (Figure 3C). A general overview of each species' individual performance in the uncapped and PMM capped TT is given in Table 4.

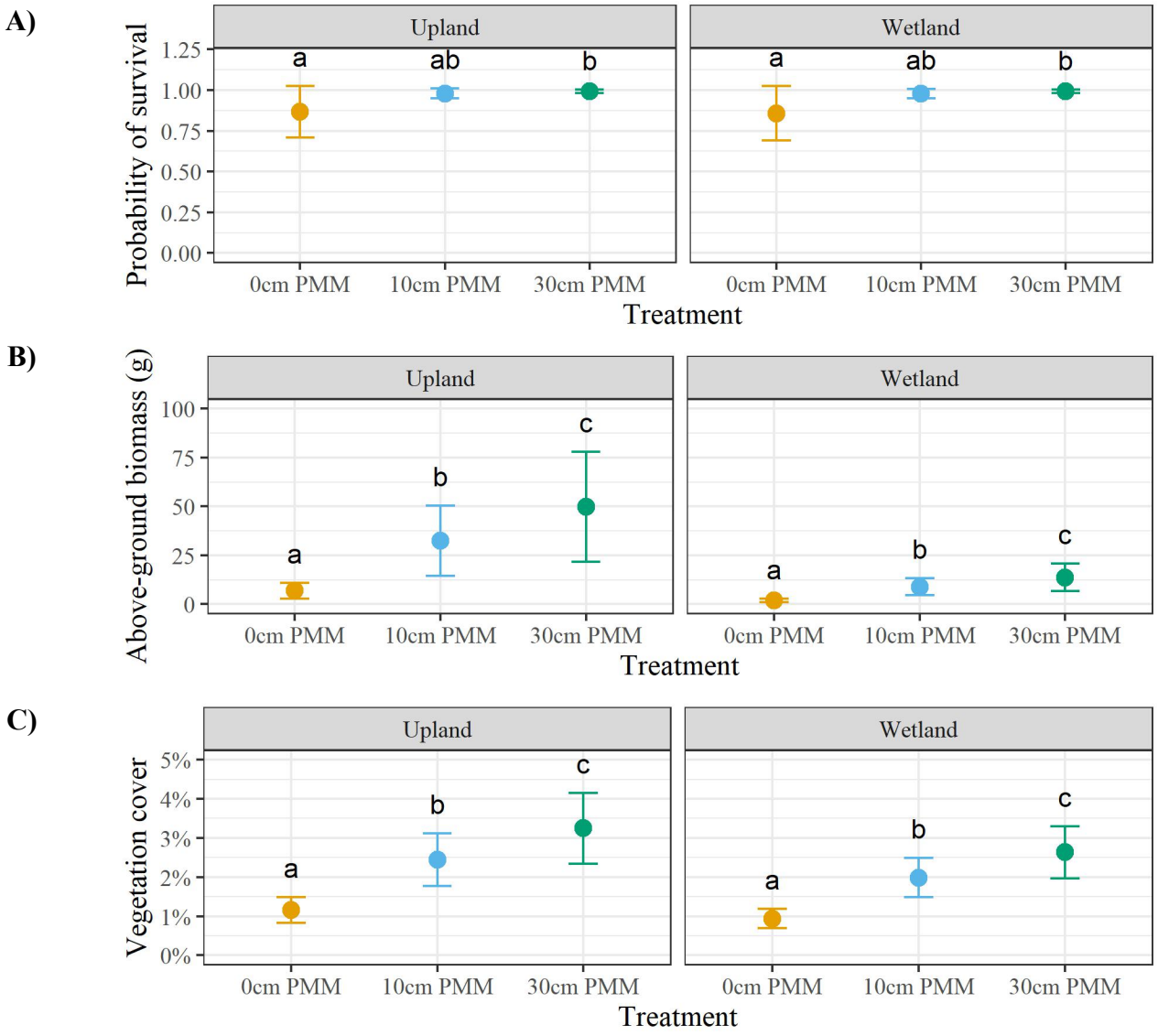

Figure 2. Probability of survival (A), above-ground biomass (B), and vegetation cover (C) per treatment at the end of Year 3 for 0 cm PMM (yellow), 10 cm PMM (blue), and 30 cm PMM (green) within the upland and wetland communities. Error bars represent one standard error of the mean. Different letters within the same vegetation community represent means that are significantly different ($P < 0.05$).

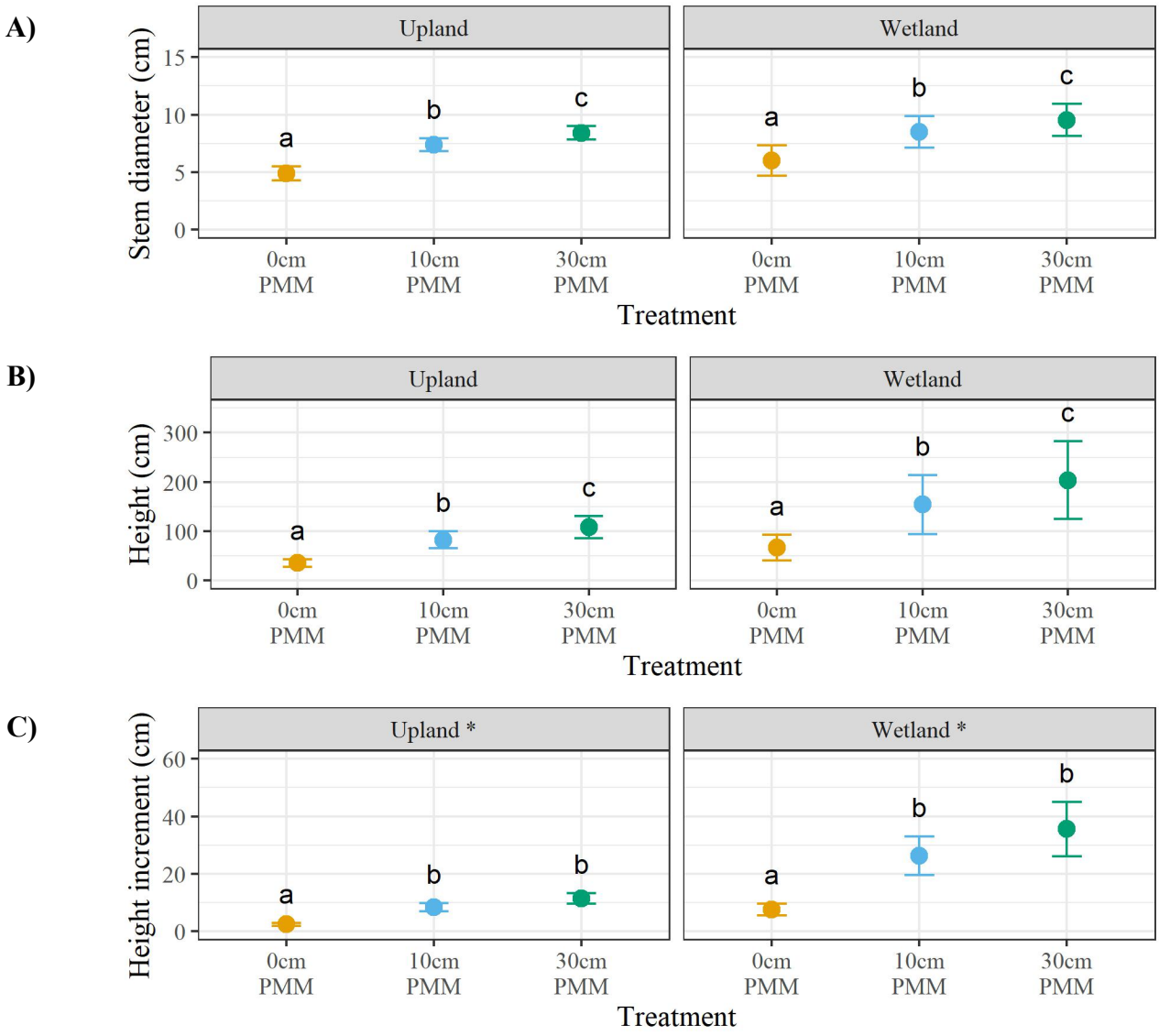

Figure 3. Mean stem diameter (A), height (B), and height growth increment (C) of woody species within the upland and wetland communities, at the end of Year 3 per treatment; 0 cm PMM (yellow), 10 cm PMM (blue), and 30 cm PMM (green). Error bars represent one standard error of the mean. Differing letters between means indicate a significant difference ($P < 0.05$) and the * indicates significant differences ($P < 0.05$) between upland and wetland communities.

Table 4. General performance, based on survival and growth, of each species in uncapped thickened tailings (TT) and TT capped with peat-mineral mix (PMM) (10 - 30 cm).

	Species	Performance in uncapped TT	Performance in TT capped with PMM (10-30 cm)
Upland community	***Populus tremuloides***	Moderate survival (58%)* and moderate (~20 g) above-ground biomass with heights ~ 0.6 m	High survival (100%)† and increased above-ground biomass (~80g) and height compared to uncapped, heights ~ 1.4 m
	Pinus banksiana	Low survival (17%)* and low above-ground biomass (~3 g) with heights < 0.3 m	High survival (100%)† and increased above-ground biomass (~30g) compared to uncapped, heights ~ 0.5 m
	Cornus sericea	Low survival (33%)* and low above-ground biomass (~6 g) with heights < 0.5 m	High survival (96%)† and increased above-ground biomass (~80g) and height with increasing PMM depth, heights ~ 1.2 m
	Elymus trachycaulus	High survival (100%)* but low (~7g) above-ground biomass	High survival (100%)† but similar above-ground biomass to uncapped (~8 g)
Wetland community	***Salix bebbiana***	High survival (100%)§ but low above-ground biomass (~3 g) with heights < 0.5 m	High survival (100%)# and increased above-ground biomass (~160 g) and height with increasing PMM depth, heights ~ 2.5 m
	Scirpus microcarpus	Low survival (25%)* and low (~5 g) above-ground biomass	Moderate survival (75%)† and increased above-ground biomass (~15g) with increasing PMM depth
	Triglochin maritima	High survival (100%)* but very little (< 1g) above-ground biomass	High survival (100%)† and increased above-ground biomass compared to uncapped but still low (~3g)
	Rumex salicifolius	High survival (100%)* but very little (< 1g) above-ground biomass	High survival (96%)† and increased above-ground biomass (~5g) with increasing PMM depth
	Carex aquatilis	High survival (100%)* but low above-ground biomass (~2g)	Moderate survival (58%)† and increased above-ground biomass (~9g) compared to uncapped

* *n* = 12 plants, † *n* = 24 plants, § *n* = 8 plants, # *n* = 16 plants

DISCUSSION

Plant response to TT tailings

Plant survival in the uncapped TT remained high (~85%) over the three growing seasons for both plant communities (Figure 2A) despite the TT exhibiting high PHCs and low essential nutrients (Table 1). Five species, *C. aquatilis, E. trachycaulus*, *R. salicifolius, S. bebbiana*, and *T. maritima*, maintained 100% survival over three years in the uncapped tailings (Table 4).

While plant survival was high in the uncapped TT, Year 3 above-ground biomass per column was low (< 20 g) and vegetative cover of each individual plant was < 2% of the column area (Figure 2B,C), indicating the inhibiting effect of TT on plant growth. The limited growth response of plants in uncapped TT further demonstrates that TT alone is not an ideal growth medium for supporting plant establishment.

Plant response to PMM cap and cap thickness

Results from this study indicate that adding a thin (10-30 cm) PMM reclamation cap above TT greatly improves plant survival and growth of both upland and wetland plant communities. The addition of either a 10 cm or 30 cm PMM cap increased the probability of surviving three growing seasons to > 98% for both plant communities (Figure 2). The 10 cm PMM cap significantly increased above-ground biomass, vegetation cover, diameter, and height

compared to the uncapped tailings for both plant communities and an increase in PMM thickness to 30 cm significantly improved these metrics compared to the 10 cm PMM cap (Figure 2 & 3).

Similar greenhouse column studies also found that thin reclamation caps of peat reclamation material and till significantly improved growth on treated tailings. Luna Wolter & Naeth (2014) found that soil caps (either PMM or LFH [upland surface soil]) improved the growth of native grasses on mature fine tailings (MFT) and Lalonde et al. (2020) found that soil caps (PMM, FFM [upland surface soil] or both) improved the growth of *P. tremuloides* and *S. bebbiana* on treated fine tailings. The PMM cap may help to mitigate plant stress caused by PHCs in the tailings (Samad et al., 2022) while also providing a good rooting medium with plant-available nutrients and available water.

An increase in the PMM cap thickness from 10 cm to 30 cm significantly improved plant growth in both the upland and wetland communities. Soil cover thickness has been found to influence soil moisture dynamics, with thicker cover soils retaining more water (Sutton & Price, 2020; Syncrude Canada Ltd., 2013). Lalonde et al. (2020) noted that volumetric water content generally increased with soil capping depth, although capping depth effects were not evident in that 16-week study. In a reclamation field study using various subsoil and topsoil capping treatments above lean oil sands overburden, enhanced growth on thicker capping depths (> 30 cm) was observed in the third growing season (Stack et al., 2020).

There were no differences in survival and growth response metrics between the wetland and the upland communities, except for the incremental growth of woody species, where the wetland incremental growth was significantly larger than the upland incremental growth. This difference was driven by the prolific growth rate of *S. bebbiana* in the wetland community.

Plant response over time

The plant growth response of the different communities to different TT capping treatments was assessed statistically only at the end of the experiment (Year 3); however, there were some general trends in the data across time that also merit discussion.

Most species that experienced mortality in the uncapped tailings saw some mortality in Year 1 except for *S. microcarpus,* where plant death did not occur until Year 3. Furthermore, differences in plant growth responses to treatment often became more distinct in Year 2 and 3 compared to Year 1. This delayed response is likely a result of plant roots extending from their soil plugs into the TT, or from the PMM into the TT, increasing the root area exposed to TT at different times, depending on the treatment. These findings highlight the importance of long-term monitoring of greenhouse or field studies to gain a better understanding of plant response to different tailings capping designs.

Another observation was that vegetation cover and yearly incremental growth of woody species generally decreased over time. Together, these results indicate that plant growth was slowing down over time. Because column disassembly at the end of the experiment showed that root development was not limited by column size, it is likely that the growth reduction was associated with the increased root exposure to tailings or a depletion of nutrients over time. Despite the observed drop in vegetative cover with time, there was an observed build-up of dead plant tissue from the previous years' growth in the column that is expected to cycle carbon and nutrients back into the soil over longer timeframes as it decomposes and contributes to soil development. In the field, natural physical and biological processes are expected to alter the physical and chemical properties of the cap and tailings over time (Huang et al., 2015).

Top performing species

Tests for statistically significant differences between species were not carried out in this analysis since the objective of this study was to evaluate the effect of the capping treatments on plant performance. However, descriptive statistics were completed to highlight differences among species, which give an indication of the ability of some species to survive and grow in capped TT.

In the upland community, *P. tremuloides* and *C. sericea* were the top performing species in terms of survival and above-ground biomass in the capped TT. While all upland species in the study achieved high survival rates, the woody species generated more above-ground biomass compared to the grass, *E. trachycaulus*. Furthermore, *P. tremuloides* and *C. sericea* each doubled the mean height of *P. banksiana,* achieving heights over 1.5 m tall on TT capped with 30 cm PMM. Lalonde et al. (2020) also found that capping treated fine tailings with cover soil substantially improved survival and growth of *P.*

tremuloides (Lalonde et al., 2020). *C. sericea* has demonstrated the ability to tolerate oil sands tailings and tailings water relatively well compared to other species (Renault et al., 1998, 1999, 2000) and has been grown successfully on various reclamation sites from container seedlings (Alberta Environment, 2010). *P. tremuloides* and *C. sericea* are both tolerant of a wide range of soil moistures and textures (Hardy BBT Limited, 1989). As such, they are widespread across Alberta and are often early colonizers of disturbed areas (Alberta Environment, 2010; Hardy BBT Limited, 1989). Their ability to reproduce vegetatively (*C. sericea* from sprouts or root shoots and *P. tremuloides* through vigorous root suckering), make them good candidates for revegetating reclamation sites (Hardy BBT Limited, 1989).

In the wetland community, *S. bebbiana* and *S. microcarpus* were the top performing species in terms of survival and above-ground biomass in the capped TT. *T. maritima* achieved high survival rates but very low above-ground biomass across all treatments, while *C. aquatilis* survival dropped on the capped TT compared to uncapped, potentially due to competition with *S. microcarpus*. *S. microcarpus* was a top performing species in the capped tailings in terms of survival and above-ground biomass. *S. microcarpus* is a perennial wetland sedge that establishes quickly and spreads rapidly from rhizomes, potentially outcompeting other species (Smreciu et al., 2013; Turnbull & Bridgham, 2015). As such, it may be useful for revegetation of reclaimed TT tailings deposits. *S. bebbiana* was the tallest woody species in this study, reaching more than 3 m tall on the TT capped with 30 cm PMM. *S. bebbiana* is an adaptive species tolerant of a wide range of soil conditions (Hardy BBT Limited, 1989). As such, *S. bebbiana* performed similarly well in other studies with capped treated tailings (Lalonde et al., 2020). The ability of *S. bebbiana* to easily reproduce vegetatively also make it a good candidate for reclamation (Alberta Environment, 2010).

CONCLUSION

This mesocosm greenhouse study evaluated the ability of upland and wetland plant communities to grow on TT and compared the plant growth response to growth on TT capped with PMM. Initial characterization of the TT material found elevated concentrations of PHCs, nutrient deficiencies, and unfavourable physical properties, posing potential challenges for plant growth; however, plant survival was high across all treatments although growth was limited. Results from this study indicate that a thin (10 cm) reclamation cap comprised of PMM can significantly improve vegetation growth on TT compared to uncapped TT. Furthermore, plant growth response increases significantly by increasing the PMM cap thickness to 30 cm. The top performing species, in terms of survival and above-ground biomass on capped tailings, were *P. tremuloides* and *C. sericea* in the upland community and *S. bebbiana* and *S. microcarpus* in the wetland community. The survival and growth response to the capping treatments were similar between the upland and wetland communities.

Although the study was limited to a small sample size, three growing seasons, and the reduced complexity of an isolated column system lacking the full range of hydrological and climatic factors which influence plant growth and nutrient cycling, this work contributes to the understanding of the reclamation capability, and best reclamation practices for TT. In addition, these findings support the requirement of a soil reclamation cap over TT tailings to improve growth of both upland and wetland plant communities. Additional greenhouse and field research on optimal capping depth of TT will inform TT reclamation best practice.

We would like to acknowledge technical assistance from Craig McMullen, Kaitlyn Trepanier, Caren Jones, and Danica Long.

REFERENCES

Alberta Energy Regulator. (2018). *Decision 20180716A: Imperial Oil Resources Limited; Application for Kearl Mine's Tailings Management Plan* (No. 20180716A; p. 76). Alberta Energy Regulator.

Alberta Energy Regulator. (2020). *State of Fluid Tailings Management for Mineable Oil Sands, 2019*. Alberta Energy Regulator.

Alberta Energy Regulator. (2022). *Directive 085: Fluid Tailings Management for Oil Sands Mining Projects*. Alberta Energy Regulator. https://www.aer.ca/regulating-development/rules-and-directives/directives/directive-085

Alberta Environment. (2010). *Guidelines for Reclamation to Forest Vegetation in the Athabasca Oil Sands Region*. Terrestrial Subgroup of the Reclamation Working Group od the Cumulative Environmental Management Association.

Armstrong, S. A., Headley, J. V., Peru, K. M., Mikula, R. J., & Germida, J. J. (2010). Phytotoxicity and naphthenic acid dissipation from oil sands fine tailings treatments planted with the emergent macrophyte *Phragmites australis*. *Journal of Environmental Science and Health, Part A*, *45*(8), 1008–1016. https://doi.org/10.1080/10934521003772436

Bolker, B. M., Brooks, M. E., Clark, C. J., Geange, S. W., Poulsen, J. R., Stevens, M. H. H., & White, J.-S. S. (2009). Generalized linear mixed models: A practical guide for ecology and evolution. *Trends in Ecology & Evolution*, *24*(3), 127–135. https://doi.org/10.1016/j.tree.2008.10.008

Boswell, J. E. S., Gidley, I. D. C., Jeeravipoolvarn, S., Pellerin, K. D. O., & Vietti, A. (2015). *Oil sands thickened tailings – remedies from an international perspective*. 16.

Brooks, M., E., Kristensen, K., Benthem, K., J. ,van, Magnusson, A., Berg, C., W., Nielsen, A., Skaug, H., J., Mächler, M., & Bolker, B., M. (2017). GlmmTMB Balances Speed and Flexibility Among Packages for Zero-inflated Generalized Linear Mixed Modeling. *The R Journal*, *9*(2), 378. https://doi.org/10.32614/RJ-2017-066

COSIA. (2012). *Technical Guide for Fluid Fine Tailings Management*.

Cossey, H. L., Batycky, A. E., Kaminsky, H., & Ulrich, A. C. (2021). Geochemical Stability of Oil Sands Tailings in Mine Closure Landforms. *Minerals*, *11*(8), 830. https://doi.org/10.3390/min11080830

Cutter, J. L. (2013). *Investigating the phytotoxicity of oil sand tailings water formed during atmospheric fines drying processing*. University of Saskatchewan.

Demoz, A. (2022). Geotechnical Properties Determination of Thickened Fluid Fine Tailings. *Geotechnical and Geological Engineering*, *40*(4), 1887–1898. https://doi.org/10.1007/s10706-021-01998-3

Farnden, C. (2021). *Reclaimed Upland Vegetation Community Trends on Syncrude's Mine Sites* (p. 74). Syncrude Canada Ltd.

Fox, J., & Weisberg, S. (2019). *An R Companion to Applied Regression*.

Gelman, A., & Hill, J. (2006). *Data Analysis Using Regression and Multilevel/Hierarchiacal Models*. Cambridge University Press.

Grant, J., Huot, M., Lemphers, N., Dyer, S., & Dow, M. (2013). *Beneath the surface: A review of key facts in the oilsands debate*. Pembina Institute for Appropriate Development. https://www.deslibris.ca/ID/236478

Hardy BBT Limited. (1989). *Manual of Plant Species Suitability for Reclamation in Alberta* (Reclamation Research Report RRTAC 89-4). Alberta Land Conservation and Reclamation Council.

Headley, J. V., Barrow, M. P., Peru, K. M., & Derrick, P. J. (2011). Salting-out effects on the characterization of naphthenic acids from Athabasca oil sands using electrospray ionization. *Journal of Environmental Science and Health, Part A*, *46*(8), 844–854. https://doi.org/10.1080/10934529.2011.579857

Headley, J. V., Peru, K. M., Mcmartin, D. W., & Winkler, M. (2002). Determination of Dissolved Naphthenic Acids in Natural Waters by Using Negative-Ion Electrospray Mass Spectrometry. *Journal of AOAC INTERNATIONAL*, *85*(1), 182–187. https://doi.org/10.1093/jaoac/85.1.182

Huang, M., Barbour, S. L., & Carey, S. K. (2015). The impact of reclamation cover depth on the performance of reclaimed shale overburden at an oil sands mine in Northern Alberta, Canada. *Hydrological Processes*, *29*(12), 2840–2854. https://doi.org/10.1002/hyp.10229

Imperial Oil Resources Limited. (2020). *Kearl Oil Sands Mine: Fluid Tailings Management Report for 2019*.

Lalonde, R. S., Pinno, B. D., MacKenzie, M. D., & Utting, N. (2020). Capping dewatered oil sands fluid fine tailings with salvaged reclamation soils at varying depths to grow woody plants. *Canadian Journal of Soil Science*, *100*(4), 546–557. https://doi.org/10.1139/cjss-2019-0120

Lenth, R. (2020). *emmeans: Estimated Marginal Means, aka Least-Squares Means* (R package version 1.4.8). https://CRAN.R-project.org/package=emmeans

Ma, G., Jia, J., Qi, Z., & Peng, S. (2021). Unconventional Oil Ores around the World: A Review. *IOP Conference Series: Earth and Environmental Science*, *621*(1), 012009. https://doi.org/10.1088/1755-1315/621/1/012009

McKenna, G., Mooder, B., Burton, B., & Jamieson, A. (2016). *Shear strengthand density of oil sands fine tail-ings for reclamation to a borealforest landscape*. IOSTC Interna-tional Oil Sands Tailings Confer-enc, Lake Louise, AB.

Omari, K., Pinno, B., Utting, N., & Li, E. (2020). Growth of Common Plants of Boreal Reclamation Sites in Oil Sands Tailings Cake Mixes and Process Water. *Land*, *10*(1). https://doi.org/10.3390/land10010025

R Core Team. (2021). *R: A language and environment for statistical computing*. R Foundation for Statistical Computing. http://www.R-project.org/

Renault, S., Lait, C., Zwiazek, J. J., & MacKinnon, M. (1998). Effect of high salinity tailings waters produced from gypsum treatment of oil sands tailings on plants of the boreal forest. *Environmental Pollution*, *102*, 177–184.

Renault, S., MacKinnon, M., & Qualizza, C. (2003). Barley, a Potential Species for Initial Reclamation of Saline Composite Tailings of Oil Sands. *Journal of Environmental Quality*, *32*(6), 2245–2253. https://doi.org/10.2134/jeq2003.2245

Renault, S., Paton, E., Nilsson, G., Zwiazek, J. J., & MacKinnon, M. D. (1999). Responses of Boreal Plants to High Salinity Oil Sands Tailings Water. *Journal of Environmental Quality*, *28*(6), 1957–1962. https://doi.org/10.2134/jeq1999.00472425002800060035x

Renault, S., Zwiazek, J. J., Fung, M., & Tuttle, S. (2000). Germination, growth and gas exchange of selected boreal forest seedlings in soil containing oil sands tailings. *Environmental Pollution*, *107*(3), 357–365. https://doi.org/10.1016/S0269-7491(99)00167-0

Rowland, S. M., Prescott, C. E., Grayston, S. J., Quideau, S. A., & Bradfield, G. E. (2009). Recreating a Functioning Forest Soil in Reclaimed Oil Sands in Northern Alberta: An Approach for Measuring Success in Ecological Restoration. *Journal of Environmental Quality*, *38*(4), 1580–1590. https://doi.org/10.2134/jeq2008.0317

Samad, A., Pelletier, G., Séguin, A., Degenhardt, D., Muench, D. G., & Martineau, C. (2022). Understanding Willow Transcriptional Response in the Context of Oil Sands Tailings Reclamation. *Frontiers in Plant Science*, *13*, 857535. https://doi.org/10.3389/fpls.2022.857535

Smreciu, A., Gould, K., & Wood, S. (2013). *Boreal Plant Species for Reclamation of Athabasca Oil Sands Disturbances—Updated December 2014* (OSRIN Report TR-44; p. 23). Oil Sands Research and Information Network, University of Alberta, School of Energy and the Environment.

Stack, S., Jones, C., Bockstette, J., Jacobs, D. F., & Landhäusser, S. M. (2020). Surface and subsurface material selections influence the early outcomes of boreal upland forest restoration. *Ecological Engineering*, *144*, 105705. https://doi.org/10.1016/j.ecoleng.2019.105705

Stack, S., Yarmuch, M., & Landhäusser, S. M. (2021). Species-specific responses to targeted fertilizer application on reconstructed soils in a reclaimed upland area. *Canadian Journal of Soil Science*, *101*(1), 45–61. https://doi.org/10.1139/cjss-2019-0136

Sutton, O. F., & Price, J. S. (2020). Soil moisture dynamics modelling of a reclaimed upland in the early post-construction period. *Science of The Total Environment*, *718*, 134628. https://doi.org/10.1016/j.scitotenv.2019.134628

Syncrude Canada Ltd. (2013). *South Bison Hill Soil Capping Research Synthesis*.

Turnbull, L. C., & Bridgham, S. D. (2015). Do Two Graminoids, the Invasive *Phalaris arundinacea* and the Native *Scirpus microcarpus* , Have Similar Ecosystem Effects in a Wetland? *Soil Science Society of America Journal*, *79*(3), 957–967. https://doi.org/10.2136/sssaj2014.08.0335

Wickham, H., Averick, M., Bryan, J., Chang, W., McGowan, L., François, R., Grolemund, G., Hayes, A., Henry, L., Hester, J., Kuhn, M., Pedersen, T., Miller, E., Bache, S., Müller, K., Ooms, J., Robinson, D., Seidel, D., Spinu, V., … Yutani, H. (2019). Welcome to the Tidyverse. *Journal of Open Source Software*, *4*(43), 1686. https://doi.org/10.21105/joss.01686

Wilson, G. W., Kabwe, L. K., Beier, N. A., & Scott, J. D. (2018). Effect of various treatments on consolidation of oil sands fluid fine tailings. *Canadian Geotechnical Journal*, *55*(8), 1059–1066. https://doi.org/10.1139/cgj-2017-0268

Wytrykush, C., Vitt, D. H., McKenna, G., & Vassov, R. (2012). Designing landscapes to support peatland development. In *Reclamation and resoration of Boreal ecosystems* (pp. 161–178). Cambridge University Press.

Zhuang, J., McCarthy, J. F., Perfect, E., Mayer, L. M., & Jastrow, J. D. (2008). Soil water hysteresis in water-stable microaggregates as affected by organic matter. *Soil Science Society of America Journal*, *72*(1). https://doi.org/10.2136/sssaj2007.0001S6

Zuur, A. F., Hilbe, J. M., & Ieno, E. N. (2013). *A beginner's guide to GLM and GLMM with R: a frequentist and Bayesian perspective for ecologists*. Highland Statistics Ltd.

GROWTH AND SURVIVAL OF NATIVE WETLAND SPECIES IN SHALLOW CAPPED CENTRIFUGE TAILINGS AND CO-MIX TAILINGS: A MESO-SCALE GREENHOUSE STUDY

Dani Degenhardt[1], Angeline Van Dongen[1], Jessica Hudson[1], Nicolas Utting[2], and Stefan G. Schreiber[3]
[1]Natural Resources Canada, Canadian Forest Service, Northern Forestry Center, Edmonton, Canada
[2]Natural Resources Canada, CanmetEnergy, Devon, Canada
[3]EnviroStats Solutions Inc., Edmonton, Canada

ABSTRACT

This three-year meso-scale greenhouse study used 55-gallon columns to evaluate the survival and growth of boreal wetland communities on centrifuged tailings (CF) and co-mixed tailings (CM) with different reclamation cover soil capping designs. The CF tailings were capped with a shallow layer (0-30 cm) of peat reclamation material (PRM) and CM tailings were capped with a shallow layer (0-5 cm) of PRM above (0-35 cm) of reclamation subsoil (till). After three growing seasons, plant survival and growth on CF tailings showed significant improvement with a 10 cm PRM cap compared to the uncapped tailings, and plants growing on a 30 cm PRM cap outperformed those on the 10 cm PRM cap. Plant growth on CM tailings was significantly improved with a soil reclamation cap containing 5 cm PRM and at least 15 cm till. Among the seven native wetland species included in this study, the top performing species on the capped treated tailings were *Salix bebbiana*, *Scirpus microcarpus,* and *Carex aquatilis.*

INTRODUCTION

Oil sands deposits in Alberta represent the world's fourth largest reserves of crude oil (Government of Alberta, 2022). Where these deposits are located less than approximately 70 m below ground, open pit mining is utilized to extract the resource (CAPP, 2022). The Clark Hot Water extraction process creates a tailings by-product, which is a mixture containing sand and a fluid component consisting of water, silt, clay and some residual hydrocarbons and salts. The tailings are distributed hydraulically in storage facilities (in-pit and out-of-pit), which serve two important purposes; they are the primary source of recycle water in the bitumen extraction process, and as containment for the tailings (BGC Engineering Inc., 2012). Oil sands mines must reclaim their mine sites, including tailings ponds that are no longer in use and are built to closure design specifications, to produce a landscape with a self-sustaining ecosystem including local vegetation and wildlife habitat (Government of Canada, 2013). Oil sands operators have several decades of experience reclaiming overburden dumps and sand dominated tailings, such as Syncrude Canada Ltd. (Syncrude) South Bison Hill and Gateway Hill (Grant et al., 2013; Syncrude Canada Ltd., 2013).

Fluid fine tailings (FFT) are a liquid suspension of oil sands fines in water with a solids content greater than 2% but less than the solids content corresponding to the liquid limit (COSIA, 2012). FFT are dominated by fine-grained material (e.g. silt and clay dominated particles < 45 µm) and also contain dissolved inorganic salts, residual bitumen, and soluble organic compounds, including naphthenic acids (NAs) (Kasperski & Mikula, 2011). Under normal conditions, consolidation of the fines and loss of the excess pore-water takes decades for sufficient settling to achieve a geotechnical strength that is trafficable for equipment to complete reclamation (e.g. soil capping).

To accelerate the consolidation process, various techniques have been implemented to create a trafficable surface for reclamation. One such technique is the creation of centrifuge (CF) tailings, a tailings cake produced from the addition of a coagulant (e.g., gypsum), organic polymers (polyacrylamides), and centrifugation (BGC Engineering Inc., 2012). Another technique involves mixing FFT with saline-sodic overburden, a clay shale material overlying oil sands ore, to create co-mixed (CM) tailings. These methods are expected to increase the strength, stability, and structure of the deposit, thereby accelerating the transformation of tailings slurry into trafficable deposits that are ready to reclaim. CF and CM tailings are placed in contained structures or cells to create deep deposits that are > 2 m thick and more commonly 20 m at the end of deposition (COSIA, 2022; Syncrude Canada Ltd., 2020). Full-scale production of tailings using these treatment technologies is relatively new and large-scale reclamation of these deposits is now underway.

There are two types of caps commonly used in tailings reclamation: a substrate cap over the treated tailings (e.g. coarse tailings or suitable overburden material), which is intended to buffer any deleterious constituents in the tailings (e.g. elevated salinity, NAs and residual bitumen) and a soil reclamation cap that provides a medium for revegetation. In some cases, both caps would be applied (e.g. Sandhill Fen reclamation area) (Vitt et al., 2016). Current regulatory approvals for treated FFT reclamation requires soil reclamation placement of 0.8-1.0 m of suitable overburden (or tailings sand which meets the chemical criteria for suitable overburden), overlain by 0.2 m of coversoil (Alberta Energy Regulator, 2020). Although there are specific regulatory requirements of soil reclamation placement for treated FFT, there is a lack of understanding on how capping materials and depths will influence reclamation objectives. Furthermore, these deposits will continue to undergo self-weigh consolidation, which will result in settlement of the landscape and release of process water overtime. Since reclamation of these tailings deposits is still in its infancy, there are opportunities to find innovative, cost effective, and commercially viable reclamation strategies to reclaim treated FFT deposits and achieve end land use targets and closure certification.

In the mineable oil sands region of NE Alberta (Athabasca Oil Sands Region), wetlands make up over 60% of the natural landscape and are dominated by peatland landforms (bogs and fens) (Rooney & Bayley, 2011; Vitt et al., 2016). In a mine closure scenario, fines-dominated tailings deposits, such as treated FFT, may be a suitable substrate for wetland development, establishing a (near) surface water table from surface runoff and precipitation inputs, as well as from upward seepage of pore water from tailings consolidation.

In the past decade, there have been some large-scale constructed fen research projects led by oil sands operators including the Sandhill Fen, constructed by Syncrude, where composite tailings were capped with several meters of hydraulically and mechanically placed coarse tailings, followed by fine-grained clay till subsoil (0.5 m thickness) and peat coversoil (0.5 m thickness) reclamation materials (Syncrude Canada Ltd., 2020; Wytrykush et al., 2012). Common boreal fen species were seeded at Sandhill Fen including a variety of sedges, arrow grasses, rushes, *Beckmania syzigachne*, and *Betula glandulosa*, while natural ingress of native species also occurred (Syncrude Canada Ltd., 2020; Wytrykush et al., 2012).

There has been limited research considering the impacts of plant growth and survival in treated fine tailings (e.g., CF and CM tailings) capped with reclamation coversoil. Omari et al. (2020) considered the growth of a native species in reclamation soils mixed with CF tailings and found that the CF and peat mixture supported the highest aboveground biomass (Omari et al., 2020). Lalonde et al. (2020) considered the implication of the thickness of reclamation soil caps on the growth of woody species (*Salix bebbiana* and *Populus tremuloides*) overlying CF tailings. The preceding studies have considered growth of vegetation on treated FFTs; however, these studies were limited to a small container (< 3 L) and relatively short growth duration (a couple of months). Controlled greenhouse studies provide an opportunity to assess performance of different wetland species in CF and CM tailings with different soil reclamation capping prescriptions. In addition, relatively thin soil reclamation caps provide an opportunity to evaluate plant growth response with a root zone that is affected by the tailings and any constituents that are released from the tailings into the above soil reclamation cover. The objective of this three-year meso-scale greenhouse study was to understand the effects of CF and CM tailings on survival and growth of native wetland species and the potential improvement in plant response with the addition of a relatively thin soil reclamation cap above the tailings.

MATERIALS AND METHODS

Materials

Materials for this study were provided by an oil sands operator and included CF tailings, PRM, till (mineral subsoil), FFT, and Clearwater formation (Kc) overburden. The CM tailings were created in-house by crushing the Kc to pass a #4 mesh size (24.76 mm) and then mixing it with FTT at a 0.4 (by weight) Kc:FTT ratio and curing at room temperature for 24 hours. This generated CM tailings with ~70% solids (by weight) and ~10 kPa shear strength.

Experimental design

Columns were assembled in 55-gallon (208 L) plastic cylindrical barrels (54 cm in diameter and 90 cm in height).

For the CF tailings, three capping treatments were evaluated (Figure 1). Each column was planted with

one of two fen communities: woody fen or graminoid fen. Each fen community was comprised of four different species. The woody fen community included *Salix bebbiana* Sarg. (Bebb's willow), *Betula pumila* var. *glandulifera*, Regal (Dwarf birch), *Scirpus microcarpus* J. Presl and C. Presl (Small-fruited bulrush), and *Rumex occidentalis* S. Watson, (Western dock). The graminoid fen community included *Salix bebbiana* Sarg., (Bebb's willow), *Scirpus microcarpus* J. Presl and C. Presl, (Small-fruited bulrush), *Triglochin maritima* L, (Sea-side arrow grass) and *Beckmannia syzigachne* (Steud.) Fernald (Slough grass). Each of the three capping depth treatments with the two plant communities were replicated four times for a total of 24 columns.

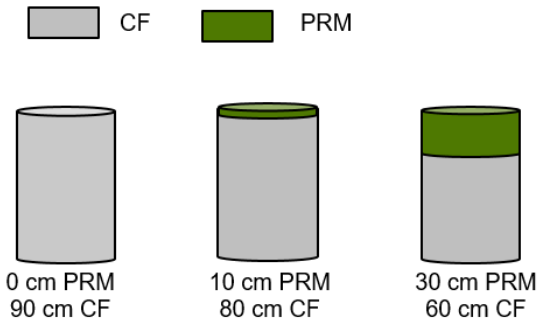

Figure 1. Tailings capping treatments with varying depths of peat reclamation material (PRM) on top of centrifuge tailings (CF) in columns

For the CM tailings, five capping treatments were evaluated (Figure 2). Different capping thicknesses were created using only a thin layer of PRM (5 cm) over top of increasing amounts of till. The 5 cm PRM / 85 cm till treatment does not contain any CM tailings and was included as a control representing plants growing without the influence of tailings. Each column was planted with a wetland community comprised of four species: *Salix bebbiana* Sarg. (Bebb's willow), *Carex aquatilis* Wahlenb. (water sedge), *Triglochin maritima* L, (Sea-side arrow grass) and *Beckmannia syzigachne* (Steud.) Fernald (Slough grass). Each of the five capping treatments was replicated four times for a total of 20 columns.

All columns were planted in May 2019 with three individual plants per species for a total of 12 plants per column. Species were planted as soil-rooted seedlings in 170 mL peat plugs. No fertilizer was used post-planting. Over-head irrigation was applied consistently to all treatments to mimic precipitation. Column temperature and moisture were monitored and greenhouse conditions were altered to mimic a typical growing season over the study period.

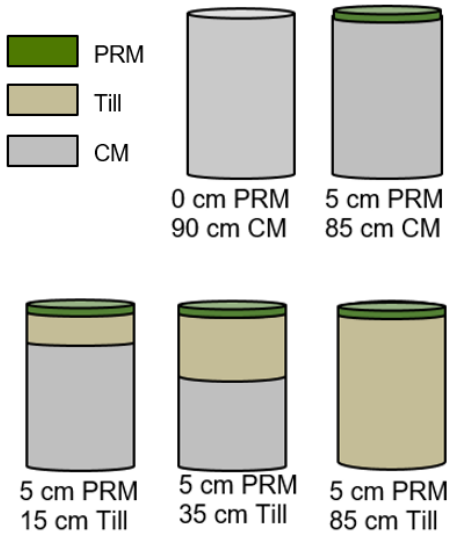

Figure 2. Tailings capping treatments with carrying depths of peat reclamation material (PRM) and till on top of co-mixed tailings (CM) in columns.

Initial material characterization

Composite samples of the CF, CM, PRM, and till were collected prior to column assembly to characterize the materials (Table 1). The CF and CM tailings used in this project were fines-dominated tailings with sands to fines ratios (SFR) < 1 (Table 1). Total exchangeable cations were mainly comprised of Ca^{2+} and Na^{+} (Table 1). In the CF tailings, electrical conductivity (EC) is rated Poor, and petroleum hydrocarbons (PHCs) (F1 to F4) exceeded Alberta Tier 1 guidelines (Alberta Environment and Parks, 2019; Canadian Council of Ministers of the Environment, 2007) (Table 1). In the CM tailings, EC is rated Fair, while boron and PHCs (F1-F3) exceed Alberta Tier 1 guidelines (Alberta Environment and Parks, 2019; Canadian Council of Ministers of the Environment, 2007) (Table 1). The naphthenic acids (NAs) concentration was ten folds higher in CF tailings compared to CM tailings (Table 1).

Basic physiochemical analysis was determined for the PRM coversoil and till reclamation materials and included pH, EC, sodium adsorption ratio (SAR), cation exchange capacity (CEC), exchangeable cations and available nutrients (Table 1). The PRM's values are within the general range of PRM coversoil used for reclamation in this region

(MacKenzie & Quideau, 2012; Schott et al., 2016; Stack et al., 2020, 2021).

Table 1. Centrifuge tailings (CF), co-mixed tailings (CM), peat reclamation material (PRM) and till physiochemical properties expressed as mean ± standard deviation.

	Parameter	*CF Tailings (n=8)*	*CM Tailings (n=7)*	*PRM (n=8)*	*Till (n=5)*
Physio-chemical	pH	7.8±0.1	7.6±0.1	6.2±0.4	8.4±0.1
	Electrical Conductivity (dS/m)	7.0±0.9	3.5±0.2	0.2±0.1	0.2±0.01
	Sodium Adsorption Ratio	4.3±0.3	5.4±0.6	0.5±0.2	0.8±0.1
	Cation Exchange Capacity (cmol/kg)	19±8	20±5	49±12	9±2
	Solids (%)	59±1.7	71±3		87±1
	Sand to Fines Ratio	0.44±0.1	0.55±0.1		1.1±0.3
	% sand (>45 µm)	30±5	34±6		45±12
	% silt (2 - 45 µm)	54±5	38±4		29±9
	% clay (<2 µm)	16±4	28±4		25±4
	Total Organic Carbon (mg/kg)			13.7±3.5	
	Total Carbon (mg/kg)			15.7±3.6	
Inorganics	Exchangeable Ca^{2+} (mg/kg)	2,698±666	3,735±400	6,320±1283	4,908±421
	Exchangeable Na^{+} (mg/kg)	922±165	1,385±138	89±41	222±33
	Exchangeable K^{+} (mg/kg)	131±26	198±28	51±14	66±31
	Exchangeable Mg^{2+} (mg/kg)	478±96	826±111	1,157±290	437±105
	Extractable P (mg/kg)	6±6	8±2	5.7±1	1.4±0.5
	Extractable S (mg/kg)	235±144	403±82	72±17	40±1
	NO_3-N (mg/kg)	38±4	32±9	29±16	39±12
	NH_4-N (mg/kg)	64±14		24±9	
	Total Nitrogen (mg/kg)			0.3±0.1	
Trace metals	Boron (mg/kg)	2.6±3	8.8±1		
	Barium (mg/kg)	2.2±0.8	1.8±0.1		
	Copper (mg/kg)	0.06±0.02	0.1±0.04		
	Iron (mg/kg)	7.4±7	0.7±0.1		
	Manganese (mg/kg)	0.5±1.4	5.1±2		
	Strontium (mg/kg)	1.6±4.0	20±8		
	Zinc (mg/kg)	0.5±0.3	1.0±0.1		
Organics	PHC F1 C6-C10 (mg/kg)	4,279±1,423	581±114		
	PHC F2 C10-C16 (mg/kg)	8,331±1,171	570±114		
	PHC F3 C16-C34 (mg/kg)	41,938±5,861	1,357±213		
	PHC F4 C34-C50+ (mg/kg)	37,838±6,406	2,757±407		
	PHC F5 (mg/kg)	19,900±4,598	2,907±756		
	Naphthenic Acids* (mg/kg)	3,717±770	321±80		
	Bitumen (%)	4.8±1.0	0.5±0.2		

* Naphthenic acids analysed using Headley et al.'s method (Headley et al., 2002, 2011)

Assessment and monitoring

Vegetation assessments were conducted at the time of planting and at the peak (August) of each growing season and included evaluations of plant survival and vegetative cover for plants of all species as well as stem diameter, height, and growth increment (leader growth) for the woody species (*S. bebbiana* and *B. pumila*). Vegetative cover was assessed as the percent of the total circular area of the column covered by each individual plant.

At the end of Year 3, composite samples of the tailings, PRM, and till were collected from each treatment for physiochemical analysis. In addition, the living aboveground biomass was collected for each species from each column for total

aboveground biomass. The weight per species was determined after drying for three days at 40°C.

Data analysis

Data analysis and visualizations were carried out using the R language and environment for statistical computing (R Core Team, 2021), the *glmmTMB* package (Brooks et al., 2017) as well as the *tidyverse* packages (Wickham et al., 2019). Separate analyses were conducted for CF and CM tailings treatments. Linear and generalized linear mixed-effects models (Bolker et al., 2009; Gelman & Hill, 2006; Zuur et al., 2013) were used to model the effect of capping treatment on survival, above-ground biomass, plant cover, and woody species growth (stem diameter, height, height increment). The random effect used for all models was "column" to account for non-independent measurements within each column. Furthermore, whenever possible, species nested in the community was used as an additional random term. Wald chi-square tests were conducted to test the fixed effects for their significance via the *Anova()* function of the *car* package (Fox & Weisberg, 2019). Estimated marginal means were calculated using the *emmeans* package (Lenth, 2020) based on the fitted models. P-values for multiple mean comparisons were adjusted using the Tukey method.

RESULTS

Changes in substrate properties

There were some notable changes in the physical and chemical properties of the CF and CM tailings after three growing seasons. The initial vane shear strength of the CF tailings was 2.5 ± 0.3 kPa (Table 2), below the 5 kPa limit that approximates the liquid limit of a cohesive deposit, and is often used to gauge the trafficability of treated tailings prior to initiating terrestrial reclamation (Alberta Energy Regulator, 2022). By the end of Year 3, the vane shear strength of the tailings had increased to between 20 and 39 kPa, depending on the treatment (Table 2). The initial vane shear strength of the CM tailings was 5.8±2.6 kPa and increased to between 31 and 53 kPa depending on the treatment (Table 3).

The EC, exchangeable Na^+ concentration, and extractable S and NO_3^- concentrations and the NAs concentrations in the CF tailings decreased over time across all treatments (Table 2). Over the course of the experiment, the SAR was consistent across the three years, while the concentrations of exchangeable K^+ increased across all treatments (Table 2) over time. The F1 PHC fraction decreased to below the detection limit and the F4 PHC fraction was reduced to almost half of its initial concentration across all treatments by the end of Year 3, respectively (Table 2), while the F2, F3 and F5 PHC fractions stayed consistent during the experiment.

The exchangeable Na^+ concentration and extractable S and NAs concentrations in the CM tailings decreased over time across all treatments while the concentrations of exchangeable K^+ increased across all treatments (Table 3). The F4 and F5 PHC fractions decreased while the F3 PHC fraction increased across all treatments by the end of Year 3 (Table 3).

Table 2. Chemical properties of centrifuged tailings (CF) and peat reclamation material (PRM) expressed as mean ± standard deviation at the beginning of the experiment (Initial) and at the end of Year 3 (Final) for each CF treatment: 0, 10, and 30 cm PRM. DL = Detection Level.

Parameters	***Initial*** *(n=8)*	***Final***		
		0 cm PRM (*n*=2)	10 cm PRM (*n*=2)	30 cm PRM (*n*=2)
Centrifuge tailings				
Vane shear (kPa)*	2.5±0.3	34±14	20±7	39±16
pH	7.8±0.1	7.6±0.1	7.9±0.1	7.4±0.4
Electrical conductivity (dS/m)	7.0±0.9	5.8±1.1	3.7±1.7	4.4±1.7
Sodium adsorption ratio (SAR)	4.3±0.3	5.2±1.3	4.8±0.9	4.3±0.2
Exchangeable Ca^{2+} (mg/kg)	266±119	167±104	259±214	158±113
Exchangeable Na^+ (mg/kg)	1211±112	696±363	596±242	520±122
Exchangeable K^+ (mg/kg)	58±7	113±13	110±14	86±12
Exchangeable Mg^{2+} (mg/kg)	96±36	79±50	78±50	154±142
Extractable S (mg/kg)	697±284	446±31	364±100	475±301

NO_3-N	6.1±4.5	2.2±1.3	2.9±0.5	3.5±1.9
PHC F1 C6-C10 (mg/kg)	4,279±1,423	<DL	<DL	<DL
PHC F2 C10-C16 (mg/kg)	8,331±1,171	8,703±770	8,695±1,473	9,220±3,009
PHC F3 C16-C34 (mg/kg)	41,938±5,861	44,100±1,817	42,750±7,778	44,675±13,622
PHC F4 C34-C50+ (mg/kg)	37,838±6,406	18,775±369	17,775±3,279	18,650±5,698
PHC F5 (mg/kg)	19,900±4,598	19,200±2,918	17,900±1,920	19,450±7,547
NA (mg/kg)	3,717±770	2,079±899**	711±487**	1,152±450**
Peat Reclamation Material				
pH	6.2±0.4	-	6.8±0.1	5.9±0.1
Electrical conductivity (dS/m)	0.2±0.1	-	4.0±1.0	1.0±0.2
Sodium adsorption ratio (SAR)	0.4±0.2	-	4.1±0.8	1.5±0.1
Exchangeable Ca^{2+} (mg/kg)	15.7±3.6	-	294±78	80±26
Exchangeable Na^{+} (mg/kg)	13.6±3.5	-	504±182	80±6
Exchangeable K^{+} (mg/kg)	55±32		161±16	173±150
Extractable S (mg/kg)	66±19		1050±179	315±53
NO_3-N	29±17		2.5±2.2	4.6±1.5

*n=4, **n=6

Table 3. Chemical properties of co-mixed tailings (CM), peat reclamation material (PRM), and till expressed as mean ± standard deviation at the beginning of the experiment (Initial) and at the end of Year 3 (Final) for all CM treatments; 0 cm PRM, 5 cm PRM, 5 cm PRM / 15 cm till, and 5 cm PRM / 35 cm till. DL = Detection Level.

Parameters	***Initial*** *(n=7)*	***Final***				
		0 cm PRM (*n*=1)	5 cm PRM (*n*=1)	5 cm PRM 15 cm Till (*n*=1)	5 cm PRM 35 cm till (*n*=1)	5 cm PRM 85 cm till (n=1)
Co-mixed tailings						
Vane shear (kPa)*	5.8±2.6	53±15	41±28	31±8	31±9	22±6
pH	7.6±0.1	7.9	8.1	7.9	6.4	-
Electrical conductivity (dS/m)	3.5±0.2	8.1	5.7	5.7	5.6	-
Sodium adsorption ratio (SAR)	5.4±0.6	6.5	5.3	4.9	5.1	-
Exchangeable Ca^{2+} (mg/kg)	3735±400	254	298	296	179	-
Exchangeable Na^{+} (mg/kg)	1385±138	1043	705	749	610	-
Exchangeable K^{+} (mg/kg)	198±28	171	118	189	-	-
Exchangeable Mg^{2+} (mg/kg)	826±111	143	93	92	84	-
Extractable S (mg/kg)	403±82	1010	366	607	-	-
PHC F1 C6-C10 (mg/kg)	581±114	<DL	<DL	<DL	<DL	-
PHC F2 C10-C16 (mg/kg)	570±114	667±218	731±322	365±28	563±322	-
PHC F3 C16-C34 (mg/kg)	1357±213	4190±1259	4385±1266	3075±375	3935±1393	-
PHC F4 C34-C50 (mg/kg)	2757±407	1820±580	1885±544	1005±163	1534±786	-
PHC F5 (mg/kg)	2907±756	1390±608	1790±622	1330±424	1756±868	-
NA (mg/kg)	321±80	151±47**	137±80**	165±46**	239±91**	-
Peat reclamation material						
pH	6.2±0.4	-	8.0	6.4	6.0	6.5
Electrical conductivity (dS/m)	0.2±0.1	-	6.8	1.7	1.5	0.6
Sodium adsorption ratio (SAR)	0.4±0.2	-	5.8	2.5	2.1	1.1
Exchangeable Ca^{2+} (mg/kg)	15.7±3.6	-	262	86	72	33
Exchangeable Na^{+} (mg/kg)	13.6±3.5	-	875	176	125	38
Extractable Mg (mg/kg)	1276±331	-	93	39	37	14

Till						
pH	6.2±0.4	-	-	8.4	8.4	8.7
Electrical conductivity (dS/m)	0.2±0.1	-	-	3.6	2.0	0.6
Sodium adsorption ratio (SAR)	0.4±0.2	-	-	4.0	2.9	1.6
Exchangeable Ca^{2+} (mg/kg)	15.7±3.6	-	-	138	96	25
Exchangeable Na^{+} (mg/kg)	13.6±3.5	-	-	411	224	68
Exchangeable K^{+} (mg/kg)	55±32	-	-	84	81	72
Extractable Mg (mg/kg)	66±19	-	-	52	34	7
Total S	-	-	-	334	129	42
NO_3-N	29±17	-	-	9.5	1	<DL

*n=4, **n=6

After three growing seasons, EC and SAR increased in PRM samples and till samples from both the CF and CM columns (Tables 2 and 3). Concentrations of exchangeable Ca^{2+} and Na^{+} also increased over time in PRM and till from both CF and CM tailings (Tables 2 and 3). These increases were greater in the thinner capping treatments compared to the thicker capping treatments (Tables 2 and 3).

Plant growth response in CF tailings

Survival of all species in both communities and across all treatments was high after Year 1; however, after the second growing season, all *B. syzigachne* and most of *B. pumila* in the uncapped columns had died (data not shown). By the end of Year 3, only *S. bebbiana* and *T. maritima* maintained high survival rates (75-100%) in the uncapped treatment (data not shown). Plant survival after three years growing in the uncapped treatment was significantly lower ($P < 0.001$) than for species growing in the capped treatments (Figure 3A). There was no significant difference in plant survival between the two PRM cap treatments, with high survival rates >90% in both treatments after Year 3 (Figure 3A).

Aboveground biomass at the end of the third growing season was also significantly higher ($P < 0.001$) in the capped treatments compared to the uncapped treatment and increased with increasing depth of PRM (Figure 3B). Overall, *S. bebbiana* produced the most aboveground biomass after Year 3, followed by *B. pumila,* and *S. microcarpus* while *T. maritima, R. occidentalis*, and *B. syzigachne* contributed little aboveground biomass across all treatments (data not shown).

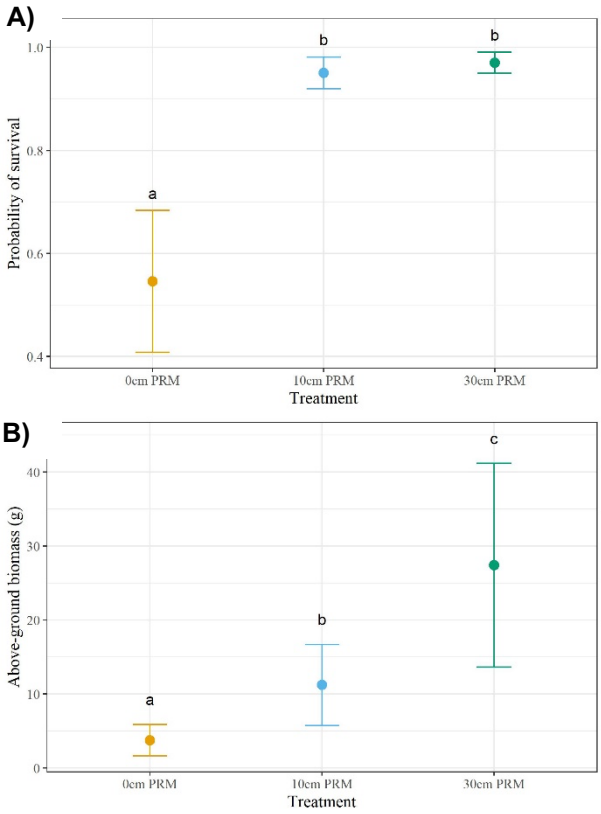

Figure 3. Probability of survival (A) and above-ground biomass (B) at the end of Year 3 for each treatment on CF tailings; 0 cm peat reclamation material (PRM) (yellow), 10 cm PRM (blue), and 30 cm PRM (green). Error bars represent standard error of the mean. Differing letters between means indicate a significant difference ($P < 0.05$).

For the two woody species, *S. bebbiana* and *B. pumila*, their mean stem diameter, mean height, and mean incremental height growth were significantly greater ($P < 0.001$) in the capped treatments compared to the uncapped treatment for all three

growing seasons (Figure 4). Mean stem diameters and heights increased each year, but incremental height growth was lowest in Year 3 (Figure 4). After the third growing season, these three parameters were significantly greater in the 30 cm PRM treatment compared to the 10 cm PRM and uncapped treatment.

Figure 4. Mean stem diameter (A), height (B), and height growth increment (C) of woody species, *Salix bebbiana* and *Betula pumila*, at the end of each year per treatment on CF tailings; 0 (yellow), 10 (blue), and 30 cm PRM (green). Error bars represent standard error of the mean. Differing letters between means indicate a significant difference ($P < 0.05$).

Plant growth response in CM tailings

Survival of all species was high after Year 1 across all treatments; however, by the end of Year 3, there was some plant mortality observed within all treatments except in the 5 cm PRM / 85 cm till control (data not shown). The probability of survival after three growing seasons was significantly higher in the 5 cm PRM / 15 cm till treatment compared to plants growing in the uncapped tailings ($P = 0.026$), although there were no other significant differences in survival probability across treatments (Figure 5A). It should be noted that, because all species survived in the 5 cm PRM / 85 cm till treatment, variance could not be properly modelled within that treatment (Figure 5A). For the treatments that included till, the depth of the till did not influence the probability of plant survival, with high survival rates (> 90%) achieved across all treatments containing till (Figure 5A). Aboveground biomass at the end of the third growing season was not significantly different ($P = 0.107$) across treatments (Figure 5B).

After the first growing season, mean vegetation cover was significantly higher ($P < 0.001$) in the 5 cm PRM / 15 cm till and 5 cm PRM / 35 cm till treatments compared to the uncapped tailings and the 5 cm PRM / 85 cm till treatment (Figure 6). Over time, vegetation cover decreased slightly within all treatments. By the end of the study, the 5 cm PRM / 15 cm till and 5 cm PRM / 35 cm till treatments had significantly higher ($P < 0.001$) vegetation cover than both the uncapped tailings and the 5 cm PRM treatments, while vegetation cover in the 5 cm PRM

/ 85 cm till was not significantly different from any of the treatments (Figure 6).

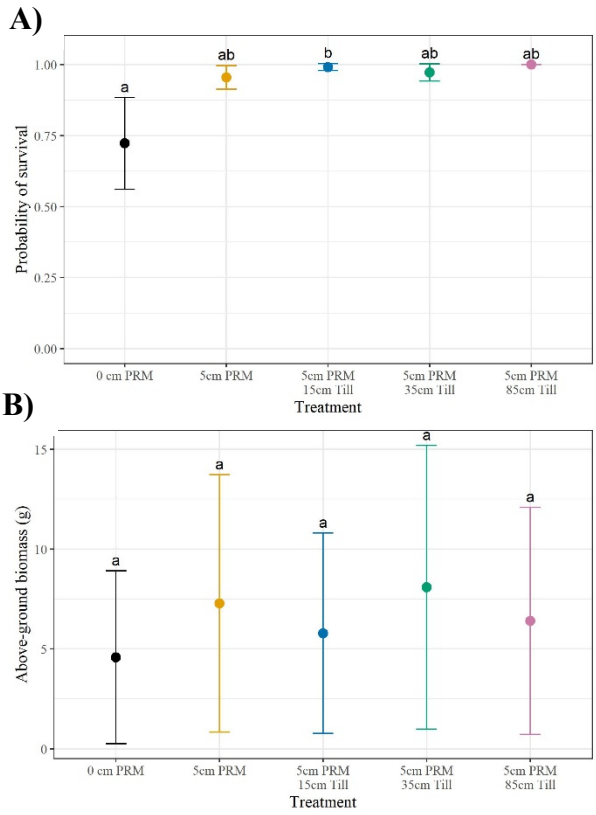

Figure 5. Probability of survival (A) and aboveground biomass (B) per treatment in CM tailings at the end of Year 3 for 0 cm PRM (black), 5 cm PRM (orange), 5 cm PRM / 15 cm till (blue), 5 cm PRM / 35 cm till (green), and 5 cm PRM / 85 cm till (pink). Error bars represent standard error of the mean. Differing letters between means indicate a significant difference ($P < 0.05$).

Differences in *S. bebbiana* mean stem diameter and height between treatments became more apparent over time (Figure 7A, B). By Year 3, the 5 cm PRM treatment saw improved stem diameter, height, and incremental growth compared to the uncapped tailings; however significantly greater mean diameter (P =0.018), height (P < 0.001), and incremental growth (P < 0.001) were achieved in the three till treatments compared to the treatments without till (Figure 7A, B, C). Mean stem diameters and heights increased each year, but incremental height growth was lowest in Year 3 (Figure 7).

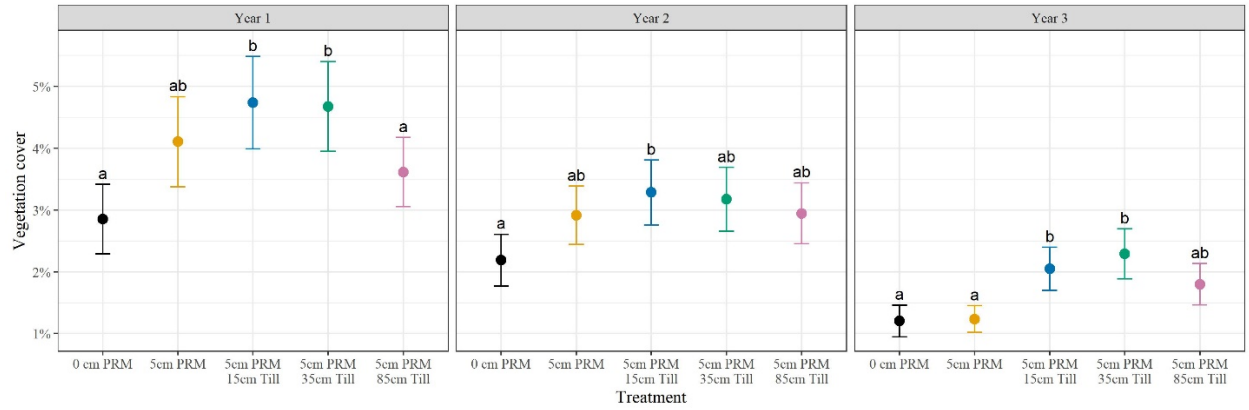

Figure 6. Mean vegetation cover at the end of each year per treatment in CM tailings; 0 cm peat reclamation material (PRM) (black), 5 cm PRM (orange), 5 cm PRM / 15 cm till (blue), 5 cm PRM / 35 cm till (green), and 5 cm PRM / 85 cm till (pink). Error bars represent standard error of the mean. Differing letters between means indicate a significant difference ($P < 0.05$).

Figure 7. Mean stem diameter (A), height (B), and height growth increment (C) of *Salix bebbiana* at the end of each year per treatment; 0 cm peat reclamation material (PRM) (black), 5 cm PRM (yellow), 5 cm PRM / 15 cm till (blue), 5 cm PRM / 35 cm till (green), and 5 cm PRM / 85 cm till (pink). Error bars represent standard error of the mean. Differing letters between means indicate a significant difference ($P < 0.05$).

DISCUSSION

Plant response to CF and CM tailings

The physio-chemical properties of CF and CM tailings (Table 1), which include elevated salinity and PHCs and low available plant nutrients, can negatively impact plant growth and survival (Renault et al., 1998, 2000, 2003, 2004). The CF tailings had higher EC, higher NAs and residual petroleum hydrocarbons compared to the CM tailings, while CM tailings had a higher SAR, Na^+ concentration, and higher boron concentration than the CF tailings.

In the uncapped CF tailings, survival remained high in Year 1, but then dropped to 55% (Figure 3A) by Year 3. Plants growing in uncapped CF tailings achieved significantly lower above-ground biomass, cover, and woody species growth compared to plants growing in capped CF tailings.

In the uncapped CM tailings, survival remained relatively high after 3 years (72%; Figure 5A). Furthermore, Year 3 above-ground biomass in the uncapped CM tailings was not significantly different from biomass in the tailings with various capping designs (Figure 5B). Mixing overburden with the FTT created a CM tailings deposit with lower concentrations of PHCs and NAs relative to the CF tailings. However, growth limitations associated with CM tailings were evident in the reduced vegetation cover in the uncapped and thinly capped (5 cm PRM) tailings compared to the tailings with thicker caps (5 cm PRM / 15 cm till or 5 cm PRM / 35 cm till) (Figure 6). Furthermore, the stem diameter, height, and height incremental growth of *S. bebbiana* after Year 3 were all significantly lower in the uncapped tailings compared to the other treatments (Figure 7).

Samad et al. (2022) grew *Salix* directly on oil sands tailings in a similar meso-scale greenhouse study and found an alteration in physiological and

transcriptomic responses associated with stress compared to those grown in treatments capped with PRM or mineral subsoil material (Samad et al., 2022). Salinity can induce bio-chemical changes which produce reactive oxygen species (e.g. hydroxyl radicals, superoxide, and hydrogen peroxide) that are known to kill plant cells (Ashraf, 2004; Francois & Maas, 1999; Munns & Tester, 2008). Furthermore, reductions in plant growth hormones have been observed in plants growing in saline environments (Javid et al., 2011; Miransari & Smith, 2014). The elevated PHCs in the tailings can also affect plant growth. Soils contaminated with crude oil have been found to impact seedling growth, specifically decreasing plant biomass and shoot growth while reducing water use efficiency (Renault et al., 2000). Additionally, the presence of PHCs in soil can lead to reduced nitrogen availability as PHC degrading soil microbes compete with plants for nitrogen (Correa-García et al., 2018). Finally, high concentration of NAs in the CF and CM tailings likely impacted plant growth and despite the decrease observed in Year 3, NA levels likely still contributed to the phytotoxicity of the tailings (Armstrong et al., 2010).

Taken together, several elevated, deficient and/or restrictive parameters of CF and CM tailings resulted in plant growth limitations relative to the soil reclamation cap treatments; however, determining the relative magnitude of each individual contribution or their cumulative effects on plant response cannot be determined in this study. These constraints further demonstrate that CF and CM tailings alone (e.g. no soil reclamation cover) are not an ideal growth medium for plant growth.

Plant response to reclamation cap

The PRM cap on CF tailings significantly improved plant survival over three growing seasons and significantly increased above-ground biomass and vegetation cover. Mean stem diameter, height, and height increment growth were also significantly larger for the woody species in the treatments with PRM caps compared to the uncapped CF treatment.

The addition of a cap on the CM tailings, such as 5 cm of PRM, resulted in very high plant survival rates (> 90%) after three years (Figure 5A). The 5 cm PRM cap alone provided a minimal increase in plant growth overall; survival, above-ground biomass, and cover were not significantly different between the 5 cm PRM cap and the uncapped tailings. However, the 5 cm PRM cap did significantly benefit *S. bebbiana* growth (height, diameter, height increment) relative to growth in the uncapped tailings (Figure 7).

These findings are consistent with other greenhouse tailings capping studies; Luna Wolter & Naeth (2014) found that coversoil caps (either PRM or upland surface soil coversoil) improved the growth of native grasses on mature fine tailings (MFT) and Lalonde et al. (2020) found that soil caps (PRM and/or upland surface soil coversoil) improved growth of *P. tremuloides* and *S. bebbiana* on CF tailings.

PRM coversoil material is predominantly organic peat soil which is a suitable coversoil material for reclamation that holds moisture and provides essential plant-available macro- and micronutrients. The soil reclamation cap likely helped to provide a suitable root zone for plant growth relative to CF and CM substrates, providing nutrients, while having lower salinity and PHCs. The PRM used may also contain beneficial root-associated microorganisms that can promote plant growth and reduce environmental stress through enhanced nutrient cycling and uptake, phytohormones production, and contaminants degradation (Correa-García et al., 2018).

Plant response to reclamation cap thickness

Plant growth response differences between the 10 and 30 cm PRM cap depth on CF tailings became evident at the end of Year 3 when the thicker PRM cap had significantly higher aboveground biomass and vegetation cover. In addition, the woody species stem diameter, height, and growth increment were significantly higher in the 30 cm PRM cap compared to the 10 cm PRM cap after Year 3.

On the CM tailings, the additional layer of 15 or 35 cm of till beneath the 5 cm PRM cap, substitutes some of the tailings in the column with suitable overburden (subsoil) reclamation material, and yielded significantly higher vegetation cover compared to both the uncapped CM tailings and the CM tailings capped with only 5 cm PRM (Figure 3). *S. bebbiana* diameter, height, and height increment generally increased with increasing cap thickness; however, there were no significant differences between the 5 cm PRM / 15 cm till or 5 cm PRM / 35 cm till after Year 3 in terms of height and height increment growth (Figure 3). In most cases, there was little difference in plant response between the two thicker caps (either 15 or 35 cm till) and the

plant response in these thicker caps was also very similar to the plant response from the control columns which lacked CM tailings. These findings indicate that, over the course of this 3-year study, the 5 cm PRM / 15 cm till cap improved plant growth, but beyond this thickness, increases in cap thickness did not correspond to increases in plant growth, at least in the first three growing seasons of this study.

The current study further supports the need for a soil reclamation cap over CF and CM tailings to improve wetland species (and likely all plant species) survival and growth. The reclamation regulatory requirements of a suitable soil reclamation cap for CF tailings (20 cm of coversoil plus 100 cm of subsoil) and CM tailings (20 cm coversoil and 80 cm subsoil) (Alberta Energy Regulator, 2020) provides significantly more root zone for plant growth relative to those used in this study.

Plant response over time

This three-year study showed that plant response in the first growing season is a mere snapshot of plant establishment and that monitoring in subsequent years is especially important as roots spread further into tailings with increasing resource demands and chemical constituents present in the tailings impact water quality and the soil reclamation cover, which in turn affects the root zone for plant growth. In this study, significant plant growth differences between the two PRM coversoil treatments in the CF tailings were not evident until the end of Year 3. Capping treatment differences on CM tailings also became more apparent over time. For example, vegetation cover in the 5 cm PRM cap was similar to the thicker cap treatments in Year 2, but by the end of Year 3, cover in the 5 cm PRM treatment dropped and became significantly lower compared to treatments with thicker caps (Figure 3). While the peat-filled plugs provided seedlings in all treatments with a good rooting medium, the delayed differentiation of plant growth response variables by treatment may be due in part to plant roots extending deeper into the column as the plants grow and resources become limited relative to the treatments that had a higher proportion of tailings within the column.

It is also noteworthy that vegetation cover and woody species' height increment growth dropped between Year 1 and Year 3 across all treatments on both CF and CM tailings. Because the drop in vegetation cover and decrease in growth were observed across all treatments, even in the control columns, we can conclude that the CM tailings are not solely responsible for this response. Photos taken of below-ground biomass during the experiment take-down show that, while many roots extended to the base of the column, the container was not crowded and not a limiting factor for root growth. As such, the decrease in cover and growth may be associated with nutrient limitations. All cap treatments in the CM tailings only included 5 cm PRM, which likely became devoid of nutrients by the third growing season. In addition, plant physiology may contribute to the reduction in growth rates observed in the woody species as some species may slow down growth after the first few years or reaching a steady state after a certain height. The initial plant growth response observed in our study may overestimate long-term growth estimates if the soil profile is unable to meet increasing resource requirements and highlight the importance of selecting an appropriate reclamation soil depth that meets the requirements of the vegetation community. Despite the drop in vegetative cover with time, there was an observed build-up of plant tissue from the previous years' growth that is expected to cycle carbon and nutrients back into the soil over time as it decomposes. In the field, the physical and chemical properties of the cap and tailings are expected to change over time with natural physical and biological processes, further highlighting the importance of long term field studies (Huang et al., 2015).

Top performing species

Tests for statistically significant differences between species were not carried out in the analysis since the objective of this paper was to evaluate the capping material and depth on plant performance. However, descriptive statistics were completed to highlight differences among species, which give an indication of the ability of some fen wetland species to survive and grow.

On the CF tailings, *T. maritima* and *S. bebbiana* demonstrated high survival rates even in uncapped tailings, although *T. maritima* biomass at the end of year three was low across all treatments. *S. bebbiana* and *S. microcarpus* survival and growth were improved with a PRM cap and these species were the top performing species in terms of cover and biomass at the end of Year 3 in the capped CF tailings. On the CM tailings, all species demonstrated high survival rates on the capped tailings, but *S. bebbiana* and *C. aquatilis* achieved the highest above-ground biomass after Year 3 and are thus considered top performing species.

Salix species are natural colonizers of highly disturbed areas and have been found to survive harsh conditions on mine sites (Mosseler et al., 2014). *S. bebbiana* is tolerant of a wide range of soil textures and moisture conditions and has been found on barren, acidic, metal contaminated soils (Hardy BBT Limited, 1989). Lalonde et al. (2020) recorded high (100%) survival rates of *S. bebbiana* when grown directly in CF tailings for 16 weeks (Lalonde et al., 2020). In the CF tailings, 75% of *S. bebbiana* plants survived three growing seasons in the uncapped tailings, although growth was limited. The PRM cap greatly improved *S. bebbiana* growth and survival in CF tailings. In the CM tailings, a thin cap greatly improved survival probability for S. bebbiana, which increased from 42% to 92% with the addition of a 5 cm PRM cap. By the end of Year 3, S. bebbiana achieved the highest above-ground biomass in both the CF and the CM tailings columns and may be successful in CF and CM tailings reclamation.

S. microcarpus is a perennial wetland sedge that spreads rapidly from rhizomes (Turnbull & Bridgham, 2015). In our study, *S. microcarpus* survival and growth improved greatly in the capped treatments, likely due to its low tolerance for salinity (USDA, 2022). In the capped CF tailings, *S. microcarpus* was a top performing species in terms of cover and above-ground biomass and has potential for use in CF tailings reclamation.

C. aquatilis was another top performing species in this study with high survival rates and above-ground biomass on capped CM tailings. The increased vegetation cover and above-ground biomass of *C. aquatilis* compared to the other wetland grasses (*B. syzigachne* and *T. maritima*) is associated with its prolific reproduction; *C. aquatilis* is a biannual and produces new rhizomatous shoots twice per year, spreading out in a mat from the main plant (Koropchak et al., 2012). *C. aquatilis* is a promising candidate for reclamation because it is a foundational species for early peatland communities, has a wide distribution across the boreal, and has a wide range of environmental tolerances, including soil type, organic matter content, and water depth (Koropchak et al., 2012). As such, this species was a large component of the seed mixed used at Sandhill fen, where sodium concentrations have been increasing over time (Vitt et al., 2020). In greenhouse studies, *C. aquatilis* has demonstrated a high tolerance for sodium with concentrations up to 1650 mg L^{-1} (Glaeser et al., 2021; Vitt et al., 2020). Based on its performance in this study, *C. aquatilis* may be a key species for successful reclamation of capped CM tailings deposits.

CONCLUSIONS

This study evaluated the ability of select wetland species to grow in CF and CM tailings and compared this plant growth response with treatments that had the addition of a soil reclamation cap. Results from this study found that CF and CM tailings had select elevated constituents and nutrient deficiencies that negatively affected plant growth. Furthermore, this study found that the addition of a relatively thin reclamation cap of PRM significantly improved the growth and survival of wetland species in CF tailings compared to uncapped tailings. In addition, we found that a 20 cm reclamation cap comprised of 5 cm of PRM above 15 cm of till above CM tailings significantly improved vegetation cover and growth on CM tailings compared to uncapped or thinly capped tailings. Many plant responses to the different capping treatments were not evident until Year 3, indicating the importance of longer term studies in understanding plant response for reclamation of substrates in closure landscapes. The top performing species, in terms of survival and growth, were *S. bebbiana*, *S. microcarpus,* and *C. aquatilis,* which have potential for use in CF and CM tailings reclamation. Although laboratory column studies like this one have limited capability to infer to actual reclamation field conditions, this study contributes to the understanding of the reclamation capability, potential environmental risks, and best reclamation practices of CF and CM tailings. As reclamation of treated fine tailings continues, there will be opportunities to conduct additional research studies and long-term monitoring activities.

ACKNOWLEDGEMENTS

We would like to acknowledge technical assistance from Craig McMullen, Kaitlyn Trepanier, Caren Jones, and Danica Long. We appreciate the feedback received from Marty Yarmuch and Craig Farnden.

REFERENCES

Alberta Energy Regulator. (2020). *Environmental Protection and Enhancement Act Approval No. 26-03-00*.

Alberta Energy Regulator. (2022). *Directive 085: Fluid Tailings Management for Oil Sands Mining Projects*. Alberta Energy Regulator. https://www.aer.ca/regulating-development/rules-and-directives/directives/directive-085

Alberta Environment and Parks. (2019). *Alberta Tier 1 Soil and Groundwater Remediation Guidelines*. Land Policy Branch, Policy and Planning Division.

Armstrong, S. A., Headley, J. V., Peru, K. M., Mikula, R. J., & Germida, J. J. (2010). Phytotoxicity and naphthenic acid dissipation from oil sands fine tailings treatments planted with the emergent macrophyte *Phragmites australis*. *Journal of Environmental Science and Health, Part A*, *45*(8), 1008–1016. https://doi.org/10.1080/10934521003772436

Ashraf, M. (2004). Some important physiological selection criteria for salt tolerance in plants. *Flora - Morphology, Distribution, Functional Ecology of Plants*, *199*(5), 361–376. https://doi.org/10.1078/0367-2530-00165

BGC Engineering Inc. (2012). *Oil Sands Tailings Technology Deployment Roadmap* [Project Report - Volume 2].

Bolker, B. M., Brooks, M. E., Clark, C. J., Geange, S. W., Poulsen, J. R., Stevens, M. H. H., & White, J.-S. S. (2009). Generalized linear mixed models: A practical guide for ecology and evolution. *Trends in Ecology & Evolution*, *24*(3), 127–135. https://doi.org/10.1016/j.tree.2008.10.008

Brooks, M., E., Kristensen, K., Benthem, K., J.,van, Magnusson, A., Berg, C., W., Nielsen, A., Skaug, H., J., Mächler, M., & Bolker, B., M. (2017). GlmmTMB Balances Speed and Flexibility Among Packages for Zero-inflated Generalized Linear Mixed Modeling. *The R Journal*, *9*(2), 378. https://doi.org/10.32614/RJ-2017-066

Canadian Council of Ministers of the Environment. (2007). Canadian Soil Quality Guidelines for the Protection of Environmental and Human Health: Summary tables. In *Canadian environmental quality guidelines*. Canadian Council of Ministers of the Environment.

CAPP. (2022). *Oil Extraction*. CAPP | A Unified Voice for Canada's Upstream Oil and Gas Industry. https://www.capp.ca/oil/extraction/

Correa-García, S., Pande, P., Séguin, A., St-Arnaud, M., & Yergeau, E. (2018).

Rhizoremediation of petroleum hydrocarbons: A model system for plant microbiome manipulation. *Microbial Biotechnology*, *11*(5), 819–832. https://doi.org/10.1111/1751-7915.13303

COSIA. (2012). *Technical Guide for Fluid Fine Tailings Management*.

COSIA. (2022). *Deep Deposit Design Guide for Oil Sands Tailings* (p. 260). Canada's Oil Sands Innovation Alliance - Deep Deposit Working Group.

Fox, J., & Weisberg, S. (2019). *An R Companion to Applied Regression*.

Francois, L. E., & Maas, E. V. (1999). Crop Response and Management of Salt-Affected Soils. In M. Pessarakli (Ed.), *Handbook of Plant and Crop Stress, Second Edition* (Vol. 19990540, pp. 169–201). CRC Press.

https://doi.org/10.1201/9780824746728.ch8

Gelman, A., & Hill, J. (2006). *Data Analysis Using Regression and Multilevel/Hierarchiacal Models*. Cambridge University Press.

Government of Alberta. (2022). *About oil sands*. https://www.alberta.ca/about-oil-sands.aspx

Government of Canada. (2013). *Oil Sands: A strategic resource for Canada, North America, and the global market*.

Grant, J., Huot, M., Lemphers, N., Dyer, S., & Dow, M. (2013). *Beneath the surface: A review of key facts in the oilsands debate*. Pembina Institute for Appropriate Development.

https://www.deslibris.ca/ID/236478

Hardy BBT Limited. (1989). *Manual of Plant Species Suitability for Reclamation in Alberta* (Reclamation Research Report RRTAC 89-4). Alberta Land Conservation and Reclamation Council.

Headley, J. V., Barrow, M. P., Peru, K. M., & Derrick, P. J. (2011). Salting-out effects on the characterization of naphthenic acids from Athabasca oil sands using electrospray ionization. *Journal of Environmental Science and Health, Part A*, *46*(8), 844–854. https://doi.org/10.1080/10934529.2011.579857

Headley, J. V., Peru, K. M., Mcmartin, D. W., & Winkler, M. (2002). Determination of Dissolved Naphthenic Acids in Natural Waters by Using Negative-Ion Electrospray Mass Spectrometry. *Journal of AOAC INTERNATIONAL*, *85*(1), 182–187. https://doi.org/10.1093/jaoac/85.1.182

Huang, M., Barbour, S. L., & Carey, S. K. (2015). The impact of reclamation cover depth on the performance of reclaimed shale overburden at an oil sands mine in Northern Alberta, Canada. *Hydrological Processes*, *29*(12), 2840–2854. https://doi.org/10.1002/hyp.10229

Javid, M., Sorooshzadeh, A., Moradi, F., Sanavy, M., Mohammad, S. A., & Iraj, A. (2011). The Role of Phytohormones in Alleviating Salt Stress in Crop Plants. *Australian Journal of Crop Science*, *5*, 726–734.

Kasperski, K. L., & Mikula, R. J. (2011). Waste Streams of Mined Oil Sands: Characteristics and Remediation. *Elements*, *7*(6), 387–392. https://doi.org/10.2113/gselements.7.6.387

Lalonde, R. S., Pinno, B. D., MacKenzie, M. D., & Utting, N. (2020). Capping dewatered oil sands fluid fine tailings with salvaged reclamation soils at varying depths to grow woody plants. *Canadian Journal of Soil Science*, *100*(4), 546–557. https://doi.org/10.1139/cjss-2019-0120

Lenth, R. (2020). *emmeans: Estimated Marginal Means, aka Least-Squares Means* (R package version 1.4.8). https://CRAN.R-project.org/package=emmeans

MacKenzie, M. D., & Quideau, S. A. (2012). Laboratory-based nitrogen mineralization and biogeochemistry of two soils used in oil sands reclamation. *Canadian Journal of Soil Science*, *92*(1), 131–142. https://doi.org/10.4141/cjss2010-070

Miransari, M., & Smith, D. L. (2014). Plant hormones and seed germination. *Environmental and Experimental Botany*, *99*, 110–121. https://doi.org/10.1016/j.envexpbot.2013.11.005

Mosseler, A., Major, J. E., & Labrecque, M. (2014). Growth and survival of seven native willow species on highly disturbed coal mine sites in eastern Canada. *Canadian Journal of Forest Research*, *44*(4), 340–349. https://doi.org/10.1139/cjfr-2013-0447

Munns, R., & Tester, M. (2008). Mechanisms of Salinity Tolerance. *Annual Review of Plant Biology*, *59*(1), 651–681. https://doi.org/10.1146/annurev.arplant.59.032607.092911

Omari, K., Pinno, B., Utting, N., & Li, E. (2020). Growth of Common Plants of Boreal Reclamation Sites in Oil Sands Tailings Cake Mixes and Process Water. *Land*, *10*(1). https://doi.org/10.3390/land10010025

R Core Team. (2021). *R: A language and environment for statistical computing*. R Foundation for Statistical Computing. http://www.R-project.org/

Renault, S., Lait, C., Zwiazek, J. J., & MacKinnon, M. (1998). Effect of high salinity tailings waters produced from gypsum treatment of oil sands tailings on plants of the boreal forest. *Environmental Pollution*, *102*, 177–184.

Renault, S., MacKinnon, M., & Qualizza, C. (2003). Barley, a Potential Species for Initial Reclamation of Saline Composite Tailings of Oil Sands. *Journal of Environmental Quality*, *32*(6), 2245–2253. https://doi.org/10.2134/jeq2003.2245

Renault, S., Qualizza, C., & MacKinnon, M. (2004). Suitability of altai wildrye (Elymus angustus) and slender wheatgrass (Agropyron trachycaulum) for initial reclamation of saline composite tailings of oil sands. *Environmental Pollution*, *128*(3), 339–349. https://doi.org/10.1016/j.envpol.2003.09.009

Renault, S., Zwiazek, J. J., Fung, M., & Tuttle, S. (2000). Germination, growth and gas exchange of selected boreal forest seedlings in soil containing oil sands tailings. *Environmental Pollution*, *107*(3), 357–365. https://doi.org/10.1016/S0269-7491(99)00167-0

Rooney, R. C., & Bayley, S. E. (2011). Setting reclamation targets and evaluating progress: Submersed aquatic vegetation in natural and post-oil sands mining wetlands in Alberta, Canada. *Ecological Engineering*, *37*(4), 569–579. https://doi.org/10.1016/j.ecoleng.2010.11.032

Samad, A., Pelletier, G., Séguin, A., Degenhardt, D., Muench, D. G., & Martineau, C. (2022). Understanding Willow Transcriptional Response in the Context of Oil Sands Tailings Reclamation. *Frontiers in Plant Science*, *13*, 857535. https://doi.org/10.3389/fpls.2022.857535

Schott, K. M., Snively, A. E. K., Landhäusser, S. M., & Pinno, B. D. (2016). Nutrient loaded seedlings reduce the need for field fertilization and vegetation management on boreal forest reclamation sites. *New Forests*, *47*(3), 393–410. https://doi.org/10.1007/s11056-015-9522-4

Stack, S., Jones, C., Bockstette, J., Jacobs, D. F., & Landhäusser, S. M. (2020). Surface and subsurface material selections influence the early outcomes of boreal upland forest restoration. *Ecological Engineering*, *144*, 105705. https://doi.org/10.1016/j.ecoleng.2019.105705

Stack, S., Yarmuch, M., & Landhäusser, S. M. (2021). Species-specific responses to targeted fertilizer application on reconstructed soils in a reclaimed upland area. *Canadian Journal of Soil Science*, *101*(1), 45–61. https://doi.org/10.1139/cjss-2019-0136

Syncrude Canada Ltd. (2013). *South Bison Hill Soil Capping Research Synthesis*.

Syncrude Canada Ltd. (2020). *Sandhill Fen Watershed: Learnings from a Reclamation Wetland on a CT deposit. Appendix C of Composite Tailings Capping Knowledge Synthesis*. Syncrude Canada Ltd.

Turnbull, L. C., & Bridgham, S. D. (2015). Do Two Graminoids, the Invasive Phalaris arundinacea and the Native Scirpus microcarpus, Have Similar Ecosystem Effects in a Wetland? Soil Science Society of America Journal, 79(3), 957–967. https://doi.org/10.2136/sssaj2014.08.0335

USDA, NRCS. (2022). *The PLANTS Database*. National Plant Data Team. http://plants.usda.gov

Vitt, D. H., House, M., & Hartsock, J. A. (2016). Sandhill Fen, an initial trial for wetland species assembly on in-pit substrates: Lessons after three years. *Botany*, *94*(11), 1015–1025. https://doi.org/10.1139/cjb-2015-0262

Wickham, H., Averick, M., Bryan, J., Chang, W., McGowan, L., François, R., Grolemund, G., Hayes, A., Henry, L., Hester, J., Kuhn, M., Pedersen, T., Miller, E., Bache, S., Müller, K., Ooms, J., Robinson, D., Seidel, D., Spinu, V., … Yutani, H. (2019). Welcome to the Tidyverse. *Journal of Open Source Software*, *4*(43), 1686. https://doi.org/10.21105/joss.01686

Wytrykush, C., Vitt, D. H., McKenna, G., & Vassov, R. (2012). Designing landscapes to support peatland development. In *Reclamation and resoration of Boreal ecosystems* (pp. 161–178). Cambridge University Press.

Zuur, A. F., Hilbe, J. M., & Ieno, E. N. (2013). *A beginner's guide to GLM and GLMM with R: a frequentist and Bayesian perspective for ecologists*. Highland Statistics Ltd.

MONITORING NATIVE PLANT ESTABLISHMENT ON TREATED FLUID FINE TAILINGS USING WORLDVIEW-3 SATELLITE DATA

Benoit Rivard[1], Amanda Schoonmaker[2], Jilu Feng[1], and Michael G. Lipsett[1].
[1]University of Alberta, Edmonton, Alberta, Canada; [2]Center for Boreal Research, NAIT

ABSTRACT

This study is part of a broader one relating plant development and growth to improvements in soft tailings deposit performance, under field conditions. Here we ask whether high spatial resolution remote sensing data, specifically Worldview-3 satellite imagery, can be used to quantitatively assess aspects of vegetation growth. To our knowledge, it is a first attempt to use remote sensing imagery to characterize vegetation on oil sands soft tailings. Specifically, we make use of two methods of analysis applied to Worlview-3 satellite imagery to examine tailings vegetation abundance. The first method involves the development of quantitative predictive models via the correlation of satellite data to field data. Predicted leaf biomass compared to ground values result in a R^2 of 0.64 and an RMS is 40.89 (g/m^2). When this model is applied to the Worldview satellite imagery it yields a modeled map of leaf biomass distribution with finer detail than achieved from field surveys. The second method is semi quantitative and examines the relative distribution across the scene of spectral endmembers extracted from the imagery with three endmembers highlighting respectively the distribution of broad leaf vegetation, grasses in various states of vigor, and soil. Using Specim IQ ground based hyperspectral imagery we also show that the distribution of 6 plant species (*Carex, Rumex, Typha, Elymus, Hordeum* and *Salix*) can be mapped in detail. Finally, the paper discusses the value and limitations of the findings for revegetation planning and monitoring.

INTRODUCTION

The oil sands of northern Alberta comprise the third-largest proven reserves of petroleum in the world (Alberta Energy, 2014). Two barrels of water are typically required to produce a barrel of bitumen from oil sands resulting in large volumes of tailings, consisting mostly of water with sand, silt, clay, and residual bitumen. When the tailings are discharged into the tailings pond, the coarse sand particles settle quickly unlike the remaining fine solids. This mixture densifies to about 30 wt% fines or fines-plus-water within a few years forming fluid fine tailings (FFT) (MacKinnon 1989). The FFT remains saturated for decades because of its very slow natural consolidation rate (MacKinnon, 1989; Kasperski, 1992). Dewatering and eventual reclamation of oil sands fluid fine tailings deposits is thus one of the greatest challenges faced by oil sands operating companies in Alberta, Canada. Planting vegetation is a potential method to dewater saturated tailings structures and increase soil strength through a root bed that acts as a natural reinforcing geotextile.

A key tailings management challenge for flocculated and centrifuged material is the rate at which dewatering occurs once placed into a final deposit. For thick lifts, there may be insufficient surcharge to load the deposit to dewater under gravity alone. Also, a common problem with tailings that are treated through centrifugation or flocculant-addition processes is the development of a surficial crust that slows evaporative drying deeper in the deposit. For densification and consolidation near the surface (less than 2 m depth), vegetation may allow both dewatering and some temporary strength benefit through a fibrous root structure.

Early-successional woody species, such as willows and poplars, have been used extensively for reclamation to stabilize soil in British Columbia (Polster, 1997). It was clearly demonstrated over 20 years ago that plants are capable of dewatering composite tailings (CT) from oil sands and copper mining (Silva, 1999). Wu (2009) tested plant

dewatering capability for five native grasses & found some species (*Agropyron* spp.) took up water from the high-water content CT tailings, yielding higher solids content and strength after 15 weeks.

The consistent and strong performance observed in both CT and FFT, for the *Agropyron* genus and for *Elymus trachycaulus* (synonym = *Agropyron trachycaulus* ssp. *trachycaulus*) specifically (Renault et al., 2004; Wu, 2009; Yucel et al., 2016) aligns with observations of its strong salinity tolerance observed in natural systems (Purdy et al., 2005). Although not widely studied on mine tailings to-date, another group of species, willows (*Salix* spp.) have been successfully grown in dredged sediment studies (Vervaeke et al., 2001; Smith et al., 2009) and have shown capacity to dewater these similarly soft deposits (Smith et al., 2009). The tolerance of this genus to fluctuating water tables and ability to regenerate from any part of the plant (root, shoot or seed) make it well suited to tailings deposits, with *Salix interior* having been grown successfully in treated FFT under greenhouse conditions (Yucel et al. 2016).

In a 2020 global systematic review of remote sensing studies of mine site rehabilitation for ecological outcomes McKenna et al. (2020) reported three papers (Gillanders et al., 2008; Zhang et al., 2014; Chasmer et al., 2018) relevant to oil sands tailings examining land cover changes using decimeter spatial resolution satellite imagery (Landsat, SPOT, RapidEye), none examining vegetation growth on soft tailings. Here we ask whether high spatial resolution remote sensing data, specifically Worldview-3 satellite imagery, can be used to quantitatively assess aspects of vegetation growth. To our knowledge, it is a first attempt to use remote sensing imagery to characterize vegetation on oil sands soft tailings. Specifically, we make use of two methods of analysis applied to Worlview-3 satellite imagery to examine tailings vegetation abundance. The first method involves the development of quantitative predictive models via the correlation of satellite data to field data. The second method is semi quantitative and examines the relative distribution across the scene of vegetation and soil spectral endmembers extracted from the imagery. Lastly, we examine the feasibility of mapping the distribution of specific plant species using ground based hyperspectral imagery. Finally, the paper discusses the value and limitations of the findings for revegetation planning and monitoring.

MATERIALS AND METHODS

Site description

The field pilot study was conducted in a self-contained centrifuge cake deposit (30 m width x 60 m length x 4 m deep) at an oil sands mine site in Alberta, Canada (Fig. 1). A detailed description regarding the design and setup of this deposit can be found in Smith et al. (2018). Briefly, the deposit was poured in January 2016 and allowed to go through a full year cycle with evaporative drying and freeze-thaw conditions. Due to the configuration of the test cell with sloped sides, the central most part of the deposit experienced longer periods of inundation than the periphery of the deposit, this was an ongoing challenge throughout the study and resulted in segregation of plant species by moisture condition.

In spring 2017, the deposit was initially vegetated with two species: slender wheatgrass (*Elymus trachycaulus*) which was seeded and sandbar willow (*Salix interior*) which was planted as rooted seedling or unrooted stem cutting in discrete treatment plots with a section of the deposit left unplanted. Learnings from the 2017 growing season informed on supplemental planting that was conducted in spring 2018 and 2019 where an additional grass species was seeded (tufted hairgrass, *Deschapmsia caespitosa*) and additional species were hand planted including: Bebb's willow (*Salix bebbiana*), water sedge (*Carex aquatilis*), Bebb's sedge (*Carex bebbi*), western dock (*Rumex occidentalis*), slough grass (*Beckmania schyziachne*), and common reed (*Phragmites australis* subsp. *Americanus*) plants (refer also to Smith et al. (2018) and Schoonmaker et al. (2021) for additional details on planting). Of note, due to extensive flooding, cattails (*Typha* spp.) were

present throughout the deposit through natural ingress.

Figure 1. Photographs of the field plot taken in September of 2017 (top) and 2018 (bottom).

Field measurements

A deposit-scale sampling grid (3-m intervals) was utilized to capture the spatial variability in vegetation development due to differences in tailings deposit thickness. The same basic sampling scheme was utilized in 2018; therefore, the measurement and sampling points were offset 0.5 m between years to ensure we did not repeatedly clip vegetation at the same location. At each of these points, the following was collected in early September in both years:

- Vegetation percent (%) cover (which is estimated by visually determining the % of the area covered by vegetation in a 0.5 x 0.5-m quadrat) by genus.
- Total aboveground leaf mass (by genus) was clipped into paper bags, except for grasses, which were grouped as a single biomass pool (this was predominantly composed of *Elymus trachycaulus* but there were other species present sporadically through the deposit including: *Calamagrostis canadensis*, *Hordeum jubatum* and *Beckmania schyziachne*.
- Adjacent to the quadrat, a few leaves were collected and stored in a plastic bag and refrigerated until return to the lab for determination of leaf area. A single composite sample was collected for each plant species observed.

Laboratory measurements

Aboveground biomass was initially air-dried on the bench and then uniformly dried in an oven to weight constancy at 70°C. Total plant dry weight was determined to the nearest 0.1 g but in cases where the sample was very small (< 1 g), a different scale was used, and dry weight was measured to the nearest 0.0001 g. The relationship between leaf mass and surface area was determined on a subset of leaves of individual species that were collected in the field concurrent with vegetation clipping for biomass. These samples were stored frozen (-4°C) after field collection to preserve the leaf structure and shape. For the determination of leaf area, individual leaves from each species were placed on a flatbed scanner and WinFOLIA™ software was used to estimate the leaf area from the scanned image. The scanned leaves were then oven-dried at 70 °C and weighed to the nearest 0.0001 g. The ratio of leaf area: leaf mass on this subsample of leaves was used to scale-up the total leaf mass harvested from individual 0.5 x 0.5 m quadrats into a total leaf area estimate. The total leaf area (m^2) per quadrat was divided by 0.25m^2 to determine leaf-area index (LAI) per sampling point.

Satellite data and analysis methodology for vegetation abundance

Description of satellite data

Satellite data from Worldview 3 was selected for this study given the combined high spatial resolution of the imagery and the number of spectral bands available to detect the distribution of plants on the tailings deposit. The data obtained for this investigation encompass atmospherically corrected (ACOMP) orthorectified (Standard 2a format) Panchromatic (B&W) and 8 band multispectral visible near-infrared imagery at a spatial resolution of 0.30m and 1.24m respectively.

Two methods of satellite image analysis were used to examine tailings vegetation abundance. The first method involves the development of quantitative predictive models via the correlation of satellite data to field data. The second method is semi quantitative in that it is not constrained by field data but examines the relative distribution across the scene of spectral endmembers extracted from the imagery.

Predictive models and ensuing maps

For the development of a quantitative predictive model of vegetation abundance we made use of regression analysis to relate satellite image data to field observations. The satellite data comprised band values for the eight available spectral bands and we derived a normalized difference vegetation index (NDVI) calculated as (Rnir-Rred)/(Rnir+Rred) and a simple ratio index (SRI) calculated as Rnir/Rred. Rnir and Rred are the reflectance values of the corresponding band in multispectral imagery (band 7: 770-895nm and 5: 630-690nm respectively). We tested predictive models for each of the three available field data including: vegetation % cover, leaf biomass, and LAI. Best variable selection (Cyprian, 2009) was used to determine which band or spectral index should be included in the model to improve the correlation coefficient (R). Multiple linear regression was then used to estimate the model parameters.

Relating satellite data to field data required coregistration of these data and resampling of the satellite data. First the Panchromatic imagery, being of highest detail, was registered to the field sampling grid described in section 2.2. The multispectral imagery was then co-registered and resampled to the 0.30 m pixel size of the Panchromatic imagery on which the field grid was overlaid. A circular region of interest (ROI) of 1.2m in diameter, approximating the 1.2x1.2m pixel size of the multispectral imagery, was then positioned in the lower left quadrant of each 3x3m grid cell. The pixels values (NDVI and bands) encompassed by each ROI were averaged to generate the 106 input data points to the models. These were then portioned into 100 points for model development (e.g., calibration) and 6 points for model testing. The 6 testing points are in a single row in the middle of the field grid that encompasses all vegetation types as well as water and exposed soil. Predictive models were then implemented on the multispectral imagery resampled at 0.30m to produced predictive maps. Lastly a krigging procedure was applied to these maps to facilitate comparison with field maps generation using spatial interpolation. For this purpose, a linear component semi-variogram model (anisotropy ratio=1.0 and anisotropy slope=1.0) was used with 80 x 190 output grids to match the resolution of resampled worldview 3 pixels.

Generation of endmember abundance maps

The second analysis methodology of the Woldview-3 imagery aims to identify distinct spectral endmembers relevant to vegetation mapping and map their distribution in the scene. To derive an image endmember set from the 8 band multispectral data, the spatial-spectral endmember extraction (SSEE) algorithm was used, and the image was divided into equal spatial subsets (each subset = 11x11 pixels) (Rogge et al., 2007; Rogge and Rivard, 2010; Rogge et al., 2012). This method is designed to discern spectrally similar endmembers that occupy different portions of the scene. The first 10 endmembers selected explain over 99% of the 8 band simplex volume and as discussed in the results, 6 relate to vegetation or

vegetation, soil, or mixtures of both. Mapping the distribution of each endmember was conducted using a spectral angle mapper (SAM) algorithm that treats spectra as multidimensional vectors and computes the angle between spectral pairs (Kruse et al., 1993). For this purpose, the spectrum from each pixel of the image was compared to that of each endmember. Endmember spectra with the smallest SAM angle to a given pixel spectrum indicates the greatest similarity and this is conveyed as a color map per endmember where greatest similarity is shown in red and lowest similarity in blue.

Hyperspectral data and analysis methodology for species mapping

VNIR (400–1000 nm) spectral images of vegetation at the site were acquired under clear sky conditions on the 12th of September 2019 between 11 am and 1.45 pm using a Specim IQ hyperspectral camera mounted on a tripod. Integration time was 6 ms and 25 seconds were required for acquisition of an image. The camera acquires data over 204 bands at a 3 nm spectral bandwidth. Radiance data was obtained by applying appropriate gains and offsets. These data were then converted to reflectance by ratioing each pixel spectrum to that of an average spectrum for a Spectralon panel of 99% reflectance measured concurrently.

Samples of *Carex, Rumex, Typha, Elymus, Hordeum* and *Salix* were collected during the field imaging campaign and sub-millimeter resolution imagery of these samples was obtained in the laboratory the same day using a Specim SisuROCK™ hyperspectral scanner (a linescan imager) at the University of Alberta. The scanner contains a 256 spectral by 320 spatial pixels detector array that acquires data at a 6.3 nm sampling interval and a 10 nm spectral bandwidth. A 99% reflectance Spectralon™ white panel was measured concurrently with the vegetation targets, and radiance data were converted to reflectance by normalizing to the radiance data of the white panel. These high-resolution imagery of the six species of interest enabled the selection of spectra of each species for over 1000 pixels used to compute an average spectrum per species. Examination of these spectra (not shown) indicated that the 6 species of interest presented distinct spectral characteristics that should enable their mapping from Specim IQ spectral imagery.

On that basis, the processing of the Specim IQ imagery to derive an abundance map for each species was initiated with an unsupervised K-means classifier using 10 classes. Using a greater number of classes than the number of species accounted for intraclass (e.g., intra species) spectral variability where more than one spectral class may define the distribution of a given species (e.g. leaves vs stems). The pixels for each class were then averaged to produce a spectral endmember as an input to the spectral angle mapper (SAM) algorithm to derive an image distribution map for each species. A SAM angle threshold of 0.2 radian was used for all endmembers. We chose to use the results of the unsupervised classification to define the endmembers rather that the laboratory spectra acquired from plant samples because the plants displayed intraclass spectral variability that could not be captured by the limited size of our plant sample suite.

RESULTS

The analysis of the Worldview-3 satellite data for vegetation abundance is presented followed by the analysis of the field hyperspectral data for species mapping.

Worldview-3 data for vegetation abundance

Correlation of NDVI with ground data

A scatterplot of leaf biomass against % vegetation ground cover reveals two data trends (Fig. 2) where the first trend is displayed by grasses and spans a wide range of % cover and a restricted range (<100 g/m2) of leaf biomass (lowest trend on the figure). A similar pattern can be seen for plots involving above ground biomass and LAI (not shown). The second trend is defined by the highest leaf biomass

values (upwards of 350 g/m2) and broader leaf vegetation (e.g. *Salix, Rumex, Typha*) that spans a more restricted range in % cover and a wider range of the other three variables. This resulted in poor correlation of % vegetation ground cover with NDVI (not shown) and for this reason we did not pursue a predictive model for % vegetation ground cover. However, we found good correlation (and a single data trend) when examining NDVI with leaf biomass (Fig. 2), LAI and above ground biomass (not shown).

Predictive model and related maps

Predictive models were pursued for above ground biomass, LAI and leaf biomass. Figure 3 illustrates a scatterplot of predicted versus observed values for the calibration and testing data of leaf biomass. These data display a R^2 of 0.64, the same obtained for the data using the LAI model and considerably better than that for Above Ground Biomass (0.53), since NDVI is primarily sensitive to the foliar component of vegetation. The predictive model for leaf biomass uses reflectance data for band 3 (547nm), band 4 (604nm), band 7 (824nm), band 8 (913nm) and two vegetation indices (NDVI and SR). Figure 4 provides a comparison of observed leaf biomass (e.g., field data) and values predicted by applying the above model to the Worldview-3 imagery. The first observation relates to the level of detail portrayed by both maps, with the map generated from ground data being considerably coarser (one 0.5 x 0.5 m point per 3 x 3 m grid cell). Nevertheless, one can track the "Hot spots" of the coarse resolution ground map in the higher resolution satellite map. Subsequent field visits have confirmed that the satellite map provides a realistic detailed view of leaf biomass distribution and improved the detection of smaller patches of dense vegetation that were missed with the coarser scale ground data collection.

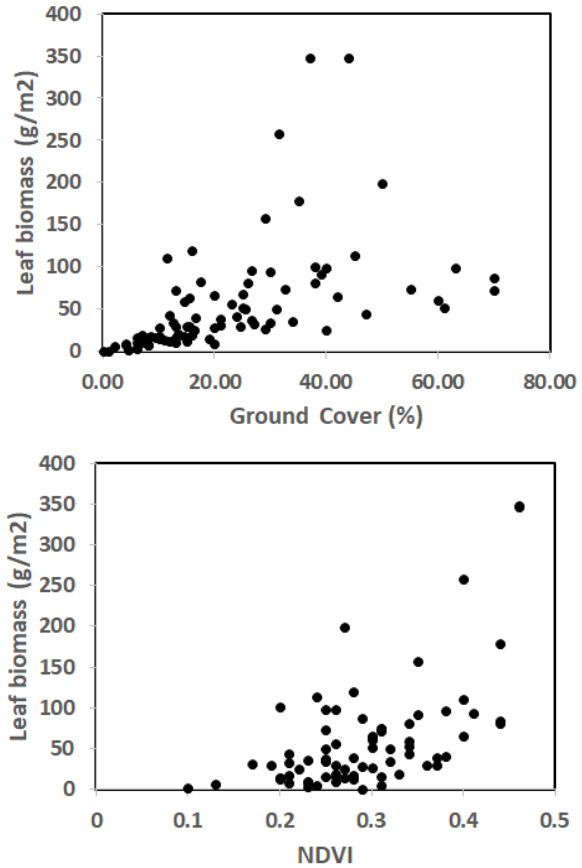

Figure 2. Scatter plots of % ground cover (area covered by leaves) versus leaf biomass (top), and NVDI versus leaf biomass (bottom).

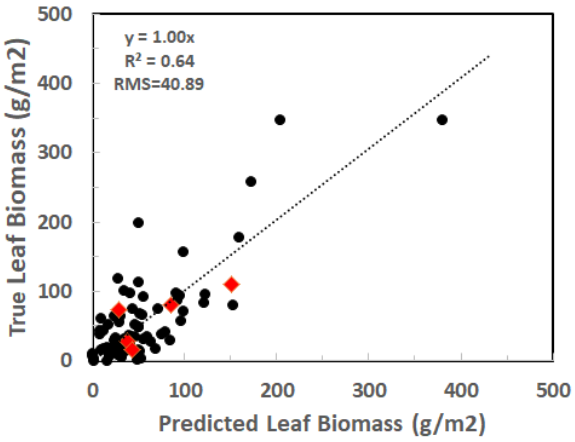

Figure 3. Scatterplot of predicted and observed values for Leaf biomass. The best fit line shown is set to a zero intercept and the RMS is for the samples used for model development. Black dots were for model development (e.g., calibration) and red dots were for model testing.

Spectral unmixing and related maps

Six endmember spectra relate to vegetation or vegetation, soil, or mixtures of both. The abundance maps of three of these endmembers (#2, 3, 8) is shown on figure 5. The spectra (not shown) of endmember #3 is characteristic of broad leaf vegetation displaying a strong pigment absorption near 680nm. The spectra of endmember #7 is similar but highlights vegetation along the perimeter of the site. Endmembers #2 and #10 correspond to that of grasses in various states of vigor and/or age. The spectra and abundance maps of endmembers #8 and #9 are very similar and highlight the distribution of soil sensed amongst the vegetation cover, in this case primarily where grasses occur as seen by the co-occurrence of high abundances of soil and grasses in abundance maps of endmembers #8 and #2 respectively.

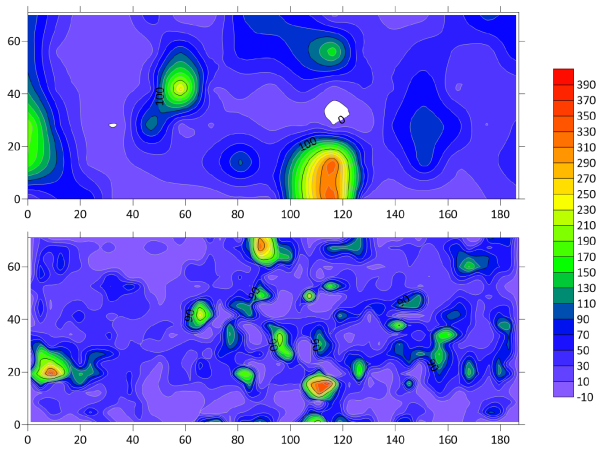

Figure 4. Leaf biomass (g/m^2) spatially interpolated based on field point measurements (top) and estimated from Worldview 3 satellite data (bottom).

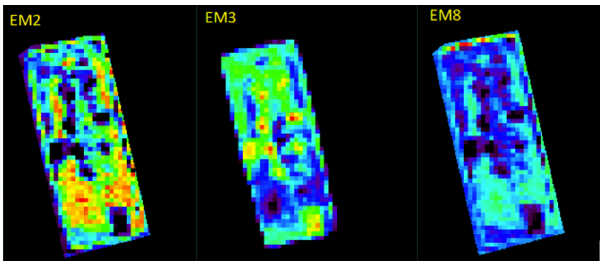

Figure 5. Relative abundance maps of endmembers #2 (grasses), 3 (broader leaves) and 8 (soil). Red is highest abundance and dark blue is lowest abundance.

Hyperspectral imagery for species mapping

The analysis of the Specim IQ imagery yielded detailed distribution maps of *Carex, Rumex, Typha, Elymus, Hordeum* and *Salix*. Figures 6 and 7 present imagery respectively acquired at 7-45m (foreground-background) and 1.2m to showcase different scales of observation. The results also illustrate the challenge of obtaining species distribution maps from the distribution of spectral classes, a reflection of intraclass variability. Specifically, figure 6 offers a perspective view where four species are mapped, two of which (*Rumex and Elymus)* required 2 classes or more for mapping to account for different age classes and associated structural changes in these species as they grow. In addition, the classification that was predominantly *Typha* also included *Carex* (central-left portion of image, Figure 6). The close-up example of figure 7 shows three species, all requiring more than one class to map their distribution. At a short stand-off distance of 1.2m finer detail is captured than in figure 6 and spectral differences between leaves and stems emerge and can be captured by different spectral classes as seen for *Salix*, whereas only a single class was required to describe this species in figure 6.

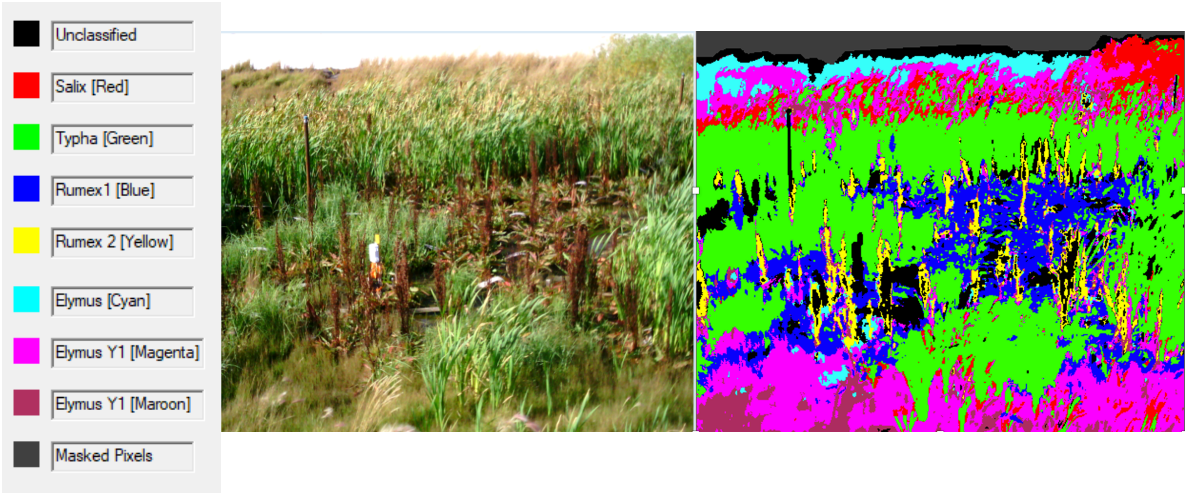

Figure 6. Specim IQ imagery and resulting detailed distribution maps of *Rumex, Typha, Elymus,* and *Salix*. The imagery was acquired at 7-45m (foreground-background).

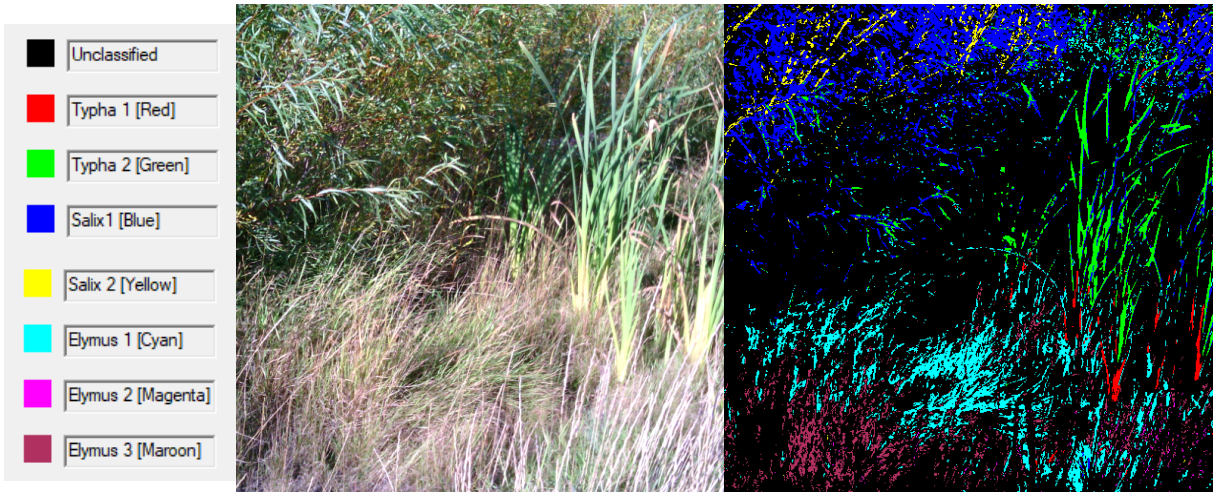

Figure 7. Specim IQ imagery and resulting detailed distribution maps of *Typha, Elymus,* and *Salix* (Willow). The imagery was acquired at 1.2m.

DISCUSSION

Value and limitations of leaf biomass satellite predictions for planning and monitoring

This case study illustrated that satellite imagery was able detect, with reasonable accuracy, the relative abundance (expressed as either LAI or biomass) of vegetation in this test deposit. A major advantage of this technique is that it can capture information with a greater degree of resolution compared with ground surveys which inherently only sample a small subset of the target site. Operationally, being able to accurately capture the relative abundance of vegetation with remote imagery has significant value in assessing success and for planning re-entry where patches of vegetation failed to establish. Relying only on ground surveys would potentially result in vegetation establishment gaps being missed; an issue which could be problematic when utilizing vegetation as a tailings dewatering or surface strengthening treatment approach.

We found that ground cover data of vegetation was not a useful parameter for correlation with NDVI due to the variation in the relationship between leaf biomass and cover inherent to the varying species groups within the study area. It is also possible that the qualitative assessment of % cover has a greater degree of inherent error relative to destructive harvest of leaf biomass directly as leaf biomass and leaf-area index (which was derived from leaf biomass) were more useful parameters to correlate with NDVI.

While promising, the world-view image maps required a predictive model to first be calibrated to ground data, which still necessitates that some ground information is provided. In soft tailings deposits, this may initially pose to be quite a challenge to physically access, however, it may be sufficient to train the model on similar classes of vegetation in more accessible locations surrounding the deposit. These could be in drainage ditches or potentially in targeted patches, in readily accessible areas, and planted concurrent with a large-scale field deposit.

Value of species level mapping from hyperspectral imagery

Hyperspectral imagery proved to be relatively good indicator associated with numerous vegetation groups (genus-level) though many of these groups were represented by more than one spectral class and at greater distances some vegetation groups became less distinct (*Typha* and *Carex*, Fig. 6). In general, this was driven by dichotomies in plant morphology in some instances as well as differing plant life stages in other cases. *Salix* (willow) was associated with two spectra representing either leaves or woody tissues (Fig. 7), *Typha* showed variation in spectra related to the leaf growth base (lighter in color relative to upper portions of leaves) versus fully expanded leaves (Fig. 7) and in *Rumex* the leaves were distinct from the flowering stem (which also contained seeds) (Fig, 6). For *Elymus*, two spectra were associated with different age classes of plants as the study site was seeded over two years and each age class of grass had distinct spectra (Fig 6) as well as distinction associated with leaf tissues versus seed producing tissues (Fig. 7). Lastly, future studies could consider more extensive sampling of plants to better quantify intraclass variation in the spectra, this would likely facilitate a greater degree of resolution in identifying individual species groups as well as distinction between groups.

Using hyperspectral imagery to detect broad vegetation groups has utility in its own right for species documentation as well as what these species are indirect indicators of in terms of surface and subsurface moisture conditions within a tailings deposit. For example, *Typha* is a strong indicator of extensively flooded conditions while the dominant grass in this site was *Elymus trachycaulus* which had low tolerance to extended periods of flooding and was more associated with side slopes and drier parts of the deposit.

CONCLUSIONS

This study examined whether high spatial resolution remote sensing data, specifically Worldview-3 satellite imagery, could be used to quantitatively assess aspects of vegetation growth. A predictive model for leaf biomass uses reflectance data for band 3 (547nm), band 4 (604nm), band 7 (824nm), band 8 (913nm) and two vegetation indices (NDVI and SR). Predicted leaf biomass compared to ground values results in a R^2 of 0.64 and an RMS of 40.89 (g/m^2). When this model was applied to the Worldview-3 satellite imagery it yielded a modeled map of leaf biomass distribution with finer detail than achieved from field surveys. Subsequent field visits have confirmed that the satellite map provides a realistic detailed view of leaf biomass distribution. Using three spectral endmembers extracted from the Worldview-3 imagery allowed us to highlight respectively the distribution of broad leaf vegetation, grasses in various states of vigor, and soil. From Specim IQ ground based hyperspectral imagery we also showed that the distribution of 5 plant species (*Carex, Rumex, Typha, Elymus,* and *Salix*) can be mapped in detail. In principle, the

results of this study support the use of remote imagery as well as hyperspectral cameras as a tool for vegetation detection in soft tailings deposits. In future studies, satellite monitoring capability would be best demonstrated via a multitemporal (e.g. multi-year) study. This would enable an assessment of the predictive capability in other deposits and across multiple years ideally without having to recalibrate the model every year though we would want to conduct repeat validation to assess portability of the model across deposits and plant communities.

Access to drones with hyperspectral cameras could be used to bridge across scales and characterize species distribution for target areas defined by the predictive mapping generated from satellite data. This technology is now readily accessible.

ACKNOWLEDGMENTS

The authors would like to acknowledge the Institute for Oil Sands Innovation (IOSI) at the University of Alberta, Imperial Oil and CNRL their support of this research.

REFERENCES

Alberta Energy, 2014. Alberta's oil sands: the facts. Government of Alberta, Edmonton, Alta.

Chasmer, L., Baker, T., Carey, S.K., Straker, J., Strilesky, S., Petrone, R., 2018. Monitoring ecosystem reclamation recovery using optical remote sensing: Comparison with field measurements and eddy covariance. Sci. Total Environ., **642**: 436–446.

Gillanders, S.N., Coops, N.C., Wulder, M.A., Goodwin, N.R., 2008. Application of Landsat satellite imagery to monitor land-cover changes at the Athabasca Oil Sands, Alberta, Canada. Can. Geogr, **52**: 466–485.

Kasperski, K.L., 1992. A review of properties and treatment of oil sands tailings. AOSTRA Journal of Research, **8**: 11–15.

Kruse, F. A., Lefkoff, A.B, Boardman, J.W., Heidebrecht, K.B., Shapiro, A.T., Barloon, P.J., Goetz, A.F.H., 1993. The spectral image processing system (SIPS)–interactive visualization and analysis of imaging spectrometer data. Remote Sens. Environ., **44**: 145–163.

McKenna, P.B., Lechner, A.M., Phinn, S., Erskine, P.D., 2020. Remote sensing of mine site rehabilitation for ecological outcomes: A global systematic review. Remote Sensing, **12**: 3535-3569.

MacKinnon, M.D., 1989. Development of the tailings pond at Syncrude's oil sands plant: 1978–1987. AOSTRA Journal of Research, **5**: 109–133.

Polster, D.F., 1997. Restoration of landslides and unstable slopes: considerations for bioengineering in interior locations. Proceedings of the 21st Annual British Columbia Mine Reclamation Symposium, Cranbrook, BC. pp. 153-166.

Purdy, B.G., Macdonald, S.E., Lieffers, V.J., 2005. Naturally saline Boreal communities as models for reclamation of saline oil sand tailings. Restoration Ecology, **13**: 667-677.

Renault, S., Qualizza, C., MacKinnon, M., 2004. Suitability of altai wildrye (Elymus angustus) and slender wheatgrass (Agropyron trachycaulum) for initial reclamation of saline composite tailings of oil sands. Environmental Pollution, **128**: 339-349.

Rogge, D. M., Rivard, B., Zhang, J., Harris, J., Feng, J., and Sanchez, A., 2007. Integration of spatial–spectral information for the improved extraction of endmembers. Remote Sens. Environ., **110**: 287–303.

Rogge, D.M., Rivard, B., 2010. Iterative spatial filtering for reducing intra-class spectral variability and noise. In IEEE GRSS workshop on hyperspectral image and signal processing: Evolution in remote sensing, Reykjavik, Iceland, June 14–16, 1–4.

Rogge, D., Bachmann, M., Rivard, B., Feng, J., 2012. Spatial sub-sampling using local endmembers for adapting OSP and SSEE for large-scale hyperspectral surveys. IEEE J. Sel. Top. Appl. Earth Observ. Remote Sens., **5**: 183–195.

Schoonmaker, A., Chigbo, C., Walton-Sather, K., Abdulnabi, A., Beier, N., Laberge, S., Smith, W., 2021. Plant growth on oil sands tailings from the bench-scale to a field pilot: Part 1 plant development patterns. Tailings and Mine Waste Conference, Banff AB.

Silva, M.J., 1999. Plant dewatering and strengthening of mine waste tailings. PhD thesis, Department of Civil and Environmental Engineering, University of Alberta.

Smith, K.E., Banks, M.K., Schwab, A.P., 2009. Dewatering of contaminated sediments: Greenhouse and field studies. Ecological Engineering, **35**: 1523-1528.

Smith, W., Olauson, E., Seto, J., Schoonmaker, A., Nik, R.M., Freeman, G., McKenna, G., 2018. Evaluation of strength improvement and dewatering technologies for a soft oil sands tailings deposit. International Oil sands Tailings Conference, Edmonton, Alberta, Canada.

Vervaeke, P., Luyssaert, S., Mertens, J., De Vos, B., Speleers, L., Lust, N., 2001. Dredged sediment as a substrate for biomass production of willow trees established using the SALIMAT technique. Biomass and Bioenergy, **21**: 81-90.

Wu, S., 2009. A greenhouse study of selected native plant species for dewatering CT. MSc thesis, Department of Civil and Environmental Engineering, University of Alberta.

Yucel, K., Schoonmaker, A., Degenhardt, D., Kaur, J., Khadka, B., 2016. Utilization of plants to dewater and stabilize mature fine tailings. Proceedings from the International Oil Sands Tailings Conference. December 4-7th 2016, Lake Louise, Alberta.

Zhang, Y., Guindon, B. Lantz, N.; Shipman, T., Chao, D., Raymond, D., 2014. Quantification of anthropogenic and natural changes in oil sands mining infrastructure land based on RapidEye and SPOT5. Int. J. Appl. Earth Obs. Geoinf,. **29**: 31–43.

SESSION 5

COMPLIANCE WITH TAILINGS MANAGEMENT FRAMEWORK OBJECTIVES
A 3RD PARTY PERSPECTIVE

Jim Blum
JGBlum Consulting Ltd.

ABSTRACT

This paper is a follow-on to an earlier critique of the effectiveness of D085 in dealing with the accumulation of fluid fine talings by the oil sands mining industry (Blum et al (2018)). Much of the regulatory background is contained in that paper. This paper provides an analysis of developments over the subsequent 4 years. Data is drawn from a summary report prepared by the Regulator (AER (2021)); including specific examples from individual Operators.

All of the problems previously identified remain to this day. Fluid Tailings (FT) inventories continue to expand; no new technologies for dealing with this growth have been commercialized; and tailings that are still fluid continue to be removed from the inventory in defiance of a specific instruction contained in Directive 085. Meanwhile the Author has not seen any Operator file a terrestrial reclamation alternative as required under the Regulations. The Regulator paints a rosy picture of inventories remaining within the overly generous allowable limits that have essentially been defined by each Operator; and continues to expand the timelines for submission of terrestrial alternatives for reclamation; which should have been included in the first Tailings Management Plans (TMPs) filed in 2016.

A primary concern for the Indigenous Peoples on whose lands these projects are based is the explosion of Pit Lakes onto the proposed closure landscape. A keynote address at IOSTC 2018 (Hyndman, McKenna & Sawatsky) made a case for a pit lake closure landscape. Indigenous Peoples do not buy into this concept, and repeated requests for a Forum with Industry and the Regulator to explain Industry's position have gone unanswered.

The Author recognizes the probable need for a single End Pit Lake per mine site for passive water treatment and return. But the reclamation proposals under review paint an entirely different picture. For example: the 3 mines in the vicinity of Kearl Lake propose a total of 7 pit lakes plus a compensation lake. The combined areas of these new water bodies amount to approximately 8 times the area of Kearl Lake. The Tailings Management Framework (TMF) requires the landscape to be returned to boreal forest; and Indigenous Communities have been promised a landscape having equivalent productivity compared to the pre-disturbance terrain. Increasingly it appears that instead they will get an approximation to "Waterworld." Pit lakes containing tailings are a nightmare scenario for Indigenous Communities. In particular, the concept of such features forming part of the closure landscape is not acceptable.

INTRODUCTION

Background

The issues surrounding tailings management and reporting are presented in the Author's previous paper. The problems arise from the nature of the fine mineral fraction of the processed ore, dispersed in the bitumen extraction process. This fines fraction forms fluid tailings, termed FT, or sometimes FFT, for fluid fine tailings. Extensive large strain consolidation testing of FT samples shows a logarithmic reduction in permeability with decreasing void ratio such that settlement to form a stable soil is impossible without an intervention. Any such intervention is compounded in difficulty by the vast scale of the enterprises.

The TMF sets out the general objectives for the transformation of tailings deposits into a reclaimed boreal forest landscape; while Directive 85 (D085) prescribes parameters for filing tailings management plans (TMPs) and for annual reporting through TMRs (tailings management reports).

The TMRs are collated by the Regulator and summarized annually (State of Fluid Talings Management for Mineable Oil Sands). The lag in reporting is such that the following analysis is based on 2020 data and published in September of 2021. A later version should be available, but not in time for the preparation of this paper.

Overview

The presentation of data commences in Section 7 of the report, titled Regional Fluid Tailings Status. FT volumes are shown graphically by site over a 7-year period. What is immediately apparent is the FT growth continues. This is alarming, as the intent of the Directive is that no growth beyond a projected 10-year maximum production of "zero treated" FT from the introduction of the Regulation (or after the start-up of a new Operation). While this growth is within the permitted allowance, it should be borne in mind that some of the "allowed" limits on accumulation were based on zero secondary tailings treatment whatsoever. So, any exceedance would amount to total failure of the TMPs.

The other point to note is that the bulk of accumulated tailings is debited to Suncor and Syncrude's base plants, the longest running Operations. A numerical breakdown by site and then by storage area is given in Appendix 3 Fluid Tailings Volume Data. The total in Appendix 3 is for 1.4 billion m^3 for all the sites, slightly more that shown in the graph.

This confusion in data reporting is referenced in footnotes which may or may not be an adequate explanation. But the problem with this type of reporting is that there is no standard, particularly with reference to the solids content of the reported volumes. This leads in to a concern expressed to Operators over the review of TMRs. The Author has requested an annual fines mass balance to give a clear picture of FT operations. This request has repeatedly been denied on the basis that it is not a requirement under D085. That particular argument completely ignores the entitlement of Indigenous Peoples to have full disclosure and a meaningful annual consultation.

The final point or caveat to note is that due to the COVID pandemic, Operators applied for and received waivers to avoid conducting full pond investigations in 2020. The intent of the waivers being to limit the number of personnel on each site. Thus, some of the presented data is based on best estimates. Operators were required to subsequently reconcile this data with more complete field surveys to be performed in 2021. Since the 2021 report was not available at the time of writing, the outcome was not known.

SITE ANALYSES

Suncor – Base Plant

The analysis by AER of Suncor's performance is best described as confusing. For example – Section 8.1 para 2: Suncor's FT inventory is within the approved profile using "unapproved" RTR criteria, but exceeds the allowable by 13 Mm^3 using "approved" criteria (paraphrased).

It's not clear as to why this is stated in this fashion. One possibility is that the criteria are under still review. The other possibility is that Suncor is applying RTR criteria to PASS (passive aquatic storage structure) treated tailings to allow FT meeting those criteria to be removed from the FT inventory. This contravenes D085 Section 9.8.2 which clearly states that water-capped tailings cannot be removed from the FT inventory.

The Author is not aware of any Operator having filed a terrestrial reclamation alternative, as AER has deferred the requirement from submission of the first TMPs (due back in 2016) to dates ranging from 2025 to 2027. Therefore, it can be reasonably assumed that any deep fine-grained deposit such as PASS will be water-capped.

An attempt can be made to balance the data presented for Suncor against a calculated rate of FT production. For the period 2018 through 2020, Suncor would have been expected to generate roughly 66 Mm^3 of New FT, based on an earlier mining estimate. For the same period, Suncor reported (from Table 1) that 14 Mm3 of FT were treated by thin-lift drying, and 65.7 by PASS. This suggests a net reduction in total FT. This is borne out by comparing the data in Figures 5 & 6, which indicate a gain in New FT of about 80 Mm^3, and a reduction of Legacy FT of 85 Mm^3, also a net overall reduction.

However, Para 8.1.1 states that improved accuracy of pond bottom surveys resulted in an increase of reported FT of 7.5 Mm^3 from 2019 to 2020. Note that the same paragraph states that consolidation of FT is not accounted for in the FT inventories. This statement does not make a lot of sense, as inventories are based on measurement; thus, any consolidation will be accounted for in the measurement!

This could be much more easily reported by an annual fines mass balance.

It is important to note that Table 3 shows Suncor Base Mine as contributing 21% of the total FT inventory among all Operations. The inventory continues to grow; and the actual growth is probably under-reported. A further example of this is for Pond 5 (see Table 3) which managed to lose 20 Mm^3 of FT after 2016. This is almost certainly the result of achieving RTR criteria; while the actual deposit will not commence reclamation until the mid-2030s. The point to be emphasized here is that RTR simply does not mean ready to reclaim.

Footnote: Since the preparation of this segment, Suncor has provided an explanation as to why their PASS tailings should be removed from inventory. It relies on a narrow interpretation of the Directive – which refers to tailings "treated" by water capping. Suncor maintains that water-capping is not a part of the treatment process; but rather that they are creating a fine-grained deposit with surface drainage. Of course – the counter argument is that when these tailings are finally water-capped, that they will once more be part of the FT inventory. Currently they are applying to have their RTR criteria relaxed, possibly to enable them to further circumnavigate the Directive. However, this form of closure satisfies neither the Indigenous Peoples, nor the intent of the TMF; and should be a concern for all Albertans, including the Regulator.

Syncrude – Mildred Lake

The data presented for Mildred Lake is extremely concerning. Their FT inventory at almost 550 Mm^3 represents 39% of all FT for Industry (Table 3). The rate of FT treatment averaged over the most recent 5 years of record shows about 2 Mm^3/yr for CT and about 5 Mm^3/yr for the centrifuges.

The Author has calculated FT production based on MLX data at about 25 Mm3/yr for the reported period; rising to a peak of about 30 Mm^3/yr by 2030. Thus, it is not surprising to see that Syncrude's Mildred FT inventory has increased by almost 75 Mm^3 over the same 5-year period. This figure represents 28% of the FT growth for all operations.

A rough check of the figures indicates that at 25 Mm^3/yr FT production and 7 Mm^3/yr treatment, the inventory gain should be about 18 Mm^3/yr. This can be compared with the actual gain reported at 15 Mm^3/yr. Given that there are more than 500 Mm^3 in storage, this discrepancy can easily be attributed to consolidation.

AER does acknowledge that Syncrude is exceeding its approved profile for Legacy tailings. Based the treatments in place, only Legacy tailings are treated. However, since the overrun is below the "trigger" point – no remedial action is required.

This is astounding from a 3rd party viewpoint, and can be summarized by observing that if there is light at the end of the tunnel; it must be an oncoming train!

Syncrude reports that almost 30 Mm^3 of treated FT attained RTR status in 2020. The bulk of this was centrifuge cake which had attained 50% solids by weight. Since it appears that Syncrude intends to reclaim both CT and cake as landforms, this did not raise the issue of "approved" vs. "unapproved" RTR criteria. However, it is noted that cake at 50% solids has a void ratio of about 2.7:1. This means that a deep deposit will need to shrink by about 50% of its volume to perform as a geotechnically defined soil. This will necessitate careful landform design to ensure the deposit does not form another pit lake.

Syncrude – Aurora North

Aurora North shares a slight advantage with Jackpine – which is that both operations produce froth which is shipped offsite for treatment. The froth contains some fines which form FT at the destination site, rather than at the origin. The amount is not reported; highlighting another benefit of a site wide fines mass balance.

The calculation of probable FT production for Aurora North indicates that an average of about 17 Mm3/yr of New FT would be generated for the period reported with no treatment. Aurora utilizes CT as the treatment process; which draws on Legacy FT as a feed to the process. Table 1 shows that about 70 Mm3 of FT was treated in this way over the 5-year period 2016 – 2020.The profiles presented (Figures 9 & 10) agree with this analysis, showing a steady increase in New FT and a corresponding decrease in Legacy FT.

In 2020, CT production was curtailed, resulting in an increase in overall inventory. This decision was made in response to the COVID pandemic. Unfortunately, this is a reflection of a somewhat cavalier attitude towards the need to control FT inventories.

Aurora remained within its allowed limit of FT inventory, which was the probable rationale for cutting back on treatment. It is apparent that Aurora has sufficient treatment capacity in place to effect zero overall FT growth.

CNUL – Muskeg River

Muskeg River Mine (MRM) is an interesting case in so far as the data presented only tells a part of the story. Without treatment, MRM would be expected to produce about 10 Mm^3/yr of FT. Figure 5 indicates an allowable 10-year accumulation of 69 Mm^3 or about 7 Mm^3/yr. So far MRM has accumulated 43.8 Mm^3 or about 7.3 Mm^3/yr. This suggests that they should be reporting above the allowable; contrary to what is shown in Figure 5. This example illustrates the generous allowance that AER is prepared to approve.

Any reviewer of this information would be concerned about the future as it appears to predict an exceedance of the permissible within a few years.

However, MRM has filed a new Fluid Tailings Management Plan Amendment (FTMPA 2022); in which they indicate the phasing in of centrifuges in 2025 to address the current shortfall in treatment capacity.

Table 1 carries an entry for treatment of tailings by thickening, with a volume summation of 133.5 Mm^3 over the 7 years of tabulation. This is a singularly useless piece of data, since neither solids content (SC) nor sand-to-fines (SFR) is included.

However, a guess can be made at the true meaning. SC for thickened tailings is offered for the first 4 years at an average of about 23%. This equates to a specific gravity of about 1.17, giving a calculated mass of 156 Mtonnes. At 23% solids, the solids mass is about 36 Mtonnes. SFR can be guessed to be at 0.8:1; resulting in a treated mass of 20 Mtonnes over 7 years. This is roughly one quarter of the fines mined over that same period, which seems promising.

But the thickener performance, which has to be a factor in determining if these fines are truly “treated” is another story. The defining factor is the ratio f_w, defined as “fines / (fines + water)”, in this case, calculated at 17%. The target in a conventional thickener is close to 35%. It can be argued that the thickener is actually a clarifier, and the thickened underflow is a dilute slurry devoid of significant treatment.

Despite the poor thickener performance, the end result of co-disposing (through separate discharges) of thickened tailings with either whole tailings or coarse tailings is showing promise. In addition, MRM is treating a modest quantity of fines by thin lift drying.

CNUL - Jackpine

The Jackpine Mine (JPM) is remarkable from a tailings standpoint; commissioned in 2010, so far it has accumulated less than 30 Mm^3 of New and Legacy FT. The mine has been assisted in this by the transfer of froth containing some fine tailings to MRM. The magnitude of this is not known as CNUL does not provide a fines mass balance, despite repeated requests.

JPM relies mainly on thickened tailings to achieve its objective, plus a small amount of centrifuged product. These streams are co-disposed with either whole tailings or cyclone underflow, as is practiced at MRM. It would appear that this is a simple but effective technique.

CNRL - Horizon

The data presented in the AER report can be misleading. In the case on Horizon, this is especially so. Table 1 reports that over 425 Mm^3 of FT have been treated by non-segregating tailings (NST) processes in the years 2018-2020. In the same period, the operation would have been expected to produce about 72 Mm^3 of FT without treatment. Yet for this period, the site accumulated about 40 mm^3 of New FT while reducing the Legacy FT volume by about 2 Mm^3.

Footnote “h” to Table 1 indicates that while the Table refers to “treated FT volumes”; the value reported is for NST volumes. Calculation of the volume of actual FT contained within this requires so many assumptions as to render the result meaningless.

Instead, it is necessary to examine Figure 15; which indicates that the FT inventory has increased by about 15 Mm^3/yr over the reporting period, against a predicted volume of 24 Mm^3/yr for the “zero treatment” case.

Figure 16 shows a very small reduction in Legacy FT, probably attributable to a variant of the NST

process. For the uninitiated, NST results from a combination of thickener underflow with cyclone underflow. This resembles a whole tailings stream in composition, except that the solids content is increased and the fines have been flocculated.

The variants include eNST (for enhanced), meaning that CO_2 has been injected downstream to improve dewaterability; and esNST (enhanced spiked), signifying the addition of some reclaimed higher density FT to increase the fines content of the stream.

The reporting is further confused by the addition of NRU (Naphtha Recovery Unit) tailings in the volume of treated FT in Table 1, whereas the text (para 8.6.1) states that NRU tailings have not been removed from the FT inventory as no RTR criteria have been approved. (Note that NRU tailings result from froth treatment – some sites refer to these as TSRU (Tailings Solvent Recovery Unit) tailings, depending on the froth treatment process in place at that site.)

Horizon has an interesting technology under development called IPEP (In-Pit Extraction Process). Little is known about this (though possibly based on Bitmin) and the pilot was shut down in 2020 due to a combination of COVID and low oil prices. It is hoped that this is being resurrected, and that more information and a field visit will be forthcoming.

Imperial - Kearl

During the consultation phase of the Kearl TMP, Imperial frequently used the phrase “under promise and over deliver”. While this might be appropriate for a team in the Olympics, whose performance is largely influenced by others, it became tedious for a situation over which Imperial had full control. The result of this mindset was that Kearl was granted an allowance of 180 Mm^3 of FT storage; which can be compared against a “zero treatment” accumulation of 200 Mm^3 in 10 years.

Imperial has managed to restrict FT growth to 75 Mm^3 in what amounts to 6 years of operation, and is well within their target. This is the result of lower than planned production coupled with the generous FT inventory allowed.

Imperial reports that their thickeners are not achieving the desired underflow solids content in the range of 40 to 50%. Given that MRM, JPM and Fort Hills are struggling to exceed the low 20’s, this is hardly a major concern. However, the Author has expressed concern in the past that the thickeners are undersized for the intended duty. This is contradicted by Imperial’s assertion that they are unable to feed sufficient fines to the thickeners. This has been ongoing since start-up. It is impossible to ignore the inference that had this been a process limitation in the production of bitumen froth; it would have been resolved immediately.

Suncor – Fort Hills

The section on Fort Hills provides an example of the lack of rigour exercised in administering the Regulations for tailings management. Table 1 provides no data for Fort Hills, as none is available, except for a reference under para. 8.8.1 of 30 Mm^3 of New FT; also delineated in Figure 18.

There is no direct reference to the existence of a TMP for Fort Hills; but para. 8.8.2 refers to submission of an “updated” TMP to be submitted within 2 years of the start of the PASS technology demonstration, but no later than Sept 30th 2026. The need for a PASS pilot is puzzling since the process is reported as having been in commercial operation at Suncor’s Base Mine since 2018.

Figure 18 shows an approved profile for New FT with a trigger at 125 Mm^3. A rough calculation based on the mine plan indicates that the first 10 years of operation would result in the generation of about 165 Mm^3. Thus, Fort Hills can meet its initial target by treating 25% of the fines that would be produced without treatment, and will not exceed the Total Volume Trigger with zero treatment.

The report notes that PASS is the only intended technology to be applied at Fort Hills; but that this is not an approved technology, and that no RTR criteria have been established. This suggests that Fort Hills has no research on tailings available to establish the relevance of PASS at this operation, compared to Suncor’s Base Mine!

It is also noted that Fort Hills started production in December of 2017. This would suggest that by the 2020 reported data; 3 years of inputs should have been made available.

Para. 8.8 refers to the need for Suncor to submit feasible alternative treatment technologies and a plan to manage the volume of FT to be treated by PASS and subsequently water-capped. A reasonable reader might interpret this to mean that a terrestrial reclamation alternative is required, as

specified in Directive 085, and in accordance with the intent of the TMF.

However, given that PASS treated tailings, though intended (as referenced in the above paragraph), have been interpreted as not treated by water capping, the above requirement is probably meaningless. Suncor can meet this by suggesting that they use centrifuges, or co-disposal, or thin-lift drying, or any other number of technologies to meet the phrasing of this requirement.

AER notes a concern that the thickeners are not operating to specification. This would put Fort Hills on par with MRM and JPM in this regard. The degree to which the thickeners are off target is not mentioned.

REPORT CARD

The top performer is undoubtedly CNUL's Jackpine Mine. This has been in operation for 10 years, and yet has accumulated only 30 Mm^3 of FT; representing slightly more than 2% of the total. The key to this success would appear to be the use of co-disposal of treated fines streams with coarser material in separate but adjacent discharges. The transfer of fines in froth sent to MRM is also helping the performance.

In last place is Syncrude Mildred Lake. Syncrude has been producing since 1978; and in the 42 years to 2020 have stockpiled almost 550 Mm^3, or slightly more than 13 Mm^3/yr. The rate of treatment shows little hope of halting this growth. No doubt Syncrude's defence will reference their bitumen output over the same period. The Author would welcome ready access to data to rank total FT inventory to cumulative bitumen production.

The dark horse among the companies reporting is Suncor. AER recognizes this in their differentiation between "approved" and "not approved" inventories. The Author perceives this as an end-run around the prohibition of removal of water-capped FT from their inventory; while proposing to treat these same tailings by water-capping in the reclamation phase. Suncor has 21% of the combined FT inventory, but has been operating for the longest time – 53 years from 1967 to 2020. This might cause the FT inventory to look better on the basis of accumulation per barrel of bitumen.

Syncrude's Aurora North is doing reasonably well despite having an inventory exceeding 140 Mm3. The key point is that growth over the last 6 years is only 30 Mm^3. As with JPM, Aurora is able to transfer some fines in froth to another site.

MRM was on a collision course with its allowed FT inventory limit, but has proposed remedial action. This needs to be closely monitored.

Horizon has accumulated 150 Mm^3 of FT in only 11 years of operation, including 80 Mm^3 in the last 6 years. While a small amount of Legacy FT is being used in the esNST process, a more aggressive treatment approach is warranted.

Kearl is within their generous allowance. However, their inventory is increasing at about 12.5 Mm^3/yr and action is needed.

CONCLUSIONS

It is immediately apparent that the growth of FT inventories continues. In the past 6 years, 325 Mm^3 has been added to the combined inventory. This amounts to 23% of the current total. Directive 85 was in place for 5 of these years.

It is also apparent that Industry fully expects that water-capping of FT deposits will become an approved technology for reclamation of mine sites, ignoring the objections of Indigenous Communities. This prediction is supported by the absence of any terrestrial alternative to water-capping, despite the requirement for this specified in D085.

The analysis indicates that the worst offenders are the senior operations at Syncrude Mildred Lake and Suncor Base Mine. Other operations are achieving some success in reducing the rate of FT accumulation.

However, it is worth noting that the Directive calls for the FT inventory to eventually reduce to 5-years of "normal" production at the end-of-mine-life, and to be on a trajectory for (terrestrial) reclamation within 5 years of that date. To meet the profiles specified in the Directive, Operators must first reach a state whereby they are capturing all of the FT produced in any given year. They are then required to treat additional volumes of FT inventory to reduce the overall volume from the 10-year peak allowance to a 5-year EOML volume limit. No Operator appears to be heading in that direction.

Analysis of the relative impact of treatment processes is hampered by the refusal of Operators to provide requested fines balances. The variance in both sand-to-fines ratio (SFR) and solids content of the various deposits makes any determination of actual fines treated impossible to be accurately assessed.

REFERENCES

Compliance with TMF Objectives – Fact or Fantasy – An Indigenous Peoples' Perspective. J Blum et al. IOSTC 2018.

State of Fluid Tailings Management for Mineable Oil Sands, 2020. Alberta Energy Regulator, September 2021.

Directive 085 (D085) – Fluid Tailings Management for Oil Sands Mining Projects. Alberta Energy Regulator. Revised October 12th, 2017.

Lower Athabasca Region (LARP) – Tailings Management Framework (TMF) for the Mineable Athabasca Oil Sands. Alberta Government. March 2015.

Reclamation sketches associated with various TMP submissions.

GOVERNMENT POLICY AND REGULATORY INFLUENCE ON OIL SANDS TAILINGS INNOVATION

Jonathan Matthews, Magpie Consulting Inc. Calgary, Alberta, Canada

ABSTRACT

For fifty-five years the production and management of fluid tailings (FT) from oil sands mining operations has been recognized by mine operators, regulatory agencies, the Government of Alberta (GoA), the Government of Canada (GoC), Indigenous communities, and various environmental non-governmental organizations (eNGOs) as a significant environmental concern. As the number and scale of oil sands mining operations has increased, so has public scrutiny and pressure to reduce FT volumes.

The GoA responses to these pressures are reflected in GoA policies, evolving oil sands tailings regulations, and Alberta Energy Regulator (AER) project approval conditions. This paper will provide a summary of the evolution of tailings regulations, with a focus on how the Energy Resources Conservation Board (ERCB) Directive 074 (D-074), GoA Tailings Management Framework for the Mineable Athabasca Oil Sands (TMF), AER Directive 085 (D-085), and AER project approval conditions, have consistently promoted more tailings innovation to reduce the production and accumulation of FT.

ERCB D-074 created legislative requirements that resulted in rapid development and deployment of tailings technologies to meet GoA performance requirements. In contrast, D-085, which replaced D-074, does not drive oil sands mine operators to transform more FT into trafficable landforms. Consequently, industry progress on reducing FT has diminished since D-074 was rescinded.

Within this context, the paper concludes that the current GoA tailings policy and regulatory framework do not demand tailings innovation but rather hope for it. There are no current governmental or regulatory requirements or incentives to develop and deploy novel technologies that reduce the environmental footprint of oil sands tailings.

Nor does the AER's Mine Financial Security Program (MFSP) incentivize tailings innovation. Securities required by the operators are very modest relative to future reclamation costs thus operators can minimize the net present cost (NPC) of reclamation by delaying reclamation activities rather than proactively reducing FT volumes and liabilities.

Despite the absence of regulatory requirements or incentives for oil sands tailings innovation, oil sands mine operators are motivated to explore novel tailings technology opportunities. As reflected in the Canadian Oil Sands Innovation Alliance's (COSIA) 2021 Annual Report, oil sands mine operators are still seeking innovative solutions to transform FT into terrestrial landscapes in a sustainable manner, motivated to:

- improve cost competitiveness, and,
- enhance corporate environmental, social, and governance (ESG) excellence.

By responding proactively to the consistent public pressure to reduce FT volumes, oil sands mining operators can enhance shareholder and stakeholder support for continued extraction of oil from the minable Athabasca oil sands deposits in northern Alberta.

INTRODUCTION

The production of fluid tailings[1] (FT) is a consequence of conventional oil sands mining and aqueous bitumen extraction processes (AER, 2021). The volume of FT has increased every year

[1] For those reviewing background materials, the lexicon for the tailings deposits of primary concern has evolved over the years. This evolution will be reflected in lexicon changes in technical documents discussing oil sands tailings. What is called fluid tailings was first known as sludge. Sludge nomenclature evolved into mature fine tailings (MFT) which in turn evolved into fluid fine tailings (FFT). With AER Directive 085, FFT has evolved to fluid tailings (FT). Despite the rebranding, the issue is that there are suspensions comprised of water and clay mineral fines that are highly resistant to settling and eventually consolidation without engineering interventions and the composition of the FT does present numerous environmental hazards that require careful management and eventual mitigation. In most cases sludge, MFT, FFT, and FT are interchangeable for this discussion.

since 1967 (Environmental Defence & CPAWS, 2022) (CEC, 2020) (AER, 2022).

FT are defined as *"…any fluid discard from bitumen extraction facilities containing more than five mass percent suspended solids and having less than an undrained shear strength of five kilopascals."* (AER, 2017).

The primary logistical challenges associated with oil sands FT are described by Gray et al (2009); "*The sludge poses two problems. First, it accumulates continuously with time, so the ponds need to grow in size and depth: Increasing amounts of land must be disturbed for sludge storage, and more fresh water must be drawn from the Athabasca River, thereby requiring careful management of water inventory. Second, the accumulated sludge is too fluid to bear any weight at all, so it presents environmental concerns. The sludge must eventually be treated to produce a self-supporting solid matrix that can bear weight before the landscape can be remediated to support vegetation and wildlife."* (Murray Gray, 2009)

In addition to the increasing volumes of FT, stakeholders have expressed a range of concerns associated with oil sands FT, including:

- uncertainty respecting the viability of water capping of FT, including PASS, and an absence of viable FT management contingencies if the use of water capping of FT is not approved for industry-wide (The Royal Society of Canada Expert Panel, 2010) (Blum, 2018),
- fugitive emissions (Environmental Defence Canada & CPAWS, 2022) (Pembina Institute, 2017),
- potential seepage of toxic constituents in FT into undisturbed lands and waterways (Environmental Defence & CPAWS, 2022) (Rougeot, 2021),
- a call for more demonstration of reclamation of oil sands FT into landscapes suitable for terrestrial reclamation (Blum, 2018) (Rougeot, 2021) (Pembina Institute, 2017) (The Royal Society of Canada Expert Panel, 2010),
- Alberta taxpayer exposure to substantial future reclamation liabilities due to a weak mine financial securities program (Bakx, 2021) (CEC, 2020),
- risk of release of FT from tailings storage due to loss of containment integrity (Pembina Institute, 2010),
- acid generation potential of pyritic minerals concentrated in froth treatment tailings (FFT) (Van Dongen, 2021), and,
- hazards associated with naturally occurring radioactive materials in minerals concentrated in FFT (Suncor Energy Inc. Oil Sands, 2022).

This paper can't do justice to providing an objective assessment of all these concerns however the paper can propose that most of these concerns can be reduced, if not alleviated, if the sufficient water is removed from the FT such that the resulting product has geotechnical integrity. A companion paper will provide examples that support the validity of this assertion (Matthews, Fluid Tailings Thermal Drying: More Promising Than You Might Think, 2022).

Against this backdrop, the oil sands industry has been working with governments and academic institutions for decades to explore various means to treat the FT such that it can be incorporated into sustainable reclaimed landscapes and mitigate the other concerns identified. Despite a concerted collaborative effort, most solutions developed and deployed to date fall short of expectations and more innovation is needed (AER, 2021) (Pembina Institute, 2017) (COSIA, 2021).

The oil sands mine operators, through Canada's Oil Sands Innovation Alliance (COSIA), have identified three focus areas to improve tailings management:

- reduce the accumulation of FT tailings within tailings ponds through the development of new and improved tailings management practices,
- treatment of process affected water, the water which remains once the solids are removed, and,
- accelerating the reclamation of the resulting tailings deposits so that they can be incorporated into the final reclaimed landscape (COSIA, 2021).

There has been encouraging progress on developing technologies that improve FT management however FT inventories continue to grow. Increasing FT volumes and continuing uncertainties respecting the viability of eventual FT reclamation garner negative local, provincial, national, and international attention (The Royal Society of Canada Expert Panel, 2010) (Pembina Institute and Water Matters, 2009) (Pembina Institute, 2017) (GoA, 2015) (CAPP, 2021).

As discussed, there are number of concerns respecting FT, including a need to confront and

mitigate fugitive GHG emissions from FT deposits. The governments of Alberta and Canada, oil sands mine operators, and key stakeholders have shown that fugitive emissions from oil sands tailings ponds are a significant potential contributor to annual GHG emissions from oil sands mines. Reducing overall GHG emissions from oil sands operations is currently the most prominent ESG initiative for the oil sands mining industry (Oil Sands Pathways to Net Zero, 2021). Therefore, it is appropriate to discuss the source and scale of fugitive GHG emissions from tailings deposits.

A paper published by the GoA proposes that GHG emissions from fluid tailings could be as high as 6.0 kg CO_2e per barrel of bitumen produced (Burkus Z. , 2014). This is approximately 17% of the total GHG footprint for a current best-in-class oil sands mine operation, excluding upgrading related emissions. The fugitive GHG emissions are primarily carbon dioxide and methane associated with decomposition of residual solvents that are discharged to the tailings settling basins as a constituent of froth treatment tailings.

Cumulative fugitive GHG from oil sands tailings ponds have varied between approximately 740,000 and 1,930,340 tonnes CO_2e, each year, from 2011 to 2020. For some operators, fugitive GHG emissions from tailings ponds have represented up to 89% of total annual fugitive emissions reported (AEP, 2021). Generally, the oil sands mine sites with the longest operating history have the highest emissions, irrespective of the current annual bitumen production rates, because the onset of fugitive emissions can take a decade or more to commence (Van Dongen, 2021).

Some researchers have used alternative fugitive emissions measurement techniques to conclude that the fugitive emissions might be underreported by approximately 64% due to the nature of industry standard emissions measurement techniques (Yuan You, 2021).

Thus, innovations with the potential to materially reduce fugitive emissions from oil sands tailings deposits should be highly synergistic and supportive of the industry drive to zero net GHG emissions by 2050. Those technologies that have the potential to reduce fugitive GHG emissions from tailings ponds and reduce FT volumes should be of top priority for R & D efforts by the oil sands tailings innovation community.

OIL SANDS TAILINGS REGULATIONS AND POLICY LANDSCAPE

Oil sands tailings regulation has evolved significantly since 1967. The oil sands tailings regulation landscape is simple, in principle, i.e., tailings management commitments are made by operators during project approval processes and then project specific tailings management requirements are included as project approval conditions. Additional industry-wide regulatory compliance requirements are introduced through AER Directives or in the form of amendments to mine specific approvals. Thus, almost all oil sands tailings regulations are managed through Oil Sands Conservation Act (OSCA) approval conditions and D-085 requirements.

This paper is focused on synergies between operator approval conditions, tailings directives, and the evolution of tailings management technologies and practices. Within this context, the discussion will focus on the GoA TMF, ERCB D-074[2], the AER MFSP, and AER D-085 as the policy and regulatory instruments with the greatest potential to influence the tailings innovation priorities of the oil sands mine operators.

ERCB Directive 074

In response to stakeholder concerns respecting rapidly increasing volumes of FT and other environmental concerns respecting FT, the ERCB issued *Directive 074: Tailings Performance Criteria and Requirements for Oil Sands Mining Schemes* in February 2009. Directive-074 was introduced with an intention to *"… slow the growing volumes of fluid tailings and the proliferation of tailings ponds."*. (Energy Resources Conservation Board (ERCB), 2009)

When ERCB[3] D-074 was being finalized for public release in 2008 the oil sands mature fine tailings[4] inventory was 740 million cubic metres (ERCB, 2008) and new oil sands mining operations were in the project application and approval stages. In issuing D-074, the GoA and ERCB wanted to

[2] Now rescinded/retired as of 2016

[3] Alberta Energy Resources Conservation Board, now known as the Alberta Energy Regulator)

[4] For this discussion, mature fine tailings and fluid fine tailings are synonymous

prevent MFT inventories ever exceeding one billion cubic metres. Confounding this ambition, the AER reported in 2021 that fluid tailings volumes increased by 80 million cubic metres from 2019 to 2020 and that cumulative FT volumes exceeded 1.4B m^3, representing a doubling of the fluid tailings inventory since D-074 was released[5], and reinforcing the need to find solutions that will reduce FT inventories to support an improved balance between social, environmental, and economic performance.

The long-term goals identified in D-074 included:

- minimize and eventually eliminate long-term storage of FT in the reclamation landscape,
- incorporate FT tailings into trafficable landscapes suitable for terrestrial reclamation,
- reduce containment of FT in external tailings disposal area during operations,
- reduce process-affected waste-water volumes on mine sites,
- enhance process water recovery to increase energy efficiency and reduce fresh-water import,
- reduce resource sterilization associated with above grade tailings ponds facilities, and,
- ensure that the liabilities for tailings management are managed through reduced FT inventory and more rapid reclamation of tailings facilities.

D-074 required that all oil sands mine operators capture at least 50% of the tailings fines run-off from mined oil sands in dedicated disposal areas (DDAs) in a way that within one year the deposits would have an undrained shear strength of at least 5 kPa and the deposits would be trafficable and ready for reclamation within five years of the end of tailings deposition.

When D-074 was issued, oil sands mine operators were concerned that the regulatory requirements would not be achievable within the timeframes stipulated. This created a sense of urgency among oil sands mine operators and research partners to form collaboration alliances and increase resource allocations to accelerate the research, development, and implementation of FT reduction technologies. Notable responses to the innovation demanded by D-074 included the inaugural International Oil Sands Tailings Conference (IOSTC) in December 2008, and formation of the Oil Sands Tailings Consortium (OSTC), in December 2010.

In 2013 the ERCB concluded that no oil sands mine operators were fully achieving D-074 requirements, noting that *"The volume of fluid tailings, and the area required to hold fluid tailings, continued to grow, and the reclamation of tailings ponds was further delayed.".* On March 13, 2015, the application and enforcement of D-074 was formally suspended by AER[6]. The bulletin rescinding D-074 noted that the GoA was planning to publish a policy framework that would complement and expand upon D-074 requirements to *"…ensure that fluid fine tailings are reclaimed as quickly as possible and that current inventories are reduced.*" (ERCB, 2013).

D-074 did accelerate the development and deployment of novel FT treatments before being rescinded. Large-scale deployment of thin lift subaerial drying and centrifugation technologies was a direct response to D-074 requirements.

Tailings Management Framework for Mineable Athabasca Oil Sands

The suspension of D-074 was accompanied by release of the GoA's *Tailings Management Framework for Mineable Athabasca Oil Sands (TMF)* which indicated that the principles and objectives outlined in the TMF would be used to guide oil sands tailings regulation until a new tailings directive could be released. (AER, 2015)

The stated goal of the Government of the TMF is*: "Fluid tailings accumulation is minimized by ensuring that fluid tailings are treated and reclaimed progressively during the life of a project and all fluid tailings associated with a project are ready-to-reclaim within 10 years of the end of mine life of that project. The objective will be achieved while balancing environmental, social, and economic needs".*

The overarching policy objective of the TMF is *"… reducing the amount of fluid tailings on the landscape more quickly, and of having tailings*

[5] Despite the objectives of the TMF and D-085, it is apparent that the objective of treating fluid tailings to limit total FT inventory to below 1B m^3 has failed.

[6] The merger of Alberta Energy Resources Conservation Board and Alberta Environment and Sustainable Resource Development to form Alberta Energy Regulator was proclaimed on June 17, 2013.

ready to reclaim within an acceptable timeframe" [7] (Government of Alberta, 2015).

One of the key principles articulated within the framework relates to technological innovation, i.e., *"The framework drives the application of technology, and technological innovation, understanding, and certainty around fluid tailings treatment options."* The TMF also affirms the GoA's environmental principles, including *"Continuous improvement and the use of best available technology."*[8] for tailings management. Within the context of managing the uncertainty of yet unproven technologies the TMF requires that *"…fluid tailings volume profiles submitted with technologies that have yet to be proven will require contingency plans for treatment, including alternative technology options for meeting requirements"* (GoA, 2015)[9].

A key tenant of the TMF is *"…to drive innovation and proving of technology with the intent of enhancing certainty around fluid tailings treatment, and the eventual achievement of the outcomes of this framework."* (GoA, 2015).[10]

Within the TMF guidance for setting FT volume profiles, the GoA lists factors to be considered in assessing tailings management technologies, including:

- *"All plans should be based on the most advanced and demonstrated technologies.",*
- *"Fluid tailings accumulation must be managed and minimized through the life of the project.",*
- *"Tailings management plans will steward toward a safe, stable, and sustainable final landscape."*, and,
- *"Tailings management plans need to balance potential impacts to air, land, and water as well as ensure that the operations remain cost effective.".*[11]

With respect to net environmental effects of tailings management technologies, several evaluation criteria are noted in the TMF including:

- tailings footprint,
- timeliness of reclamation,
- water use intensity,
- water quality,
- greenhouse gas emissions, and,
- energy intensity.

AER MFSP

The MFSP is a liability management tool that is intended to shelter Albertans from the potential burden of oil sands and coal mine closure costs. The intent of the program is to ensure that the companies that own and operate coal and oil sands mines will have the financial resources to complete satisfactory closure and reclamation without transferring the financial burden to Alberta taxpayers (AER, 2022).

The MFSP should protect Alberta taxpayers from the risk of inheriting future costs of mine reclamation efforts. However, some stakeholders are concerned that the securities posted for the current oil sands mine operations fall significantly short of the actual liability, especially in the context of the highly uncertain future costs of remediation and reclamation of oil sands FT deposits (Yewchuk, 2021).

In 2022 the total of cash deposits, letter of credit guarantees, and demand forfeiture bonds for all eight active oil sands mining operations was $913M (AER, 2022). In contrast, in 2018 the VP of Closure and Liability at the AER delivered a presentation that indicated that the liability for mining closure and reclamation was estimated internally by the AER to $130 B (AB POL ECON, 2018). Much of this $130B is attributable to reclamation of oil sands tailings, with soft tailings and FT in many cases attracting the highest cost per hectare reclaimed. Environmental Defence Canada (EDC) used sparse GoA and industry sources to estimate that in 2016 the liability attributable to FT was $44.5B, excluding an additional $6.8B liability for land reclamation

[7] Given the context of the TMF replacing Directive-074 it seems reasonable to assume that the government had concluded that efforts to reduce fluid tailings inventories and to make tailings ready to reclaim in an acceptable timeframe has not yet been validated as achievable with status quo operator plans and technologies.

[8] Noting however neither the TMF nor the subsequent D-085 provide a description of what criteria will be used in identifying or selecting the best available technologies for oil sands fluid fine tailings treatment processes.

[9] Since water capped fluid tailings, and variations thereof, are not currently considered proven technologies there is a need to have an alternate plan the event that water capping strategies are not satisfactorily demonstrated to meet the needs of the TMF.

[10] The corollary to this key tenant is that technologies that demonstrate potential to reduce FT inventory and enable more rapid stabilization and reclamation of fine tailings should be given a high priority in oil sands tailings research efforts.

[11] The GoA has not yet provided guidance on how the cost of a FT treatment processes would be evaluated within the broader context of assuring that oil sands mining operations remain cost effective, nor who would make such determinations using objective, transparent criteria

(Environmental Defence Canada and NRDC, 2022)[12].

AER Directive 085

The TMF was followed by the release of AER's *Directive 085: Fluid Tailings Management for Oil Sands Projects* on July 14, 2016. D-085 serves as the current enforcement vehicle of the TMF. The TMF and D-085 require that the Directive *"…must be reviewed by the AER every five years…",* and that, *"…the AER will engage industry, indigenous communities, as part of this review. To promote transparency, the results of this review will be made publicly available…"*. Since all oil sands mine operators submitted the first D-085 TMPs were filed in November 2016, the public review process should be commencing soon.

Directive 085 states that after an early production phase for new mines *"…it is expected that growth of fluid tailings will closely match the rate of treatment so that, on average, fines can be managed to a treated state as they are produced."* (AER, 2017). AER D-085 also instructs that *"The approved fluid tailings management plans must[13] be reviewed every five years or as necessary over the course of the mine life. This review will ensure that the profiles and thresholds are in line with projections and reflect current technology, new knowledge, and continuous improvement.",* and that, *"As identified by the TMF, the AER will engage industry, indigenous communities, and other stakeholders as part of this review. To promote transparency, the results of this review will be made publicly available, including the AER website."*. (AER, 2017).

AER Directive 085 instructs that *"Fluid tailings are considered ready to reclaim (RTR) when they have been processed with an accepted technology, placed in their final landscape position, and meet performance criteria[14]. RTR is intended to track treated fluid tailings performance during the operational stage of the deposit to ensure that the deposit can be reclaimed as predicted in the life-of-mine closure plan, in the time predicted. To evaluate whether active treated tailings deposits are on the predicted trajectory to allow them to be removed from the fluid tailing inventory, they must achieve approved performance criteria. Each treated tailings deposit will have approved indicators that must be measured to determine if the performance criteria has been achieved."* (AER, 2017).

Directive 085: Progress Update

The AER has reported that the total FT inventory decreased in 2021 – the first time since commercial oil sands operations began in 1967 – from 1,351 Mm^3 in 2020 to 1345 Mm^3 in 2021 (AER, 2022). In fact, the FT inventory continued to grow, as will be discussed. The crux of the issue is that operators can choose to report reduced FT inventory by renaming some of the FT as ready to reclaim tailings (RTR), even if the tailings deposits still meet the AER definition of FT (Blum, 2018).

There is no easy method to extract the true volume of FT using the D-085 annual reporting requirements because the AER reports do not require operators to report the total inventory of FT on each site before moving the FT volumes from the FT ledger to the RTR ledger. However, for the 2021 reporting year we can assess two significant RTR deposits – one at Suncor Base Plant and one at Syncrude Mildred Lake – to get a better sense of the true total FT inventory for the 2021 reporting year.

In 2022, Suncor reported that between 2018 and 2021 86.9 Mm^3 of permanent aquatic storage structure (PASS) tailings met the RTR criteria. (Suncor Energy Inc. Oil Sands, 2022). Thus, this volume was excluded from the FT inventory for Suncor's Base Plant numbers. Strength values are not reported for the PASS deposit however Suncor does provide a cross section showing %solids versus elevation and %fines versus elevation. Analysis of these plots shows that more than 90% of the PASS deposit has a solids content between 0 and 60% and a fines content between 50% and 100%[15]. This material would be classified FT using the AER definition. Therefore, Suncor FT inventory

[12] GoA or industry sources would be preferred to estimate the future reclamation liabilities for various types of FT deposits however these are not readily available in the public domain

[13] Emphasis on 'must' added by the author

[14] Readers may be interested to know that some deposits currently acceptable for the RTR designation, and removal from the reported FT inventory, may not be known to be reclaimable within ten years of mine closure, as is also required by AER Directive 085. For example, centrifuged tailings being placed in a deep pit at Syncrude typically have a solids content of less than 55wt% solids and may require more than a century before they are normally consolidated and exhibiting geotechnical strength that is supports reclamation objectives in a cost-effective way

[15] Although perhaps not sensical to have a deposit comprised of at least 50% clay but with no solids, this is the information provided in Suncor' report. The point is that almost of PASS deposit tailings are FT based on the AER definition.

for 2021 is at least 78.2 Mm^3 higher[16] than indicated in the AER report.

Similarly, in 2022, Syncrude reported that since commencing commercial scale centrifugation at Base Mine operations 28.6 Mm^3 of centrifuge cake had been produced that exceeded the RTR criteria of 50wt% solids. In 2021 the average solids content of produced centrifuge cake 52.8% solids, including approximately 5% bitumen as solids (Suncor Energy (Syncrude) Operating Inc., 2022).[17] The centrifuge cake was deposited into the NMSPE Deep Cake cell was approximately 45 m thick at the deepest point. Solids content is shown to vary between 40wt% and 60wt% solids with a SFR of <1 which means the entire deposit will have an undrained shear strength of less than 5 kPa and is FT according to the current AER definition.

Thus, looking at the Suncor and Syncrude reporting examples, it is reasonable to assume that the overall fluid fine tailings for the industry in 2021 was at least 1,451.8 Mm^3 (9.1 billion barrels) [18].

There are more scenarios where total FT has been under-reported in the 2021 AER summary however the point of this discussion is to advise the reader *sometimes* reports of reduced FT inventories are more about semantics than actual FT reductions[19], which can lead to misleading media coverage.

A case in point is a June 7, 2022, Canadian Energy Centre headline which read *"Oil sands shrinking volume of legacy tailings ponds: Total legacy tailings down 24% in last five years"*. (Canadian Energy Centre, 2022). This headline and the associated story are misleading.

The first sentence of the article indicates that *"New technologies and practices are improving the environmental performance of Canada's oil sands industry, with producers removing more than 270 million cubic meters of "legacy tailings" from the environment over the last five years.".* In no instances, however, have tailings been removed from the environment. All the solids and water associated with the legacy FT are still very much in the environment. In some cases, such as thin lift drying product or composite tailings, the legacy FT have been incorporated into tailings deposits that are no longer fluid. However, a significant portion of this 'reduction' in legacy tailings is attributable to simple relabeling of FT to RTR, as was done with Suncor's PASS and Syncrude's centrifuge cake, without changing the fluid nature of the tailings.

It is important to challenge such coverage because repetition of such misleading statements has a high potential to be perceived as a disingenuous distortion of the facts, which has a potential to erode stakeholder trust in the GoA, AER, and oil sands mine operators. [20]

MINE OPERATOR TAILINGS INNOVATION PRIORITIES

There are currently eight active oil sands mining projects. Each project has submitted a tailings management plan (TMP) to the AER and received approval, with conditions, through the OSCA:

- CNUL Muskeg River mine (AER, 2018),
- CNRL Horizon (AER, 2017),
- CNUL Jackpine mine (AER, 2018),
- Imperial Kearl (AER, 2018),
- Suncor Millennium Mine (AER, 2017),
- Suncor Fort Hills (AER, 2019),
- Syncrude Mildred Lake (AER, 2019), and,
- Syncrude Aurora North (AER, 2018).

There are a lot of details in each of the approvals however all approvals have identified concerns including:

- the viability of water capped FT deposits,
- uncertainties respecting the viability of the reclaiming of tailings deposits within ten years of the end of mining for each project, and,
- the need to improve FTT management options.

[16] 86.9 Mm^3 x 90% = 78.2 Mm^3

[17] It may interest some readers to note that the average feed content to the centrifuge plant was 50.8% solids - including approximately 5% of bitumen as solids - in the 2019 operating year. No feed solids concentrations have been provided for the 2020 or 2021 operating years.

[18] 1,345 Mm^3 +28.6 Mm^3 + 78.2 Mm^3 = 1,451.8 Mm^3

[19] For clarity, Syncrude and Suncor are reporting faithfully and accurately according to D-085 requirements. The point being made is that the D-085 reporting requirements have been established in a manner that will almost certainly lead to consistent underreporting of the volume of fluid fine tailings, industry wide.

[20] The author recognizes that it is challenging for those seeking to understand Directive 085 reporting as the semantics are often confusing, reports are lengthy due to D085 requirements, and true assessment of gains being made to accelerate mitigation of the environmental concerns and impacts of FT is lacking.

Within this context, the TMF states that *"…until it is determined whether or not the technology is a successful treatment method, plans will be required to consider alternatives",* and, *"…technologies that have yet to be proven will require contingency plans for treatment, including alternative technology options for meeting requirements."* (GoA, 2015).

To date, the AER has not published a formal position on which technologies included in the approved D-085 TMPs have been determined by the AER to be proven technologies. Despite requiring a plethora of data reporting from the oil sands mine operators the AER has not commented on the efficacy of any of the mine operator' efforts to deliver on D-085 and the objectives of the TMF, other than to comment on volume threshold performance. Nor has the AER provided an update with respect to their intention to establish best available technologies (BAT) for oil sands tailings as discussed in the TMF. The AER does continue to require that all operators proposing water capping of tailings develop terrestrial reclamation alternatives.

TAILINGS INNOVATION PRIORITIES SUMMARY

Consistent throughout oil sands mine approvals, D-074, the TMF, and D-085 is an expectation that oil sands mine operators will continue to seek technologies that reduce FT volumes, reduce environmental footprint, and accelerate the pace of stabilization and reclamation of oil sands tailings. Despite encouragement of further innovation to reduce FT, there currently no GoA policy instruments or AER regulations requiring, or incentivizing, oil sands mine operators to develop and deploy novel FT reduction technologies.

The GoA and AER have indicated an intention to establish a BAT inventory to meet the ambitions of the TMF however thus far there has been no indication that this intention is being actioned. Nor has the AER issued public statements to differentiate proven technologies from unproven technologies or indicate what criteria they would contemplate in making such determinations. Establishing clear positions on these issues could provide clarity on expectations that could lead to increased focus on innovation initiatives considered critical to delivering on the GoA TMF ambitions.

Public communications from oil sands mine operators indicate they remain committed to improving upon incumbent technologies and developing and deploying promising novel technologies (CAPP, 2021) (Canada's Oil Sands Innovation Alliance , 2021) however the tailings plans being submitted by oil sands mine operators under D-085 are primarily based on combinations of incumbent technologies such as thickened tailings, composite tailings, non-segregating tailings, centrifuged tailings, and water capping of FT[21] (AER, 2022).

Industry tailings innovation efforts are summarized in annual COSIA progress reports, available publicly from the COSIA website. These summaries fail to provide an opinion on to what extent COSIA's R & D efforts are progressing deliver on COSIA's top three tailings innovation priorities. The last time the oil sands tailings innovation community provided a summary on the tailings innovation landscape and identified specific strategic innovation priorities together with recommended 'high priority' contenders was with the publication of the Tailings Roadmap that was commissioned by the Oil Sands Tailings Consortium (OSTC) in 2010 (CTMC, 2012) (COSIA, 2021) (Gidley & Boswell, 2013) (GoA, 2015).

PERFORMANCE CRITERIA FOR ASSESSING NOVEL FLUID TAILINGS PROCESSES FOR OIL SANDS MINING OPERATIONS

ERCB D-074, the TMF, and AER D-085 all indicate a bias and encouragement for innovations that reduce FT. Looking across more than a decade of evolving regulation and government policy – which should also reflect the interests of Indigenous groups and eNGOs – it is apparent that all parties are supportive, in principle, of deployment of technologies that demonstrate potential to transform FT into trafficable tailings that can support terrestrial reclamation in a reasonable time span.

Other outcomes desired of novel FT treatment processes include:

[21] Including Suncor's 'permanent aquatic storage structure' which entails water capping of polymer amended fluid fine tailings.

- mitigation of fugitive carbon dioxide and methane emissions associated with the decomposition of residual solvents and flocculants in fluid tailings deposits (Suncor Energy Operating Inc, 2021),
- recovery and reuse of water from fluid tailings deposits to enhance freshwater conservation.
- optimization of water content for trafficability (AER, 2017) (Hyndman, 2019),
- recovery and reuse of heat from warm extraction tailings and hot froth treatment tailings streams (Murray Gray, 2009), and,
- optionality to mitigate health, safety, and environmental hazards, associated with the concentration of naturally occurring radioactive and pyritic minerals in froth treatment tailings (Van Dongen, 2021) (Suncor Energy Inc. Oil Sands, 2022).

CONCLUSIONS

Government policies, oil sands mine approvals, and current tailings regulations encourage continued technology development to reduce FT volumes but do not require it. There is currently an absence of explicit regulatory or GoA policy influence on the oil sands tailings innovation agenda, in contrast to the more specific tailings performance outcomes that were required by D-074.

Since implementing D-085 the AER has been focused on compliance with status quo – that is, delivery on commitments made in approved D-085 TMPs. The oil sands mine operators alone are driving the tailings innovation agenda, motivated to develop and deploy of tailings innovation opportunities that enhance the bottom-line and support corporate ESG objectives as a mean of shoring up shareholder confidence in the continued viability of oil sands mining operations.

The GoA and AER have declared their intentions to review the efficacy of the current tailings regulatory regime to deliver on the TMF ambitions and to define BATs for oil sands tailings operations. Both initiatives are overdue. Engaging key stakeholders on these topics has the potential to accelerate the development and deployment of novel tailings technologies that strongly enhance the sustainability of the oil sands mining industry, to the benefit of all key stakeholders.

Despite the wishes of the GoA, the AER, and impacted stakeholders, the inventory of FT continues to rise. Rising FT inventories lead to increased risk of environmental damage through uncontrolled release and increased future closure and reclamation cost liabilities.

Against this backdrop, the oil sands mine operators have identified through COSIA three key tailings innovation priorities to address through collaborative innovation:

- Development of new and improved tailings technologies to mitigate the accumulation of fluid fine tailings,
- Treatment of process affected water, and,
- Acceleration of reclamation of oil sands tailings deposits to facilitate incorporation into functional landscapes (COSIA, 2021).

Within this context, the collaborative oil sands tailings innovation ecosystem should prioritize the following:

- reduce FT production,
- reclaim more water from FT for reuse,
- transform FT into reclamation substrates that are amenable to terrestrial reclamation,
- reduce fugitive emissions, including GHG, from tailings deposits, and,
- mitigate acid generation potential and naturally occurring radiation hazards associated with froth treatment tailings.

Economic benefits of highest synergistic potential include:

- reduced dam construction costs due to reduced FT inventory,
- reduced fluid tailings management and monitoring costs,
- reduced future closure and reclamation costs, and,
- increased mine operations efficiency (i.e., fewer tonne-kilometres of materials movement will reduce mine fleet fuel and operating expenses).

Meaningful tailings innovation progress will only happen when:

- the GoA and regulator articulate objective, achievable, and time-bound tailings performance improvement requirements such that industry efforts to innovate are recognized and rewarded, and,
- oil sands mine operators remain fully committed to challenging the status quo through objective

analysis including genuine technical and economic investigation of alternatives, coupled with a willingness to invest in first-of-a-kind technology deployment initiatives that have the potential to further enhance the sustainability of oil sands mining operations.

If the GoA and AER wish to enhance industry efforts to achieve the overarching TMF goal of *"… reducing the amount of fluid tailings on the landscape more quickly, and of having tailings ready to reclaim within an acceptable timeframe"* it should pass judgement on the capacity of incumbent technologies to deliver on the ambitions of the TMF, establish best available technologies (BATs) for oil sands tailings, and incentivize deployment of technologies that deliver strongly on the TMF ambitions.

REFERENCES

AB POL ECON. (2018, November 5). Environmental Liabilities-Part 2 AER Bombshell. Retrieved from AB POL ECON: http://abpolecon.ca/2018/11/06/environmental-liabilities-part-2-aer-bombshell/

AEP. (2021). Area Fugitive Emissions from Oil Sands Mining Operations, 2011 to 2020. Communicated to author via spreadsheet from Alberta Energy and Parks. Edmonton: Alberta Energy and Parks.

AER. (2015, March 13). Bulletin 2015-11. Retrieved December 5, 2021, from Alberta Energy Regulator Bulletins: https://static.aer.ca/prd/documents/bulletins/Bulletin-2015-11.pdf

AER. (2017, December 18). Approval of Canadian Natural Resources Limited Application for Horizon Oil Sands Processing Plant anmd Mine Tailings Plan. Retrieved from Alberta Energy Regulator: Tailings Notices and Decisions: https://static.aer.ca/prd/documents/decisions/2017/20171218A.pdf

AER. (2017, October 12). Directive 085: Fluid Tailings Management for Oil Sands Mining Projects. Retrieved DEcember 5, 2021, from Alberta Energy Regulaor Directives.

AER. (2017, October 25). Suncor Energy Inc. Applications for Millennium Operational Amendment and Base Plant Tailings Management Plan. Retrieved from Alberta Enery Regulator Tailings Notices and Decisions: https://static.aer.ca/prd/documents/decisions/2017/20171025A.pdf

AER. (2018, June 13). Alberta Energy REgulator Tailings Notices and Decisions. Retrieved from Approval of Syncrude Canada Ltd. Application for Aurora North Tailings Management Plan: https://static.aer.ca/prd/documents/decisions/2018/20180613A.pdf

AER. (2018, May 23). Approval of Canadian Natural Upgrading Limited Application for Jackpine Mine. Retrieved from Alberta Energy Regulator: Tailings Notices and Decisions: https://static.aer.ca/prd/documents/decisions/2018/20180523B.pdf

AER. (2018, May 23). Approval of Canadian Natural Upgrading Limited: Application for Muskeg River Mine Tailings Management Plan. Retrieved from Alberta Energy Regulator: Tailings Notices and Decisions: https://static.aer.ca/prd/documents/decisions/2018/20180523A.pdf

AER. (2018, July 2018). Approval of Imperial Oil Resources Limited Application for Kearl Mine's Tailings Management Plan. Retrieved from Alberta Energy Regulator Tailings Notices and Decisions : https://static.aer.ca/prd/documents/decisions/2018/20180716A.pdf

AER. (2019, February 25). Alberta Energy Regulator Tailings Notices and Decisions. Retrieved from Fort Hills Energy Corporation Application for Fort Hills Tailings Management Plan: https://static.aer.ca/prd/documents/decisions/2019/20190225A.pdf

AER. (2019, July 16). Alberta Energy Regulator Tailings Notices and Decisions. Retrieved from Approval of Syncrude Canada Ltd. Mildred Lake Extension Project and Mildred Lake Tailings Management Plan: https://static.aer.ca/prd/documents/decisions/2019/2019ABAER006.pdf

AER. (2019, February). Fort Hills Energy Corporation: Application for Fort Hills Tailings Management Plan. Retrieved December 5, 2021, from AER Decisions, Decision 20190225A: https://static.aer.ca/prd/documents/decisions/2019/20190225A.pdf

AER. (2021, December 5). Tailings. (Alberta Energy Regulator) Retrieved December 5, 2021, from

Alberta Energy Regulator: https://www.aer.ca/providing-information/by-topic/tailings

AER. (2022, 11 08). Annual Mine Financial Security Program Submissions. Retrieved from Alberta Energy Regulator: https://static.aer.ca/prd/documents/liability/AnnualMFSPSubmissions.pdf

AER. (2022, 11). Mine Financial Security Program. Retrieved from AER Liability MAnagement Programs and Processes: https://www.aer.ca/regulating-development/project-closure/liability-management-programs-and-processes/mine-financial-security-program

AER. (2022, October). State of Fluid Tailings Management for Mineable Oil Sands, 2021. Retrieved December 6, 2021, from Reports: https://static.aer.ca/prd/documents/reports/State-Fluid-Tailings-Management-Mineable-OilSands.pdf

Bakx, K. (2021, December 6). Banned for decades, releasing oilsands tailings water is now on the horizon. (Canadian Broadcasting Corporation) Retrieved 02 08, 2022, from CBC News: https://www.cbc.ca/news/business/bakx-oilsands-tailings-release-mining-effluent-regulations-1.6271537

Blum, J. (2018). Compliance with TMF Objectives-Fact or Fantasy - an Indigenous People's Perspective. Sixth International Oil Sands Tailings Conference (p. 6). Edmonton: University of Alberta Geotechnical Centre.

Burkus, Z. (2014, November). GHG Emissions from Oil Sands Tailings Ponds: Overview and Modelling Based on Fermentable Substrates. Part II: Modeling of GHG Emissions from Tailings Ponds Based on Fermentable Substrates. Retrieved 02 08, 2022, from Oil Sands Research and Information Network: https://era.library.ualberta.ca/communities/e4fdd15f-c21d-4612-a2f7-bfec3fdfc1de/collections/97c301ec-5099-45ae-8eed-7b6c55616fbf

Burkus, Z. J. (2014, November). GHG Emissions from Oil Sands Tailings Ponds: Overview and Modelling Based on Fermentable Substrates. Part I: Review of the Tailings Ponds Facts and Practices. Retrieved December 5, 2021, from Educationa and Research Archive: Oil Sands Research and Information Network: https://era.library.ualberta.ca/communities/e4fdd15f-c21d-4612-a2f7-bfec3fdfc1de/collections/97c301ec-5099-45ae-8eed-7b6c55616fbf

Canada's Oil Sands Innovation Alliance . (2021, December 6). Tailings Management. Retrieved from Canada's Oil Sands Innovation Alliance: https://cosia.ca/initiatives/tailings

Canadian Energy Centre. (2022, June 7). Canadian Energy Centre Environment. Retrieved from Oilsands shrinking volume of legacy tailings ponds: Total legacy tailings down 24% in last five years: https://www.canadianenergycentre.ca/oil-sands-shrinking-volume-of-legacy-tailings-ponds/

Canadian Natural. (2021, April 30). Canadian Natural Jackpine Mine 2020 Fluid Tailings Management Report. Retrieved December 5, 2021, from Alberta Energy Regulator.

Canadian Natural. (2021, April 30). Horizon Oilsands Mine and Processing Plant: 2020 Annual Fluid Tailings Management Report. Retrieved December 5, 2021, from AER Company Tailings Management Reports: https://static.aer.ca/prd/documents/oilsands/CompanyTailingsManagementReports-2020.zip

CAPP. (2021, December 6). Canadian Association of Petroleum Producers. Retrieved from CAPP: https://www.capp.ca/explore/tailings-ponds/#:~:text=The%20Government%20of%20Alberta%2C%20through%20the%20Tailings%20Management,the%20accumulation%20of%20fluid%20tailings%20on%20the%20landscape.

CEC. (2020). Alberta Tailings Ponds II. Factual Record regarding Submission SEM-17-001. Montreal: Commission for Environmental Cooperation.

CEC. (2020). Alberta Tailings Ponds II. Factual Record regarding Submission SEM-17-001. Montreal, Canada: Commission for Environmental Cooperation.

COSIA. (2021). 2020 ANNUAL REPORT: INNOVATIVE SOLUTIONS FOR SUSTAINABLE OIL. Retrieved from COSIA: https://cosia.ca/sites/default/files/2021-06/2020COSIA_AnnualReport.pdf

COSIA. (2021). Tailings Management. Retrieved September 6, 2021, from Canada's Oil Sands Innovation Alliance: https://cosia.ca/initiatives/tailings

CTMC. (2012, June 22). OIL SANDS TAILINGS TECHNOLOGY DEPLOYMENT ROADMAP,

Project Report - Volume 2, Component 1 Results. Retrieved December 5, 2021, from Canada's Oil Sands Innovation Alliance: https://cosia.ca/sites/default/files/attachments/Tailings%20Roadmap%20Volume%202%20June%202012.pdf

CTMC. (2012, June 28). OIL SANDS TAILINGS TECHNOLOGY DEPLOYMENT ROADMAP, Project Report - Volume 3, Component 2 Results. Retrieved December 5, 2021, from Canada's Oil Sands Innovation Alliance.

CTMC. (2012, June 29). OIL SANDS TAILINGS TECHNOLOGY DEPLOYMENT ROADMAP, Project Report - Volume 4, Component 3 Results. Retrieved December 5, 2021, from Canada's Oil Sands Innovation Alliance.

CTMC. (2012, June 26). OIL SANDS TAILINGS TECHNOLOGY DEPLOYMENT ROADMAP, Project Report - Volume 5, Component 4 Result. Retrieved December 5, 2021, from Canada;s Oil Sands Innovation Alliance.

CTMC. (2012, June 12). OIL SANDS TAILINGS TECHNOLOGY DEPLOYMENT ROADMAPs, Project Report - Volume 1, Project Summary, June 22, 2012. Retrieved December 5, 2021, from Canada's Oil Sands Innovation Alliance: https://cosia.ca/sites/default/files/attachments/Tailings%20Roadmap%20Volume%201%20June%202012.pdf

CTMC. (2012, June). Technology Scoring Sheets. Retrieved December 5, 2021, from Canada's Oil Sands Innovation Alliance (COSIA).

Energy Resources Conservation Board (ERCB). (2009, February 3). Directive 074:Tailings Performance Criteria and Requirements for Oil Sands Mining Schemes. Retrieved December 3, 2021, from Impact Assessment Agency of Canada (IAAC): https://iaac-aeic.gc.ca/050/documents_staticpost/59540/81944/Tab7_-_ERCB_Directive_on_Tailings_Performance.pdf

Environmental Defence & CPAWS. (2022, May). 50 Years of Sprawling Tailings:Mapping decades of destruction by oil sands tailings. Retrieved from Environmenal Defence Canada: https://environmentaldefence.ca/report/50-years-of-sprawling-tailings/

Environmental Defence Canada & CPAWS. (2022, May). 50 Years of Sprawling Tailings. Retrieved from Environmental Defence: https://environmentaldefence.ca/wp-content/uploads/2022/05/TailingsPondsReport_edcv2_web.pdf

Environmental Defence Canada and NRDC. (2022, November). One trillion litres of toxic waste and growing: Alberta's tailings ponds. Retrieved from Environmental Defence Canada: https://environmentaldefence.ca/wp-content/uploads/2017/06/EDC-and-NRDC-One-trillion-litres-of-toxic-waste-and-growing-Albertas-tailings-ponds-June-2017.pdf

ERCB. (2008, December 7 to 10). Oil Sands Tailings: Regulatory Perspective. Retrieved December 5, 2021, from 1st International Oil Sands Tailings Conference: https://sites.google.com/a/ualberta.ca/iosct2008/

ERCB. (2013, June). 2012 Tailings Management Assessment Report: Oil Sands Mining Industry (PDF) (Report). Retrieved December 5, 2021, from Oil Sands Information Portal (OSIP): http://osipfiles.alberta.ca/datasets/158/TailingsManagementAssessmentReport2011-2012.pdf

Gidley, I., & Boswell, J. (2013). A model for technology development in oil sands tailings. Retrieved 12 8, 2021, from https://papers.acg.uwa.edu.au/p/1363_42_gidley

GoA. (2015, March 03). Lower Athabasca Region : tailings management framework for the mineable Athabasca oil sands. Retrieved December 5, 2021, from Alberta Open Government Publications: https://open.alberta.ca/publications/9781460121740#summary

Government of Alberta. (2015, March 03). Lower Athabasca Region : tailings management framework for the mineable Athabasca oil sands. Retrieved December 5, 2021, from Alberta Open Government Publications: https://open.alberta.ca/publications/9781460121740#summary

Hyndman, A. S. (2019, August 22). Fluid Fine Tailings Processes: Disposal, Capping, and Closure Alternatives . Retrieved December 5, 2021, from Recent Events: http://mckennageotechnical.com/news.html#:~:text=Fluid%20Fine%20Tailings%20Processes%20%E2%80%94%20Disposal%2C%20Capping%2C%20and,Sands%20Tailings%20Conference%20in%20Edmonton%20in%20December%202018.

Imperial. (2021, April 30). Kearl Oil Sands Mine: Fluid Tailings Management Report for 2020.

Retrieved December 5, 2021, from Company Tailings Management Reports: https://static.aer.ca/prd/documents/oilsands/CompanyTailingsManagementReports-2020.zip

Jason Hamelehle, R. J. (2021). Regeneration of filter press fabrics in the mining sector. Banff: Tailings and Mine Waste Conference 2021.

Matthews, J. (2008). Objectives of D-074, discussions with senionr ERCB representatives (Houlihan and Lord). Fort McMurray.

Matthews, J. (2022, December 6 - 9). Fluid Tailings Thermal Drying: More Promising Than You Might Think. International Oil Sands Tailings Conference. Edmonton, Alberta, Canada: University of Alberta.

McKinley, J., Sellick, A., Dawson, R., & and Hyndman, A. (2018, June). Fluid Fine Tailings Management Methods: An Analysis of Impacts on Mine Planning,Land, GHGs, Costs, Site Water Balances and Recycle Water Chloride Concentrations. Retrieved December 5, 2021, from Canada's Oil Sands Innovation Alliance.

Monica Ansah Sam, E. D. (2021). Filter press technology commercial scale pilot - geotechncal deposit performance. Tailings and Mine Waste Conference 2021. Banff, Alberta: Tailings and Mine Waste Conference 2021.

Morsch, B. F. (2021). Regeneration of filter press fabrics in the mining sector. Banff: Tailings and Mine Waste Conference,2021.

Murray Gray, Z. X. (2009, March 01). Physics in the oil sands of Alberta. Retrieved December 5, 2021, from Physics Today, Volume 62, Issue 3: https://doi.org/10.1063/1.3099577

Oil Sands Pathways to Net Zero. (2021). We need to get to net zero. (Oil Sands Pathways to Net Zero) Retrieved 01 30 , 2022, from Oil Sands Pathways to Net Zero: https://www.oilsandspathways.ca/

Pembina Institute. (2010, 12 October). Could the Hungarian tailings dam tragedy happen in Alberta? Retrieved from Pembina Blog: https://www.pembina.org/blog/could-hungarian-tailings-dam-tragedy-happen-alberta

Pembina Institute. (2017, March 13). Backgrounder. Retrieved December 5, 2021, from Review of Directive 085 Tailings Management Plans: https://www.pembina.org/reports/tailings-whitepaper-d85.pdf

Pembina Institute and Water Matters. (2009, December). Reports. Retrieved December 6, 2021, from Tailings Plan Review — An Assessment of Oil Sands Company Submissions for Compliance with : https://www.pembina.org/reports/tailings-plan-review-report.pdf

Rougeot, A. (2021, November 16). In the thick of it: Living on the frontlines of Alberta's toxic tailings lakes. (Environmental Defence) Retrieved 02 08, 2022, from Environmental Defence Climate Change: https://environmentaldefence.ca/2021/11/16/in-the-thick-of-it-living-on-the-frontlines-of-albertas-toxic-tailings-ponds/

Spiller, P. P. (2021). Future of tailings management. Banff: Tailings and Mine Waste Conference 2021.

Stantec. (2021, December 20). Material and Energy Balance for an Oil Sands Surface Mining and Bitumen Extraction Reference Facility. Retrieved 02 14, 2022, from Canada's Oil Sands Innovation Alliance: https://cosia.ca/sites/default/files/attachments/Material_and_Energy_Balance_for_an_Oil_Sands_Surface_Mining_and_Bitumen_Extraction_Reference_Facility.pdf

Suncor Energy (Syncrude) Operating Inc. (2022, April 29). 2021 Mildred Lake Tailings Management Report . Retrieved from 2021 Company Tailings Management Reports: https://www.aer.ca/providing-information/by-topic/tailings

Suncor Energy Inc. Oil Sands. (2022, April 30). 2021 Base Plant Fluid Tailings Management Report. Retrieved from AER Tailings Measurement System Plans for Oil Sands Mines: https://www.aer.ca/providing-information/by-topic/tailings

Suncor Energy Operating Inc. (2021, April 30). 2020 Fort Hills Fluid Tailings Management Report. Retrieved December 5, 2021, from Compnay Tailings Management Reports: https://static.aer.ca/prd/documents/oilsands/CompanyTailingsManagementReports-2020.zip

Syncrude. (2021). 2020 Sustainability Fact Sheet: Operations and Performance. Retrieved 01 18, 2022, from Syncrude: https://syncrude.ca/wp-content/uploads/2021/09/Fact-Sheet-_Operations-and-Performance-2020.pdf

Syncrude Canada Ltd. (2021, April 30). 2020 Mildred Lake Tailings Management Report. Retrieved December 5, 2021, from AER Reports.

Syncrude Canada Ltd. (2021, April 30). 2020 Syncrude Aurora North Tailings Management Annual Report. Retrieved December 5, 2021, from Alberta Energy Regulator: https://static.aer.ca/prd/documents/oilsands/CompanyTailingsManagementReports-2020.zip.

The Royal Society of Canada Expert Panel. (2010, December). Environmental and Health Impacts of Canad's Oil Sands Industry. Retrieved December 5, 2021, from Documents: https://rsc-src.ca/sites/default/files/RSC%20Oil%20Sands%20Panel%20Main%20Report%20Oct%202012.pdf

Van Dongen, A. S. (2021). A Deep Look into the Microbiology and Chemistry of Froth Treatment Tailings: A Review. Microorganism. Microorganisms, 9(5). Retrieved from https://doi.org/10.3390/microorganisms9051091

Yewchuk, D. (2021, 10 19). Another Year Gone Under the Mine Financial Security Program. Retrieved from University of Calgary Faculty of Law Blog: https://ablawg.ca/2021/10/19/another-year-gone-under-the-mine-financial-security-program/

Yuan You, R. M. (2021). Methane emissions from an oil sands tailings pond: a quantitative comparison of fluxes derived by different methods. Atmospheric Measurement Techniques, 14, 1879-1892. Retrieved from https://amt.copernicus.org/articles/14/1879/2021/amt-14-1879-2021.pdf#:~:text=Tailings%20ponds%20in%20the%20Alberta%20oil%20sands%20region,ployed%20under%20current%20regulatory%20compliance%20monitoring%20pro-%20grams.

WHAT DO WE MEAN BY "SAFE CLOSURE" FOR OIL SANDS TAILINGS FACILITIES?

Gord McKenna, McKenna Geotechnical Inc, Delta, BC, Canada

ABSTRACT

The 2020 Global Industry Standard on Tailings Management (GISTM) identifies the need to design, construct, operate, and reclaim tailings facilities to achieve "safe closure," which can be defined as "a closed tailings facility that does not pose ongoing material risks to people or the environment." Everyone wants safe closure, but just what does safe closure of a tailings landform mean in practice? What does it mean to an operator, to a design engineer, to a regulator, to an insurance company, and to local communities and future users of the land? How will we all agree whether it is safe?

The mining industry is working to define safe closure and describe good practices for new and existing tailings facilities. This paper explores the challenges and describes the use of the landform design process, with a focus on oil sands tailings facilities. It establishes a clear design basis that is acceptable to all and a process for designing, constructing, and monitoring the facility against the design objectives. The paper also describes the use of an operation, surveillance, and monitoring program that, in collaboration with local communities, manages the long-term residual risks.

INTRODUCTION

A key requirement of the Global Industry Standard on Tailings Management (GISTM 2020) is "safe closure" for tailings facilities. This requires a closed tailings facility that does not pose ongoing material risks to people or the environment, has been confirmed by an Independent Tailings Review Board (ITRB), and signed off by the Accountable Executive (AE).

This paper explores the notion of safe closure for oil sands tailings facilities through the lens of landform design (see LDI 2021). After providing background information, it parses the definition of safe closure, argues that safe closure involves more than dam safety in perpetuity, and provides a process to design, construct, operate, monitor, and maintain tailings facilities that meet this requirement.

While the landform design process can be applied to all mining landforms and landscapes (the minesite scale), this paper provides examples and guidance tailored to the oil sands mining region in northeastern Alberta, Canada. The key to success is providing clarity in what is promised and then diligently delivering on those commitments.

Background

A global tailings review was recently convened in response to recent tailings dam failures. A broad multidisciplinary team produced the GISTM document, which develops and builds on 15 principles, many of which apply to "all phases of the tailings facility lifecycle, including closure and post-closure."

Many mining companies outside the oil sands have formally adopted the GISTM requirements and are now on a tight schedule to bring operating and closed tailings facilities into compliance. The GISTM has applied a fresh viewpoint on the post-closure performance of tailings facilities, broadening the mandate of professionals and managers to the consideration of long-term landscape performance, not only during reclamation design and construction, but throughout the lifecycle of each tailings facility. As many facilities are already in operation and many others are already closed and reclaimed, these new requirements will result in the need to at least partially retrofit or redesign a large number of facilities.

In particular, GISTM Requirement 5.2 requires operators to "develop a robust design that considers the technical, social, environmental, and local economic context, the tailings facility consequence classification, site conditions, water management, mine plant operations, tailings operational and construction issues, and that demonstrates the feasibility of safe closure of the tailings facility. The design should be reviewed and updated as performance and site data become available and in response to material changes to the tailings facility or its performance."

Notably, a facility that is demonstrated to be in a state of safe closure is exempt from the section of

GISTM Requirement 3.2 that requires the operator to "periodically review and refine the tailings technologies and design, and management strategies to minimize risk and improve environmental outcomes."

The GISTM Conformal Protocols (ICMM 2021a) also indicate that "safe closure elements typically include geotechnical, hydrotechnical and geochemical risks, which should be documented in the [design basis memorandum] or may be included in a supporting separate closure plan report."

Numerous international standards also apply to the design, operation, closure, and reclamation of tailings facilities (e.g., ANCOLD 2019; APEC 2018; CDA 2013, 2019; IBRAM 2014; ICMM 2019, 2021b; ICOLD 2013, 2018; MAC 2019). Specific regulatory requirements vary by jurisdiction, and the mine may have additional commitments to the regulator and local communities.

Tailings management throughout the lifecycle of a facility is multifaceted. Teck (2022) provides a useful list of practices for the safe and secure management of tailings facilities. The list identifies six levels of protection: surveillance technology, staff inspections, annual performance reviews, third-party reviews, internal governance reviews, and independent tailings review boards. As discussed below, the level of each of these activities varies over the lifecycle of the landform/landscape. After safe closure, the level of management is presumably small and care, responsibility, and liability for such sites may be theoretically suitable for transfer to the Crown or state.

Oil sands tailings framework

The oil sands region of northeastern Alberta contains 10 of the world's largest mines, which together produce 3.5 million tonnes of ore per day (AER 2022). They extract bitumen from the Cretaceous sands to produce synthetic crude oil. Each mine has numerous large tailings facilities, many of which are external to the mine pits, and more that involve hydraulic tailings backfilling into mined-out pits. Many oil sands tailings facilities use tailings sand dykes to contain potentially mobile tailings, fluid tailings, and process-affected water. Others have dykes that consist of compacted lean oil sands.

Dozens of large tailings facilities are active in the region, and several have been fully stabilized and reclaimed (e.g., Russell 2010; Syncrude 2020; CNRL 2021). Most facilities have a history of extensive progressive reclamation of the downstream dyke slopes. Slingerland et al. (2018) discuss the long-term performance of reclaimed tailings dams in Alberta.

The regulatory environment in Alberta has significant influence on mining activity. It requires that an operator "reclaim specified land, and … obtain a reclamation certificate" (GoA 2021). It defines reclamation as "the stabilization, contouring, maintenance, conditioning, reconstruction, and revegetation of the surface of the land to a state that permanently returns the EPEA approved footprint to an equivalent land capability" and requires that the approval holder "reclaim disturbed land to a self-sustaining, locally common boreal forest ecosystem, integrated with the surrounding area" (AER 2020b).

The Alberta Energy Regulator (AER) provides a detailed approach to closing dams that shares many of the ideals related to GISTM safe closure, including avoiding ponded water, passing floods, no unsafe storage of flowable tailings, no conditions that allow for internal erosion, and no future conditions that could make the facility unsafe (AER 2020a). Practically speaking, most of these require that the tailings facility be designed for closure from the start, rather than being retrofit.

While oil sands operators have not have publicly committed to GISTM requirements, they structure their tailings management to align with MAC (2019) and CDA (2013; 2019), which are evolving to better align with the GISTM (see Suncor 2021).

Regardless of the stated degree of compliance, the principles of safe closure are of interest to the oil sands industry and its practitioners as each keeps up with (and sometimes leads) the rapidly evolving international state of practice. Requirements for the closure of oil sands tailings facilities (and mining landforms generally) have many facets beyond that required in the GISTM; the requirement of safe closure is likely necessary but not sufficient for successful reclamation for oil sands tailings facilities. Successful reclamation is "that which satisfies the needs of all involved: the mining company, the regulator, Indigenous Peoples, and local communities" (LDI 2021).

What's different after safe closure?

The ICMM (2021) Conformance Protocols indicate:

- "The Standard strives to 'achieve the ultimate goal of zero harm to people and the environment with zero tolerance for human fatality.'

- Operators [are] to take responsibility and prioritize … safety … until a facility meets the criteria of safe closure.

- Once a tailings facility is deemed to be in a state of safe closure it no longer needs to be subject to self-assessments or third-party audits.

- Validation of conformance with the Standard should continue until a closed tailings facility is deemed to be in a state of 'safe closure.'"

Essentially, after safe closure, the level of monitoring and review/audits decreases. Presumably, the residual risk is also low. Levels of monitoring and review would presumably be similar to those of the rest of the reclaimed landscape, and presumably the CDA (2013) dam safety guidelines would no longer apply (see OSTDC 2014).

Other ideas on tailings closure

Others have previously weighed in on themes similar to the GISTM safe closure concept. For example:

- CEMA (2005) provides a short but comprehensive checklist of landscape performance requirements for landform design and closure of oil sands projects.

- Brett (2009) notes the basic requirement of mine waste disposal is to provide "safe, stable and economic storage … presenting negligible public health and safety risks and acceptably low social and environmental impacts during operation and post-closure."

- CTMC (2012) and Williams (2021) highlight the need to select tailings technologies that support acceptable long-term tailings performance and minimize the risks at all stages of the tailings lifecycle (again highlighting the importance of designing with the end in mind).

- APEC (2018) notes that "closed mines must be made reasonably safe from risks to humans and wildlife … If a specific project area cannot reasonably be made safe, access controls may be needed to prevent inadvertent entry."

- CDA (2019) emphasizes the need to provide safe and long-term storage of tailings, protect the environment from release of water, and manage effluent to meet discharge requirements.

- LDI (2021) suggests the use of a design basis memorandum (DBM) to define just what will be achieved with the design, construction, reclamation, and details of the aftercare of mining landforms.

PARSING THE DEFINITION OF SAFE CLOSURE

Fiscor (2021) notes that the GISTM definition of safe closure "is a bit ambiguous" and that companies will need to develop guidance on what it means.

The following sections attempt to parse the definition of safe closure by looking at the elements of the GISTM guidance quoted above. It seems clear that the GISTM has left interpretation of the elements to the mining companies, their shareholders, and stakeholders. The guidance in this section is designed to help others write their own definitions and answer their own questions (see Figure 1).

Closed tailings facility

Closure definitions abound and continue to evolve; each has strengths and weaknesses. Some definitions indicate that closure is a point in time, some that it is a phase of activity, another that it is a process.

ICOLD (2013) defines closure of a tailings facility as a phase: "the planned final cessation of tailings disposal into the tailings dam and the modification/engineering of the tailings dam with the objective of achieving long term physical, chemical, ecological and social stability and a sustainable, environmentally appropriate after-use."

LDI (2021) defines mine closure as the date of final ore processing (when the mill shuts down). This event is a major milestone in the socioeconomic life of both the mine and the local community (e.g., Neil et al. 1992). Closure of a tailings facility is similarly defined as the last day of tailings deposition or the last day the facility is used as an operating water pond. At this point, the decommissioning and post-closure reclamation phase begins and involves removal of infrastructure, final reclamation, water treatment, and transition to long-term care (aftercare).

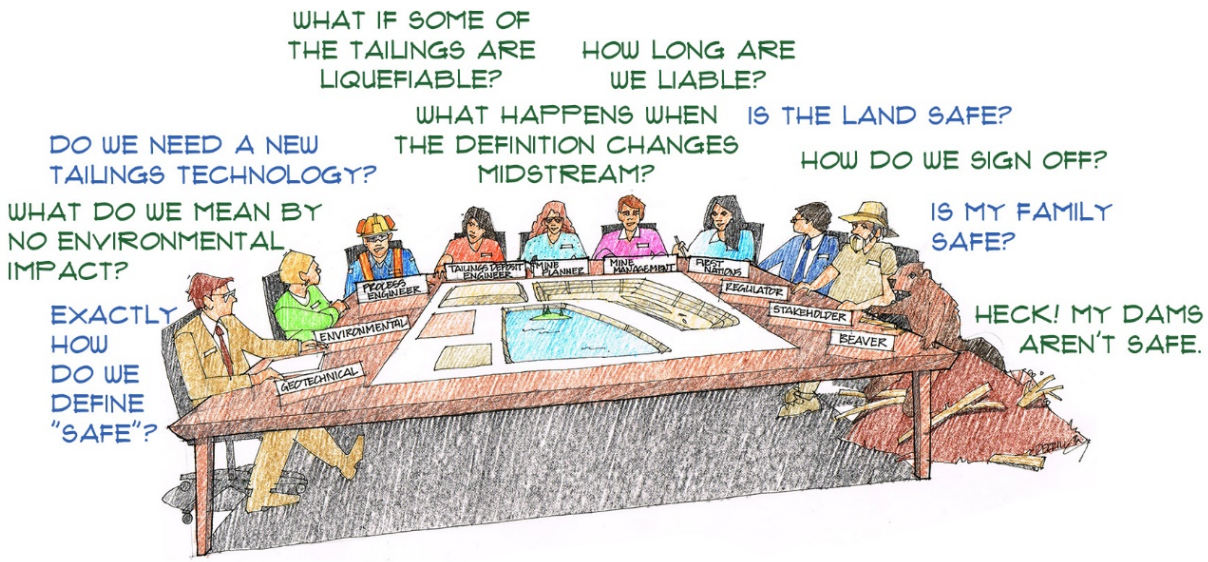

Figure 1. Design team questions about GISTM "safe closure" for tailings facilities.

The GISTM defines closure as occurring after operation (and after any interim closure period) and involves regrading, demolition, and reclamation. Post-closure (also known as passive care) activities include relinquishment, reprocessing, relocation, or removal with "permanently closed facilities that have been configured for their perpetual form/state)."

Many tailings facilities with acid rock drainage concerns have a permanent water cap, creating the need for a trade-off between geochemical and geotechnical risk levels. Martin (2011) notes "tailings impoundments incorporating water-retaining dams and a flooded/saturated condition within the impoundment are not, in geotechnical terms, ever truly closed." Writing in a summary of the state of the art for water-capped tailings, Bjelkevik (2005) concludes "criteria for long term stable tailings dams can hardly be defined today." The GISTM definition of safe closure therefore precludes long-term water capping of tailings contained by dams. Brett (2009) argues that a risk assessment can be used to guide design for the acceptable long-term performance of such facilities. Given the large number of such facilities operating well, opportunities exist for updated guidance.

In Alberta, GoA (2018) and AER (2020) define closure as "a process of modifying and establishing a configuration for a dam or canal with the objective of achieving long-term physical, chemical, ecological, and social stability, and a sustainable, environmentally appropriate after-use." The closure period does not begin until the regulator issues an authorization. GoA (2018) goes on to define decommissioning as "complete removal or breach of a dam or canal so that the structures can no longer retain, store, or divert water, including water containing another substance such as fluid waste or flowable tailings that may pose safety or environmental concern."

A tailings facility has come to mean not just tailings dams storing liquids or potentially mobile materials, but, at least in British Columbia, any mining facility that stores "residue remaining from preparation of a concentrate of minerals or coal" (MEM 2017). In practice, the following situations may all be considered targets requiring safe closure (even where there is no risk of sudden catastrophic failure):

- slurried tailings stored below grade or behind a low berm
- filtered tailings including coarse coal rejects
- waste rock facilities that have layers of process reject, zones of tailings or waste-rock/tailings co-disposal
- planned, operating, and closed facilities
- permanently water-capped tailings
- long-closed tailings facilities with few credible failure modes.

The challenge of defining closure for oil sands tailings facilities is complicated by the fact that such facilities often contain large volumes of fluid tailings that are scheduled for reprocessing over years or decades and are capped with water that is usually part of the water-recycling system that feeds the bitumen extraction plant. Even when the fluid tailings and water are removed, the remaining surface is only safe to access once carefully capped with tailings sand, overburden, or other mine waste (e.g., McKenna et al. 2016; Syncrude 2020). A surface-water drainage system, including an outlet channel, is typically installed during the capping phase. At that point, the deposit is covered with reclamation material as a growth media and revegetated.

For an oil sands tailings facility, GISTM safe closure would require first that the tailings facility be closed. It would seem logical to assume that such a facility is no longer receiving tailings, no longer has an inventory of fluid tailings, and no longer has an inventory of water. It would also be reasonable to assume that the operational infrastructure has been removed, and that the capping, reclamation, and surface-water drainage system has been installed.

Material risk and failure modes

Nixdorf, in his description of the current standards of material risk, writes that: “material risk is not a subject which is determinable by review of statute but has been developed through common law. It is defined as a grave or detrimental consequence of treatment, regardless of the infrequency of its occurrence” (Nixdorf 1990).

This definition seems to align with a “significant consequence” (rather than the “risk = probability × consequences” definition used in the dam safety world). Here, the notion of a credible failure mode, as defined in the GISTM, is relevant. It includes “technically feasible failure mechanisms given the materials present in the structure and its foundation, the properties of these materials, the configuration of the structure, drainage conditions and surface water control at the facility, throughout its lifecycle.” Practitioners appear to be slowly coming to a consensus on the practical aspects of this definition, and it may be useful to substitute the notion of credible failure mode for material risk for safe closure.

The GISTM seems to imply that all credible geotechnical and hydrologic failure modes need to be resolved. It also identifies the need to consider geochemical risks, implying that the impacts of contaminated seepage from the facility need to be considered for safe closure. Process-affected seepage water can impact onsite and offsite wetlands, waterbodies, and streams, soils and covers, and onsite or offsite groundwater and aquifers. It would be reasonable to consider such impacts in determining whether safe closure has been achieved, especially given that a major function of a tailings facility is to limit the impact of the tailings and its pore waters on the environment (CDA 2019).

Schafer (in press) describes a list of key geotechnical failure modes for closed tailings facilities: foundation failure, internal erosion, overtopping, seismic liquefaction, slope instability, spillway failure, and static liquefaction. The thesis also notes that there is a small subset of credible failure modes for reclaimed tailings landforms. These geotechnical and hydrologic failure modes are similar to those identified for oil sands tailings dams by OSTDC (2014).

McKenna (2002) describes more than 150 failure modes for reclaimed landscapes, including physical, chemical, and biological modes and failure to meet intended functions. Failure modes combine to form failure scenarios with complex event trees. For example, tailings seepage can contaminate covers on tailings slopes, leading to loss of vegetation, which can in turn lead to gully erosion, slumping, and perhaps even catastrophic failure, as well as the ultimate failure to achieve intended land uses. Holden et al. (2019) describe dozens of failure modes that are part of the normal geological and ecological evolution of natural and reclaimed landscapes. Schafer (in press) describes a method for including various timeframes in risk assessments of closed tailings facilities, using examples from the oil sands.

Additionally, regulations and mine permits, including those in Alberta, typically demand of mines much more than merely controlling material risks from catastrophic geotechnical and hydrologic events, or minimizing the impacts of process-affected waters from tailings facilities. In Alberta (and most jurisdictions) mines are required to meet land use objectives. The most common land use objectives relate to wildlife habitat, but can include any of 150 or more land uses, depending upon what the mine has promised (e.g., OSMELUC 1998; Pearman 2009; McKenna et al. 2015).

In terms of safety, designers also guard against dusting, or metalliferous uptake in vegetation affecting people and wildlife; other human health and ecological risks; and erosion that exposes mine wastes and causes sediment loading (both onsite and off) that affects streams, wetlands, and lakes. In some cases, the resulting fan deposition causes blockages and stream avulsion. In other cases, infilling of wetlands introduces contaminants and elevated levels of suspended sediments that threaten fish and other aquatic life.

What is clear is that safe closure as defined by the GISTM is an important part of successful reclamation, but that is only half the battle. Designers and operators need to avoid situations in which managers aim only for safe closure for tailings when the ultimate goal is so much more; successful reclamation requires a declared suite of conditions to be achieved beyond just safe closure.

People and the environment

The GISTM requires the protection of people and the environment. While defining these might at first seem straightforward to practitioners, two key aspects need to be specified.

We recognize “people” as those working on or using the reclaimed landscape and those working, living in or using the area surrounding the minesite. But there is considerable debate about how to consider future villages or towns downstream of a tailings facility. Declaring just who is being protected is important for any discussion of residual risk. The GISTM safe closure framework appears to inherently protect current and future populations.

With respect to defining “environment,” additional clarity is usually wise. Most members of local communities would assume the environment includes the reclaimed minesite and surrounding area (and some may choose not to distinguish between them). But miners and regulators typically distinguish between offsite and onsite environments, with a compliance point at the mine property/lease boundary. The difference, often poorly communicated, can be crucial. Onsite post-reclamation environmental impacts (such as erosion, impacts on groundwater and surface water due to seepage of contaminated water, and metal uptake in vegetation) can sometimes be greater and more immediate than similar offsite impacts. Again, clarity and understanding are needed for each site.

A definition of safe closure

The GISTM requires an Independent Tailings Review Board (ITRB) or senior independent reviewer and the Accountable Executive (AE) to confirm the facility has reached safe closure. This implies a formal review and signoff of the design, construction, reclamation, and performance — ideally over several stages during the decades-long lifecycle of a tailings facility.

These professionals will need a clearly stated definition of safe closure, and one adapted to the specific facility in question. They will also need extensive documentation of design, construction, and performance. Provision of such records may be simpler for new facilities than for old ones, particularly as historical record-keeping has not typically been designed to support a case for safe closure.

The history of signoff requirements highlights the evolution of review board mandates (McKenna 2022). Historically, review boards provide private, independent, non-binding advice to the mine owner to help manage geotechnical risks (e.g., McKenna 1998; Burnett and McKenna 2022). British Columbia, the Canadian province west of Alberta, now requires review boards for all tailings facilities and inclusion in the mine’s annual report to the regulator of “signed acknowledgement by the members of the Board, confirming that the report is a true and accurate representation of their reviews.” (MEM 2017).

The GISTM asks boards to provide confirmation that a state of safe closure has been achieved. The board’s first questions will presumably be: “What are the specific requirements? To whom is this assurance being delivered? Who will rely upon it?” It is unclear under what circumstances a board will be able to provide such assurance, particularly for an existing facility. Furthermore, there is a paucity around the world of regulatory signoff on reclamation success for even simple mining landforms (LDI 2021), much less for complex tailings facilities and dams (see Morgenstern 2012). To support any decision for signoff by the regulator and the independent reviewers, many sites will require extensive site investigations (OSTDC 2014), perhaps similar in effort to the initial tailings site investigation for dam design.

Even the engineer of record (EOR) may not have the skills or the team to provide assurance, unless they are experienced in mine closure, and the

expected performance requirements are well defined. Straker and McKenna (2022) make the case for a reclamation designer of record (RDOR) supported by a multidisciplinary reclamation review board (RRB), who, working alongside the EOR and the ITRB, may be able to provide broader coverage of the requirements for safe closure. The signoff process would be led by the geotechnical and landform design teams and be a joint product of the AE, the EOR, the RDOR, and the two boards.

Presumably, signoff on safe closure would also require review and buy-in from the regulator and local communities.

Level of risk acceptance

Engineers and geologists often have a different definition of “safe” than that of others. Many people may view “safe” as an absolute: Webster’s dictionary defines safe as “secure from threat of danger, harm, or loss.”

Technical people sometimes fail to realize that the level of risk acceptance varies widely (Slovik 1987). Risk acceptance matrices based on f-n curves and expected annual costs vary not only from company to company (or even within companies), but from person to person (Shafer in press). More importantly, the regulator has its own risk tolerance, as would a person living at the toe of a tailings dam, especially a person who has not directly benefited from the mining and may not understand the hazards. Schafer (in press) describes the limitations of engineering risk assessments and provides some solutions regarding risk acceptance.

There is a need to discuss and come to a collective understanding of what safe closure means to local individuals and communities, to the regulator, to designers, and to management.

ADDITIONAL CHALLENGES

Beyond the challenges listed above (the need to define safe closure, having good records, finding qualified people to provide assurance, uncertainty in future performance, and issues of liability associated with all of these), several other challenges associated with the safe closure of oil sands tailings facilities are worth exploring.

In most oil sands tailings facilities, loose saturated tailings sand is stored permanently above the elevation of the natural landscape. Other layers of

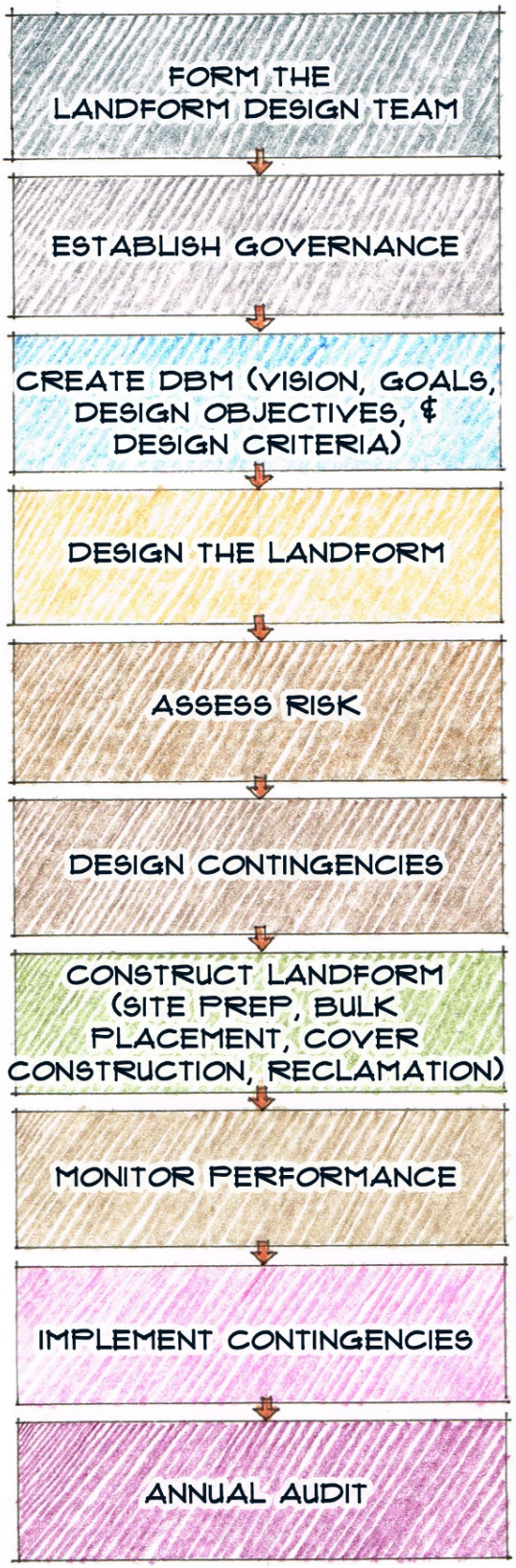

Figure 2. Landform design process.

reprocessed tailings can be susceptible to liquefaction or softening and may be mobile. The presence of such layers complicates signoff on safe closure.

Much of the wording in the GISTM relates to reducing risks to as low as reasonably practicable. Most hazards may not qualify for this approach. These include hazards such as excessive gully erosion, control of long-term seepage, consequences of blockage of even deep channels by beaver dams, impacts of re-mining, or the cumulative impacts of evolution of reclaimed mining landscapes over centuries. Which credible failure modes need to be as low as practicable is a key consideration.

Experience shows that few mines can continue to meet their reclamation requirements in the absence of ongoing landscape monitoring and maintenance (McKenna 2002; LDI 2021). A major risk reduction strategy is to design the reclaimed landscape to require only minimal maintenance, then fund and carry out long-term monitoring and maintenance on the critical areas. Within Alberta, for example, recognizing the need for long-term monitoring and maintenance has proven to be a challenge for the existing regulatory framework. Elsewhere, the benefits from and the need for long-term maintenance of reclaimed mining landscapes is widely recognized. Bonding for long-term maintenance remains a challenge elsewhere (Cassie and McKenna 2016).

A PATH FORWARD

Fortunately, several tools and processes are available that will aid in the quest for safe closure to meet the GISTM, or more specifically, for declaring and negotiating the elements that will lead to the creation, confirmation, and acknowledgement of safe closure. The resulting processes and requirements will vary from site to site and continue to evolve.

Landform design can be applied to new or existing tailings facilities to achieve safe closure (McKenna 2002; LDI 2021). The process has been developed and tested over the past two decades at numerous sites around the world, and in the oil sands region in particular. It provides a logical framework to address the opportunities and challenges posed by the need to create safe closure.

LDI (2021) describes landform design as “the integrated, multidisciplinary design and construction of mining landforms and landscapes, directed by a dedicated team working with different mine operations groups and others over the life of the mine and beyond. The focus is on achieving successful reclamation … it achieves signoff on completion, confirming that all mining operations and reclamation for a landform or landscape have been satisfactorily completed, and that the residual risks are acceptable to all parties. Landform design allows all parties to work together to manage costs and risks, minimize liability, and produce progressively reclaimed landscapes with confidence and pride.”

Figure 2 shows the landform design process. Ensuring safe closure for tailings requires several elements:

- A multidisciplinary design team that shepherds the tailings facility/landform through the process, a team that will be needed for decades. Ideally it is formed before the facility is designed, but in many cases will be formed after deposition has begun, given the preponderance of tailings landforms that are already partially constructed.

- A DBM (often called a design basis or design basis memorandum) is created (e.g., Ansah-Sam et al. 2016). This document includes the vision, goals, objectives, and design criteria for the tailings facility and is key to safe closure as it defines what is being promised and how it will be measured. It forms the basis for the engineering risk assessment, and for the monitoring program.

- Patterned after Peck’s (1969) geotechnical observational method and extending adaptive management, the landform design process involves designing to the DBM, assessing risks, and designing contingencies should the intended performance not be met. The process includes performance monitoring to demonstrate the tailings landform is being built to design and performing as intended (two keys to safe closure).

- An annual independent audit, perhaps by the review boards, to keep the project on a trajectory such that signoff by the boards, the AE, and representatives of the local community and the regulator is possible, essentially confirming the results of the annual audits and the construction and reclamation records reports.

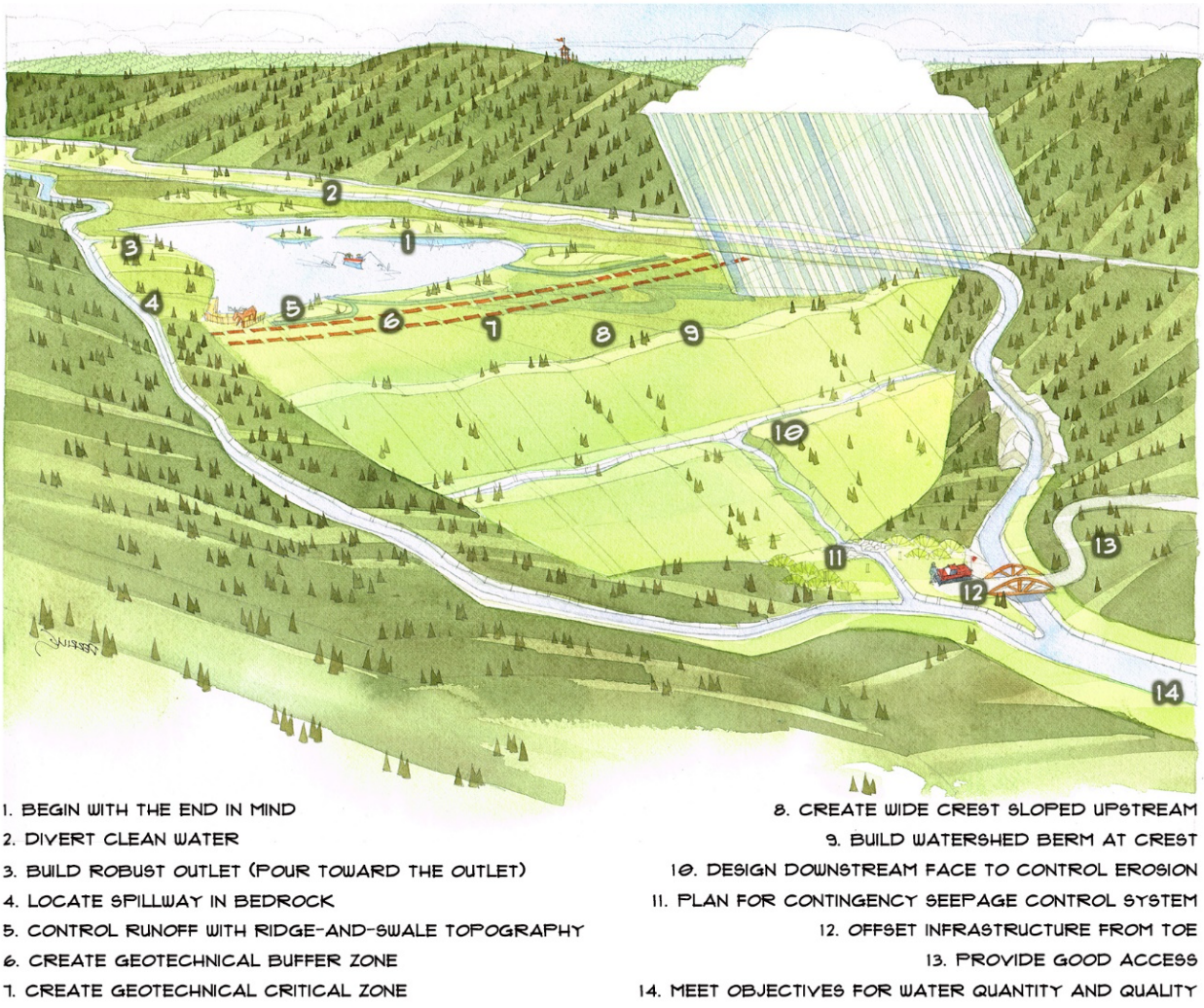

Figure 3. Performance measures obtained from model results (from McKenna and Van Zyl 2020).

The landform design process works best where it is integrated with the geotechnical and hydrotechnical dam design. Ideally there is both an RDOR and an EOR (working closely together) supported by a RRB and an ITRB (with some overlapping membership) throughout the lifecycle of the facility.

Industry, academia, and the Landform Design Institute (landformdesign.com) are developing general and specific guidance on design, and there is already a rich literature on specific elements. For example, SME (2022) provides a chapter on designing tailings facilities for closure, McKenna and Van Zyl (2020) provide advice and a case history on landform design of tailings facilities, and the GoWA (2020) closure planning guidance provides an excellent framework for the design and planning of mine sites and individual mining landforms. Crossley et al. (2011) provides details on how to develop an operations, maintenance, and surveillance manual for reclaimed mining landforms.

A GRAPHIC EXAMPLE

Figure 3 depicts a tailings facility that has benefitted from landform design with examples of practical landform elements (Pollard and McKenna 2018) and design processes intended to create a landform that can be confirmed as safe closure. Many of

these elements are most effective (and low in cost) if designed with the end in mind (and before the facility is constructed) but many can be retrofit to existing facilities. Additional details and case histories are available (e.g., Russell et al. 2010; CEMA 2012; and Ansah-Sam et al. 2017).

KEY MESSAGES

- Safe closure is not yet well defined. Practitioners have the opportunity to provide clarity and adapt the definitions to their own sites.
- Form a multidisciplinary team to guide the landform design, a team that will work closely alongside the geotechnical and/or hydrotechnical dam design team. Appoint an RDOR to work alongside the dam safety EOR. Appoint an RRB to work in parallel with the ITRB. Involve local communities and regulators in the process (see Daly et al. 2021).
- Forge a DBM for landform design that includes a vision, nested goals, specific objectives, and design criteria that define what constitutes successful safe closure and the many other requirements for reclaimed landforms. Ideally the landform and dam designs share the same DBM, but in practice this may be two complementary documents, each updated over time.
- Design, assess, monitor, steward, and sign off against the DBM. Recognize this is a decadal- or even century-long process.
- Design to minimize maintenance, but also to foster the inevitable long-term monitoring and maintenance required of tailings landforms. Maintenance is key to managing residual risks and providing for ongoing safe closure.
- Reclaim progressively so you can learn as you go and establish trust within the company, with the regulator, and with local communities.
- Be careful not to over commit. The best intentions have led industry and the regulator to promise or expect too much from even well-reclaimed mining landforms and landscapes. There is a risk that tailings people who are new to landform design and mine closure, and to the desire to achieve safe closure, will repeat the mistakes of past generations of reclamation specialists who have overcommitted and generally under-delivered on achieving successful reclamation.

ACKNOWLEDGEMENTS

The author is indebted to Derrill Shuttleworth of Gabriola Island for his illustrations and David Wylynko and James Hrynyshyn of West Hawk Associates for their editing of this paper.

REFERENCES

AER. 2020a. Decommissioning, closure, and abandonment of dams at energy projects. Manual 019. Jan 2020. Alberta Energy Regulator. Edmonton. 22 pp.

AER. 2020b. Syncrude Canada Environmental Protection and Enhancement Act Approval for Mildred Lake, Aurora North, and Aurora South. Dated 2020-06-18. Alberta Energy Regulator. Edmonton. 120 pp.

AER. 2022. Alberta Energy Outlook, Crude bitumen, statistics, and data. ST98:2002 released in May 2022. Alberta Energy Regulator. Edmonton.
ANCOLD. 2019. Guidelines on tailings dams – planning, design, construction, operation, and closure – revision 1 and its addendum.

Ansah-Sam M, Hachey L, McKenna G, and Mooder B. 2016. The DBM approach for setting engineering design criteria for an oil sands mine closure plan. International Oil Sands Tailings Conference. Lake Louise. University of Alberta Geotechnical Group, Edmonton. 11 pp.

Ansah-Sam M, Olauson E, and McKenna G. 2017. Closure landform design for an oil sands external tailings facility. Tailings and Mine Waste Conference 2017.

APEC. 2018. Mine closure checklist for governments. Asia-Pacific Economic Cooperation. APEC Mining Task Force. Singapore. Feb 2018. 104 pp.

Bjelkevik A. 2005. Water cover closure design for tailings dams: state of the art report. Luleå University of Technology. Luleå Research Report 2005:19. 103 pp.
Brett DM. 2009. Water covers for tailings and waste rock – designing for perpetuity. Mine Closure 2009. Australian Centre for Geomechanics. pp. 485-492.

Burnett A and McKenna G. 2022. Celebrating 50 years: the Syncrude Geotechnical Review Board. CDA Canadian Dam Association Conference, St Johns.

Cassie J and McKenna G. 2016. Mine closure planning, design, and implementation: from hand-waving to reality. Planning for Closure 2016. Santiago. Gecamin. Santiago. 9 pp.

CDA. 2013. Dam safety guidelines (2013 edition). Canadian Dam Association. 88 pp.

CDA. 2019. Application of dam safety guidelines to mining dams (2019 edition). Canadian Dam Association. 59 pp.

CEMA. 2005. Landscape design checklist: revised RSDS government regulator version. Cumulative Environmental Management Association. Fort McMurray. 8 pp.

CEMA. 2012. Oil Sands End Pit Lakes Guidance Document. Cumulative Environmental Management Association. Fort McMurray. 494 pp.

CNRL. 2021 report to stakeholders. Canadian Natural Resources Ltd. Calgary. 52 pp.

Crossley C, Russell B, van Zyl D and McKenna G. 2011. Developing an operation, maintenance, and surveillance manual for the post-closure management of tailings facilities. Mine Closure 2011. Lake Louise. Australian Centre for Geomechanics. Perth. 10 pp.

CTMC. 2012. Oil sands tailings technology deployment roadmap: project report – volume 2, Component 1 Results. Consultant's report to Alberta Innovates – Energy and Environment Solutions. Consortium of Tailings Management Consultants. Calgary. June 22, 2012. 112 pp.

Daly C, L'Hommecourt J, Arrobo B, McCarthy D, Donald G, and Gerlach SG. 2021. Toward a co-reclamation framework in collaboration with Indigenous Peoples. Landform Design Quarterly. Fall 2021. pp 2-5.

Fiscor S. 2021. Newmont implements global industry standard for tailings management. Engineering and Mining Journal. October 2021.

GISTM. 2020. The Global Industry Standard on Tailings Management. https://globaltailingsreview.org/wp-content/uploads/2020/08/global-industry-standard-on-tailings-management.pdf. Accessed 2022-05-01.

GoA. 2018. Alberta dam and canal safety directive. AEP Water Conservation 2018 No 3 issued 2018-12-11. Government of Alberta. Edmonton. 50 pp.

GoA. 2021. Environmental protection and enhancement act (EPEA). Revised statues of Alberta 2000. Chapter E-12. Current as of 2021-12-08. Government of Alberta. Edmonton. 172 pp.

GoWA. 2020. Mine closure plan guidance – how to prepare in accordance with part 1 of the statutory guidelines for mine closure plans. Government of Western Australia. Department of Mines, Industry Regulation, and Safety. Version 3. 74 pp.

Holden A, Provost H, Pollard J, McKenna G, and Wells PS. 2019. Evolution of landforms in reclaimed landscapes in the surface mineable Athabasca oil sands. Tailings and Mine Waste Conference. Vancouver. 16 pp.

IBRAM. 2014. Guide for mine closure planning. Instituto Brasileiro de Mineracao. Brasilia: Brazilian Mining Association. 225 pp.

ICMM. 2019. Integrated mine closure: good practice guide. Second edition. International Council on Mining and Metals. London. 132 pp.

ICMM. 2021a Tailings management good practice guide. International Council on Mining & Metals. London. 128 pp.

ICMM. 2021b. Conformance protocols: global industry standard on tailings management. International Council on Mining & Metals. London. 108 pp.

ICOLD. 2013. Sustainable design and post-closure performance of tailings dams. Bulletin 153. International Congress on Large Dams. Paris. 92 pp.

ICOLD. 2018. Dam decommissioning guidelines. International Commission on Large Dams. Paris. 143 pp.

LDI. 2021. Mining with the end in mind: Landform design for sustainable mining. Position Paper TR-01. Landform Design Institute. Delta, BC, Canada. 78 pp.

MAC. 2019. A guide to the management of tailings facilitates. Version 3.1. Mining Association of Canada.

Martin TE. 2011. Mine waste management in wet, mountainous terrain: some British Columbia

perspectives: Part II – creating, managing, and judging our legacy. Tailings & Mine Waste Conference. Vancouver. 22 pp.

McKenna G and Van Zyl D. 2020. Closure and reclamation. Chapter VIII Management of Tailings: Past Present & Future. Towards Zero Harm: A Compendium of Papers Prepared for the Global Tailings Review. London.

McKenna G, Abbott R, Nahir M, O'Kane M, Seto J, and Straker J. 2015. Post mine land uses for northern mines. The Northern Latitudes Mining Reclamation Workshop: Reclaiming the North. Juneau, AK. PowerPoint slide deck. 26 pp.

McKenna G, Mooder B, Burton B, and Jamieson A. 2016. Shear strength and density of oil sands fine tailings for reclamation to a boreal forest landscape. International Oil Sands Tailings Conference. Lake Louise. University of Alberta Geotechnical Group. Edmonton.

McKenna G. 1998. Celebrating 25 Years. Syncrude's Geotechnical Review Board. Geotechnical News. Volume 16. pp. 34-41.

McKenna G. 2002. Landscape engineering and sustainable mine reclamation. PhD Thesis. Department of Civil and Environmental Engineering. University of Alberta. Edmonton. 660 pp.

McKenna G. 2022. Building and operating a successful geotechnical review board. CDA Canadian Dam Association Annual Meeting. St John's. 29 pp.

MEM. 2017. Health, safety, and reclamation code for mines in British Columbia. Ministry of Energy and Mines. Victoria, BC. 365 pp.

Morgenstern NR. 2012. Oil sands mine closure – the end game. David C. Sego Symposium. Edmonton. University of Alberta Geotechnical Centre. Edmonton. pp 85-99.

Neil C, Tykkyläinen M and Bradbury J. 1992. Coping with closure: an international comparison of mine town experiences. Routledge, New York, 427 pp.

Nixdorf D. 1990. Current standards of material risk. Journal of the Canadian Chiropractic Association. Volume 34(2). pp 87-89.

OSMELUC. 1998. Report and recommendations: Committee report for consideration by the Alberta Government, the Oil Sands Mining Industry, and the Regional Municipality of Wood Buffalo. Oil Sands Mining End Land Use Committee. Fort McMurray. 48 pp.

OSTDC. 2014. De-Licensing of oil sands tailings dams – technical guidance document. Oil Sands Tailings Dam Committee. Edmonton. 46 pp.

Pearman G. 2009. 101 things to do with a hole in the ground. Eden Project. Post Mining Alliance. Cornwall. 69 pp.

Peck RB. 1969. Advantages and limitation of the observation method in applied soil mechanics. Geotechnique. Volume 19(2). pp 171-187.

Pollard J and McKenna G. 2018. Design of landform elements for mine reclamation. BC Mine Reclamation Symposium. Williams Lake. 9 pp.

Russell B, McKenna G, Leblanc M, Wells PS, and Anderson HB. 2010. Design and construction of the reclamation surface for the first oil sands tailings pond. Mine Closure 2010, Vina del Mar. Australia Centre for Geomechanics, Perth. 13 pp.

Schafer H. In press. Risk management for tailings dam safety: consideration for long-term and post-closure timelines. PhD Thesis. Department of Civil and Environmental Engineering. University of Alberta. Edmonton.

Slingerland N, Schafer H, and Eaton T. 2018. Long-term performance of tailings dams in Alberta. Geotechnical News. March. pp. 50-53.

Slingerland NM. 2019. Geomorphic landform design and long-term assessment of tailings storage facilities in the Athabasca oil sands. PhD Theses. Department of Civil and Environmental Engineering, University of Alberta. Edmonton. 337 pp.

Slovik P. 1987. Perception of risk. Science. Volume 236. pp. 280-285.

SME. 2022. Tailings management handbook: a life-cycle approach. Society for Mining, Metallurgy & Exploration. Edited by Morrison KF. 1024 pp.

Straker J and McKenna G. 2022. The case for a reclamation designer of record. BC Mine Reclamation Symposium. 15 pp.

Suncor 2021. Annual information form 2021. Suncor Energy Inc report dated 2022-02-23. 140 pp. https://sec.report//Document/311337/000155837022002013/su-20211231xex99d1.htm. Accessed 2022-09-30.

Syncrude 2020. Syncrude Canada Ltd. Composite tailings capping knowledge synthesis. regulatory submission dated 2022-09-02. Syncrude Canada Ltd. Fort McMurray. 814 pp.

Teck. 2022. Tailings management and our sustainability strategy. Internet website. https://www.teck.com/sustainability/sustainability-topics/tailings-management. Accessed 2022-10-02.

Williams DJ. 2021. Lessons from tailings dam failures — where to go from here? Minerals. Volume 11:853. 35 pp.

SESSION 6

ASSESSMENT TOOL FOR LANDFORMS CONTAINING POTENTIALLY FLOWABLE TAILINGS

Glen Miller[1], Bhamisha Ramdharry[2], Scott Martens[3], Catherine Isaka[3], Alistair James[4], Anthony Burnett[1], Douglas Bell[5], Jack Law[1], Jennifer Haverhals[6], Norm Eenkooren[2], Paul Cavanagh[6], and Wayne Mimura[1]
[1]Syncrude Canada Limited, [2]Suncor Energy Inc, [3]Canadian Natural Resources Limited, [4]Hatch Dynamic Earth Solutions, [5]Westmoreland Coal Company, [6]Imperial Oil

ABSTRACT

Oil sands tailings containment facilities are closed and reclaimed at the end of their operational life and transitioned into landform configurations. Flowable tailings that were stored within the facility may be removed, mitigated, or contained within the interior of the facility so that they do not pose an unacceptable risk in the closure landform. Alberta dam safety regulations and guidelines do not explicitly define the material characteristics that constitute flowability or provide other detailed requirements for the consideration of flowable tailings at closure, and there is therefore a need to address flowable tailings in the process of closing and reclaiming tailings facilities. To achieve successful closure outcomes where potentially flowable tailings are present, an alignment on the technical criteria for flowable tailings will be required between dam owners, regulators, and other stakeholders.

This paper offers a tool for assessing the flowability of tailings in a Tailings Storage Facility (TSF) that has been modified from an 'operational' to a 'closure landform' configuration. The first part of the assessment is a series of steps and a flow chart to assess if the tailings contained in a TSF have material properties that could be considered to be flowable. This includes the consideration of tailings gradation, cohesion, density states, saturation conditions, and undrained shear strengths. The second part of the assessment tool offers a framework for a 'facility-scale' and closure-focused Failure Mode and Effects Analysis (FMEA), a Risk Assessment (RA) (with focus on geometry and other inputs/characteristics to determine risk level and acceptability), and a flow risk mitigation plan (or facility closure re-design) to reduce the risks to As Low As Reasonably Practicable (ALARP).

This work is a result of the collaboration between the different members of the Dam Integrity Advisory Committee's Closure and Reclassification subcommittee, and the goal of the paper is to help facilitate discussions and an eventual definition of industry standards and best practices related to the dam abandonment and de-registration process for TSFs containing potentially flowable tailings.

INTRODUCTION

The incorporation of flowable tailings is a design element for various oil sand closure landform configurations. The flowability of tailings contained within the facility needs to be assessed at several time frames in the design and closure process to confirm that the tailings do not pose an unacceptable risk in the closure landform. To achieve successful closure outcomes where potentially flowable tailings are present, an alignment on the technical, geometric, and risk criteria for the acceptable configuration and state of flowable tailings is required between dam owners, regulators, and other stakeholders.

This paper proposes a tool to assess the flowability of tailings and consists of a series of steps that can be used to establish the flowability potential outside the tailings facility, assess the risks posed by the potential mobility of flowable tailings to people, environment, and infrastructure, and compare the results with acceptable or ALARP requirements. The paper also provides case studies that showcase flowability assessments conducted for different closure configurations.

The paper relies on principles established in the 2014 Oil Sands Tailings Dam Committee (OSTDC) guidance document (Oil Sands Tailings Dams Committee, 2014), the 2018 Alberta Dam and Canal Safety Directive (ADCSD) (Government of Alberta, 2018), and the 2019 Alberta Energy Regulator (AER) Manual 019 (Alberta Energy Regulator, 2020). It is recommended that the user of the tool outlined in this document be familiar with the principles of dam and tailings facility closure and abandonment as outlined in the above referenced documents.

FLOWABLE TAILINGS TYPE

Flowable tailings may be encountered in both terrestrial and aquatic closure landforms. Terrestrial closure landforms may be created from tailings facilities that are considered either 'in-pit' or 'external' during their operational phase, while aquatic closure landforms are expected to be predominantly created from 'in-pit' tailings facilities.

Terrestrial Closure Landforms

Flowable tailings types that could exist in terrestrial closure landforms include liquefiable coarse tailings, treated fine tailings, and mature fine tailings. These tailings can be located immediately behind a dam (for example, in an upstream constructed dam) or in isolated pockets at great distances from the dam (for example, in sand storage facilities).

The typical configuration of flowable tailings in a tailings facility includes containment by overburden dams, tailings sand constructed dams, in-situ pillars, or a combination of the aforementioned. A granular cap is typically required over the tailings deposit as part of the closure design, and may be established using a single or combination of capping materials such as coarse tailings, petroleum coke, or overburden material.

Case studies 1 and 2 illustrate the various configurations in which flowable tailings may be encountered in terrestrial closure landforms.

Aquatic Closure Landforms

Flowable tailings types that could exist under the water cap in aquatic closure landforms include liquefiable coarse tailings, untreated fine tailings, treated fine tailings, and mature fine tailings.

The typical configuration of flowable tailings in an aquatic closure landform includes containment by constructed materials (overburden or interburden fill inside a mined-out pit), in-situ materials, or a combination of both.

A significant water cap depth (3 to 5+ m) is typically established over flowable tailings. The water cap can be considered as being equivalent to reclamation soil in a terrestrial closure configuration, and it is where ecological activities are supported.

Case study 3 illustrates the typical configuration in which flowable tailings are planned to be established in aquatic closure landforms.

TIMELINES FOR COMPLETING A FLOWABILITY ASSESSMENT

When to carry out a flowability assessment

Figure 1 shows a schematic of a tailings facility's later lifecycle stages and the proposed timelines at which flowability assessments may be appropriate to be completed.

It is recommended that the assessment of flowable tailings within a closure landform be started early in the facility planning process and be completed at least twice at key points during the life cycle development of the tailings facility.

The first assessment is conducted during the closure landform design that culminates in an FMEA and RA. The timing for this could vary but the assessment is expected to be required to support a dam decommissioning, closure and abandonment (DCA) plan per Section 9.6 of the 2018 ADCSD. This submission is required for the AER to authorize the execution of activities described in the dam/facility decommissioning, closure and abandonment plan. The DCA plan is expected to be prepared and submitted to the AER 5 to 10 years before the closure topography is completed for a landform. The characteristics of the tailings deposit in the assessment would be based on as-built information at the facility under review and/or on tailings characteristics from a similar facility.

The second assessment is conducted following the completion of the facility's closure activities plus some period of active care, typically 5 to 10+ years after facility closure and reclamation/revegetation have been completed (this can be sooner for some facilities). This assessment should be revisited using the facility's as-built geometry and as-measured deposit and facility parameters/values. The exact timing for this could vary but it would be expected to support the submission of a closure completion report per Section 9.10 of the ADCSD. This submission is required for the AER to authorize the abandonment and de-registration of the facility as a dam and transfer regulatory oversight from the Water Act to Oil Sands Conservation Rules (OSCR) regulations (per Section 9.11).

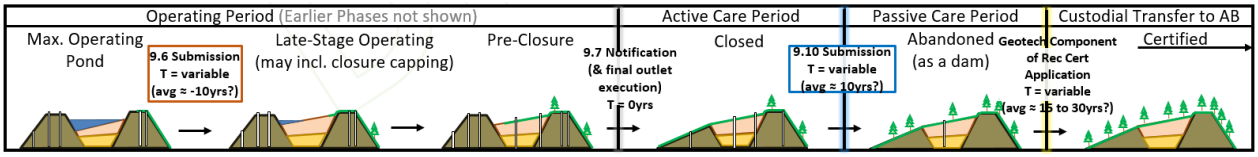

Figure 1: Schematic of Tailings Facility with Flowable Tailings – ETF Scenario of Transition from Operating to Closure

There is potentially a third key flowability assessment point in support of Reclamation Certification and Custodial Transfer of the closure landform that could be expected to occur towards the end of the passive care phase, 10 to 20+ years after closure and reclamation/revegetation have been completed. Similarly to the assessment made to support facility abandonment, this assessment would use performance data collected over the passive care period that would be expected to show improving performance (decreasing risk) since abandonment in order to further support transfer of ownership. The characteristics of the tailings deposit in the assessment would be based on as-measured data from the results of surface and subsurface investigations and instrumentation programs.

Timeframes for consideration when conducting a facility's/landform's flowability assessment

The performance of the closure landform and flowable tailings within must be considered at several time-steps between initial closure and the recommended 1,000 year design life. It is expected that the confidence in the flowability assessment results will increase with the advancement of as-built tailings characterization, the measurement of landform performance, and the validation of models developed at the design stage.

The following timeframes should be considered for potential failure modes at the closure design assessment phase:

1. Consider estimated deposit conditions and closure performance at initial closure: T ≈ 0 to 20 years. T = 0 marks the end of the operating period and the beginning of the active care period.
   At this stage, reservoir remediation, landforming, and reclamation placement are complete. The final outlet is constructed, and final landform drainage regime is established.

2. Consider estimated deposit conditions and closure performance in mid to far future: T ≈ 50 to 100+ years.
   This is not necessarily a set number of years or single time-step, it is a placeholder for time-steps where possible landform changes may be expected to occur over time between T = 0 and T = 1,000 years. For example, 95% of predicted consolidation modelled to occur at approximately 250 years after facility closure.

3. Consider estimated deposit conditions/closure performance in far future: T ≈ 1,000 years.
   This is post-settlement when vegetation has matured, riprap has degraded, no underdrains are functional, overburden has fully softened, and when soft tailings has likely reached maximum consolidation (including water-capped tailings for aquatic landforms). The phreatic surface has also been observed to reach steady-state based on a hydrological assessment with consideration for climate change endpoints.

ASSESSMENT TOOL FOR POTENTIALLY FLOWABLE TAILINGS – DESCRIPTION OF STEPS

Figure 2 shows the assessment tool flow path for evaluating potentially flowable tailings in a closure landform.

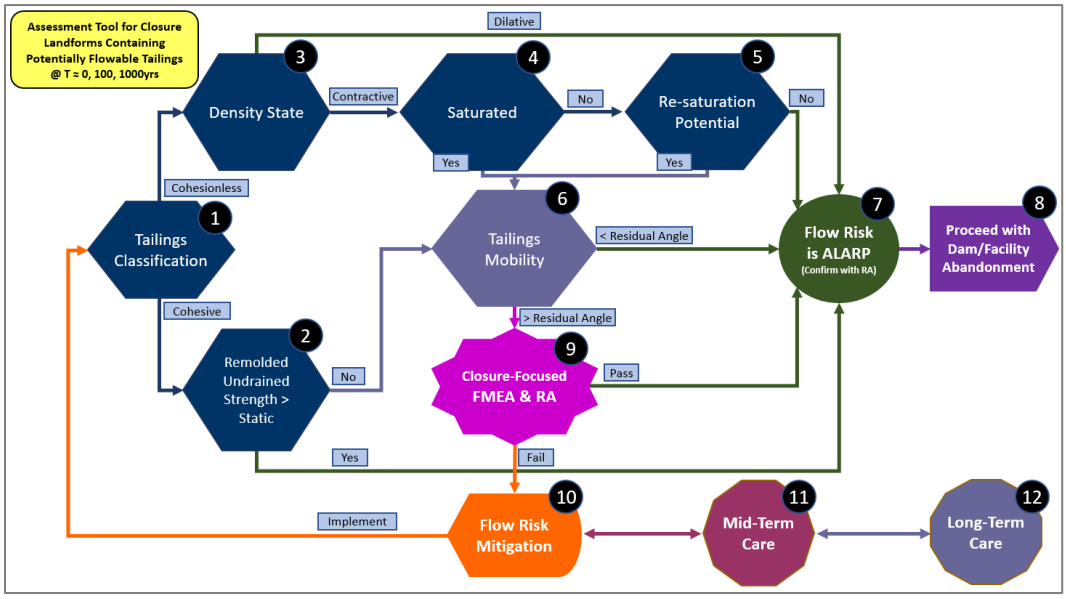

Figure 2: Flowability Assessment Tool

The composition and physical properties of the tailings will vary spatially across the pond and with depth. It is therefore advisable to identify regions of potentially flowable tailings which have similar properties and run the different regions through the flow chart.

The 12 assessment steps highlighted in Figure 2 are described in detail below:

Step 1: Tailings Classification

The demarcation between cohesive and cohesionless materials can be determined by:

- Plasticity Index, PI
  - Boundary between sand like and clay like material is PI = 7% - 12%.
- Soil Behaviour Type (SBT) Index, Ic
  - Soils with Ic <2.6 are considered cohesionless; and
  - Soils with Ic >2.6 are considered cohesive.
  - Coarse grained soils are typically characterized by having a Soil Behaviour Type Index, Ic less than 2.6.

For cohesive material, proceed to Step 2. For cohesionless material, proceed to Step 3.

Step 2: Remoulded Undrained Strength

If the material is cohesive, the remoulded undrained strength is an important criterion in the assessment of the flowability of the tailings. The remoulded undrained strength is measured using field vane shear tests, and cone penetration test (CPT) programs. The material may be vulnerable to flow if the remoulded strength is less than the static shear stress.

Note that the static shear stress is a function of load on the tailings, and in the case of added loading due to closure landforms, the static shear stress will vary along the slope of the embankment fill.

If the remoulded undrained strength is equal to or less than the static shear stress, proceed to Step 6. If the remoulded undrained strength is greater than the static shear stress, proceed to Step 7.

Step 3: Density State

If the material is cohesionless, the CPT tip resistance can be used to determine the density state of coarse grained soils to evaluate the potential for flow liquefaction. The concept of “clean sand equivalent” is also used to extend the evaluation of the density state for a wide range of sandy soils (Robertson P.K. & Wride, 1998). The normalized cone resistance for a clean sand equivalent, $Q_{tn,cs}$ of 70 is considered to be the boundary between contractive and dilative soils. Soils with $Q_{tn,cs}$ < 70 are considered contractive and those with $Q_{tn,cs}$ > 70 are considered dilative.

The potential for flow liquefaction can also be characterized in terms of the in-situ density state using the in-situ state parameter, ψ. A ψ of - 0.05 or less is required to prevent flow liquefaction.

If the tailings material is contractive, proceed to Step 4. If the tailings material is dilative, proceed to Step 7.

Step 4: Degree of Saturation

Saturation conditions in coarse grained materials present a key factor for the potential for liquefaction, and therefore flowability. The subject of degree of saturation as it impacts the potential for liquefaction is not yet fully understood and is currently under study. Until the results of these studies are obtained, tailings deposits below the phreatic surface are considered to be saturated, whereas those above the phreatic surface are considered to be partially saturated (and may be unsaturated). There is also a general understanding in the oil sands industry that materials with > 85% degree of saturation may be liquefiable, though recent and preliminary research indicates that partially saturated oil sand tailings at higher degrees of saturation may be significantly resistant to liquefaction. The user could alternatively use this criterion based on their professional judgement and previous experience.

It is expected that uncertainties will be encountered regarding the location and variability of the phreatic surface within the landform. In addition, perched water tables are expected to be present within the tailings deposits. An assessment of the location of the phreatic surface within the landform may be recommended during detailed site investigations.

If the tailings material is partially saturated or unsaturated, proceed to Step 5. If the tailings material is saturated, proceed to Step 6.

Step 5: Re-saturation Potential

If the coarse-grained tailings is considered to be partially saturated or unsaturated at the time of the flowability assessment, it must be demonstrated that the potential for re-saturation during the closure timeframe is minimal.

If the potential for re-saturation exists, proceed to Step 6. If the potential for re-saturation is minimal, proceed to Step 7.

Step 6: Tailings Mobility Beyond the Facility Boundary

The extent of potential flow of tailings beyond the tailings facility is imperative in assessing tailings mobility. If the flowable tailings only exist below the post-liquefaction back scarp angle, then they would not flow even if the perimeter containment structure was compromised through erosion, anthropogenic activities, or some other process. In order for tailings to flow, the tailings should both be physically and geometrically flowable.

Step 7: Flow Risk is Acceptable or ALARP

This condition represents an acceptable or ALARP condition for the tailings deposit/closure landform and could be expected to allow a closure designer/facility owner to continue planning the development of the closure design without first confirming with an FMEA and RA. As mentioned in previous sections, the DCA plan and completion report for a closure landform will require an FMEA and RA so this activity is never actually ‘skipped’. Proceed to Step 8.

Step 8: Continue with Dam/Facility Closure and Abandonment

The owner/operator could now proceed with closure and abandonment if the high-level assessment of tailings characteristics and closure landform configuration indicate that the risks associated with the closure landform are acceptable or ALARP. Depending on the physical status of the facility/closure landform at the time of assessment, this may be the continued design/planning development, inclusion of a design/plan in a Life of Mine Closure Plan (LMCP), a submission to the AER according to Sections 9.6 (DCA Plan), or 9.10 (Completion Report) of the 2018 ADCSD.

Step 9: Failure Mode and Effects Analysis (FMEA) and Risk Assessment (RA)

If the tailings are both physically and geometrically flowable (Step 6), an FMEA and RA must be completed based on the information available, to understand the risks of the release of contents from the closure landform to the surrounding environment.

If all the residual risks identified in the FMEA and RA are determined to be acceptable or ALARP, proceed to Step 7 and 8.

If the residual risks identified in the FMEA and Risk Assessment are not acceptable or ALARP, proceed to Step 10.

Step 10: Flow Risk Mitigation

Flow risk or other mitigation measures may be required to address residual risks which are not acceptable as identified in the FMEA and RA process. This could be in the form of design/plan revisions or in the form of physical modifications. The understanding that additional time may be needed between closure and abandonment (active care), and/or between abandonment and custodial transfer (passive care) is covered in Steps 11 and 12, respectively.

Depending on the type and scale of mitigation(s) to be implemented and timeframes, proceed back to Step 1 or 9 to assess the effect of the flow mitigation measure(s).

If the flow mitigation measures are not implemented or are unsuccessful for any reason, then proceed to Steps 11 and/or 12, as appropriate.

Step 11: Mid-Term Care

This step characterizes a temporary state when the flow risk mitigation measure of a 'non-passing' risk is under way or is required to be conducted in the future. Mid-term care may also apply if immediate or complete flow risk mitigation is impractical, and a longer period of time is required for the flowable tailings or the landform to develop the required conditions to pass the FMEA and RA. The timeframe for this could range between 20 and 80 years.

Step 12: Long-Term Care

If there are no practical means to reduce risks to a level that would support the AER's approval of the dam/facility's abandonment, then the tailings facility and associated dams will require long-term or perpetual care. The Operator would be required to develop and implement a long-term care specific Operation, Maintenance, and Surveillance manual. Other dam safety related reporting would also be required. The timeframe for long-term care may be 100 years or longer, and for some structures the likely scenario is perpetual care.

A tailings facility requiring long-term or perpetual care would likely be expected to be reconfigured in the most optimal way to support the dam's/facility's abandonment, be reclaimed and revegetated, and appear to be a non-dam closure landform (versus an operating tailings facility). During this time, periodic re-evaluations could be conducted to assess whether the tailings deposit was improving such that that a dam/facility abandonment could be approved.

CASE STUDIES

The case studies presented below are hypothetical examples of actual tailings dams and facilities in the oil sands industry. The flowability assessments for case studies 1 and 3 were conducted at the closure design stage, whereas, the flowability assessment for case study 2 was conducted for a closure landform that has already been constructed. The timeframe that each facility is being assessed for spans from initial closure design to long-term closure (> 1,000 years).

Case 1: 'In Pit', Terrestrial Closure Landform

Facility Description

The tailings facility is contained by an in-situ pit wall to the west and south, with the surrounding topography sloping towards the facility. Overburden dams, constructed using both engineered and non-engineered fills, make up containment on the north and east sides of the facility. The north dam consists of a very wide containment geometry on the upstream side, and the downstream area to the north was backfilled to create a terrestrial closure configuration with similar final drainage elevation to the internal valley. An aquatic closure landform will be established to the east of the facility. Figure 3 shows a typical section through the facility.

The typical section shows an idealized infilling plan of a relatively deep (up to 50 m) homogeneous Composite Tailings (CT) deposit with a relatively thin (up to 5 m) sand cap. The closure topography of this facility is planned to be a relatively shallow, hummocky valley with dendritic surficial drainage regime, which allows runoff to report to an adjacent aquatic closure landform (end pit lake) to the east via the closure drainage outlet. The engineered outlet features a sinuous and relatively narrow (8 m to 12 m invert width) low-flow channel within a much wider flood plain (approximately 100 m wide), and a low channel gradient excavated through engineered dam fills.

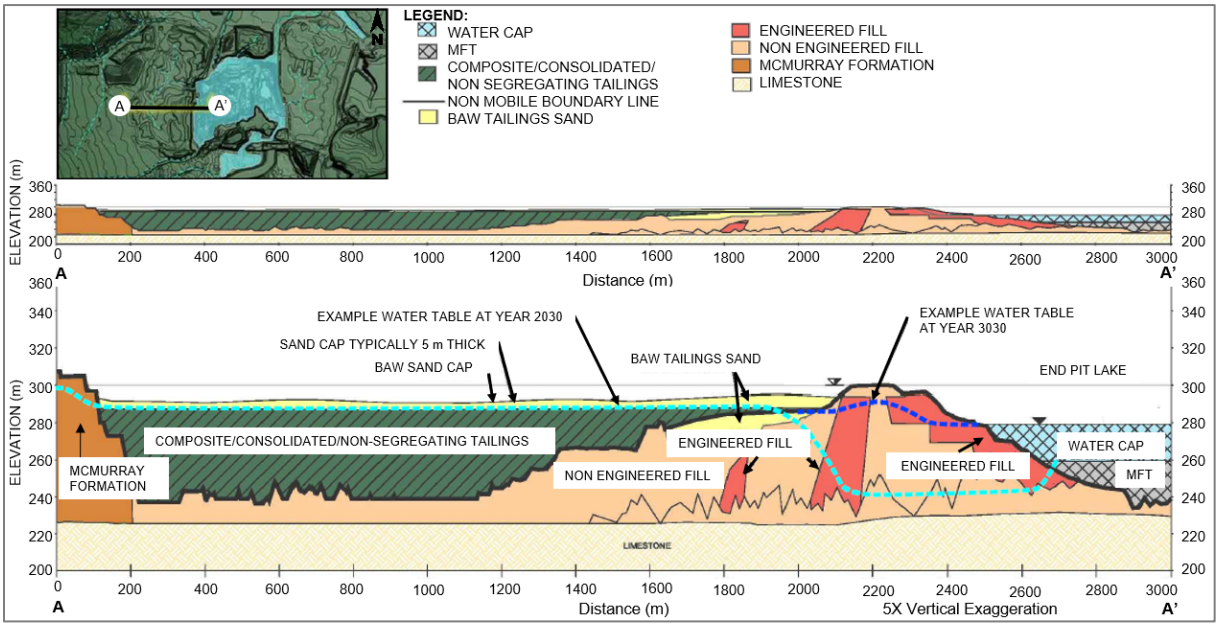

Figure 3: In-Pit Terrestrial Closure Example

A flowability assessment was conducted for this structure as follows:

Step 1: Tailings Classification

The tailings within the structure were gypsum-amended CT. These tailings are considered to be cohesionless (Soil Behaviour Type indices expected to be less than 2.6). Proceed to Step 3.

Step 3: Density State

Based on deposit characterization of a similar facility with a sand-capped CT deposit, it is expected that the majority of the CT-type tailings within this facility could be characterized as contractive.

The tailings in the area of interest are categorized as contractive. Proceed to Step 4.

Step 4: Degree of Saturation

Based on predictive hydrologic modelling of a similar tailings facility that has been converted to closure landform, the estimated phreatic surface within the tailings deposit could be assumed to mimic the surficial topography at a depth of up to 3 m below surface. The short-term (at closure) and long-term (1,000 years after closure) phreatic surfaces through the dam/east side of closure landform are estimated from the seepage modelling completed for the dam.

Figure 4 shows the plan views of the modelled phreatic surface depths. Proceed to Step 6.

Step 6: Tailings Mobility Beyond the Facility Boundary

The Factor of Safety and probability of appropriate scale/geometry of failure mode required to cause exposure of mobile tailings must be considered. For this facility, a significantly large scale failure with significantly large displacement/slumping of the containment structure would be required to expose CT.

Given the considered (non-credible) post-failure geometry, an assumed backscarp angle of 6% and flowout angle of 2%, and ignoring the existence of reclamation soils and vegetation, tailings flow beyond the 'post-failed' containment structure is not expected. The assessment could proceed to Step 7, however, this assessment required a similar level of judgement to the one for Step 9.

The low probability of such a consequential failure had to be considered in this step, and highlights the degree of overlapping steps built into this assessment process. Proceed to Step 7.

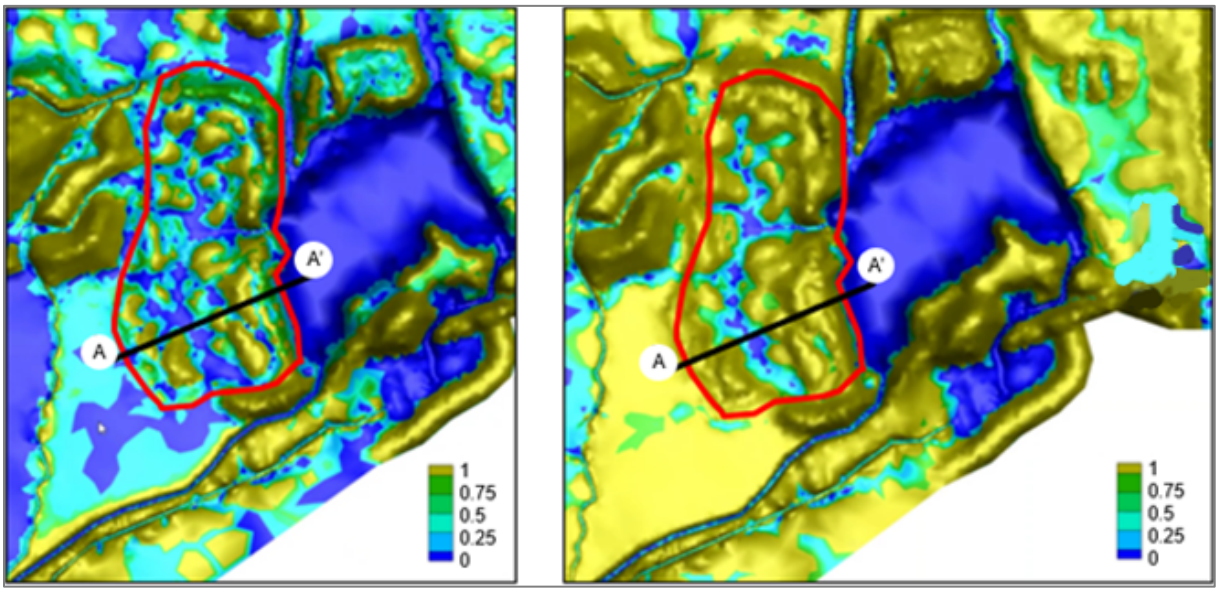

Figure 4: Case 1 – Plan Views of Modelled Depth-to-Phreatic Surface under 'Historical Wet' Conditions (Left) and 'Historical Dry' Conditions (Right)

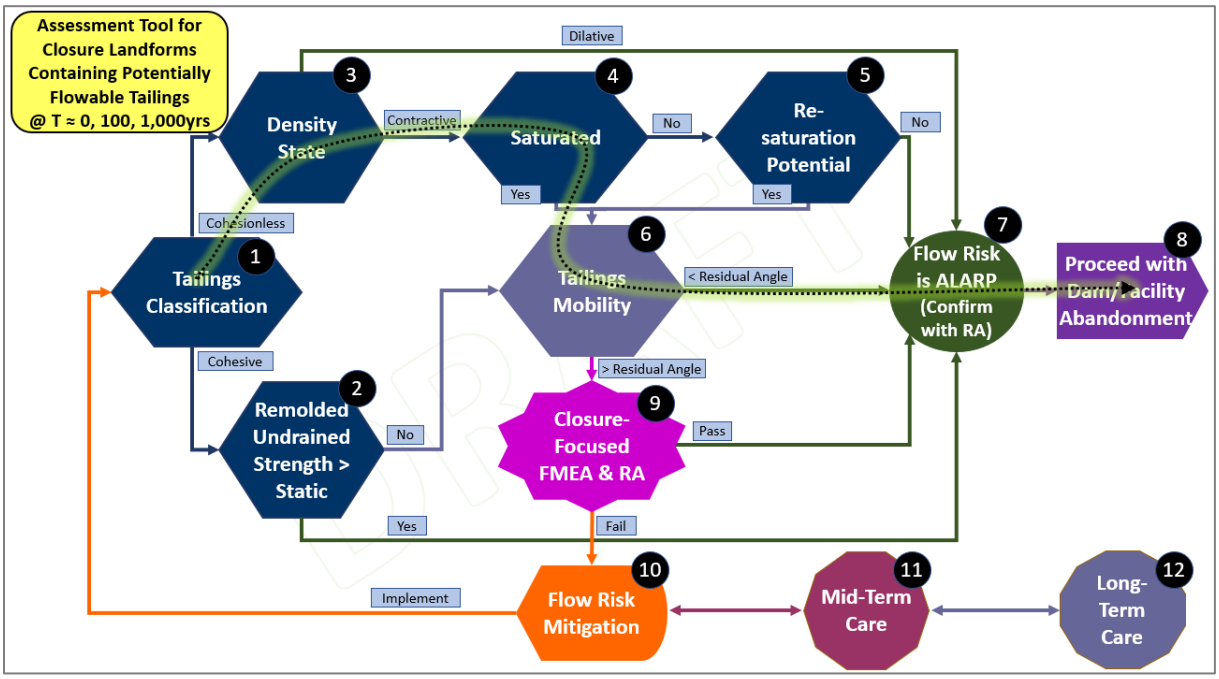

Figure 5: Flow Path through Assessment Steps for Case 1

Step 7: Flow Risk is ALARP

Acknowledging the assessment tool's recommendation that a closure-focused FMEA & RA be completed for every tailings facility, 'early' arrival at this step may indicate that failure modes related to liquefiable tailings are either 'less concerning' or 'non-credible' and may help to prioritize certain other design elements and/or assessments. Proceed to Step 8.

Step 8: Proceed with Dam/Facility Abandonment

This step may have several forms depending on the timing of the assessment (for example, in support of closure design versus in support of dam abandonment).

Since the facility in this case study is in the design phase, this step would be comprised of continued efforts to conduct engineering evaluation of the closure design, a closure-focused FMEA and RA, and the preparation and submission of a dam DCA plan according to Section 9.6 of the 2018 ADCSD. Figure 5 shows the path through the flowability assessment chart for Case 1.

Case 2: 'Ex Pit', Terrestrial Closure Landform

Facility Description

The scenario considered in this case study is an external tailings facility retaining potentially flowable tailings. The facility was designed and constructed using the upstream construction method. The structure is comprised of a starter dyke, tailings cell sand forming a 200 m wide dilative shell around the perimeter of the dyke, and a tailings beach consisting of both a beach above water (BAW) and beach below water (BBW). The structure has an ultimate dyke crest elevation of El. 306 m with overall slopes ranging from 8H:1V to 12.5H:1V. The localized features within the final closure landscape are constructed to El. 309 m.

The facility served as an operating tailings pond for 10 years and contained coarse tailings beach sand and Fluid Tailings (FT) during the operational phase. No treated tailings were deposited in the structure. Towards the end of its operating phase, all FT and nearly all soft fines-rich material was transferred out of the facility as the pond was infilled with Coarse Sand Tailings (CST). The infilling process was conducted to displace potentially flowable tailings and to create a trafficable surface in order to support future closure and reclamation activities.

Following the successful completion of the infilling process, the structure's final landform has been constructed and reclamation (reclamation soil placement and vegetation planting) has taken place. The closure landform includes a surface water drainage system which consists of a main drainage channel running in the north-south direction, and four collector channels running in the east-west direction, directing surface water runoff within the catchment area towards the main channel. The main channel drains its water into a seepage collection pond, located at the south-end of the structure. The plan view of the facility and surface drainage features are shown on Figure 6.

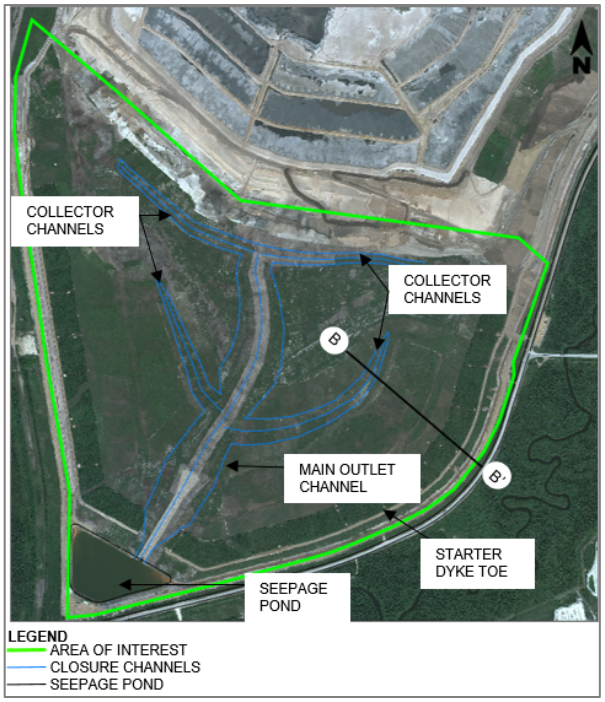

Figure 6: Plan View of an Out of Pit Terrestrial Closure Example

Figure 7 shows a typical cross section (B-B') through the facility, highlighting the overburden starter dyke, tailings cell sand, and tailings beach where potentially flowable tailings are located.

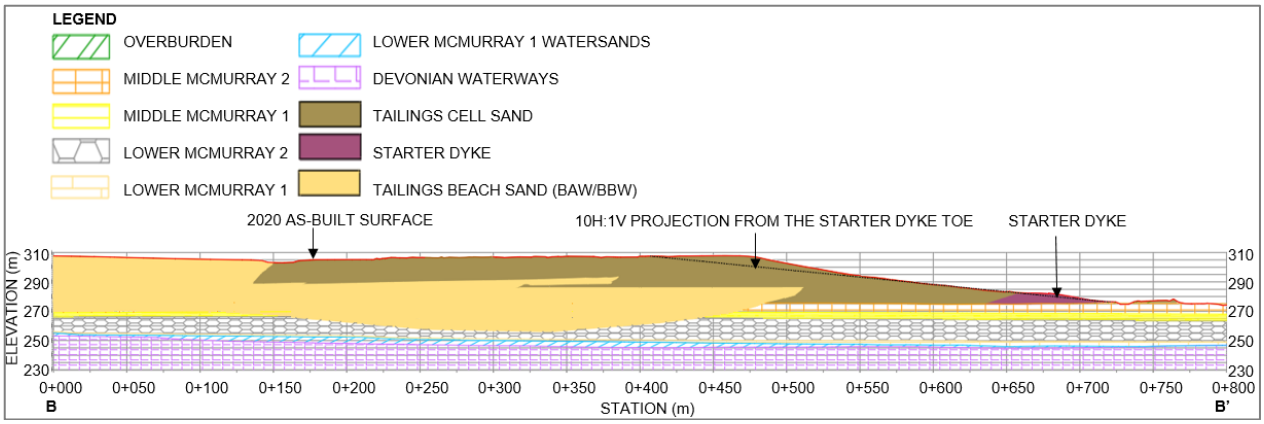

Figure 7: Cross Section View of an Out of Pit Terrestrial Closure Example (B-B')

A flowability assessment was conducted for this structure as follows:

Step 1: Tailings Classification

During operations, routine testing and material characterization tests were completed to characterize the deposit and to fulfill the AER reporting requirements as part of Directive 085. CPT programs were conducted during infilling to confirm and characterize the quality of the tailings within and below the reclamation platform, and to assess the extents of potentially liquefiable material.

The Soil Behaviour Type of the tailings material varied spatially across the pond and with depth. A region of interest within the facility (the critical section) was identified to be a section along the main outlet channel, shown on Figure 6. This area was determined to be the critical section because it had the easiest flow path for liquefied tailings and is the area where the dilative material is the thinnest, since the dilatant shell was excavated to establish the main outlet channel.

Figure 8 shows the pre and post-construction geometry along the main outlet channel.

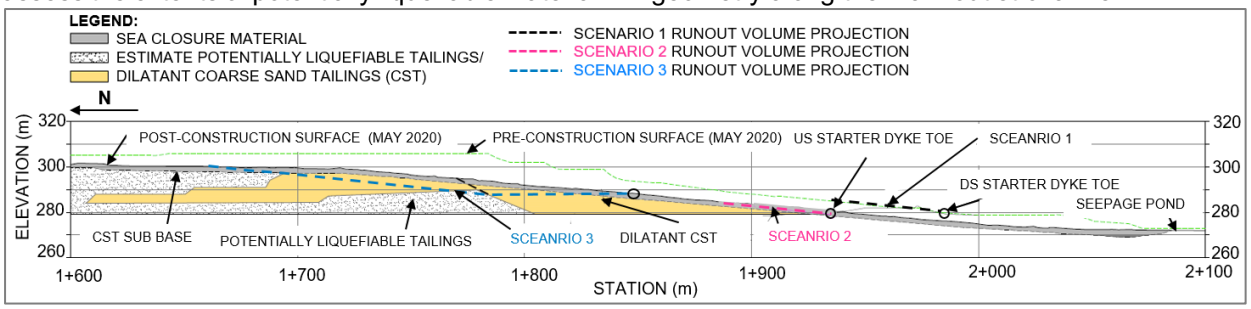

Figure 8: Runout Assessment Scenarios Conducted for an Out of Pit Terrestrial Closure Example

An analysis was conducted on 20 CPT locations which were within a close proximity to the main outlet channel to determine the variation of the Soil Behaviour Type Index (Ic) with depth and across the pond. The Ic varied as follows:

- 81% of the data points had an Ic <2.6, and were considered cohesionless; and
- 19% of the data points had an Ic >2.6, and were considered cohesive.

Spatially, the distribution of the potentially cohesionless materials was extensive and the tailings in the area of interest were therefore categorized as cohesionless. The results of this analysis aligns with the tailings deposition history described earlier, where FT was removed from the facility and replaced with sand dominated materials (CST), which are cohesionless. Proceed to Step 3.

Step 3: Density State

The normalized cone resistance for a clean sand equivalent, Qtn,cs varied with depth as follows:

- 40% of the data points were in the potentially contractive zone (Qtn,cs <70); and
- 60% of the data points were in the dilative zone (Qtn,cs >70).

There is sufficient contractive material that the potential for flow instability requires further evaluation. Proceed to Step 4.

Step 4: Degree of Saturation

The measurements of the degree of saturation for the facility were not available, however, the phreatic surface within the facility was found to vary between El. 280 m and El. 306 m, according to the CPTs and piezometers installed within the facility. The elevation of the phreatic surface along the main outlet channel ranged between El. 290 m and El. 306 m. The BBW deposits above the phreatic surface were considered to be unsaturated, and the BBW below the phreatic surface were considered saturated.

The elevation of the phreatic surface could reduce the potential for flow instability, but there is still a sufficiently thick saturated zone that the potential for flow instability requires further assessment. Proceed to Step 6.

Step 6: Tailings Mobility Beyond the Facility Boundary

A tailings runout assessment was conducted to evaluate the volume and distance that the flowable tailings would travel if a liquefaction event occurred behind the main channel. A significant rainfall event causing erosion and over steepening of the main channel outlet leading to liquefaction was considered to be the credible failure mechanism. The main channel outlet was designed for the 10,000 year return period precipitation event, so this failure mechanism described is very unlikely to occur within the design life of the closed facility (1,000 years). Nonetheless, it is considered for this flow instability assessment.

Other failure mechanisms such as overtopping and construction loading-related mechanisms were considered but were deemed to be non-credible since the pond was removed through the infilling process and construction was complete. of 10H:1V was selected. This angle was considered to be a conservative selection based on the characteristics of the MRM tailings and comparable case histories. The runout assessment considered three scenarios shown on, which are described as follows:

In Scenario 1, the back-slope projection angle of 10H:1V was projected from the downstream toe of the starter dyke, along the main channel. This scenario can be considered to represent the most likely case failure scenario. A 10H:1V slope was also projected from the downstream toe of Section B-B', as shown in plan view on Figure 6 and section view on Figure 7. This was done to represent the most likely case failure conditions through another section (non-critical section) of the structure.

In Scenario 2, the back-slope projection angle of 10H:1V was projected from the upstream toe of the starter dyke, along the main channel. In this scenario, the potential back-slope projection would not intersect potentially liquefiable tailings and would primarily consist of dilatant coarse sand tailings, reclamation material, riprap, and bedding materials. These materials are not contractive and/or saturated, and therefore would not flow.

In Scenario 3, the back-slope projection angle of 10H:1V was projected from the mid-slope where the potentially liquefiable tailings were nearest to the excavated surface of the main channel. This scenario can be considered to represent the reasonably worst case failure scenario. The assumed post-failure slope of 10H:1V is steeper than the dyke's existing slopes along the main channel. These materials are not contractive and/or saturated, and therefore would not flow.

Additionally, if the potential volumes from Scenarios 2 and 3, which are primarily confined to the dilatant CST and channel construction fill did run out and/or erode, they could be contained by the available capacity in the seepage pond shown on Figure 6.

At this point, the flowability assessment could proceed to Step 7 (Flow risk is ALARP). However similarly to Case 1, the assessment in Step 7 for this case study required a similar level of judgement to the one in Step 9 (Closure focused FMEA and RA). Proceed to Step 9.

Step 9: Failure Mode and Effects Analysis (FMEA) and Risk Assessment

A risk assessment was conducted for this facility to comply with the 2018 ADCSD Sections 5.17, 9.6, and 9.10 requirements. As discussed in Step 6 above, tailings are very unlikely to flow and any run out volumes could be contained by the available capacity in the seepage pond.

With the likelihood of the runout event being low, the impact to fisheries, wildlife habitats, rare or endangered species, unique landscapes, or sites of cultural significance would be short term and with minimal affects and impacts. For these reasons, the risks associated with potentially flowable tailings were found to be “Low”. Proceed to Step 7.

Step 7: Flow Risk is ALARP

According to the discussions in Steps 6 and 9, the flow risk for this facility was deemed to be at ALARP. Proceed to Step 8.

Step 8: Proceed with Dam/Facility Abandonment

The operator for this facility submitted a DCA plan to satisfy the requirements in Section 9.6 of the 2018 ADCSD. The DCA plan provided a plan for decommissioning, closure and abandonment and also included a closure-focused FMEA. This plan was approved by the AER.

The operator also completed an application to lower the consequence classification of the structure from “Extreme” to “Significant”, as per Parts 3.3 and 3.4 of the 2018 ADCSD. This application was also approved by the AER. The operator has submitted a Construction Completions Report and is in the process of applying to deregister the dam as per Parts 9.10 and 9.11 of the 2018 ADCSD. The facility will be in active care until it is deregistered as a dam, and then passive care until a reclamation certificate is obtained.

Figure 9 summarizes the flow path through the assessment steps for Case 4.

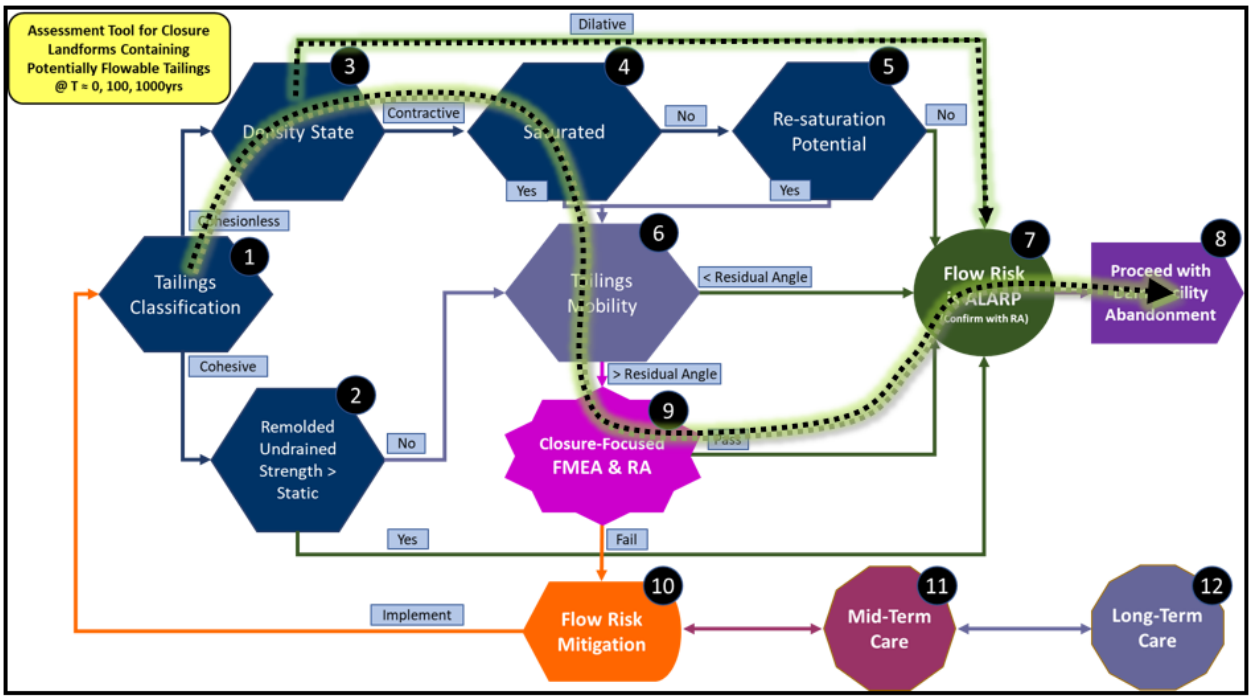

Figure 9: Flow Path through Assessment Steps for Case 2

Case 3: ‘In Pit’, Aquatic Closure Landform

Facility Description

An in-situ pit wall containment exists for north, south, and west of this aquatic closure landform. To the east, multiple in-pit tailings dams and pits exist

with infilled terrestrial closure configurations. The focus for this case study will be on the west side containment structure which is an in-situ pillar separating the end pit lake from an adjacent river, as shown on Figure 10.

The cross section across the facility shows an infilling plan of relatively deep (40 m to 50 m) homogeneous FT deposit with an initial water cap of 5 m. This condition represents an initial condition that is expected to occur 10 to 20 years prior to the final closure outlet for the lake being established (could be additional 5 m to 8 m).

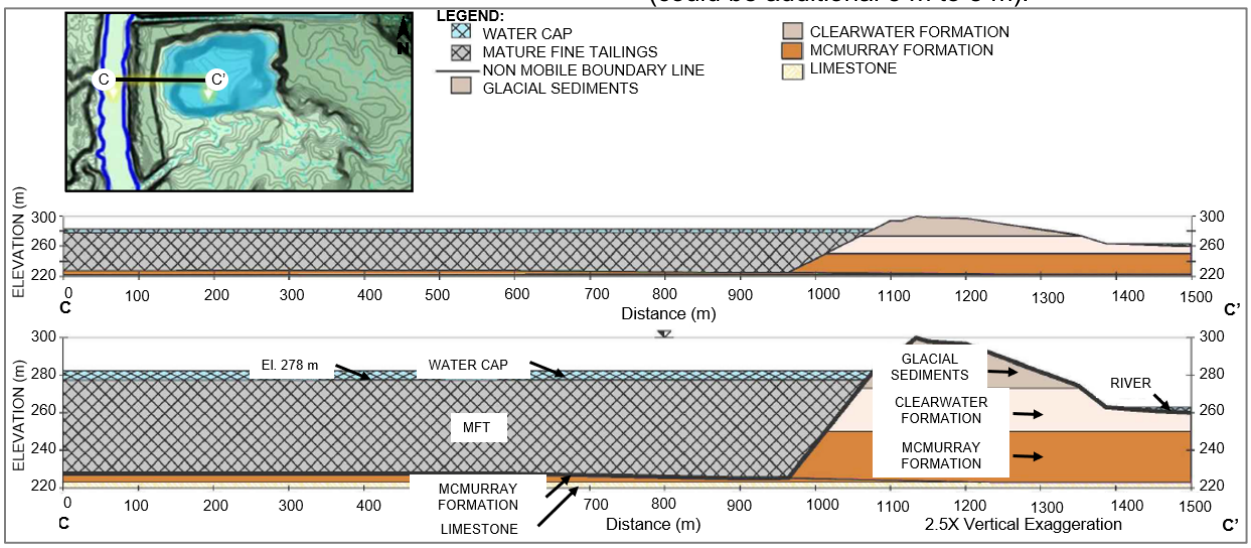

Figure 10: In-Pit Aquatic Closure Example

The elevation of the FT at T = 0 should therefore take this into account by considering FT consolidation and resulting elevation. Future time frames must also consider the degree of FT consolidation and elevation, as necessary. Note that FT infilling plan is based around maximum consolidation of FT (approximately 15 m total) leading to a final elevation equal to an adjacent river (and expected to occur over approximately 30 to 40 years). It should be noted that the surficial elevation of the water cap is expected to be maintained as a function of the sill elevation of the lake's outlet channel. In other words, the water cap deepens as FT consolidation occurs.

The final closure drainage outlet is planned to be established through an adjacent in-pit, terrestrially closed tailings facility and then through the in-situ pillar that makes up the west boundary of the facility. This is currently designed as an engineered outlet channel featuring a sinuous and relatively narrow (8 m to 12 m invert width) low-flow channel within a wide flood plain (approximately 180 m wide) with low channel gradient.

A flowability assessment was conducted for this structure as follows:

Step 1: Tailings Classification

The tailings within the structure were FT. These tailings are considered to be cohesionless (Soil Behaviour Type indices expected to be less than 2.6). Proceed to Step 3.

Step 3: Density State

Based on deposit characterization of a similar facility, this material is expected to be contractive. The tailings in the area of interest are therefore categorized as contractive. Proceed to Step 4.

Step 4: Degree of Saturation

The deposit is considered to be saturated because of the presence of a water cap. Proceed to Step 6.

Step 6: Tailings Mobility Beyond the Facility Boundary

For this case study, the FT deposit is the focus of mobility assessment and the water cap is not included. For other reasons, it will be critical that this aquatic closure landform is designed and constructed in such a way that the volume of water cap does not pose any dam-style failure modes at

closure in order to support facility closure and abandonment.
Some details on the magnitude and rate of the FT consolidation are provided earlier in this section. At closure milestones T = + 30 to 40 years, the volume of FT that is able to flow out of this facility if the entire in-situ pillar was removed is zero. At T = 0, the volume and mobility would represent a considerable consequence of failure. Proceed to Step 9.

Step 9: Failure Mode and Effects Analysis (FMEA) and Risk Assessment

Depending on the results of the engineering evaluations completed to support assessments of this design at T = 0, the risks associated with the failure modes related to tailings mobility may not be considered ALARP.

This could lead to the operator proceeding to Step 10, which could include a form of tailings treatment that accelerates consolidation or to Step 11, where the operator acknowledges a longer period of active care in order to wait for deposit conditions to improve and to support facility abandonment.

It could be expected that a longer period of active care could be required for this type of landform to allow for consolidation of FT to reach a suitable elevation as determined by the Operator, and accepted by the AER to support facility abandonment.

Figure 11 summarizes the flow path through the assessment steps for Case 3.

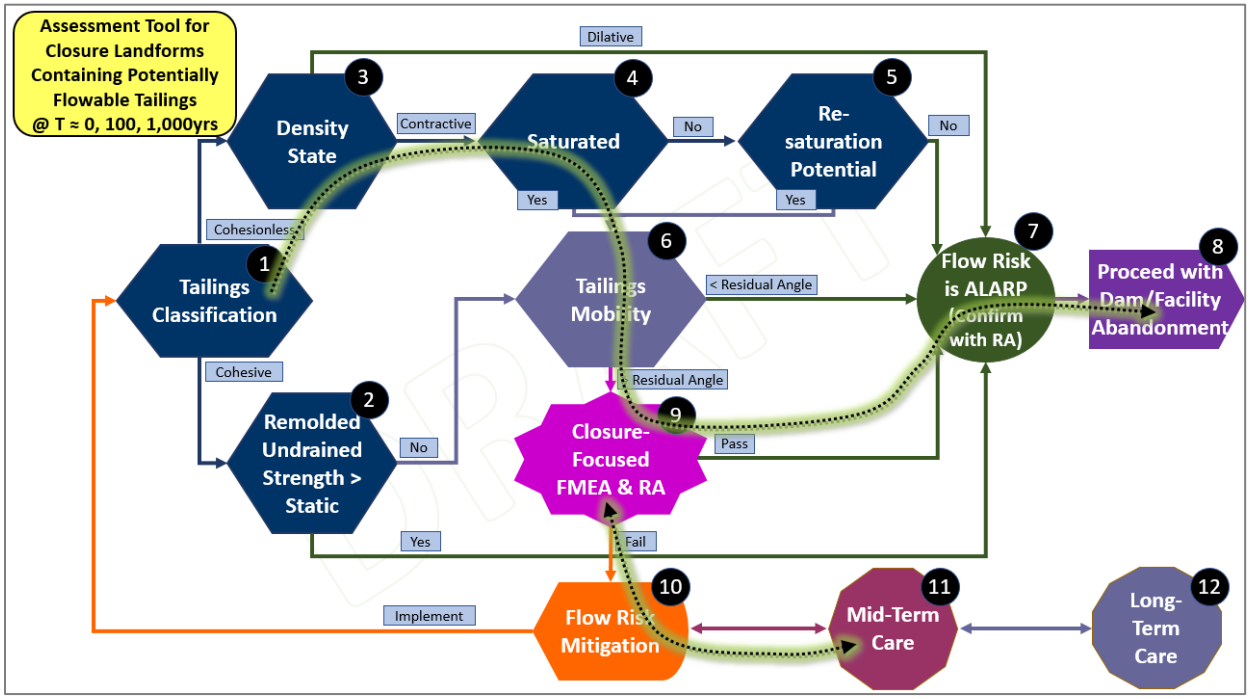

Figure 11: Flow Path through Assessment Steps for Case 3

REFERENCES

Alberta Energy Regulator. (2020). Decommissioning, Closure, and Abandonment of Dams at Energy Projects.

Government of Alberta. (2018). 2018 Alberta Dam and Canal Safety Directive.

Oil Sands Tailings Dams Committee. (2014). De-licensing of Oil Sands Tailings Dams. Technical Guidance Document.

Robertson P.K. , & Wride, C. (1998). Evaluating cyclic liquefaction potential using the cone penetration test. Canadian Geotechnical Journal, 35(3): 442–459.

COMPARING ADAPTIVE MANAGEMENT AND THE OBSERVATIONAL METHOD FOR MINE CLOSURE AND RECLAMATION

Abigail Paul, Nicholas Beier, and David Barsi
University of Alberta, Edmonton, Alberta, Canada

ABSTRACT

Adaptive management has emerged as an approach to mine closure and reclamation with dozens of applications referenced in papers and policy documents. In theory, adaptive management reduces uncertainty over time by using performance to inform decision-making, though many critics claim that is not meeting expectations. The observational method, a well-established method in geotechnical engineering for using performance to inform design, offers a point of comparison to better understand and potentially improve adaptive management approaches to closure and reclamation.

A comprehensive literature review was conducted to identify the similarities and differences between adaptive management and the observational method with specific reference to mine closure and reclamation. It is proposed that incorporating contingency measures from the observational method into adaptive management allows it to exist within a risk management framework. Stakeholder engagement was identified as a strength of adaptive management, though clarity on the approach is needed to satisfy stakeholders and fully realize benefits. Criteria should be set in advance to define when adaptive management is no longer needed. While a potentially powerful tool, adaptive management is not appropriate for all closure and reclamation challenges, and its limitations must be recognized before selecting it as an approach.

INTRODUCTION

Mine closure and reclamation projects involve considerable uncertainty due to their scope and complexity. In the Athabasca oil sands region specifically, the reclamation of hundreds of square kilometres of disturbed land and mine waste structures, including tailings storage facilities and their associated dams, is a subject of ongoing research. To deal with this uncertainty, adaptive management (AM) has been proposed as an approach to closure and reclamation in many policies and standards worldwide, including in Alberta. The Alberta Energy Regulator (AER), whose mandate includes oil sands mine closure and reclamation, refers to adaptive management in both Specified Enactment Direction 003: Direction for Conservation and Reclamation Submissions (SED 003) and Directive 085: Fluid Tailings Management for Oil Sands Mining Projects (AER 2017, 2018).

In theory, AM offers a flexible approach to reducing uncertainty over time by using observed performance to inform decision-making. In practice, critics have argued that adaptive management is not satisfying the expectations of both industry and community stakeholders. The practice of using observations to inform design is an existing idea in geotechnical engineering and is a cornerstone of the well-established observational method (OM). It is proposed that by comparing AM and the OM, AM approaches to mine closure and reclamation can be better understood and potentially improved. A comprehensive literature review was conducted to identify similarities and differences between the two methods.

ADAPTIVE MANAGEMENT

Origins

AM is typically traced back to the work of Holling et al. (1978). It was originally conceived as a novel approach to environmental assessment and natural resource management. Holling et al. (1978) proposed that uncertainty regarding the impacts of a project could be reduced over time by implementing controlled, targeted experiments to understand specific environmental responses. The goal of these experiments was to learn about the system and subsequently use the knowledge gained to refine the management strategy over time. Central to this approach was the use of models, both more sophisticated mathematical approaches and simple conceptual approaches, as a planning tool. Key recommendations on AM from this foundational work include:

- The project or policy design process should incorporate environmental considerations from the start.

- Information on the uncertain effects of the project or policy should be collected through experimentation. The goal of these experiments is to learn from change. These experiments should be controlled and targeted at understanding specific responses.
- Monitoring and remedial actions are integral to the design from the beginning and should be considered before the project or policy is implemented.
- The relative cost of assuming that uncertainty can be designed out compared to monitoring and mitigation of unexpected effects should be considered.

AM described and defined

Since the publication of Holling et al. (1978), AM has been defined and described in dozens of publications spanning the disciplines of ecology and environmental management (CEMA 2012). AM is often simply described as 'learning by doing.' A figure from Williams et al. (2009) (the United States Department of the Interior's technical guide on AM) is used in many sources (e.g. AER, 2018) to illustrate the iterative structure and key steps of an AM approach (Figure 1). This is a simplification of the comprehensive summary of AM provided by Williams et al. (2009). Stakeholder engagement is an element of AM that is not included in this figure but is described in detail in Williams et al. (2009) and other contemporary sources. While the importance of stakeholders was not stressed in early works, stakeholder engagement has become central to contemporary applications of AM.

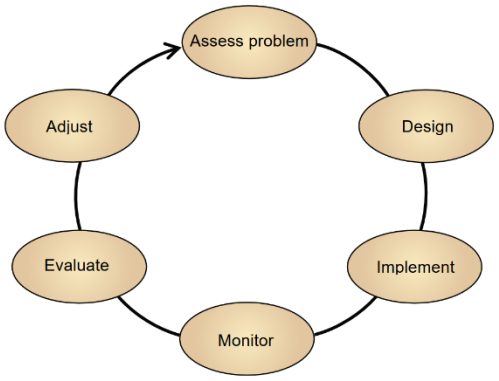

Figure 1. AM cycle (Williams et al. 2009)

Two definitions of AM relevant to the context of this paper are those presented in SED 003 and the Global Industry Standard on Tailings Management (GISTM) (italics added for emphasis):

- SED 003 (AER 2018): "A *management approach* that involves the *monitoring* and *evaluation* of performance followed by any necessary actions to achieve the intended *performance objectives*. [AM] also allows *information to be fed back into the planning and design process* so that future performance will meet the intended outcomes."
- GISTM (Global Tailings Review 2020): "A structured, iterative process of robust *decision-making* with the aim of *reducing uncertainty* over time via system *monitoring*. It includes the implementation of *mitigation* and *management measures* that are responsive to changing conditions, including those related to climate change, and the results of monitoring throughout the tailings facility lifecycle. The approach supports alignment on decisions about the tailings facility with the changing social, environmental and economic context and enhances opportunities to develop resilience to climate change in the short and long term."

The definition presented in SED 003 is of particular importance because this document sets the environmental regulatory requirements for oil sands mines in Alberta (AER 2018). The GISTM presents a multi-national perspective on AM for mine waste facilities.

Applications

AM was originally developed for environmental assessment and management, though Holling et al. (1978) believed that the approach applied to a wider range of problems. Case studies describing the original application and development of AM in Holling et al. (1978) include forestry in New Brunswick, fisheries in British Columbia, watershed development in Venezuela, and economic development in an Austrian ski town.

In recent decades, AM has been applied to mine closure and reclamation. While AM was not specifically developed with mine closure and reclamation in mind, Morrison-Saunders et al. (2016) suggest that closure and reclamation planning is similar to the consideration of impacts at the environmental assessment stage, which provides a basis for its application.

Typical applications of AM to mine closure and reclamation vary by region. AM has been used as a strategy for re-vegetation in Australia (Cummings et al. 2005, Grigg 2012, Bell 2020). In the United States, large-scale watershed restoration in areas of extensive historical mining has employed an AM approach (US EPA 2002, Bell et al. 2007, Faulkner et al. 2010). Applications in Canada are broader in scope. For example, at oil sands mines, AM has been used or proposed for impacts related to wildlife and fish, emissions, health and safety, surface water management, climate change, reclamation, and as an overall management strategy (Olszynski 2017).

AM has also been referenced in recent policy and guidance documents, standards, and other items of regulatory interest. A summary is presented in Table 1 (located at the end of the paper).

Challenges and limitations

Holling et al. (1978) had a grand and revolutionary vision for AM, describing it as following in the tradition of "prehistoric man's exploration of fire and the modern scientist's development of hypotheses and experiments." Contemporary takes on AM are markedly cooler, with many sources claiming that it has failed to live up to expectations (CEMA 2012). Two specific challenges are dealing with uncertainties in the long term and disagreement on the meaning of AM.

Long-term uncertainties

AM is intended to be a long-term approach. SED 003 refers to a landform design process that follows AM principles and lasts "several decades" (AER 2018). Some sources go further and define AM as a specific phase or time period in the mine lifecycle (INAP 2017, ISO 2021b). Changing conditions and logistical considerations over this timeframe introduces significant uncertainty. Challenges include maintaining documentation, data management, financing, monitoring, and maintenance over the long term. There can also be a significant time lag between when a management action is implemented and when the response is observed (Williams et al. 2009).

Uncertainties that must be considered in the AM approach are not limited to the actual performance of the reclaimed landscape. This is demonstrated by the challenges faced at Sullivan Mine, a metal mine located in British Columbia that operated for nearly one hundred years before closing in 2001 (Peterson et al. 2015). The mine is widely known for the extensive treatment and remediation measures put in place to manage acidic drainage, which includes an "adaptive site-wide risk management plan" for groundwater, surface water, vegetation, and aquatic life. Changes in site conditions, surrounding land use, weather, regulatory policy, and mine closure and reclamation requirements have all posed challenges to AM at this site.

Lack of clarity

As has been demonstrated in this paper, there is a large body of literature defining and describing AM. Despite this (or arguably because of this), there is considerable confusion on what it really means. Gouin (2017) and Olszynski (2017) have identified a lack of clarity on AM to be a barrier to its effective implementation specifically for oil sands closure and reclamation projects in Alberta.

Olszynski (2017) reviewed the application of AM to environmental impact assessments for coal and oil sands mines in Alberta through a legal lens. It was found that AM was not being applied effectively, if at all: "definitions and conceptions of [AM] vary, with most proponents erroneously invoking it as a general or routine strategy that ensures effective mitigation; little or no attention is being paid to experimental design; objectives, indicators, and thresholds for adaptation are generally missing, especially at the environmental assessment stage. […] [N]one of the projects assessed here had much to show in terms of actual learning."

This lack of clarity is not just a concern for mine operators. Gouin (2017) examined the perspectives of a diverse group of stakeholders (including operators, Indigenous groups, government officials, researchers, practitioners, and environmental groups) on AM in Alberta's oil sands. AM was found to be "undefined and open to interpretation in Alberta," leading to distrust and uncertainty between stakeholders.

The OBSERVATIONAL METHOD

Origins

The observational method (OM) was first described by Peck (1969), who credited Karl Terzaghi with developing the approach. The method was specifically developed for geotechnical engineering projects. In the OM, the design is based on the most probable conditions as assessed from a site

exploration. As construction proceeds, the project is monitored, and the observed behaviour is compared against the expected behaviour. If observations deviate from the most probable conditions, the design is modified to suit the actual observed conditions. Critically, these design modifications or contingency measures have been planned for every foreseeable deviation from the most probable conditions.

The OM described and defined

The specific steps of the OM as described by Peck (1969) are:

- "Exploration sufficient to establish at least the general nature, pattern and properties of the deposits, but not necessarily in detail.
- Assessment of the most probable conditions and the most unfavourable conceivable deviations from these conditions. In this assessment geology often plays a major role.
- Establishment of the design based on a working hypothesis of behaviour anticipated under the most probable conditions.
- Selection of quantities to be observed as construction proceeds and calculation of their anticipated values on the basis of the working hypothesis.
- Calculation of values of the same quantities under the most unfavourable conditions compatible with the available data concerning the subsurface conditions.
- Selection in advance of a course of action or modification of design for every foreseeable significant deviation of the observational findings from those predicted on the basis of the working hypothesis.
- Measurement of quantities to be observed and evaluation of actual conditions.
- Modification of design to suit actual conditions."

Many sources refer directly to Peck (1969) rather than present their own definition of the OM. An exception is the GISTM, which defines the OM as: "a continuous, managed, integrated, process of *design, construction control, monitoring and review* that enables *previously defined modifications* to be incorporated during or after construction as appropriate. All of these aspects must be demonstrably robust. The key element of the [OM] is the *proactive assessment* at the design stage of *every possible unfavourable situation* that might be disclosed by the monitoring programme and the development of an *action plan or mitigative measure* to reduce risk in case the unfavourable situation is observed. This element forms the basis of a *performance-based risk management approach*. The objective is to achieve greater overall safety" (italics added for emphasis) (Global Tailings Review 2020).

Applications

The OM is widely used in geotechnical engineering applications, including dams, foundations, excavations, and tunnels (Lacasse and Höeg 2019). This approach is also used for the design, construction, and operation of tailings storage facilities. For example, the largest tailings dam in Europe (located at the Zelazny Most mine in Poland) is constructed and operated according to the OM (Lacasse and DiBiagio 2019).

The relevance of the OM to oil sands closure and reclamation is to the stability of tailings dams after mining operations are complete. In a series of interviews with practitioners in Alberta, Schafer et al. (2020) found that the OM was viewed as critical to the success of long-term monitoring and maintenance of tailings dams. On an international scale, the GISTM requires the implementation of a monitoring system to apply the OM over the facility lifecycle (Global Tailings Review 2020). This system monitors for potential failure modes and verifies design assumptions.

The OM has also been applied to landform design for closure and reclamation in the oil sands (CEMA 2012). For example, Suncor applied the OM to cap Wapisiw Lookout (Pond 1) and Pond 5 (Pollock et al. 2010, McKenna and van Zyl 2020). The development and implementation of contingency plans are key to the application of the OM to landform design. McKenna and van Zyl (2020) state: "[i]n the same way that a pre-designed toe berm may be a contingency for dam safety on dams with poor foundation conditions, shallow wetlands may be a contingency for reclamation for pockets of beaches that have undergone differential settlement."

Challenges and limitations

Peck (1969) claimed that the OM would improve cost and time savings for geotechnical projects without compromising safety, though the application of engineering judgement was needed to realize these benefits. Designers must be able to predict the potential failure modes of the structure and select appropriate quantities to monitor. They must also develop contingency measures be prepared to apply them quickly. Peck (1969) cautions against relying on the OM to guard against brittle failure modes, which can occur rapidly and without warning. Clearly, the use of the OM is not to be taken lightly.

Identification of failure modes

The OM assumes that "all failure modes are well understood in advance and that contingencies can be designed" (CEMA 2012). This is no small undertaking; over 200 potential failure modes are possible in the context of landform design for reclaimed mine landscapes (LDI 2021). This list must then be narrowed down to credible or technically feasible failure modes (Global Tailings Review 2020). Methods such as a failure modes assessment and failure modes effects analysis (FMEA) have been developed to screen and evaluate potential failure modes, though these activities require substantial technical effort and expertise (McKenna and van Zyl 2020). An example application of FMEA to a tailings dam closure plan is presented in Schafer et al. (2022).

Brittle behaviour of mine waste

Peck (1969) states in the first description of the OM that it is not appropriate to guard against brittle failure. This is because brittle materials can fail quickly and catastrophically with little warning. The implications of this limitation to mining projects have been demonstrated by the well-publicized failures of multiple tailings storage facilities in the past decade. For example, the failure of Feijão Dam I in Minas Gerais, Brazil was attributed in part to brittle behaviour (Robertson et al. 2019). Notably, the failure occurred after deposition into the facility ceased and the tailings surface had been covered with soil and vegetation. This limitation is reflected in the GISTM, which states that the OM applies to only non-brittle failure modes (Global Tailings Review 2020).

DISCUSSION

Current regulations and policy guidance documents include requirements and recommendations for an AM approach to mine closure. This trend seems likely to continue as demonstrated by references to AM in the GISTM and ISO 21795 (Global Tailings Review 2020, ISO 2021a, 2021b). In theory, AM offers a flexible approach in which uncertainty is reduced over time by using monitoring results to inform closure and reclamation strategies. In practice, critics have argued that AM is not satisfying expectations (CEMA 2012).

The OM offers a point of comparison to AM. Both are iterative approaches to dealing with uncertainty relevant to mine closure and reclamation in the oil sands and elsewhere. Conceptual differences between AM and the OM that have arisen based on their original intent, history of application, and other factors are summarized in Figure 2.

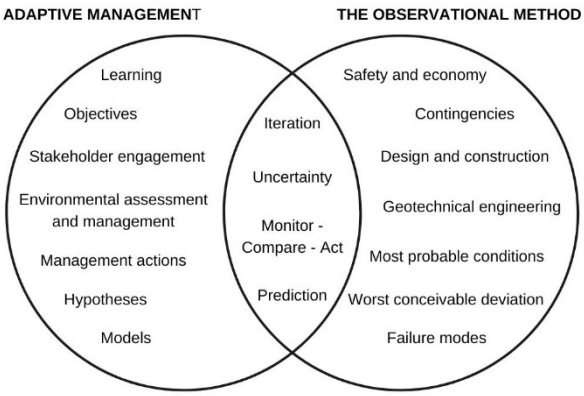

Figure 2. Venn diagram of AM and the OM

The idea of improving AM by incorporating elements of the OM has been previously discussed by McKenna et al. (2016), who propose "true [AM] […] based on the geotechnical OM where risks are identified in advance, contingencies developed and costed in full, and the monitoring program supports timely identification of any performance deficiencies which are remediated as they arise." A modified AM approach for end pit lakes at oil sands mines based on the OM is presented in CEMA (2012).

The two approaches are shown side by side in Figure 3. The specific steps are based on descriptions in Williams et al. (2009) and Peck (1969), for AM and the OM, respectively.

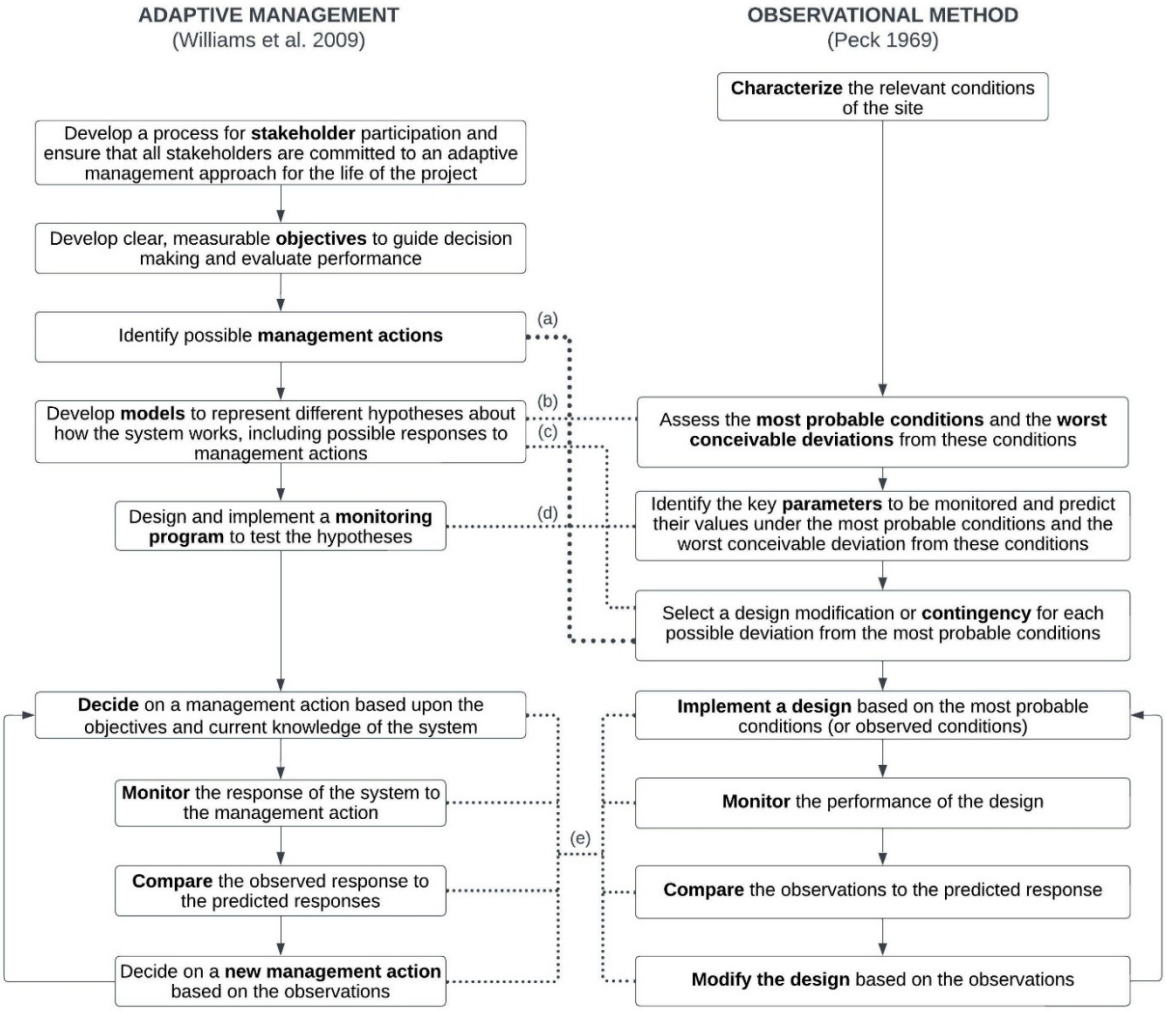

Figure 3. Comparison of steps in AM and the OM

Major similarities between specific steps in the approaches are represented as dashed lines:

(a) Management actions and contingency plans play similar roles in AM and OM, respectively; they are both measures to improve performance. What distinguishes them is their level of detail and intent. Management actions are less detailed because the goal of taking the action is to learn about the response. They are also not necessarily planned in advance. For example, a management action could be planting vegetation on a slope to determine the effect on stability. By comparison, contingency plans are as detailed as possible and are explicitly planned in advance. For example, constructing a toe berm from a designated material stockpile because monitoring results indicate instability.

(b) The "most probable conditions" and "worst conceivable deviations" in the OM are examples of models of system behaviour in AM.

(c) Models are used to assess possible contingency measures before implementation.

(d) The OM implements a monitoring program to test two "hypotheses" by predicting parameters under the "most probable conditions" and the "worst conceivable deviations".

(e) Both AM and the OM iterate through cycles of monitor – compare – act. A key distinction between the methods is decision-making. Iteration in AM involves deciding to take a specific management action which may not have been prepared in advance. In the OM, a fully developed contingency plan is implemented based on the observations. Ideally, no decision-making is required.

From this comparison, an AM approach to mine closure and reclamation may be better understood and potentially improved. Key ideas and suggestions are summarized as follows.

Incorporating risk

A relative strength that the OM has over AM is the proactive consideration and implementation of contingency measures for deviations in observed performance. Selecting the design based on "probable" conditions and "reasonably foreseeable" deviations is aligned with a contemporary risk management approach in which failure modes are considered based on their probability (e.g. Schafer et al., 2021). The GISTM recognizes the OM as "the basis of a performance-based risk management approach" (Global Tailings Review 2020).

Elements of the OM have been embraced in descriptions of AM in policy documents outside of Alberta (Table 1). Descriptions of AM in Australian mining policy and guidelines are notable for their risk-informed approach with specific mention of trigger levels. AM has been identified as a strength of mine closure and reclamation regulations in Australia (Morrison-Saunders et al. 2014). A progressive closure and reclamation framework in which plans are submitted before the start of mining is key to the Australian approach (Morrison-Saunders and Pope 2013, Morrison-Saunders et al. 2014). Australian sources additionally refer to management intervention in the form of contingency plans or controls (Government of Western Australia 2013, NSW Government 2013, Australian Government 2016). Some international standards and guidelines take a similar view of AM to Australian sources. ISO 21795 explicitly links AM to risk and mitigation measures are directly referred to in the definition of AM presented in the GISTM (Global Tailings Review 2020, ISO 2021b).

Descriptions of AM in Albertan policy documents are more general and describe a method of iteration over the long term to fill knowledge gaps (Alberta Government 2015, AER 2018). In practice, Olszynski (2017) describes a lack of thresholds and indicators in AM plans for coal and oil sands mines in Alberta. Incorporating contingency measures responsive to explicitly defined indicators would allow AM to exist within a broader framework of risk management for closure and reclamation.

Embracing stakeholder engagement

Stakeholder engagement is the first and arguably most important step of an AM approach. The OM is comparatively more focused on the technical aspects of design and construction. Brown (2005) suggests that collaboration between stakeholder groups is key to implementing AM. Case studies describing the importance of stakeholder engagement to AM in mine closure and reclamation can be found in Bell et al. (2007), Grigg (2012), and Jensen and Hylland (2019). This interaction goes both ways: stakeholder engagement is necessary for a successful AM approach, and a successful AM approach is necessary to satisfy stakeholders (Ott 2017).

This two-way interaction provides some insight as to why AM approaches have often not met expectations. Stakeholders in oil sands mining projects reported that their involvement in AM approaches was limited (Gouin 2017). Consequently, negative perceptions of AM among stakeholders were found to be a barrier to the application of AM in the oil sands. While stakeholder engagement is a relative strength of AM, further work is required in ensuring that AM approaches do not stumble at this critical first step.

Converging on stability

An endpoint to the iterative stage of monitor – compare – act is often missing from descriptions of AM and the OM. However, it is not desirable to be stuck in this loop indefinitely. A risk-informed AM approach to mine closure and reclamation could link the end of the iterative cycles to achieving a certain risk threshold. This could correspond to steady state, stable conditions or a similar risk level as tolerated by the public for similar natural landforms.

Many have commented on how AM approaches are improved by defining closure criteria or reclamation endpoints. These criteria should be site-specific, flexible, and developed as early as possible (Koontz et al. 2009, Poscente and Charette 2011). Flexibility is necessary to allow regular updates as learning occurs through AM. Defining these criteria allows for both the evaluation of the AM strategy and a mechanism for risk assessments (Watson et al. 2017, Young et al. 2019).

In a mine closure and reclamation context, ending the iterative stage does not necessarily mean a "walkaway closure" scenario. Long-term perpetual care as proposed by Morgenstern (2012) may be

more appropriate. This could involve transitioning to "reactive" management as described in INAP (2017) in which monitoring and action occur in response to specific conditions, such as extreme weather events. Remote monitoring may be appropriate for these applications. Guidance on transitioning out of adaptive management can also be found in ISO (2021b).

Recognizing the limitations of adaptive management

Even with the improvements suggested above, AM is not suitable for every problem and retains many of its existing limitations. Williams et al. (2009) present a problem-scoping key that can be used to determine if AM is appropriate for a particular problem. AM should not be used unless all of the criteria listed below are satisfied:

- A management decision is to be made
- Stakeholders can be engaged
- Management objective(s) can be explicitly stated
- Decision-making is complicated by uncertainty regarding potential management impacts
- Monitoring can be used to inform decision-making
- Progress can be measured in achieving the stated management objective(s)
- Management actions can be adjusted as learning occurs
- The AM process is aligned with the relevant legal framework

For example, brittle failure modes fall outside of both the OM and AM. Referring to the criteria proposed by Williams et al. (2009), monitoring cannot be used to inform decision-making and management actions cannot be adjusted because the failure occurs too quickly. It is suggested that these failure modes should be considered outside of this framework by applying conservative design criteria (Global Tailings Review 2020).

CONCLUSION

AM has been referenced in recent policy documents and will likely continue to be a part of mine closure and reclamation practice, despite legitimate criticisms. The application of AM can be a controversial topic, though realizing its benefits may provide a pathway to success for complex closure and reclamation scenarios. Comparison with the OM, a well-established method in geotechnical engineering, offers some insight as to how AM may be improved. From this comparison, the following are recommended:

- Explicitly define contingency measures for deviations in observed performance to incorporate risk.
- Embrace stakeholder engagement, recognizing that it is critical to the success of AM.
- Consider the endpoint of an AM approach and develop criteria to finish the iterative cycle.
- Be aware of the limitations of AM, recognizing that it is not appropriate for all closure and reclamation challenges.

ACKNOWLEDGEMENTS

Financial support of this research was provided by the AER. The authors would also like to thank Tim Eaton (AER), Scott Martens (Canadian Natural Resources Limited), and Gord McKenna (McKenna Geotechnical Inc.) for their support of this research.

Table 1. AM in mine closure guidelines and policy

International	
GISTM (Global Tailings Review 2020)	• Enhance climate resiliency over lifecycle through AM • Update management using AM if impacts have changed • Performance monitoring program to be designed, implemented, and operated following AM
ISO 21795-1: Mine closure and reclamation planning – Part 1: Requirements (ISO 2021a)	• AM allows for adjusting methods that do not meet objectives through a cycle of implementation, monitoring, and making changes while learning (including from stakeholder engagement) • AM applied over the mine life (including during progressive reclamation and post-closure) to enable continuous improvement
ISO 21795-2: Mine closure and reclamation planning – Part 2: Guidance (ISO 2021b)	• AM is used to confirm long-term stability of reclamation measures • The objectives of AM are to identify risks from changes to closure measures and to apply critical controls to manage these risks • Key elements of AM include failure modes and effects analyses (FMEA); monitoring plans; performance criteria, goals, and predictions; critical controls; and lessons learned • Minimize reliance on AM with robust and resilient engineering • AM is a phase of the mining lifecycle between "closure and reclamation implementation" and "post-closure and reclamation operations and maintenance" (AM may continue post-closure)
Global Cover System Design Technical Guidance Document (INAP 2017)	• AM occurs over a site-specific time period after closure of a covered mine waste landform (part of the operational period may be included if reclamation began before closure)
Australia	
Western Australia Water in Mining Guideline (Government of Western Australia 2013)	• AM framework is objectives and outcomes • AM works by evaluating the effectiveness of a strategy against stated objectives, then modifying it as needed • AM mechanisms include triggers, responses, and contingencies • AM is used to ensure that impacts do not exceed approved levels
Leading Practice Handbook: Mine Rehabilitation (Australian Government 2016)	• AM is to reduce uncertainty using a risk-based approach with trigger levels to identify where management actions are needed
ESG3: MOP Guidelines (NSW Government 2013)	• AM is "based on evaluating the probability of an event occurring; evaluating the consequence; and using a risk-based approach to determine trigger levels (both upper and lower) where response or action is required" • The use of performance indicators allows for AM in response to poor performance or unexpected results
Alberta	
SED 003 (AER 2018)	• AM is used to mitigate the impacts of hydrogeological knowledge gaps in closure plans • Apply AM by updating reclamation plans over the project life • Post-closure landscape design must adopt AM principles and requires a long-term, multidisciplinary, iterative approach
Directive 085: Fluid Tailings Management for Oil Sands Mining Projects (AER 2017)	• Approval conditions in tailings management plans support AM
Lower Athabasca Region - Tailings Management Framework (Alberta Government 2015)	• Cumulative effects management follows an AM model that includes learning and adapting to changing stakeholder expectations • Development of tailings reclamation criteria is an iterative process with learning through AM (where knowledge gaps exist)

REFERENCES

AER. 2017. Directive 085: Fluid Tailings Management for Oil Sands Mining Projects.

AER. 2018. Specified Enactment Direction 003: Direction for Conservation and Reclamation Submissions.

Alberta Government. 2015. Lower Athabasca Region - Tailings Management Framework for the Mineable Athabasca Oil Sands.

Australian Government. 2016. Leading Practice Handbook: Mine Rehabilitation

Bell, K.Y., Stokes, C.L., Miller, F., and Faulk, K.L. 2007. Adaptive Watershed Management in the Copper Basin: Evaluation of Early Successes. National Meeting of the American Society of Mining and Reclamation, Gillette, Wyoming, June 2-7, 2007. 24 pp.

Bell, S.A.J. 2020. Translocation of threatened terrestrial orchids into non-mined and post-mined lands in the Hunter Valley of New South Wales, Australia. Restoration Ecology, **28**(6): 1396–1407.
Brown, M.T. 2005. Landscape restoration following phosphate mining: 30 years of co-evolution of science, industry and regulation. Ecological Engineering, **24**(4): 309–329.

CEMA. 2012. End Pit Lakes Guidance Document.
Cummings, J., Reid, N., Davies, I., and Grant, C. 2005. Adaptive Restoration of Sand-Mined Areas for Biological Conservation. Journal of Applied Ecology, **42**(1): 160–170.

Faulkner, B.B., Price, K.R., Russell, F.D., and Miller, F.K. 2010. Land and water restoration of the Copper Basin of Tennessee. National Meeting of the American Society of Mining and Reclamation, Pittsburgh, Pennsylvania, June 5-11, 2010. 13 pp.
Global Tailings Review. 2020. Global Industry Standard on Tailings Management.

Gouin, C. 2017. Managing uncertainty: An examination of adaptive management and progressive reclamation in Alberta's mineable oil sands. Master's Thesis, Norwegian University of Life Sciences, Ås, Norway.

Government of Western Australia. 2013. Western Australian water in mining guideline.

Grigg, A. 2012. Adaptive rehabilitation management and a drying climate: unique challenges for Alcoa's bauxite mine rehabilitation in southwestern Australia. 7th International Conference on Mine Closure 2012, Brisbane, Australia, September 25-27, 2012. 8 pp.

Holling, C.S., Bazykin, A., Bunnell, P., Clark, W.C., Gallopin, G.C., Gross, J., Hilborn, R., Jones, D.D., Peterman, R.M., Rabinovich, J.E., Steele, J.H., and Walters, C.J. 1978. Adaptive environmental assessment and management.

INAP. 2017. Global Cover System Design Technical Guidance Document.

ISO. 2021a. ISO 21795-1: Mine closure planning and reclamation planning - Part 1: Requirements.
ISO. 2021b. ISO 21795-2: Mine closure and reclamation planning - Part 2: Guidance.

Jensen, T., and Hylland, K. 2019. Environmental Adaptive Management: Application on Submarine Mine Tailings Disposal. Integrated Environmental Assessment and Management, **15**(4): 575–583.
Koontz, D., Fourie, A., and Tibbett, M. 2009. Evolving closure criteria throughout the life of mine. 4th International Conference on Mine Closure, Perth, Australia, September 9-11, 2009. 8 pp.

Lacasse, S., and DiBiagio, E. 2019. Two Observational Method Applications: An Ideal Solution for Geotechnical Projects with Uncertainty. 8th International Conference on Case Histories in Geotechnical Engineering, Philadelphia, Pennsylvania, March 24-27, 2019. 12 pp.

Lacasse, S., and Höeg, K. 2019. In praise of monitoring and the Observational Method for increased dam safety. ICOLD 87th Annual Meeting and Symposium, Ottawa, Ontario, June 9-14, 2019. 13 pp.

LDI. 2021. Mining with the end in mind: Landform design for sustainable mining.
McKenna, G., Straker, J., and O'Kane, M. 2016. Custodial transfer of reclaimed mines: barriers and opportunities. 40th Annual Technical and Research Committee on Reclamation Mine Reclamation Symposium, Penticton, British Columbia, September 19-22, 2016. 13 pp.

McKenna, G., and van Zyl, D. 2020. Chapter VIII: Closure and Reclamation. Towards Zero Harm - A compendium of papers written for the Global Tailings Review. pp. 109–125.

Morgenstern, N.R. 2012. Oil sands mine closure - The end game: An update. 3rd International Oil Sands Tailings Conference, Edmonton, Alberta, December 3-5, 2012. pp. 12.

Morrison-Saunders, A., Gorey, P., Doepel, D., Mtegha, H., and McHenry, M.P. 2014. Enhancements in mine closure planning in Western Australia and possible applications for Africa. 9th International Conference on Mine Closure, Johannesburg, South Africa, October 1-3, 2014.11 pp.

Morrison-Saunders, A., McHenry, M.P., Rita Sequeira, A., Gorey, P., Mtegha, H., and Doepel, D. 2016. Integrating mine closure planning with environmental impact assessment: challenges and opportunities drawn from African and Australian practice. Impact Assessment and Project Appraisal, **34**(2): 117–128.

Morrison-Saunders, A., and Pope, J. 2013. Mine closure planning and social responsibility in Western Australia: Recent policy innovations. 2nd International Conference on Social Responsibility in Mining, Santiago, Chile, November 5-8, 2013. 9 pp.

NSW Government. 2013. ESG3: Mining Operations Plan (MOP) Guidelines.

Olszynski, M.Z.P. 2017. Failed Experiments: An Empirical Assessment of Adaptive Management in Alberta's Energy Resources Sector. UBC Law Review, **50**(3): 697–796.

Ott, T. 2017. Finding the interface between mining, people, and biodiversity: a case study at Richards Bay Minerals. Journal of the Southern African Institute of Mining and Metallurgy, **117**(1): 1–5.

Peck, R.B. 1969. Advantages and Limitations of the Observational Method in Applied Soil Mechanics. Géotechnique, **19**(2): 171–187.

Peterson, R.A., Humphries, S.A., and Unger, M.L. 2015. Adaptive risk management and lessons learned : post-closure at the "mighty" Sullivan mine. 10th International Conference on Mine Closure, Vancouver, Canada, June 1-3, 2015. 12 pp.

Pollock, G., Liu, X., McRoberts, E., Williams, K., Wells, P.S., and Fournier, J. 2010. Suncor oil sands tailings pond capping project. 14th Annual Tailings and Mine Waste Conference, Vail, Colorado, October 17-20, 2010. 13 pp.

Poscente, M., and Charette, T. 2011. Criteria and indicator framework for oil sands mine reclamation. 6th International Conference on Mine Closure, Lake Louise, Canada, September 18-21, 2011. 8 pp.

Robertson, P.K., de Melo, L., Williams, D.J., and Wilson, G.W. 2019. Report of the Expert Panel on the Technical Causes of the Failure of Feijão Dam I.

Schafer, H.L., Beier, N.A., and Macciotta, R. 2021. A Failure Modes and Effects Analysis Framework for Assessing Geotechnical Risks of Tailings Dam Closure. Minerals, **2021**(11): 1234.

Schafer, H.L., Beier, N.A., and Macciotta, R. 2022. Applying a Generalized FMEA Framework to an Oil Sands Tailings Dam Closure Plan in Alberta, Canada. Minerals, **2022**(12): 293.

Schafer, H.L., Macciotta, R., and Beier, N.A. 2020. Tailings dam closure scenarios, risk communication, monitoring, and surveillance in Alberta. CIM Journal, **11**(1): 80–90.

US EPA. 2002. EPA Superfund Record of Decision: Bunker Hill Mining & Metallurgical Complex.

Watson, A.S., Merovich, G.T., Petty, J.T., and Gutta, J.B. 2017. Evaluating expected outcomes of acid remediation in an intensively mined Appalachian watershed. Environmental Monitoring and Assessment, **189**: 339.

Williams, B.K., Szaro, R.C., and Shapiro, D. 2009. Adaptive Management: The U.S. Department of the Interior Technical Guide.

Young, R., Manero, A., Miller, B., Kragt, M., Standish, R., and Boggs, G. 2019. A framework for developing mine-site completion criteria in Western Australia. The Western Australian Biodiversity Science Institute.

FLUID TAILINGS THERMAL DRYING: MORE PROMISING THAN YOU MIGHT THINK

Jonathan Matthews, Magpie Consulting Inc. Calgary, Alberta, Canada

ABSTRACT

Canadian oil sands mining operations contribute strongly to Canadian energy security and prosperity. Canada will continue to need oil from Canadian oil sands mines for decades to come, even as environmental performance expectations increase. Reducing GHG emissions and fluid tailings (FT) associated with oil sands mining operations could enhance stakeholder and shareholder support for oil sands mining operations.

Fluid Tailings Thermal Drying (FTTD) offers the potential to convert FT into immediately trafficable deposits, enhance water reclamation and conservation efforts, and accelerate the establishment of healthy and self-sustaining terrestrial, wetland, and aquatic ecosystems while enhancing overall efficiency of oil sands mining operations and reducing fugitive GHG emissions such that overall GHG emissions from oil sands mining operations decline.

Additional potential environmental benefits include better management of the acid generation potential and naturally occurring radioactivity associated with minerals concentrated in froth treatment tailings (FTT), reduced risk of FT discharge from tailings storage compounds due the loss of containment integrity, and reduced potential for harmful interaction due to wildlife contact with FT.

FTTD will be most energy and cost efficient when coupled with a preliminary concentration step such as pond settling, centrifugation, thickening, accelerated dewatering, and thin lift fines drying and where the recovered heat is used to offset incumbent sources of hot water such as auxiliary boilers. FTTD could be especially attractive to mine sites with upgrading facilities, which may have 'surplus' heat that can be used to drive the drying process.

In short, FTTD has the potential to be a 'poster child' for COSIA's goal to *"… significantly reduce greenhouse gas emissions, significantly reduce water use, minimize land disturbances, and reclaim land faster.",* especially given the potential to also reduce oil sands mining operating expenses.

This paper will describe FTTD and provide two conceptual FTTD implementation scenarios that illustrate significant potential to enhance the environmental., social, and governance (ESG) performance of oil sands mining operations.

Contrary to widely held belief, implementation of FTTD can contribute to reduced GHG emissions for oil sands mining operations.

INTRODUCTION

Purpose

The purpose of this paper is to challenge preconceived notions and biases respecting the potential of FTTD processes.

There are currently two 'immutable truths' about commercial oil sands mining operations:

- bitumen extraction requires hot water, and,
- aqueous extraction produces FT.

This paper explores the potential to exploit the untapped synergy between these two truths. By thinking of the FT as a primary source of hot water for extraction processes, rather than a waste stream to be dealt with after bitumen extraction, it may be practical to curtail FT, reduce GHG emissions, and accelerate reclamation efforts while reducing operating costs.

The paper has been written to spark dialogue within the oil sands tailings innovation community and encourage a more comprehensive, transparent, and objective assessment benefits of FTTD.

This paper does not presume to *conclude* that the net environmental and economic benefits are positive for oil sands operations. Rather, the paper seeks to illustrate realistic implementation scenarios where the application of FTTD appears to have a *high potential* to enhance the environmental

and economic performance of oil sands mining operations.

The ideal outcome of this discussion would be formation of a collaborative multi-disciplinary initiative charged with the task of determining which FTTD implementation scenarios warrant further development and demonstration.

Background & Context

FT management is a significant economic burden for oil sands mining operations. Large volumes of FT require construction of costly impoundments, are a source of fugitive GHG emissions, hinder mine operations efficiency, and hinder progressive reclamation efforts. (McKinley, Sellick, Dawson, & and Hyndman, 2018).

All key stakeholders support efforts to transform FT into trafficable tailings that can support terrestrial reclamation in a reasonable time. A summary of the issues associated with oil sands FT, including government policy and regulations influencing the FT innovation landscape, are provided in a companion paper (Matthews, Government Policy and Regulatory Influence on Oil Sands Tailings Innovation, 2022) so that this discussion can focus on assessing the potential of thermal drying of FT.

Within this context, oil sands operators have identified three top priorities for collaborative tailings innovation:

- addressing the accumulation of fluid fine tailings (FFT) within tailings ponds through the development of new and improved tailings management technologies,
- treating process affected water, and,
- accelerating the reclamation of the resulting tailings deposits (COSIA, 2021).

Other outcomes desired of novel FT treatment processes include:

- mitigation of fugitive GHG emissions from FT (Suncor Energy Operating Inc, 2021),
- enhanced mine operations efficiency (McKinley, Sellick, Dawson, & and Hyndman, 2018),
- reduced FT management and reclamation costs (McKinley, Sellick, Dawson, & and Hyndman, 2018),
- recovery and reuse of water from fluid tailings deposits to enhance freshwater conservation efforts (COSIA, 2021),
- establishing optimum tailings water content to facilitate trafficability (Alberta Energy Regulator, 2017) (Hyndman, 2019),
- recovery and reuse of heat from warm extraction tailings and hot froth treatment tailings streams (Murray Gray, 2009), and,
- optionality to mitigate concerns associated with minerals that represent environmental and health risks, especially naturally occurring radiative minerals and potentially acid generating mineral constituents concentrated in the froth treatment tailings streams (Van Dongen, et al., 2021).

The FTTD implementation scenarios presented in this paper will demonstrate that FTTD has the potential to contribute to mitigation of all the challenges listed above while maintaining the primary focus of the three COSIA tailings innovation priorities.

FTTD PROCESS INTRODUCTION

An elegant potential solution to overcoming the challenge of clay fines suspension stability is to drive the water from the solids via evaporation in a controlled and efficient manner. FTTD delivers on this opportunity with precision. No chemicals are required so the primary operating expenses associated with FTTD are personnel, electricity for pumps and blowers, and heat. These costs are expected to be modest relative to the numerous significant benefits expected with FTTD.

In the simplest manifestation of FTTD, the FT is split into a solids stream and a vapor stream by evaporating the water from the FT in a drying vessel. The flue gas is ‘scrubbed’ in a cyclone to remove any fine particles and the water vapor in the flue gas can be recovered through condensation for reuse in plant operations. The solids stream is dry, readily compactable using heavy earth moving equipment, and requires much less storage volume and engineering controls.

Thermal drying processes are used extensively at industrial scale across a range of application types including mineral processing and food processing. The technology is mature and there are no significant technical uncertainties to suggest that the process will not be effective in treating oil sands FT.

Dispersion dryers are the preference for oil sands mining applications. Unlike spray dryers, dispersion dryers can process fluid fine tailings solids concentrations up to 65wt% solids without dilution. The FTTD drying circuit can accommodate a wide range of FT compositions (i.e., mineralogy, particle size distribution, and water & hydrocarbon content), The final target solids content can be tuned to deliver optimal water content and favourable geotechnical properties. The ability to treat a wide range of slurry concentrations makes dispersion thermal drying of FT amenable to receiving slurry directly from incumbent primary thickening processes, including:

- high density FT reclaimed from settling ponds, e.g. 45 – 65wt% solids at Canadian Natural's Horizon Mine (Canadian Natural, 2021), 40-50wt% solids fluid tailings at Fort Hills (Suncor Energy Operating Inc, 2021), and 45.7wt% fluid tailings used as feed to Syncrude centrifugation operations (Syncrude Canada Ltd, 2021),
- high-rate and/or paste thickener underflow, e.g., Average SG = 1.41 for Horizon thickener underflow is approximately 47wt% solids concentration. (Canadian Natural, 2021), design basis of 40 – 50wt% solids for Imperial Oil's Kearl Mine (Imperial, 2021),
- accelerated dewatering product at 50 – 60wt% solids (Syncrude Canada Ltd, 2021),
- centrifuge cake, e.g., 54.7wt% average solids content for Syncrude's 2020 centrifugation cake (Syncrude Canada Ltd, 2021), and,
- thin lift sub-aerial deposits at 40 – 65wt% solids.

FTTD treatment of FT that has been pre-concentrated will reduce the energy required per tonne of solids processed. CAPEX and OPEX will be inversely proportional to the dryer feed solids content for a given solids throughput rate. Therefore, the bias in developing FTTD scenarios is to feed the drying circuit with the densest FT available.

Figure 1 illustrates the FFTD concept. In this illustration the process is used to treat 50wt% solids FT such that a trafficable 80wt% solids tailings deposit is created[1]. The heart of the process is a dryer which enables rapid drying of high moisture wet cakes, pastes, or slurries. The FT stream is introduced to a hot air stream by a mechanical screw auger where high-speed dispersion plates rotate and spread material into a thin layer along the periphery of the dryer. A heated air stream passes through and conveys the wet material, flashing off moisture. The water is separated from the fine mineral solids. The solids stream is dry to the touch after just a few moments in the dryer, enabling high throughput from a modest equipment footprint.

The dispersion drying process creates small granules of dry solids and the particle size can be tuned through equipment design and piloting efforts. The FTTD solids produced is drier than necessary to facilitate rapid and low-cost compaction, capping, and reclamation. This means that only a portion of the FT needs to be fed to FTTD to convert all the FT into a trafficable deposit. The implementation scenarios to be presented will combine FT and FTTD solids in proportions that produce a deposit that is trafficable and amenable for terrestrial reclamation.

The FTTD product can be transported to the final disposition point and blended with FT before placement, or the FTTD solids and FT can be blended at the FTTD plant before transportation to the final disposition site. In either scenario, the final product will be managed such that it is trafficable with heavy mine equipment and amenable to terrestrial reclamation.

Given the extreme priority to reduce the overall GHG footprint of oil sands mining operations it is essential to integrate processes such the net GHG emissions are reduced for mining operations. By looking at opportunities for heat recovery and reuse coupled with mitigation of fugitive GHG emissions from oil sands tailings ponds there appear to be legitimate FTTD implementation pathways with the potential to enhance the economic and environmental performance of oil sands mining operations. These opportunities will be discussed in the thermal drying scenario discussions.

FTTD Literature Review

The concept of separating FT into a water stream and a solids stream seems an obvious option to evaluate given the desire to reduce FT and to reclaim water for reuse. However, there is little discussion in the public domain that explores the

[1] Noting that the 80% final solids target may be more aggressive than needed to achieve all the benefits of the drying process. As will be discussed in the paper, CNRL has reported tailings deposits from pressure filtration trials with an average 63% solids content were deemed trafficable with a D6 dozer

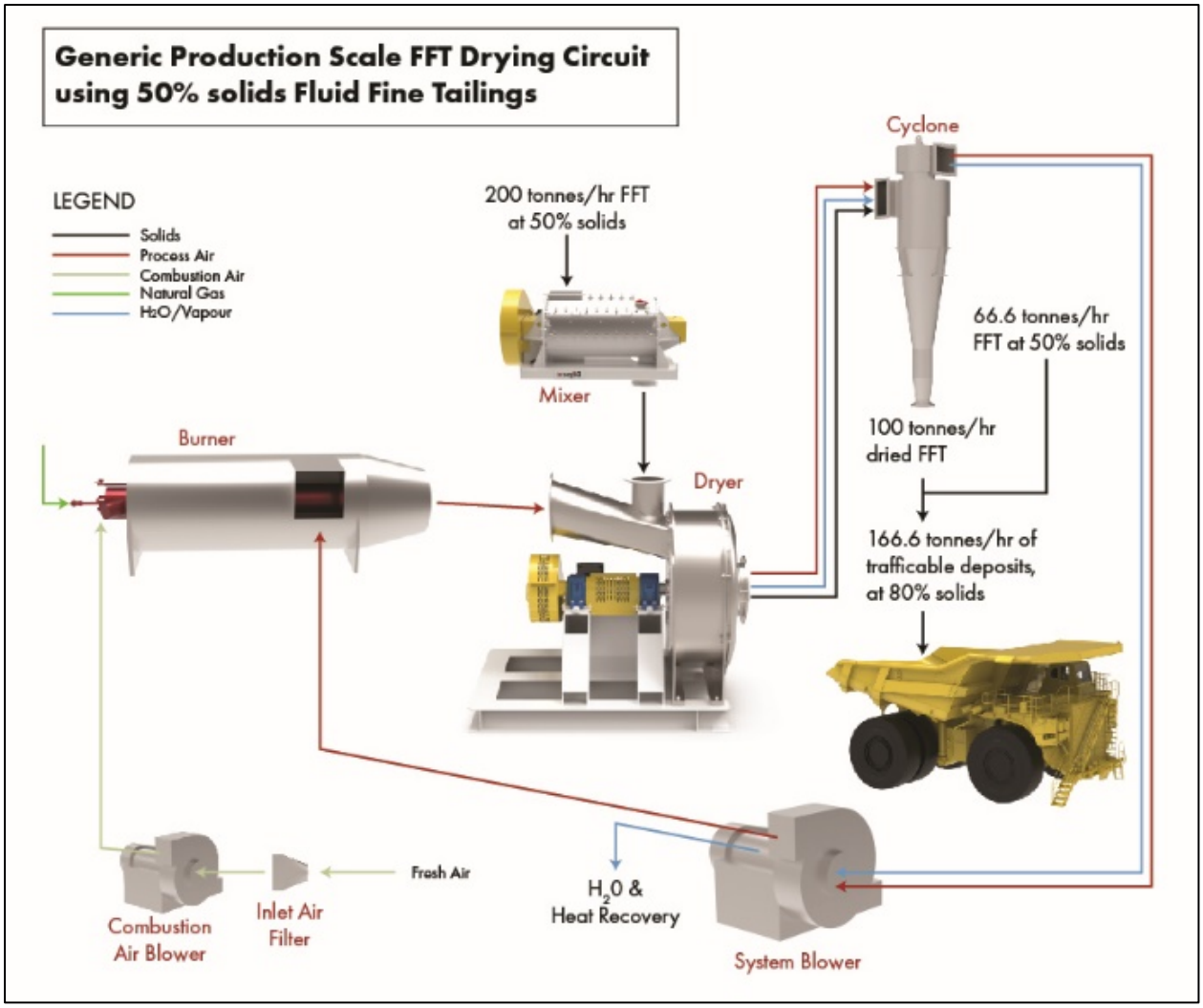

Figure 1. Generic Production Scale Fluid Tailings (FFT) Drying Circuit

potential of thermal drying of FT in an oil sands context. Below is a summary of the information found in the public domain.

Discussion of the application of thermal drying of oil sands FT first appears in the public domain in 2012 in a paper presented at the Third International Oil Sands Tailings Conference (IOSTC) titled *"The MITD Process for Dealing with MFT"* (Bonem, 2012)[2]. The paper concluded that drying of MFT using a thermal process, coupled with heat recovery from the drying process, showed potential to help oil sands mine operators meet the ERCB D-074 tailings strength performance requirements[3].

The concept of thermal drying of MFT was included in the 2012 Tailings Technology Roadmap Assessment. The technology was flagged as a high potential technology and was recommended as a high priority for further evaluation by the oil sands operators (CTMC, 2012).

Since the road map was published, pilot scale work has been done using oil sands FT. This work demonstrated that the MITD process is effective in separating FT into a solids stream and a vapor/water stream as proposed (Bepex LLC, 2021).

[2] MITD stands for MFT to Immediately Trafficable Deposits, where MFT is synonymous with FT; this is synonymous with FTTD.

[3] ERCB D-074 and associated FT strength performance criteria were rescinded in 2015

A 2018 report, commissioned by COSIA, evaluated the economics of five different tailings technology deployment scenarios. One of the scenarios evaluated was centrifugation of MFT followed by thermal drying of the centrifuge cake. The report concluded that *"Thermal drying could be an attractive component of FFT management if high energy recovery and reuse can be achieved without negating other energy efficiencies.*", and, *"Economics and energy efficiency for method feasibility requires recovery of 80% of the thermal-drying heat[4].".* With respect to the thermal drying scenario the report also notes *"The process has been piloted for COSIA by BEPEX but unlike the other tailings treatment technologies it has not been implemented at commercial scale"*.[5] The report concludes that the net mining costs decreased by adding a thermal drying step after centrifugation of FT. That is, the overall economics were improved by drying the centrifuge cake because of reduced materials handling costs, reduced fluid containment requirements, and enhanced mine efficiencies[6] (McKinley, Sellick, Dawson, & and Hyndman, 2018).

All public sources found in this literature review indicated that FTTD of oil sands FT has potential to enhance the economic and environmental performance of oil sands mining operations.

Synergies with In-Pit Extraction Process (IPEP)

The benefits of fines drying reported by McKinley et al (2018) are echoed in CNRL's description of the benefits In IPEP which is being developed by CNRL[7] because it produces dry stackable tailings, with no fluid tailings. Eliminating FT facilitates operational efficiencies including the *"Potential to reduce production costs by approximately $1 to $2/ barrel while substantially reducing tailings management costs and liabilities",* and *"Reduce GHG emissions by up to 40% in bitumen production compared to conventional oil sands mining…"*, and, *"Accelerate reclamation, reduce and avoid fugitive emissions, and potentially eliminate the need for future fluid tailings ponds through the production of dry stackable tailings."* (CNRL, 2021).

Deployment of FTTD has the potential to deliver incremental sustainability improvements that are comparable to IPEP. FTTD could also be used to complement IPEP by a local source of hot water for the extraction process and by reducing the size and complexity of the fines drying circuit.

FTTD IMPLEMENTATION SCENARIOS

The paper considers two conceptual FTTD implementation scenarios:

1. Thermal drying of FT after coagulation, flocculation, and centrifugation. An alternative to this scenario, scenario 1A, will consider by-passing chemical treatment and centrifugation, thereby feeding the centrifuge feed directly to FTTD, and,
2. Feeding 100% of froth treatment tailings (FTT) to the FTTD process, after an initial 'black box' concentration step.

Effective management of the energy footprint of FTTD is important. The gross environmental footprint is a function of energy consumed in the drying process. For the scenarios considered in this paper it is assumed that the heat source is from combustion of natural gas with air and that electricity will be necessary to run the pumps and blowers. The combination of combustion and electrical demand will define the gross energy and GHG emissions footprint of the FTTD process for the scenarios reviewed and it is assumed that 90% of the heat used to affect separation of water from solids is recovered for reuse[8]. The recovered heat will offset natural gas that would otherwise be consumed in support of bitumen extraction activities, for example though use of auxiliary boilers.

The scenario discussions assume that there is no 'surplus'[9] heat available on the mine site. If specific mine sites do have 'surplus' heat, for example from on-site upgrading operations, the surplus heat could

[4] This paper will present two conceptual implementation scenarios where the integration of FTTD into existing oil sands mine operations has the potential to exceed the 80% heat recovery threshold.

[5] Although thermal drying has not been implemented at commercial scale in an oil sands setting the technology has been deployed at commercial scale across a range of mineral processing applications, including drying of kaolin slurries.

[6] Potential cost savings would be higher if monetary value were assigned to the benefits of enhanced water conservation, reduced tailings liability costs, accelerated reclamation at lower cost, and reduced fugitive GHG emissions potentials.

[7] With generous financial support from the GoC and GoA,

[8] There are different potential pathways to achieving 90% heat recovery. To determine the optimal pathway would it is necessary to assess current and future site-specific energy balances.

[9] In this context 'surplus' means heat that exceeds operational needs of the integrated mine site operations.

be used to enhance the potential of FTTD by using the surplus heat for FT drying operations.

Target Solids Content

There is a need to establish a target solids content for the FTTD deposits. The strategy used for all scenarios is to blend FTTD solids and FT in proportions such that the final product is at an optimum solids content that is trafficable.

This paper leverages Canadian Natural's 2019 experience piloting pressure filtration of FFT (Canadian Natural, 2021) to establish a target water content for trafficability of treated FT. CNRL treated FT with coagulants and flocculants and then extracted water from the FT using pressure filtration technology.

Canadian Natural reports that the FT treated using pressure filtration had a solids content ranging from 50 to 70 wt%, averaging 63 wt% solids for the 2019 pilot program. With an average of 63 wt% solids, the filtered tailings were found to be "… *immediately trafficable with a D6 dozer.*", and *"…able to immediately produce upland reclamation ready products from FFT"*. The pressure filtration deposits were found to have peak vane strengths of 15 to 60 kPa within one to three months of placement and 40 to 88 kPa one year after placement (Canadian Natural, 2021). A trafficability threshold of 63 wt% solids for centrifuged FT will seem low to the geotechnical community, even for a low ground pressure D6, however the vane strengths reported after one to three months and after one year clearly indicate that the deposits had developed sufficient geotechnical integrity to be considered trafficable.

As another reference point, Syncrude has indicated in regulatory filings that the expected final solids content of centrifuged FT deposits scheduled for capping and terrestrial reclamation *"… will be in the range of 70 – 75 percent"*. These are projected values after deep CFT deposits have undergone decades of consolidation and have been surcharged with capping materials (AER, 2019).

CNRL did not report the detailed composition of the FT used in the pressure filtration trial, so it is assumed that Syncrude's FT and CNRL's FT have similar mineralogical profiles, particle size distributions, and hydrocarbon contents. Thus, the solids content at which the treated FT becomes trafficable is assumed to be the same for either feed stream used in the scenarios analyses, irrespective of the source and history of the FT.

To accommodate for the various uncertainties, this paper targets a solids concentration of 67% solids for the final blended FTTD product to be considered in the implementation scenarios. This is 4% higher than the trafficability threshold reported by CNRL for pressure filtered product and 3 to 8% lower than the values proposed by Syncrude for normally consolidated centrifuge cake deposits.

In practice, the optimal solids content for a specific FT composition can only be determined with confidence via field trial demonstrations where the effects of clay mineralogy, particle size distribution, climate effects, deposition rates, and lift thicknesses on geotechnical performance can be assessed.

If a higher target FTTD product density is required than the 67 wt% used in the scenario evaluations it is a simple matter to tune the ratios of untreated FT and FTTD processed FT, without significantly impacting the overall material and energy balance calculations or net GHG emissions footprint.

Calculating Net GHG Footprint

The predictions for Scenarios 1, 1A, and 2 have been calculated using a dispersion drying energy balance model that was made available to the author for the purpose of assessing these scenarios. A detailed description of the model is beyond the scope of this paper however key parameters used for calculating the gross and net energy and GHG emissions footprint of the thermal drying process are:

- Specific heat of water: 4186.7 J/kg^{o}C
- Specific heat of solids: 284 J/kg^{o}C
- Specific heat of steam: 1884 J/kg^{o}C
- Specific heat of methane: 3349. J/kg^{o}C
- Electrical demand: 50.3 kWh per tonne of solids processed
- Ambient air temperature: 10^{o}C
- FT feed temperature: 10^{o}C
- FTTD Outlet temperature: 116^{o}C
- Heat recovered from combustion: 90%
- 0.395 tonnes CO_2e emitted per MWh of electricity used
- 50.2 kg CO_2e per GJ of methane combusted.

Mitigation of Fugitive GHG Emissions

A discussion of the nature and scale of fugitive GHG emissions from oil sands tailings is presented in a companion paper (Matthews, Government Policy and Regulatory Influence on Oil Sands Tailings

Innovation, 2022). This paper presumes that the reader has reviewed the companion for background on fugitive GHG emissions from oil sands tailings.

For simplification, the scenario discussions will assume that FT is derived from naphtha-based froth treatment processes and that all fugitive GHG emissions estimates are calculated using the Burkus model described in the companion paper.

The reference cases will assume an anaerobic depositional environment for the FT whereby most of the solvent with undergo methanogenesis to produce methane as the primary emission.

The FTTD implementation scenarios will assume an aerobic environment for the FTTD solids where a small fraction of the solvents may volatilize, and the rest of the solvent will undergo aerobic decomposition to produce primarily CO_2.

The differences between the FTTD implementation scenario and the reference case will be presented for each scenario to show that drying of FT containing residual solvents has the potential to reduce the magnitude of fugitive GHG emissions from oil sands tailings.

Other environmental benefits

Additional potential environmental benefits can be contemplated due to the conversion of FT into trafficable tailings using FTTD, including:

- reduced risk of FT discharge from tailings storage facilities, in the event of loss of containment integrity,
- mitigation of acid generation potential associated with pyritic minerals concentrated in FTT,
- improve management and mitigation of OH&S hazards associated with naturally occurring radioactive materials (NORMS) concentrated in FTT,
- reduced potential for harmful interaction due to wildlife contact with FT,
- faster establishment of healthy and self-sustaining terrestrial, wetland, and aquatic ecosystems.

The scenario evaluation discussions will constrain the discussion of the environmental benefits of FTTD to reduced FT volumes, reduced GHG emissions, and water recovery potential. The scenarios represent forecasts only and the magnitude of benefits realized will depend on the composition, age, and treatment of the FT being treated. Future discussions of FTTD can be expanded to include more detailed evaluation of the full breadth of potential environmental benefits.

FTTD IMPLEMENTATION SCENARIOS

Two conceptual FTTD implementation scenarios are presented:

- Scenario 1 contemplates treating centrifuge cake using FTTD. An alternative version, Scenario 1A, contemplates by-passing the centrifuge, thereby avoiding the expense associated with centrifugation.
- Scenario 2 contemplates treating froth treatment tailings (FTT) with thermal drying, after an initial preliminary dewatering step.

There is a reference case for each scenario. The reference case serves as a proxy for status quo operations so that the net effects of FTTD can be evaluated.

Reference Case for FTTD Scenario 1 and 1A

Scenario 1 and 1A use Syncrude's experience with centrifugation of FT for reference. Centrifugation of FT is an incumbent FT treatment technology being used by Syncrude and Canadian Natural (Syncrude, 2021) (Canadian Natural, 2021). Centrifugation of FT results in an incremental densification of the FT however the centrifuge cake produced is not trafficable and will require decades to consolidate if produced as deep deposits (Hyndman, 2019) (Canadian Natural, 2021).

The centrifuge reference case uses information reported for MFT centrifuge operations at Syncrude's Mildred Lake operations. Syncrude's 2019 centrifugation experience guides the FFT composition assumptions, and Syncrude's 2020 centrifugation operation experience guides the FFT throughput assumptions.

For Scenarios 1 and 1A the mass of FT processed by Syncrude's centrifuge plant in 2020 will be converted to trafficable tailings using FTTD. In 2020 Syncrude processed 4.1 Mm^3 of FT at the Mildred Lake Centrifuge Plant and produced 3.4 Mm^3 of CFT with an average solids content of 54.7 wt% solids, representing a dry solids throughput of 2.81

MT per hour[10] (Syncrude Canada Ltd, 2021). The FT composition was not reported for 2020 however in 2019 the FT feed to the centrifuge plant averaged 45.7 wt%[11] solids, so this value is used as the feed solids concentration for the reference case. The FT was treated with coagulant and polyacrylamide flocculants prior to centrifugation. The CFT product (aka 'cake') was placed in a dedicated mine pit (Syncrude Canada Ltd., 2020). Consolidation of the centrifuge cake is expected to take several decades before the mineral solids are considered consolidated (AER, 2019) (Hyndman, 2019).

In 2020 Syncrude reported that the total mass of mineral solids added to the FT inventory was 15.8 MT (Syncrude Canada Ltd, 2021) and the total bitumen production was 118.8 Mbbls (Syncrude, 2021). Thus, on average 133 kg of mineral solids reported to FT per barrel of bitumen produced. In the reference case 2.81 MT of mineral solids are processed at the centrifuge plant, representing 17.8%[12] of the 2020 production total at Mildred Lake operations. This infers Scenario 1 is reducing the FT inventory associated with the production of approximately 21 Mbbls of bitumen[13].

Syncrude runs light diluent at their Mildred Lake operations so the Burkus model predicts the fugitive GHG emissions attributable 21 Mbbls of bitumen would be 107,610 T CO_2e.[14]

Syncrude does not report on naphtha contents for the FFT fed to the centrifuge plant, so this calculation assumes that the diluent content in Syncrude's FFT is homogenous. The actual diluent content in the FFT fed to CFT, and the associated fugitive GHG emissions footprint potential, may be higher since all the FTT for Syncrude's Mildred Lake and Aurora North mining operations have been discharged into in the Mildred Lake Settling Basin settling for years, effectively increasing expected diluent content per tonne of mineral solids treated using centrifugation. Conversely, the diluent content may be lower than modelled since there have already been decades of fugitive methane emissions from the Mildred Lake Storage Basin.

Scenario 1 FTTD after centrifugation

For application Scenario 1 (Figure 2) a portion of CFT is treated using FTTD. The FTTD solids are then blended with the remaining CFT to create a trafficable deposit. The proportion of CFT directed to the dryer was calculated such that the final solids content of the recombined tailings will be a trafficable deposit at 67wt% solids, per the earlier discussion of CNRL's experience with pressure filtered FT[15].

In Scenario 1 FTTD is used to treat 1.37 Mm^3 of CFT cake at 54.7 wt% solids. Thus, 1.37 Mm^3 of CFT is treated over the course of a year to give an average CFT feed rate of 157 m^3/hr (238 T/hr)[16]. Two streams will leave the thermal drying plant: 130 T/hr of dry mineral solids and 94 T/hr of water vapor and combustion exhaust gases. The vapor is cooled and condensed to produce hot water to support operational needs.

Next, 130 tonnes/hr of FTTD solids are mixed with 349 tonnes/hr of CFT cake to transform 3.36 MT tonnes of CFT cake, with no meaningful strength, into 2.5 Mm^3 of trafficable fines tailings while producing almost 1 Mm^3 of hot clean water over the course of a year.

In reference case 1, the CFT product is placed in a deep storage cell where consolidation is expected to take several decades before the mineral solids are considered consolidated (Hyndman, 2019). In Scenario 1, 41% of the CFT is processed using FTTD and the FTTD solids are blended with the remaining 59% of CFT to produce a final trafficable deposit at 67 wt% solids. In this scenario all the CFT produced by Syncrude in 2020 would be transformed into trafficable tailings.

Scenario 1A FTTD of Centrifuge By-Pass

For Scenario 1A (Figure 3) all FT by-passes the centrifuge plant. Thus, 54% of the FT is fed directly to FTTD, without any treatment using coagulants or

[10] CNUL reported production of 1.4 Mm^3 of centrifuge cake (0.88 MT of fine solids) at the JackPine Mine for the 2019 – 2020 reporting period in the 2020 AER State of Tailings Report.
[11] 2019 Average FFT To Centrifuges was 0.3 MT (5%) bitumen, 3.0 MT (49%) water, 2.8 MT (46%) solids, with the mineral solids fraction comprising 0.3 MT (11%) coarser than 44 um and 2.5 MT (89%) finer than 44 um).
[12] That is 2.81 MT of solids processed using centrifugation versus 15.8 MT of mineral solids reported in new FFT inventory for Syncrude in 2020
[13] That is 17.8% x 118.8 Mbbls of bitumen
[14] That is 5.1 kg CO_2e per barrel of bitumen produced x 21.1 Mbbls = 107,610 T CO_2e
[15] For simplicity, it is assumed that the CFT is comprised only of mineral solids and water for solids content calculations. In practice the bitumen will remain with the solids fraction. The bitumen is not expected to have a meaningful impact on the geotechnical properties of the FTTD deposit nor the thermal efficiency of the drying process.
[16] Assuming steady treatment over the course of one year 1.2 Mm^3 would require drying of 137 m^3/hr of CFT. At 54.7% solids x 1.51 T/m^3 of CFT = 207 T/hr of 54.7% solids centrifuge cake

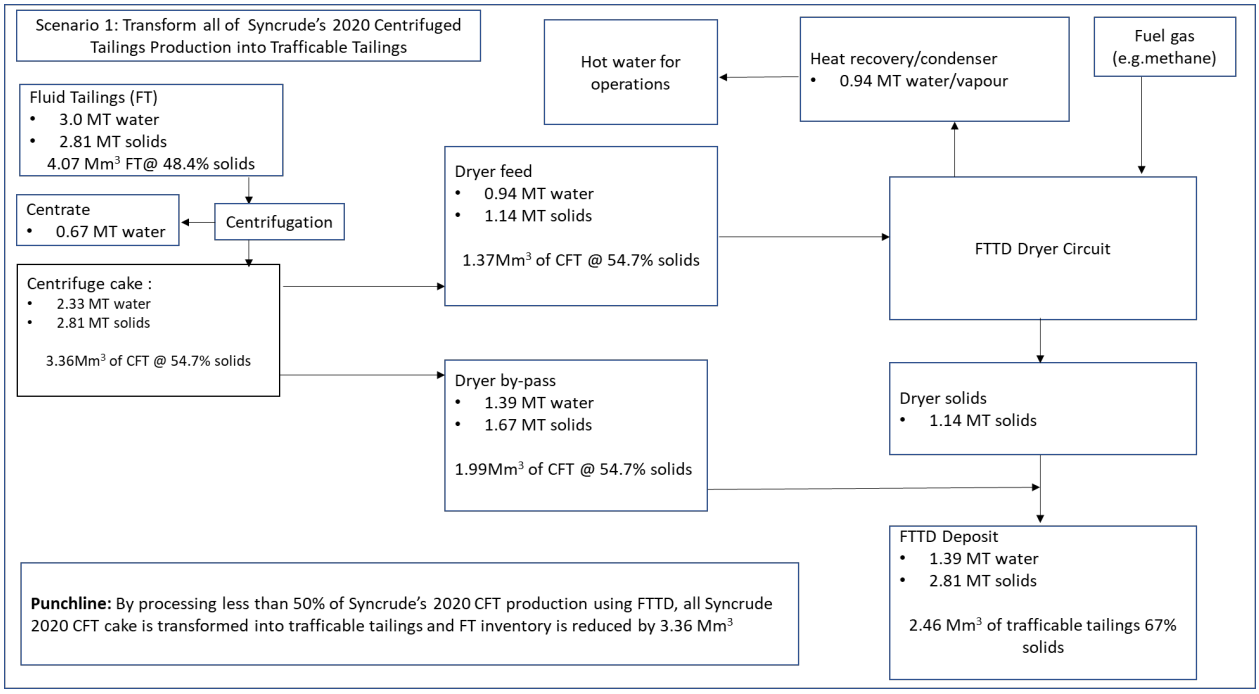

Figure 2. Scenario 1: FTTD Centrifugation

flocculants. The FTTD solids stream is then combined with the remaining 46% of FT to create a final deposit at 67 wt% solids.

As in Scenario 1, the proportion of FT to FTTD is managed such that the final solids content of the combined tailings will be a trafficable deposit at 67wt%. In this scenario all coagulation, flocculation, and mechanical centrifugation steps are eliminated.

In Scenario 1A 2.2 Mm^3 of FT at 48.4 wt% solids are treated using FTTD. Processing 2.2 Mm^3 over the course of a year gives an average hourly feed rate of 252 m^3/hr (359 T/hr)[17] to the FTTD plant. Two streams leave the FTTD plant comprising 173 T/hr of dry mineral solids and 186 T/hr of water vapor and combustion exhaust gases. The water in the vapor can be cooled and condensed to produce hot water to support operational needs. The 173 T/hr of dry solids are mixed with 306 T/hr of FT to transform 4.07 Mm^3 of centrifuge plant feed into 2.45 Mm^3 of trafficable tailings while reclaiming 1.6 Mm^3 of water over the course of the year.

Scenario 2 Reference Case

The reference case for Scenario 2 is derived from Stantec's "Material and Energy Balance for an Oil Sands Surface Mining and Bitumen Extraction Reference Facility" report (Stantec, 2021). Stantec's report supplies four heat and material balances based on ore grade (low or high) and type of froth treatment process (naphthenic or paraffinic) for a generic 200,000 bbl/day bitumen production plant.

For Scenario 2 the "COSIA Mining & Extraction High Grade - Naphthenic Froth Treatment - Material and Energy Flow" material balance prepared by Stantec is used as the source of the FTT properties[18].

The Stantec model indicates there are 1,019 tonnes/hr of NRU comprised on 2wt% bitumen, 76 wt% water, 22 wt% solids, and 0.4wt% diluent at a temperature of 40C.

The material balance assumes no further treatment of the FFT other than end-of-pipe tailings discharge to a tailings settling basin where the bitumen, naphtha, and mineral solids will contribute to the formation of FT.

The Burkus model is used to estimate fugitive GHG emissions for the Scenario 2 reference case. The reference case treats 100% of the FFT from a

[17] Assuming steady treatment over the course of one year 1.2 Mm^3 would require drying of 137 m^3/hr of CFT. At 54.7% solids x 1.51 T/m^3 of CFT = 207 T/hr of 54.7% solids centrifuge cake

[18] In the report the froth treatment tailings are referred to as Naphtha Recovery Unit (NRU) Tailings

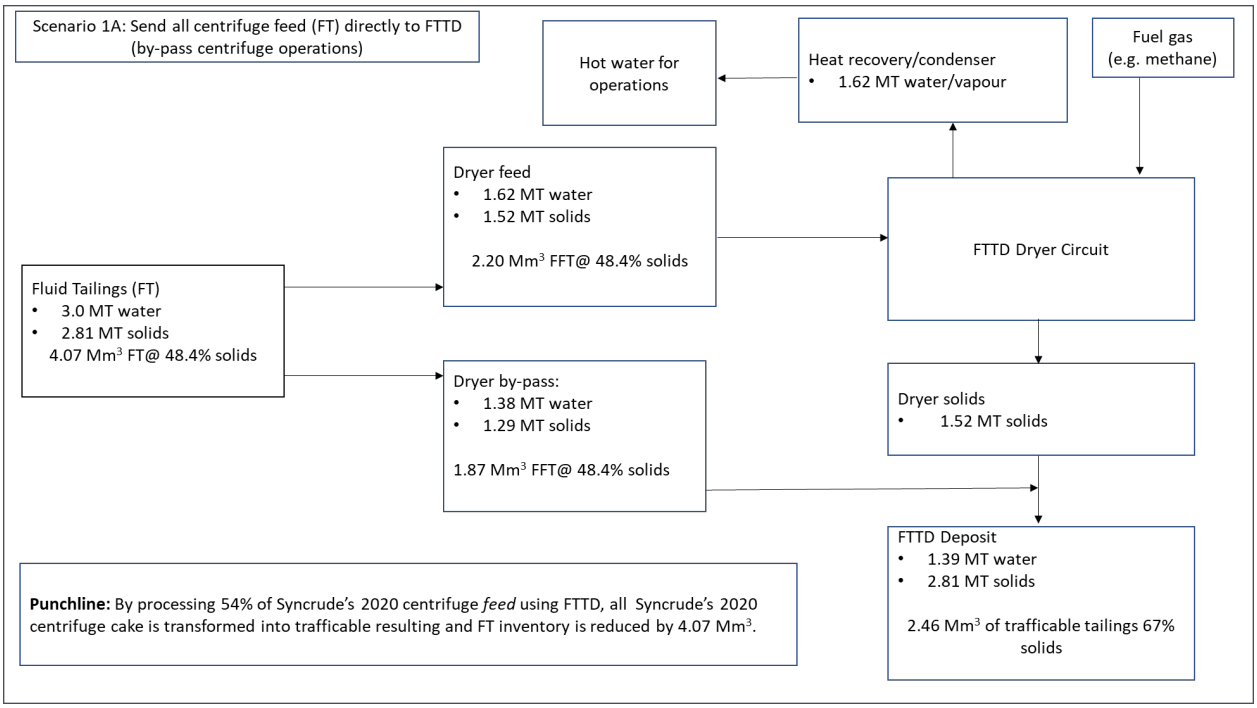

Figure 3. Scenario 1A, By-Pass Centrifuge Plant, CFT Feed direct to FTTD

generic 200,000 bbls bitumen per day production plant, using light naphtha froth treatment tailings.

Therefore, using the Burkus model the expected fugitive GHG emissions attributable to the fluid tailings deposited straight to a tailings management facility is 372,300 T CO_2e per year[19].

Environmental Footprint, Scenarios 1 and 1A

The fines drying model was used to estimate the thermal and electric demands of the thermal drying process as a function of feed solids concentration, feed solids temperature, and final target solids content. The reference case attributed 107,610 T of fugitive CO_2e emissions to the CFT produced, excluding the GHG emissions associated with the centrifugation plant operation.

Fugitive GHG emissions are reduced by up to 82% by treating the CFT with FTTD and placing the FTTD product subaerially to prevent methanation. Thus, the net abatement value for Scenarios 1 and 1A is 88,242[20] T of CO_2e. For the assumptions made, the *net* GHG emissions reduction for Scenarios 1 and 1A are 52,741 T CO_2e/yr (Figure 4), and 35,901 T CO_2e/yr (Figure 5), respectively. The GHG abatement for Scenario 1A would be greater if the effect of removing the centrifuge step were included in the analysis.

Scenario 2 NRU/FTT Treated with FTTD

For Scenario 2 (Figure 6) it is assumed the NRU[21] tailings undergo a preliminary treatment to increase the solids content to 50 wt% solids. The preliminary dewatering step is a 'black box' for this discussion. The preliminary 'black box' concentration might be conventional gravity settling in a dedicated NRU receiving pond, thin lift drying, flocculation and thickening in a paste thickener, accelerated dewatering, or even centrifugation.

Given the low solubility of the naphtha in water and the close association of the bitumen with the fine mineral solids it is assumed that 533.9 m^3 of water per hour is removed from the froth treatment tailings by the 'black box' dewatering step, prior to thermal drying and the balance of water, naphtha, bitumen, and mineral solids are directed to thermal drying or

[19] 5.1 kg CO2e /bbl of bitumen x 200k bbls bitumen/day x 365 days/yr x 1 tonne/ 1000 kg = 372,300 tonnes CO2e per year

[20] Fugitive GHG emissions for Scenario 1 and 1A reference cases is 143,796 tonnes CO_2e. Preventing methanation through strategic deposition could facilitate a 82% so the abatement potential is 107,610 T CO_2e x 82% = 88,240 T CO_2e.

[21] Consider FTT, NRU, and FT as synonymous for this discission

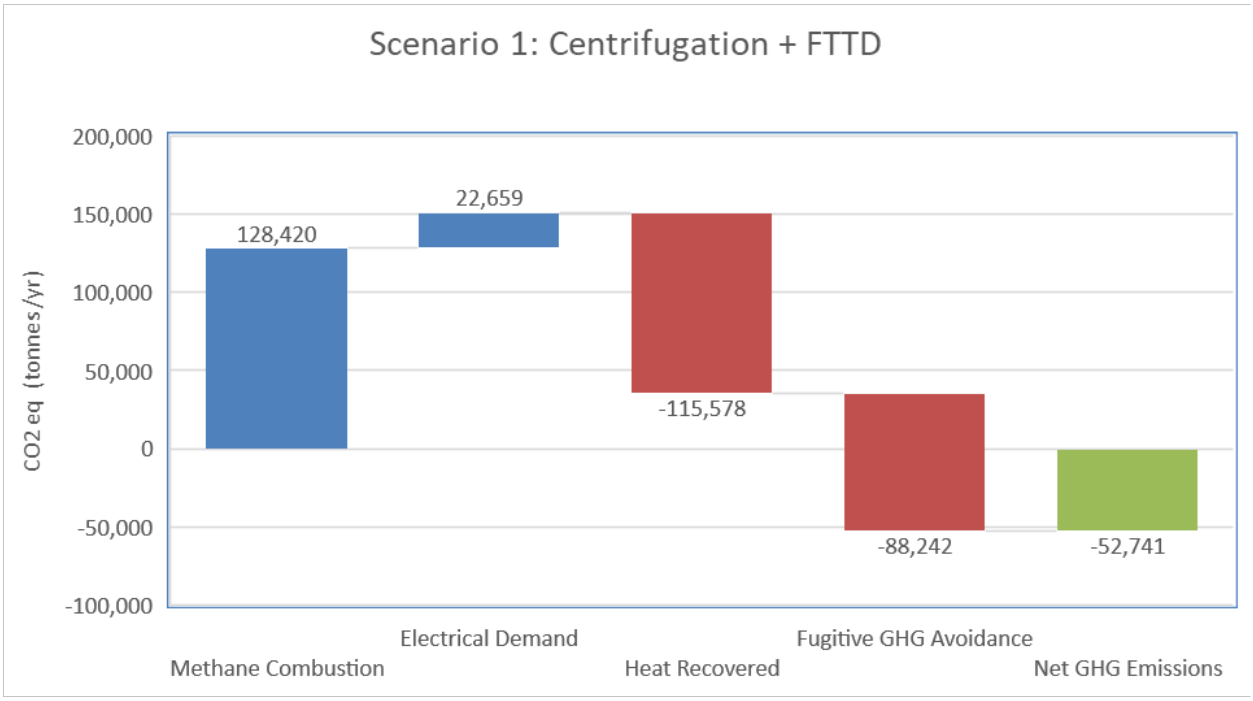

Figure 4. Scenario 1 GHG Emissions Waterfall Plot

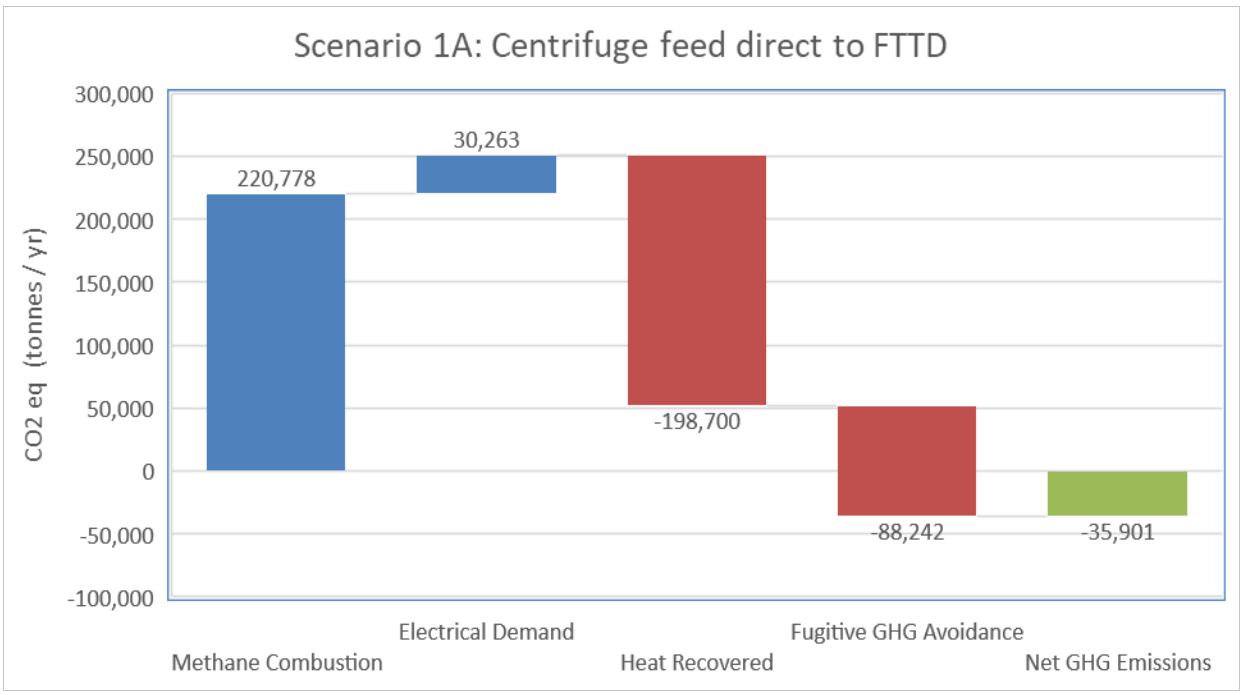

Figure 5. Scenario 1A GHG Emissions Waterfall Plot

the thermal drying by-pass. Thus, the 50 wt% FT that is fed to FTTD is comprised of 20.4 T/hr bitumen, 240.5 T/hr water, 224.2 T/hr solids, and 4.1 T/hr naphtha.

Scenario 2 targets a final solids concentration of 67 wt% solids so that 247.5 T/hr of the partially dewatered FTT tailings will be fed to the FTTD process at 50 wt% solids and then blended with the 241 T/hr of the FTTD by-pass to produce a final

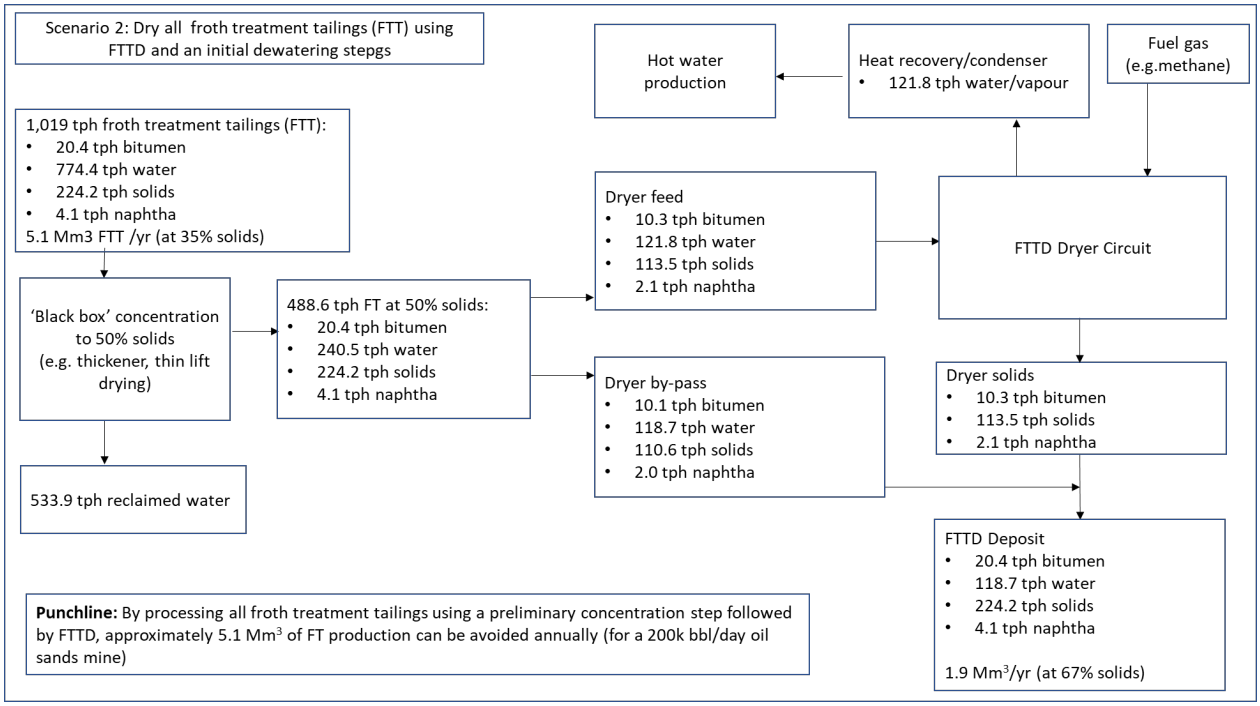

Figure 6. Scenario 2 FTTD after 'Black Box' Concentration Step

product volume of 213.4 m^3/hr (1.9 Mm^3/yr) of trafficable tailings. It is assumed that the FTTD product is placed in sub-aerial thin lift deposits to enhance aerobic decomposition of residual diluent to carbon dioxide, rather than anaerobic decomposition to methane.

Scenario 2 Environmental Footprint

The fines drying model has been used to estimate the thermal and electric demands of the FTTD process as a function of feed solids concentration, feed solids temperature, and final target solids content.

The Scenario 2 reference case predicts 372,300 T/yr of CO_2e fugitive emissions from NRU tailings. By treating the NRU tails with FTTD and placing the solids in subaerial thin lifts, the fugitive GHG emissions could be reduced by as much as 82% (Burkus Z. , 2014). Thus, the fugitive GHG emissions abatement potential for Scenario 2 is 305,286[22] T CO_2e/yr and the net GHG emissions reduction potential for Scenario 2 is 269,127 T CO_2e/yr (Figure 7). That is, the GHG avoidance potential associated with methanation abatement, is greater than the gross footprint of the FTTD process. This means processing FTT with the FTTD process might deliver net GHG reductions, even if no heat was recovered from the FTTD process.

Implementation Cost Considerations

To be a contender technology, FTTD needs to enhance both environmental performance and cost competitiveness. Detailed discussions of implementation costs should be evaluated on specific implementation scenarios that include mine operator verified costing parameters.

The primary operating expense of FTTD will be attributable to the net cost of purchased energy and GHG emissions tariffs. If flowsheets can be developed that lead to a net reduction in GHG emissions, as has been shown to be possible, then the overall future cost of GHG tariffs will decrease and a host of additional cost reductions will become available to the mine operators.

Preliminary evaluations indicate that the CAPEX requirements of an FTTD plant would be modest relative to other tailings technology deployment initiatives.

The best way to map-out the full cost-benefit picture of FTTD will be through case-specific studies that

[22] 372,300 T CO_2e x 82% = 305,286 T CO_2e

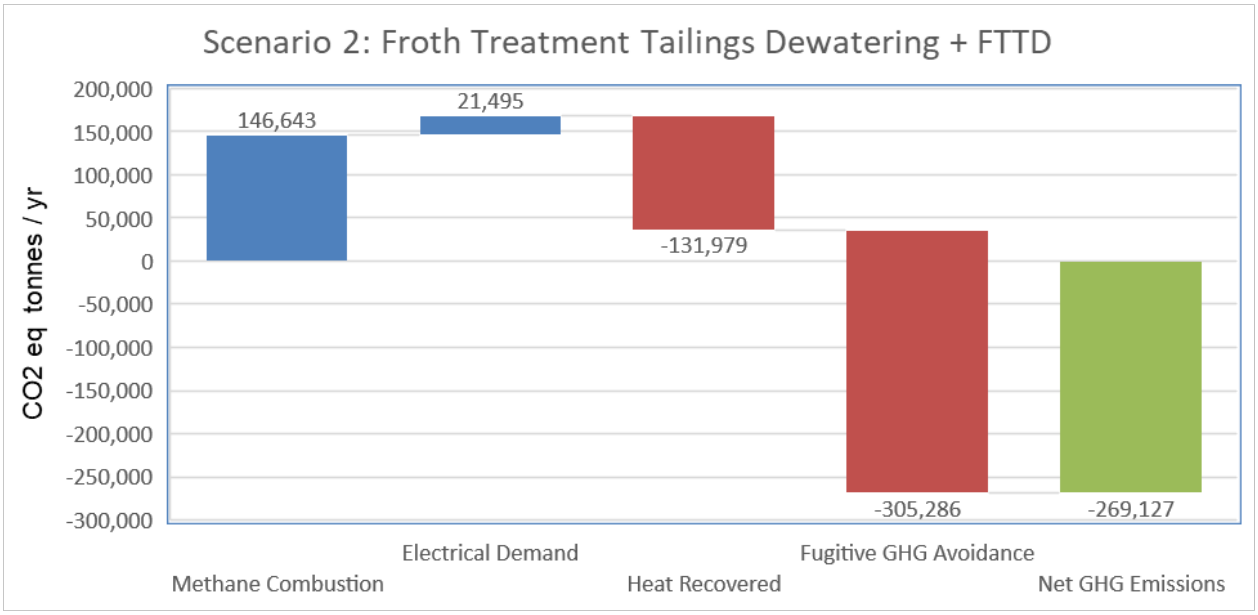

Figure 7. Scenario 2 GHG Emissions Waterfall Plot

include direct involvement of mine operations subject matter experts and cost estimators.

FTTD Implementation Scenarios Summary

Thermal drying of FT offers the potential to deliver a best available technology platform that complements technologies already included in D-085 applications.

The coupling of FFTD with fines settling, thin lift drying tailings, thickener underflow, accelerated dewatering product, and pressure filtration are other FTTD applications worthy of evaluation based on the promise shown in the two FTTD scenarios evaluated.

ARISING OPPORTUNITIES: OIL SANDS PATHWAYS TO NET ZERO

The main environmental footprint associated with the implementation of FTTD drying is GHG emissions associated with the combustion of natural gas to provide heat. As the scenario discussions have illustrated there are credible pathways to deliver a net GHG reduction by reusing the heat recovered from FTTD and by reducing fugitive GHG emissions from tailings ponds.

The Oil Sands Pathways to Net Zero Alliance (OSPNZA) has a goal to reduce net emissions from oil sands mining operations to zero GHGs by 2050 using *"…multiple parallel pathways…"* including *"… electrification, fuel substitution and energy efficiency to carbon capture, process improvements and the implementation of emerging technologies"* (Oil Sands Pathways to Net Zero, 2021).

This collaborative industry and government effort to reduce GHG emissions will create synergies between FTTD and GHG emissions abatement efforts. Many of the investments that will be necessary to reduce the GHG emissions associated with oil sands mining operations could facilitate further reduction of the net GHG footprint of FTTD operations. There are a multitude of possible FFTD implementation pathways with the potential to reduce net GHG emissions from oil sands mining operations, including:

- operating FTTD to mitigate production of fugitive GHG emissions from tailings,
- use of 'surplus' heat' on mine sites to reduce the gross energy requirements of FTTD,
- use of FTTD as an integrated component of novel bitumen extraction process flowsheets such as IPEP,
- integration of FTTD into large-scale carbon capture and sequestration developments planned by all current oil sands mine operators, and,
- utilization of electric heaters using 'low GHG electricity sources' (e.g., carbonate fuel cells)

in-lieu of combustion of hydrocarbons for FTTD heating needs.[23]

CONCLUSIONS

Oil sands mine operators are motivated to improve ESG performance through development and deployment of novel tailings technologies. By responding proactively to the FTTD implementation opportunities identified, oil sands mine operators have a unique opportunity to boost ESG performance.

The paper uses publicly available information to construct and analyze conceptual FTTD implementation scenarios and concludes that FTTD treatment of FT has significant potential to enhance the ESG performance of oil sands mine operators, especially within the context of high synergy potential with the OSPNZA mission.

Expected environmental benefits of FTTD include:

- reduced volume of FT,
- incorporation of solids in FT into reclamation substrates that support faster progressive terrestrial reclamation,
- reduced fugitive GHG emissions from tailings, and,
- enhanced recovery and reuse of water.

Additional environmental benefits could include:

- mitigation of acid generation potential and naturally occurring radiation hazards,
- reduced risk of FT discharge from tailings storage facilities, and,
- reduced potential for harmful interaction due to wildlife contact with FT.

Expected economic benefits include:

- reduced dam construction costs due to reduced fluid tailings inventory,
- reduced closure and reclamation costs,
- reduced fluid tailings management and monitoring costs, and,
- increased mine operations efficiencies (i.e., fewer tonne-kilometres of materials = lower mine fleet OPEX).

RECOMMENDATIONS

The oils sands innovation community, the GoA, and other impacted stakeholders are encouraged to review the findings of this paper with a sense of enthusiasm for finding novel ways to help oil sands mining operators improve upon environmental performance while remaining globally cost competitive.

.

In the spirit of innovation excellence, it would be helpful for the various claimholder and stakeholder groups to provide an independent critique which identifies points of agreement, contention, and outright disagreement, if any, with the conclusions presented.

FTTD treatment of FT warrants further evaluation and oil sands mine operators are encouraged to establish a multi-stakeholder ‘validation taskforce’ through COSIA with a mandate to develop a strategy to mature the full potential of FTTD including synergies with the OSPNZ initiative.

REFERENCES

AER. (2019, February). Fort Hills Energy Corporation: Application for Fort Hills Tailings Management Plan. Retrieved December 5, 2021, from AER Decisions, Decision 20190225A: https://static.aer.ca/prd/documents/decisions/2019/20190225A.pdf

AER. (2019, September 17). The Father of Oil Sands Extraction: Dr. Karl Clark’s patent proved vital to Alberta’s energy future. Retrieved from Resource Stories with energy: https://resource.aer.ca/stories/the-father-of-oil-sands-extraction#:~:text=The%20Father%20of%20Oil%20Sands%20Extraction%20Alberta%20-,a%20patent%20for%20a%20game-changing%20oil%20sands%20technology.

Alberta Energy and Parks. (2021). Area Fugitive Emissions from Oil Sands Mining Operations, 2011 to 2020. Communicated to author via spreadsheet from Alberta Energy and PArks. Edmonton: Alberta Energy and Parks.

[23] A key benefit of using electric heating versus combustion of natural gas with methane is that the FTTD process gas would be steam rather than moist air, facilitating easier recovery and repurposing of the recovered energy

Alberta Energy Regulator (AER). (2015, March 13). Bulletin 2015-11 . Retrieved December 5, 2021, from Alberta Energy Regulator Bulletins: https://static.aer.ca/prd/documents/bulletins/Bulletin-2015-11.pdf

Alberta Energy Regulator. (2017, October 12). Directive 085: Fluid Tailings Management for Oil Sands Mining Projects. Retrieved DEcember 5, 2021, from Alberta Energy Regulaor Directives.

Alberta Energy Regulator. (2021, September). State of Fluid Tailings Management for Mineable Oil Sands, 2020. Retrieved December 6, 2021, from Reports: https://static.aer.ca/prd/documents/reports/2020-State-Fluid-Tailings-Management-Mineable-OilSands.pdf#:~:text=In%202020%2C%20monitoring%20and%20reporting%20of%20fluid%20tailings,requirements%20during%20the%20initial%20phases%20of%20the%20pandemic.

Alberta Energy Regulator. (2021, December 5). Tailings. (Alberta Energy Regulator) Retrieved December 5, 2021, from Alberta Energy Regulator: https://www.aer.ca/providing-information/by-topic/tailings

Bakx, K. (2021, December 6). Banned for decades, releasing oilsands tailings water is now on the horizon. (Canadian Broadcasting Corporation) Retrieved 02 08, 2022, from CBC News: https://www.cbc.ca/news/business/bakx-oilsands-tailings-release-mining-effluent-regulations-1.6271537

Bepex LLC. (2021, 06 01). Personal Communications. Oil sands FTTD pilot experience. Minneapolis, MN, USA.

Bonem, J. a. (2012). The MITD Process for Dealing with MFT. Proceedings of the Third International Oil Sands Tailiongs Conference (p. 10). Edmonton: University of Alberta Geotechnical Centre.

Boswell, J. A. (2012). The Oil Sands Tailings Technology Roadmpa Project: The Identification and Improvement of Tailings Technology Suites, and Pathways for Technology development. The ThirdInternational Oil Sands Tailings Conference (p. 10). Edmonton: Univesity of Alberta.

Burkus, Z. (2014, November). GHG Emissions from Oil Sands Tailings Ponds: Overview and Modelling Based on Fermentable Substrates. Part II: Modeling of GHG Emissions from Tailings Ponds Based on Fermentable Substrates. Retrieved 02 08, 2022, from Oil Sands Research and Information Network: https://era.library.ualberta.ca/communities/e4fdd15f-c21d-4612-a2f7-bfec3fdfc1de/collections/97c301ec-5099-45ae-8eed-7b6c55616fbf

Burkus, Z. J. (2014, November). GHG Emissions from Oil Sands Tailings Ponds: Overview and Modelling Based on Fermentable Substrates. Part I: Review of the Tailings Ponds Facts and Practices. Retrieved December 5, 2021, from Educationa and Research Archive: Oil Sands Research and Information Network: https://era.library.ualberta.ca/communities/e4fdd15f-c21d-4612-a2f7-bfec3fdfc1de/collections/97c301ec-5099-45ae-8eed-7b6c55616fbf

Canada's Oil Sands Innovation Alliance . (2021, December 6). Tailings Management. Retrieved from Canada's Oil Sands Innovation Alliance: https://cosia.ca/initiatives/tailings

Canadian Natural. (2021, April 30). Canadian Natural Jackpine Mine 2020 Fluid Tailings Management Report. Retrieved December 5, 2021, from Alberta Energy Regulator.

Canadian Natural. (2021, April 30). Horizon Oilsands Mine and Processing Plant: 2020 Annual Fluid Tailings Management Report. Retrieved December 5, 2021, from AER Company Tailings Management Reports: https://static.aer.ca/prd/documents/oilsands/CompanyTailingsManagementReports-2020.zip

CAPP. (2021, December 6). Canadian Association of Petroleum Producers. Retrieved from CAPP: https://www.capp.ca/explore/tailings-ponds/#:~:text=The%20Government%20of%20Alberta%2C%20through%20the%20Tailings%20Management,the%20accumulation%20of%20fluid%20tailings%20on%20the%20landscape.

CNRL. (2021). In Pit Extraction Process for Tailings. Retrieved from Technology and Innovation Cases Studies Booklet: https://www.cnrl.com/upload/media_element/1279/38f7f53e080e/technology-and-innovation-case-studies-booklet_2021_w.pdf

Commission for Environmental Cooperation. (2020). Alberta Tailings Ponds II. Factual Record regarding Submission SEM-17-001. Montreal, Canada: Commission for Environmental Cooperation.

COSIA. (2021, August). Maintaining Permeability for Contnuous Mature Fine Tailings Dewatering. Retrieved from 2020 Tailings Research Report: https://cosia.ca/sites/default/files/attachments/2020%20Tailings%20Research%20Report_Final_August%202021_Final.pdf

COSIA. (2021). Tailings Management. Retrieved September 6, 2021, from Canada's Oil Sands Innovation Alliance: https://cosia.ca/initiatives/tailings

CTMC. (2012, June 22). OIL SANDS TAILINGS TECHNOLOGY DEPLOYMENT ROADMAP, Project Report - Volume 2, Component 1 Results. Retrieved December 5, 2021, from Canada's Oil Sands Innovation Alliance: https://cosia.ca/sites/default/files/attachments/Tailings%20Roadmap%20Volume%202%20June%202012.pdf

CTMC. (2012, June 28). OIL SANDS TAILINGS TECHNOLOGY DEPLOYMENT ROADMAP, Project Report - Volume 3, Component 2 Results. Retrieved December 5, 2021, from Canada's Oil Sands Innovation Alliance.

CTMC. (2012, June 29). OIL SANDS TAILINGS TECHNOLOGY DEPLOYMENT ROADMAP, Project Report - Volume 4, Component 3 Results. Retrieved December 5, 2021, from Canada's Oil Sands Innovation Alliance.

CTMC. (2012, June 26). OIL SANDS TAILINGS TECHNOLOGY DEPLOYMENT ROADMAP, Project Report - Volume 5, Component 4 Result. Retrieved December 5, 2021, from Canada;s Oil Sands Innovation Alliance.

CTMC. (2012, June 12). OIL SANDS TAILINGS TECHNOLOGY DEPLOYMENT ROADMAPs, Project Report - Volume 1, Project Summary, June 22, 2012. Retrieved December 5, 2021, from Canada's Oil Sands Innovation Alliance: https://cosia.ca/sites/default/files/attachments/Tailings%20Roadmap%20Volume%201%20June%202012.pdf

CTMC. (2012, June). Technology Scoring Sheets. Retrieved December 5, 2021, from Canada's Oil Sands Innovation Alliance (COSIA).

Energy Resources Conservation Board (ERCB). (2009, February 3). Directive 074:Tailings Performance Criteria and Requirements for Oil Sands Mining Schemes. Retrieved December 3, 2021, from Impact Assessment Agency of Canada (IAAC): https://iaac-aeic.gc.ca/050/documents_staticpost/59540/81944/Tab7_-_ERCB_Directive_on_Tailings_Performance.pdf

Energy Resources Conservation Board (ERCB). (2013, June). 2012 Tailings Management Assessment Report: Oil Sands Mining Industry (PDF) (Report). Retrieved December 5, 2021, from Oil Sands Information Portal (OSIP): http://osipfiles.alberta.ca/datasets/158/TailingsManagementAssessmentReport2011-2012.pdf

Energy Resources Conservation Board. (2008, December 7 to 10). Oil Sands Tailings: Regulatory Perspective. Retrieved December 5, 2021, from 1st International Oil Sands Tailings Conference: https://sites.google.com/a/ualberta.ca/iosct2008/

Gidley, I., & Boswell, J. (2013). A model for technology development in oil sands tailings. Retrieved 12 8, 2021, from https://papers.acg.uwa.edu.au/p/1363_42_gidley

Government of Alberta. (2015, March 03). Lower Athabasca Region : tailings management framework for the mineable Athabasca oil sands. Retrieved December 5, 2021, from Alberta Open Government Publications: https://open.alberta.ca/publications/9781460121740#summary

Hyndman, A. S. (2019, August 22). Fluid Fine Tailings Processes: Disposal, Capping, and Closure Alternatives . Retrieved December 5, 2021, from Recent Events: http://mckennageotechnical.com/news.html#:~:text=Fluid%20Fine%20Tailings%20Processes%20%E2%80%94%20Disposal%2C%20Capping%2C%20and,Sands%20Tailings%20Conference%20in%20Edmonton%20in%20December%202018.

Imperial. (2021, April 30). Kearl Oil Sands Mine: Fluid Tailings Management Report for 2020. Retrieved December 5, 2021, from Company Tailings Management Reports: https://static.aer.ca/prd/documents/oilsands/CompanyTailingsManagementReports-2020.zip

Jason Hamelehle, R. J. (2021). Regeneration of filter press fabrics in the mining sector. Banff: Tailings and Mine Waste Conference 2021.

Matthews, J. (2008). Objectives of D-074, discussions with senionr ERCB representatives (Houlihan and Lord). Fort McMurray.

Matthews, J. (2022). Government Policy and Regulatory Influence on Oil Sands Tailings Innovation. International Oil Sands Tailings Conference. Edmonton: University of Alberta.

McKinley, J., Sellick, A., Dawson, R., & and Hyndman, A. (2018, June). Fluid Fine Tailings Management Methods: An Analysis of Impacts on Mine Planning,Land, GHGs, Costs, Site Water Balances and Recycle Water Chloride Concentrations. Retrieved December 5, 2021, from Canada's Oil Sands Innovation Alliance.

Monica Ansah Sam, E. D. (2021). Filter press technology commercial scale pilot - geotechncal deposit performance. Tailings and Mine Waste Conference 2021. Banff, Alberta: Tailings and Mine Waste Conference 2021.

Morsch, B. F. (2021). Regeneration of filter press fabrics in the mining sector. Banff: Tailings and Mine Waste Conference,2021.

Murray Gray, Z. X. (2009, March 01). Physics in the oil sands of Alberta. Retrieved December 5, 2021, from Physics Today, Volume 62, Issue 3: https://doi.org/10.1063/1.3099577

Oil Sands Pathways to Net Zero. (2021). We need to get to net zero. (Oil Sands Pathways to Net Zero) Retrieved 01 30 , 2022, from Oil Sands Pathways to Net Zero: https://www.oilsandspathways.ca/

Pembina Institute. (2017, March 13). Backgrounder. Retrieved December 5, 2021, from Review of Directive 085 Tailings Management Plans: https://www.pembina.org/reports/tailings-whitepaper-d85.pdf

Pembina Institute and Water Matters. (2009, December). Reports. Retrieved December 6, 2021, from Tailings Plan Review — An Assessment of Oil Sands Company Submissions for Compliance with : https://www.pembina.org/reports/tailings-plan-review-report.pdf

Qi, L. (2022, 10 01). Maintaining Permeability for Continuous Mature Fine Tailings Dewatering. Retrieved from cognit.ca: https://cognit.ca/en/research/project/206123

Rougeot, A. (2021, November 16). In the thick of it: Living on the frontlines of Alberta's toxic tailings lakes. (Environmental Defence) Retrieved 02 08, 2022, from Environmental Defence Climate Change: https://environmentaldefence.ca/2021/11/16/in-the-thick-of-it-living-on-the-frontlines-of-albertas-toxic-tailings-ponds/

Spiller, P. P. (2021). Future of tailings management. Banff: Tailings and Mine Waste Conference 2021.

Stantec. (2021, December 20). Material and Energy Balance for an Oil Sands Surface Mining and Bitumen Extraction Reference Facility. Retrieved 02 14, 2022, from Canada's Oil Sands Innovation Alliance: https://cosia.ca/sites/default/files/attachments/Material_and_Energy_Balance_for_an_Oil_Sands_Surface_Mining_and_Bitumen_Extraction_Reference_Facility.pdf

Suncor Energy Operating Inc. (2021, April 30). 2020 Fort Hills Fluid Tailings Management Report. Retrieved December 5, 2021, from Compnay Tailings Management Reports: https://static.aer.ca/prd/documents/oilsands/CompanyTailingsManagementReports-2020.zip

Syncrude. (2021). 2020 Sustainability Fact Sheet: Operations and Performance. Retrieved 01 18, 2022, from Syncrude: https://syncrude.ca/wp-content/uploads/2021/09/Fact-Sheet-_Operations-and-Performance-2020.pdf

Syncrude Canada Ltd. (2021, April 30). 2020 Mildred Lake Tailings Management Report. Retrieved December 5, 2021, from AER Reports: https://www.aer.ca/providing-information/by-topic/tailings

Syncrude Canada Ltd. (2020, April 30). 2020 Mildred Lake Tailings Management Report. Retrieved from 2019 Mildred Lake Tailings Management Report.

Syncrude Canada Ltd. (2021, April 30). 2020 Syncrude Aurora North Tailings Management Annual Report. Retrieved December 5, 2021, from Alberta Energy Regulator: https://static.aer.ca/prd/documents/oilsands/CompanyTailingsManagementReports-2020.zip.

The Royal Society of Canada Expert Panel. (2010, December). Environmental and Health Impacts of Canad's Oil Sands Industry. Retrieved December 5, 2021, from Documents: https://rsc-src.ca/sites/default/files/RSC%20Oil%20Sands%20Panel%20Main%20Report%20Oct%202012.pdf

Van Dongen, A., Samad, A., Heshka, N., Rathie, K., Martineau, C., Bruant, G., & Degenhardt, D. (2021). A Deep Look into the Microbiology and Chemistry of Froth Treatment Tailings: A Review. Microorganisms, 9(5). Retrieved from https://doi.org/10.3390/microorganisms9051091

Yuan You, R. M. (2021). Methane emissions from an oil sands tailings pond: a quantitative comparison of fluxes derived by different methods. Atmospheric Measurement Techniques, 14, 1879-1892. Retrieved from https://amt.copernicus.org/articles/14/1879/2021/amt-14-1879-2021.pdf#:~:text=Tailings%20ponds%20in%20the%20Alberta%20oil%20sands%20region,ployed%20under%20current%20regulatory%20compliance%20monitoring%20pro-%20grams.

SESSION 7

INSIGHTS INTO DUTCH VACUUM CONSOLIDATION METHODS AND THEIR ABILITY TO IMPROVE STABILITY OF SOFT CLAY DEPOSITS FOR FILL PLACEMENT

Jeroen Dijkstra[1] and Ebi Meshkati[2]
[1]Cofra B.V., Amsterdam, The Netherlands, [2]R&D Boskalis B.V. (former Deltares), Papendrecht, The Netherlands

ABSTRACT

Clay-rich soft sediments are increasingly used within construction projects across the globe, from construction on soft mud layers and the beneficial use of dredged materials originating from estuaries and waterways to the rehabilitation of clay-rich waste deposit areas from mining or processing operations. To minimize construction delays and potential hazardous environmental and/or social risks, managing such sediments (e.g., by confining, preloading or capping) is often required. However, the main challenge is their extremely low strength (< 5kPa) and slow consolidation, hence dealing with storage volume, delayed strength increases of, and placement of granular layers on, material with poor work- and trafficability.

Vacuum consolidation is a proven technology to speed up the consolidation process and accompanying strength gain in such deposits without the placement of surcharge. Over the past decades, the performance of this technology has been constantly improved and multiple installation methods have been developed. This paper presents some of the recent developments in the design and installation of vacuum consolidation technology, using examples from executed projects in civil engineering works on soft clay-rich deposits.

INTRODUCTION

Soft soils strength improvement is vital to the successful placement of sand caps and controlling the residual settlement of fills and deposits [Jacobs 2012]. The Deltaic origin of the Dutch subsoil, with very soft clay and peat layers down to 20m below the surface, together with the extensive worldwide experiences in reclaiming very soft clay/mud deposits, has considerably advanced both the theoretical and practical knowledge of Dutch ground improvement engineers and researchers in improving the strength gain of very soft soils. Part of this advancement is owed to the use of vacuum consolidation, which is often used to enhance the properties of the low strength ground, providing strength gain for specific layers without the use of a surcharge. The goal of such applications is to provide a stable subsoil for capping and ultimately a controlled residual settlement after construction.

This paper provides an overview of the main vacuum consolidation installation methods accompanied by examples from both Dutch and international projects performed for civil engineering applications. Opportunities, limitations, and brief design takeaways of various installation methods are presented with an attempt to bridge the applicability of the technology to oil sands tailings.

CONSOLIDATION

Highly permeable soils like sand or coarse tailings when subjected to a new higher stress state can rapidly adjust to loads and accommodate a fast compression / reduction in voids due to their ability to easily drain the excess porewater expelled by the stress rearrangement of particles. Saturated low permeable soils like clay, peat, and mature fine tailings (MFT) do not have such drainage ability and thus show a delayed compression when loaded.

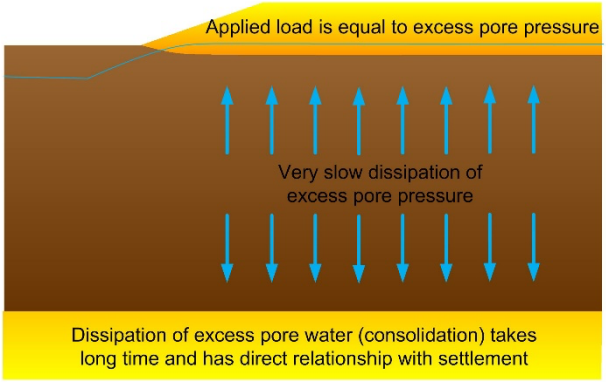

Figure 1. Dissipation of excess pore pressure without any measures

The low permeability of the soil prevents the incompressible water, filling the complete voids between the particles, to dissipate from the voids; and hence, prevents the particles to move into a denser equilibrium state. The load, in the case the soil matrix is not adjusted to it, is mainly transferred to the water reflecting in so called excess porewater pressure. With time the excess pressure slowly dissipates as the water flows out of the soil matrix, allowing for the volume change to occur. This process continues until the stress state equilibrium is reached and the water pressure equals the hydrostatic pressure. This process of dissipation of excess pore pressure and adjusting to a new stress condition, also known as consolidation, can take up to years depending on the thickness, permeability and compressibility of the deposit [Bjerrum, 1967].

In construction projects, the time to have the soil naturally adjusted to new loads is often not available and thus additional measures are required to shorten the construction times. The most common and often also the most economical solution used to reduce the consolidation period is the creation of artificial drainage paths, in which the water can freely drain and even-out pressure differences.

These artificial drainage paths can be made in the form of granular inclusions and are generally created by the use of prefabricated vertical drains (PVD), also known as wick drains. The vertical drains patented by Kjellman in 1945 have been used for many decades and have proven their efficiency in thousands of projects worldwide, with currently over 100 million meters of PVD installed on construction projects on a yearly basis. The drains can be installed using land, hybrid or water-based equipment up to depths of over 60m below the surface and even through dense sand layers, using heavy push rig types.

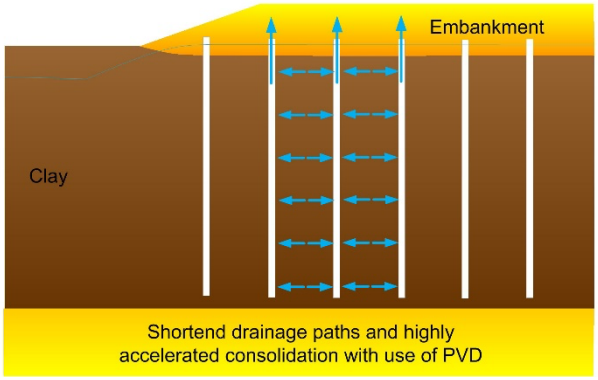

Figure 2. Dissipation of excess pore pressure with prefabricated vertical drains

With the application of the shorter dissipation paths from the installed PVD, allowing the excess pore water to dissipate over much shorter distances, the consolidation process may accelerate to a few months or even weeks when the PVD is placed at close center to center distances as the flow path is squared in the consolidation formulae as per Terzaghi's consolidation theory (i.e. a flow path of 2m (2^2=4) will consolidate 4/9 times faster compared to a flow path of 3m (3^2=9). Especially in thick deposits like tailing ponds, the time gains can be enormous when the flow paths of tens of meters are reviewed against the drainage paths of only a few meters.

PREFABRICATED VERTICAL DRAINS (PVD)

The basic principle of a vertical drain is its ability not only to create free flow conditions over the height of a drain under deformed/buckled conditions [Dijkstra 2014], but also to even-out any water pressure differences between the surrounding soil and the drain itself whilst keeping the soil particles out of the vertical drainage channels of the core.

The commonly used vertical drain types consist of a plastic core with individual flow channels, through which water can freely flow, and a filter that is wrapped around or glued to the core with the function of filtering the water and retaining any soil particles that flow with the water towards the drain. Tests have shown [Dijkstra 2012, Kochx 2011] that in fine-grained soils, the filter has its main filtration function in the first hours after installation till the formation of a natural soil filter. Afterwards it mainly acts as a separator. The combined interaction between the core and filter, i.e. elongation of the filter into the flow channels, creep deformation of the core under pressure and the development of the flow paths under buckling, determine the final discharge capabilities of the PVD and is a function of the material properties (core and filter) of the PVD (i.e. the plastic compound used), the geometrical properties of the core, the effective stress, temperature, gradient applied and time.

The most common standards (EN 15237 2007, ASTM 4716, ISO/CD 18325 2014) have prescribed laboratory tests in which most of the before-mentioned parameters are specified. The outcome of these tests however, shown ultimately in the specification of a PVD as a discharge capacity under a fixed pressure, time and gradient, will only

provide the end user with a single dot within a three-dimensional plane. i.e., during the lifetime of a PVD, the pressure build-up, affected by the amount of water (flow speed), the deformation of the flow channels by the buckling and the effective stresses deforming the core and pushing the filter into the core, will move with the changing boundary conditions over this plane. This makes that, also because the specified discharge tests, or even the specified values in the declarations, are not easy to compare with each other, it can even easily be debated whether the provided data point is the actual discharge flow of the PVD at the specific translated field conditions.

Although the material behavior of a PVD is complex, particularly in relation to the flow resistance on a detailed level, a decent quality vertical drain will always be capable of draining the provided water from the soil by creation of an equilibrium state (i.e. pressure profile inside the drain). Most western drain types will provide an equilibrium state in which the water has no obstruction, or only a few kPa of resistance at the bottom of a drain at the start of the consolidation process, to allow for a situation where the water can freely flow from the soil and validity of the governing calculation models is provided.
However, over the past years the specified discharge capacities of the vertical drain types, especially in Asia, have reduced due to large market volumes and a strong focus on material costs, to the point where certain drain types will no longer automatically provide the free flow assurance anymore. In this specific situation, with an underperforming PVD, a high volume of water flowing through the drain will lead to a higher gradient and a pressure built-up inside the drain in order to reach the equilibrium state. This will result in a lower pressure difference between the drain and the surrounding soil, leading to a lower amount of water flowing towards the drain (Darcy's law) and a delay in the consolidation time. It is therefore key to check the discharge capacity and specify a required discharge that fits the PVD lifetime, taking into account the predicted settlement behavior. The settlement is a function of the amount of water that needs to flow through the drain and effective stress development with time. The highest flow requirements often occur at the lowest stresses, while the lowest flow requirements are near the end of the consolidation at the highest stress situation. It is not recommended to take the highest discharge and specify this against the highest effective pressure.

Next to the discharge it is important that water can enter the PVD. In order to keep soil particles out of the core and prevent chemical, biological or particle clogging of the filter, its properties are of importance, especially tailing applications as various chemicals could be present, which could influence the behavior of the filter by, for example, chemical clogging. There is, so far, no standardized apparatus to test this clogging behavior. A unique testing principle is often adopted and used in several laboratories (Blond 2017, Dijkstra 2016, Yao 2010)) to test filters placed on a mesh with soil. Most documented tests with these tools involve tests with MFT.

Figure 3. Preparation of the MFT test on Filter conform the methods described in REF

The testing principle involves the placement of soil or sludge material on top of the placed filter fabric and consolidating the material from the top, using pressurized balloons, water or weights. After the consolidation testing, the filters can be investigated on their clogging behavior. The obtained results showed that after being in contact with MFT, the water permeability of the filters reduced considerably when compared to the initial value [Dijkstra 2016]. Although it was observed that a part of the filter was potentially clogged with tar-rich material, the permeability proved to be more than sufficient for the application. This was confirmed by the results of the PVD installation on one of the MFT ponds in Fort Mc Murray, where several millions of meters of PVD have successfully been installed and used [Robertson 2013].

From the final consolidation results, and moreover the undrained shear strength development over time in the pond, obtained in the oil sands [Robertson 2013] it can clearly be noticed that when

there is no pressure difference between the surrounding soil and the drain, e.g., only a light weight cap of minimal thickness, there is little volume change, effective stress increase (only the equivalent of the weight of the platform) and ultimately corresponding strength increase. Hence, additional measures are required to create a strength increase in the top layer, like the application of vacuum consolidation, to be able to place thicker fill layers without taking additional measures like the use of high strength geotextiles, placement of a cap during long-term frost conditions or hydraulically place sand caps.

VACUUM CONSOLIDATION THEORY

The pressure difference between the drain and the surrounding soil is, like with normal PVD, the driving mechanism of vacuum consolidation. This was found within 7 years after the invention of the vertical drain by Kjellman in 1945 when he invented the vacuum consolidation principle.

The name vacuum is however somewhat misleading as the method relies on lowering of the atmospheric pressure of maximal 90% at the pump, but more commonly 70% to 80%. This pressure lowering is at the location of the pumps (i.e. the location where the water table is within the pump system). The pressure lowering is, as the drainage and pump system is a closed environment and filled with water up to the location where it is pumped from the system, transferred to the water and distributed as per Pascal's law throughout the system.

The concept of effective mobilized atmospheric pressure is used to explain the working principle of vacuum consolidation. The effective mobilized atmospheric pressure in the soil $P_{a\text{-}eff}$ is equal to the pump pressure $P_{a\text{-}pump}$ corrected for flow losses in the system P_{flow} and the height difference between the location where the lower air pressure is transferred to the water and the initial hydrostatic level, i.e., ground water level, H_{vacuum}, as shown in formula [1]. For the various vacuum system this is schematically shown in figure 8, 12 and 16.

$$P_{a\text{-}eff} = P_{a\text{-}pump} - P_{flow} - H_{vacuum} \cdot g \cdot \gamma_{water} \quad [1]$$

In which:

$P_{a\text{-}eff}$ Effective mobilized atmospheric pressure acting on the soil [kPa] assuming no well resistance

$P_{a\text{-}pump}$ Mobilized atmospheric pressure pump pressure [kPa]

P_{flow} Flow losses in the system [kPa]

H_{vacuum} Height difference between water air level inside the pump and the ground water level. [m]

g Gravity [m/s2]

γ_{water} Unit weight of water [kN/m3]

The effective mobilized atmospheric pressure has the advantage that it acts as an isotropic surcharge onto the soil. At a given time t_1, the mobilized atmospheric pressure inside the drain $P_{a\text{-}eff}$ is equal to a surcharge load acting on the soil without any load spreading with depth as per [2].

$$\Delta\sigma'(t_1) = U(t_1).(\Delta\sigma_s + P_{a\text{-}eff}) \quad [2]$$

In which

$\Delta\sigma'(t_1)$ Increase of effective stress at t_1 [kPa]

$U(t_1)$ Degree of consolidation at t1 [-]

$\Delta\sigma_s$ Weight conventional surcharge [kPa]

$P_{a\text{-}eff}$ Mobilized atmospheric pressure [kPa]

This means that the total applied pressure (surcharge load plus vacuum load) acts on the soil and compresses the soil matrix. This implies that when no surcharge is used, the mobilized atmospheric pressure alone can consolidate soft compressible materials that can maintain a lowering of the pressure (e.g., are low permeable). This concept was confirmed during trials performed in The Netherlands where the SHANSEP theory was checked with the sole application of mobilized atmospheric pressure [Vink 2019]. It was found that the undrained shear strength increases from the sole application of a lowering of the atmospheric pressure complies with the governing relation between effective stress increase and undrained shear strength development [3].

$$\Delta\tau\,(t_1) = 0.22\,\Delta\sigma'(t_1) \quad [3]$$

In which

$\Delta\tau\,(t_1)$ Increase of undrained shear strength at t_1 [kPa]

$\Delta\sigma'(t_1)$ Increase of effective stress at t_1 [kPa]

During the trials two vacuum installation methods were trialed: the liner vacuum system and the drain-to-drain vacuum system called BeauDrain-S. (which are explained later in the manuscript). The outcome was comparable for both vacuum systems. Figure 4 provides a snip of the test data where the blue and red lines give the theoretical prediction based on SHANSEP theory and the dots the laboratory and direct measurements over a period after shutting down the pumps in order to see if the undrained shear strength increase remains in the ground and

is not reduced by the swelling that often occurs after the unloading and returning to atmospheric pressure condition. Both laboratory data (Direct simple shear test, in short DSs) and in-situ data (ball cone penetrometer tests) provided similar results and confirmation that the lowering of atmospheric pressure in a vacuum drainage system leads to an increase of undrained shear strength (S_u) following the relations provided in equations [2] and [3].

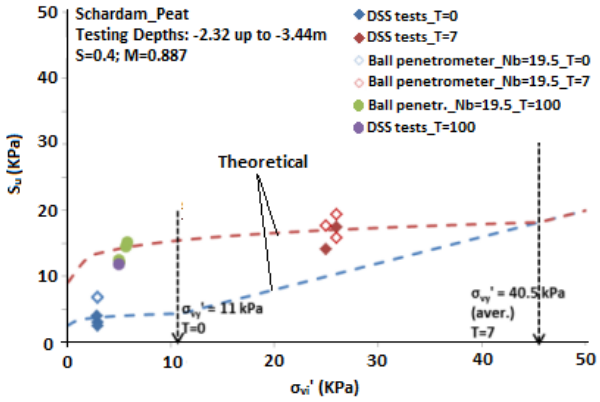

Figure 4. Example of Beaudrain-S area (Peat): DSS results, theoretical SHANSEP line & correlation Ball cone resistance, source: POV-M (2017)

The conclusion of the research is also that the principle as described above in equations [2] and [3] is valid for all vacuum installation methods. This is because the difference between the different vacuum methods is only the ability of each system to seal the vacuum drains from ingress of air or water from permeable layers, which layers are treated by the pressure lowering and how they deal with the flow losses in the system.

Each of the systems, see Figure 5, will be discussed separately accompanied with examples in the following sections.

VACUUM CONSOLIDATION INSTALLATION METHODS

There are three main so-called vacuum installation methods in the market:

- The liner vacuum system
- The BeauDrain system
- The drain to drain system

Each vacuum method has its own advantages and disadvantages, but also its particulars that are required to make the application a success and if not adhered to the efficiency of vacuum would reduce considerably. The basic concept of all the systems is that a horizontal distribution system is

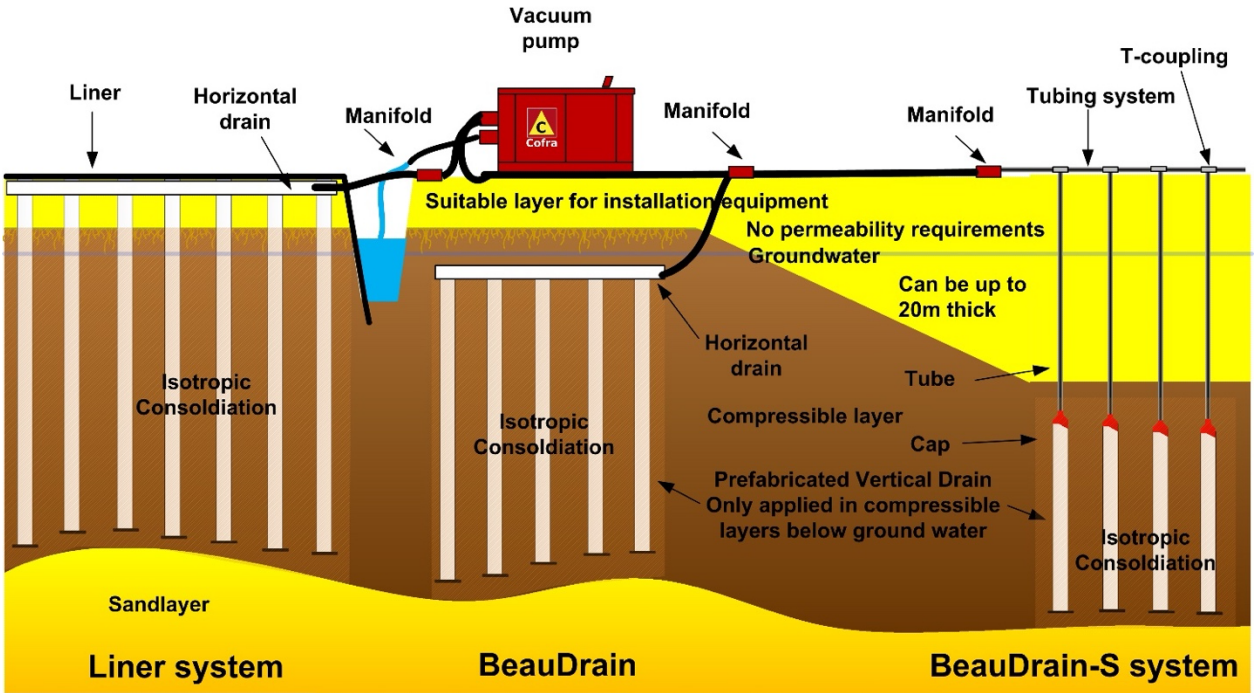

Figure 5. Three vacuum system

present which will, during the operation by the lowering the air pressure, be filled with water.
The water transfers the applied reduction of the atmospheric pressure at the pumps, as per Pascal's law, to each vertical drain installed into the compressible material. These systems will be explained one by one in the following sections.

Liner vacuum system

The basic particular of the liner vacuum system is that a liner is used to seal the treated area from the air. This involves the creation of an impervious seal on the surface after the installation of the vertical and horizontal drain system respectively in the subsoil and working platform.

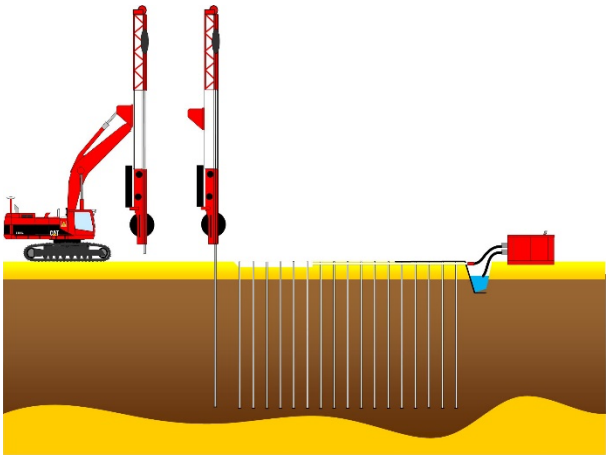

Figure 6. Basic installation method of the liner vacuum system

Liner vacuum has, as far as the authors are aware of, only been applied using working platforms accessible for PVD installation equipment. This is mainly due to the need to install the horizontal drainage system, pull the liner over the vacuum areas and create surrounding trenches. There are options to apply the system over waterlogged areas, but this requires considerable additional adjustments to the concept to assure the vertical drains are all connected to the vacuum system and the system is completely sealed from air or excess water ingress. The application using a working platform is therefore discussed herein.

For the main application of the liner vacuum it is required to place a working platform on top of the soft clay layers to be able to install the vertical drains with land based equipment. It should be noted that with deeper drains, the installation units often also become heavier and require thicker working platforms (up to 2m of sand on soft soil for installation depths over 30m). Besides the function to act as platform for the base unit installing the drains, the platform is also used to connect each vertical drain to horizontal drains. There have been projects where the horizontal and vertical drains were not connected and instead multiple layers of horizontal drains have been applied. Such adjustments in installation method require additional permeability prerequisites for the working platform in order to be permeable enough not to delay the discharge of the water from the vertical drain to the horizontal drain.

Figure 7. Installation of the sealing liner in a liner vacuum project

After the installation of the vertical and horizontal drain system, trenches are constructed around the treated area to make sure the liner, that will be used to seal the soil body from the surrounding air ingress, is extended into the compressible material and below the ground water table. The system of horizontal drains is either led through the liner or is guided though the trench to be connected to pumps. Recent developments in the system include the development of a sub pump system which is located inside the working platform and separates the water and air/gas outflow to enhance the vacuum [Bergado, 2022]. It has been found that the sub pump system reduces the flow path and hence flow losses in the system, but also lowers the location where the water is pumped from the system, with the result of reducing the height difference between the location where the atmospheric pressure is transferred to the water and the ground water level (see equation [1]). The schematic view of the pressure development with depth given a certain ground water level is provided in Figure 8.
The liner vacuum system works well with a high-water table (limited loss in effective vacuum pressure) and when large areas need to be

consolidated (placement of liner is labor intensive and trenches need to made). The inclusion of the working platform in the vacuum system leads to the most effective pressure transfer into the soil from the three vacuum systems around as the complete soft layers are subjected to a pressure drop including the working platform.

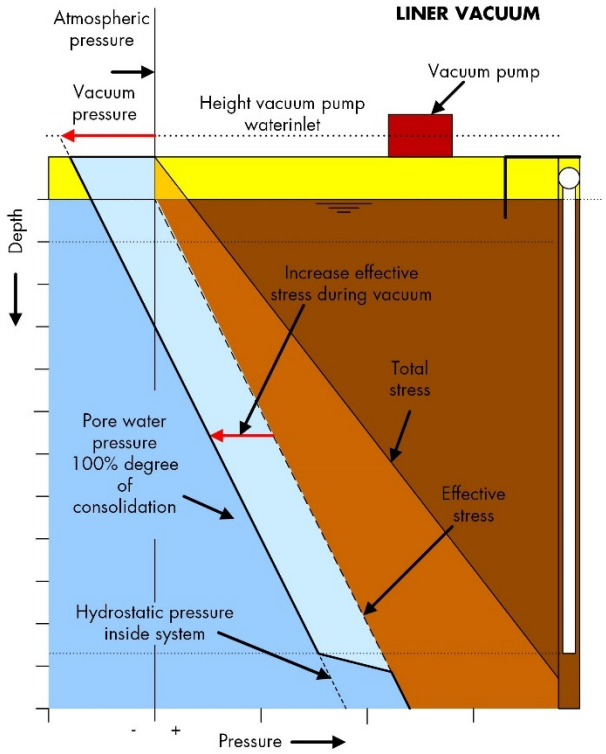

Figure 8. Pressure development of the liner vacuum system

A disadvantage is that the liner could remain buried in the ground creating an impervious layer in the subsurface after construction. Geotextiles are also required to protect the liner from being punctured. When a puncture has occurred the complete vacuum area is affected, which can be problematic particularly if layers of surcharge are already placed.

As an example, to show the efficiency of the liner vacuum system, the graph shown in Figure 9 provides moisture content development and undrained shear strength increase under 80kPa vacuum loading and 30kPa surcharge achieved in a project related to the expansion of the internal airport in Bangkok. In this project a total of 800.000m2 of vacuum consolidation was executed, using vacuum and drains down to 10m below the surface [Bergado 2022]. Measurements in the center between the drains shows an undrained shear strength increase between 15 up to 20kPa. Reviewing the SHANSEP theory [3], an effective stress increase has been reached of 70 to 90kPa. This corresponds with the requirements, loads and to other measurements taken during the project.

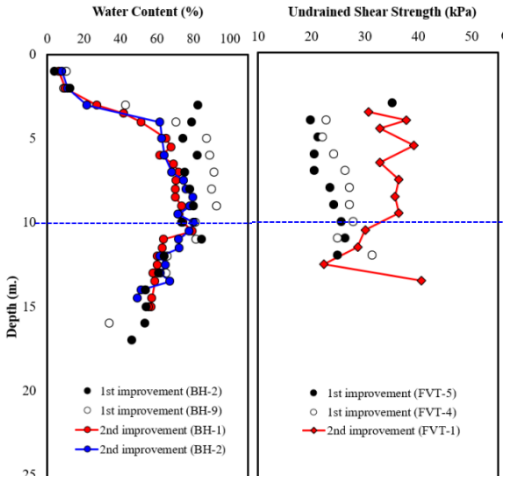

Figure 9. Undrained shear strength and moisture content development after vacuum preloading

BeauDrain vacuum system

The main distinctive feature of the BeauDrain system is that this system is installed in a single workflow. During this process, both the vertical and horizontal drains are installed below the ground water in the soft compressible soil. The horizontal drain is automatically connected to the top of a vertical drain inside the plough and installed in the same work operation, as part of the production process.

Figure 10. BeauDrain installation equipment

The system was developed in The Netherlands and has mainly been applied to Dutch construction projects. Installation is usually carried out from a working platform. Having said that, the system is easily adjustable to be used from a pontoon or hybrid installation tool allowing deployment on sludge depots or tailing ponds. An image of the installation equipment is shown in Figure 10.
The installation machine utilizes a uniquely designed plough to pull a horizontal (collecting) drain at a maximum depth of 2.5 m beneath the installation level (depending on the thickness of the working platform and the groundwater level). To make sure the horizontal drain is sealed from air ingress from the passage of the plough, the first section leading to the surface is sealed from air ingress by an extendable closed connection and a strip of membrane is installed on top of the horizontal drain to improve the sealing between the atmosphere and the horizontal drain. After the installation of a predetermined number of drains, installation is ceased, and the plough is led to the surface. The initial blinded section of the drain is led to the collection pipe and ultimately the vacuum pump.

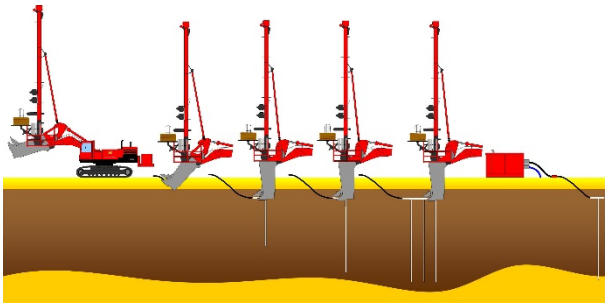

Figure 11. Basic installation method of the liner vacuum system

The BeauDrain system works best in very soft material as in this system the soil needs to deform and close the insert remnant after the passage of the plough. In stiffer grounds the trench has a higher risk to remain open which affects the vacuum, as air leaks can occur through the cut in the soil. More than the liner vacuum system, the BeauDrain system requires a high groundwater table to assure the horizontal drain is completely buried and saturated up to the blinded section of the drain. This is a prerequisite for ensuring vacuum in the system. As the system consists of parallel screens (lines) of vertical drains each separately connected to a dedicated horizontal drain, a leak can ultimately be resolved by just disconnecting the malfunctioning single line from the system. This saves the rest of the lines as access to the system is not possible other than the collecting tubes at the surface at the end of each line. A main advantage of the system is that the area, after installing a line can immediately receive vacuum and the surface can be crossed by any equipment as the entire line and its components are buried underneath the surface. For active sludge depots or tailing ponds this has the advantage that operations can continue as planned and the system can be buried without any constraints.

The lower position of the horizontal drain within the soil profile, compared to the liner vacuum system, leads to a different pressure development in the soil. The top layer will not receive vacuum as this layer acts as sealing medium for the system. The vacuum will only start at the depth of the horizontal drain, see Figure 8. This is why the surface consolidation in the BeauDrain system is a bit less effective compared to the liner vacuum system. The distance to the drain end the surface is however in most cases very short to assure a normal consolidation behavior in this section.

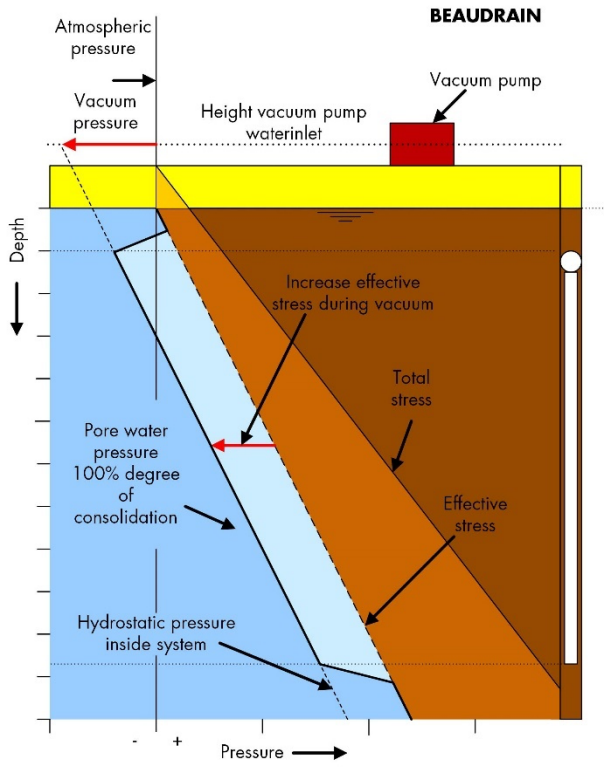

Figure 12. Pressure development of the BeauDrain vacuum system

Flow losses in the BeauDrain system are in the same range as the liner vacuum system. The maximum length of a line is related to the diameter

of the horizontal drain same as the distance to the pump in the liner vacuum system. It is key to keep the flow in the drain in a laminar condition to avoid large flow losses.

A fine example of the capabilities of the BeauDrain vacuum system is a construction project described in Dijkstra 2015. The BeauDrain vacuum system was used to control the stability of an 18m high embankment on top of very soft organic peat layers with strengths below 5kPa.

During the consolidation period an average volume reduction of 40 to 60% was achieved with absolute settlement up to 4 meters. It has been possible to use a fast lifting schedule of 0.5 to 0.75m of sand a week on this very soft subsoil. This was possible thanks to the effect of vacuum on the effective stress increase in the first lifts where the vacuum acts as a surcharge, but not as a driving force for instability. Figure 13 provides a short summary of the compression, settlements and embankment heights in the project.

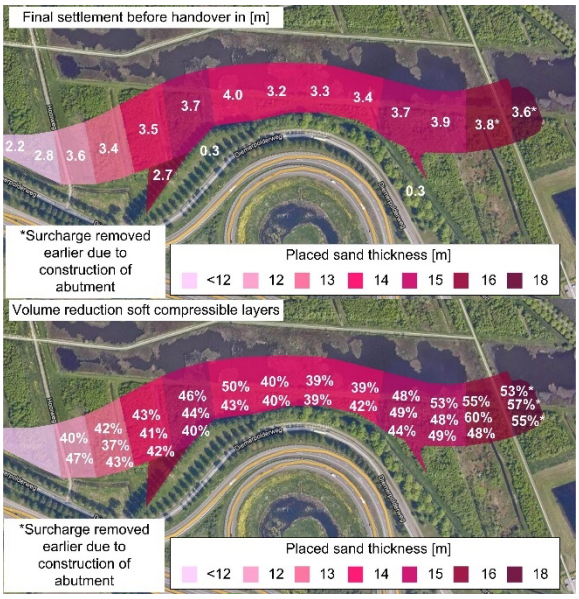

Figure 13. Measured settlements, top image, and compression rates bottom image

Drain to drain vacuum system

The distinctive feature of the Drain to drain vacuum system, also called BeauDrain-S (Single) system, is that the vertical drain consists of a normal PVD section extended by an ethylene tube (impervious) to cross the permeable layers and the non-saturated layers. The length of PVD and ethylene tube sections depend on site conditions and the application. Each single vertical drain is individually designed and can differ in ethylene length and PVD length. Each single ethylene tube, present at the surface after installation, is separately connected at the surface to the vacuum system. The system is ideal to be used on small or irregular areas as each single PVD is connected to the system. The use of the ethylene tube offers the advantage that thick sand layers can be crossed and the vacuum can be applied only the sections where the vacuum needs to be applied without the need to blind the sand layers using trenches. A good example for the BeauDrain-S system is a project executed in Singapore where a total drain length of 30m was installed using over 12m of ethylene tube to cross a sand key on a new reclamation site. The drain was only applied to the deep soft clay thanks to predesigned lengths of ethylene tailored to the need of the project.

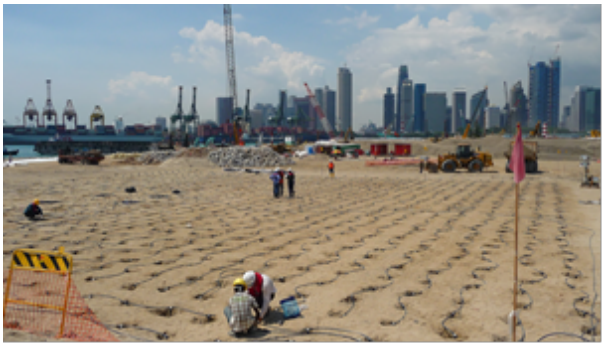

Figure 14. BeauDrain-S from the surface with lines connecting the single drains

The installation of the BeauDrain-S vacuum system is performed with the same equipment as for regular PVD installation. The drains are prefabricated with predetermined lengths of ethylene tubing and pulled into the installation sets. The ethylene hose is installed across the thickness of the working platform and, depending on the groundwater level, extended half a meter into the sealing clay or peat layer. After installation, only the ethylene tubes protrude above the installation platform. After the tubes have been cut to length, the BeauDrain-S drains are connected to each other in lines by means of couplings. These pipes are connected to a vacuum pump at the edge of the field via a manifold and collection pipe. Figure 15 shows the installation process on site.

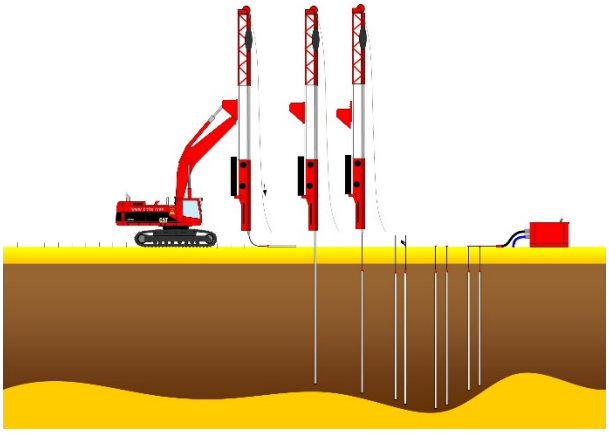

Figure 15. Basic installation method of the liner vacuum system

Similar to the BeauDrain vacuum system, the top section of the soil will also remain without vacuum as the ethylene tube is located over this section. The pressure profile of the system is provided in Figure 16.

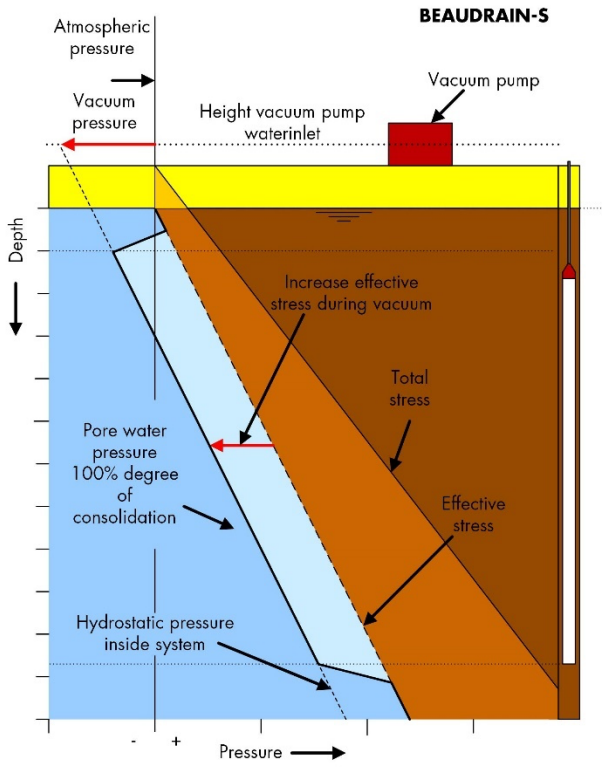

Figure 16. Pressure development of the BeauDrain-S vacuum system

The BeauDrain-S system relies on the closure of the installation hole; hence care should be taken when medium stiff to stiff clay layers are present at the surface. In these scenarios, the installation location has a larger risk to remain open and the vacuum cannot be reached by an excessive inflow of air. Due to the use of small diameter tubes, the maximum number of drains that can be connected to a single line is limited and depends on the expected settlements. Despite the limitations related to the soil conditions and the limited line length, it is used in many projects. This has mainly to do with the flexibility both in the area but also in the section where vacuum is applied. The BeauDrain-S system is ideal to be applied to dike reinforcement projects as there is no liner involved, and the large plough is not ideal to be applied to the narrow winding installation stretched often involved with dike reinforcement projects. The vacuum is hence used to create strength without applying large berms. Figure 17 shows the increase in resistance of a ball penetrometer after the treatment [Vink 2019]

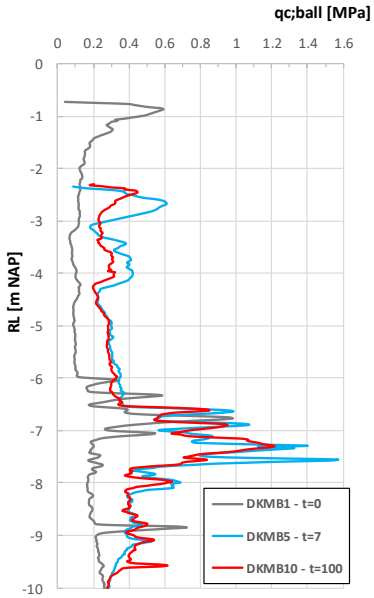

Figure 17. Ball penetrometer results before and after consolidation in the Beaudrain-S section [Vink 2019]

The BeauDrain-S system has also been successfully utilized to create strength in a hydraulically placed sludge depot in Bremerhafen where the material was too soft for placing a cap with the equipment on site. The dredged material was found to only have an undrained shear strength (0.1 to 0.5kPa) at the top of the newly placed material. [Nooy van de Kolff 2010]. The vacuum system proved to be crucial to the project. Thus, it was installed from floating pontoons after which the area was drained from the surface water. Using special tools the single ethylene tubes were connected to lines, and the vacuum system was applied from pontoons on the water.

Figure 18. Tubes after installation, ready to be connected

Figure 18 provides an image of the area after installation of the single vacuum drains. Note that a first capping layer was already placed before the contractor noticed that the major deformations took place, and a vacuum was required to be able to meet the functional requirements of the project. After a few months of pumping, the first lifts of dry sand could be placed, and the strength increased up to 5 kPa. In addition, the system released and removed (part of) the gas dissolved in the organic-rich sludge.

CONCLUSION

Vacuum consolidation has proven itself to be a mature solution for the treatment of soft compressible material as used in civil engineering practice. The prefabricated vertical drain has also proven its use in current capping projects. With the use of the demonstrated strength increases from vacuum projects performed with the different vacuum systems for civil engineering applications, a link can be made to potential application of vacuum consolidation in the oil sands sector for the capping of tailing ponds. Although the conditions would differ from the current application areas, there are certainly possibilities for each of the described systems to be used in tailings (e.g., MFT), each with its particulars and requirements to overcome the well-known challenges encountered in tailings ponds such as the presence of bitumen, gas formation, changes in soil conditions and so on. Listing of the exact particulars and how these can be overcome is by itself a separate study. A table has been provided in which a general comparison is made between the systems. Note that the classification is based on the opinion of the authors.

Table 1: Classification for the use if the systems in various conditions

	Liner	BeauDrain	Drain to drain
Soil type			
Stiff material	++	+	-
Soft material	++	++	++
Size			
Small	-	-/+	++
Medium	++	++	++
Large	++	++	-/+
Location			
Dry platform	++	++	++
Hybrid platform	-	++	++
Water based	-	++	+
Tailing ponds	-	++	+
MFT			
Bitumen	++	++	++
Cold winter	-	+/-*	-
Heterogeneity	++**	+**	++
Subareal/sub-Aqueous	-	+	+
flocculated/un-treated materials	++	++	++
Collection water	++	++	++
Size of the pond	++**	++**	-

* System is buried under the ground. Frozen section is 0.6m to 1.2m

** System should be used in compartments

REFERENCES

Bjerrum, L., 1967, Seventh Rankine Lecture: Engineering geology of norwegian normally-consolidated marine clays as related to settlements of buildings, Geotechnique 17, 1967: 81-118

Bergado D., Jamsawang P. 2022, Vacuum-PVD improvement: a case study of the second improvement of soft Bangkok clay on the subsiding ground, International Journal of Geosynthetics and Ground Engineering IGGE Volume 7 issue 4

Blond E., Dolez P. 2017. Evaluation of Geotextile Performance for the Filtration of Fine-Grained Tailings, Geotechnical Frontiers 2017

Dijkstra, J.W., 2012. Clogging potential of Mebradrain filters when used in Suncor MFT. Cofra B.V. Confidential report.

Dijkstra, J.W. , Bodamer, R. 2014 Determination of the discharge capacity of buckled PVD's, 10ICG Berlin Germany

Dijkstra, J.W., 2015. Design, construction and monitoring of 18m thick embankment on top of very soft peat using BeauDrain vacuum consolidation, XVI ECSMGE Edinburgh

Dijkstra, J.W., Vink, J-W. 2016 Clogging potential of Mebradrain vertical drain filters in mature fine tailing material, EuroGeo6 Lubliana

Jacobs, W., Dykstra, C., Kesteren W. 2012 In situ hydraulic capping of soft tailings. Proc. of the 3rd international oil sands tailings conference, Edmonton, Canada.

Kjellman W. 1945 United States Patent 2482673
With title: Drainage system

Kjellman W. 1952 Consolidation of clayey soils by atmospheric pressure. Proceedings of the Conference on Soil Stabilization, Massachusetts Institute of Technology, USA, pp. 258–263.

Kochx, A. 2011 The effect of filter jacket clogging on the performance of prefabricated vertical drains in soft soils, Thesis TU Delft

Nooy van der Kollf, A. Lesemann, D. Petereit K. The use of dredged sludge as a fill in the osthaven Bremerhaven, Germany, PIANC MMX Congress Liverpool UK 2010

Robertson 2013 pond 5 wick drain performance assessment - confidential report

Vink J-W, Dijkstra J.W., de Bruijn H.T.J., Van M.A., 2019, Vacuum consolidation trials to validate strength increase of peaty subsoil for dike stability ECSMGE2019, Reykjavik Iceland

Yao, Y., van Tol, AF., Everts, HJ., & Mulder, A. (2010) Filtration tests on PVD filter jackets in fine oil sands tailings, 14th international conference on tailings and mine waste, Vail, Colorado, USA

CHEMICALLY-ENHANCED MODIFICATIONS TO IMPROVE DEWATERING PERFORMANCE FOR OIL SANDS TAILINGS

Miguel Pelaez, Xihui Yin and Thomas Fenderson
Kemira Chemicals, USA

ABSTRACT

Mechanical technologies can be used in combination with chemical treatment to accelerate the dewatering and settling of fluid and mature fine tailings from the oil sands extraction process. Polyacrylamide-based flocculants have been used to obtain dewatered tailings with relatively high solid content in combination with selected mechanical processes. Higher solid content is desired to maximize dewatering performance, however, this introduces transportation challenges for current and future deposition areas. In this work, improving dewatering performance and mitigating hydraulic transportation challenges were addressed separately.

Several process additives, in combination with a polyacrylamide-based flocculant, were found to further enhance dewatering while maintaining the quality of the released water. The sequence of additive addition was proven to impact the synergy between the flocculant and the additives. With the chosen sequence of addition, higher solids content can be achieved.

In parallel, several dispersants were evaluated for their effectiveness in reducing the yield stress of the dewatered tailings and the impact on long-term settling. Rapid incorporation of the selected chemistry, with low mixing energy and time, led to a significant yield stress reduction of the dewatered tailings. Long-term gravity settling tests indicated that samples treated with the selected chemistry can re-gain yield stress after gravity settling. The gain was higher with chemical treatment and additional dewatering was observed. The quality of the released water improved with the optimum dosage of the additive compared to no chemical treatment.

INTRODUCTION

For decades, oil sands mining companies have developed and implemented technologies to reclaim fluid fine tailings (FFT) and mature fine tailings (MFT) (BGC Engineering, 2010). Polymers have been widely employed to chemically treat tailings in different dewatering applications (Mamer 2010; Vedoy et al., 2015). In order to further increase dewatering rate and solids content when using polymer to treat oil sands tailings certain inorganic additives (i.e., coagulants) have been introduced and shown improved dewatering and consolidation (Pelaez et al. 2016; Mahmoudkhani et al. 2012). The selection of suitable secondary additives can fully maximize the treatment performance by further increasing solid content based on cumulative or synergistic effects.

For instance, the use of ionic liquids has been proven effective as an auxiliary additive together with a polyacrylamide-based polymer to treat oil sands tailings (Fenderson et al., 2021). The synergetic effect produced by the polymeric flocculant and the auxiliary agent resulted in a reduction of the released water solids content and improved the settling rate of the flocculated material. Moreover, a polymer dosage reduction can be obtained, while still meeting the desired performance criteria, in the presence of selected ionic liquids.

A hydrophobic additive, named hydrophobic modifying agent (HMA), provided improved performance for the dewatering of oil sands tailings after initial treatment with flocculant and/or coagulant (Yuan et al., 2015). Introducing a hydrophobic component on the flocculated fine tailings yielded enhanced floc, hydraulic conductivity and porosity which translates into higher dewatering and consolidation after filtration.

Aluminate salts can be combined with silicate to condition tailings that can increase dewatering and settling rate after the addition of a organic polymer. This technology, defined as chemically induced micro agglomeration (CIMA), requires long conditioning time between the two inorganic chemicals in order to be effective. However, by reversing the order of chemical addition, the produced flocculated tailings can have similar performance to CIMA treated tailings but without conditioning time (Sakuhuni et al., 2019)..

Therefore, the order of chemical addition is a key parameter that can have an impact in the overall performance.

While high dewatering, settling and solid content can be achieved with chemical aids, several operational challenges arise: 1) The yield stress can increase exponentially as the solid content increases in the treated samples (see Figure 1, original data). This can have a significant impact on the selection of the final deposition area due to the logistics of transporting a paste rather than slurry tailings (BGC Engineering, 2010), 2) the process efficiency can be affected based on equipment selection, cost and energy consumption due to the considerable volume of treated tailings generated. For instance, head losses increase significantly when solids concentration are increased during slurry transport due to the type of flow regime observed. Moreover, the higher solids treated tailings may be thixotropic displaying a lower yield stress once sheared and will create conflict on the type of pump used during transport due to lack of consistency (centrifugal vs positive displacement pump). If the disposal site is some distance away it may be beneficial to pump slurry with lower solids content (Watson et al, 2010) which can impact the consolidation performance. An alternative is to reduce the yield stress while attempting to maintain the high solids from the tailings treatment operation.

Rheology modifiers are designed to change the interparticle interaction force, which is composed of van der Waals, electrostatic, hydrophobic, hydration, and other forces (Cruz et al., 2019). One type of rheology modifiers are known as dispersants which can have several different functions: 1) interact with particle surface, 2) provide steric interference, 3) prevent coagulation/flocculation and/or 4) reduce the slurry yield stress. Dispersants may be either organic or inorganic, and they generally affect the state of particle aggregation or dispersion. Inorganic dispersants act primarily by affecting the surface charge of mineral particles and, thus, control the magnitude of electrostatic attraction/repulsion between particles. The action of organic dispersants is a combination of electrostatic and steric forces (see Schematic 1). Those steric forces are higher with low molecular weight polymers rather than high molecular weight polymers (Klein & Pawlik, 2005).

Dispersants can enhance the fluidity of mineral slurries and hence enable them to be pumped at much higher concentrations (Melorie et al., 2018). The use of single component system such as polyacrylate, phosphate-based, polymethacrylate and polystyrene sulphonate to control rheology of mineral suspensions has been widely studied. Leong (2021) employed NaOH-phosphate-based composite inorganic dispersants to reduced concentrated iron ore tailings viscosity and yield stress for ease of pumping. Yield stress reduction of more than 90% was observed at optimum dosages.

Concentrated kaolin slurries in seawater with alkaline pH were treated with sodium tripolyphosphate (STPP) to enhance dispersion (Leiva et al., 2021). A highly saline environment increases drastically the yield stress of kaolin slurries and STPP was able to cause a significant reduction, from 231 Pa to 80 Pa at a characteristic dosage of 0.53 kg/ton. Focused beam reflectance measurement (FBRM) was employed to verify the dispersion of particles, through chord length analysis, after STPP was applied. A reduction in zeta potential also indicated the interaction between STPP and the kaolin particles that led to an increase in electrostatic repulsions between them.

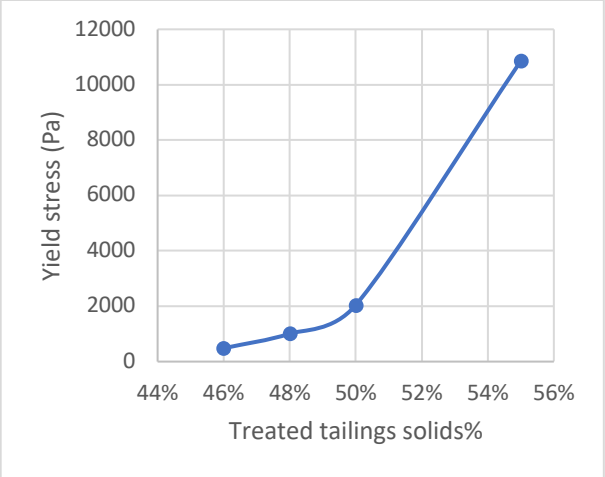

Figure 1. Correlation between solids% and yield stress on treated tailings.

Herein, this study aims at 1) introducing secondary additives to boost the solid content of the tailings and 2) assessing different chemistries that can provide a yield stress reduction on the high solids treated tailings for transportation while determining the impact on dewatering and long-term settling.

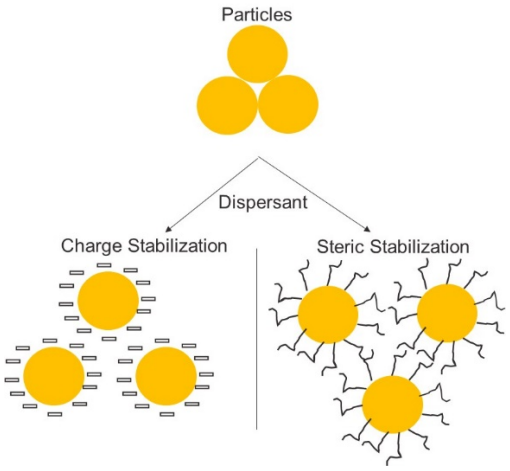

Schematic 1. Dispersant mechanisms for slurry modifications.

EXPERIMENTAL

a) Additives for enhanced dewatering testing

FFT with solids content of 26% was obtained from an oil sands producer in Alberta, Canada. The material was homogenized with an overhead mixer before flocculation tests. A specific sample was withdrawn and pre-mixed at 300 rpm for 2 min and then each additive, according to the established sequence of injection, was added into the FFT and mixed for 1 min followed by the addition of Kemira's flocculant E-4993SK, which is an anionic dry polymer. Additive 1 is a conventional acid-containing coagulant and Additive 2 is a novel inorganic agent in salt form.

The flocculated material was transferred to a 50 ml centrifuge tube and then centrifuged at 910 rcf for 2.5 min. After centrifugation, the solids of the released water and treated tailings were weighed and then placed in an oven to dry at 100 °C. After drying, the weight was recorded and the solids % was obtained for the released water and the treated tailings.

b) *Yield stress reduction testing*

Commercially-treated tailings were obtained from an oil sands producer in Alberta, Canada. The solids content ranged from 46-51%. Prior to testing, the material was homogenized manually with a spatula to minimize disruption of the floc structure and the initial yield stress was measured with a Brookfield Rheometer DV3T (Vane series spindle; 0.1 rpm). Polymeric-based dispersants (Dispersants 1 & 2) were compared with a conventional non-polymeric dispersant (Dispersant 3).

The lab-scale tests were carried out using an overhead mixer with a Phipps-Bird paddle stirrer. A predetermined dosage of dispersant was added into the sample and mixed at low energy. The yield stress was measured after a fixed mixing time. The yield stress reduction % was calculated from the initial and final yield stress measurement. For the dewatering measurements, a capillary suction time (CST) apparatus from OFITE was used. The filter paper was Fisherbrand P8 (coarse, fast). A modified slump test was used to determine flowability. The treated sample was placed in a cut open centrifuge vial and lifted vertically. Inductively coupled plasma mass spectrometry (ICP-MS) analysis was used to measure selected elements from the released water after long-term settling.

RESULTS AND DISCUSSION

a) Additives for enhanced dewatering

Several process additives, in combination with the flocculant, were found to be capable of improving the solid content of the mechanically-assisted treated tailings while maintaining or lowering the released water solids % (see Table 1). When using the optimum flocculant dosage only, a 43.6% solids content was achieved under laboratory conditions. When adding the optimum dosage of Additive 1 only after the flocculant, the solids% improved to 48.6% (+5.0% increase) while with Additive 2 only the cake solids% was 46.7%.

Two different injection sequences for the additives were examined. Results suggested that adding Additive 2 followed by Additive 1 (both at optimum dosage) after flocculation provided a superior performance compared to Additive 1 followed by Additive 2. This indicates a synergistic effect between the additive(s) and flocculated tailings in a specific sequence. When combined together in an A2-A1 sequence, the solids further increased to 50.5% (+7.1% increase compared with flocculant only treatment). It should be noted that with the addition of these additives, in both injection sequences, no reduction on released water clarity was observed. The solids% of released water were similar.

Table 1. Effect of additive(s) in released water and treated tailings solids%.

Injection Sequence	Released water solids%	Treated tailings solids%
F	0.36%	43.6%
F-A1	0.35%	48.6%
F-A2	0.42%	46.7%
F-A1-A2	0.37%	47.7%
F-A2-A1	0.36%	50.5%

These laboratory-scale results suggest that when using mechanically-assisted technologies, dewatering performance can be improved by using additives along with a polymeric flocculant. Depending on the interaction between the additives, flocculant and clay particles, the injection sequence could have significant impact on the dewatering performance. However, if additives are implemented into the operation process, the higher solids content introduces transportation challenges for current and future deposition areas. Mitigating these hydraulic transportation challenges were addressed in the next section separately.

b) *Yield stress reduction*

It was observed that rapid incorporation of the selected chemistry, with low mixing energy and time, led to a significant yield stress reduction of the dewatered tailings, as shown in Figure 2. Higher yield stress reduction was observed at lower dosages for both polymer-based dispersants (Dispersant 1 & 2) compared to the conventional Dispersant (Dispersant 3), as shown in Figure 1.

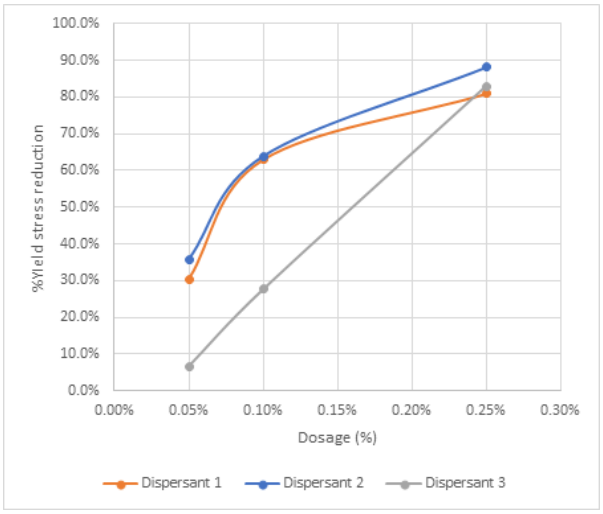

Figure 2. Yield stress reduction (%) of treated tailings with different dispersants.

For tailings, a lower yield stress translates to higher flowability. The modified slump test provided a visual indication on the effect of the dispersant addition in the treated tailings. Figure 3 shows that, based on ring diameter, the flowability improved when adding Dispersant 1 vs no treatment with dispersant (control). Also, it can be seen that the flowability was higher when increasing the Dispersant 1 dosage.

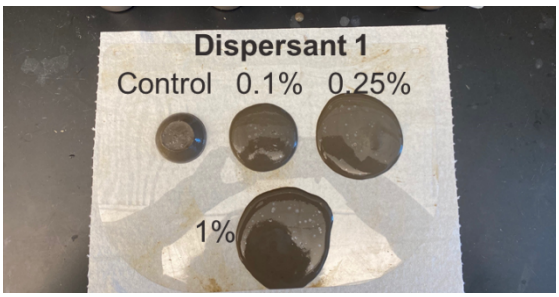

Figure 3. Flowability using different dispersant concentrations (0.1, 0.25 & 1%) vs control.

The immediate dewatering of the samples treated with Dispersant 2 is shown in Figure 4. An increase on the CST was observed with higher dosage compared to control (mixing only). This indicates that introducing Dispersant 2 will reduce the initial dewatering compared to no treatment and higher dosage of the dispersant will further reduce dewatering. However, the differences were not very high.

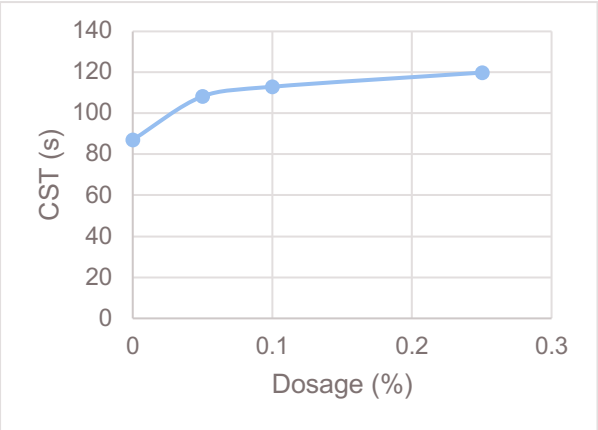

Figure 4. Capillary suction time (CST) with different dosages of Dispersant 2.

Continued dewatering and strength gain were evaluated by determining the yield stress after the treated sample was transferred to a covered glass beaker (60 ml) for gravity settling. After 2 months of settling, released water was observed and the solids % and yield stress were determined after removing this layer of water. For all the samples, including the control, there was an increase in the yield stress after 2 months. However, the yield stress was higher for the samples treated with Dispersant 1 & 2 compared to the control. Also, the solids % were slightly higher when the sample was treated with the dispersants indicating that the samples with dispersant released more water than the control. This could be due to the rearrangement of clay particles from face-edge stacking to face-face after treated by dispersant (Cruz et al., 2019). The samples with dispersant continue to gain yield stress and it was proportional to the dosage applied.

Table 2. Long-term settling of treated tailings with and without dispersants.

		Initial time			Time: 2 months	
Chemical	Dosage (%)	Solids (%)	Yield stress before mixing (Pa)	Yield stress after mixing (Pa)	Yield stress after 2 months (Pa)	Solids (%)
Control		49.6	111.4	95.7	222.4	51.9
Dispersant 1	0.05	49.6	99.8	69.4	288	52.8
Control		48.7	113.3	115.2	299.2	50.8
Dispersant 2	0.1	48.7	106.2	38.4	241.6	52.4
Control		46.1	47.7	49	254.4	49.5
Dispersant 2	0.25	46.1	39	4.64	108.4	52.7

Based on the observations in the long-term settling tests, ICP-MS was performed on the released water of selected samples to determine the concentration of elements of interest and investigate any potential improvements in water quality. Samples treated with dispersant had lower concentrations of Ca, K and Mg compared to non-treated samples (see Table 3). This is advantageous for the reuse of the released water since Ca and Mg are detrimental to the bitumen extraction process (Masliyah et al. 2004).

Table 3. Water analysis after long-term compaction.

Sample	Treatment	Ca [mg/Kg]	K [mg/Kg]	Mg [mg/Kg]	Na [mg/Kg]	S [mg/Kg]
1	Control	110	26	43	400	220
2	0.05% Dispersant 2	78	19	32	410	210
3	0.1% Dispersant 2	65	15	26	430	210

CONCLUSIONS

Two main conclusions can be drawn from this study:

1. Secondary process additives, in combination with a polyacrylamide-based flocculant, were found to further enhance dewatering while maintaining the released water quality. The sequence of addition between Additive 1, 2 and the flocculant determined the final solids content of the treated tailings. With the preferred sequence of addition, higher solids content can be achieved.

2. Chemical aids were evaluated with polymeric dispersants having the highest yield stress reduction at lower dosages compared to conventional dispersants. Rapid incorporation of polymeric dispersants was observed with low mixing energy. A slump test provided a fast evaluation of the flowability of the treated samples with and without dispersants. The dispersant reduced the initial dewatering compared to no treatment, however samples treated with dispersant can gain yield stress after gravity settling. The gain was higher than without treatment, and there was additional water released in the treated samples which led to higher solid % in the treated tailings. The quality of the released water improved with the addition of polymeric dispersant.

ACKNOWLEDGMENTS

The authors would like to thank the management of Kemira for permission to publish this work.

REFERENCES

BGC Engineering Inc., 2010. Oil Sands Tailings Technology Review. Oil Sands Research and Information Network, University of Alberta, School of Energy and the Environment, Edmonton, Alberta. OSRIN Report No. TR-1. 136 pp.

Mamer, M. (2010). Oil sands tailings technology : understanding the impact to reclamation [C]. doi:http://dx.doi.org/10.14288/1.0042580

Vedoy, D. R. L. & Soares, J. B. P. 2015. Watersoluble polymers for oil sands tailing treatment: A review. The Canadian Journal of Chemical Engineering, 93: 888-904.

Mahmoudkhani, R. Tellakula, P. Watson, T. Fenderson, K. Stewart & Y. Wu. (2012) Consolidation of Oil Sands Process Tailings by Enhanced coagulation-flocculation. Proceedings of the Third International Oil Sands Tailings Conference, Edmonton, Alberta, Canada, 121-132.

M. Pelaez and T. Fenderson. (2016) Application of Novel Polymer Combined with Inorganic Coagulation for Consolidation of Oil Sands Tailings. Proceedings of the Fifth International Oil Sands Tailings Conference, Edmonton, Alberta, Canada 214-218.

Masliyah, J., Zhou, Z.J., Xu, Z., Czarnecki, J. and Hamza, H. (2004) Understanding Water-Based Bitumen Extraction from Athabasca Oil Sands. Can. J. Chem. Eng., 82: 628-654

Watson, AH, Corser, PG, Garces Pardo, EE, Lopez Christian, TE & Vandekeybus, J (2010) A comparison of alternative tailings disposal methods — the promises and realities, in R Jewell & AB Fourie (eds), *Mine Waste 2010: Proceedings of the First International Seminar on the Reduction of Risk in the Management of Tailings and Mine Waste*, Australian Centre for Geomechanics, Perth, pp. 499-514.

Leiva,W.; Toro, N.; Robles, P.; Gálvez, E.; Jeldres, R.I. (2021) Use of Multi-Anionic Sodium Tripolyphosphate to Enhance Dispersion of Concentrated Kaolin Slurries in Seawater. Metals, 11, 1085.

Y-K Leong. (2021) Controlling the rheology of iron ore slurries and tailings with surface chemistry for enhanced beneficiation performance and output, reduced pumping cost and safer tailings storage in dam. Minerals Engineering 166, 106874.

N. Cruz, J. Forster, E. R. Bobicki. (2019) Slurry Rheology in Mineral Processing Unit Operations: A Critical Review. Can. J. Chem. Eng. 9999:1–19, 20.

B. Klein, M. Pawlik (2005) Rheology modifiers for mineral suspensions. Mining, Metallurgy & Exploration 22, 83-88.

T. Fenderson, L. Kyllonen, A. King, E. Sklavounos, F. Fournier, S. Aujla. (2021) Method and composition for treating tailings. US Patent US11001761B2.

G. Sakuhuni, C. Lin, T. T. Ngo, G. S. Forgeron, S. Cebula, A. Zahabi (2019) Oil sand tailings treatment using flocculation and treatment with a coagulant and a silicate. Canada Patent CA 3048297A1.

A. K. Melorie, D. R. Kaushal. (2018) Experimental investigations of the effect of chemical additives on the rheological properties of highly concentrated iron ore slurries. KONA Powder and Particle Journal. 35 186-199.

S. Yuan, J. Lorentz, R. Siman, Y. J. Gu. (2015) Oil sands fluid fine tailings dewatering using additives. US Patent US20160311709A1.

PSEUDO TAILINGS AND FLOCCULATED FFT (FFFT) PIPELINE TRANSPORTATION PRESSURE LOSS METHOD

Michael St-Cyr, Artem Holik, and Michael Hujber
Local Engineering, Edmonton, Alberta, Canada

ABSTRACT

Accelerated dewatering (ADW) is a proven low-cost technology to successfully treat fluid fine tailings (FFT) as an effective means of reducing tailing volumes. This dewatering technology treats FFT with coagulant followed by a flocculant addition with effective shear mixing and transport of the resulting apparent Bingham yield stress slurry to a suitable location for deposition, all within a completely closed piping system. Such systems are highly beneficial due to lower complexity, improved safety from the use of a completely closed system and the ability to treat material in a central location and transport Flocculated FFT (fFFT) a significant distance. The reduced complexity of the system also allows improved mobility of the facility once the accessible deposit locations are filled.

A major challenge with the transportation of fFFT within a closed piping system may include pressure gradients that could be unpredictable due to varying laminar fluid flow characteristics. The development of computational methods validated by actual operating data are required to accurately predict and assess overall system hydraulics and to design effective and efficient pumping systems at the high capacities required to process significant quantities of FFT.

Data from the literature indicates that flocculated FFT yield stress can vary significantly depending on mixing which in turn will affect the pressure gradients observed in the pipeline. In addition, it has been observed that in laminar flows minimum pressure gradients may be required to transport any larger solids that deposit in the pipeline. Given these complex flow situations there is need for a predictive tool that can be used in the design of such systems. This has encouraged the authors to develop an Excel based automated computational model that is easy to use and quickly produces results to allow evaluation of dynamic systems with different site conditions, essentially creating a User Interface. The use of this model has simplified the computations required to design full scale facilities that meet ADW objectives in the management of tailings.

INTRODUCTION

Background

Alberta Energy Regulator (AER) Directive 074 was first introduced to slow the growth of tailings ponds by creating standard requirements. Companies were required to track the amount of tailings they had dried using technology to remove water from the tailings and make the area accessible for reclamation. However, in 2016 Directive 085 replaces Directive 074 by tackling both existing tailings and new fluid tailings growth. Therefore, the objective is to minimize fluid tailings accumulation by ensuring that fluid tailings are treated and reclaimed progressively.

There are various proven dewatering technologies to process tailing volumes. However, the industry has sought out to develop a process with the lowest operating cost and complexity specific to the oil sands. Accelerated dewatering (ADW) technology has been considered as a low-cost tailings treatment process adapted from other areas of the industry. A closed system is accomplished all within a pipe where fluid fine tailings (FFT) are treated with a coagulant followed by a flocculant addition, mixing, and transportation to a final deposit location for dewatering. After multiple proven successes, the technology has continued to be developed and enhanced through a series of larger scale demonstration facilities.

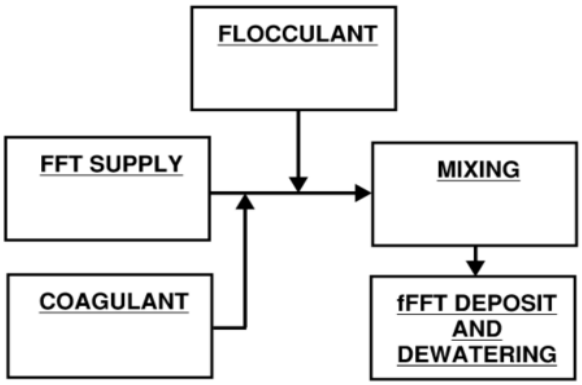

Figure 1. ADW Block Flow Diagram

ADW Design Considerations

In order to develop an effective ADW facility design, the user must first have a strong understanding of the properties that impact the transportation of the fluid to its final deposit location.

The properties of FFT (or FFT treated with a coagulant) can be estimated based on solid content but generally are provided for a site specific location. However, flocculated FFT properties are difficult to accurately predict but are very important to determine since the transportation of fFFT creates significantly higher pressure gradients than FFT or treated FFT. The ability to confidently predict the rheology is essential for establishing an appropriate flocculant injection and mixing facility location such that the hydraulic system design can accommodate the transportation of fFFT. The ideal location is to introduce flocculant and mixing near the deposit location thereby easing the pumping and piping design requirements. However, securing a nearby location within a mining environment is challenging and may force the ADW facility to be located at a significant distance away from its final deposit location. A balance between both ADW plant real estate locations and pumping design requirements needs to be carefully considered during the initial concept phase for a successful ADW implementation.

A hydraulic predictive tool is required to evaluate the numerous hydraulic conditions at various pressure gradients and pipeline profiles that need to be considered during initial facility siting determination and throughout project develop as several deposit locations may need to be evaluated. This led to the development of a computational model that was incorporated into a hydraulic calculator to interactively predict non-newtonian characteristics. The use of the computational model has been validated with actual field trial operating conditions allowing evaluation of overall hydraulic systems for effective designs and optimized pumping performance.

NON-NEWTONIAN BINGHAM FLUIDS

Fine fluid tailings are primarily made up of suspended fine solids and are typically considered as a homogenous slurry. These slurries tend to behave as non-Newtonian fluids with a yield stress that allow Bingham models to predict hydraulic performance.

$$\boldsymbol{\mu_p = \frac{(\tau - \tau_y)}{\gamma}}$$

where μp is the plastic viscosity (Pa s), τ is the shear stress (Pa), τ_y is the yield shear stress (Pa), and γ is the shear strain (s^{-1}). In comparison, for Newtonian fluids the stresses are proportional to the rate change and yield stress is omitted when determining the viscosity.

For a Bingham fluid, two models are used to predict pressure drop in either laminar or turbulent regime by determining the shear wall stress (τ_w).

For laminar regime:

$$\boldsymbol{\frac{8V}{D} = \frac{\tau_w}{u_p}\left(1 - \frac{4}{3}\varepsilon + \frac{1}{3}\varepsilon^4\right)}$$

where V is the bulk velocity (m/s), D is the hydraulic diameter (meters), and $\varepsilon = {}^{\tau_y}/_{\tau_w}$

For Turbulent regime:

$$\boldsymbol{V = V_N + \mu_* \left[2.5ln\left(\frac{1-\varepsilon}{1+\varepsilon}\right) + \varepsilon(14.1 + 1.25\varepsilon)\right]}$$

where $\boldsymbol{\mu_* = \left({}^{\tau_w}/_{\rho_m}\right)^{0.5}}$, and $\boldsymbol{Re = DV_N\rho_m\left(\frac{1-\epsilon}{\mu_p}\right)}$, *Re* is the Reynold number (unitless), ρ_m is fluid density (kg/m^3), and V_N is determined iteratively using $V_N = \left(\frac{2\tau_i}{\rho F_n}\right)^{0.5}$ where F_n is the friction factor using an initial bulk velocity input.

The laminar and turbulent Bingham models are implicit correlations where the pipeline flow rate (i.e. velocity) is typically a known variable however the shear wall stress is required to determine the pressure drop. In addition, rheology is required to determine the slurry density, plastic viscosity, and yield stress. Due to the implicit nature of the models, iteration is required to determine the shear wall that corresponds with known inputs. There are two methods to solving the shear wall stress:

1. Perform small shear wall stress step changes until the velocity matches the desired output.
2. Determine the implicit correlation roots applying the Newton-Raphson method.

In both situations, the assistance of computer programs is required to accelerate the required iterative process. The first iterative step approach takes a program longer to execute due to potentially small step changes required to gain accurate results. The second Newton-Raphson approach is considered to be much faster as each iteration step quickly converges to the result, however this method requires an initial guess to start the computation. The closer the initial guess is to the final result, the faster the computation. In addition, the second approach allows convergence to take place under defined tolerances thus improving results accuracy.

The authors have utilized the second method to develop a computation method built into the Excel Visual Basic (VBA) platform for the purpose of predicting shear wall stress for Bingham models.

With the aid of this computational method, the precise shear wall stress is determined instantly at any given condition allowing for an interactive user environment. The computational method has been built as a function within Excel which allows live input changes to result in immediate answers and works with other calculating functions. In addition, the Excel built-in goal seek feature can be used interactively with the computational method function to resolve answers quickly. The end result in a user friendly design tool that quickly and accurately allows the user to assess and troubleshoot complicated slurry hydraulic systems.

Once the shear wall stress is known it can be converted into an equivalent friction factor f_B. It is stressed that the equivalent Bingham friction factor is different from friction factor resulting from methods such as Colebrook-White and Churchill used for Newtonian fluids.

$$f_B = \frac{8\tau}{V^2 * \rho}$$

Then the equivalent friction factor can be easily applied to the overall hydraulic system equivalent length to determine the pressure losses following typical hydraulic calculation methods. The fitting equivalent length can be determined with typical industry known K factors. For large pipelines generally fittings are not all accounted for and therefore it may be more appropriate to apply an overall design factor which can be multiplied to the total equivalent length, especially during the initial design/assessment phase of a project.

$$L_f = \frac{K}{f_B * D}$$

The total equivalent length with the determined equivalent Bingham friction factor can determine the overall pressure losses.

$$dP = \frac{f_B * L_e * V^2 * \rho}{2 * g}$$

Many other fittings components can be converted into their respective K factors allowing the prediction of non-Newtonian pressure losses.

The non-Newtonian shear wall stress can be used to determine an equivalent Reynolds number and viscosity. Typically, fittings can require a Reynolds number to complete a final fitting K factor representative of the pipe size such as the 2K method. The influence of the Reynolds number is small during turbulent regime for the K factor, however attention to laminar regime should be considered for these losses as K factor in laminar flow may increase.

Furthermore, most heat transfer methods require a Reynolds number to compute the pipe inside heat transfer coefficient. The equivalent Reynolds number can provide insight to determine the pipeline heat loss for such fluids.

Fine Fluid Tailing

Generally, FFT consists of large amounts of fines and is characterized as a homogenous fluid. The rheology of FFT slurries must always be considered to properly predict pipeline pressure gradients to transport FFT to a desired location. Hence, the FFT yield stress and plastic viscosity are given inputs and site specific. Treated FFT with coagulant will further impact the rheology of the fluid depending on various factors such as, but not limited to, type of coagulant used, dosing concentration, and FFT solids content. Similarly, treated FFT yield stress and plastic viscosity are given inputs and site specific. The determination of this rheology can take a significant amount of time and lab resources and therefore clients may treat this information as confidential and proprietary.

Typically, the higher the solid contents will result in higher yield stresses and plastic viscosities. Treated FFT with coagulant may further amplify these characteristics requiring further investigation and analysis.

The calculated shear wall results determined by the computation of both Laminar and Turbulent models with respect to velocity are shown graphically below. Although the computation method does not specifically produce a graphical output this was quickly produced by incrementing the flow rate through a pipe. The following figures represent the shear wall stresses with respect to velocity through a 20 inch HDPE DR11 pipe for an approximately 33%wt and 28%wt solids.

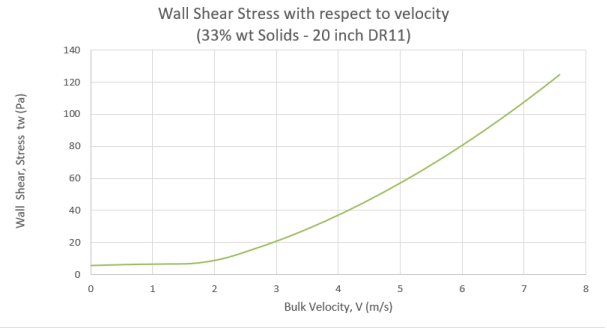

Figure 2. Shear wall with respect to Bulk Velocity for a 33%wt solids (τ_y = 5.6 Pa, u_p = 11.6 cP)

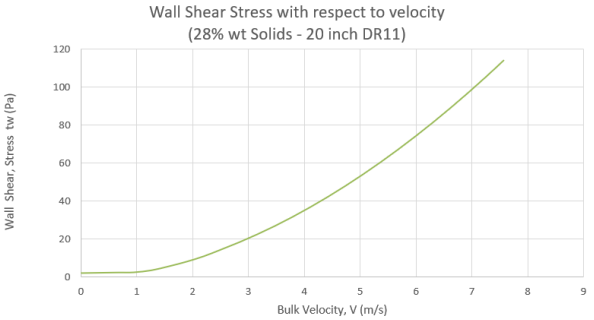

Figure 3. Shear wall with respect to Bulk Velocity for a 28%wt solids (τ_y = 2 Pa, u_p = 7.9 cP)

It is noted that a higher yield stress tends to increase the transitional velocity between laminar and turbulent regime. In addition, the transition occurs when the determined shear wall stress of the turbulent model exceeds that of the laminar model. It is interesting to note that a higher yield does not necessarily cause higher pressure gradient for all velocity ranges and could be the opposite during transitional flow regime. Therefore, it is important to evaluate all turndown conditions that can produce various operating performances. The Excel VBA design tool allows the user to evaluate these different conditions quickly and obtain an accurate understanding of the impact on the conditions as the design is developed.

FLOCCULATED FINE FLUID TAILING (FFT)

When a flocculate solution is injected into a FFT piping system, the fine particles are bound together with the polymer and dewatering occurs. The properties of the slurry change and predicting the shear stress becomes very complex. The Excel based design tool allows the user to transition from a FFT slurry to a complex slurry within the same model, allowing for the analysis of the entire system within the same sheet. This start to finish approach has enhanced the ability for the user to simultaneously evaluate and design a pipeline system for the transportation of both FFT and complex flocculated slurry.

Effective flocculation requires an adequate amount of mixing to reach optimum dewatering effect. The quality of flocculation is measured by a capillary suction time (CST) which is a simple measure of the rate at which water is released from slurry. There is also a significant cost associated with procuring and

preparing flocculant solution ready for injection use. Therefore, the optimum flocculant dosing and mixing performance must be considered to maximize the effectiveness of dewatering and achieve the best flocculation possible.

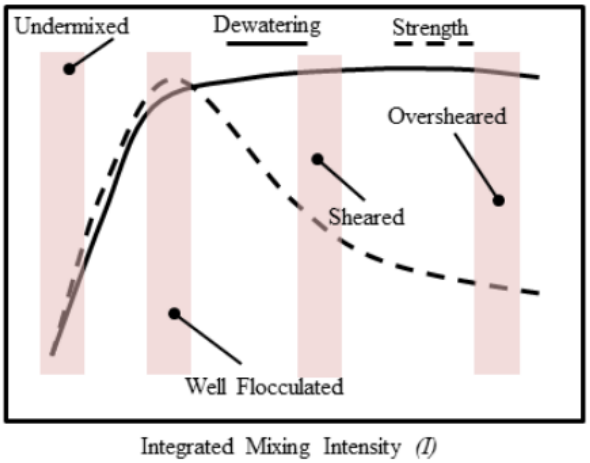

Figure 4. The relationship between the integrated mixing intensity and the mixing state

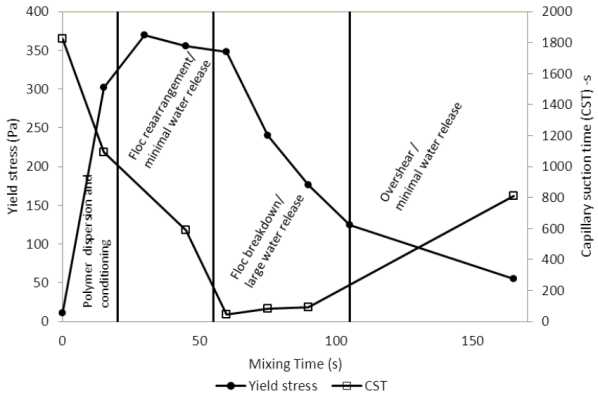

Figure 5. Shear progression curve of flocculated MFT highlighting four distinct

Data from literature shows that flocculated FFT yield stress is dependent on the amount of shear mixing. In addition, the optimum dewatering occurs when the CST is at its lowest while yield stress has been significantly decreased.

None the less, once a flocculant is introduced and mixed, the yield strength significantly increases. Thus, with such high yields stresses the utilization of the models shows that the fluid is apparently characterized as a laminar flow for a wider velocity range. The following figures hypothetically represent the wall shear stresses through a 20 inch HDPE DR11 pipe for a 26%wt solids with a yield stress of 50 Pa.

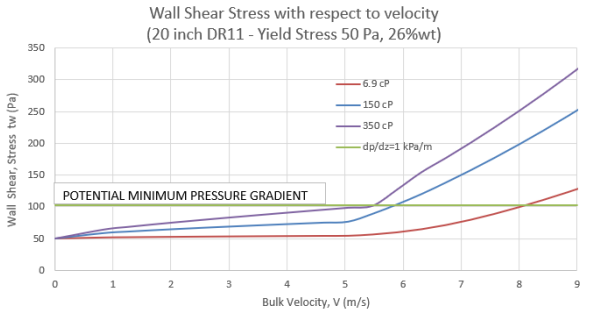

Figure 6. Shear wall with respect to Bulk Velocity for a 26%wt solids (τ_y = 50 Pa)

Marginal wall shear stress gains tend to occur during laminar regime as velocity increases. In this circumstance, the transitional velocity occurs around 5 m/s primarily influenced by the yield stress. The viscosity had marginal influence on the transition velocity from laminar to turbulent. The viscosity significantly influences the rate rise of wall shear stress and is more pronounced during turbulent regime. Typically tailing pipelines are designed with operating velocities below 5 m/s.

The flocculant FFT high yield stress is dependent of FFT quality, polymer dosing, mixing (shearing), and flocculation quality. A range of yield stresses and viscosities are required to be modeled to predict the various possible pressure gradients and overall system hydraulics. There may be situations where the fFFT requires a minimum pressure gradient of 1 kPa/m regardless of velocity as solids deposit in the line. The deposit of solids can create a new hydraulic diameter or increase the yield stress required to move the flocculated FFT.

Additional fFFT Pipeline Transportation Considerations

The Bingham models is suitable for non-settling homogenous fluids. Thus, the FFT slurry is generally treated as a pseudo homogenous fluid and Bingham models can generate good pressure drop predictions. When a flocculant is introduced to FFT the solids begin to settle towards the invert of a pipeline potentially creating a new hydraulic diameter. The settled flocculated solids at the invert of the pipe are moving as a sliding bed which can

require a minimum pressure gradient to be transported in a pipeline.

If the minimum pipeline pressure gradient is exceeded, the settled bed will be transported through the pipeline as a sliding bed. If the determined pressure gradient is lower than the minimum pressure gradient, solids will accumulate on the pipe invert thereby increasing the pipeline pressure gradient until one of the following occurs:

1. The pressure gradient exceeds the minimum pressure gradient required to transport the bed under laminar flow conditions.
2. The velocity above the bed increases sufficiently to generate turbulence to suspend the coarse particles and erode the bed.
3. The system pressure rises to a point where preventative action is necessary to avoid pipeline blockage.

The shear wall stress is proportional to the pressure gradient. If the required minimum pressure gradient and pipeline diameter are fixed values, then the shear wall stress can be determined.

$$\frac{dP}{dz} = \frac{4\tau}{D}$$

If the fluid is transported under laminar regime, velocities at lower viscosities only marginal increases in pressure gradients will result until the laminar to turbulent transition occurs. The laminar to turbulent transitions will occurs at higher velocities where pipelines do not generally operate.

Various pipeline diameters can be used to transport fFFT where a potential settled bed can form particularly in larger pipelines. Therefore, a balanced pipeline sizing approach must be considered as larger pipe sizes will not necessarily reduce the pressure gradient.

When applying the Bingham models a plastic viscosity and yield stress must be known to determine the final shear wall stress. A higher viscosity can be used to explain the higher pressure gradients at a known conditions or more conservatively use high enough yield stress that represent the minimum potential pressure gradient. A flocculated FFT presents many operating challenges as a sliding bed may accumulate additional solids until its minimum pressure gradient is satisfied. If the system cannot provide sufficient pressure to move the settling bed, then a blockage is surely to occur. Therefore, it is important to model various operating conditions to ensure the pipeline system can adequately move the sliding bed without further accumulation of solids. In addition, fFFT pressure gradients can be impacted by the FFT solid quality thus standardization of the FFT feed must be maintained to ensure a manageable pressure gradient that can form.

CONCLUSION

There are certainly additional efforts required to refine and predict flocculated FFT flow behaviors especially within the transition zones. The predictive tool used the Bingham models at higher yield stress to determine the pressure gradients. However, flocculated FFT may require a minimum pressure gradient to move a sliding bed.

Given the complex nature of non-newtonian fluids, a predictive tool has been developed to facilitate the hydraulic design of closed pipe ADW systems. The use of the tool has dramatically improved the ability for the designer to assess and adjust the hydraulic system design for various ADW turndown conditions and objectives quickly and accurately. This is very beneficial for designing ADW piping systems that will continuously be adjusted and altered as the facility and deposition locations change to meet the varying demands of tailing management.

REFERENCES

Shook, C.A and Roco M.C. (1991). Slurry Flow: Principle and Practice.

Scott E. Webster, Wayne A. Brown, Babak Derakhshandeh, Neville Dubash, Clara Gomez, and Christian N. Veenstra (2016). A Comprehensive Control Scheme For Dynamic Inline Flocculation of Oil Sands Tailings.

P.S. Wells, A. Revington, O. Omotoso (2011). Mature fine tailings drying — technology update

Robert Cooke. Laminar Flow Settling: The Potential For Unexpected Problems.

SESSION 8

ON THE MAGNITUDE AND RATE OF AGEING IN BOTH SOFT SOILS AND OIL SANDS TAILINGS

Arazooben Patel and Paul H. Simms
Carleton University, Ottawa, Ontario, Canada

ABSTRACT

Remoulded or freshly deposited soft soils and clayey mine tailings are young materials by their nature and may exhibit the characteristics of ageing. The ageing phenomenon can induce significant changes in the mechanical properties of the soft deposits such as an increase in peak strength and a decrease in compressibility. This may be very important for the deep deposits of re-deposited soft soils of low hydraulic conductivity where slow consolidation over a long period can be influenced by ageing. The ageing phenomenon can, therefore, have important implication for the reclamation of such deposits. This research aims to evaluate both the magnitude and rate of ageing in both soft soil and oil sands tailings. It was apparent that the magnitude of ageing increases as the initial water content decreases for the selected range of water content between 2-1.25 times the liquid limit of tested soft soil. A strong relationship between small strain elastic shear modulus and fall cone shear strength was observed. Moreover, samples of different water contents when remoulded, and allowed to re-age, generated almost identical patterns of strength recovery, pointing to a robust physical process being responsible for the ageing behaviour in soft soils. The rate of ageing in the studied materials was analyzed using concepts developed from ageing experiments in colloidal science, and an empirical relationship was proposed to determine the final ageing strength based on the strength measured after an “Early Equilibrium Stage (EES)”. It was observed that maximum ageing strength could vary close to 5 times the strength measured at the end of the “early equilibrium stage”. This should allow for relatively rapid estimation of the potential for ageing to alter the dewatering and strength development in the existing tailings deposits.

INTRODUCTION

Remoulded or freshly deposited soft soils and clayey mine tailings are young materials by their nature and, consolidation is the dominant dewatering mechanism in these materials upon deposition in the impoundments. However, due to the poor geotechnical properties of these materials such as low hydraulic conductivity, low shear strength, and higher water content, it takes a longer time for the consolidation to come to an end. During that time, these young materials may exhibit time-dependent effects such as creep (deformation at constate effective stress) or ageing. The ageing phenomenon can induce significant changes in the mechanical properties of the soft materials such as an increase in peak strength or stiffness and post-peak strength while reducing the compressibility. Whereas conventional practice designs deposition plans of young material employing the large strain-consolidation theory. Therefore, the predicted long-term behavior of these young materials may not be accurate and differ from behavior observed in the real field deposits.

The ageing phenomenon has been long documented in natural soils (Skempton and Northey, 1952; Leonard and Altschaeffl,1964, Schmertman,1991; Mitchell and Soga, 2005). It is also reported for different kinds of tailings and dredged sediments by many researchers including Banas (1991), Suthaker and Scott (1997), Jeeravipoolvarn (2005), Jeeravipoolvarn et al., (2009), Miller (2010), Igbinedion (2020), Salam (2020), Patel et al., (2021), Zeng et al., (2015), Shahriar et al., (2018), Peng et al., (2021), Ren et al., (2022). Moreover, the increase in sensitivity and decrease in compressibility due to ageing are also reported in pilot studies conducted on flocculated and centrifuged FFT. Interestingly, Salam (2020) and Igbinedion (2020) a found strong match of laboratory scale data with pilot studies. Hence, it is evident that ageing does occur in soft soils and certain kinds of tailings.

Moreover, the magnitude of ageing is speculated to influence by many factors. Banas (1991) concluded that the water content of FFT significantly influences thixotropic strength development behavior and reported a maximum thixotropic strength ratio of about 20 for the water content of 233% which is typically observed in the tailings ponds post-deposition. Suthaker and Scott (1997) also reported preconsolidation pressure of 2 kPa in aged fine tailings compared to a young sample from Syncrude

Pond. Miller (2010) recorded the development of precosnolidation pressure of 0.2 kPa in raw FFT in a 2m standpipe and attributed it to water extraction chemistry. Igbinedion (2020) noted the development of preconolidation pressure of about 10 kPa in centrifuged FFT both in 0.1m tall samples and in the large dry box. Salam (2020) also reported that the magnitude of ageing i.e., increase in sensitivity and preconsolidation pressure, is maximum for the polymer dosage which demonstrated optimum performance in short-term dewatering. Indeed Salam (2020) reported a linear relationship between thixotropic strength gain and preconsolidation pressure. Aldaeef and Simms (2019) also studied the effects of pipeline shear on the magnitude of ageing and observed poor strength development behaviour for the samples exposed to pipeline shear post-flocculation. Similarly, Patel et al., (2020) also demonstrated that higher energy input during sample preparation of soft soils could deteriorate the long-term strength development behavior under low consolidation stresses. Recently, Patel et al. (2021) also identified the conditions necessary for ageing to occur in flocculated FFT and discussed both positive and negative implications of ageing on long-term behaviour.

Similarly, Zeng et al. (2015) and Shahriar and Jadid (2018), Salam (2020), and Alam et al. (2021) also reported changes in compressibility with time and increase in thixotropic strength ratio in dredged sediments/ reconstituted soft soils. Recently, Ren et al. (2021) reviewed numerous studies conducted to understand the thixotropic behavior in soft clays and attempted to develop a correlation between thixotropic behavior and some index properties of soft soils. However, no well-established relationships were proposed. Additionally, Zhang et al. (2017) and Tang et al., (2020) also proposed empirical relationships to quantify the rate of thixotropic strength gain in remoulded natural clays-

$$q_u = A \times t^B \qquad [1]$$

Where q_u is ageing strength and t is ageing time. A and B are the thixotropic coefficients.

$$q'_u(t) = q'_u(0) S_t (k_0 + k_1 w + k_2 \rho) \log t + \frac{q_u}{S_t} \qquad [2]$$

Where q'_u (t) is ageing strength corresponding to the ageing time t, in kPa; q'u (0) is the remoulded strength in kPa; q_u is a strength of undisturbed soil, S_t is the sensitivity of the soil; w is a water content and ρ is a density of the sample (with dimension removed); k_0, k_1 and k_2 are dimensionless model parameters

However, the power-law relationship Eq.1 requires knowledge of thixotropic strength development data (q_u) over time, t, to determine the relationship constants. The strength recovery model proposed by Tang et al., (2020) Eq.2 also requires information on the intact state of the natural soil such as undisturbed strength(q_u) and sensitivity (s_t). Therefore, such empirical relationships cannot be directly applied to young materials which are yet to age.

Researchers also demonstrated that due to ageing, small strain stiffness increases linearly with logarithmic of time after EOP (Anderson and Wood ,1976; Athanasopoulos, 1993). Hence, based on that Anderson and Stokoe (1978) proposed that the slope of the linear portion during secondary compression can provide quantitative information on the rate of ageing and proposed an empirical relationship to estimate time-dependent changes in in-situ soil.

$$G_{\max(field)} = G_{\max(EOP)} + I_G * \log\left(\frac{t_c}{t_p}\right) \qquad [3]$$

Where $G_{max\ (field)}$ is change in small strain stiffness with time. G_{EOP} is small strain stiffness measured after EOP. I_G is the rate of secondary increase, obtained after EOP and time must be one log cycle apart. T_c and T_p are ageing time and time required to reach EOP respectively.

This relationship could potentially be applied to young materials. However, the only limitation would be the time required to reach EOP and determination of I_G parameter as both take a longer time for young materials. Hence, it may not be applied directly to young materials. Therefore, the quantification of magnitude and rate of ageing in young materials remains a challenging task.

Thus, to investigate the magnitude and rate of ageing in young materials, in the current study, soft Leda clay samples were prepared at different initial water contents and time-dependent changes such as undrained shear strength and small-strain stiffness were tracked over a period of 100 days. Based on the data obtained from soft Leda clay samples, data reported by different researchers, and concepts developed from the ageing experiments conducted on ideal colloidal suspensions, an empirical relationship is proposed to quantify both the magnitude and rate of ageing in soft soils and FFT.

Ideal colloidal suspensions and their comparison with young materials

Colloidal suspensions typically consist of small solid particles (10nm ~ 10 μm radius) in a liquid. (Cianci et al., 2006; Weeks, 2017). They are often referred to as dispersion as colloidal particles remain 'dispersed' in a liquid phase. They stay in the dispersed unless temperature, the chemical composition of the dispersing medium, and volume fraction (fraction of total volume occupied by the solid particles) are changed. The clay-water system is a typical example where clay particles having charged surface forms a colloidal suspension when mixed with the water (Michell, 1961).

There exist three different phases of colloidal suspensions: sol, gel, and glass. Sol phase has very small particles in a continuous liquid medium and is inhomogeneous in nature compared to liquid due to temporal cluster. However, upon the addition of polymer or electrolyte, the attractive or charge-stabilized particles cluster together into flocs and act as a denser liquid that exhibits yield stress and viscoelasticity; often regarded as a colloidal gel (Mewis and Wanger, 2009). The glass phase of the colloidal suspension is a function of particle packing fraction (1-porosity) rather than the amount of polymer or electrolyte addition in the suspension.

The phases observed in the ideal colloidal suspension can be correlated to the young materials observed in the field of geotechnical engineering such as soft soils or fluid fine tailings. Although the size of the colloidal particles is relatively smaller and homogenous in ideal colloidal suspensions compared to particles size distribution observed in the soft soils and fluid fine tailings, raw FFT can be related to the sol phase of the ideal colloidal suspension as clay particles essentially remain dispersed due to addition of dispersing agent during the bitumen extraction process. Such a stable state is responsible for the poor geotechnical properties of FFT. However, during the treatment when polymer or salt is added to FFT, clay particles flocculate in the light of attraction forces and form flocs or a network of flocs which eventually settle down under gravity and improve the geotechnical properties of the FFT noticeably. Hence, it closely relates to the gel phase of colloidal suspensions.

Colloidal gel and glass are out of equilibrium systems; as a result, they frequently evolve with time such as viscosity changes with time, due to network restructuring (Manely,2005). Thus, during the rest or ageing period, typically, at fixed density and in the absence of drainage, they display thixotropic behaviour, i.e., their elastic shear modulus and yield stress increase with time. They exhibit the elastic response below the yield stress and above which it freely flows (Ovarlez and Chateau, 2008; Bonacci et al., 2020). Researchers from the colloidal science have made significant progress to understand the fundamental concepts of ageing behaviour in colloidal gels and quantify the rate of ageing in different colloidal systems (Manley et al., 2005; Rich et al., 2011; Pujala and Bohidar, 2013; Au and Leong, 2015; Bonacci et al.,2020). Some important studies would be discussed later in the paper.

MATERIAL AND METHODS

Leda clay

The Leda clay used in this study was collected from the Navan landfill in Ottawa. The typical properties of the Leda clay are summarized in the following table (Aldeef and Rayhani, 2017)

Table 1. Characteristics of Leda clay

Characteristic	Values
Initial solids content (%)	64
Initial water content (%)	56
Specific gravity	2.7
Liquid limit (%)	55
Plastic limit (%)	25
Plasticity index (%)	30
Clay content (%)	71
D_{90}, D_{60}, D_{50}, D_{10} (μm)	10,1,<1,<1
Clay mineralogy	Illite (83%), Kaolinite (11%)

Sample preparation

Leda clay samples were prepared at three different initial water contents – 111.4 % (2 LL), 83.25 % (1.51 LL), and 67.10 % (1.22 LL) by adding a predetermined amount of deionized water into the soft remoulded natural Leda clay.

Natural undisturbed Leda clay was placed on a metal dish and disturbed through kneading for 50-55 minutes to obtain a soft plastic remoulded clay and then a pre-determined amount of deionized water was added to reach the targeted water contents and hand-mixed again for another 50-55 minutes. Samples were then stored in air-tight

containers for 48-72 hours to achieve homogenous distribution of water content. After that samples were again hand-mixed for 15-30 minutes to eliminate the effects of consolidation and bring the sample to the well reproducible initial state.

After achieving a well-defined reproducible state, remoulded Leda clay samples were then deposited into 13 cm tall and 7.5 cm diameter polypropylene columns. The columns were kept covered using parafilm at the top and the space between the cover and sample was kept to a minimum to prevent the escape of the water vapor and the prepared samples were stored at room temperature (21± 2◦C) in the air-tight container. Temperature changes recorded using 5TE were also minimal. For each water content, two different sets of samples were prepared (Figure 2).

Testing methods

The undrained shear strength of Leda clay samples was measured using a fall cone. Prior to fall cone testing bleed water from the sample surface was removed. The cone used had a mass of 40 g and an angle of 60◦. A cone factor (K) of 0.4 is used based on cone angle and roughness (Hansbo, 1957; Koumoto and Houlsby 2001). The undrained shear strength was calculated based on cone penetration using the following equation proposed by Hansbo(1957):

$$S_u = \frac{kmg}{d^2} \qquad [4]$$

Where S_u is undrained shear strength in kPa; k is dimensionless cone factor; m is the mass of cone in gm; g is gravitational acceleration in 9.81 m/s^2, and d is a cone penetration depth in mm.

To get accurate and representative values, three measurements were taken each time approximately 2 cm apart from each other and the wall of the column in undisturbed state. For remoulded strength measurements, samples were remoulded thoroughly for 3-5 minutes with the help of a spatula, and then cone penetration was recorded. During remoulded strength measurements, samples were remoulded for each measurement, and measurements were taken until the maximum penetration value or constant values for penetration is recorded (typically 4-5 measurements). Usually, the maximum value of penetration depth is used to determine the remoulded shear strength.

To examine small-strain stiffness and to track changes in viscoelastic properties, stress-controlled amplitude sweep test was performed on remoulded Leda clay samples using HAAKE viscotester iQ with a vane rotor. The important features of the HAAKE viscotester iQ with vane rotor are that it allows to run the test on the sample in its original container directly and the vane rotor can be inserted into the sample with very minimal sample disturbance. The vane had four thin blades attached with a central shaft and a radius of 11 mm and a length of 16 mm. The vane fixture was lowered into the sample up to 2 cm from the sample surface after removing the bleed water and then oscillated at a constant frequency of 1.6 Hz but at an increasing value of stress. When the sample was being sheared by a vane, the resulting deformation in the sample was estimated and expressed in terms of elastic shear modulus (G') and viscous modulus (G"). G' was calculated from the recoverable strain during each oscillation, whereas G'' was calculated from the measured irrecoverable strain. Amplitude sweep tests were performed in both undisturbed and remoulded states.

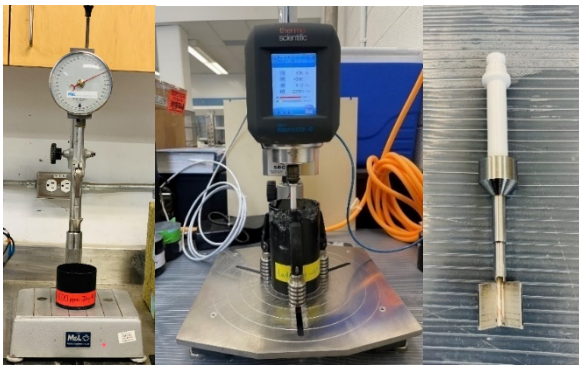

Figure 1. Fall cone device, Oscillatory rheometer, and vane rotor from right to left respectively

Water content of the Leda clay samples also measured at 105◦C by collecting subsamples carefully from each 1 cm throughout the depth of the samples to develop water content/ density profile.

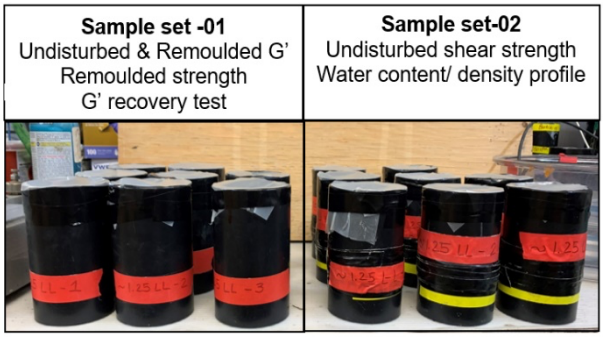

Figure 2. Two different sets of samples for each water content.

RESULTS AND DISCUSSION

Pore water pressure and water content

To track the EOP, a pore water sensor was installed at 0.02 m from the bottom in one of the samples of 2LL Leda clay. Figure 3 shows the changes in PWP after deposition in 0.092 m tall samples. 2LL sample reached to expected hydrostatic pressure around 25 days showing the arrival of EOP and stayed close to it afterwards.

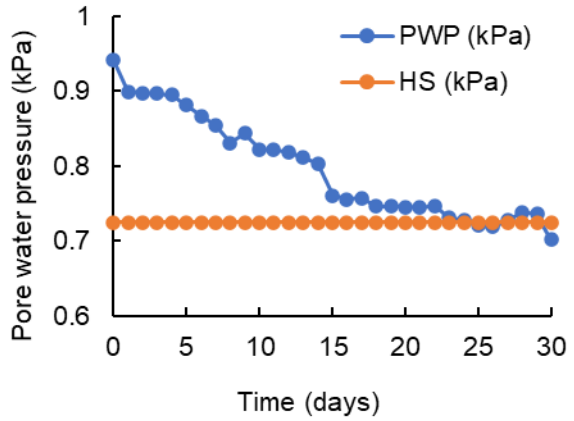

Figure 3. Change in PWP after deposition in 2LL Leda clay samples

The water content/ density profile generated over time from all of the samples demonstrated that for 2LL samples water content declined from 111.4 % to 109.2 % within first 28 days and remained nearly constant throughout the testing period. Such decline also well aligned with the PWP data. Both 1.51 LL and 1.22 LL samples demonstrated insignificant water content changes of approximately 1.2 % during the study period. Moreover, the water content profiles also demonstrated uniform changes throughout the elevation for both 1.51 and 1.22 LL samples.

Undrained shear strength

Both undrained and remoulded strengths were measured using fall cone device over time. Figure 4 shows the development in undrained shear strength over a period of 100 days in Leda clay samples prepared at three different initial water contents. As can be observed, both 1.51 and 1.22 LL samples reported almost the same magnitude of undrained shear strength after 100 days. However, undrained shear strength increased gradually over time in 1.51 LL samples. Whereas 1.22 LL samples demonstrated the majority of changes in the first 14 days.

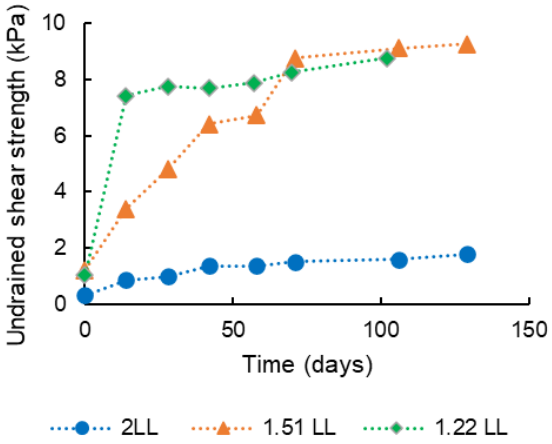

Figure 4. Development of undrained shear strength in Leda clay sample over time

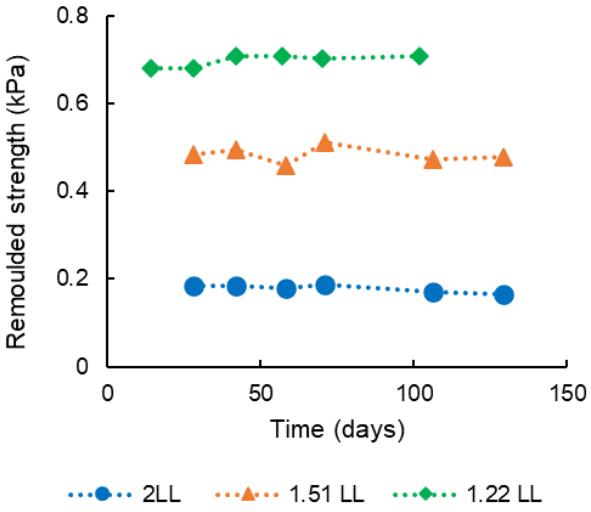

Figure 5. Remoulded strength of Leda clay samples

Figure 5 shows the remoulded strength measured over time for all of the samples. Remoulded strength remained nearly constant throughout the test period, but undrained shear strength increased with time. Hence, it clearly shows that strength gain in undisturbed state is mainly due to the ageing effects (Banas,1991; Salam,2020; Tang et al.,2020). Similar to observation drawn by many researchers e.g., Skempton and Northey (1952), the magnitude of thixotropic strength gain increased with decreasing water content.

Amplitude sweep test

Amplitude sweep tests were also performed on replicate Leda clay samples to track changes in viscoelastic properties with time in response to small strain shear. Figure 6 shows the example of typical results obtained from stress-controlled amplitude sweep tests performed on 2LL Leda clay samples. As can be observed that both linear elastic range and magnitude of elastic shear modulus (G') increased with time which clearly depicts the changes occurring in soil structure over time (Mizani, 2016).

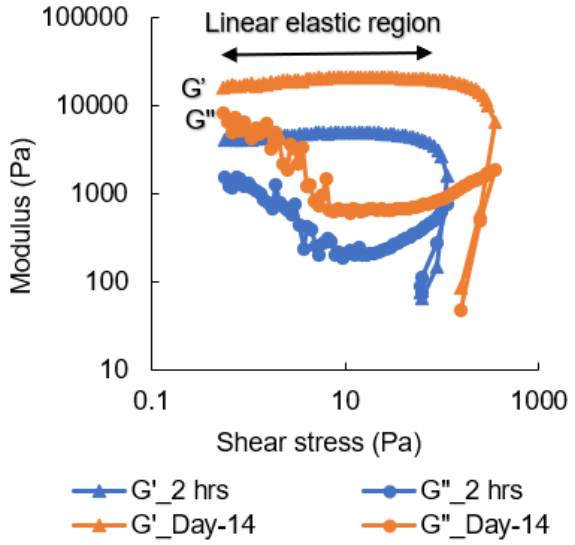

Figure 6. Results from Amplitude sweep test

A total of 30 amplitude sweep tests were performed on undisturbed Leda clay samples. From each test result, the maximum value of G' is taken from the true elastic region and plotted over time in Figure 7. Similar to undrained shear strength development, G' increased as water content decreased. Interestingly, the 1.25 LL samples which demonstrated minimal changes in undrained shear strength after 14 days of ageing, reported a continuous increase in G' with time. Moreover, the G' development trend was observed to be very similar to undrained shear strength development for both 2LL and 1.51 LL samples. Hence, when plotted together a strong relationship between G' and Su was observed (Figure 8). G' increased roughly by 25 times the undrained shear strength measured by fall cone. A similar relationship was also reported by Patel et al., (2020) for soft Leda clay samples. The ratio of small strain shear modulus (G') to undrained shear strength is often regarded as rigidity index, an indicator of stiffness. It has been used by researchers to determine important marine soil properties (Tea and Houlsby,1991; Randolph et al., 2005; Low et al.2010, etc.). Additionally, Peng et al. (2020 &2021) postulated that the rigidity index is specific to material (G_{max}/S_u) and does not change during ageing period based on tests conducted on six different soft clays for 64 days. Hence, such relationship between G_{max} and S_u could be very helpful at the field scale to track time-dependent changes in FFT as they emerge from the deposit.

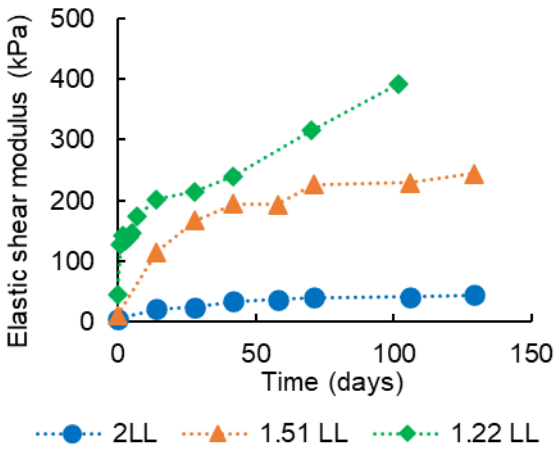

Figure 7. Change in G' over time

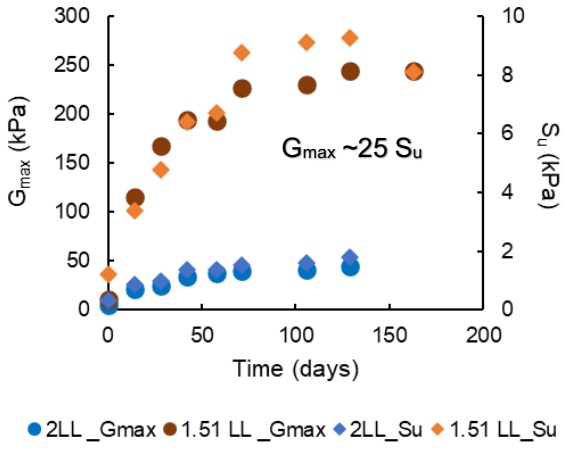

Figure 8. Relationship between G_{max} and S_u

In addition to undisturbed measurements, a total of 30 amplitude sweep tests were also performed on remoulded Leda clay samples. Similar to remoulded strength data, the changes in G' were minimal throughout the test and remained nearly constant. In contrast, G' increased with time in an undisturbed state. Hence, an increase in G' was also due to ageing effects. Anderson and Wood (1975) attributed such an additional increase to a stronger

physical-chemical bonding between the clay particles. It has also been reported by many researchers including Afifi and Richart (1973), Kokusho et al. (1982), and Athanasopoulos G.A., (1993) that when samples are loaded at constant effective stress, after the EOP, small strain stiffness increases with logarithmic of time during secondary compression. Such a linear relationship between G' after EOP and logarithmic of time is also observed for the remoulded Leda clay samples under smaller effective stresses due to their self-weight.

G' recovery test

To track the recovery rate, amplitude sweep tests were performed within the linear elastic range of the remoulded Leda clay samples. To conduct the recovery test, after undisturbed measurements Leda clay samples were remoulded thoroughly and allowed to re-age for a certain period. During the re-ageing period, samples were tested multiple times within the linear elastic range and on different locations of the sample surface to avoid sample disturbance and to obtain accurate measurements of G' respectively. After each measurement, bleed water was added back to the top of the sample (if there is any) and stored. Additionally, samples were kept covered also during the rheometer testing to avoid loss of sample mass due to evaporation, and the mass of the sample was tracked throughout the test to account for the sample loss due to the testing. At the end of each recovery test, samples were remoulded again to determine the remoulded G' and gravimetric water content was also measured. The remoulded G' values at the end of the recovery test and water content were used to track the changes in the samples that occurred during the test other than due to ageing effects such as void ratio change. Figure 9 shows an example of the raw data obtained from multiple amplitude sweep tests. Where linear elastic region was first determined from the amplitude sweep test performed on remoulded sample at the beginning of the test. For the 2LL samples, it was close to 20 Pa, thus all the samples were sheared up to only 10 Pa during the recovery test to avoid sample disturbance and stay within the true elastic region. As can be seen from Figure 9 that the values of G' recovered gradually with time and reached the same value after 7 days of the re-ageing period. Thus, after 7 days of the re-ageing period when the sample was remoulded again and G' was measured, it reported a somewhat higher value than the original values for remoulded samples. Such difference was confirmed by the water content change at the end of the test, water content declined from 109.5% to 108.3%. Thus, it emphasized that the amplitude sweep test is capable to represent the changes in the sample very accurately even at smaller water content changes. The same steps were followed for each recovery test on the Leda clay samples prepared at different initial water contents. The water content varied up to 1.5% during the recovery test for all Leda clay samples.

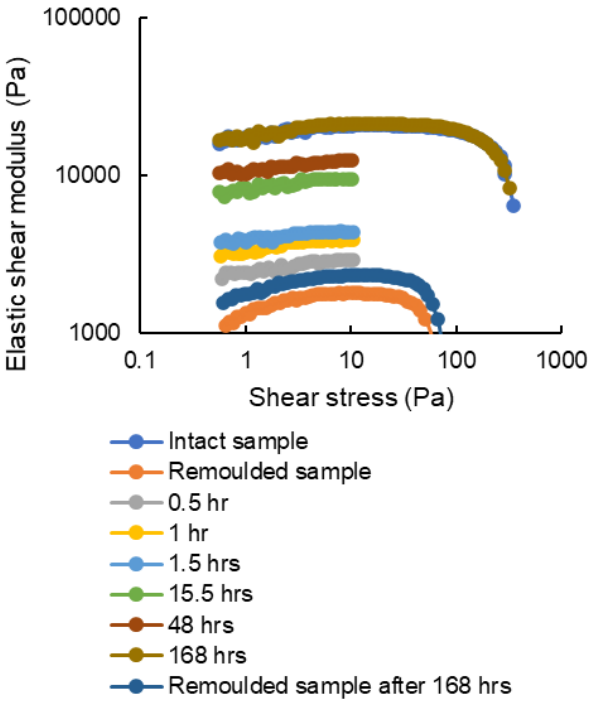

Figure 9. G' recovery test on 14-day old 2LL Leda clay sample

Figure 10 shows the summary of several amplitude tests for 2LL samples at different ages. Where x-axis corresponds to the original ageing time and re-ageing time is shown based on it. For an example, 14 days old sample was allowed to re-age for another 7 days, so its re-ageing period is shown up to 21 days on the graph considering day-14 as day-0 of re-ageing period. Also undisturbed and remoulded (shown with solid lines) shows the value of the G' obtained in the intact and remoulded state of the original samples. The rate of recovery was observed between those two points for a particular sample. Most of the samples recovered its original aged G' value within the original ageing time. Interestingly, Re-ageing of the samples developed almost an identical pattern of G' recovery, pointing to a robust physical phenomenon being responsible for the ageing behaviour. Similar recovery patterns are also recorded for both 1.5 LL and 1.25 LL Leda clay samples.

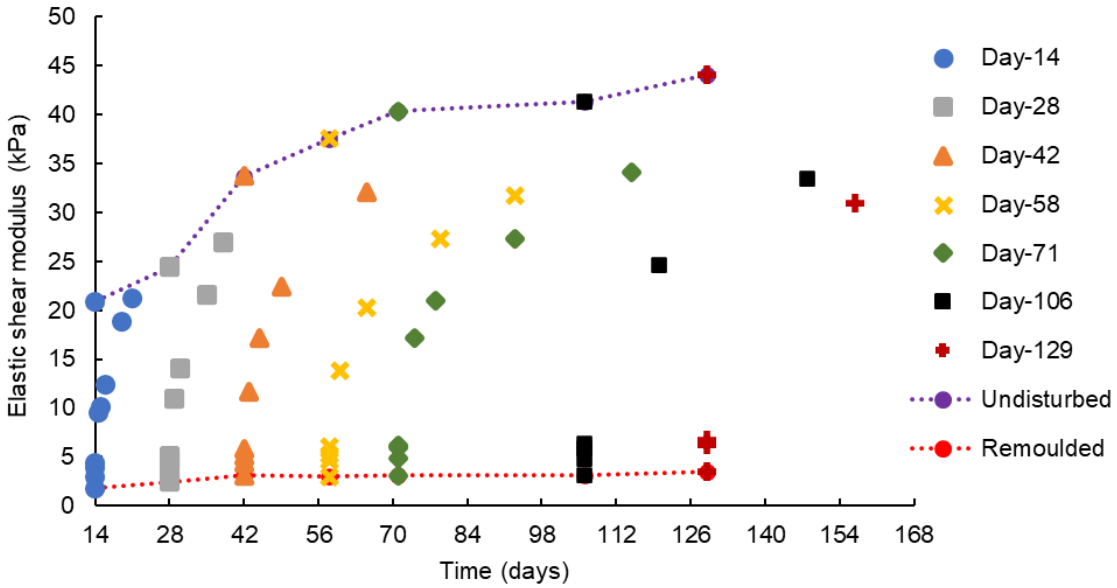

Figure 10. Summary of G' recovery tests in 2LL Leda clay samples

RATE OF AGEING

As discussed earlier, there exists very limited information on the rate of ageing in natural clays. Typically, the rate of ageing is less important for natural clays as geotechnical engineers are generally more interested in in-situ properties of natural clays and differences observed between their undisturbed and corresponding remoulded or reconstituted state, rather than how and at what rate, natural soil reached in-situ/undisturbed state. On the other hand, the rate of ageing is very important for soft soils as they are young material by the nature and yet age. Therefore, the knowledge of the rate of ageing in soft soil may provide information on how long it would take for deposits to reach targeted undrained shear strength which in turn is very important for subsequent deposition and reclamation plans. It can also allow for the rapid estimation of the potential for ageing to alter the dewatering and strength development behaviour in the existing tailings deposits. Of course, the determination of how quick and how far tailings would move during failure conditions also depends on both undisturbed and remoulded strengths (Alex et al., 2022). Hence to quantify the rate of ageing in young materials, the concepts developed from the ageing experiments conducted on colloidal suspensions were used.

Au and Leong (2015) studied the ageing behaviour in Laponite gels prepared at different concentrations of Laponite clay and a salt. They reported two modes of ageing in the Laponite gels. An initial rapid increase in the yield stress which plateaus, followed by a gradual increase in yield stress which also eventually plateaus. The first equilibrium state denoted as the "Surface Chemical Equilibrium (SCE)" state, is attributed to the time required for saturation of clay surface by ions after initial sample preparation. Upon reaching the surface equilibrium state, the second phase is considered as the ageing phase. Both electrolyte and solids concentrations have strong effects on both phases of ageing. A high concentration of electrolyte and solids displayed a larger SCE state yield stress, shorter time to reach the SCE state, and larger final ageing strength.

Recently, Bonacci et al. (2020) postulated that pastes of civil and environmental engineering are dense and contain enough ion concentration to screen coulombic repulsion, thus allowing attractive van der Waals forces to bring the particles into solid-solid contact, which may strongly influence the macroscopic properties and their evolution. Bonacci et al. (2020) put forward the concept of contact-driven ageing in the paste or dense colloidal suspension. They studied the ageing behaviour in silica gels and polymer latex suspensions prepared at moderate ionic strength and different packing fractions. They reported an increase in elastic shear modulus quasi-logarithmic with time following the equation:

$$G' \cong \left(\log\left(\frac{t}{\tau}\right)\right)^{\frac{4}{3}} \quad [5]$$

Where G' is elastic shear modulus; t is ageing time and τ is characteristic ageing time.

However, when the confocal microscope was used to access the microstructure changes at different ageing times, the particles remained essentially at the same position and the microstructure was observed to be constant during mechanical ageing. Whereas G' increased with time. Hence, Bonacci et al. (2020) emphasized that the microstructure rapidly stabilizes due to the formation of irreversible contacts; then, ageing (increase in G') proceeds due to the contact stiffening and it could be a general occurrence in many systems. Recently, Peng et al. (2021) also shed light on the role of solids contacts in thixotropic hardening in both remoulded natural and artificial clays based on the concept proposed by Bonnaci et al. (2020).

Based on the concepts developed by Au and Leong (2015) and Bonacci et al., (2020), the following empirical relationship is proposed for young materials-

$$Su = Su_{EES} + A * Su_{EES} \log\left(\frac{t}{\tau}\right)^5 \quad [6]$$

Where $S_{u\ EES}$ is shear strength at the end of the Early Equilibrium Stage (EES). A is a constant. S_u is ageing shear strength at any ageing time, t, in days. τ is characteristics time in days and always taken as 1 to make the equation dimensionally consistent.

In the proposed relationship pre-EES strength development is attributed to the particle rearrangement inducing development of more close attractive contacts, while later ageing is due to progressive stiffening of existing contacts in place (Bonacci et al., 2020). Therefore, the correlation of EES to later ageing may be because the EES state defines the number of contacts between clay particles, while further ageing is largely due to the stiffening of those existing contacts. Hence, the proposed relationship is a function of EES strength. The value of shear strength at EES is obtained using the concept developed by Au and Leong (2015). EES is the point before which the changes in undrained shear strength/ elastic shear modulus are the minimum and after that undrained shear strength / elastic shear modulus increases rapidly.

An example to determine EES is shown in Figure 11 for the Leda clay sample prepared at water content close to 1.55 LL. As can be seen, the G' increased after deposition and then stayed at a stable value until around day 14. However, after 14 days noticeable increase in G' was observed over time. Hence, the value of EES is typically taken from the stable values of G' which is 60 kPa here. It is important to note here that the SCE concept proposed Au and Leong (2015) differs for young materials. Here, we postulate that EES is related to a certain degree of consolidation which is required for close contacts to develop among clay particles. It has also been observed from the multiple data sets that samples often reach EES at relatively stable water contents. Therefore, in the absence of continuous strength measurement data, water content data may provide a reasonable assumption for the arrival of EES.

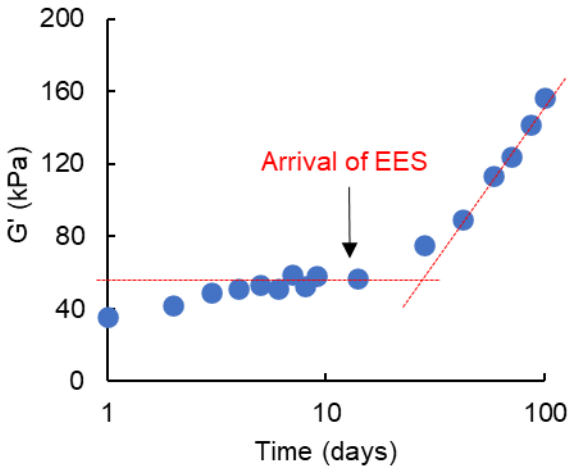

Figure 11. Determination of EES in 1.55 LL Leda clay samples

The proposed relationship is then applied to Leda clay samples prepared at different initial water contents. Figure12 shows the normalized G' (G'/ G'_{EES}) values for Leda clay samples over time. All of the data sets were fitted using a constant value of A = 0.05 and the values of EES were determined separately for each data set based on the technique shown in Figure 11. Surprisingly, the rate of ageing appeared to be the same for all of the Leda clay samples regardless of initial water content. Such observation well matched with the conclusion drawn by Manley et al., (2005) for very dilute silica gels. They postulated that regardless of the packing fraction, the rate of ageing remains nearly constant for a same material.

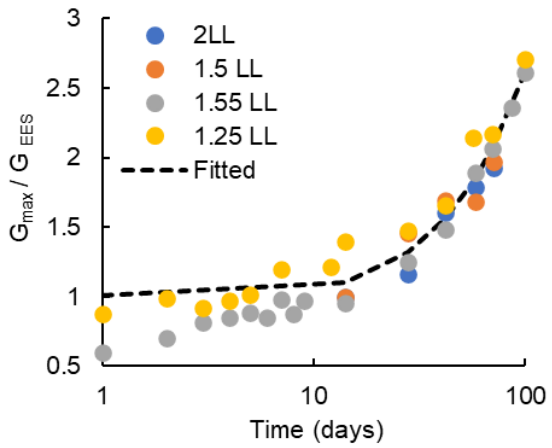

Figure 12. Normalized G' data for Leda clay fitted using Eq. 6

The proposed relationship was also applied to the undrained shear strength data of flocculated FFT samples (Figure 13). However, the values for the constant, A, changed this time for different flocculated samples and varied between 0.03 and 0.1. Here, Shell FFT _800 ppm data are obtained from Patel et al. (2021), Shell FFT _1000 ppm data from Salam (2020), and a separate study was conducted for Syncrude FFT to develop a data set where Syncrude FFT samples were flocculated at an initial solids content of 47.5 %.

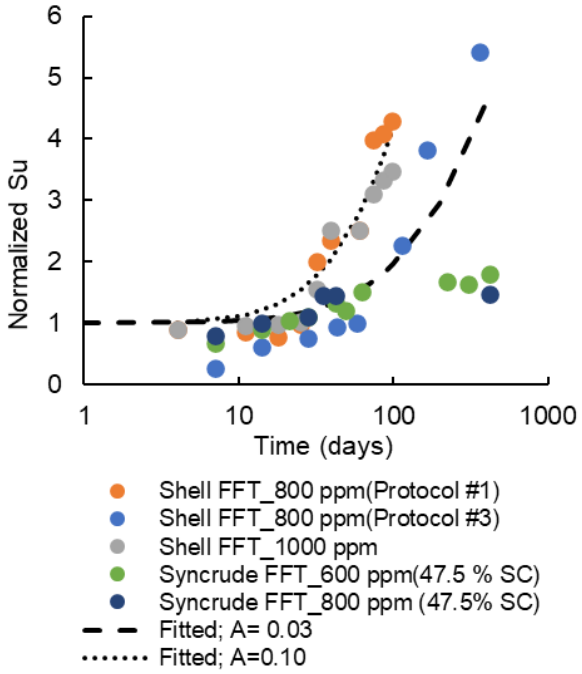

Figure 13. Normalized Su data for fFFTs fitted using Eq. 6

Later, based on the values of constant obtained from the above datasets, both upper (0.10) and lower bounds (0.03) were defined for the proposed relationship. Then, the data available from the literature were used to determine how well the data fits within those two bounds and to test the generality of the proposed relationship.

Figure 14 shows the summary of different data sets from this study as well as from the literature. Based on 18 different data sets and over 200 data points, it was observed that the proposed relationship has the potential to provide a rapid estimation of ageing undrained shear strength of young material. Additionally, the maximum magnitude of ageing varied between 5-6 times the strength measured at EES for different materials. Hence, the proposed relationship can provide the estimation of both rate and magnitude of ageing in relatively short periods of time based on the values obtained for EES strength.

CONCLUSIONS

The experimental study was conducted to evaluate the magnitude and rate of ageing in both soft soils and FFT. Soft Leda clay samples were prepared at three different initial water contents to understand the role of initial water content on the magnitude of ageing and prepare data sets to quantify the rate of ageing. The major finding from this study includes:

1. Magnitude of ageing strongly depends on the initial water content of the samples. Both undrained shear strength and elastic shear modulus increased with decreasing water content and ageing time.
2. A strong relationship between undrained shear strength measured using a fall cone and small-strain shear modulus measured using an oscillatory rheometer was observed for Leda clay samples; G_{max} ~ 25 S_u. Such relationship can be a good indicator to track time-dependent changes in FFT as they emerge from the deposits.
3. Identical pattern of G' recovery was observed from several amplitude sweep tests, pointing to a robust physical phenomenon being responsible for the ageing behaviour.
4. Similar to the observation drawn by Au and Leong (2015), two separate phases of ageing are also observed to exist in both soft soils and fFFT.

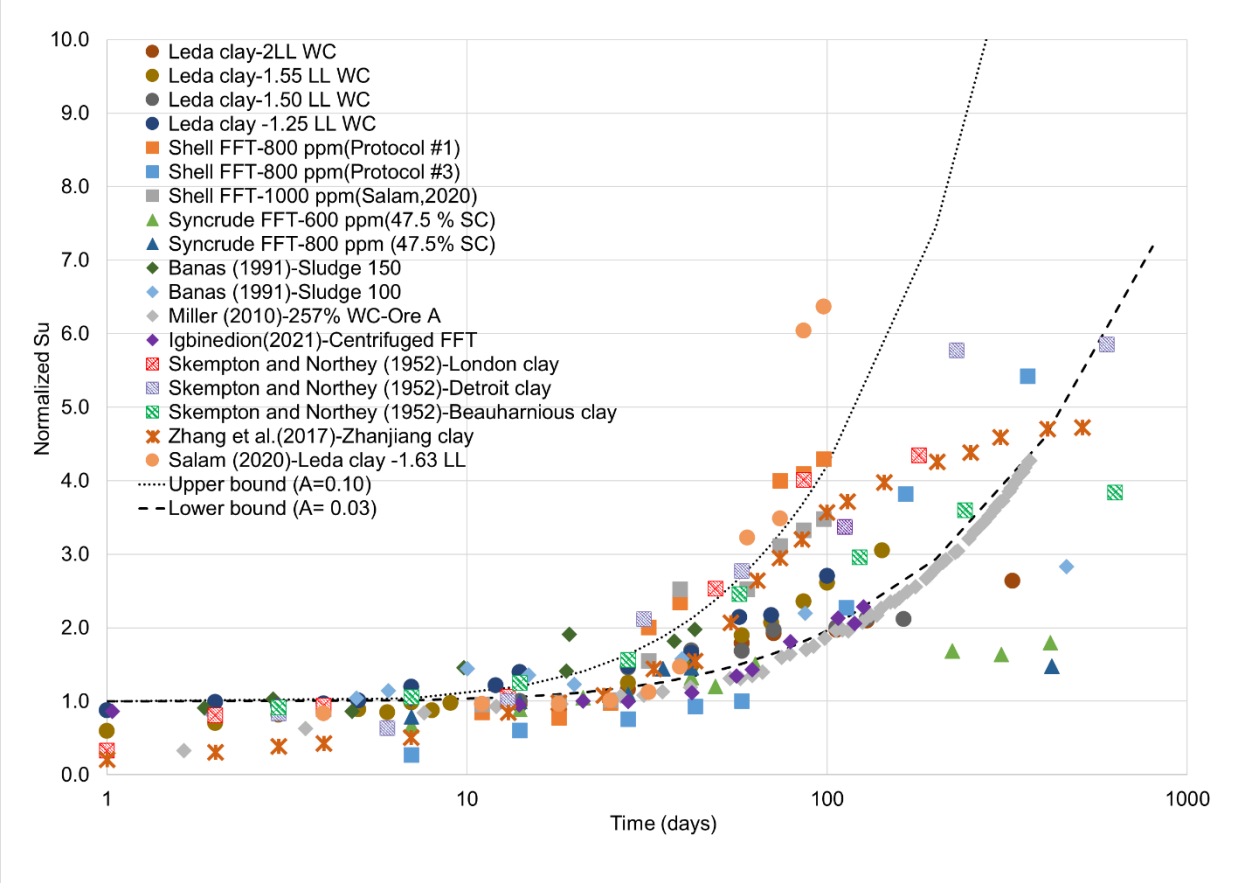

Figure 14. Summary of different data sets fitted using Eq. 6

5. The proposed empirical relationship was developed based on the concepts proposed by Au and Leong (2015) and Bonacci et al. (2020). The pre-EES strength development may be due to particle rearrangement including more close attractive contacts, while later ageing is due to progressive stiffening of existing contacts in place. Therefore, the correlation of EES to later ageing, maybe because the EES state defines the number of contacts, while further ageing is largely due to the stiffening of those existing contacts.
6. Based on the 18 different data sets it was observed that maximum ageing could vary between 5-6 times the strength measured at the end of EES. It may be possible to estimate the magnitude of ageing in a relatively short period of time based on the values observed for EES strength. It would also be feasible to refine the exiting consolidation models to accurately predict the longer-term behaviour of tailings deposits.

ACKNOWLEDGMENTS

The authors are grateful to Dr. Mohammad Rayhani, Associate Professor at Carleton University for supplying Leda clay samples. This work is funded by an NSERC Collaborative Research and Development grant supported by Canada's Oil Sands Innovation Alliance (COSIA).

REFERENCES

Afifi, S.S., Richart, F.E. (1973). Stress history effects on shear modulus of soils. Soils and Foundations 13 (1), 77–95.

Alam, M. K., Shahriar, A. R., Islam, M. S., Islam, N., & Abedin, M. Z. (2021). Experimental investigation on the strength and deformation aspects of thixotropic aging in reconstituted clays. *Geotechnical and Geological Engineering*, *39*(3), 2471-2486.

Aldaeef, A.A., & Simms, P.H. (2019). Influence of pipeline transport on sedimentation and consolidation of flocculated Fluid Fine Tailings. Proceedings of GeoSt.John's 2019, 72n^{d} Canadian Geotechnical Conference, Newfoundland, Canada.

Anderson, D.G., Stokoe, K.H. (1978). Shear modulus: a time dependent soil property. Dynamic Geotechnical Testing. Special Testing Publication, vol. 654. ASTM, Philadelphia, 66–90.

Anderson, D.G., Woods, R.D. (1976). Time-dependent increase in shear modulus of clay. Journal of the Geotechnical Engineering Division, ASCE 102 (5), 525–537.

Athanasopoulos, G.A. (1993), Effects of ageing and overconsolidation on the elastic stiffness of a remoulded clay. Geotechnical and Geological Engineering.

Au, P.K., and Leong, Y.K. (2015) Surface chemistry and rheology of Laponite dispersions -Zeta potential, yield stress, ageing, fractal dimension and pyrophosphate. Applied clay science,107,36-45.

Banas, L. C. (1991). Thixotropic behaviour of oil sands tailings sludge (Master's thesis). The University of Alberta, Edmonton, Alberta.

Bonacci, F., Chateau, X., Furst, E. M., Fusier, J., Goyon, J., & Lemaître, A. (2020). Contact and macroscopic ageing in colloidal suspensions. Nature Materials, 1-6.

Cianci, G.C., Courtland, R.E. and, Weeks, E.R., (2006). Correlations of structure and dynamics in an ageing colloidal glass.

Hansbo, S. (1957). New approach to the determination of the shear strength of clay by the fall-cone test

Igbinedion, D. (2020). Ageing and Large-scale consolidation in centrifuged Cake oil sands tailings (Masters Thesis), Carleton University, Ottawa, ON.

Jeeravipoolvarn, S. (2005). Compression behaviour of thixotropic oil sands tailings (Master's thesis). The University of Alberta, Edmonton, Alberta.

Jeeravipoolvarn, S., Scott, J. D., & Chalaturnyk, R. J. (2009). 10 m standpipe tests on oil sands tailings: long-term experimental results and prediction. Canadian Geotechnical Journal, 46(8), 875-888.

Kokusho, T., Yoshida, Y., Esashi, Y. (1982). Dynamic properties of soft clay for wide strain range. Soils and Foundations 22 (4), 1–18.

Leonards, G. A., & Altschaeffl, A. G. (1964). Compressibility of clay. Journal of the Soil Mechanics and Foundations Division, 90(5), 133-156.

Low, H. E., T. Lunne, K. H. Andersen, M. A. Sjursen, X. Li, and M. F. Randolph. (2010). Estimation of intact and remoulded undrained shear strengths from penetration tests in soft clays. Géotechnique 60 (11):843–859.

Manley, S., Davidovitch, B., Davies,R.N., Cippelletti, L., Bailey,A.E., Christianson, R.J., Gasser, U., Parasad,V., Serge, P.N., Doherty, M.P., Sankaran, S., Jankovsky, A.L., Shiley,B., Bowen, J., Eggers, J., Kurta, C., Lorik, T., and Weitz, D.A. (2005). Time-dependent strength of colloidal gels. Physical review letters, PRL95,048302.

Mewis, J., & Wagner, N. J. (2012). *Colloidal suspension rheology*. Cambridge University Press.

Miller, W. G. (2010). Comparison of geoenvironmental properties of caustic and noncaustic oil sand fine tailings. (Ph.D. Thesis, the University of Alberta).

Mitchell, J.K. (1961). Fundamental aspects of thixotropy in soils. Transactions of the American Society of Civil Engineers, 126 (1),1586-1620.

Mizani, S. (2016). Experimental Study and Surface Deposition Modelling of Amended Oil Sands Tailings Products (Doctoral dissertation). Carleton University, Ottawa, Ontario, Canada

Ovarlez, G. and Chateau, X. (2008). Influence of shear stress applied during flow stoppage and rest period on the mechanical properties of thixotropic suspensions. Physical review, E77,061403.

Patel, A., Aldaeef, A.A., Simms, P.H. (2021). Ageing in soft soils and clayey tailings. Proceedings of the Twenty-Fifth International Conference on Tailings and Mine waste, 7-10 November 2021, Banff, Alberta, Canada. Page no: 813-823.

Patel, A., Salam, A.M., Aldaeef, A.A., Simms, P.H. (2020). Sample preparation and ageing in soft soils. Proceedings of GeoNiagara 2020, 73rd Canadian Geotechnical Conference, Ontario, Canada.

Peng, J., D. J. DeGroot, Y. Cao, and G. Zhang. (2020). Rigidity index of soft remolded clays during thixotropic hardening. In Proc., 4th Int. Symp.on Frontiers in Offshore Geotecnics. London: International Society for Soil Mechanics and Geotechnical Engineering.

Peng, J., Luo, S., Wang, D., Cao, Y., DoGroot, D.J., Zhang, G. (2021). Multiple Thixotropisms of Liquid-Limit Consistency of Clays Unraveled by Multiscale Experimentation. ASCE Journal of Geotechnical and Geoenvironmental Engineering, 148(1): 04021165.

Pujala, R. and Bohidar, H.B. (2013). Slow dynamics, hydration, and heterogeneity on Laponite dispersions. Soft matter, 9,2003
.
Randolph, M. F., M. Cassidy, S. Gourvenec, and C. J. Erbrich. (2005). Challenges of offshore geotechnical engineering. In Proc., 16th Int. Conf. on Soil Mechanics and Geotechnical Engineering, 123–176. Amsterdam, Netherlands: IOS Press.

Ren, Y., Yang, S., Anderson, K., Yang, Q. and Wang, Y. (2021). Thixotropy of soft caly: A review. Engineering Geology,287 (2021),106097.

Rich, J.P., Lammerding, J., Mckinley, G.H., and Doyle, P.S. (2011) Nonlinear microrheology.

Salam, M. (2020). Effects of polymers on short- and long-term dewatering of oil sands tailings (Doctoral dissertation), Carleton University, Ottawa, ON.

Schmertmann, J.H. (1991). The mechanical ageing of soils. Journal of Geotechnical Engineering, V.117, P.26151

Shahriar, A. R., & Jadid, R. (2018). An experimental investigation on the effect of thixotropic aging on primary and secondary compression of reconstituted dredged clays. Applied Clay Science, 162, 524-533.

Shahriar, A. R., Abedin, M. Z., & Jadid, R. (2018). Thixotropic aging and its effect on 1-D compression behavior of soft reconstituted clays. Applied Clay Science, 153, 217-227.

Skempton, A.W. and Northey, R.D. (1952). The sensitivity of clays. Geotechnique, 3(1), 30-53.

Suthaker, N. N., & Scott, J. D. (1997). Thixotropic strength measurement of oil sand fine tailings. Canadian Geotechnical Journal, 34(6), 974-984.
Tang, B., Zhou, B., Xie, L., Yin, J., Zhao, S., and Wang, Z. (2021). Strength recovery model of clay during Thixotropy. Advances in Civil Engineering, Volume 2021.

Teh, C. I., and G. T. Houlsby (1991). An analytical study of the cone penetration test in clay. Géotechnique 41 (1): 17–34.

Weeks, E. R. (2017). Introduction to the colloidal glass transition.

Xia, X., Patel, A., Simms, P.H. (2022). Modelling post-failure runout of tailings and soft clay using thixotropic rheology. Proceedings of 8th Canadian Geohazards conference 2022, Quebec, Canada.

Zeng, L. L., Hong, Z. S., & Cui, Y. J. (2016). Time-dependent compression behaviour of dredged clays at high water contents in China. Applied Clay Science, 123, 320-328.

A META-ANALYSIS OF POTENTIAL PRE-CONSOLIDATION BEHAVIOUR IN OIL SANDS TAILINGS

Ahlam Abdulnabi[1], Trempess Moore[1], Sam Proskin[1], Nicholas A. Beier[2] and David C. Sego[2]
[1]Thurber Engineering Ltd., Calgary, Alberta, Canada
[2]University of Alberta, Edmonton, Alberta, Canada

ABSTRACT

Regulatory policy in Alberta limits the volume of fluid fine tailings that oil sands operators can deposit annually. Therefore, operators have explored and deployed an array of technologies to dewater and reclaim tailings to trafficable landforms. Literature speculates that some of these technologies apply a temporary stress to the tailings. In geotechnical terms this temporary stress can be interpreted as an apparent pre-consolidation pressure, impeding tailings' volume reduction until this stress is overcome. This paper investigates the potential pre-consolidation pressure (σ_p') as an artifact of some tailings dewatering treatments.

Compressibility curves from 112 large strain consolidation tests on different treated and untreated oil sands tailings were assessed. A code in programming language R was utilized to determine the pre-consolidation pressure for each compressibility dataset using four different methods. Results indicate that the pre-consolidation pressure for all of the polymer-amended, flocculated and thickened tailings was non-existent regardless of the σ_p' evaluation method employed. However, some untreated oil sands tailings and centrifuge cake specimens (undergoes chemical amendment with centrifugation) exhibit a slight apparent pre-consolidation pressure at low effective stress. Moreover, preconsolidation pressures up to 60 kPa can be present when tailings undergo freeze-thaw in the field. The geotechnical implications of this behaviour on reclamation efforts are discussed. Furthermore, the correlation of the effective vertical stress to the corresponding shear strength of the tailings is presented for the available datasets.

INTRODUCTION

Alberta Energy Regulator estimates a total of 1.3 billion cubic meters of new and legacy fluid fine tailings (FFT) in the State of Fluid Tailings Management for Mineable Oil Sands, 2019 report. Regulatory policy in Alberta requires oil sand operators to limit FFT volumes to be deposited in ponds per AER directive 085 to ensure that FFT are treated and reclaimed progressively during the life of a project. What makes oil sands tailings a challenge compared to other mining tailings is a combination of i) low solids content in the slurry; ii) high fines content; iii) and the dispersed nature of these fines (silt and clay-sized 44-45 micrometres or less in diameter) that remain suspended in the ponds due to the extraction process (Royal Society of Canada's report 2010). Untreated, these tailings deposits take decades to settle, only to a consistency of soft mud due to their characteristic slow consolidation and high compressibility. Therefore, the process of consolidation needs to be understood fully to plan tailings depositional schemes, determine storage capacities, and design for closure (COSIA 2012).

Jeeravipoolvarn (2010) alludes to a potential apparent pre-consolidation pressure (σ_p') in FFT at low void ratios. Beier (2015) suggests that this σ_p' in FFT may hinder the self-weight consolidation process by manifesting as pseudo strength, therefore slowing down dewatering. He reasons that such a pattern may inevitability have implications on the geotechnical behaviour and thus reclamation efforts.

Typically, slurries such as FFT are rarely overconsolidated, and therefore, should follow the virgin compression line regardless of their initial void ratio. However, certain initial conditions, such as electrochemical interactions, tortuous drainage, and thixotropic strength, among others, may lead to the development of a pre-consolidation pressure in clay slurries (Khan and Azam, 2017).
In the literature, the onset of an apparent pre-consolidation behaviour in oil sands FFT is attributed to different factors, including:

i. high thixotropic strength gain (Suthaker and Scott, 1997);
ii. thixotropic gel strength (Jeeravipoolvarn 2005, and 2010);
iii. development of thixotropic shear strength in FFT at large void ratios (Miller, 2010)
iv. an artifact of strain rate (Watanabe et al. 2012)

v. chemically-induced flocculation (Herweyen et al. 2017) or cementation (Wang, 2017).
vi. thixotropic re-alignment of particles (Hurtado, 2018),
vii. strain rate and structuration in reconstituted/remoulded natural clay (Qi et al. 2018)
viii. freezing induced overconsolidation when tailings are exposed to freezing temperatures (Proskin 2018).

Despite the lack of consensus as to why such behaviour may exist in FFT, little effort is directed at whether this behaviour is limited to certain tailings treatment strategies. Either way, understanding the magnitude of pre-consolidation pressure is critical to judge its implications for reclamation. Simply because it has been known for decades that pre-consolidation behaviour governs the compressibility of clay slurries, causing delayed consolidation and the progress of a reserve resistance against compression under additional loads even in normally consolidated clays (Bjerrum, 1967).

Furthermore, the magnitude of pre-consolidation pressure is instrumental in geotechnical engineering for predicting settlement since vertical effective stress higher than σ_p'must be applied to the deposit in order to cause the breakdown of interparticle bonds, which would then result in consolidation settlement (Boone 2010).

Compressibility curves of FFT are typically based on large strain consolidation (LSC) tests following finite strain theory (Gibson et al. 1967). LSC captures the large deformations that the tailings undergo, especially during the prolonged self-weight consolidation phase (Pollock 1988).

The purpose is mainly directed at answering one central question: Do oil sands tailing exhibit pre-consolidation pressure? If so, what is the magnitude of this pressure and is it associated with a certain dewatering technology?

This paper presents a meta-analysis of 112 large strain consolidation tests performed on various treated and untreated oil sands tailings over the past 37 years. Compressibility curves, shown in Figure 1, were individually examined for the existence (or lack thereof) of an apparent pre-consolidation pressure (σ_p'). The magnitude of σ_p' was determined using four different methods. Estimating σ_p' is often problematic since it relies heavily on graphical techniques that are subject to operator bias. Boone (2010) illustrates the fundamental difficulties and uncertainties associated with estimating σ_p'. Therefore, the graphical and statistical capability of the coding language 'R' was applied (R Core Team, 2014). R is an open-source computing environment that receives contributions (i.e., packages) from researchers and experts in various fields of science worldwide. The R package 'soilphysics' (da Silva and de Lima 2015) was utilized to determine σ_p' for all treated and untreated tailings compressibility datasets using four methods. Practical implications of the variation in the σ_p' outcome depending on the utilized method is discussed.

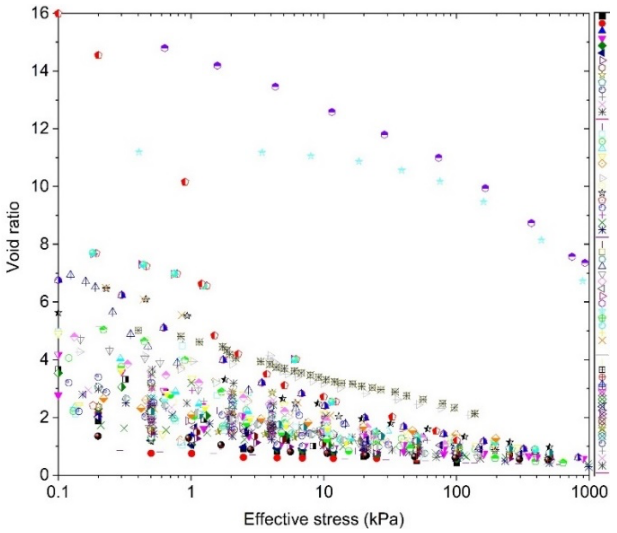

Figure 1. The variation compressibility curves investigated in this paper (identifying individual series is not the intention of this figure hence the absence of a legend).

DETERMINING PRE-CONSOLIDATION PRESSURE

Over fifteen methods exist for estimating the pre-consolidation pressure in soils (Kirstein 2010). Determining the pre-consolidation pressure, irrespective of the method adopted, involves mathematical manipulation of the compressibility by dividing it into elastic deformations (recoverable) and plastic deformations (irreversible), i.e., virgin compression curves. These estimates are typically done graphically from a compression curve. Four methods were adopted in this paper using the 'soilphysics' package in R in order to limit operator bias. The methods are Casagrande (1936), Pacheco Silva (ABNT,1990), Dias Junior and Pierce (1995) regression methods, and Arvidsson and

Keller (2004) Method. Details on the methods are presented in Figure 2 and are described in the following sections.

Casagrande's method (1936)

Casagrande's graphical method estimates σ_p' by i) determining the maximum curvature point (MCP) of the semilogarithmic compressibility relationship; ii) drawing a horizontal line (depicted in orange in Figure 2), a tangent line (purple) and their bisector (pink) at the MCP; iii) extending the straight line of the virgin compression curve (VCL) (blue) in direction to smaller stresses as seen in Figure 2. The pre-consolidation pressure is the stress value in the horizontal axis associated with the intersection point of the VCL extension and the bisector.

Casagrande's method, by virtue of being graphical, is fraught with difficulty even when the statistical approach is employed, given the subjectivity in obtaining these lines, especially when the curvature is subtle and user intervention is necessary. This is especially crucial in some of the FFT data that had pseudo curvature discussed later in the paper when the shapes of compression curves are analyzed.

Pacheco Silva's method (1990)

The pre-consolidation pressure can be determined by i) drawing a horizontal line passing through the initial void ratio of the specimen (green); ii) extending the straight-line portion of the virgin compression curve (blue) until it intercepts the green line; iii) from the point of intersection of green and blue lines, draw a vertical line down until it intercepts the e – log p′ curve; iv) from this point draw a horizontal line until it intercepts the blue line; and then v) the stress value in the horizontal axis associated with this point is the pre-consolidation pressure.

Dias Junior and Pierce regression method (1995)

This method fits the recompression line and VCL each by a regression line. The number of points assigned to create the regression lines can range from 3 to 5. The fit has to start with the smallest and highest applied stress for recompression and virgin compression lines, respectively. This method was not applicable for some FFT data due to the unique compression curve shape that resulted in erroneous estimates of σ_p', discussed in later sections.

Arvidsson and Keller method (2004)

This method defines the pre-consolidation pressure as the abscissa intercept of VCL (blue line in Figure 2) with a horizontal line drawn from the initial void ratio (green). Purely mathematical algorithm can be utilized to determine these two lines in order to obtain σ_p'. Therefore, this method eliminated much of the uncertainty associate with Casagrande's graphical method.

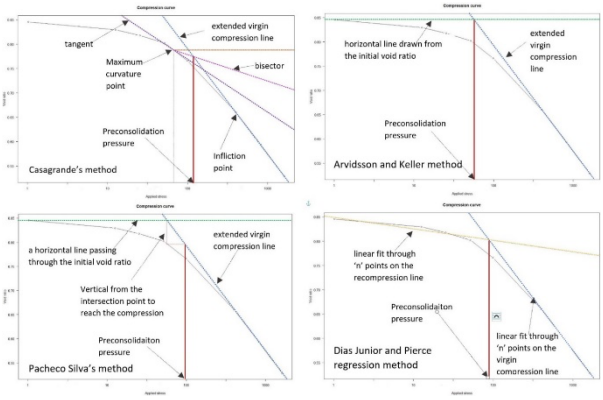

Figure 2. Graphical representation of each pre-consolidation pressure determination method in soilphysics R package.

STUDY METHODS

This study was limited to publicly available large strain consolidation tests conducted based on the multi-step load procedure adopted at the University of Alberta. The authors were careful to include tests completed with the same method due to the understanding that tests methods may impact results due to the lack of standardization of testing slurry consolidation (Jeeravipoolvarn et al. 2015). Selection also considered comparable pre-testing sample handling (such as storage, release water management, homogenization prior to element testing etc.) and sub-sampling. An important point to emphasize is that all of these datasets are based on conventional large strain consolidation tests (multi-step loading), which offer direct measurement, and it does not include complicated data interpretation.

The data analyzed in this paper come with their own limitations, operator error and uncertainties. As such, some of the datasets were limited to 100 kPa effective stress during the large strain consolidation tests (Proskin 1998 and Zhang 2012) as examples. Regardless of the method employed to estimate

pre-consolidation pressure, the virgin compression lines are interpolated based on the available data points. There may be implications on the accuracy had the test been extended further than 100 kPa. This is especially crucial for the frozen-thawed tailings, whether in the laboratory or the field.

The paper investigates datasets for over 112 compressibility curves of different types of treated and untreated oil sands tailings spanning over 37 years. The authors recognize that it is important to have each dataset's characteristics, e.g., particle size distribution, clay content and clay to water ratio, and the like. However, a comprehensive comparative analysis of all these characteristics and index properties was not possible due to the lack of characterization data from the various studies assessed herein.

The authors are aware of the variety of mineralogy and tailings treatments the candidate tailings underwent as additional factors that should be considered. However, a detailed discussion of these nuances would necessarily need a dedicated article.

Finally, the authors maintained the same naming conventions in the original source. For example, datasets referred to as 'MFT' are coming from older theses and publicly available papers where this term was still being used to refer to mature fine tailings. To distinguish different datasets for the same material, a number designation is appended to the name to indicate a different dataset, hence different compression curves.

Similarly, FFT refers to fluid fine tailings; TT refers to thickened tailings; COF cyclone overflow; ILTT refers to in-line thickened; PT refers to polymer treated, FT refers to frozen then thawed tailings, fFFT refers to flocculated FFT, and cake refers to centrifuge cake. Pre-consolidation pressure magnitudes of the different datasets are presented in Table 2. The only exception is Sorta's (2015) data, which is based on a beam centrifuge test.

RESULTS

Out of the 112 datasets investigated, approximately 55% (63 datasets) exhibited an apparent pre-consolidation pressure. The following sections categorize the variation of apparent pre-consolidation pressure in different treated and untreated oil sands tailings based on the estimation method and treatment type.

Variation in pre-consolidation pressure due to σ_p' estimation method

Figure 3 illustrates the mean and standard deviation in pre-consolidation pressure for the same compression curve using different methods. Tailings solvent recovery unit (TSRU) (Masala et al. 2012) exhibited the highest mean pre-consolidation pressure among the datasets (69 kPa). This was closely followed by the several cores taken from field tailings pond reported in Proskin (1998). The highest apparent pre-consolidation pressure from these cores was 58 kPa.

When tailings undergo freeze-thaw in the field, they undergo thaw strain offsetting the compression curve from the never-frozen tailings state downward on the void ratio scale. Frozen-thawed tailings' compressibility looks concave at low effective stress followed by gradually straightening portion at higher effective stress. This behaviour may indicate overconsolidated tailings undergoing recompression at low effective stress followed by a 'virgin' compression at high stresses. Chamberlain 1980's method postulates that the virgin compression line from the never frozen must be utilized when assessing pre-consolidation pressure in frozen soils. This recommendation was followed in each assessment of compressibility curves of tailings undergoing freeze-thaw, whether freezing occurs in the lab or the field.

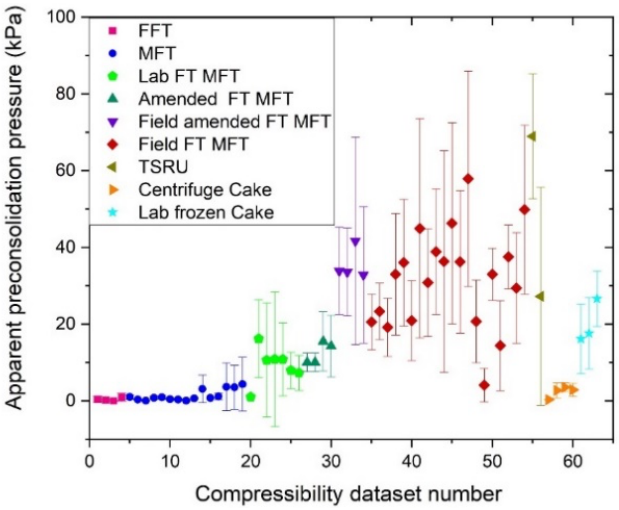

Figure 3. Variation in estimated preconsolidation pressure for the same compressibility curve based on different methods

One crucial point to identify is the following: if the straight portion of the frozen-thawed tailings'

compression curve was treated as a virgin compression line, the preconsolidation pressure results would be erroneous, and not appreciable (<1 kPa). The observed variation was up to ±28 kPa in some cases. Most of those highly variable are tailings subjected to freeze-thaw in the field. No consistent pattern of deviation was observed between estimation methods; this was highly dependent on each dataset's unique shape of the compressibility curve. Further details on the shapes are discussed later.

Another important point to emphasize here is that during the assessment of the pre-consolidation pressure graphs, it was clear that certain σ_p' evaluation methods were not appropriate for specific datasets. For example, some compression curves had a downward sloping 'L' shape that the algorithm for the regression method interpreted as convex and hence presented unrealistic results.

Variation in pre-consolidation pressure due to tailings treatment

Figure 4 illustrates the pre-consolidation pressure variation for different datasets grouped by treatment technique. The presented preconsolidation pressures in Figure 4 are from the same estimation method (Casagrande), along with the normal distribution of preconsolidation pressure values for each particular type/ treatment of each tailings. For ease of assessment, the datasets were divided into treated and untreated categories denoted by the treatment method.

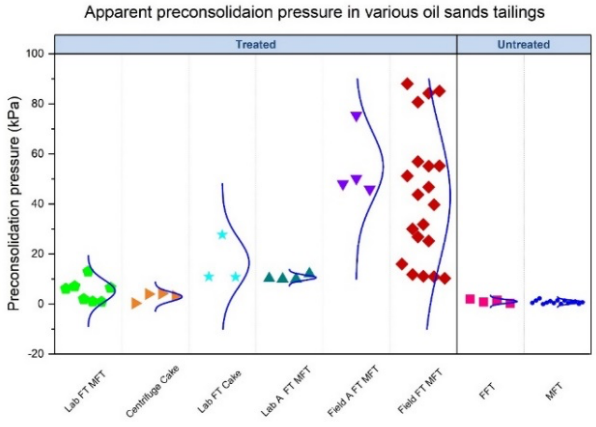

Figure 4. Performance measures obtained from the model results.

DISCUSSION

Overall, no evidence of a correlation between pre-consolidation pressure and chemical treatments of oil sands tailings was observed. In fact, all of the polymer-amended tailings displayed zero pre-consolidation pressure, and the same is true for thickened tailings.

Untreated FFT that did exhibit a pre-consolidation pressure averaged 1 kPa with ± 0.7 kPa deviation among the several FFT datasets, as seen in pink squares in Figure 4. Several more recent FFT datasets do not exhibit any measurable pre-consolidation pressure.

All older untreated MFT datasets exhibited an average pre-consolidation pressure of 0.8 kPa with ± 0.6 kPa variation between the different MFT datasets, as seen in blue circles in Figure 4. This was consistent with values reported throughout the literature not exceeding 2 kPa (Jeeravipoolvarn 2010).

All publicly available centrifuge cake compression data exhibited a mean pre-consolidation pressure of 3 kPa and a standard deviation of 1.5 kPa across datasets presented in orange triangles in Figure 4. However, the reader is reminded that these results only pertain to four unique centrifuge cake datasets. One of these centrifuge cake datasets was subjected to three freeze-thaw cycles in a laboratory flume setting (shown as blue stars Lab FT Cake in Figure 4). The average preconsolidation pressure was 16 kPa with ± 8 kPa. About an order of magnitude increase in σ_p' was observed from the never frozen cake to the first cycle of freeze-thaw. Furthermore, the σ_p' almost doubled from the second freeze-thaw cycle to the third. However, no conclusive inferences can be made here claiming that centrifuge dewatering somehow generates a behaviour in oil sands tailings or that the successive freeze-thaw compounds the pre-consolidation pressure. More compressibility curves of centrifuge cake datasets need to be investigated to generate a larger sample size (statistically) for complete analysis.

Four datasets of chemically amended with acid and quick lime then frozen-thawed MFT were presented in Proskin 1998 (depicted in teal triangles or Field A FT MFT in Figure 4). The mean pre-consolidation pressure was 10 kPa with (± 1 kPa) variation among datasets. The authors note that these specimen were subjected to a single cycle of freeze thaw and

the chemical amendment was conducted in a laboratory setting.

Field chemically amended tailings with acid and quick lime then subjected to atmospheric freeze-thaw (Proskin 1998) are shown as purple triangles in Figure 4. These exhibit half an order of magnitude higher pre-consolidation than those chemically treated then frozen-thawed in a laboratory setting. The average pre-consolidation pressure is 55 kPa with ±12 kPa variation among the four datasets.

Laboratory frozen-thawed MFT (Sego and Dawson 1992; Proskin 1998; and Zhang 2012) had a mean pre-consolidation pressure of 5 kPa (± 4 kPa) across the 7 different datasets. These sets are depicted as green pentagons (Lab FT MFT) in Figure 4.

Interestingly, thawed cores from tailings ponds in the field exhibited about an order of magnitude higher pre-consolidation pressure than those frozen-thawed in the laboratory. This may be due to slow freezing and thawing rates and longer time in a frozen state in the field than in the laboratory. Proskin (1998) offers detailed insight into the dynamics of freezing and thawing rates in the field compared to those in the laboratory and moisture migration time. The average pre-consolidation pressure of thawed cores was 49 kPa, with ±24 kPa variation among cores from the same pond taken at different points in time. These are depicted as red diamonds (Field FT MFT) in Figure 4.

Compression curves shapes

During the graphical assessment of σ_p'Four unique shapes of the compression curves were detected in the various oil sands tailings investigated, as summarized in Figure 4 that can be described as follows:

i. The classical compression curve
ii. the inverted S-shape
iii. the lightning bolt
iv. the downward sloping L

Datasets that exhibited shape 1 were some of the untreated FFT, TSRU, and centrifuge cake tailings. These were the simplest datasets to analyze for σ_p'. They feature a well-defined curvature and clear virgin compression line. Older MFT datasets manifested a distinct 'S-shape' for the e-logp curve, e.g., (Pollock 1988 and Suthaker 1995). This type of curve is iconic to sensitive clays, and it features three zones: i) up to a certain stress level, the tailings show very little deformation with the application of additional load; ii) after the infliction point is surpassed, large settlements are observed; iii). after a certain stress level, the slope once again decreases. Estimating the σ_p' in this shape of e-logp will be highly dependent on defining the points used to construct the virgin compression line (VCL). If all points on both zone 2 and 3 were employed to fit VCL, then σ_p' value is questionable at best. For this type of compression curve shape, only the steep portion (zone 2) was utilized for VCL. Cyclone overflow compression curves data seemed to exhibit this shape as well.

Compression curves for centrifuge tailings that were subjected to more than one cycle of freeze-thaw exhibited a distinctive lightning bolt shape, as seen in Figure 5. The shape features two clear, nearly parallel slopes separated around effective stress of ten kPa.

Compression curves for all investigated thickened and polymer-treated tailings datasets show the downward sloping L shape. Two zones can be identified; the first is where very large settlement happens up to certain vertical stress then the slope decreases.

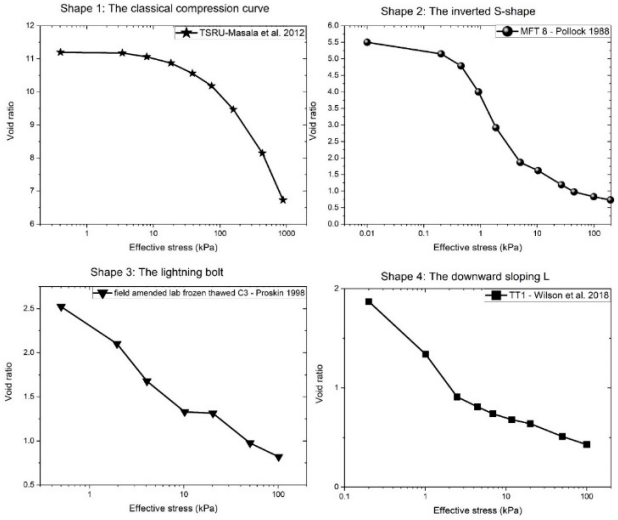

Figure 5. General shapes of the compressibility curves observed in the 112 datasets investigated in this paper.

Practical implications of preconsolidation pressure presence in oil sands tailings

The utility of accurate estimation of the pre-consolidation pressure manifests itself in two distinct ways, namely in shear strength and volume estimates.
Geotechnical literature is replete with evidence that pre-consolidation pressure is a crucial parameter for analyzing and predicting settlement behaviour and short-term stability challenges in soft clays (Jamiolkowski et al. 1985; Ladd and Foote 1974; Mesri and Godlewski 1977; Wroth 1984). The two facets, strength and settlements, are key for the design of tailings storage facilities for accurately reflecting the volume requirement and overall geotechnical performance. Geotechnical practitioners ought to be aware of knowing the pre-consolidation pressure to help better design a TSF.

Time dependency of pre-consolidation pressure

Igbinedion and Simms (2020) present evidence that pre-consolidation pressure in centrifuged tailings increased with time, and very high creep was observed as the pre-consolidation pressure was exceeded. This is consistent with literature where Mesri (1975) links thixotropic behaviour in remoulded or reconstituted clay to the structuration effect leading to a subsequent increase in pre-consolidation pressure over time. This connection is evident in tailings ponds, with thixotropic ageing linked with slow dissipation of excess pore water pressure leading to low effective stress development; these low effective stresses contribute to the development of an over-consolidated structure (structuration) that affects dewatering of tailings (Miller, 2010; Somogyi et al., 1977; Jeeravipoolvarn, 2010). Although both phenomena are similar, the difference between both is that the structuration effect leads to a stiffer clay sample, while thixotropy results in strength gain (Qi et al., 2018).

Compression rate effects on pre-consolidation pressure

Some literature links the pre-consolidation pressure to the compression rate. Therefore, in the case of oil sands FFT slurry, it is primarily a function of the self-weight settlement. This necessarily is governed by the initial hindered settlement and saturated hydraulic conductivity. A higher initial void ratio with the same sample thickness implies a relatively higher rate of compression compared to a lower void ratio; the higher pre-consolidation pressure belongs to the higher initial void ratio Suthaker (1995). The three sets of the same MFT starting with different void ratios confirm this observation. They produced slightly different σ_p' with a mean of 0.8 kPa and 0.5 kPa standard deviation. Some methods generated a higher σ_p' for a higher initial void ratio.

The 'correct' σ_p' paradigm

The pursuit of a single 'correct' value of the pre-consolidation pressure seems like a futile exercise even when dealing with classical soils. This is one of the reasons the authors decided to employ several methods to evaluate σ_p'. The goal was not to obtain the "correct" value but rather to explore which method should be utilized based on its repeatability and lack of ambiguity. Both Pacheco Silva's and Arvidsson & Keller's methods were quite straightforward with no issues. However, as one would expect, Casagrande's methods proved fairly inconsistent and operator-dependent, especially in the S-shape compressibility curve.

The potential of a σ_p' in oil sands tailings can be vital to understand the overall settlement behaviour, especially at high void ratios. However, it is not possible to pinpoint single stress at which pre-consolidation can be overcome, but rather a range for practitioners when designing and planning tailings storage facilities.

Su / σ_v' correlation
Shear strength (Su) is commonly evaluated from transformation models based on clay properties, such as pre-consolidation pressure (σ_p') (e.g. Mesri 1975; Jamiolkowski et al. 1985) or plasticity (e.g. Hansbo 1957; Chandler 1988). Many transformation models are empirical or semi-empirical, obtained by data fitting through regression analysis. Terzaghi's (1966) $Su/\sigma_p'=0.22$ correlation has been disputed in the literature (e.g. Mesri 1989).

Figure 6 illustrates the effective stress versus shear strength regression fit from available large strain consolidation datasets that presented shear strength development with effective stress.

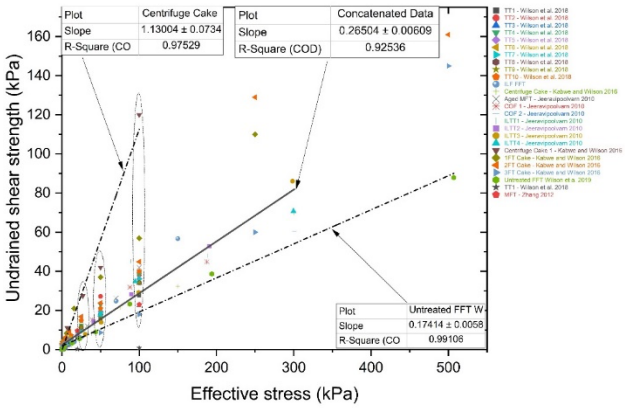

Figure 6. Undrained shear strength correlation to effective vertical stress.

An overall Su / σ_v' = 0.26 was observed from all concatenated data. However, it is important to emphasize the highly variable nature of the regression fit when looking at the processing used to produce the tailings, as underscored in Figure 6. The following ranges can be reported for Su / σ_v' =

- 0.22 – 1.13 for centrifuge cake
- 0.23 – 0.28 for in-line thickened tailings
- 0.27 – 0.39 in thickened tailings
- 0.20 – 0.25 in cyclone overflow tailings
- Up to 0.41 in "old" FFT

The datasets of undrained shear strength of tailings utilized in this paper are measured in the laboratory using the miniature vane shear test in accordance with ASTM standard (ASTM D4648) - standard test method for laboratory for saturated fine-grained clayey soil.

CONCLUSIONS

A review of publicly available data on large strain consolidation compressibility curves of various treated and untreated oil sands tailings was carried out. Over 112 datasets were evaluated for potential pre-consolidation pressure. Some untreated fluid fine tailings and mature fine tailings specimens exhibited slight pre-consolidation pressure. All of σ_p' values were lower than 2 kPa, except for 3 types of tailings. The three exceptions were TSRU, centrifuge cake and tailings undergoing freeze-thaw. Freeze-thaw dewatering of tailings resulted in the highest pre-consolidation pressure with higher variability in σ_p' stemming from datasets of a field core. Cores from the same tailings pond show high variability, much in excess of specimens frozen-thawed in a laboratory setting. The correlation between the undrained shear strength and the effective vertical stress was variable. Specific correlations pertinent to each type were presented. The only evidence that the tailings processing caused pre-consolidation pressure existed in centrifuge cake. However, none of the flocculated tailings exhibited measurable pre-consolidation pressure. All polymer-amened datasets showed zero pre-consolidation pressure. However, none of the datasets presented here were subjected to freeze-thaw cycles, which appears to be the main source of mechanical preconsolidation pressure.

ACKNOWLEDGMENTS

The authors would like to thank the Natural Sciences and Engineering Research Council (NSERC) for funding this research project. Special thanks to Dr. Louis Kabwe of the University of Alberta for assisting in acquiring some of the LSC datasets.

REFERENCES

Abdulnabi, A. Amoako,K. Moran, D. Vanadara, K. Aldaeef, A. Esmaeilzadeh, A. Beier, N. Soares, J and Simms, P. 2021. Evaluation of candidate polymers to maximize geotechnical performance of oil sands tailings. Canadian Geotechnical Journal. 59(3): 359-371. https://doi.org/10.1139/cgj-2020-0714

Alberta Energy Regulator (AER) 2017. Directive 085: Fluid Tailings Management for Oil Sands Mining Projects. Available from: https://www.aer.ca/documents/ directives/Directive085.pdf. Accessed on April 10, 2020.

Alberta Energy Regulator (AER) 2020. State of fluid tailings management for mineable oil sands, 2018. Available from: https://www.aer.ca/documents/oilsands/2018-State-Fluid-Tailings-Management-Mineable-OilSands.pdf. Accessed on February 7, 2021.

Amoako, K. A., 2020. Geotechnical Behaviour of Two Novel Polymer Treatments of Oil Sands Fine Tailings. Master of Science thesis, University of Alberta, Edmonton.

Arvidsson, J.; Keller, T. 2004. Soil precompression stress I. A survey of Swedish arable soils. Soil & Tillage Research, 77:85-95.

Beier, N. A. 2015. Development of a Tailings Management Simulation and Technology Evaluation Tool. PhD thesis. University of Alberta. Edmonton. [electronic resource]

Bjerrum, L. 1967 Engineering Geology of Norwegian Normally-Consolidated Marine Clays as Related to Settlements of Buildings Géotechnique doi 17:2, 83-118 https://doi.org/10.1680/geot.1967.17.2.83

Boone, S. J. 2010. A critical reappraisal of preconsolidation pressure interpretations using the oedometer test. Canadian Geotechnical Journal, 47, 281 - 296.

Bowles, J. A. 1986. Engineering Properties of Soils and their Measurements, 3rd edition. McGraw - Hill Book Company, Inc. NY, 218pp.

Casagrande, A. 1936. The determination of the pre-consolidation load and its practical significance. In: Proceedings of the International Conference on Soil Mech. and Found. Eng. (ICSMFE), Cambridge, MA, 22-26 June 1936, vol. 3. Harvard University, Cambridge, MA, USA, pp. 60-64.

Chandler, R. (1988). The in-situ measurement of the undrained shear strength of clays using the Field Vane and BT Vane Shear Strength Testing in Soils: Field and Laboratory Studies. ASTM International, 1988.

Core Team, R., 2014. R: A Language and Environment for Statistical Computing. R Foundation for Statistical Computing, Vienna, Austria, ISBN: 3-900051-07-0. Available from: ⟨http://www.R-project.org⟩.

COSIA – Canadian Oil Sands Innovation Alliance 2012. Technical Guide for Fluid Fine Tailings Management. Oil Sands Tailings Consortium, August 30, 2012, 131 pp.

da Silva, A. R., de Lima, R. P. 2015. soilphysics: An R package to determine soil preconsolidation pressure. Computers and Geosciences Journal. V 84 pp 54 – 60. 10.1016/j.cageo.2015.08.008.

Dias Junior, M.S., Pierce, F.J., 1995. A simple procedure for estimating pre-consolidation pressure from soil compression curves SoilTechnol.8,139–151.

Gibson, R.E., England, G.L. and Hussey M.J.L. 1967. The theory of one-dimensional consolidation of saturated clays. I. Finite non-linear consolidation of thin homogeneous layers. Géotechnique, 17(3): 261–273.

Hansbo, S. 1957 A new approach to the determination of the shear strength of clay by the fall-cone test. Royal Swedish Geotechnical Institute Proceedings No.14 (SGI Proceedings). Stockholm. Retrieved from http://urn.kb.se/resolve

Herweynen, W., Bareither, C., and Scalia, J. 2017. Salinity effects on the consolidation behavior of kaolin. Proceedings of Tailings & Mine Waste 2017, Banff, Alberta, Canada. University of Alberta, Edmonton, Canada.

Hurtado, O. 2018. Desiccation and Consolidation in Centrifuge Cake Oil Sands Tailings. Master of Applied Science thesis. Department of Environmental Engineering. Carleton University, Ottawa, ON.

Jamiolkowski, M., Ladd, C.C., Germaine, J.T., and Lancelotta, R. 1985. New developments in field and laboratory testing of soils. In Proceedings of the 11th International Conference on Soil Mechanics and Foundation Engineering. A.A. Balkema. pp. 57–153.

Jeeravipoolvarn, S. 2005. Compression Behaviour of Thixotropic Oil Sands Tailings. M.S.c. thesis, Department of Civil and Environmental Engineering, University of Alberta, Edmonton, AB.

Jeeravipoolvarn, S. 2010. Geotechnical behavior of in-line thickened oil sands tailings. PhD thesis. University of Alberta. Edmonton. [electronic resource].

Kabwe, L. and Wilson, G. W. 2016. Large Strain Consolidation Testing of Frozen and Thawed Fluid Fine Tailings Centrifuged Cake Prepared for Syncrude Canada Ltd.

Kabwe, L. Abdulnabi, A. Wilson, G. W., Beier, N. A. Scott, J. D. 2019. Geotechnical and unsaturated properties of metal mines and oil sand tailings In Proceedings of Tailings and Mine Waste 2019 November 17-20, 2019, Vancouver, Canada.

Khan, S. F., Shahid, A. 2016. Determination of consolidation behaviour of clay slurries. International Journal of Mining Science and Technology. 26. 10.1016/j.ijmst.2015.12.014.

Masala, S., Langseth, J., Smyth, K, Dunmola, A., Mckay, D., and Clark, J. 2012. TSRU tailings pilot-scale thickening and deposition trials. In Proceedings of the 3rd International Oil Sands Tailings Conference, Edmonton, Alberta, Canada, 3-5 December 2012, pp. 333-342.

Mesri, G. 1975. “New design procedure for stability of soft clays. Discussion, J. of the Geotech. Eng. Div., ASCE,10 1(4),40 9-412.

Mesri, G., and Shahien, M. 1994. Discussion of "Pre-consolidation versus aging behavior of Kaolinite clay" Journal of Geotechnical Engineering, 120(9): 1643–1645. doi:10.1061/(ASCE)0733-9410(1994)120:9(1643).

Mesri, G. 1989. A reevaluation of Su(mob) = 0.22σ’p using laboratory shear tests. Canadian Geotechnical Journal 26: 162-164.

Miller, W.G., Scott, J.D. and Sego, D.C., 2011. Effect of extraction water chemistry on the consolidation of oil sands fine tailings. CIM Journal 1(2): 113-129.

Pacheco Silva, F. 1970. A new graphical construction for determination of the pre-consolidation stress of a soil sample. In Proceedings of the 4th Brazilian Conference on Soil Mechanics and Foundation Engineering, Rio de Janeiro, Brazil. pp. 225–232.

Pollock, G. 1988. Large Strain Consolidation of Oil Sand Tailings Sludge, M.S.c. thesis, Department of Civil and Environmental Engineering, University of Alberta, Edmonton, AB.

Proskin, S. 1998. A Geotechnical Investigation of Freeze-Thaw Dewatering of Oil Sands Fine Tailings. PhD thesis, University of Alberta.

Qi, S. and Simms, P., 2018. Hydro-mechanical coupling in dewatering simulations for mine tailings management. In Proceedings of the 7th international conference on unsaturated soils (pp. 1157-1162).

Qi, S., Salam, M. A., and Simms, P. 2018 Creep and structuration in tailings and in natural clays IOSTC Edmonton AB December 9-12 2018.

Royal Society of Canada Expert Panel. 2010. Executive Summary: Environmental and Health Impacts of Canada's Oil Sands Industry Rep. Ottawa, Ontario, Canada.

Sego D.C., and Dawson R.F., 1992. Influence of freeze-thaw on behaviour of oil sand fine tails. Submitted to Alberta Oil Sands Technology and Research Authority. 77p.

Stienwand, K. 2021. Influence of Chemical Amendments on the Long-term Geotechnical Behaviour of Oil Sands Fine Tailings. M.S.c. thesis, Department of Civil and Environmental Engineering, University of Alberta, Edmonton, AB.

Suthaker, N. N and Scott, J.D. 1997. Thixotropic strength measurement of oil sand fine tailings. Canadian Geotechnical Journal 34(6): 974-984.

Suthaker, N. N. 1995. Geotechnics of Oil Sand Fine Tailings, Ph.D. thesis, Department of Civil and Environmental Engineering, University of Alberta, Edmonton, AB.

Wang, Yixuan, "A study on chemical stabilization of Oil Sands Mature Fine Tailings" (2017). Electronic Thesis and Dissertation Repository. 4937. https://ir.lib.uwo.ca/etd/4937.

Watanabe, K., Udaka, K., Nakatani, Y. and Leroeil, S. 2012. Long-term consolidation behaviour interpreted with isotache concept for worldwide clays. Soils Found., 52: 449-464.

Wilson, G.W., Kabwe, L.K., Beier, N.A., and Scott, J.D. 2018. Effect of various treatments on consolidation of oil sands fluid fine tailings, Canadian Geotechnical Journal, 55(8): 1059-1066.

Zhang, Y. 2012. Laboratory study of freeze-thaw dewatering of Albian mature fine tailings. M.Sc. Thesis Department of Civil and Environmental Engineering, University of Alberta, Edmonton, AB.pp

CONSOLIDATION-CREEP MODELING IN OIL SANDS TAILINGS DEPOSITS

Narges Gheisari[1], Paul Simms[1], Shunchao Qi[1], Fergus Murphy[2], Gordon Gjerapic[3] and Dobroslav Znidarcic[3]
[1]Carleton University, Ottawa, Ontario, Canada, [2]Suncor Energy Inc., Calgary, Alberta, Canada
[3]University of Colorado, Boulder, Colorado, USA

ABSTRACT

Oil sands tailings can exhibit time-dependent behaviours that result in the variation of compressibility with time. Therefore, slightly increasing the complexity of large-strain consolidation model to account for such effects may have justification as more confident predictions of tailings dewatering can be realized despite some additional parameterization. In this paper, the experimental observations of flocculated fluid fine tailings in two different studies (one a long-term laboratory study, and the other a pilot study) are modeled using two formulations of creep and large-strain consolidation. One is based on the existing elastic visco-plastic model (EVP) of Yin and Graham, and the second model is named CONCREEP which empirically describes the change in the compression curve over time, both embedded in a large-strain consolidation framework (UNSATCON). The modeling results indicate that both consolidation-creep models improve fits to all measured data (settlement, void ratio, and excess pore-water pressure), compared to the large-strain consolidation model. The creep parameters can be determined by using a rigorous division of data into "calibration" and "validation" sets. The sensitivity of the results to establish uncertainty of the parameters is evaluated. Numerical simulations were also performed on hypothetical full-scale deposits of tailings using consolidation-creep and large-strain consolidation models. The implications of the model projections and uncertainty for tailings deposit trajectories in settlement, density, effective stress, and strength, are discussed.

INTRODUCTION

The extraction of bitumen from oil sands deposits produces a significant volume of fine-grained tailings, which results in many technical and environmental problems for oil sands operators. Canadian Government (2018) reported that oil sands production has accumulated 650 million cubic meters of Fluid Fine Tailings (FFT) that are impounded in 176 km^2 of tailings ponds. To accelerate and improve dewatering properties, some dewatering technologies can be used, however, consolidation is still the dominant dewatering mechanism. So, an accurate consolidation analysis plays a critical role in the management of such deposits, as it estimates depth profiles of density and strength, and rate of settlement (Carrier 1983). Currently, the consolidation of soft soil deposits such as the various types of tailings, is often studied analytically or numerically based on Gibson's one-dimensional (1D) finite strain consolidation theory for saturated soils (Gibson et al. 1967). Although the large-strain consolidation theory is widely used for the management of tailings, it might be somewhat inaccurate for certain cases, especially for tailings deposits with low hydraulic conductivity and long drainage paths, where substantial settlement can be expected over periods of years to decades. At this time scale, time-dependent effects, such as creep may become important in predictions of long-term deformation. For these cases, large-strain consolidation analysis alone might not be sufficient for predicting dewatering or volume change in soft deposits (Sills 1998, Jeeravipoolvarn 2009). There is ample evidence in the literature that oil sands tailings can exhibit a significant time-dependent behaviour that can alter the compressibility curve over time. For example, the time-dependent behavior has been reported in polymer amended FFT, by Salam et al. (2017) who ran several short (10 cm high) column tests on fFFT. Also, creep has been proposed to explain the slow dissipation of pore-water pressures in oil sands tailings (Jeeravipoolvarn et al. 2008, Chaudhary et al. 2015).

Many studies have been conducted to investigate creep in clays, and several numerical analyses have been developed to incorporate creep into small-strain consolidation models. The most common creep model is based on the concept of secondary compression (C_α) proposed by Buisman (1936) in which void ratio decreases linearly with time under a constant effective stress. Bjerrum (1967) expanded on Buisman's observations and showing that creep in normally consolidated or lightly over-consolidated clays can be approximated by a series of parallel lines in the $e - \log\sigma'_z$ space, where e, and

σ_z' denote void ratio and vertical effective stress respectively. Each line corresponds to a delayed compression state at a given strain rate. New loading results in the soil "returning" to higher lines instantaneously, due to the increase in strain rate. This "isotache" concept was formalized later in general EVP models (Yin and Graham,1989, 1994), who adopted the "equivalent time" (i.e., the time following the EOP consolidation available for creep) to define these parallel lines that are uniquely related to a visco-plastic or total strain rate. A comprehensive review of the isotache creep models and their advantages and limitations can be found in Liingaard et al. (2004).

Znidarcic (2015), however, based on experimental evidence proposed that the compression curve does not shift in parallel across the full range of effective stress, but the creep effects diminish with the increasing effective stresses. This creep concept was incorporated into the numerical code CONCREEP (Gjerapic et al 2021).

One of the goals in this paper is to evaluate these two main concepts of how the compressibility curve changes in the context of oil sands tailings consolidation. To this end, the two different models are applied to two cases, for which the data has been previously published: a 5-meter column experiment undertaken by Suncor (Murphy et al. 2021), and the 13.8 m pilot tests (large caissons) undertaken by multiple oil sands companies (Gheisari et al. 2020). Both tests are on flocculated fluid fine tailings (fFFT).

The two creep models are briefly described, followed by their calibration / application to each case. The calibrated models were then used to analyze a hypothetical deposition scenario. Finally, the two models are compared, with a goal of optimizing each model for practical usage.

DESCRIPTION OF CREEP MODELS

Yin and Graham model

Yin and Graham's model (henceforward YG), for which concepts have been discussed above, was incorporated into a large-strain consolidation model embedded in UNSATCON. This section provides a brief review on the formulation of the YG model and its numerical implementation.

The YG model combines an elastic part for the recoverable deformations with a time-dependent plastic part for the non-recoverable deformations. The important concepts in the YG model include equivalent time, reference timeline, instant timeline, and limit timeline, as illustrated in Figure 1. The instant timeline is only relevant to the instantaneous elastic component of strain. To find the viscos-plastic strain, the compression curve varies from a reference timeline as a function of the strain rate. Generally, as the time required for consolidation increases, so the effective compression curve shifts down, the limit timeline being the lowest possible apparent compression line. By using the same logarithmic creep vs time relationship, all the timelines are parallel, and each is related to a unique creep strain rate (Yin and Graham 1994). Lastly, the elastic deformation of the material is assumed to follow the instant timeline, and effective stress changes are exclusively linked to the elastic part.

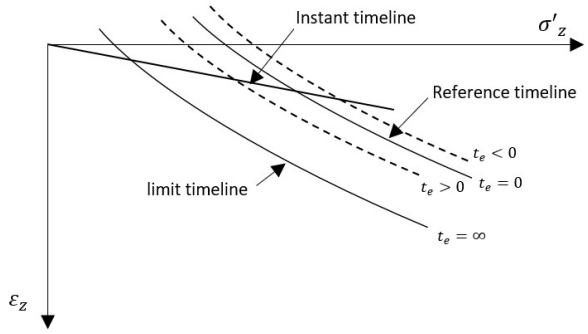

Figure 1. Illustration of important concepts in YG model

For 1D consolidation analysis in UNSATCON, the YG formulation is cast in terms of the void ratio rate change allowing for the calculation of visco-plastic strain using a general $\dot{e} - \sigma_z'$ relationship:

$$\dot{e} = -\frac{\kappa}{\sigma_z'}\dot{\sigma_z'} - \frac{\psi}{t_0} exp\left[\frac{e-e_0}{\psi}\right]\left(\frac{\sigma_z'}{\sigma_{z0}'}\right)^{\frac{\lambda}{\psi}} \quad (1)$$

where e_0 is initial void ratio corresponding to the initial effective stress σ_{z0}', which defines the position of the reference timeline in the space $\varepsilon_z - \ln \sigma_z'$, λ and κ are compression and re-compression indices or slopes of $e - \ln \sigma_z'$ curves in the normally consolidated and over consolidated ranges, corresponding to reference and instance timeline, respectively; ψ is creep parameter, t_0 is intrinsic time parameter related to the creep rate of the reference timeline.

In UNISATCON, the piecewise formulation outlined by Fox and Berles (1997) was followed to develop a

mass-conservative formulation to simulate 1D large-strain-consolidation of saturated soft soil deposits. The associated nonlinearities are addressed by solving the flow-continuity equation for water mass conservation through a finite-difference scheme in a piecewise-linear manner. UNSATCON uses void ratio (as strain state of large deformation) in the global analysis which after each time step in the discretized configuration is calculated by the finite-difference method and then used to update the σ_z' according to the adopted constitutive relationship. For consolidation-creep analysis, however, the constitutive integrations must be performed to find the stress increment $d\sigma_z'$ from an increment de over a time step dt, through solving the ordinary differential equations derived from the respective constitutive models. Different numerical integration techniques, including fully implicit, implicit with Taylor expansion and explicit algorithms, are adopted to verifying numerical accuracy. The constitutive equation of YG model (i.e., Eq. (1)) was reformulated, to calculate the $d\sigma_z'$ as:

$$d\sigma_z' = \frac{\sigma_z'}{\kappa} de + \frac{\sigma_z'}{\kappa} \frac{\psi}{t_0} exp\left[\frac{e-e_0}{\psi}\right] \left(\frac{\sigma_z'}{\sigma_{z0}'}\right)^{\frac{\lambda}{\psi}} dt \quad (2)$$

where de is void ratio change over the current time step dt, whose values for the specific case might be significantly large and cannot be regarded as infinitesimal. The equation coefficients are not constant but depend on $d\sigma_z'$ and e. To account for this nonlinearity, a forward Euler's explicit algorithm was developed, which divides the increment into many sub-increments and evaluates the coefficients at the beginning of each sub-increment from the previous time step. The errors are controlled by automatically adjusting the sub-increment size. Then, the current σ_z', is updated by adding $d\sigma_z'$ to its value in the previous time step.

CONCREEP model

A time-dependent constitutive relationship for soil's compressibility was introduced by Gjerapic et al. (2021) and implemented into a numerical model CONCREEP. The model is based on Gibson's large-strain consolidation theory (1967). The model parameters can be determined from a series of step loading consolidation tests and direct measurement of hydraulic conductivity. The family of time-dependent compressibility curves corresponding to different times is defined as Eq. (3):

$$e = A(\sigma_z' + Z)^B \quad (3)$$

where A, B and Z are described as algebraic function of time to allow for time-dependency of constitutive properties as below:

$$A = A(t) = A_f + (A_0 - A_f)\left\{a_1\left[\left(\frac{1}{a_1}\right)^{\frac{1}{a_2}} + t\right]^{a_2}\right\} \quad (4)$$

$$B = B(t) = B_f + (B_0 - B_f)\left\{b_1\left[\left(\frac{1}{b_1}\right)^{\frac{1}{b_2}} + t\right]^{b_2}\right\} \quad (5)$$

$$Z = Z(t) = Z_f + (Z_0 - Z_f)\left\{z_1\left[\left(\frac{1}{z_1}\right)^{\frac{1}{z_2}} + t\right]^{z_2}\right\} \quad (6)$$

According to above equations, at initial time (t=0), parameters A, B and Z are defined based on their initial values A_0, B_0 and Z_0, and A_f, B_f and Z_f are limiting values of parameters at infinite time. Other parameters including a_1, a_2, b_1, b_2, z_1 and z_2 are determined by fitting laboratory data to Equations 4, 5 and 6.

For implementation of CONCREEP 's constitutive relationships in UNSATCON, the compressibility function defined by (Eq. 3) was expressed as:

$$\sigma_z' = \left[\left(\frac{e}{A}\right)^{\frac{1}{B}}\right] - Z \quad (7)$$

to determine and update effective stress.

PILOT STUDY

The pilot study involved deposition and monitoring of different types of fFFT generated from surface mining of oil sands deposits containing bitumen in Northern Alberta, Canada (Tailings Consolidation Casing Experimental Pilot Project, Albian Sands Mine Site, August 2015). The tailings were deposited into a steel casing approximately 2.75 m in diameter and 13 m in height. If the tailings were instantaneously deposited at their initial density (initial e=4.67 or w=210%), the initial height of the tailings would be 13.8 m, however, the deposition occurred over 12 days. No flux was allowed at the bottom and the accumulated water at the top due to self-weigh was not removed. Thus, the tailings column remained saturated over the entire time. The tailings–water interface, density, and pore-water pressures (PWP) were monitored over 3 years.

Parameters for large-strain consolidation model in pilot study

Figure 2 illustrates the in-situ compressibility relationship in pilot study which clearly shifts with time: for example, the e corresponding to the σ_z' of

8 kPa varies between end of Year 1 to end of Year 3 from about 2.4 to 1.8. However, for the conventional large-strain consolidation analysis, a time-invariant compressibility curve was assumed. the adopted compressibility curve was determined by fitting a power function through reported in-situ data:

$$e = 3.8\,\sigma_z'^{-0.238} \quad (8)$$

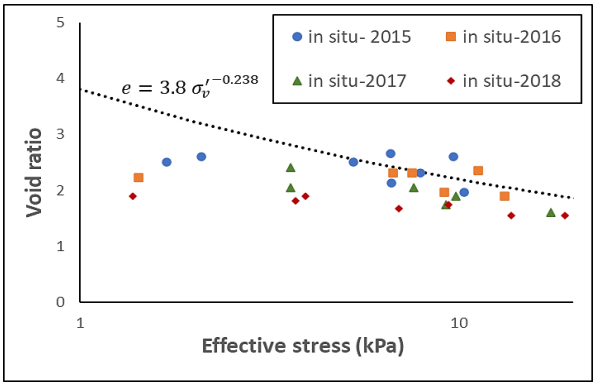

Figure 2. Compressibility function obtained from in-situ compressibility data in pilot study

Using the large-strain consolidation predictions, Qi and Simms (2020) developed a robust method for back-calculating the hydraulic conductivity from settlement data. With this method, the estimated of hydraulic conductivity for pilot data is:

$$k = 2.2 \times 10^{-10} e^{8}\ (\frac{m}{s}) \quad (9)$$

It should be noted that, for pilot study different sets of compressibility and hydraulic conductivity were obtained using different calibration methods to reduce uncertainty. The details of these methods and numerical results of large-strain consolidation analyses (using obtained sets of compressibility and hydraulic conductivity) can be found in Gheisari et al. (2020).

Parameters for YG model in pilot study

For YG model, the compression index (λ) was fitted using the slope of in-situ compressibility curves in $e - ln\sigma_z'$ plots, and the recompression index (κ) was estimated using an appropriate ratio of $\frac{\kappa}{\lambda}$ which ranges from 0.1 to 0.2. The initial effective stress (σ_{z0}') corresponds to the initial void ratio was assumed a small value (=0.1 kPa). For creep behaviors in YG model, two parameters including creep parameter (ψ) and reference time (t_0) and were calibrated based on model predictions at constitutive level. It is known that the compressibility curves (timelines) in YG models are a set of parallel lines corresponding to different strain rates. The locations of lines are shifted by t_0, and the distance of lines is affected only by ψ. The observed settlement behavior over time (i.e., the compressibility curves shifting down over time due to creep) can be used to estimate creep parameter (ψ) during the calibration process. Meanwhile, the average experimental strain rate ($\frac{de}{dt}$) for each year was estimated from the measured data, and then used to determine t_0 by fitting the analytical model prediction to the recorded measurements. Figure 3 compares the observed compressibility data with the modeled compressibility relationships for years 2015 to 2018 obtained from calibration the YG model. Table 1 summarizes the obtained YG model parameter.

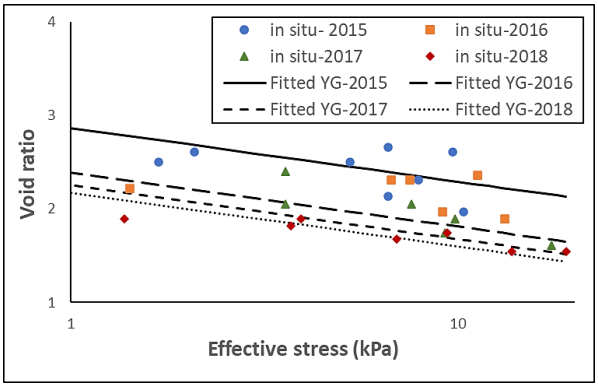

Figure 3. Calibrating YG model using in-situ compressibility data in pilot study

Table 1. Parameters for YG model in pilot study

Lambda (λ)	0.25
Kappa (κ)	0.04
Creep parameter (ψ)	0.2
Reference time (t_0) (s)	2E+3

Parameters for CONCREEP model in pilot study

Similar to the YG model, the in-situ compressibility curves were used to calibrate CONCREEP model parameters. Figure 4 compares the observed compressibility data with the modeled ones. The calibrated CONCREEP model parameters are summarized in Table.

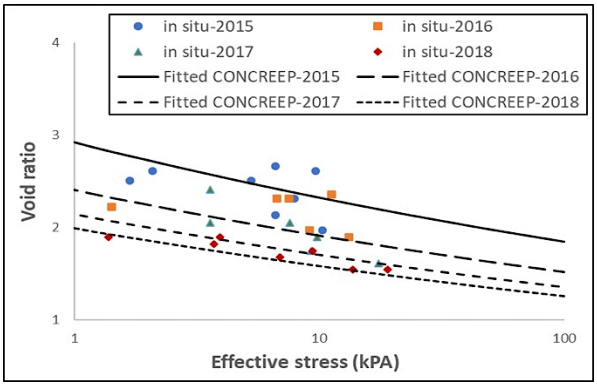

Figure 4. Calibrating CONCREEP model using in-situ compressibility data in pilot study

Table 2. Parameters for CONCREEP model in pilot study

A_0	3	a_1	1200
A_f	1.5	a_2	-1.1
B_0	-0.1	b_1	5
B_f	-0.105	b_2	-1.1
Z_0	1	z_1	0.1
Z_f	0.001	z_2	-1

Numerical results for pilot study

The consolidation analysis was conducted for instant deposition of 13.8 m tailings for 1100 days under self-weight consolidation using both the large-strain consolidation and the consolidation-creep models (YG and CONCREEP models) embedded in UNSATCON. No drainage at the bottom, and no decantation at the top were assumed as boundary conditions. Therefore, the height of water remained constant, and the tailings is fully saturated for the entire time of simulation. Table 3 shows the basic properties of fFFT deposition in pilot study which was used for numerical modeling. Figure 5 compares the simulated height of mudline over time with the observed height, and Figures 6 and 7 illustrate the depth profile of void ratio and excess PWP after 1100 days. It is observed that the large-strain consolidation model overestimated the dissipation of PWP despite the settlement predictions bracketing the observed data. Furthermore, the measured settlement curve is not flat but indicates a continuing deformation when approaching the end of the simulated period confirming the effect of time in shifting of the compressibility curves (which is also evidenced by the experimental compressibility data reported in Figure 2). Therefore, it appears that the large-strain consolidation analysis by itself (i.e., without accounting for time effects) cannot properly characterize the pilot results. Therefore, accounting for creep in the consolidation analyses is expected to provide a better physical description of the problem, and consequently, result in a better agreement between observed and simulated behaviour. Both YG and CONCREEP models predicted similar mudline heights (Figure 5) and void ratio (vs. depth) profiles (Figure 6). The CONCREEP model predicted somewhat higher excess PWP than YG model resulting in a better overall agreement the CONCREEP model and the measured data (Figure 7).

Table 3. Initial condition and specific gravity of fFFT deposition in pilot study

Thickness of deposition (m)	13.8
Initial void ratio	4.67
Initial effective stress (kPa)	0.1
Specific gravity	2.22

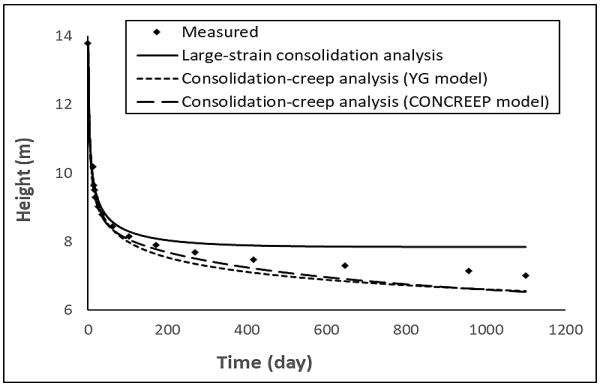

Figure 5. Predicted height for pilot study

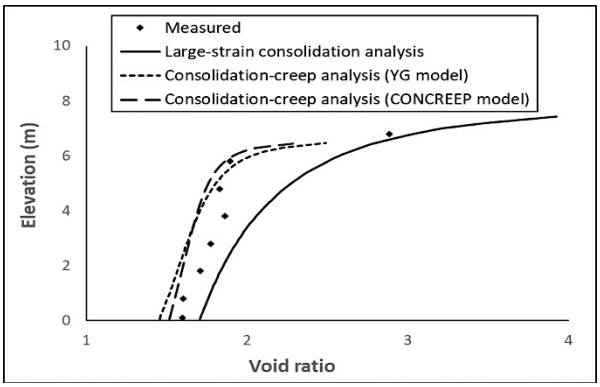

Figure 6. Predicted depth profile of void ratio at day of 1100 day for pilot study

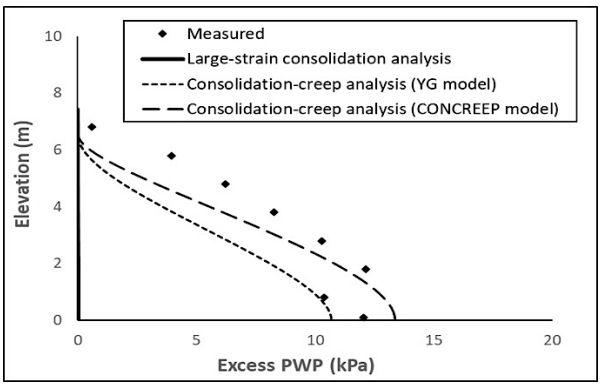

Figure 7. Predicted depth profile of excess PWP at day of 1100 day for pilot study

Laboratory study

The long-term laboratory experiment was conducted as a part of Suncor's tailings technology development project to monitor the consolidation behavior of fFFT. The tailings were deposited into a column with the height of 5 m and the diameter of 0.61 m. The filling process lasted for 6 hours. There was no drainage at the bottom and no decantation was allowed at the top, so the tailings remained saturated over the entire duration of experiment. The settlement, void ratio, and PWP at different depth were measured over several months. The experimental observations were then analyzed using CONCREEP model by Murphy et al. (2021). Their modeling results will be compared with the consolidation-creep predictions obtained from YG model in following sections.

Parameters for large-strain consolidation model in laboratory study

The Seepage Induced Consolidation (SIC) test is a rapid technique for determining compressibility and hydraulic conductivity functions in low density slurries which was first developed for phosphatic clays (Abu-Hejleh, et al., 1996), but it is also well suited for testing of oil sands tailings samples (see Znidarcic et al., 2011). Murphy et al. (2021) performed a series of SIC tests on fFFT samples in the laboratory to obtain compressibility and hydraulic conductivity relationships of tailings deposited in the 5-meter column experiment (see Figures 8 and 9). For large-strain consolidation analysis in this paper, the linear logarithmic and power functions were fitted to curves in Figures 8 and 9 resulting in the compressibility and hydraulic conductivity functions as follows:

$$e = -0.67 \ln(\sigma'_z) + 4.02 \quad (10)$$

$$k = 2 \times 10^{-10} \; e^{6.6} \; \left(\frac{m}{s}\right) \quad (11)$$

Figure 8. Compressibility function obtained from SIC test (Murphy, et al. 2021)

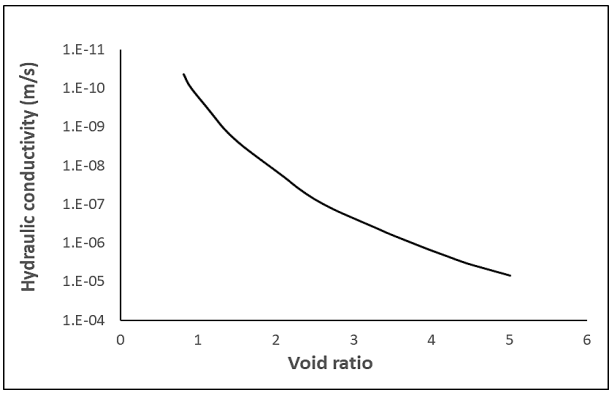

Figure 9. Hydraulic conductivity obtained from SIC test (Murphy, et al. 2021)

Parameters for YG model in laboratory study

The procedure to obtain the YG model parameters for pilot study was also followed for the 5-meter column experiment (laboratory study). Compressibility data for the 5-meter column experiment (used to calibrate the YG model parameters) are illustrated in Figure 10. The calibrated YG model parameters are summarized in Table 4.

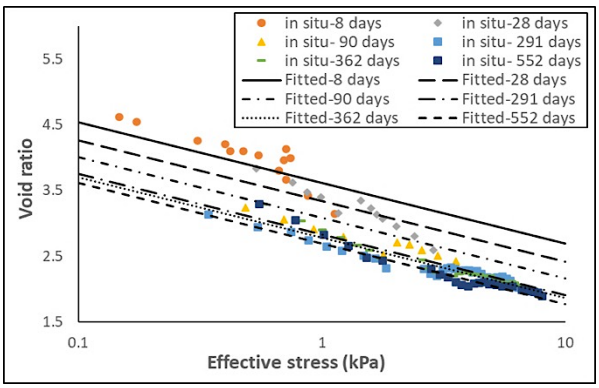

Figure 10. Calibrating YG model using compressibility data for laboratory study

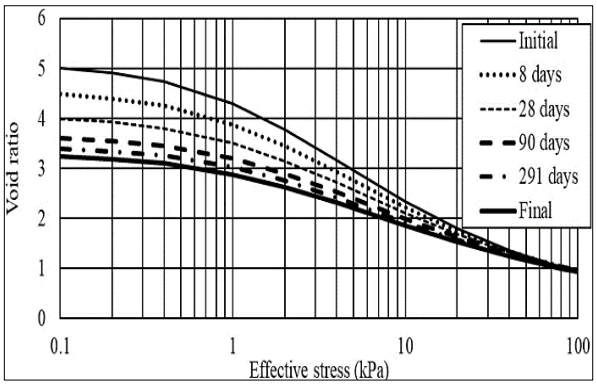

Figure 11. Calibrating CONCREEP model using compressibility curves at different times for laboratory study (Murphy, et al. 2021)

Table 4. Parameters for YG model in laboratory study

Lambda (λ)	0.4
Kappa (κ)	0.04
Creep parameter (ψ)	0.2
Reference time (t_0) (s)	5E+4

Table 5. Parameters for CONCREEP model in laboratory study (Murphy, et al. 2021)

A_0	6.93	a_1	8
A_f	4.1	a_2	-0.8
B_0	-0.436	b_1	20
B_f	-0.32	b_2	-1
Z_0	2	z_1	1
Z_f	2	z_2	-1

Parameters for CONCREEP model in laboratory study

Murphy, et al. (2021) assumed that the creep is more significant at shallower depths of the column with the effects of creep progressively diminishing towards zero as the effective stress approaches 100 kPa. They also adopted the effective stress of 0.1 kPa as the lowest stress to fit CONCREEP parameters using SIC measurements on representative tailings samples (samples of tailings material used to fill the 5-meter column). A series of SIC measurements conducted at different loads and at different loading durations were used to calibrate CONCREEP parameters and to determine the corresponding set of compressibility curves illustrated in Figure 11. The calibrated constitutive parameters for fFFT in 5-meter column experiment are listed in Table 5.

Numerical results for laboratory study

The consolidation analysis was conducted for instant deposition of 5 m tailings for 670 days under self-weight consolidation using both large-strain consolidation and consolidation-creep models. No drainage at the bottom, and no decantation at the top were assumed as boundary conditions. Hence, the height of water remained constant, and the tailings remained fully saturated for the entire time of simulation. Table 6 shows the initial conditions and specific gravity of fFFT used to conduct the 5-meter column experiment. Figure 12 compares the simulated height of mudline over time with the observed height, and Figures 13 and 14 illustrate the depth profile of void ratio and excess PWP after 552 and 645 days respectively. As the numerical analyses indicated, consolidation-creep models provide more accurate predictions compared to the large-strain consolidation analysis. Both YG and CONCREEP models predicted similar mudline heights for the 5-meter column experiment demonstrating favorable agreement with the measured values (Figure 12). The YG model results indicate a better match with the experimental void ratio data at higher elevations, while the

CONCREEP model exhibits a better agreement with void ratios at the lower elevations (Figure 13). The YG model also predicted higher excess PWP than the CONCREEP model resulting in a better overall agreement between the YG model and the measured data (Figure 14).

Table 6. Initial condition and specific gravity of fFFT deposition in laboratory study

Thickness of deposition (m)	5
Initial void ratio	4.91
Initial effective stress (kPa)	0.1
Specific gravity	2.43

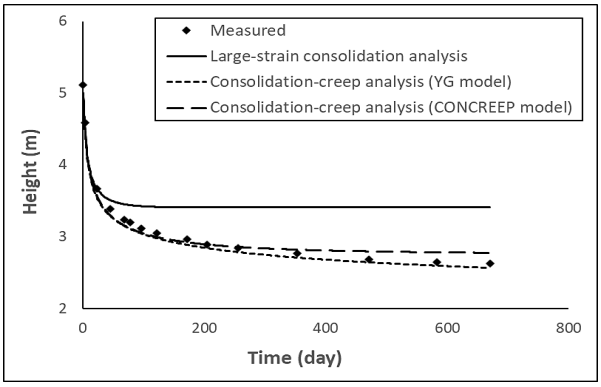

Figure 12. Predicted height for laboratory study

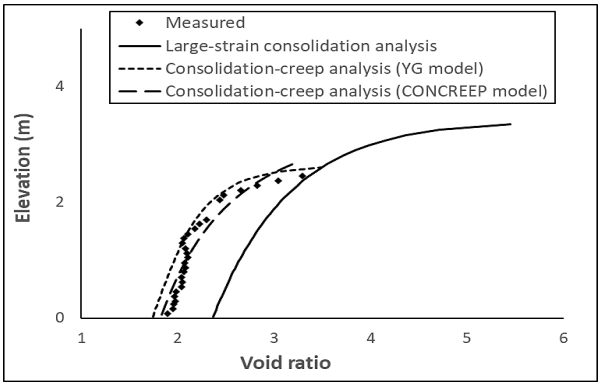

Figure 13. Predicted depth profile of void ratio at day of 552 for laboratory study

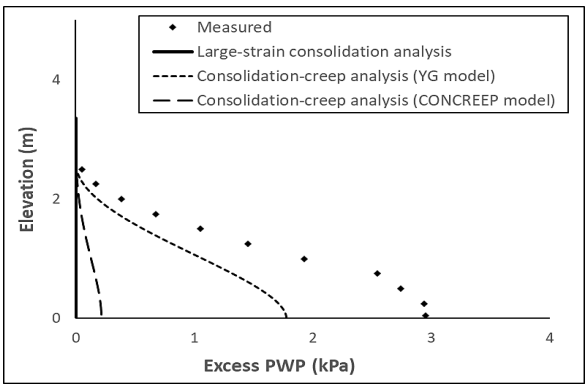

Figure 14. Predicted depth profile of excess PWP at day of 645 for laboratory study

Sensitivity analysis of YG model

In this section, the sensitivity of YG creep model to the creep parameter (ψ) is investigated and the results are compared against the measured data for the 5-meter column experiment (laboratory study). Figures 15 and 16 compare the predicted height over time, and depth profile of excess PWP after 645 days for different creep parameters respectively. As expected, the creep deformation is higher for higher creep parameters, which means the effect of creep is stronger (more significant) and the corresponding settlement is predicted to be larger for higher value of ψ. When the creep parameter is small (e.g., ψ=0.01), the deposit stops settling approximately 70 days after deposition, and the excess pore water pressure approaches zero (this observation is consistent with results of the conventional large-strain consolidation model, i.e., the model without creep). Furthermore, the height of tailings decreases continuously over time indicating larger settlement rates for higher values of the creep parameter (Figure 15). The difference between different creep parameters can be observed relatively early during the settlement process because the YG model follows the hypothesis B, in which the creep is assumed to occur since the onset (during the entirety) of the consolidation process (Leroueil, 2006).

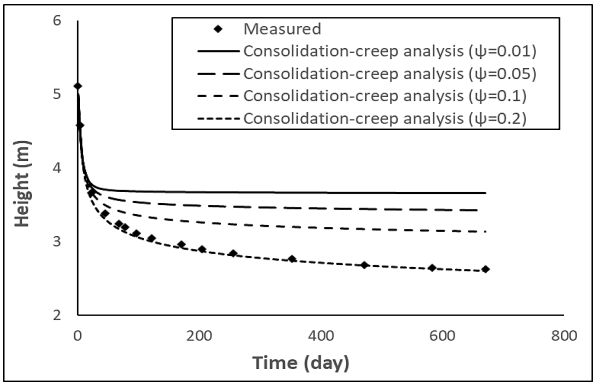

Figure 15. Sensitivity of YG model to creep parameter (ψ) in terms of settlement for laboratory study

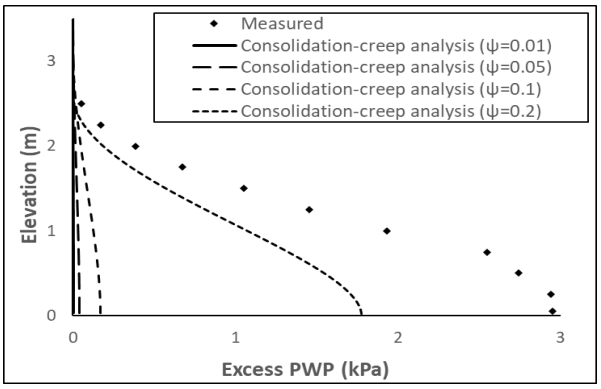

Figure 16. Sensitivity of YG model to creep parameter (ψ) in terms of depth profile of excess PWP at day of 645 for laboratory study

MODELING A HYPOTHETICAL CASE in 1D

The model parameters obtained from consolidation analyses of experimental observations such as pilot or laboratory studies can provide a range of plausible predictions for a hypothetical design case. The consolidation modeling for a hypothetical case using pilot study model's parameters was previously presented in Gheisari et al. (2020). So, in this paper, the 1D consolidation analyses for a hypothetical case was performed using model's parameters obtained from the 5-meter column experiment (laboratory study). The hypothetical simulation was assumed as a multi-layer deposition with 10 m of tailings deposited under fully saturated conditions every year during the first 5 years of operation with no decantation at the top and no drainage at the bottom imposed as boundary conditions. Both the large-strain consolidation model and the consolidation-creep models were run for an additional 100 years. Tables 7 and 8 summarize the basic properties of tailings, and models' parameters respectively.

Table 7. Basic properties of fFFT in hypothetical case

Number of depositions	5
Thickness of each deposition (m)	10
Time interval between each pour (Years)	1
Initial void ratio	4.91
Initial effective stress (kPa)	0.1
Specific gravity	2.43

Table 8. Parameters for 1D consolidation models in hypothetical case

Large-strain consolidation analysis			
Compressibility	$e = -0.67\ln(\sigma'_z) + 4.02$		
Hydraulic conductivity	$k = 2 \times 10^{-10}\ e^{6.6}\ \left(\frac{m}{s}\right)$		
Consolidation-creep analysis (YG model)			
Lambda (λ)	0.4		
Kappa (κ)	0.04		
Creep parameter (ψ)	0.2		
Reference time (t_0) (s)	5E+4		
Consolidation-creep analysis (CONCREEP)			
A_0	6.93	a_1	8
A_f	4.1	a_2	-0.8
B_0	-0.436	b_1	20
B_f	-0.32	b_2	-1
Z_0	2	z_1	1
Z_f	2	z_2	-1

Figure 17 compares the simulated height of mudline over a period of 100 years obtained from large-strain consolidation and consolidation-creep models, and Figures 18 and 19 illustrate the depth profiles of excess PWP and effective stress after 20 years respectively. The comparison indicates some differences between the settlements obtained from models with and without creep. It was observed that the consolidation-creep models predicted approximately similar settlements, though somewhat larger, than the large-strain consolidation model. While the height of mudline after 100 years was predicted to be approximately 21 m by the large-strain consolidation model, the mudline height of 19 m and 18 m were predicted by the CONCREEP and YG models. Observed differences in the excess PWP and effective stress profiles are much more significant compared to the settlement. The simulated excess PWP from the consolidation-creep analysis (YG model) is nearly 2 times of that predicted by the large-strain consolidation model (Figure 18). Consequently, the

effective stress predicted by the large-strain consolidation model is significantly higher (about 4 times higher) than predicted by the YG consolidation-creep model. The YG model estimated higher excess PWPs, and lower effective stresses compared to the CONCREEP model similarly to predictions observed for the 5-m column experiment.

The numerical modeling for a hypothetical case indicated that the consideration of creep phenomenon can lead to a significant difference in the estimated excess PWPs and the effective stresses. Considering that a precise estimation of consolidation behavior is an important requirement for a reliable tailings management, it is significant to note that the large-strain consolidation model, which ignores the effect of time-dependent behaviors, may lead to unconservative designs for tailings deposits exhibiting creep as it overestimates their strength gain during the deposition process.

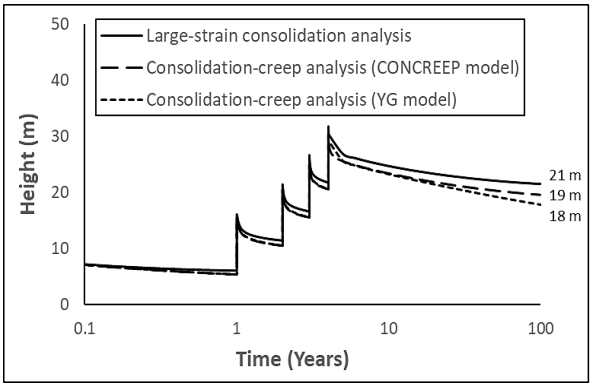

Figure 17. Predicted height for hypothetical case

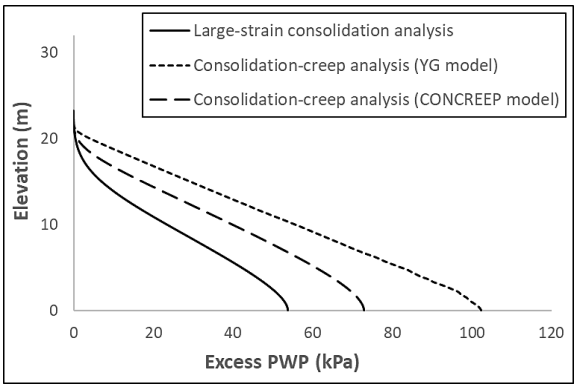

Figure 18. Predicted depth profile of excess PWP after 20 years for hypothetical case

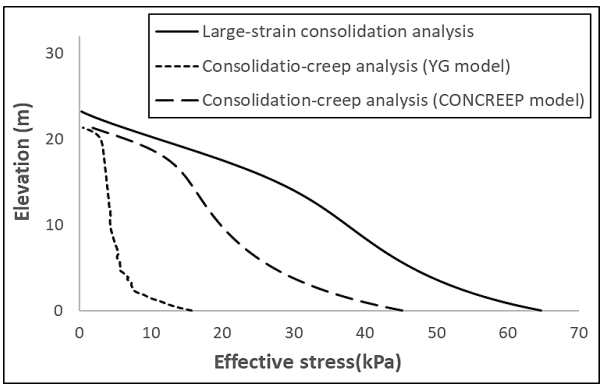

Figure 19. Predicted depth profile of effective stress after 20 years for hypothetical case

CONCLUSIONS

The paper analyzed consolidation behaviors of treated oil sands tailings using the large-strain consolidation model and two different consolidation-creep models embedded in UNSATCON. The simulations were conducted for two different studies in saturated condition. The modeling results were compared with the measured data and with those predicted with the conventional large-strain consolidation model in which the creep effects are ignored. From the analysis the following conclusions can be drawn.

(1) The conventional large-strain consolidation model may not be sufficient to predict the actual consolidation behaviors of tailings exhibiting creep, as it uses a time-invariant compressibility function. Tailings deposits with a potential for creep are likely to exhibit time-dependent behavior that may significantly affect both the magnitude and the duration of predicted settlements as well as their design strength.

(2) The recorded settlement and excess PWP data can be simulated more accurately when the effect of creep is considered into consolidation analysis.

(3) The performance of YG and CONCREEP models investigated in this study was found to be similar in terms of the settlement predictions. Observed differences in terms of excess PWP may be due to different constitutive model formulations used to describe creep effects.

(4) The 1D numerical results for a hypothetical case indicated a significant difference in consolidation results for tailings with and without creep. These

results indicate that incorporating creep in consolidation models may affect the field scale predictions in terms of excess PWPs and effective stresses with the potential to affect the initiation of reclamation plan in the field.

ACKNOWLEDGEMENT

This work is funded through a joint NSERC-COSIA Collaborative Research Development Grant awarded to the second author. Also, logistical support and data sharing by Suncor is gratefully acknowledged.

REFERENCES

Abu-Hejleh, A. N., Znidarcic, D., and Barnes, B.L., 1996, Consolidation Characteristics of Phosphatic Clays, Journal of Geotechnical Engineering, ASCE, New-York, Vol. 122, No. 4. pp. 295-301.

Bjerrum, L., (1967). Engineering geology of Norwegian normally consolidated marine clays as related to settlements of buildings. Geotechnique, 17(2), pp.83-118.

Buisman, A.S., (1936). Results of long duration settlement tests. In Proc. 1st ICSMFE (Vol. 1, pp. 103-107). Cambridge.

Carrier III, W.D., Bromwell, L.G. and Somogyi, F., (1983). Design capacity of slurried mineral waste ponds. Journal of Geotechnical Engineering, 109(5), pp.699-716.

Chaudhary, K., Fredlund, M., Lu, H. and Xu, L., (2015). Benchmarking of large-strain consolidation, sedimentation, and creep process for oil-sands tailings. Proceedings of Tailings and Mine Waste, Vancouver, BC.

Fox, P.J. and Berles, J.D., (1997). CS2: a piecewise-linear model for large-strain consolidation. International Journal for Numerical and Analytical Methods in Geomechanics, 21(7), pp.453-475.

Gheisari, N., Qi, S. and Simms, P., (2020) Consolidation–creep modeling of pilot data on deposition of flocculated fluid fine tailings, Geo Virtual conference.

Gibson, R.E., England, G.L. and Hussey, M.J.L., (1967). The theory of one-dimensional consolidation of saturated clays: 1. finite non-linear consoliildation of thin homogeneous layers. Geotechnique, 17(3), pp.261-273.

Gjerapic, G., Znidarcic, D., Peric, D., and Murphy, F.D., 2021, Development of an engineering model for consolidation and creep in tailings, Tailings and Mine Waste ‘21 conference proceedings, November 7-10, Banff, AB, Canada, ISBN: 978-1-55195-466-0, pp.841-851.

Government of Canada (2018). Public Report: Dewatering Wet Tailings Generated from Oil Sands Extraction, https://www.nrcan.gc.ca

Hinchberger, S.D. and Rowe, R.K., (1998). Modelling the rate-sensitive characteristics of the Gloucester foundation soil. Canadian Geotechnical Journal, 35(5), pp.769-789.

Jeeravipoolvarn, S., Chalaturnyk, R.J. and Scott, J.D., (2008). Consolidation modeling of oil sands fine tailings: History matching. Proceedings of GeoEdmonton’08, pp.190-197.

Jeeravipoolvarn, S., Scott, J.D. and Chalaturnyk, R.J., (2009). 10 m standpipe tests on oil sands tailings: long-term experimental results and prediction. Canadian Geotechnical Journal, 46(8), pp.875-888.

Leroueil, S., 2006, May. The Isotache approach. Where are we 50 years after its development by Professor Šuklje? 2006 Prof. Šuklje’s Memorial Lecture. In Proceedings of the XIII Danube-European Conference on Geotechnical Engineering, Ljubljana, Slovenia (Vol. 2, pp. 55-88).

Liingaard, M., Augustesen, A. and Lade, P.V., (2004). Characterization of models for time-dependent behavior of soils. International Journal of Geomechanics, 4(3), pp.157-177.

Murphy, F.D., Gjerapic, G., Znidarcic, D., and Sorta, A., 2021, Validation of an engineering model for consolidation and creep in oil sand tailings, Tailings and Mine Waste ‘21 conference proceedings, November 7-10, Banff, AB, Canada, ISBN: 978-1-55195-466-0, pp. 833-840.

Qi, S. and Simms, P., (2020). Robust methods to estimate large-strain consolidation parameters from column experiments. Canadian Geotechnical Journal, 57(5), pp.683-705.

Qi, S., Simms, P. and Vanapalli, S., (2017). Piecewise-linear formulation of coupled large-strain consolidation and unsaturated flow. I: Model development and implementation. Journal of Geotechnical and Geo-environmental Engineering, 143(7), p.04017018.

Qi, S., Simms, P., Vanapalli, S. and Soleimani, S., (2017). Piecewise-linear formulation of coupled large-strain consolidation and unsaturated flow. II: testing and performance. Journal of geotechnical and Geo-environmental engineering, 143(7), p.04017019.

Salam, M., (2020). Effects of polymers on short- and long-term dewatering of oil sands tailings (Doctoral dissertation, Carleton University).

Sills, G., (1998). Development of structure in sedimenting soils. Philosophical Transactions of the Royal Society of London. Series A: Mathematical, Physical and Engineering Sciences, 356(1747), pp.2515-2534.

Yin, J.H. and Graham, J., (1989). Canadian geotechnical journal, 26(2), pp.199-209.

Yin, J.H. and Graham, J., (1994). Equivalent times and one-dimensional elastic visco-plastic modelling of time-dependent stress–strain behavior of clays. Canadian Geotechnical Journal, 31(1), pp.42-52

Znidarcic, D., 2015, If it creeps, does it matter? Tailings and Mine Waste ‘15 conference proceedings, October 25-28, Vancouver, BC, Canada, pp.229-235.

Znidarcic, D., Miller, R., van Zyl, D., Fredlund, M., and Wells, S., 2011, Consolidation Testing of Oil Sand Fine Tailings, Tailings and Mine Waste ‘11 conference proceedings, November 6-9, Vancouver, BC, Canada, ISBN: 978-0-88865-815-9, pp.251-257.

MODELING OF TIME DEPENDENCY OF STRENGTH IN TAILINGS USING MATERIAL POINT MODELLING (MPM)- DELTAIC SAND CAPPING APPLICATION

Mario Martinelli[1,2], Ebi Meshkati[1], Dirk Luger[1], Arno Talmon[1,2], Jed Greenwood[3], Claudio Tamagnini[4]
[1]Deltares, Delft, The Netherlands
[2]Technical University of Delft, Delft, The Netherlands
[3]Barr Engineering and Environmental Science Canada, Calgary, Canada
[4]University of Perugia, Perugia, Italy

ABSTRACT

Deltaic capping of tailings involves placement of a cap by letting a hydraulic slurry of granular material such as sand flow out and spread over the tailing surface area. The slurry would flow from multiple spigots over a broad front to advance the cap onto the tailings, allowing the sand to settle and the water to be recovered for reuse. The cap is progressively built up in layers. The feasibility of (sand) capping becomes less obvious when weaker tailings deposits, e.g. treated fines-dominated tailings <5 kPa, are considered. These weak materials on the one hand can lose much of their strength with time when sheared under a given shear rate and, on the other hand, at rest can gain back a portion of their strength prior to shearing as time progresses. Standard geotechnical tools may not be able to replicate such time dependent (failure) flow and deformation behavior. Therefore, an attempt is made to develop a suitable method/constitutive model for the prediction of capping success or failure in such deposits. This paper presents how a total stress model based on von Mises viscoplastic constitutive model is extended to capture strain and time dependency of strength (i.e., strain softening strength loss, and strength gain with time at rest) in soft soils such as treated tailings. The modified total stress model is then used to perform large-strain numerical simulations of a bench-scale sand capping test. A good agreement between numerical simulations and experimental data at all loading stages is found.

INTRODUCTION

Background

The Oil Sands industry has been seeking robust, cost-effective methods to cap soft, fines-dominated tailings deposits and support reclamation activities. On strong, trafficable deposits >20 kPa, a cap can be placed with standard earth moving equipment. However, the feasibility of capping becomes less obvious when weaker deposits, e.g., treated fines-dominated tailings, are considered. The industry has faced uncertainty regarding the appropriate analytical or modelling methods to use in predicting capping success or failure on such soft materials. This uncertainty stems mostly from the question regarding how well common flow or geotechnical methods and models represent the relationships which govern the behavior of fines-dominated tailings deposits. The special aspects of the tailings as a soft geo-material possessing various properties that differentiate it from normal soils must be considered. These materials can lose so much of their strength when they are sheared that they behave as a non-Newtonian fluid and show both short- and long-term flow-like deformation processes. Additionally, with time (at rest) they may regain a portion of the strength prior to shearing. Such strain and time dependent flow-deformation behavior is known as thixotropic behavior.

The thixotropic characteristic of treated tailings cannot be easily replicated in standard flow or geotechnical tools. One may need to use one set of parameters to describe the material in the near-fluid state and another set of parameters in the stronger, more soil-like consolidated state. Depending on the properties, the behavior of material will be modelled by fluid mechanics approaches (using, for example, Delft-3D or TUDFlow3D, OpenFOAM) or by solid mechanics approaches (using finite element, finite difference, and other methods in programs like PLAXIS, ABAQUS, FLAC, MPM, etc.).

The objective of this study is to take a step towards bridging the gap between flow- and geotechnical approaches, to connect these by a constitutive model that can capture both the fluid- and solid-like flow and deformation behavior of soft sediments. To achieve that, a geotechnical total stress model

based on a von Mises viscoplastic constitutive model is modified to capture rate of change in strength as a function of time and shear rate inspired by Houska (1980) thixotropic model. This paper describes the modification applied to the von Mises viscoplastic constitutive model. Additionally, the validation of the modified model is presented. Finally, the modified constitutive model is used to replicate a scaled sand capping experiment.

THEORY AND DEFINITIONS

Shear rate dependency of strength

Soft sediments such as treated tailings tend to show higher strength (i.e., shear stress response) at higher shear rates. The increased shear stress that is generated at higher shear (strain) rates by the viscosity of the material is, compared to the static yield stress, more dominant in soft, fluid-like materials than in stronger solids-like materials such as consolidated clays. In soil mechanics, the viscosity is often neglected, but if one desires to model the materials at the boundary between fluids and solids, viscosity is an essential element. This ties in with the time-dependent creep and relaxation characteristics present in all materials to a greater or lesser degree. Creep is defined as ongoing time-dependent deformation under constant stress conditions, and relaxation is defined as the decrease of stress with time under constant strain conditions.

Time dependency of strength

Thixotropic hardening

In the absence of a change in water content, the strength of treated tailings at rest tends to increase with time. This is referred to as thixotropic hardening, structuration, or "setting". Thixotropic hardening is due to attractive forces at micro-scale levels that restore broken bonds between the smallest particles. The time scale of this effect is in order of magnitude several hours to several days, during which the strength of treated tailings may increase by approximately a few hundred Pascals.

Shear-thinning or shear softening with time

Shear-thinning is the rheological term for what is called strain softening in geotechnics. It is the phenomenon that a material, when sheared, loses strength until it reaches a (remolded) equilibrium strength. The softening process is caused by the breakdown (degradation) of the (micro-)structure that is formed by the solids in the material. Shear-thinning acts contrary to thixotropic hardening (the aggregation of structure with time). An equilibrium strength for a given shear rate is achieved when the rate of degradation and aggradation of the (micro-)structure is equal. The time scale of shear-thinning directly depends on the shear rate to which a material is subjected; at high shear rates (in rheometers), it is on order of minutes. In a slowly deforming material, this process can take days, months, or years. The amount of strength loss relative to the original peak strength is often referred to as the sensitivity of the material. The rate at which bonds are broken can be linked to the effort (energy) needed to break them and, therefore, to the amount of plastic work that is dissipated during the deformation process. Thus, time dependency of strength in soft sediments such as treated tailings consists of two components of destruction (decay of strength/viscosity) and restructuration (recovery of strength/viscosity) of a material's fabric. The term thixotropic behavior is another term for time dependent flow-deformation behavior.

Consolidation

At rest and under self-weight consolidation, tailings tend to form a strength/density profile in which the tailings' density and strength increase with depth. This strength increase with depth is due to the compression of the material under the overburden or surcharge which increases the effective stresses between particles. As such it differs from thixotropic hardening. The time scale of strength and density profile development is in the order of several months to many years and depends on the thickness of the tailing layer, its permeability and its compressibility. In this paper, the effect of consolidation on the failure or success of the sand cap is not considered. This is because the one-day time scale of the scaled capping test used for validation of the modified constitutive model was too short to allow any significant consolidation.

Structure parameter

The time dependent flow-deformation behavior (i.e., thixotropic hardening and shear softening) of a material is governed by various microscopic factors such as concentration, shape, and size distribution of the constituents, their interaction, and interdependence. Comprehensive modeling of thixotropy by considering microscopic factors is a very complicated task as it demands detailed

knowledge of the substance's microscopic physiochemical and mineral properties (Merckelbach, 2000). To overcome the extreme complexity of the problem, a lumped parameter model is used to describe the thixotropic phenomena. In this approach, the particle interaction effects and interdependence of microscopic details are summarized into a single structure coefficient (λ). This coefficient quantifies the state of the structure in the substance: λ equals unity when the fluid is fully built up and intact; λ equals zero when the fluid is thoroughly broken up (Moore 1959). Hence, the coefficient λ can be related to the strength of a substance as it specifies the structural connectivity of the substance fabric (Merckelbach, 2000).

Houska thixotropic model

Equation of State

The Houska (1980) model consists of a non-Newtonian equation of state for base condition (fully de-structured) following Herschel-Bulkley plus an additional part that mathematically describes the change in the rheology of material relative to its base condition as a function of change in the structural coefficient λ. The compacted mathematical expression of the Houska equation of state reads:

$$\tau = \tau_\infty + \lambda(\tau_0 - \tau_\infty) + (\mu_\infty + \lambda c)\dot{\gamma}^n \quad \text{(Eq. 1)}$$

where:
τ_0 = static yield stress of fully structured fluid (occurs at λ = 1);
τ_∞ = static yield stress of totally de-structured fluid (occurs at λ = 0);
n = flow index;
μ_∞ = viscosity entirely de-structured fluid (Bingham plastic viscosity if n = 1);
c = viscosity increment for fully structured fluid;
$\dot{\gamma}$ = shear rate.

Kinematic Equation
The growth and decay of structure coefficient λ is described by the kinematic equation, Moore (1959):

$$\frac{\partial \lambda}{\partial t} = a(\lambda_0 - \lambda) - b\lambda\dot{\gamma} \quad \text{(Eq. 2)}$$

where:
λ = structure coefficient [0-λ_0];
λ_0 = maximum value of structure [0-1], where Moore (1959) assumed λ_0 = 1;
a and b = coefficients of growth and decay of structure, respectively.

The first term on the right-hand side of the above equation describes the self-recovery of structure. The second term describes the shear down (shear softening) of structure related to energy dissipation during the shearing process. This equation does not explicitly describe the influence of reaggregation (or re-flocculation) in shear (Mietta et al., 2009; Sun, 2018). For a given shear rate, the growth and decay of structure (flocs) will approach an equilibrium structure defined by the equilibrium structural coefficient λ_e, which is given by:

$$\lambda_e = \frac{\lambda_0}{1+\beta\dot{\gamma}} \quad \text{(Eq. 3)}$$

where:
$\beta = b/a$;
λ_e = equilibrium structure [0 to λ_0].

The quantification of the structural coefficient enables one to quantify how flocs change in size over time (grow by accretion of clay platelets and primary particles) or decay (erosion) with dynamic conditions (shear rate, time).

Modification of total stress von Mises model

The constitutive equations of the von Mises elasto-viscoplastic model to achieve a total stress formulation of elasto-viscoplasticity with thixotropy are defined as follows: The stress rate is linked to the elastic rate of deformation by a linear elastic relation:

$$\dot{\boldsymbol{\sigma}} = \boldsymbol{D}_{el}\left(\dot{\boldsymbol{\varepsilon}} - \dot{\boldsymbol{\varepsilon}}_{vp}\right) \quad \text{(Eq. 4)}$$

where $\boldsymbol{D}_{el}$ is the elastic tangent stiffness tensor, $\dot{\boldsymbol{\varepsilon}}_{vp}$ is the viscoplastic strain rate, and $\dot{\boldsymbol{\varepsilon}}$ is the total strain rate. The viscoplastic strain rate follows from the flow rule:

$$\dot{\boldsymbol{\varepsilon}}_{vp} = \gamma_{vp}\boldsymbol{n} \quad \text{(Eq. 5)}$$

where γ_{vp} is the viscoplastic multiplier and $\boldsymbol{n}$ is the viscoplastic flow direction tensor, assumed perpendicular to the von Mises yield surface, as follows:

$$f\left(\boldsymbol{\sigma}, c_u\right) = q - 2c_u \qquad \text{(Eq. 6)}$$

where q is the deviatoric stress invariant and the viscoplastic multiplier is defined as follows:

$$\gamma_{vp} = D_r \left(OCR\right)^{-1/I_v} = D_r \left(\frac{2c_u}{q}\right)^{-1/I_v} \qquad \text{(Eq. 7)}$$

where D_r (material constant) is the reference strain rate magnitude, c_u (material constant) is the undrained shear strength in the reference conditions ($D_r = \|\dot{\varepsilon}\|$), and I_v (material constant) is the viscosity index. In geotechnical viscoplastic constitutive models, the reference strain rate magnitude is often considered equal to 1 day^{-1}, i.e., 1/86400 sec^{-1}, which is a typical duration of a load interval of the oedometer test.

The thixotropic behaviour is introduced by replacing the constants c_u and I_v with the following functions of the "structural coefficient" λ, which is considered as a state variable:

$$c_u\left(\lambda\right) = c_{u,\infty} + \lambda\left(c_{u,0} - c_{u,\infty}\right) \qquad \text{(Eq. 8)}$$

$$I_v\left(\lambda\right) = I_{v,\infty} + \lambda\left(I_{v,0} - I_{v,\infty}\right) \qquad \text{(Eq. 9)}$$

The values of λ range from 0 to 1, so the strength c_u varies between $c_{u,0}$ and $c_{u,\infty}$, respectively, the maximum and the minimum values. The same approach is used for the viscosity index I_v.

The rate of change of λ is, similar to Eq. 2, given by:

$$\dot{\lambda} = a\left(\lambda_0 - \lambda\right) - b\lambda\left\|\dot{\boldsymbol{\varepsilon}}\right\| \qquad \text{(Eq. 10)}$$

where *a*, *b*, and λ (initial value of λ_0, set to 1 in this report) are material constants.

Note that the change of λ is controlled by the total strain rate rather than the viscoplastic strain rate, as it should occur in a viscoplastic hardening law. In this case, the difference is most likely very small since in the considered materials the elastic component of the strain rate is small compared to the viscoplastic one.

THE MATERIAL POINT METHOD

The Material Point Method (MPM) is a numerical method particularly suited for large deformations with history-dependent materials. The original formulation of MPM was initially developed by Harlow (1964) for fluid mechanics, and then it was applied to solid mechanics (Sulsky et al., 1995) and dry granular materials (Wieckowski et al., 1999; Wieckowski Z., 2003). Later, the method was extended to handle saturated soils (Jassim et al., 2013), using the velocity of both solid and liquid as primary unknowns. It was shown that MPM could successfully simulate several geotechnical problems, such as cone penetration tests (Beuth & Vermeer, 2013; Ceccato & Simonini, 2015; Martinelli and Galavi, 2021), close-ended and open-ended pile installation (Phuong et al., 2016; Galavi et al., 2019), slope failure (Yerro et al., 2015), collapse of dams (Alonso & Zabala, 2011) and riverbanks (Bandara & Soga, 2015). The MPM integration scheme proposed by Martinelli and Galavi (2022) is used in this paper to simulate the sand capping process. The MPM code is a version of Anura3D developed by Deltares.

In MPM, the continuum body is represented by a cloud of points, called Material Points (MPs). They carry all information of the continuum body, such as density, velocity, strain, stress, material parameters, and external loads. They are not physical particles, like single solid grains described in the Discrete Element Method, but they represent a portion of a continuum body. A schematic representation of MPM and the background mesh is shown in Figure 1.

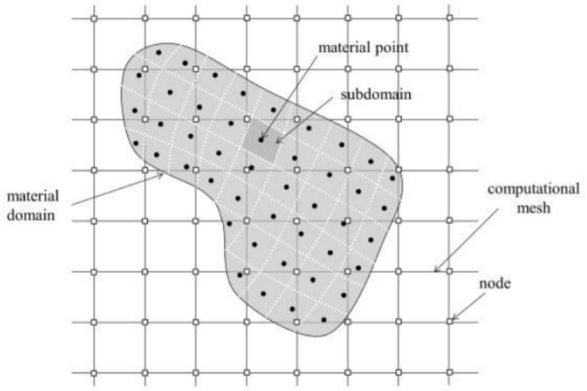

Figure 1: Spatial Discretization in MPM (Yerro, 2015)

At the beginning of each timestep, the nodal forces are computed based on the information stored at the material points by means of the shape functions. The governing equations are then solved at the nodes and afterward used to compute the strain, stress, and density, and to update the position of the material points. At the end of the timestep, the mesh is reset to the original configuration (Al-Kafaji, 2013). Thus, mesh distortion is not a limiting constraint for this model, and great flexibility in material behaviour representation is obtained because numerical formulations of material behaviours govern the movement of fluids and solids.

The one-phase dynamic MPM formulation (Al-Kafaji, 2013) is used in this study. It can analyze situations where softening causes instabilities. Because the behaviour of the Centrifuged Fluid Fine Tailings(CFFT) is described using a total stress model (von Mises model with thixotropy), this formulation is used to describe the undrained response of the soil-water mixture without the need for the degree of freedom of the water phase. A single computational cycle is described as follows:

a) Nodal accelerations are solved by the discretized form of the momentum balance equation
b) Material point velocities are computed from the nodal accelerations
c) Nodal velocities are computed as the ratio between nodal momentum and nodal mass
d) Strain increments are computed at the location of each material point
e) Stress increments are determined
f) Positions of all material points are finally updated throughout the mesh

The explicit integration scheme is conditionally stable. The size of the time step for a stable solution decreases with an increase in the material stiffness and with a decrease in the element size in the computational mesh. To speed up calculations, the maximum time step is increased by multiplying the mass matrices by a Mass-Scaling-Factor (MSF), which comprises values larger than 1. This procedure is typically used for quasi-static processes and can be applied as long as the inertia forces are not significant in the case at hand, as described in Al-Kafaji (2013).

RESULTS AND DISCUSSION

Example of constitutive model response

Fully structured material (i.e., λ =1)
Consider a simple shear test at constant volume, where the structural coefficient λ is set to 1. The condition which corresponds to the steady-state strength is characterized by $\dot{\sigma} = 0$ in Eq. 4. It can be demonstrated that, for a simple shear test in undrained condition, the steady-state shear stress (τ_f) follows the equation:

$$\frac{\tau_f}{c_u} = \left(\frac{\dot{\gamma}}{\sqrt{2}\, D_r}\right)^{I_v} \qquad \text{Eq (11)}$$

which is illustrated in the bi-logarithmic plane in Figure 2. Each line corresponds to a specific value of I_v. Eq. 11 shows that the input parameter c_u is the shear strength when the material is sheared at a shear rate $\dot{\gamma} = \sqrt{2}\, D_r$.

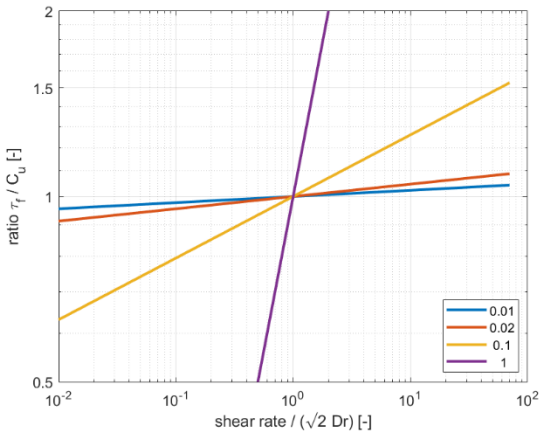

Figure 2: A Simple Shear Test: Effect of Shear Rate and Viscosity Index I_v

Thixotropic response

The thixotropic response is described by Eq. 10, which contains both contributions of strain-softening and strength increase in time. For the special case where the strain-rate is constant over time, the value of λ(t) is described by the following equation:

$$\lambda(t) = (1 - \frac{a}{a+b\|\dot{\varepsilon}\|})e^{-(a+b\|\dot{\varepsilon}\|)t} + \frac{a}{a+b\|\dot{\varepsilon}\|} \quad \text{Eq (11)}$$

An example of thixotropic response is shown in the example illustrated in Figure 3. The model parameters are summarized in

Table 2. In this example, the structural coefficient λ is not restricted, as it evolves with Eq. 10. The hypothetical soil here exhibits both peak and residual strength. The test is performed at a shear rate of 50 1/sec. If parameter *a* is set to 0, the soil exhibits only strain-rate softening behaviour as the structural coefficient continuously decreases. When both *a* and *b* are positive numbers, a strain-rate softening response is observed, and the material exhibits an increase in strength with time. Note that the value of shear stress at larger strains is higher as the parameter *a* increases.

Table 2: The Model Parameters for the CFFT

Parameter	Unit	Value
ρ	kg/m^3	1,325
E_u	kPa	1.5
ν_u	-	0.4995
$c_{u,\infty-0}$	kPa	0.01, 0.1
D_r	sec^{-1}	1/86400
$I_{v,\infty-0}$	-	0.02, 0.02
a	sec^{-1}	1e^{-3}
b	-	1e^{-3}

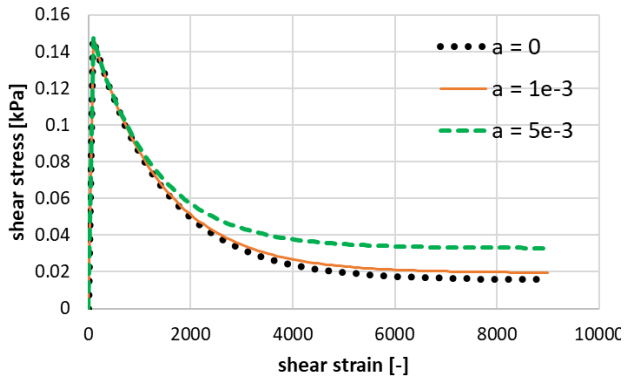

Figure 3: Simple Shear Test of a Thixotropic Material; Effect of Strength Gain in Time (parameter *a*)

The scaled sand capping test

The scaled sand capping tests were conducted by Barr Engineering and Environmental Science Canada. The inner dimensions of the aquarium were 178.5 cm long, 57.0 cm wide, and 90 cm tall. This gave the tank a maximum capacity of 916 L. Centrifuged fluid fine tailings (CFFT) with a density of 1.32 kg/m^3 were placed in the tank to a level of approximately 61 cm above the bottom of the tank before cap placement began. Five lifts of sand cap (coarse sand tailings, or CST) – two lifts of a nominal 2.5-cm thickness and three lifts of a nominal 5-cm thickness – were placed on the afternoon of January 31 with intervals of approximately one hour. Another four sand cap lifts were placed on February 1 – three lifts of a nominal 5-cm thickness and one lift of a nominal 4-cm thickness, with similar intervals. The total mass of the nine lifts was 193.3 kg. The nominal cap thickness placed was 39 cm, but the cap never reached that height, since the cap, as it was built, settled into and displaced CFFT. It pushed 20 to 30 cm into the CFFT such that the total CST thickness placed to build the cap ranged from 50 to 60 cm. Table 3 summarizes the lifts and their settlement measured during the test.

Table 3: Cap Thickness at Wall and Center of Aquarium Accounting for Settlement

Lift	Nominal Lift Thickness (cm)	Nominal Total Cap Thickness (cm)	Total Cap Thickness at Wall (cm)	Total Cap Thickness in Center (cm)
1	2.5	2.5	2.5	5.8
2	2.5	5.0	4.1	9.9
3	5.0	10.0	15.3	21.3
4	5.0	15.0	23.3	34.8
5	5.0	20.0	28.7*	38.5
6	5.0	25.0	34.2	42.7
7	5.0	30.0	39.2*	47.4
8	5.0	35.0	43.2*	51.5
9	4.0	39.0	46.9*	54.6

* Minor discrepancies in sums are due to rounding

Figure 4 shows the traces marked on the side of the aquarium for each lift of cap placed (lift 9 was placed to the bottom of the black rim around the aquarium top) and the CST-CFFT interface at the wall as the cap settled. As seen in Table 3, although no settlement was seen at the wall from placement of lift 1, there was settlement equal to

the nominal lift thickness (2.5 cm) in the center of the aquarium under the cap. Even though the targets for lifts 3 through 8 (red lines in Figure 4) were 5 cm above the current cap surface, Figure 4 shows that the spacing between those targets progressively diminished. This is because the cap had settled between the time the lift placement was complete and the time the next lift was to be placed. Lifts were generally allowed an hour to settle and equilibrate before the next lift was placed.

Figure 4: Lift 9 Cap, CST Target Height Traces, and CFFT-CST Interface Traces at Wall

MPM sand capping scaled test modelling

The sand capping scaled test is modelled using the Material Point Method. The numerical model domain is shown in Figure 5. The background mesh comprises four-node quadrilateral elements, with a uniform element size of 2.5 cm and a base and height of 175 cm and 150 cm, respectively. The thickness of the CFFT is 60 cm. The material points are evenly distributed in the computational mesh, with approximately four to nine points per element for the bottom 60 cm and approximately nine points per element for the rest of the domain.

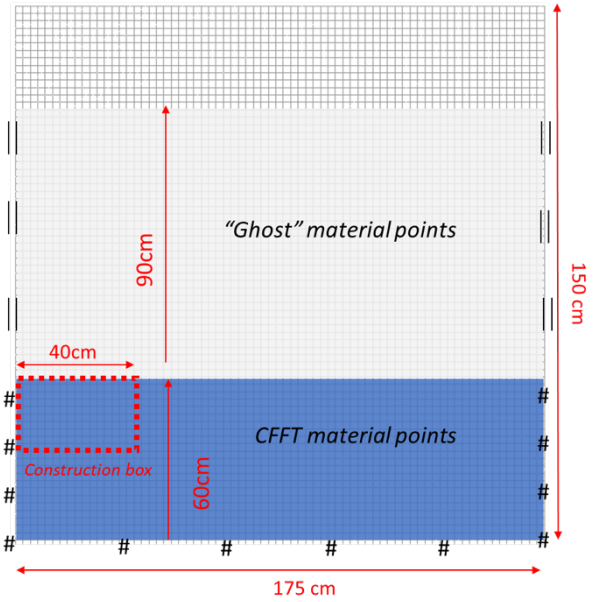

Figure 5: MPM Model of the Aquarium Test

In the MPM code, as available at the time of this study, it was not possible to add material points during the calculation process. Lacking this option, in order to simulate the sand placement process, a very light, weak, and flexible material was initially placed on top of the mud layer for the entire length of the domain. This material was called "ghost material", with a thickness (height, *h*) of 0.9 m. The capping process is simulated with a 40-cm-wide "construction box", which moves vertically with a constant velocity to convert all "ghost" material points into sand material points when they come into the construction box. The construction process is divided into nine phases, and for each phase, the construction box is activated until the total volume of the sand material points matches the one placed in the experiment (Table 4).

Table 4: Sand Volume for Each Lift

Lift no.	Lift volume (m^3/m)
1	0.0187
2	0.0119
3	0.0424
4	0.0531
5	0.0321
6	0.0224
7	0.0307
8	0.0275
9	0.0296

A standard linear elastic-perfectly plastic constitutive model with a Mohr-Coulomb failure criterion is used for the sand. The material properties are given in Table 5. The properties of the sand layer are selected in agreement with the data measured during the experimental test, where the unit weight is the average value over the nine loading steps. The response of the sand layer is modelled as drained, and no excess pore pressure develops during the simulations. A standard linear elastic model is used for the ghost material. For the ghost material, the density is only used to construct the mass matrix; the body force, due to the self-weight, is not used. The experimental tests show that there is a non-negligible adhesion between the CFFT and the aquarium wall. For this reason, the nodes on the bottom and side boundaries of the domain (only for the first 60 cm, i.e., where the CFFT is originally located) are fully fixed, representing a perfectly rough boundary. The rest of the boundary nodes are only fixed in the normal direction (i.e., a smooth boundary).

Table 5: The Model Parameter List

Parameter	Unit	Value	
		Sand	"Ghost"
ρ	kg/m^3	1,250	500
E	kPa	4,166	0.1
nu	-	0.2	0.0
c	kPa	0.0	-
ϕ	degrees	32	-

Figure 6 to Figure 10 show the construction process for lifts 1, 3, 5, 7, and 9. In all figures, the dashed lines represent the experimental observation of the ground level, which describes the surface of the tailing deposit and the sand cap.

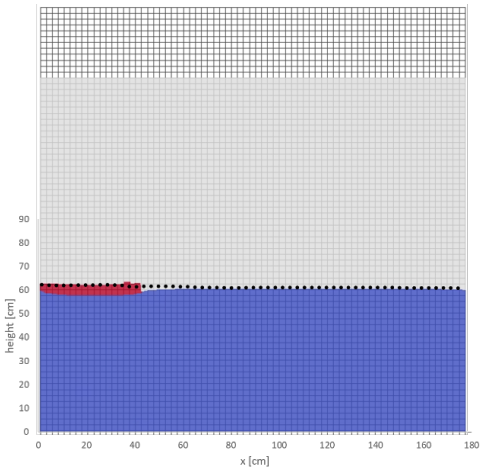

Figure 6: The Sand Capping Construction: Lift 1. The dotted line is the experimental observation.

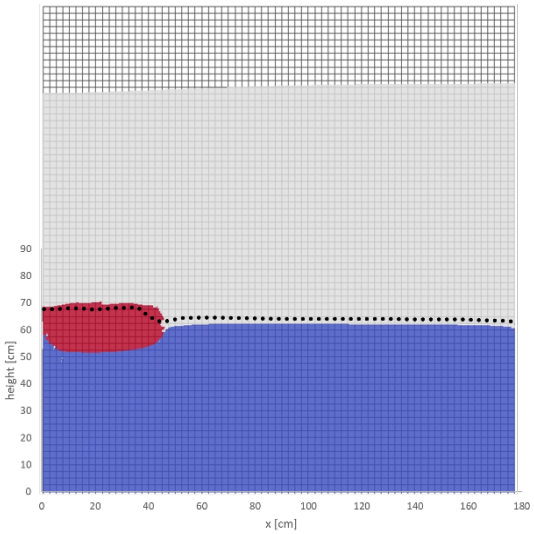

Figure 7: The Sand Capping Construction: Lift 3. The dotted line is the experimental observation.

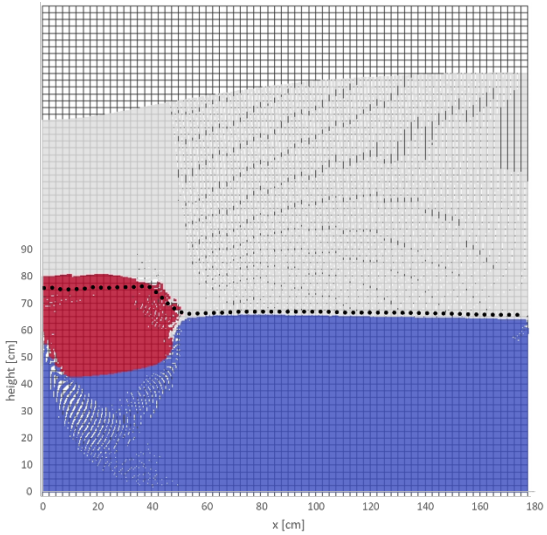

Figure 8: The Sand Capping Construction. Lift 5. The dotted line is the experimental observation.

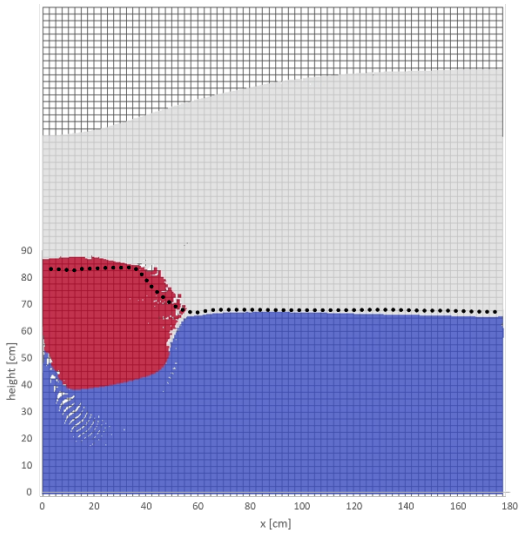

Figure 9: The Sand Capping Construction. Lift 7. The dotted line is the experimental observation.

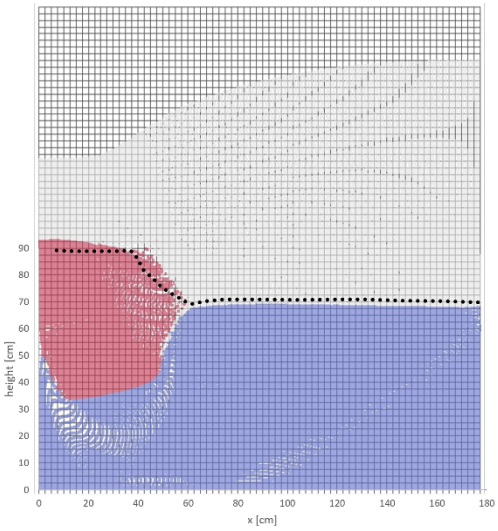

Figure 10: The Sand Capping Construction. Lift 9. The dotted line is the experimental observation.

The cumulative deviatoric strains developed in the CFFT are illustrated in Figure 11, after lift 9. During the simulation the cumulative deviatoric strains reach values which are locally in excess of 100%. The results are represented within a range from 0 and 50% and all strains higher than 50% are in the same color band. A deep-seated failure surface is developed during the construction process. The failure surface is affected by the presence of the rough bottom boundary, as it is quite close to the capping sand layer. However, the development of such a shear failure process is not clearly identified by localized shear strains. This is probably due to the ductile behaviour of the CFFT layer.

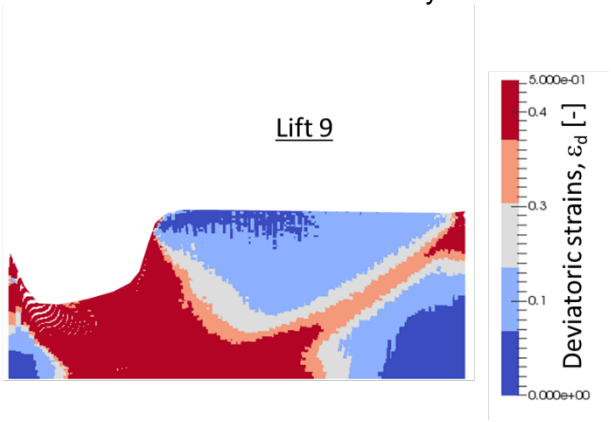

Figure 11: Cumulative Deviatoric Strains Developed in the CFFT Layer after Lift 5 and Lift 9

Overall, the numerical MPM simulations shown in Figures 6 to 10 are in good agreement with the experimental data where the position of the ground level, both for the sand cap deposit and the tailings surface are concerned. Even though the computed slope of the sand cap is generally slightly steeper than the experimental data, the toe of the sand slope is predicted well by the numerical simulations. The surface of the sand cap is also modelled with satisfactory agreement.

It is worth noting that, during the simulation, the structural parameter λ remained close to 1, as illustrated in Figure 12, so the reference strength c_u is equal to the peak value $c_{u,0}$ (in Eq. 7). This is confirmed by another simulation illustrated in Figure 13, where parameter a is set to 0 (i.e. strength gain is not considered) and parameter b is set to 0.1 (i.e. 100 times larger). The results show that the parameter λ decreases while shearing, but the value reached at the end of the simulation (i.e. lift 9) is always higher than 0.75.

This is because CFFT was fully remoulded before introducing it into the aquarium. In other words, the structural parameter λ was initially low and close to equilibrium. It follows that the results illustrated in Figures 6 to 10 can be obtained without the Houska formulation but instead with the simple rate-independent von Mises model with a shear strength $c_{u,0}$.

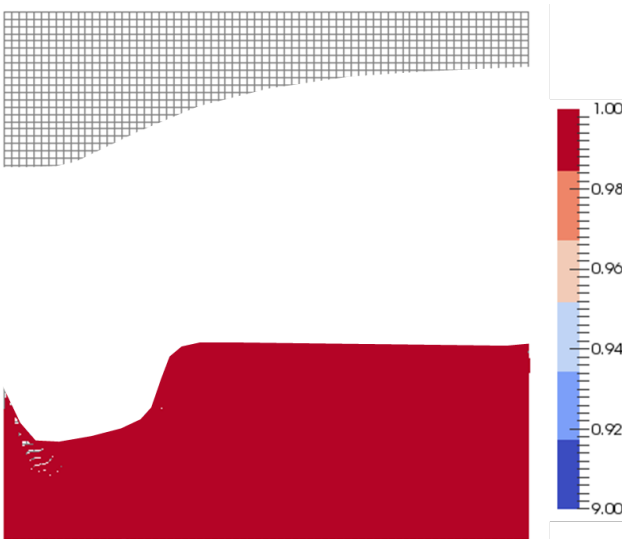

Figure 12: The Sand Capping Construction: Lift 9. Distribution of the structural coefficient λ in the tailings deposit.

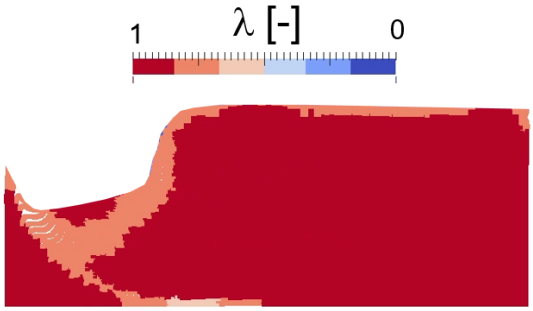

Figure 13: The Sand Capping Construction: Lift 9 with parameter a=0 and b=0.1. Distribution of the structural coefficient λ in the tailings deposit.

CONCLUSIONS

In this study, a well-established constitutive model that describes the rate-dependent response of soft soils was extended by including the time-dependent thixotropic effects on the shear strength. This constitutive model is developed in the framework of total stress analysis, which can capture the rate-dependency and thixotropy of the shear strength under the hypothesis of the undrained response of the system. The total stress thixotropic constitutive model was then used to perform large-strain numerical simulations of sand capping using MPM. The scaled sand capping test was successfully simulated, with good agreement between numerical simulations and experimental data at all loading stages.

This is a breakthrough step towards bridging the gap between the “fluid mechanics” approach and the “porous media mechanics” approach for what concerns flow-like failure problems, such as extended flow failure behavior of soft sediments. This is particularly relevant for applications like sand capping and resulting potential slope instabilities.

REFERENCES

Al-Kafaji I.K.A. (2013). Formulation of a dynamic material point method (MPM) for geomechanical problems. PhD thesis, Universität Stuttgart

Alonso E.E. & Zabala F. (2011). Progressive failure of Aznalcóllar dam using the material point method. Géotechnique, 61(9), pp.795–808

Bandara S. and Soga K. (2015). Coupling of soil deformation and pore fluid flow using material point method. Computers and geotechnics 63, 199-214.

Beuth L. & Vermeer P.A. (2013). Large deformation analysis of cone penetration testing in undrained clay. In M. Hicks, ed. Installation Effects in Geotechnical Engineering. Taylor & Francis Group, London

Ceccato F. & Simonini P. (2015). Two-phase Material Point Method applied to cone penetration for different drainage conditions, In Geomechanics from Micro to Macro. Cambridge, pp. 965–970

Galavi V., Martinelli M., Elkadi A., Ghasemi P. & Thijssen R. (2019). Numerical simulation of impact driven offshore monopiles using the material point method, in the XVII European Conference on Soil Mechanics and Geotechnical Engineering, Reykjavik, Iceland, 1 - 6 September 2019

Harlow, F. H., 1964. “The particle-in-cell computing method for fluid dynamics.” Methods in computational physics 3 (3): 319–343.

Houska, M., 1980. Engineering Aspects of the Rheology of Thixotropic Liquids. PhD-thesis (in Czech), Czech Technical University, Prague.

Jassim I., Stolle D. & Vermeer P. (2013). Two-phase dynamic analysis by material point method. International Journal for Numerical and Analytical Methods in Geomechanics numerical and analytical methods in Geomechanics, 37, pp.2502–2522.

Martinelli M. & Galavi V. (2021). Investigation of the material point method in the simulation of cone penetration tests in dry sand. Computers and Geotechnics, 2021 (130).

Merckelbach, L.M., (2000). Consolidation and strength evolution of soft mud layers, PhD-thesis, Delft University of Technology.

Mietta, F., Chassagne, C. and Winterwerp, J.C. (2009). Shear induced flocculation of a suspension of kaolinite as function of pH and salt concentration. Journal of Colloid and Interface Science 336: 134–141.

Moore, F. (1959). The rheology of ceramic slips and bodies. Transactions British Ceramic Society 58: 470-494.

Phuong N.T.V., van Tol A.F., Elkadi A.S.K. & Rohe A. (2016). Numerical investigation of pile installation effects in sand using material point method. Computers and Geotechnics, 73, 58-71

Sulsky D., Chen Z. & Schreyer H.L. (1994). A particle method for history-dependent materials. Computer Methods in Applied Mechanics and Engineering, 118(1-2), pp.179–196

Sun Y., 2018. Recovery of thickened kaolinite suspension properties through shear. MSc-Thesis. University of Alberta.

Wieckowski Z. (2003). Modelling of silo discharge and filling problems by the material point method. Task Quarterly 4: 701–721

Wieckowski Z., Youn S.-K. & Yeon J.-H. (1999). A particle-in-cell solution to the silo discharging problem. International Journal for Numerical Methods in Engineering 45 1203–1225.

Yerro A., Alonso E.E. & Pinyol N.M. (2015). The material point method for unsaturated soils. Géotechnique, 65(3), pp.201–217

SESSION 9

THE USE OF PRECIPITATED CALCIUM CARBONATE (PCC) IN FLUID FINE TAILINGS TREATMENT TO ENHANCE CIRCULAR ECONOMIES IN TAILINGS RECLAMATION

Yunhui Li[1], Catalina Romero[1], Andrea Sedgwick[1], Robert Lacey[2], and Brandon M. Smith[3]
[1]Northern Alberta Institute of Technology, Edmonton, Canada
[2]Delta Remediation, Canada
[3]Clear-Site Solutions, Canada

ABSTRACT

Our economy is based on extracting materials from the Earth and making useful products from them. During that process we generate by-products often considered to be a waste and destined for landfill. The role of the circular economy is to eliminate waste production, circulate materials and, where possible, renew natural resources. The concept is relatively simple with Company A integrating by-products from Company B as an input to Company A's existing process. However, in North America, there is a prevalent challenge in finding disposal reuse, or recycling options for the by-products of precipitation using lime – the biggest challenge being the abundance of spent lime created.

Since 2018, Delta Remediation (Delta) and Clear-Site Solutions (Clear-Site) have been researching sustainable reuse opportunities for Preciptated Calcium Chloride (PCC) which is also known as spent lime. The solidification of tailings is one considered solution for PCC. The oil sands industry has been relying on post-deposition dewatering mechanisms such as evaporation and freeze-thaw to achieve sufficient strength for eventual reclamation. Those reclamation solutions, however, may not meet engineering standards due to the formation of a crust layer on the top of treated tailings. The application of spent lime into tailings treatment for reclamation would be an alternative technology for managing soft and fluid tailings. In 2021 and 2022 Delta and Clear-Site Engaged with NAIT Center For Oilsands Sustainability (COSS) to undertake laboratory studies of the use of PCC in FFT applications The initial results of this study were promising, demonstrating that precipitated calcium carbonate (PCC) has the potential to enhance the strength gain of the oil sands tailings deposits which would accelerate the upland reclamation of the oil sands tailings. Such a process, if proven successful, would eliminate waste from one industry, circulate material to another, providing economic benefit for both companies and Environmental benefit for the planet.

INTRODUCTION

Lime is a calcium containing inorganic compound which is derived from heating limestone to over 900 degrees Celsius. When the limestone is "cooked", it becomes much more reactive than the limestone would be in its original state. When limestone has been cooked, it is known as unslaked lime or quicklime. Once the "cooked" or unslaked lime has been reacted or "used" in an industrial process, it becomes slaked lime. Although unslaked lime is used in many different industries the byprodcut (slaked lime) is most often considered waste. The most notable prodcucers of slaked lime (byprodcut) are the cement industry as well as the food and pulp and paper industries.

Slaked lime is scientifically known as Precipitated Calcium Carbonate (PCC) and is used widely for many applications (National Lime Association, 2007). PCC can be easily integrated into wastewater treatment, bio-solids, or other industrial sludges for stacking, stockpiling, as well as transportation and disposal purposes. The use of PCC in sludge management maximizes load volumes while also assisting in passing stringent leachability testing. PCC can be mixed into soils to increase stability and hardness. Soils that are not pH balanced (acidic) will become pH balanced with the use of PCC. Applications include road construction agriculture, dust suppression embankment stabilization, and soil cement.

PCC is currently considered a waste byproduct in the production of sugar. Internationally, there are alternative uses in the agricultural sector as a soil amendment but here in Canada production volume vastly surpasses practical application for agricultural use. From both an operations standpoint and also under the Environmental Protection and Enhancement Act (EPEA) waste

byproducts without viable use alternatives are destined for landfill. Alternative options may be pursued but such pursuit requires the producer to find viable and beneficial upcycling solutions.

Oil sands tailings are a byproduct of oil sands mining with present stockpiles exceeding 1.3 billion m^3 (AER, 2021). Tailings are transported and stored in large tailings ponds where fluid fine tailings (FFT) are accumulated. FFT requires decades to centuries to settle into a semi-solid material, resulting in major environmental and fiscal challenges. Upland reclamation to a dry landscape is the main reclamation technology that is targeted by Alberta Energy Regulator (AER). Meeting the required shear strength (10 kPa) for a trafficable surface within a reasonable period is the crucial step for upland reclamation (SRIN, 2010). Increased solids concentration through consolidation and/or a chemical modification could improve the strength and stability of the deposit.

This study investigated the use of PCC on polymer-treated FFT to assess the impact of PCC addition on strength gain and long-term consolidation of the FFT. PCC addition to FFT, if proven successful in FFT strength gain, would eliminate waste, circulate material, and offer clear benefits to both companies engaged in this process as well as the Canadian environment.

EXPERIMENTAL

Materials

The FFT used in this study were analyzed for composition by Dean & Stark (D&S) for bitumen, mineral, and water contents (Dean and Stark, 1920), methylene blue index (MBI) (Omotoso and Benson, 2008), fines content, reported weight percent of particles passing 44 micron (COSIA, 2015), pH, electrical conductivity (EC), major cations and anions by ion chromatography (IC) (Table 1 and Table 2). The sample of PCC was supplied and characterized by Delta Remediation (Table 3). PCC used in this study is sourced from food waste.The anionic polyacrylamide flocculant A3338, produced by SNF Canada, was used in this study. The polymer solution was prepared at a concentration of 0.45% in process effluent water (PEW). The water chemistry of the PEW is shown in Table 2.

Table 1. Characterization of FFT.

Sample	Mineral (wt%)	Bitumen (wt%)	Water (wt%)	MBI (meq/100g)	Fines (wt%)	SFR	EC (μS/cm)
FFT	44.4	1.8	53.8	7.9	70.4	0.42	1475

Table 2. FFT and PEW Characterization on water chemistry.

Sample	Li^+	Na^+	K^+	Mg^{2+}	Ca^{2+}	F^-	Cl^-	NO_3^-	SO_4^{2-}	pH
FFT	0.0	230.8	14.6	28.6	56.3	2.3	17.5	5.7	365.7	8.46
PEW	0.0	274.7	14.4	13.4	7.2	3.0	176.9	0.0	221.3	9.42

FFT Treatment with polymer and PCC

A complete polymer amendment dosage curve for the characterized FFT was conducted to determine the polymer optimal dosage (Li, et al. 2021). The FFT was treated with polymer A3338 at the optimal dosage first prior to the PCC addition. The details of the tests are as follows.

An overhead mixer with an online torque sensor and display (Heidolph Hei-Torque 100 Precision Base) was used to provide mixing during flocculation and PCC addition in a 6” metal baffled cup (Li, et al. 2022). Each flocculation was conducted using a 1 L FFT sample.

The FFT sample was mixed for 1 min at 300 rpm to pre-shear the slurry. The desired volume of polymer solution was injected using a peristaltic pump (ColeParmer DRIVE/DISP MFLX BENCH 115/230) at a fixed flow rate of 1200 mL/min. Mixing continued at 300 rpm while monitoring the torque response. When the torque reached a peak value and began to decrease, the speed was immediately decreased to 50 rpm. The final step was to condition the flocs by mixing at 50 rpm for 15 seconds.

The PCC solids were incorporated into raw FFT and flocculated FFT first by hand using a scoop with gentle folding movement. Then the material was mixed using the overhead mixer for 1 minute at 20 rpm ensuring complete PCC integration in the flocs and raw material. The dosage of PCC was based on the weight percent of the total mass of the sample (Eq. 1). The PCC incorporation time on flocculated FFT increased proportionally to the dose to avoid overshearing on flocs structure.

$$PCC\ dosage\ (\%) = \frac{Mass\ of\ PCC}{Mass\ of\ PCC + Mass\ of\ FFT} \times 100 \quad (1)$$

Table 3. Characterization of PCC.

	Old / North PCC / 0-15 / cm	Old / Miller Window PCC / 0-15 / cm	Centre / South PCC / 0-15 / cm
Organic Matter % by weight	6.3	5.5	5.9
Phosphorus Available ug/g	660	760	1600
Potassium Available ug/g	892	613	494
Nitrogen Total % dry weight	0.51	0.39	0.35
Boron Hot Water Soluble mg/kg	0.52	0.62	0.5
Mercury Strong Acid Extractable mg/kg	<0.01	<0.01	<0.01
Iron Strong Acid Extractable mg/kg	100	1180	750
Moisture Wet Weight @ 105°C %	27.8	34.7	41.8
2.0 mm sieve % Retained % by weight	8.6	15.3	4.7
250 micron sieve % Retained % by weight	41.2	58.2	45.6
pH Saturated Paste pH	8.2	8.3	8.7
Electrical Conductivity Saturated Paste dS/m at 25°C	16.1	9.6	3.7
SAR Saturated Paste	0.2	0.2	<0.1
% Saturation %	89	98	107
Calcium Saturated Paste meq/L	7.17	3.71	3.21
Calcium Saturated Paste mg/kg	128	73.1	68.9
Magnesium Saturated Paste meq/L	194	110	42.8
Magnesium Saturated Paste mg/kg	2100	1310	556
Sodium Saturated Paste meq/L	1.7	1.5	<0.43
Sodium Saturated Paste mg/kg	34	34	11
Potassium Saturated Paste meq/L	16.6	7.1	3.18
Potassium Saturated Paste mg/kg	578	273	133
Chloride Saturated Paste meq/L	3.78	2.2	0.97
Chloride Saturated Paste mg/kg	120	76	37
Sulfate-S Saturated Paste meq/L	24.9	16.5	16.6
Sulfate-S Saturated Paste mg/kg	357	259	284
Nitrate and Nitrite - N Saturated Paste meq/L	166	94.3	26.2
Nitrate and Nitrite - N Saturated Paste mg/kg	2080	1300	393
TGR Saturated Paste T/ac	<0.1	<0.1	<0.1
Iron Strong Acid Extractable mg/kg ($FeCO_3$)	109.3	1289.3	819.5
Calcium Saturated Paste mg/kg ($CaCO_3$)	194.8	111.2	104.8
Magnesium Saturated Paste mg/kg ($MgCO_3$)	5273.1	3289.4	1396.1
Sodium Saturated Paste mg/kg Na_2CO_3	45.1	90.2	29.2
Potassium Saturated Paste mg/kg K_2CO_3	451.0	426.0	207.6
Total CO_3	6073.2	5206.1	2557.1
Total inorganic (excl. water)	1.94%	1.47%	0.67%
Total organic	6.3%	5.5%	5.9%
Total water	27.8%	34.7%	41.8%
Total mass accounted for	36.04%	41.67%	48.37%

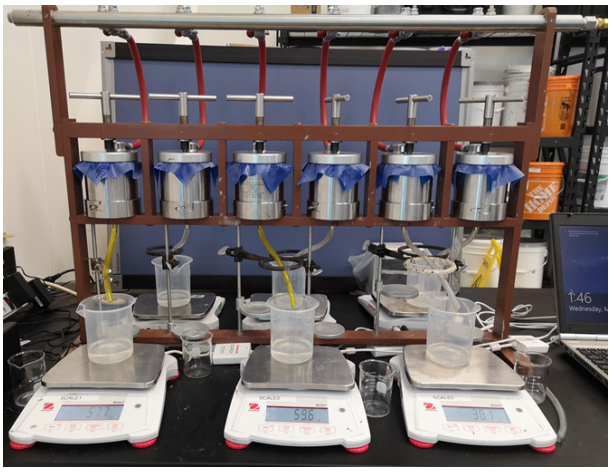

Figure 1. The photo of modified filter press setup with balances.

Pressure Filtration Test

A modified OFITE multi-unit filter press was used for filter press testing (Figure 1) (Li, et al. 2018; Li, et al. 2021; Qureshi, et al. 2021). The filter medium used was Whatman Grade #50 filter paper (particle filtration size of 2.7 μm). The 300 g samples were fed into the sample cup. Each sample cup was connected to a compressed air-line and the pressure was adjusted to the desired pressure (138 kPa / 20 psi). An elastic film was placed between the sample and the high pressure gas in each sample cup to avoid sample cracking during dewatering. The filtrate was collected and the mass of the filtrate was measured automatically along with the compression time directly to the computer.

Strength Measurement

The static yield stress was measured using the Brookfield DVIII HB, 5HB, and RST rheometers with vanes 73, 74, and VT-20-10. The maximum yield strength range for HB rheometer is 8 kPa, 5HB is 40 kPa, and RST is 69kPa.

Solids Content Measurement

The solids contents in this study were measured by placing the samples in an oven overnight at 105°C. The physically adsorbed water in the samples would be removed but chemically bonded water might be left in the samples.

Plastic Limit Testing

The thread rolling method was used to measure the plastic limit of the tailings samples (ASTM D4318-17). A filter press was used to accelerate the drying process of the samples. Plastic limits were calculated according to Eq. 2.

$$Plastic\ limit\ (\%) = \frac{Mass\ of\ water}{Mass\ of\ oven\ dry\ sample} \times 100 \quad (2)$$

RESULTS AND DISCUSSION

Optimal PCC Dosage Determination and Dewatering Performance Comparison

The optimal A3338 polymer dosage for the FFT sample was determined by testing the full dosage response curves corresponding to the net water release (NWR) after 24-hour drainage (Sadighian, et al. 2018; Li, et al. 2021). The optimal dosage for

the FFT was 1364 g/dry tonne solids and was used throughout this study (Figure 2).

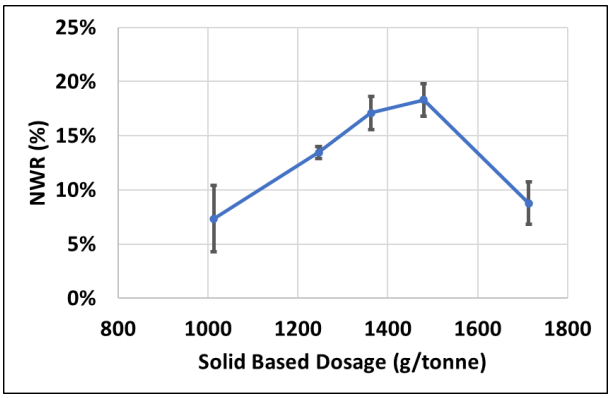

Figure 2. Dosage curves of the FFT treated with polymer A3338. Each dot is the average value of triplicate testing results. The error bars represent the 95% confidence index.

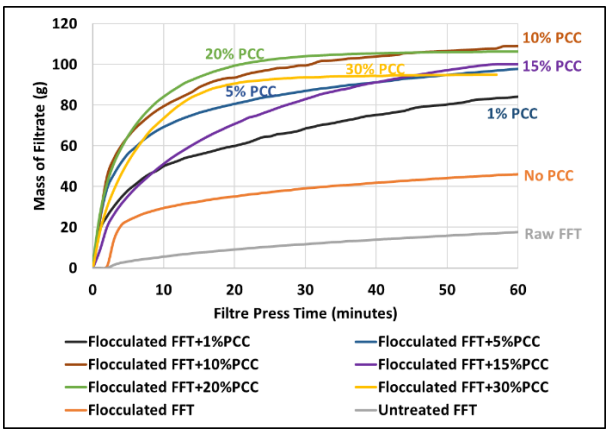

Figure 3. Filter press curves of A3338-flocculated FFT with different dosage treatments of PCC at 138 kPa.

The flocculated FFT with A3338 at the optimal dosage was then mixed with solid PCC with different dosages (by weight percent of total mass of the sample). The mixtures were then compressed by the modified filter press for 60 minutes. The filtrate flow rates were used to determine the optimal dosage of the PCC. A higher initial filtrate generating rate indicates higher dewatering performance and hence better dosage.

Figure 3 shows that both 10% and 20% of PCC in flocculated FFT had the highest flow rates. Therefore, 10% of PCC addition was determined to be the optimal dosage in this study. Figure 3 also shows that the dewatering performance greatly increased with the combination of flocculation and PCC. Even 1% PCC addition increased the dewatering performance of FFT compared with raw FFT and flocculated FFT without PCC addition.

Indication of Long-Term Consolidation

The FFT sample was treated with different additives: A3338 polymer at the optimal dosage, PCC addition at the optimal dosage, and the combination of A3338 and PCC at the respective optimal dosages. The treated FFT samples were dewatered with the modified filter press at 138 kPa along with the untreated FFT as a control test (Figure 4). The 138 kPa of gas pressure was used as an equivalent to about 5 meters of a sand cap. All three types of treatments greatly increased the filtrate flow rates compared with the untreated FFT indicating significant improvement in the dewatering performance of treated FFT. The rate of dewatering by the treatment of the combination of polymer and PCC was vastly higher than in others revealing improved filterability and consolidation rate.

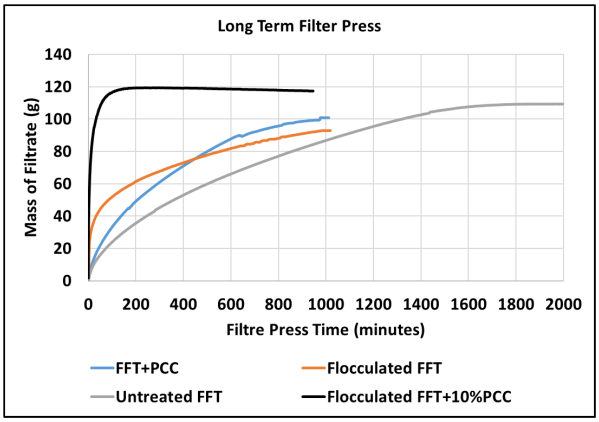

Figure 4. Filter press curves of the FFT with different treatments at 138 kPa. Each curve is the average of three sets.

The specific resistance to filtration (SRF) values of the FFT with different treatments were calculated according to Eq. 3 and compared in Table 4 (Coulson, et al. 1991; Li, et al. 2018). The linear portions of the filtration flow curves in Figure 4 were chosen for the SRF calculation. The SRF values are consistent with the dewatering performance. The combination of A3338 and PCC treatment dewatered much faster than others indicating a higher filterability. The results also indicated that PCC assisted with further improving the dewatering performance of polymer flocculated FFT.

$$SRF = (2 \times P \times A^2) \times b/(\mu \times c) \quad (3)$$

Where P is the pressure drop (Pa), A is the area of filter (50.27×10^{-4} m^2), μ is the viscosity of filtrate and assumed the viscosity of filtrate be the same as water (1×10^{-3} Pa·s), c is the concentration of solids in suspension, b is the slope of time(t)/volume(V) against volume (V) plot (t/V^2).

The solids content of the combined treatment of PPC and polymer after long-term filtration reached higher values than the treatments with polymer only and PCC only indicating a better long-term consolidation performance by the combined treatment (Figure 4) (Li, et al. 2021).

Table 4. The calculated specific resistance to filtration (SRF) values for FFT with different treatments.

Treatment	Average SRF	Standard deviation
No treatment	7.9E+13	2.1E+12
A3338	1.6E+14	1.8E+13
PCC	2.1E+14	6.4E+12
A3338+PCC	1.2E+12	2.7E+11

Development of Shear Strength

Tailings deposits designed for terrestrial reclamation must achieve sufficient strength to support surface access and reclamation (Li, et al. 2022). As water is released from FFT and solids content increases, the strength of the treated tailings increases, passing through the liquid limit and plastic limit. The combined treatment of A3338 and PCC increased the plastic limit compared with the untreated FFT and flocculated FFT (Table 5).

The solids contents and static yield stress was measured as an indicator of strength gain for different treatments (Figure 5 and 6). The combined treatment of A3338 and PCC increased greatly the yield stress of filtered cakes while keeping the comparable solids contents. Therefore, the strength gain of the combined treatment after filtration was due to the reaction between the added PCC and flocculated FFT, not just the solids addition.

Table 5. Plastic limit values of untreated and treated FFT.

Treatment	Average (%)	STDEV (%)
No treatment	16.0	0.8
A3338	18.6	0.5
A3338+PCC	20.4	0.3

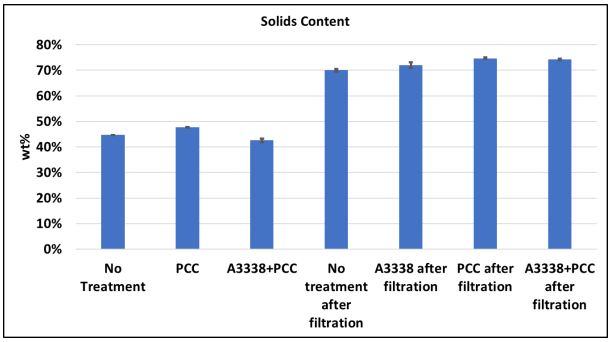

Figure 5. Solids contents of FFT with different treatments before and after filtration. Each column is the average of triplicate testing results. The error bars represent the STDEV.

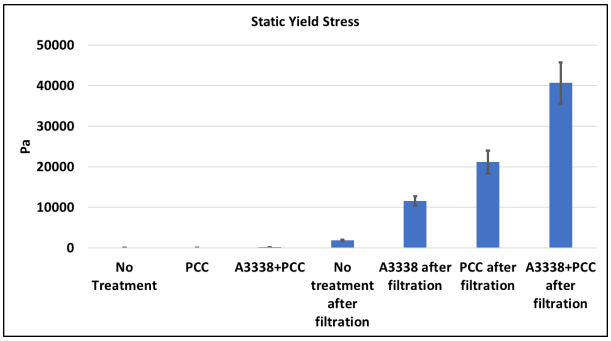

Figure 6. Static yield stress of FFT with different treatments before and after filtration. Each column is the average of triplicate testing results. The error bars represent the STDEV.

CONCLUSION AND FUTURE WORK

The effect of PCC addition to the polymer-treated FFT was investigated in this study through the characterization by pressure filtration dewatering, strength gain, and plastic limit testing. Dewatering performance was tested using the pressure filter press and the results show that 10% of PCC solids was the optimal dosage for the polymer A3338-

flocculated FFT in this study. The combined treatment of polymer and PCC on FFT increased the dewatering performance, strength gain, and long-term consolidation performance compared with no PCC addition to the FFT.

In the study, PCC was added as solids to the tailings. The dosage of PCC might decrease by adding as a slurry. Future studies will work on optimizing the process of PCC addition to the tailings in order to decrease the dosage of PCC required and simultaneously increase the strength of tailings. The feasibility of PCC transportation and addition in the tailings deposit will be explored.

Since this technology performed very well in the SRF tests, it is expected to be particularly relevant for centrifuge cake deposits as it may rapidly increase the strength of the deposit. The application of the PCC with centrifuge cake will be investigated in future studies. To ensure that this is a robust tailings treatment technology, testing on at least 3 other FFTs with different characteristics (sand to fines ratios, clay contents, and water chemistry) will also be studied.

The potential environmental benefits and/or impacts on the self-sustaining ecosystems are critical for the tailings reclamation to the upland system. Future studies will include the impact of PCC addition to tailings deposits on GHG emission and soil development,

REFERENCES

Alberta Energy Regulator (AER) 2021. State of Fluid Tailings Management for Mineable Oil Sands, 2020.

COSIA Fines Measurement Working Group 2015. Unified Fines Method for Minus 44 Micron Material and for Particle Size Distribution.

Coulson, J.M.; Richardson, J.F.; Backhurst, J.R.; Harker, J.H. 1991. Particle Technology and Separation Process. Chem. Eng. Vol. 2, 4th ed. Pergamon, Chapter 7.

Dean, E. W. and Stark, D.D. 1920. A convenient method for the determination of water in petroleum and other organic emulsions. Ind. Eng. Chem. 12: 486-490.

Li, Y.; Kaminsky, H.; Gong, X.Y.; Sun, Y.S.; Ghuzi, M.; and Sadighian A. 2021. What Affects Dewatering Performance of High Density Slurry? Minerals, 11, 761.

Li, Y.; Kaminsky, H.; Romero, C.; Gong, X.Y.; Ghuzi, M.; and Tacas, J. 2021. Assessing Dewatering Performance of Treated Fluid Fine Tailings with a Modified Bench-Scale Filter Press. Proceedings of Tailings and Mine Waste 2021, Banff, Alberta, Canada.

Li, Y.; Kaminsky, H.; Romaniuk, N.; Tate, M. 2018. Filter press modification to assess dewatering performance of fluid fine tailings. Proceedings of Sixth International Oil Sands Tailings Conference, Edmonton, Alberta, Canada: December 9-12, 2018.

Li, Y.; Kaminsky, H.; Romero, C.; Romaniuk, N.; Hariharan, N.; and Tate, M. 2021. Stabilization of flocculated fluid fine tailings by lime treatment. Proceedings of the 25th International Conference on Tailings and Mine Waste, 7-10 November 2021, Banff, Alberta, Canada.

Li, Y.; Kaminsky, H.; Dadighian, A.; Sun, Y.S.; Murphy, F.; Gong, X.Y.; Ghuzi, M.; and Rima, U. 2012. Impact of Chemical and Physical Treatment on Freeze-Thaw Dewatering of Fluid Fine Tailings. Cold Regions Science and Technology 193, 103385.

National Lime Association. 2007. Fact Sheet: Lime Terminology, Standards & Properties.

Omotoso, O.; Morin, M. 2008. Methylene Blue Procedure: Dean Stark Solids. CanmetEnergy, Devon, Alberta, Canada

Qureshi, TH; Li, Y.; Sedgwick, A.; Kaminsky, H.; Ng, J. 2021. Assessing oil sands tailings consolidation using a modified benchtop filter press. Paste 2021: 24th International Conference on Paste, Thickened and Filtered Tailings.

Sadighian, A.; Revington, A.; Kaminsky, H.; Moyls, B.; Li, Y.; and Omotoso, O. 2008. A New Protocol to Assess the Quality of Tailings Flocculation/Coagulation: A Collaboration to Improve Tailings Treatment at Suncor Energy. Proceedings of Sixth International Oil Sands Tailings, Edmonton, Alberta, December 9-12, 2008. 81 pp.

SRIN Oil Sands Research and Information Network, 2010. Review of Reclamation Options for Oil Sands Tailings Sustrates, BGC Engineering Inc.

RESIDUAL BITUMEN RECOVERY FROM FLUID FINE TAILINGS AND ENHANCED DEWATERING PERFORMANCE WITH A NOVEL TECHNOLOGY- PURETAILS

Mohammed Ghuzi[1], Yunhui Li[1], Catalina Romero[1], Andrea Sedgwick[1], George Terry[2] and Nigel Bosworth[2]
[1]Northern Alberta Institute of Technology, Edmonton, Canada
[2]Oil Solved Inc., Nisku, Alberta, Canada

ABSTRACT

Residual bitumen in fluid fine tailings can be a potential hazard to the environment and can have an adverse effect on the deposit reclamation process. In this study, a novel process called PureTails, which uses a water-derived solution (known as Energy Liquid Separation (ELS) Water), supplied by Oil Solved Inc., was used to remove the residual bitumen from a high-density fluid fine tailing (FFT). ELS Water successfully demonstrated the ability to recover bitumen from FFT resulting in a condensed layer of sediment (77.7% solids), and a mixed middle layer of water and fine silt and clays, known as middlings. These results indicate that ELS Water can simultaneously serve as a bitumen liberator and a coagulant aid. With no further treatment, the resultant sediment showed better drying characteristics when compared to the raw FFT. The dewatering of the middlings using a commercial coagulant and flocculant was found to be feasible. However, more systematic study might be required to determine the optimal coagulation/ flocculation conditions of the middlings. Overall, this investigation showed that ELS Water can recover bitumen from FFT resulting in less bitumen being deposited in the tailings ponds, and indicatively improve the long-term consolidation of the treated FFT.

INTRODUCTION

Oil sands tailings are produced during the bitumen extraction process of the surface mined oil sands ore, and they are composed of sand, silt, clay, oil sands process-affected water (OSPW), and residual bitumen. For every one cubic meter of oil sands extracted, around four cubic meters of oil sands tailings waste is produced (Siddique et al., 2006). These tailings are pumped and stored above ground in settling basins, known as tailings ponds. According to (Alberta Energy Regulator, 2020), these ponds contain over 1.3 billion m^3 of tailings that must be ready for reclamation within ten years after they become off-service. Therefore, there is a growing political and social pressure imposed on the oil sands industry to take more effective and efficient measures against the oil sands waste due to various environmental concerns.

Bitumen residues in tailings ponds are considered one of the main concerns as they can pose a direct threat to environment when biodegraded over time and hence release harmful components such as naphthenic acids, greenhouse gases, reduced sulfur compounds, and volatile organic compounds (Van Dongen et al., 2021). In addition, residual bitumen can seep and cause mats of bitumen to form on the surface of the tailings ponds, which has been already observed in the Syncrude Base Mine Lake (Syncrude, 2021). Furthermore, some studies have been reported that residual bitumen hinders the settling rate of flocculated fluid fine tailings (FFT) (Klein, 2014) and lowers the tailings hydraulic conductivity (Suthaker & Scott, 1996). As a result, the tailings dewaterability and consolidation characteristics can be negatively affected, and this can lead to a prolonged reclamation process. Bitumen may also contribute to the fouling of advanced treatment technologies such as the filter press by binding to the filter medium and hence becoming detrimental to the filtration process. Therefore, removing bitumen from tailings not only can provide cleaner tailings, reduce fugitive emissions from tailings ponds, accelerate reclamation process, but also can create economic value by increasing the bitumen recovery.

Skimming off bitumen directly from tailings ponds can be expensive due the high operating cost and difficulties in processing froth produced. Flotation is another conventional avenue for bitumen removal from tailings (Alam & Shang, 2017). However, it is inefficient to process coarser particles unless tailings are screened first. So, flotation can be costly as it may require building a flotation system before the tailings waste enters the tailings pond. Flotation also has high process requirements and can be influenced by many factors such as size and volume of gas bubbles and adhesion between gas bubbles and bitumen droplets.

Chemical treatment of tailings using aqueous solutions to recover residual bitumen prior to dewatering and deposition can be a potential solution. In the present study, we report a two-step treatment process where high-density FFT is mixed with ELS Water (water-derived chemical) to recover the residual bitumen resulting in a bitumen rich layer on the surface, condensed layer of solids at the bottom, and a mixed layer of water, silt, and clays in the middle. The middle layer (middlings) is then dewatered using aluminum sulfate as a coagulant and anionic polyacrylamide-based polymer as a flocculant. The bitumen recovery from the FFT and the dewaterability performance of the middlings were evaluated using various techniques.

EXPERIMENTAL

Materials

The FFT and process effluent water (PEW) were obtained from an existing inventory at the Centre for Oil Sands Sustainability (COSS) at NAIT. The anionic polyacrylamide flocculant (A3338) and coagulant salt (aluminum sulfate) were produced by SNF and Kemira, respectively. The aqueous solution (ELS Water) was supplied by Oil Solved Inc.. The polymeric solution with a concentration of 0.45% wt/vol was prepared by mixing the appropriate amount of A3338 powder in PEW at 300 rpm for an hour. The polymeric solution was used within 1 week after preparation.

Characterization of Materials

The raw FFT, PEW and treated FFT were characterized at COSS using different methods where applicable as follows:

Dean & Stark analysis (Dean & Stark, 1920) was used to determine the solids, water, and bitumen contents and to prepare the solids for the fines content analysis. Methylene Blue Index (MBI) was determined following the method described elsewhere (Kaminsky, 2014). Fines content was determined by the wet sieving technique at 45 µm (sieve no. 325). The pH and electrical conductivity (EC) were determined by directly immersing the pH meter (PH100 ExStick) and EC probe (Cole-Parmer traceable conductivity pocket Tester) in the targeted sample. Capillary Suction Time (CST) indicates the filterability of FFT by measuring the time it takes for water to pass through the sample slurry and flow through a filter paper and reach two electrode points (~1 cm apart). The test was performed using Type 319 Multi-purpose CST apparatus with CST filter papers of 7x9 cm (Triton Electronics) (Sadighian et al., 2018). The major cations and anions were determined on the water extracts using a Dionex™ Aquion™ Ion Chromatography (IC) System. FFT samples were directly filter pressed using an OFITE filter press to obtain water extracts. After extraction, all water was further filtered using a 0.45 µm particulate filter prior to testing (Sadighian, et al. 2018). The sodium adsorption ratio (SAR) was calculated using Eq 1, where ionic concentrations of sodium (Na^+), calcium (Ca^{2+}), and magnesium (Mg^{2+}) ions are reported in milliequivalents (mEq):

$$SAR = [Na^+] / \sqrt{[(Ca^{2+} + Mg^{2+})/2]} \quad (1)$$

The results of Dean & Stark, MBI, SFR, pH, EC, and CST for the FFT and PEW are presented in Table 1 while their associated major ions are shown in Table 2.

Table 1. Physio-chemical characteristics of FFT and PEW used in this study. Mean values ± Standard Deviation are shown where applicable with three replicates.

Property	FFT	PEW
Solids (wt%)	44.4 ± 0.6	-
Water (wt%)	53.8 ± 0.4	-
Bitumen (wt%)	1.8 ± 0.4	-
MBI (mEq/100g solids)	7.9 ± 0.4	-
Fines (<44 µm) (wt%)	70.4	-
pH	7.62 ± 0.12	9.42
EC (dS/m)	1.45 ± 0.06	1.50
CST (s)	1716 ± 91	8
Density (g/mL)	1.371	0.999

Table 2. Major ions in FFT and PEW (unit = mg/L); SAR is sodium adsorption ratio.

Ions	FFT	PEW
Sodium (Na^+)	230.8	274.7
Potassium (K^+)	14.6	14.4
Magnesium (Mg^{2+})	28.6	13.4
Calcium (Ca^{2+})	56.3	7.2
Chloride (Cl^-)	17.5	176.9
Sulphate (SO_4^{2-})	365.7	221.3
SAR	6.2	14.0

Bitumen Recovery Test by ELS Water

FFT stored in a 20 L pail was initially homogenized using a hand-drill mixer for 5 min, and then subsampled in 2000 g batches into unbaffled 2 L glass beakers with a diameter of 12.5 cm. A flat impeller with a diameter of 7.6 cm was used for mixing while an overhead mixer (Heidolph Hei-Torque 100 Precision Base) was used to control the mixing speed at 300 rpm. A series of preliminary tests were performed at room temperature to find the optimal dosage of ELS Water. The FFT was dosed at various concentrations, namely 1.1%, 2.3%, or 3.4% vol/wt-solids, using a disposable syringe and mixed for 2 min. The treated FFT was then allowed to settle for 30 min. The bitumen that rose to the surface was then skimmed off using a metal spatula and labeled as primary recovery. Additional 0.2%, 0.5% and 0.7% vol/wt-solids of ELS Water were added to the 1.1%, 2.3% and 3.4% vol/wt-solids pre-dosed samples, respectively. The samples were then mixed for 2 min and allowed to settle for 30 min. The floated bitumen was recovered in a similar fashion to the primary recovery and labeled as secondary recovery. The samples were further mixed for 6 min and allowed to settle for another 30 min for tertiary recovery. The operator's visual assessment of the thickness of sediment (bottom layer) along with the bitumen mass recovered was utilized to determine the optimal dose. The FFT samples were then treated in triplicate at the optimal dosage of ELS Water. After the bitumen recovery, the samples were allowed to settle for 24 h. The resultant middlings were then transferred to another glass beaker for coagulation and flocculation, while the densified sediment bed was kept for a drying test as illustrated in Figure 1. The recovered bitumen (primary layer) was characterized using Dean & Stark technique to determine the quality and recovery % of bitumen.

As a control sample, raw FFT was also mixed at 300 rpm with the overhead mixer, but no bitumen separation was observed.

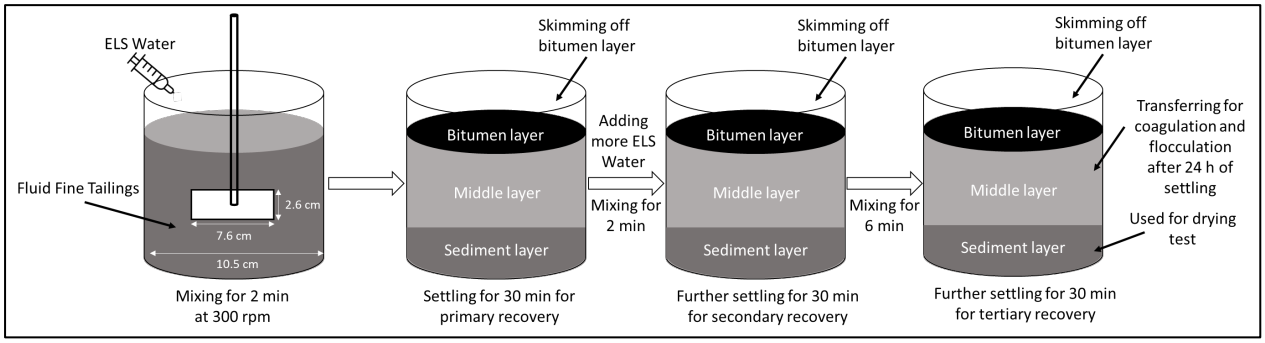

Figure 1. Schematic of the bitumen recovery process when treated with ELS Water

Coagulation and Flocculation Test of Middlings

After 24 hours of settling, the middlings layer was poured into a clean 1 L glass beaker and subsampled while being homogenized using an overhead mixer for the dewatering test. The remaining portion was used for the Dean & Stark and MBI tests. The middlings required for the coagulation and flocculation was diluted to ~10% solids by adding the appropriate amount of PEW prior to the treatment. The diluted middlings were treated following a modified version of the experimental procedure reported elsewhere (Li et al., 2021). Briefly, the sample was initially homogenized for 1 min in an unbaffled 1 L glass beaker using the Hei-torque overhead mixer and a flat impeller. The sample was then dosed with the appropriate amount of alum under continued mixing for 10 seconds at 300 rpm. The mixing speed was then decreased to 80 rpm and the mixing was continued for 13 min. At the 13 min mark, the mixing speed was increased back to 300 rpm and the appropriate amount of flocculant was immediately injected in one shot via a syringe while still mixing. Visual observation of the floc formation was indicative of optimal polymer dosage. The formed flocs were then conditioned at 10 rpm for 15 seconds for better water release. Raw FFT and diluted FFT to the same solid content as the diluted middlings were also coagulated and flocculated as control samples in a similar fashion as the diluted middlings samples but with different optimal alum and A3338 dosages. The different optimal dosages were chosen to meet the best dewatering performance of the raw FFT and diluted FFT. The dewaterability behavior of the coagulated-

flocculated samples was evaluated using CST, solids content of flocs after draining for 24 h and specific resistance to filtration (SRF) tests.

The CST tests were conducted after 24 hours of drainage by subsampling 2 mL of drained water in triplicate. The solids content of flocs was gravimetrically determined by oven-drying over night at 105°C. The remaining flocs were then used for the SRF tests which were conducted using a modified OFITE filter press with a 2.7 µm filter paper as reported elsewhere (Li et al., 2021). The samples were pressed at 20 psi using a compressed nitrogen cylinder. The mass of filtrate was recorded as a function of time using WinWedge software connected to a 0.1 g digital scale, and the solid content of the filtered cake was determined gravimetrically.

Drying Test of Sediment

A portion of the resultant sediment layer after bitumen and middling removal was used for a drying test. The sample was placed in an uncovered aluminum pan (20 cm x 20 cm x 4 cm) and the loss of water due to evaporation was measured for 11 days. A control water and raw FFT samples were also placed next to the sediment sample to compare the actual evaporation (AE) to the potential evaporation (PE) and the solids gain. AE is the mass of water removed from the treated/ untreated FFT sample while the PE is the mass of water removed from the water pan. The aluminum pans used for this test have an identical surface area.

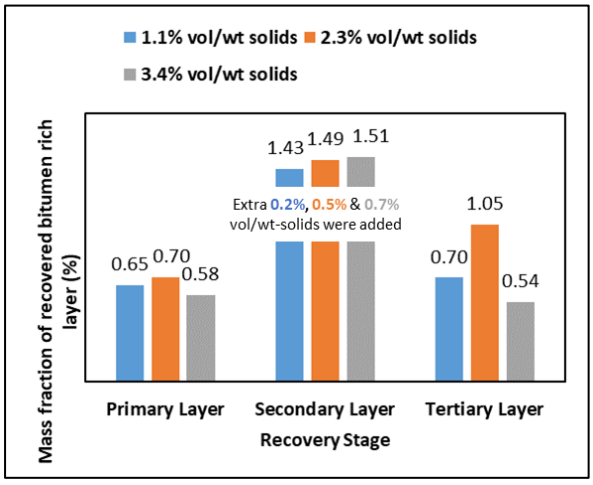

Figure 2. Amount of bitumen layer recovered at three different stages for different doses of ELS Water.

RESULTS AND DISCUSSION

Bitumen Recovery

The amount of the recovered floated bitumen-rich layer (BRL) was used as a qualitative indicator for determining the optimal dosage of ELS Water (Figure 2). All three ELS Water doses, either in the primary or secondary stage, yielded similar mass fraction of BRL (Figure 2) and hence the lowest dosage (i.e. 1.1% vol/wt-solids for primary stage and 0.2% vol/wt-solids for secondary stage) was selected for the subsequent testing where the FFT was treated in triplicate.

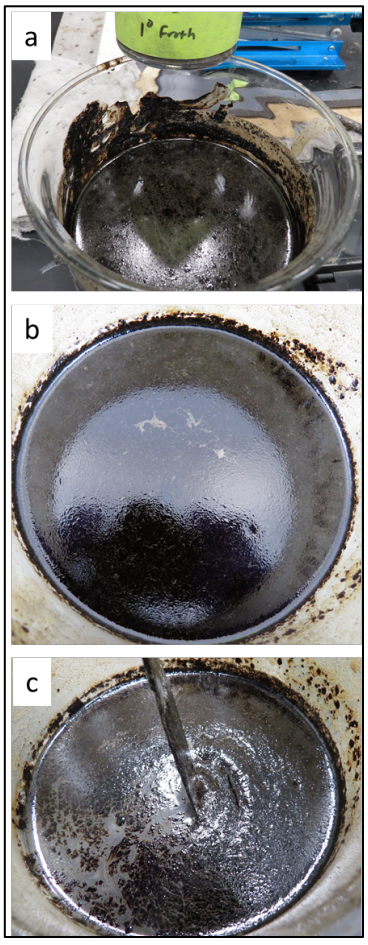

Figure 3. Floating bitumen-rich layer (BRL) at (a) primary, (b) secondary, and (c) tertiary stages after dosing FFT with ELS Water at 0.5% vol/wt-solids for the primary recovery and extra 0.2% vol/wt-solids for the secondary recovery.

Treating the FFT with the targeted amount of ELS Water produced a BRL that was collected at each

recovery stage (Figure 3). It is noteworthy that the formation of the bitumen-rich layer continued even after the tertiary extraction. The bitumen content of the primary recovery stage was analyzed, and the Dean & Stark results along with a complete mass balance of solids and water components are presented in Table 3.

Table 3. Composition of the primary bitumen-rich layer (BRL) after dosing with 0.5% vol/wt-solids ELS Water; the composition of middlings and sediments after three rounds of bitumen extraction.

Name	Solids	Water	Bitumen	Solids recovery	Water recovery	Bitumen recovery	MBI
	wt%	wt%	wt%	%	%	%	Meq/100g
Raw FFT	44.4	53.8	1.8	-	-	-	7.9
Primary BRL	17.5	41.8	39.4	0.7	1.3	37.9	-
Middlings	29.4	68.2	0.9	45.1	82.9	32.9	4.8
sediment	77.7	20.7	0.3	54.2	11.9	5.7	2.0
Mass balance	-	-	-	100.0	96.2	76.5	-

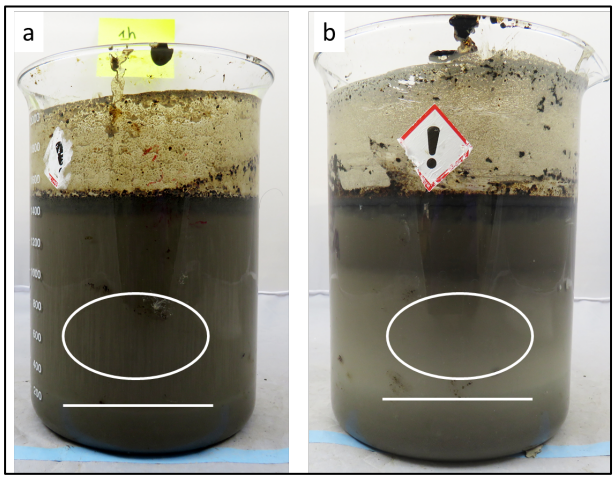

Figure 4. Settling of solids (a) immediately after bitumen extraction and (b) after sitting for 24 h; white line marks the height of the sediment bed, and the white circle shows the change in color of the middlings.

The bitumen recovery (%) on the primary BRL showed that 37.9±1.6% of bitumen was recovered from the primary froth. Although secondary and tertiary bitumen recoveries were not analyzed in this study, it was expected to achieve over 50% for the total bitumen recovery. The bitumen to solids ratio (B/S) of the primary froth was 2.3. The further cleaning of the primary froth or the improvement of the process would provide higher quality of the primary froth. Overall, ELS Water demonstrated the ability to recover the residual bitumen and produce a sediment with 77.7±1.3% solids after settling for 24 hours as shown in Figure 4. The MBI of the middlings and sediment was also determined to be 4.8 and 2.0 mEq/100 g solids, respectively, which is lower than the MBI of the original FFT (7.9 mEq/100 g solids). Lower MBI value reflects lower active clay content and hence ELS Water not only liberated bitumen from FFT but also showed a coagulation effect.

Drying Test of Sediment

After treating the FFT with ELS Water and allowing it to settle for 24 hours, a consolidated solids layer was formed (Figure 4). This layer made up 31% by weight of the treated FFT. The original FFT has a clay-to-water ratio (CWR) of 0.46 while the produced sediment layer had a CWR of 0.52.

Sadighian et al., (2018) evaluated the drying performance of three different polymers by optimally flocculating 0.40 CWR FFT. The treated FFT was placed onto a mesh sieve with a 1 mm opening and a surface area of 324 cm^2 for drying. The researchers then measured the loss of water to drainage and evaporation daily. The drying performance of the sediment layer was compared to that of the optimally flocculated FFT with the three polymers (Figure 5). Although the FFT used in this study is different from the FFT used by Sadighian et al., both FFTs had relatively similar CWR. The sediment was fully desiccated (99.3% solids) within 6 days while the chemical treatments achieved only 93% solids at best even after 20 days of drying. Hydrophilic polyacrylamide type of polymers tends to retain water in the flocs which makes it impossible to achieve 100% water removal whereas the ELS Water treatment easily achieved 100% water removal upon drying. To eliminate the difference in the evaporation rate of this study and Sadighian et al., the AE was normalized by dividing by the PE. Therefore, the non-dimensional drying curves (Figure 6) show that the drying rate drastically slowed down after achieving 6.6 CWR for the polymer-treated FFT while the drying rate was relatively constant for the sediment generated by the ELS Water treatment.

The evolution of the visual appearance of the sediment is captured in Figure 7. The dense sediment was converted from a malleable structure to a rigid one while the raw FFT was changed from a fluid-like texture to a close-to-plastic limit yet moldable texture over 11 days of drying. The dried sediment also looked relatively clean (i.e., bitumen-free) as compared to the original FFT where there

was a clear bituminous marbling pattern in the dried FFT sample (Figure 7 b & c).

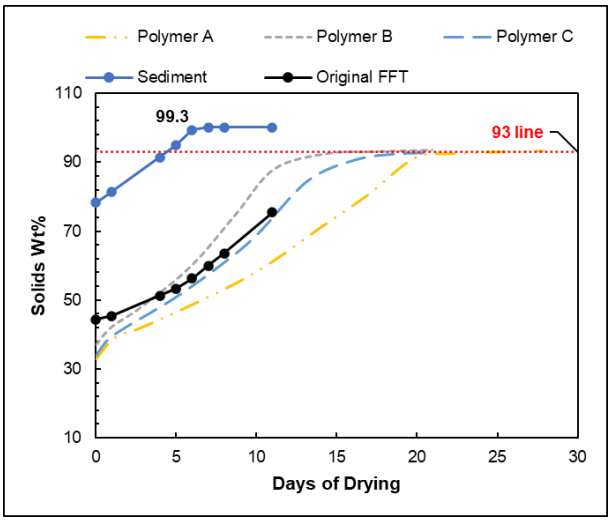

Figure 5. Solids wt% gain in sediment, original FFT, and polymer-treated FFT with polymers A, B &C (Sadighian et al., 2018) as a function of time.

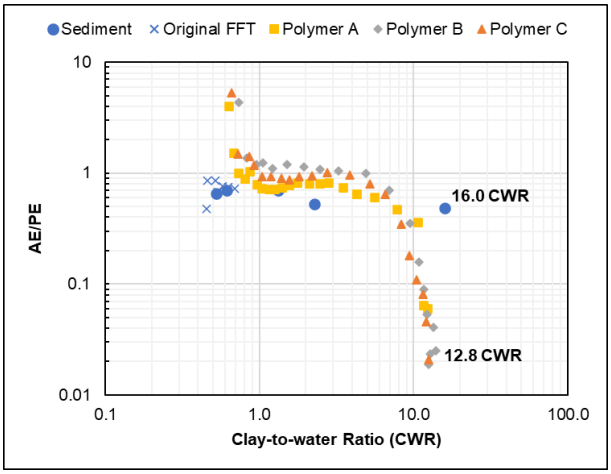

Figure 6. Non-dimensional evaporation drying curves of sediment and polymer treated FFT with polymers A, B &C (Sadighian et al., 2018) as a function of clay-to-water ratio.

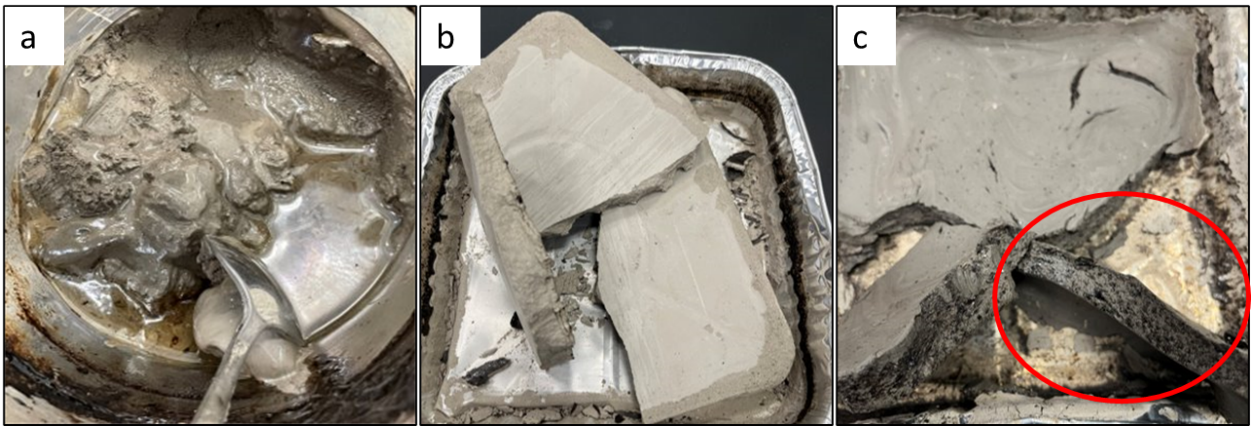

Figure 7. Physical appearance of (a) sediments after decanting the middlings, (b) sediment after 11 days of drying, (c) original FFT after 11 days of drying with bitumen marbling pattern circled in red.

Dewatering of Middlings

A preliminary coagulation and flocculation study was performed to assess the viability of dewatering the middlings layer using commercial coagulants and flocculants. Therefore, the diluted middlings (10% solids) were treated with alum and A3338 at different dosages, and their dewatering behavior was compared to that of the diluted FFT (10% solids) and original FFT (44.4% solids).

Figure **8** shows the CST results of the release water of the treated samples after 24 hours of draining. Lower CST values reflect better quality of water release. It was expected that diluted samples would show lower CST results (~ 8±1 s) compared to the treated original FFT (26±17 s) because treated diluted samples immediately released most of the diluent PEW (Figure 9). It is noteworthy that diluted middlings required less polymer on a solids basis than the diluted FFT to achieve optimal flocculation. This finding can also support the observation of the coagulation effect of the ELS Water where less

polymer solution is usually required for a pre-coagulated substrate.

The solids content of the flocs after draining for 24 hours was also reported in Table 4. The flocs of the diluted middlings achieved a solid content of ~ 20% while the flocs of the diluted FFT and original FFT achieved ~ 27% and 50% solids, respectively. The low solid content in the diluted middlings flocs, in comparison to the other samples, can be attributed to the partial removal of the coarser solids during the bitumen recovery stage. The sand-to-fines ratio (SFR) of the diluted middlings was determined to be 0.05 which is less than that of the diluted FFT (0.42 SFR) (Table 4). The resultant flocs of the draining test were further dewatered using the modified filter press to study the consolidation behavior. The flocs were pressed at 20 psi for 2 hours, and the final solids content of the filtered cake shown in Table 4 indicated that the middlings could be further treated and consolidated after bitumen and sediment removal.

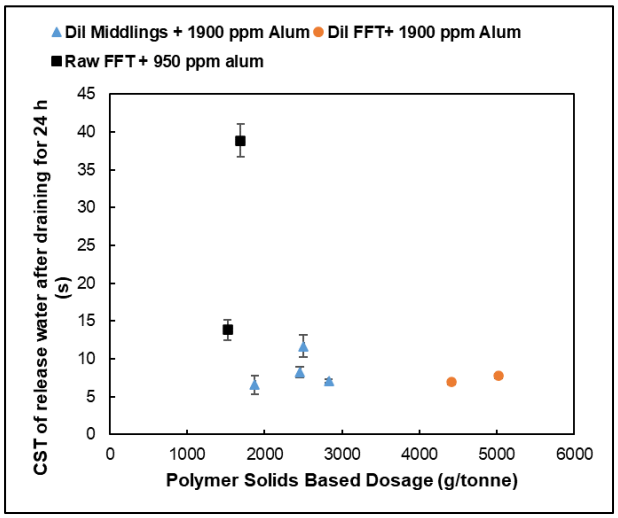

Figure 8. Capillary Suction Time (CST) of release water of flocculated samples after 24 h drainage; error bar represents standard deviation of triplicate.

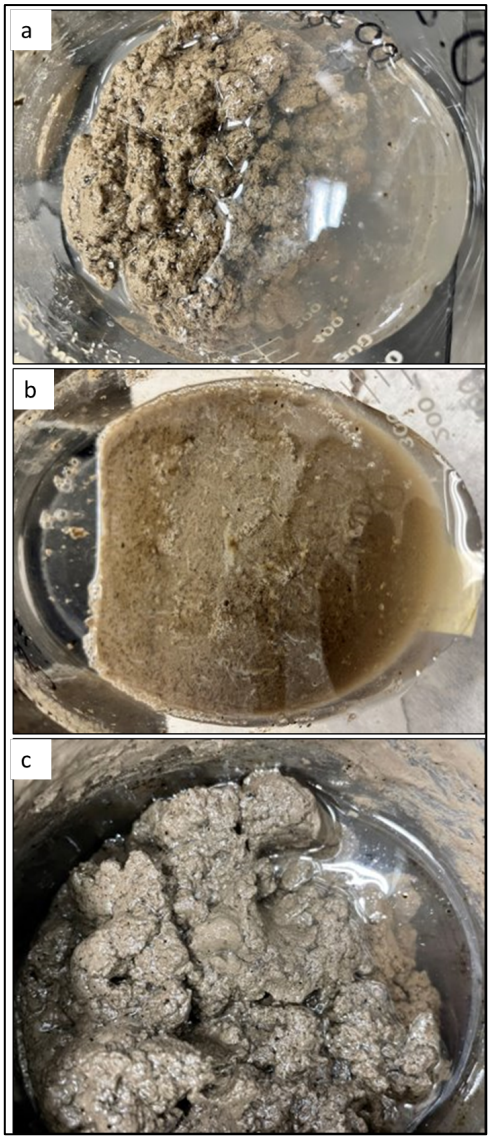

Figure 9. Water release immediately after the coagulation-flocculation treatment of (a) diluted middlings, (b) diluted FFT, and (c) original FFT

Table 4. Summary of the solids content of different substrates for different tests; SFR is sand to fines ratio while SRF is specific resistance to filtration test.

Material	Original solids	SFR	Flocs solids/ initial SRF solids	Final SRF solids	Final solids of drying test
	wt%		wt%	wt%	wt%
Raw FFT	44.4	0.42	50.0	58.6	75.5
Middlings	29.4	0.02	-	-	-
Sediment	77.7	0.73	-	-	100.0
Diluted Middlings	10.0	0.05	20.3	42.4	-
Dilute FFT	10.0	0.42	27.2	66.3	-

CONCLUSIONS AND FUTURE WORK

The effectiveness of the PureTails process, using ELS Water in bitumen removal from high-density fluid fine tailings (FFT) was evaluated, and the findings of the study can be summarized as follows:

- Dosing the FFT with the appropriate amount of ELS Water can achieve reasonable bitumen recovery resulting in relatively bitumen-free FFT.
- ELS Water demonstrated a coagulation effect where a condensed layer of solids (sediment) was formed after settling for 24 hours.
- The results of the drying test showed that the resultant sediment of the ELS Water treatment can reach 100% desiccation significantly faster than the untreated FFT.
- The resultant middlings of the PureTails treatment can be further dewatered using a commercial coagulant and flocculant.

This technology has the potential to be applied to a process for removing residual bitumen from tailings such as froth tailings and FFT resulting in a dense layer of coarse tailings at the bottom of the tailings ponds. Then only the middling layers would be required for further treatment. Further investigation will be explored to improve the removed bitumen quantity and quality from FFT and speed the bitumen recovery such as using an air flotation process during the bitumen removal. It also has potential for recovering bitumen directly from ore samples however validation of that theory is required. Also, future studies are required to evaluate the kinetics of the formation of the bitumen-rich layer and assess the robustness of this technology by investigating the effect of solids, fines, clay content, and water chemistry on PureTails' performance of bitumen removal.

REFERENCES

Alam, R., & Shang, J. Q. 2017. Removal of bitumen from mature oil sands tailings slurries by electro-flotation. Journal of Water Process Engineering, 15, 116–123.

Alberta Energy Regulator. 2020. State of Fluid Tailings Management for Mineable Oil Sands, 2019.

Dean, E. W., & Stark, D. D. 1920. A Convenient Method for the Determination of Water in Petroleum and Other Organic Emulsions. Journal of Industrial & Engineering Chemistry, 12(5), 486–490.

Kaminsky, H. (2014). Demystifying The Methylene Blue Index.

Klein, C. G. 2014. Effect of Residual Bitumen on Polymer-Assisted Flocculation of Fluid Fine Tailings [University of Alberta].

Li, Y., Kaminsky, H., Romero, C., Gong, X. Y., Ghuzi, M., & Tacas, J. 2021. Assessing Dewatering Performance of Treated Fluid Fine Tailings with a Modified Bench-Scale Filter Press. Proceedings of the Tailings and Mine Waste Conference 2021 (TMW 2021).

Sadighian, A., Revington, A., Kaminsky, H., Moyls, B., Li, Y., & Omotoso, O. 2018. A New Protocol To Assess The Quality Of Tailings Flocculation/Coagulation: A Collaboration to Improve Tailings Treatment At Suncor Energy. Sixth International Oil Sands Tailings Conference.

Siddique, T., Fedorak, P. M., & Foght, J. M. 2006. Biodegradation of Short-Chain n -Alkanes in Oil Sands Tailings under Methanogenic Conditions. Environmental Science & Technology, 40(17), 5459–5464.

Suthaker, N. N., & Scott, J. D. 1996. Measurement of hydraulic conductivity in oil sand tailings slurries. Canadian Geotechnical Journal, 33(4), 642–653.

Syncrude. 2021. New Technology Tested To Dredge Bitumen From Base Mine Lake. Syncrude.

Van Dongen, A., Samad, A., Heshka, N. E., Rathie, K., Martineau, C., Bruant, G., & Degenhardt, D. 2021. A Deep Look into the Microbiology and Chemistry of Froth Treatment Tailings: A Review. Microorganisms, 9(5), 1091.

INFLUENCE OF CLAYS AND ORGANIC-RICH SOLIDS ON TAILING BEHAVIOUR

Bussaraporn Patarachao[1]*, Ryan Way[1], Andre Zborowski[1], Judy Kung[1], Martin Couillard[1], Daniel Tyo[1], Yunhui Li[2], Heather Kaminsky[2]
[1]National Research Council Canada (NRC), Ottawa, Ontario, Canada
[2]Northern Alberta Institute of Technology (NAIT), Edmonton, Alberta, Canada

ABSTRACT

Fluid fine tailings (FFT) and mature fine tailings (MFT) are the primary tailings output generated during oil sands processing. These tailings compose of solids, water and small amounts of unrecovered bitumen. Clays and Organic-Rich Solids (ORS) composed in tailings' solids have properties and characteristics that could cause poor dewatering and consolidation rates which is the major challenge for the effective reclamation of the tailing ponds. In this study, coagulation tests and detailed characterization of the clays and ORS were performed in order to obtain better understanding of the physics and chemistry of these solids and the surrounding aqueous medium. ORS and Total clay fractions (TC) with particle size of < 2 μm was separated from a set of FFT samples. The separated solids were coagulated using aluminum sulfate (alum). Settling behavior of the clays and the ORS was monitored and recorded over a period of 24 hours. Clear differences of settling behavior were observed. The clays exhibited a consistent settling/mudline interface. The ORS settled in a much more chaotic pattern where no mudline was readily detected but rather individual clusters of particles formed and settled out of suspension. After the treatment, the supernatants and the settled solids from the test columns were collected for further characterization. XRD analysis revealed that illite and kaolinite are the main minerals in the < 2 μm clay solids while heavy minerals (siderite, pyrite, zircon, rutile and anatase) are the main minerals in the ORS. Mineralogical changes following the coagulation process reveals the effectiveness of the coagulation particularly on illite for the TC fractions and quartz for the ORS fraction. Morphological characterization of the remaining solids in the supernatant by TEM analysis shows small iron-bearing particles (<10 nm) scattered on top of clay particles in the TC fractions. These iron-bearing particles were also present in the ORS fraction along with some small quartz particles surrounded by carbon-rich particles. Increase of Ca^{+}, Mg^{2+} and K^{+} concentration in the supernatant, determined using ion chromatography technique confirmed ion-exchange reaction. The results obtained from this study provided insightful information which can be used to evaluate the effect of clays and ORS on coagulation behavior for tailings management in order to facilitate the dewatering process.

INTRODUCTION

Bitumen extraction from surface-mined oil sands deposits produces fluid tailings composed of sand, fines (silts and clays), water, and small amounts of unrecovered bitumen. Fluid fine tailings (FFT) are a primary tailing outputs generated during oil sands processing (COSIA, 2012). There are about 1360 Mm^3 legacy and new fluid tailings in 220 km^2 of active ponds as of 2020 (Alberta Energy Regulator, 2021). Numerous chemical, physical, electro-chemical, biological, and thermal methods have been tested for tailings treatment. At present, no technology that addresses FFT/MFT can be considered "mature" in the sense of showing sound technicality, environmental responsibility, and cost-effectiveness. Seeking solutions to transform tailings from waste into a substrate that speeds land and process-affected water reclamation is of paramount importance. Among the currently used chemical methods to accelerate the release of water from FFT, in-line polymer flocculation and gypsum coagulation enhanced by a solid-bowl scroll centrifugation show the best results in dewatering. However, the presence of divalent metal ions (e.g. Ca^{2+}) increases process-affected water hardness that is detrimental to the oil extraction. As a result, any tailings treatment method needs to estimate its impact on bitumen extraction via recycled water (Chalaturnyk et al. 2002). Poor dewatering and consolidation rates, primarily caused by fines and clays in tailings' solids, are known to be the major challenges for the effective reclamation of the ponds (Mamer 2010, Junqueira et al 2011). Despite many studies on tailing behavior done over the years, the physics and chemistry of these fine clay particles and the surrounding aqueous medium still have not

yet been fully understood. Organic-Rich Solids (ORS) are bi-wettable solids present in oil sands that have been previously linked with challenges in extraction and froth treatment by acting as emulsion formers. (Bensebaa et al. 2000, Kotlyar et al. 1999, Sparks et al. 2003, Couillard et al. 2020). However, to date, no studies have been done on the influence of the ORS on tailing behavior. It is important to understand the types and characteristics of solids present in tailings in order to identify whether any solids types or characteristics could lead to the observed challenge associated with tailing treatment. In this study, coagulation tests using the alum and detailed characterization of the clays and ORS were performed. The clay particles and ions interaction in the presence or absence of bitumen were also investigated.

EXPERIMENTAL

Five Fluid Fine Tailings (FFT1, FFT2, FFT3, FFT4 and FFT5) from different sources were used in this study. FFT1 is from one pond, FFT2 &FFT3 are from another pond and FFT 4& 5 are from a third pond. ORS and Total Clay (TC) fractions with particle size < 2 μm were separated from each of these samples using the toluene/water interfacial solids wettability separation technique and the clay-ultrafine separation technique, respectively (Mercier et al. 2019). In order to investigate the efficiency of coagulation in the presence or absence of bitumen, TC with bitumen fraction and TC with no bitumen fraction were separated. To separate TC with no bitumen, prior to centrifugation, the bitumen was removed from the samples using the toluene/water interfacial total solids separation technique. For separation of TC with bitumen, the samples were centrifuged directly without bitumen removal process. Particle size distribution of the TC fractions was measured on a Horiba LA950v2 laser diffraction instrument. The suspending medium was water, and the refractive index used for the solids was 1.55 with an imaginary portion of 0.1.

Bulk mineralogy of TC with bitumen, TC with no bitumen and ORS fractions, before and after coagulation treatment, was determined using XRD technique. Samples were prepared as randomly oriented powder mount in a zero background holder. XRD measurement was performed using powder X-ray diffractometer (XRD) – Bruker D8 Advance (da Vinci design) set up in Bragg Brentano geometry (theta-theta), configured with Copper (Cu) X-ray tube, Trio optics, motorized anti-scatter screen and a Lynxeye XE-T silicon strip detector. XRD data were collected with a scan range of 5 to 80 °2θ using a step size of 0.02 and count time of 1 second per step. Quantification of minerals present in the settle solids was determined from the collected XRD data using Rietveld analysis with TOPAS version 6 software (Bruker AXS, Karlsruhe, Germany).

Coagulation tests was performed by diluting 0.1 wt% of TC with bitumen, TC with no bitumen with the synthetic process water in 100 mL beaker. ORS fractions were already at 0.1 wt% and so were not diluted. The samples were homogeneously mixed using a magnetic stirrer at 400 rpm. Following homogenization, 0.146 mL of coagulant (48.76 wt% of aluminum sulfate in sulfuric acid, Kamira®) was pipetted in the 100 mL beaker and stirred for 2 minutes. Once the mixing was completed, the samples were transferred into 100 mL graduated cylinders (23 mm in internal diameter and 240 mm in height). One control column (no coagulant added) and three coagulation treatment columns were prepared for each sample. For TC with bitumen and TC with no bitumen, changes in the settling behavior were monitored by taking photos of the columns over a period of 24 hours. The height of mudline was recorded at 3, 6, 9, 12, 15, 30, 45, 60 minutes and 24 hours. The settling rate was evaluated as average of percent height of the mudline (change in height at the particular recorded time compared to the original height) over settling times. For ORS, changes in the settling behavior were monitored and virtually assessed according to opacity of the water observed over a period of 24 hours. Scales of opacity from 1 to 10 were assigned and recorded at 3, 6, 9, 12, 15, 30, 45, 60 minutes and 24 hours. The opacity scale of 10 refers to the most cloudiness while the opacity scale of 1 refers to the least cloudiness. The settling rate was evaluated based on opacity level over settling times.

Supernatant and settled solids were collected from the control and the treated columns after 24 hours for further characterization. Ion Chromatography (IC) technique was used to determine cation concentrations of calcium, magnesium and potassium (Ca^{2+}, Mg^{2+} and K^{+}) in the supernatant. Prior to IC analysis, samples were filtered using 0.45 μm Luer-Lock syringe filter into 1.5 mL vials. The supernatant from the TC fractions were diluted to $1/10^{th}$ and $1/50^{th}$ of their original concentration, while the supernatant from the ORS fractions were left at their original concentrations. A set of 7 standards were prepared using the following concentrations; 0.2, 0.5, 1, 3, 5, 10, and 25 ppm. Check standards were ran to ensure calibration

accuracy. The IC measurements were performed using Thermoscientific – Dionex ICS 5000+. The analysis was done in triplicate for each sample. Data were analyzed using the Chromeleon software version 7.

Transmission Electron Microscopy (TEM) technique was used to analyze mineralogy and morphology of the remaining solids in the supernatant. TEM specimens were prepared by depositing a drop of the solution was then placed onto a 200 mesh TEM copper grid coated with a uniform carbon support film. A FEI Titan^3 80-300 TEM operated at 300 keV, and equipped with a CEOS aberration corrector for the probe forming lens and a monochromated field-emission gun was used to acquire both high-resolution TEM (HRTEM) and annular dark-field (ADF) images. ADF images were collected using a high-angle annular dark-field (HAADF) Fischione detector in scanning transmission electron microscopy (STEM) mode. This technique provides signal intensity related mainly to the atomic number (Z) and the thickness of the region analyzed. The TEM instrument is also equipped with an energy-dispersive X-ray (EDX) spectrometer (EDAX Analyzer, DPP-II. To optimize the signal intensity, EDX spectra were acquired with the specimen tilted at 15 degrees.

RESULTS AND DISCUSSION

TC and ORS separation

Laser scattering measurements confirmed that particle sizes mostly < 2 μm were achieved for the separated TC fractions. Mean particle size of approximately 1 μm was measured for all samples as shown in Table 1. No significant difference was observed in the mean particle size of TC with bitumen and TC with no bitumen.

Amounts of the separated TC fractions and ORS fractions from all FFT samples are shown as wt% per total solids in Table 2. Samples with no bitumen contain slightly larger content of TC compared with samples with bitumen. FFT2 and FFT3 have similar quantity of TC with bitumen of ~ 25 wt% and TC with no bitumen of ~ 28 wt%. FFT4 and FFT5 have similar quantity of TC with bitumen of ~ 36 - 38 wt% and TC with no bitumen of ~ 38 - 39 wt%. FFT1 contains highest amount of TC with bitumen and TC with no bitumen of ~ 42 wt% compared to other samples. Similar quantity of ORS (~2 wt%) were separated from FFT1, FFT2 and FFT3 while much less quantity of ORS (~0.8 wt%) was separated from FFT4 and FFT5.

Table 1. Mean particle size (μm) of TC with bitumen and TC with no bitumen

	TC with bitumen	TC with no bitumen
FFT1	1.11	1.09
FFT2	0.76	1.06
FFT3	1.00	0.96
FFT4	0.83	1.20
FFT5	0.98	0.88

Table 2. Quantitative amount of TC and ORS in FFT samples (wt% per total solids)

	TC (wt%)		ORS (wt%)
	with bitumen	with no bitumen	
FFT1	41.74	42.77	2.40
FFT2	25.00	28.19	2.12
FFT3	25.00	27.76	2.43
FFT4	37.64	39.26	0.83
FFT5	36.09	37.95	0.75

The presence of twelve different minerals were identified by XRD analysis in TC with bitumen, TC with no bitumen and ORS fractions from all FFT samples. Figure 1 shows XRD patterns of TC with bitumen (a), TC with no bitumen (b) and ORS (c) separated from FFT1. The identified minerals are listed in Table 3. TC with bitumen and TC with no bitumen have similar XRD patterns (Figure 1(a) and 1(b)) showing strong diffraction peaks of illite and kaolinite clays associated with small diffraction peaks of other non-clay minerals (quartz, calcite, siderite, anatase and rutile). In contrast, XRD patterns of ORS fractions show strong diffraction peaks of quartz and other heavy minerals such as pyrite, anatase, rutile and zircon. These heavy minerals have hydrophobic characteristic and are typically concentrated in the ORS fractions (Couillard et al. 2020). Smaller diffraction peaks of illite and kaolinite clays were also identified in the XRD pattern of the ORS fractions as shown in Figure 1(c). It is noted, however, that the 001 diffraction peak of chlorite clay at 7° 2-theta (14 Å) was clearly detected in the XRD patterns of ORS fractions but not in TC fractions.

Table 3. List of minerals found in ORS and TC with bitumen and TC without bitumen

	Name	Formula
K	Kaolinite	$Al_2SiO_2O_5(OH)_2$
I	Illite	$KAl_2Si_3AlO_{10}(OH)_2$
Chl	Chlorite	$(Fe,Mg,Al)_6(Si,Al)_4O_{10}(OH)_8$
Q	Quartz	SiO_2
D	Dolomite	$CaMg(CO_3)_2$
C	Calcite	$CaCO_3$
G	Gypsum	$CaSO_4.2H_2O$
P	Pyrite	FeS_2
S	Siderite	$FeCO_3$
R	Rutile	TiO_2
A	Anatase	TiO_2
Z	Zircon	$ZrSiO_4$

Settling behaviour and settling rate

Coagulation treatment was performed using the separated ORS, TC with bitumen and TC with no bitumen. As an illustrative example, Figure 2 shows settling behaviour of TC with bitumen from FFT1 sample. Photos of the control column taken at 0 minute and 24 hours were compared with photos of the treated column taken at 6, 12, 30, 60 minutes and 24 hours. A clear and consistent settling/mudline interface were observed in the treated column at any given time during the coagulation treatment. As time increases, the water in the treated column became progressively clearer. The effectiveness of the added coagulant was evidenced by comparing the clarity of water in the control and treated column at 24 hours. It was revealed that the water of the coagulant treated column was much clearer than the supernatant of the control and has much larger settling bed. Similar settling behaviour was observed for TC with bitumen and TC with no bitumen of all other FFT samples.

The settling behaviour of ORS, on the contrary, is in stark contrast from that of the TC fractions. As an illustrative example, Figure 3 shows settling behaviour of ORS from FFT1 sample. During the first 60 minutes of coagulation treatment, the water in the treated column appeared very cloudy. No mudline was readily detected but rather individual clusters of particles formed and settled out of suspension. At 24 hours, the water became much clearer allowing for the settling bed to become visible. The settling of the treated column at 24 hours (Figure 3 (f)) is very similar to that of the control column (Figure 3 (g)) with only slightly larger settling bed and slightly clearer water. This indicates that addition of coagulant did not greatly improve settling of ORS from the FFT1 which is similarly to the ORS from FFT2 and FFT3. However, unlike what was observed in the other samples, it was noted that the water in the control columns of the ORS from the FFT4 and FFT5 remained very cloudy while the water in the treated columns became very clear after 24 hours. It is most likely that these samples contain higher amount of fine clay particles compared to the ORS from FFT1, FFT2 and FFT3. Further investigation will be required to confirm this assumption.

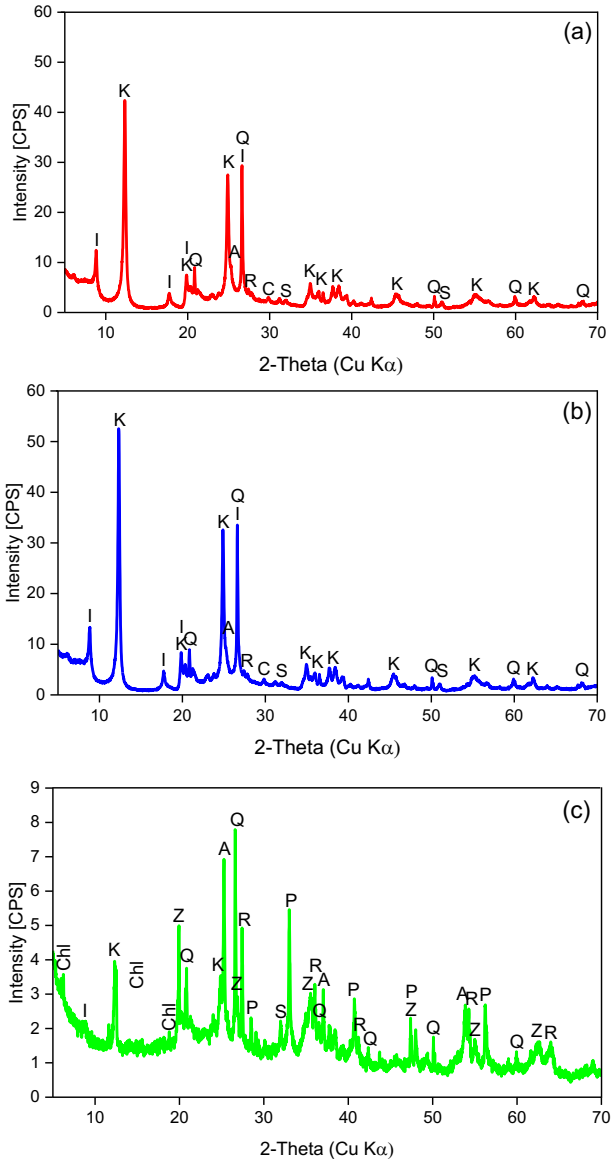

Figure 1. XRD patterns of TC with bitumen (a), TC with no bitumen (b) and ORS (c) from FFT1

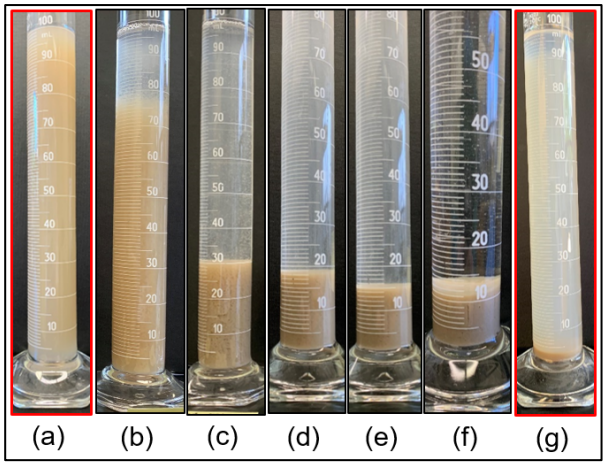

Figure 2. Settling behavior of TC with bitumen from FFT1 showing the control column at 0 min (a), treated columns at 6 min (b), 12 min (c), 30 min (d), 60 min (e), 24 hrs (f) and the control column at 24 hrs (g)

Since no mudline was readily detected in the coagulation treated columns of the ORS samples, the changes in settling behaviour was virtually assessed using opacity scale of 1 to 10 (the least to the most cloudiness). Figure 4 (a) shows opacity scale of the water in the control columns of the ORS from all five FFT samples. For FFT1, FFT2 and FFT3, the opacity scale slowly decreased from ~8 – 9 at the beginning to ~6 – 7 at 60 minutes. In contrast, the opacity scale of FFT4 and FFT5 remained unchanged at ~6 – 7 from the beginning to 60 minutes. After 24 hours, the opacity scale of FFT1, FFT2 and FFT3 dropped down to 1 which is the least cloudiness. However, the opacity scale FFT4 and FFT5 stayed higher at 6 and 5, respectively. Figure 4 (b) shows opacity scale of the water in the treated columns of the ORS from all five FFT samples. At the beginning of the coagulation treatment (0 minute), the opacity of the water in the treated columns were at higher scale of ~ 6 - 9. The highest opacity scale of 9 was assigned to the ORS from FFT1 and the lowest opacity scale of 6 was assigned to ORS from FFT5. As the coagulation treatment progressed, the opacity level of all FFTs slowly decreased to ~ 5 - 6 at 60 minutes and then dropped to 1 at 24 hours.

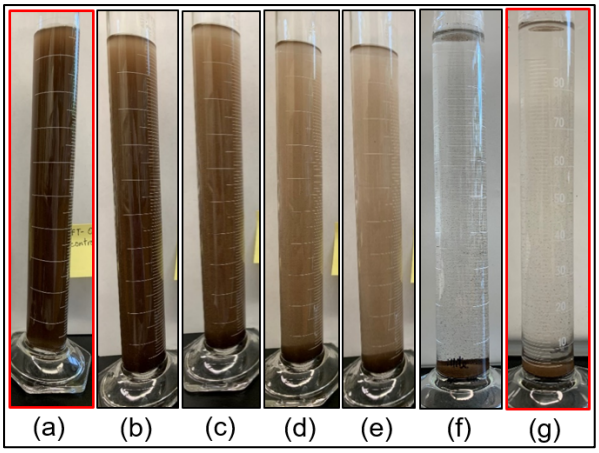

Figure 3. Settling behavior of ORS from FFT1 showing the control column at 0 min (a), treated columns at 6 min (b), 12 min (c), 30 min (d), 60 min (e), 24 hrs (f) and the control column at 24 hrs (g)

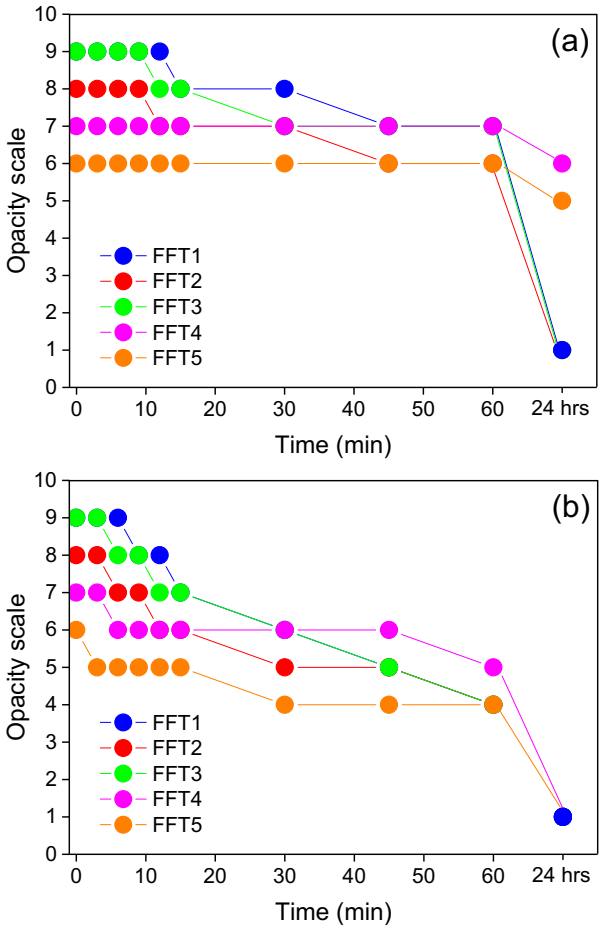

Figure 4. Assessment of ORS' settling behaviour based on opacity level of the control columns (a) and the treated columns (b)

Comparison of the opacity scale from the control and treated columns of ORS from FFT4 and FFT5 demonstrates that addition of the alum enabled the settling of solid particles as the opacity scale dropped to 1 in the treated column while it remained higher at ~5 – 6 in the control column after 24 hours. This indicates that some particle aggregation took place due to the presence of the alum but that alum didn't agglomerate the majority of the particles.

The settling rate of TC with bitumen and TC with no bitumen from the five FFT samples determined as average of percent height of the mudline are shown in Figure 5 (a) and (b), respectively. Similar settling rates were observed for both TC with bitumen and TC with no bitumen in all five samples. This is consistent with results from other studies demonstrating that the bitumen is not the primary factor in the slow initial settling of oil sands tailings. It is shown that the settling occurred rapidly within 15 minutes of coagulation treatment and progressively slowing down thereafter until reaching a plateau at the height of ~10 – 20%. Only slight reduction of percent height was observed at 24 hours compared to at 60 minutes. FFT5 sample has the highest settling rate, at any given time while FFT1 samples has the lowest settling rate compared to the other samples. It is noted that since no mudline was readily detected in the coagulation treated columns of the ORS samples, settling rate of the ORS cannot be determined. Since the settling behaviour and settling rate of TC with bitumen and TC with no bitumen were very similar, characterizations were only performed on the TC with no bitumen.

Characterization of the settled solids

Mineralogical composition results obtained by Rietveld analysis for the control and treated settled solids of TC with no bitumen are compiled in Table 4. The minerals are categorized into clay and non-clay. Clay content (wt%) is the sum of kaolinite and illite minerals. Non-clay content (wt%) is the sum of quartz, rutile, anatase and siderite minerals. It is shown that the control settled solids contain mostly clay minerals with clay content larger than 80 wt% and small amount of other non-clay minerals of less than 20 wt%. After 24 hours of coagulation test, in the treated settled solids, the clay content increased by ~ 3 – 7 wt% while the non-clay content decreased. This indicates the efficiency of coagulation test on clay minerals. Addition of the alum as coagulant in the water causes the suspended clay minerals to settle faster. Figure 6 compares quantity of individual minerals in the control and treated settled solids for each sample. For clay minerals, the amount of kaolinite is relatively the same in the control and treated settled solids for all samples. However, larger amount of illite was quantified in the treated settled solids compared to the control settled solids indicating that illite is the mineral responsible for the increase of the overall clay content in the treated settled solids. Specifically, this indicates that the added alum is more effective on illite than kaolinite.

Mineralogical composition results obtained by Rietveld analysis for the control and treated settled solids of ORS are compiled in Table 5. The minerals are categorized into hydrophilic and hydrophobic based on their wettability characteristic. Hydrophilic content (wt%) is the sum of quartz, illite, kaolinite and chlorite minerals. Hydrophobic content (wt%) is the sum of pyrite, rutile, anatase, zircon and siderite minerals.

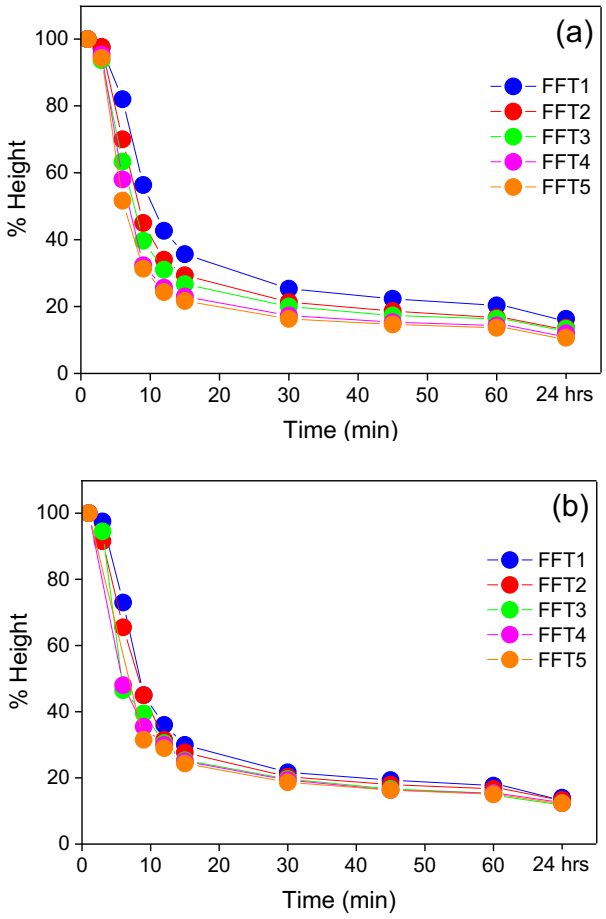

Figure 5. Settling rate of TC with bitumen (a) and TC with no bitumen (b)

Table 4. Clay and non-clay content in the settled solids of the control and treated TC with no bitumen

	Clay (wt%)		Non-Clay (wt%)	
	Control	Treated	Control	Treated
FFT1	82.66	87.09	17.34	12.91
FFT2	84.07	86.80	15.93	13.20
FFT3	84.82	89.40	15.18	10.60
FFT4	82.09	88.28	17.92	11.72
FFT5	84.59	88.83	15.41	11.16

Due to insufficient quantity of the control and treated settled solids from FFT4 and FFT5 sample, mineralogical quantification by XRD for these samples was not determined (n.d.). It is shown in Table 5 that the control settled solids of all samples contain higher amount of hydrophobic minerals (~ 56 – 64 wt%) compared to the hydrophilic minerals (~ 36 – 44 wt%). After 24 hours of coagulation test, in the treated settled solids, the hydrophilic content significantly increased by ~ 9 wt% for FFT1 but only slightly increased by ~3 wt% for FFT2 and FFT3. This indicates the efficiency of coagulation test on hydrophilic minerals. Figure 7 compares quantity of individual minerals in the control and treated settled solids for each ORS sample. Interestingly, the amount of quartz is consistently higher in the treated settled solids compared to the control settled solids. Contrary to the TC with no bitumen where the amount of quartz is consistently lower in the treated settled solids. Since quartz is categorized as hydrophilic minerals in the ORS fraction, the consistent increase in its content determined in the treated settled solids shows that quartz is the main mineral responsible for the increase of the overall hydrophilic content after 24 hours of coagulation. This indicates that the added alum is effective at treating fine quartz.

Table 5. Hydrophilic and hydrophobic minerals content in the settled solids of the control and treated ORS

	Hydrophilic (wt%)		Hydrophobic (wt%)	
	Control	Treated	Control	Treated
FFT1	41.53	50.33	58.47	49.67
FFT2	36.35	39.33	63.64	63.03
FFT3	44.29	47.58	55.72	52.41
FFT4	n.d.	n.d.	n.d.	n.d.
FFT5	n.d.	n.d.	n.d.	n.d.

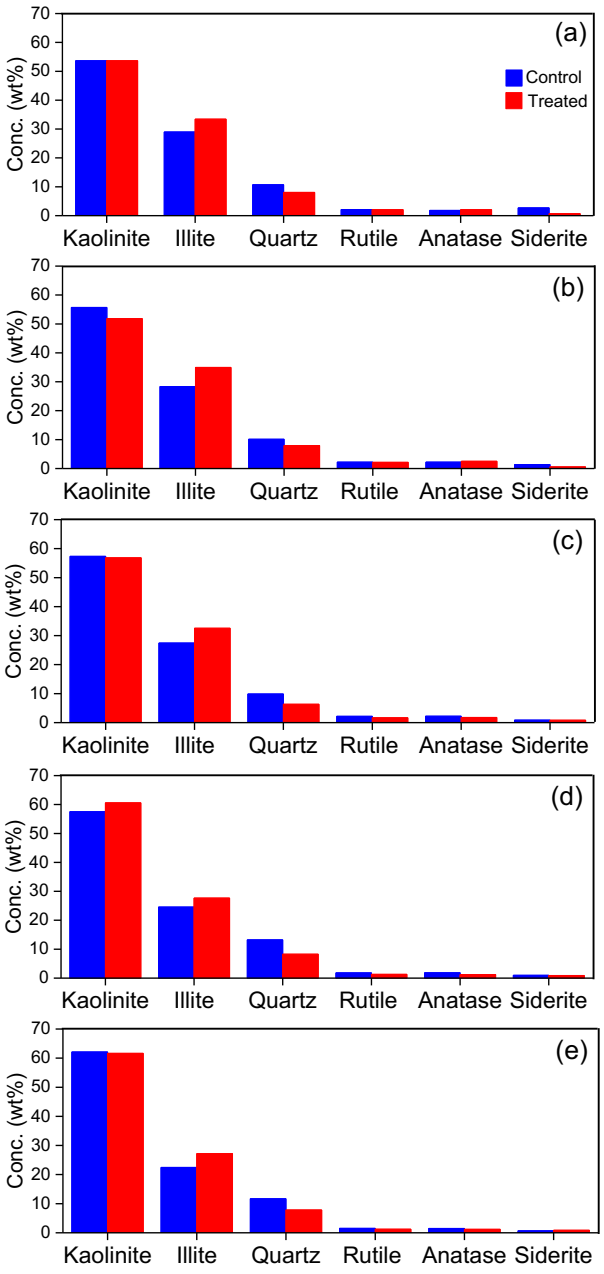

Figure 6. Mineralogical composition in control and treated settled solids of TC with no bitumen for FFT1 (a), FFT2 (b), FFT3 (c), FFT4 (d), FFT5 (e)

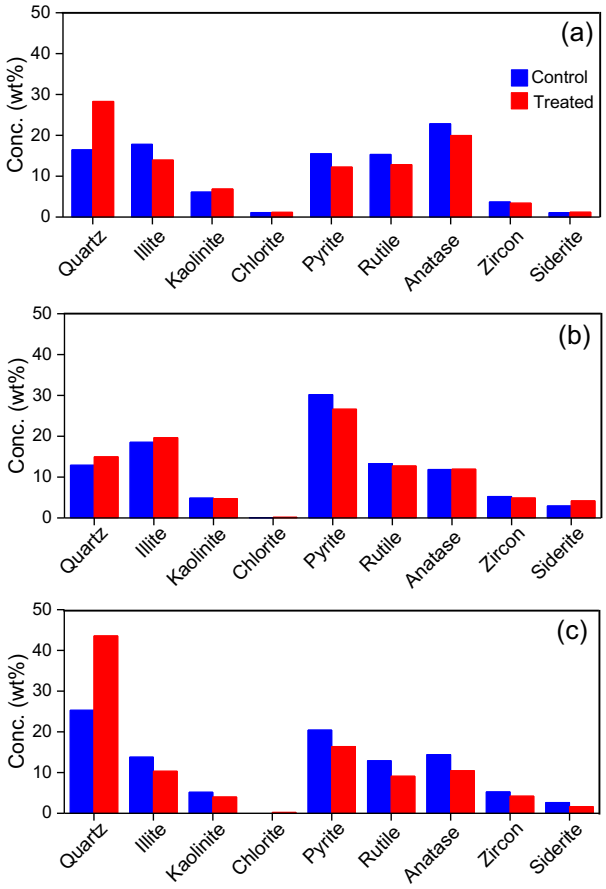

Figure. 7 Mineralogical composition in control and treated settled solids of ORS

Characterization of the supernatant

Comparison of Ca^{2+}, Mg^{2+} and K^{+} concentration in the control and treated columns after 24 hours of coagulation is as shown in Figure 8 and 9 for TC with no bitumen and ORS, respectively. For the TC with no bitumen, similar concentration of the three cations in the control supernatant was measured at ~ 8 – 15 ppm in all five samples. Slightly higher concentration were measured in the treated supernatant. In the case of ORS, varying concentration of Ca^{2+}, Mg^{2+} and K^{+} were measured at a much lower range (~0.1 – 10ppm) compared to the TC with no bitumen. In some cases the measured concentrations were less than limit of detection (< 0.2 ppm). The same trend of higher concentration in the treated supernatant compared to the control supernatant was also observed in the ORS samples except for K^{+} from sample FFT4 and FFT5 where the trend was opposite. It should also be noted and taken in to consideration that the concentration of K^{+} in these samples were very low and at the level of limit of detection.

Figure 10 shows TEM images of the remaining solids in the supernatant after 24 hours of coagulation treatment of TC with no bitumen separated from FFT1 sample. Clay particles in the range of < 100 to 500 nm were observed. EDX analysis indicates the presence of two types of clays: illite clay (Al-Si-O-K) and kaolinite clay (Al-Si-O). Very small iron-bearing particles (Fe-O) with particle sizes <10 nm are scattered on top of the clay particles. Other small particles of aluminum-sulfur-bearing (Al-S) particles were also observed. These particles are believe to be the undissolved or re-crystallized particles of the aluminum sulfate used as coagulant. Figure 11 shows TEM images of the remaining solids in the supernatant after 24 hours of coagulation treatment of ORS separated from FFT1 sample. Mostly carbon particles with various particle sizes (~10 – 200 nm) are present in the sample. Similar to the TC with no bitumen, very small iron-bearing particles (Fe-O) with particle sizes <10 nm also present the ORS. Due to high carbon signal, long acquisition time was applied for EDX analysis revealing few small particles of clay minerals associated with carbon and sulfur particles (C-Al-Si-O-S). Some small particles of quartz particles (Si-O) were also observed.

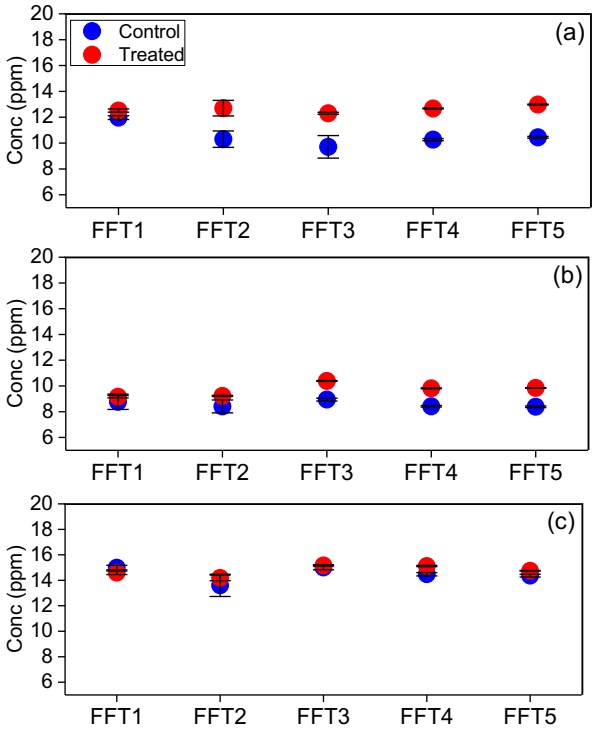

Figure 8. Concentration of Ca^{2+} (a), Mg^{2+} (b) and K^{+} (c) in the supernatant of TC with no bitumen

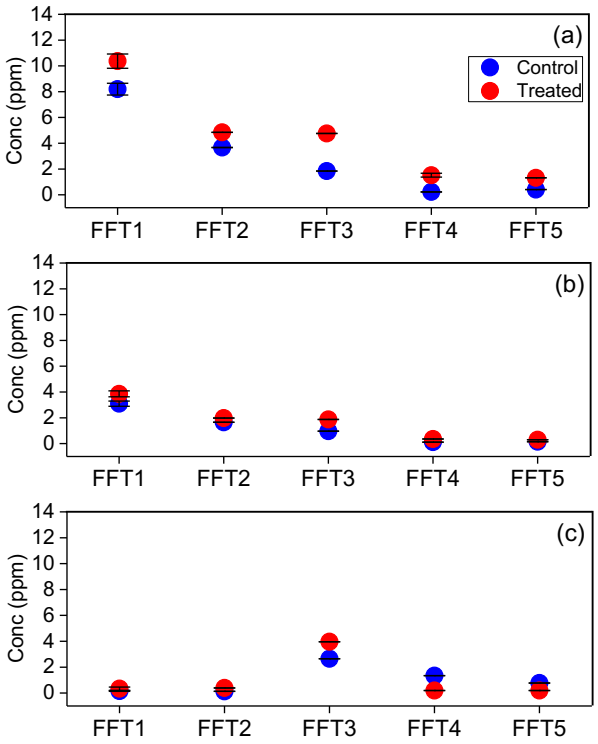

Figure 9. Cation concentration (Ca^{2+}, Mg^{2+} and K^{+}) in the supernatant of ORS after 24 hours of coagulation treatment

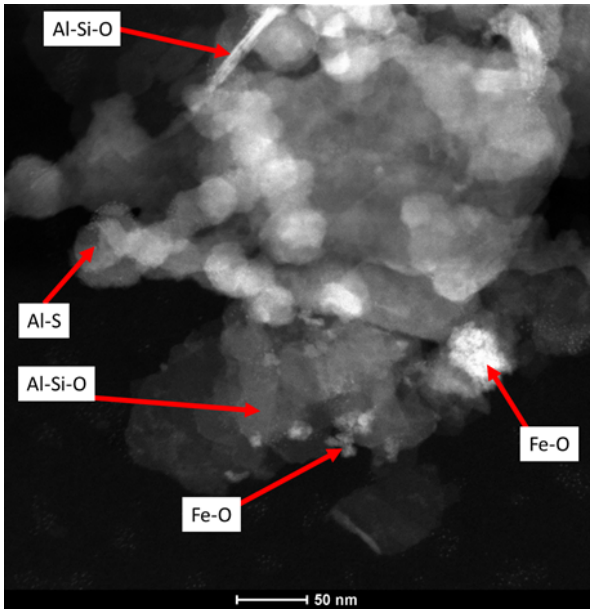

Figure 10. TEM images and EDX of remaining solids in the supernatant of the TC with no bitumen separated from FFT1 sample

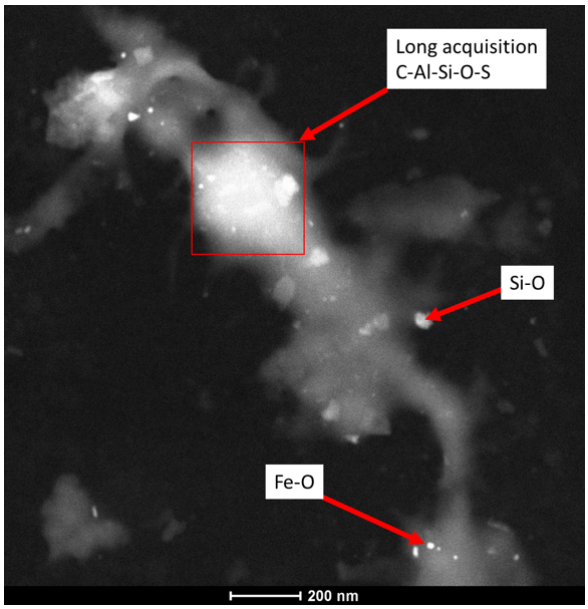

Figure 11. TEM images and EDX of remaining solids in the supernatant of the ORS separated from FFT1 sample

CONCLUSION

Following the results obtained in this study, it is shown that the presence of bitumen does not affect settling rate and behavior of the TC fractions. However, the differences in settling behavior are observed depending on wettability properties of the solids (hydrophobic vs hydrophilic). The clays exhibited a consistent settling/mudline interface while the ORS settled in a much more chaotic pattern where no mudline was readily detected but rather individual clusters of particles formed and settled out of suspension. Quantitative mineral analysis by XRD confirmed the coagulation efficiency as evidenced by the increase in clay mineral content in the settled solids of total clay fractions and the increase in hydrophilic content in the settled solids of ORS fractions after treatment. TEM analysis revealed that there are solids particles that did not settle and still remained in the supernatant of the TC and ORS even after 24 hours of coagulation treatment using the alum. For the solids collected from the supernatant of TC, small iron-bearing particles (<10 nm) are seen scattering on top of clay particles. For the solids collected from the supernatant of ORS, mostly carbon-rich particles solids are observed with small portion of iron-bearing particles (<10 nm) and quartz. It is also evidenced that the characteristic and properties (quantity, settling behavior and settling rate) of TC

and ORS separated from each of the FFTs linked to their tailings' sources. Since coagulation with alum is not an effective treatment in ORS identified so far, it is likely that these solids will have different interaction with polymers as well. Enhanced understanding of the interaction of ORS with existing tailings treatments may help improve tailings dewatering and may also have benefits in extraction & froth treatment.

REFERENCES

Technical Guide for Fluid Fine Tailings Management, Oil Sands Tailings Consortium, COSIA, August 30th, 2012

State of Fluid Tailings Management for Mineable Oil Sands, 2020, Alberta Energy Regulator, September, 2021

Chalaturnyk, R.J., Scott, J.D., Ozum, B. (2002). Petroleum Science and Technology, 20, 9&10: 1025-46

Mamer. M., (2010). Oil sands tailings technology: understanding the impact to reclamation, British Columbia Mine Reclamation Symposium Courtenay, BC, Canada

Junqueira, F.F., Sanin, M.V., Sedgwick, A., Blum, J., (2011). Assessment of Water Removal from Oil Sands Tailings by Evaporation and Under-drainage, and the Impact on Tailings Consolidation, Tailings and Mine Waste, Vancouver, BC, Canada.

Bensebaa, F., Kotlyar, L., Sparks, B., Chung, K. (2000). Organic coated solids in Athabasca bitumen: characterization and process implications. Can J Chem Eng, 78: 610-616

Kotlyar, L., Sparks, B., Woods, J. (1999). Solids associated with the asphaltene fraction of oil sands bitumen. Energy and Fuels, 13(2): 346-350

Sparks, B., Kotlyar, L., O'Carroll, J., Chung, K. (2003). Athabasca oil sands: effect of organic coated solids on bitumen recovery and quality. J Pet Sci Eng, 39(3-4): 417-430

Mercier, P.H.J., Tyo, D., Zborowski, A., Kung J., Patarachao, B., Kingston, D.M., Couillard, M., Robertson, G., McCracken, T., Ng, S. (2019). First quantification of < 2 μm clay, <0.2 μm ultrafines and solids wettability in process streams from naphthenic froth treatment plant at commercial mined oil sands operations. Fuel, 237: 961-976

Couillard, M., Tyo, D.D., Kingston, D. M., Patarachao, B., Zborowski, A., Ng, S., Mercier, P.H.J. (2020). Structure and mineralogy of hydrophilic and biwettable Sub-2 μm clay aggregates in oil sands bitumen froth. Minerals, 10, 1040: 1 – 21

The Oil Sands Tailings Research Facility (OSTRF) was established in 2003 as a direct response to the global need for improved tailings management. Through extensive interaction and collaboration with other distinguished research groups, the OSTRF provides the novel research required to develop environmentally superior tailings disposal options. With the flexibility to support concurrent interdisciplinary research projects, the facility attracts the brightest minds in the field and trains early-career, technically competent scientists and engineers—the future leaders, consultants and regulators for the oil sands industry. The OSTRF is pioneering the way to innovative, environmentally conscientious solutions for future generations.

Drs. Nicholas A. Beier, G. Ward Wilson and David C. Sego, through the OSTRF, lead instrumental initiatives to bring together academia, industry and government agencies to find environmentally sustainable solutions for oil sands development. One such initiative is the International Oil Sands Tailings Conference (IOSTC), which provides a forum for mine waste managers, engineers, regulators and researchers to present new ideas and to discuss the latest developments in the field.

The Seventh International Oil Sands Tailings Conference offers the most recent developments in oil sands tailings and management through invited speakers and select technical presentations. IOSTC'22 will feature invited speakers and select technical presentations on topics including innovations in tailings management and dewatering technologies, regulatory policy and guidelines, mine waste structure integrity and closure/reclamation considerations.

For more information about the University of Alberta Geotechnical Centre's current oil sand tailings research projects and initiatives, including the NSERC/COSIA Industrial Research Chair (IRC) in Oil Sands Tailings Geotechnique, please visit http://ualbertageotech.ca or http://ostrf.com.

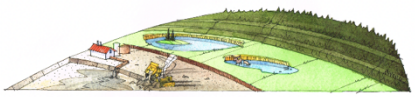

International Oil Sands Tailings Conference 2022

The UofA Geotechnical Centre

Proceedings cover photo courtesy of Syncrude Canada Ltd.